

Simple, Efficient, and Rapid Methods to Determine the Potential for Vapor Intrusion into the Home: Temporal Trends, Vapor Intrusion Forecasting, Sampling Strategies, and Contaminant Migration Routes

RESEARCH AND DEVELOPMENT

Simple, Efficient, and Rapid Methods to Determine the Potential for Vapor Intrusion into the Home: Temporal Trends, Vapor Intrusion Forecasting, Sampling Strategies, and Contaminant Migration Routes

Prepared for

U.S. Environmental Protection Agency
National Exposure Research Laboratory
Las Vegas, Nevada

Prepared by

RTI International
3040 E. Cornwallis Road
Research Triangle Park, NC 27709

and

ARCADIS U.S., Inc.
4915 Prospectus Drive, Suite F
Durham, NC 27713

EPA Contract EP-C-11-036, Task Order 013

Although this work was reviewed by EPA and approved for publication, it may not necessarily reflect official Agency policy. Mention of trade names and commercial products does not constitute endorsement or recommendation for use.

U.S. Environmental Protection Agency
Office of Research and Development
Washington, DC 20460

TABLE OF CONTENTS

1. Executive Summary	1-1
1.1 Context in Overall Research Program	1-1
1.2 Purpose and Objectives	1-2
1.3 Methods	1-2
1.4 Results and Conclusions	1-5
1.4.1 Performance of the Prediction Methods	1-5
1.4.2 Groundwater as a Vapor Intrusion Source	1-6
1.5 Considerations for Practitioners	1-7
2. Introduction	2-1
2.1 Background	2-3
2.1.1 Variability in Vapor Intrusion Studies	2-5
2.1.2 Vapor Attenuation Factors	2-10
2.1.3 Potential for Use of Radon as a Surrogate for VOC Vapor Intrusion	2-10
2.1.4 Passive VOC Sampling	2-13
2.2 Research Program Objectives	2-17
2.2.1 Continuing Objectives	2-17
2.2.2 New Objectives	2-20
2.2.3 Time Scale and Measurement of Independent and Dependent Variables	2-20
3. Methods	3-1
3.1 Site Description	3-1
3.1.1 Area Geology/Hydrogeology	3-1
3.1.2 Area Potential Sources	3-1
3.1.3 Building Description	3-6
3.1.4 Building Occupancy During Sampling	3-9
3.1.5 Investigation History	3-9
3.2 Evolution of Conceptual Site Model	3-9
3.2.1 Prior to 2011–2012 Investigations	3-10
3.2.2 After 2011–2012 Investigations (U.S. EPA, 2012a)	3-10
3.2.3 Refinements in Conceptual Site Model during the 2012–2013 Study (U.S. EPA, 2013)	3-11
3.2.4 Refinements in Conceptual Site Model During This Study (May 2013–March 2014)	3-12
3.3 Building Renovation and Mitigation	3-13
3.4 VOC Monitoring, Sampling, and Analysis	3-13
3.4.1 Indoor and Outdoor Air VOC Monitoring (Passive Samplers)	3-19
3.4.2 Subslab and Soil Gas (TO-17)	3-19
3.4.3 Groundwater	3-20
3.4.4 SSD System Stack Gas Sampling	3-20
3.4.5 FROG Portable GC	3-20
3.5 Radon Sampling and Analysis	3-20
3.5.1 Indoor and Outdoor Air Radon Sampling and Analysis (Electrets)	3-21
3.5.2 Subslab and Soil Gas Radon Sampling and Analysis (AlphaGUARD)	3-21
3.5.3 Continuous (Real-Time) Indoor Air Radon Sampling and Analysis (AlphaGUARD)	3-22

3.5.4	Consumer-Grade Radon Detector (Safety Siren).....	3-22
3.5.5	Professional Radon Detector (SIRAD).....	3-22
3.6	Physical Parameters Monitoring.....	3-23
3.6.1	On-Site Weather Station.....	3-23
3.6.2	Indoor Temperature.....	3-24
3.6.3	Soil Temperature.....	3-24
3.6.4	Soil Moisture.....	3-24
3.6.5	Groundwater and Surface Water Levels.....	3-25
3.6.6	Differential Pressure.....	3-25
3.7	Data Aggregation Methods.....	3-26
4.	Results and Discussion: Quality Assurance Checks of Individual Data Sets.....	4-1
4.1	VOC Sampling—Indoor Air, Passive Radiello—Eurofins Air Toxics, Ltd.....	4-1
4.1.1	Blanks.....	4-1
4.1.2	Surrogate Recoveries.....	4-3
4.1.3	Laboratory Control Sample Recoveries.....	4-3
4.1.4	Duplicates.....	4-4
4.2	VOC Sampling—Subslab and Soil Gas (TO-17)—U.S. EPA.....	4-4
4.2.1	Blanks.....	4-4
4.2.2	Calibration Verification.....	4-7
4.2.3	Internal Standard Recoveries.....	4-8
4.2.4	Surrogate Recoveries.....	4-8
4.2.5	Laboratory Control Sample Recoveries.....	4-8
4.2.6	Field Duplicates.....	4-9
4.3	Field Portable Gas Chromatograph (Soil Gas and Indoor Air).....	4-9
4.3.1	Blanks.....	4-10
4.3.2	Initial Calibration.....	4-10
4.3.3	Continuing Calibration.....	4-11
4.3.4	Calibration Check via Comparison to Fixed Laboratory (TO-17 versus Field PorGC).....	4-11
4.4	Radon.....	4-12
4.4.1	Indoor Air: Comparison of Electrets to Charcoal Canisters Analyzed by EPA Radiation and Indoor Environments National Laboratory.....	4-12
4.4.2	Comparison of Average of Real-Time AlphaGUARD to Electrets and Charcoal Canisters.....	4-15
4.4.3	Quality Assurance Checks of Electrets.....	4-19
4.5	On-Site Weather Station versus National Weather Service.....	4-20
4.6	Groundwater Analysis—EPA NERL.....	4-22
4.6.1	Blanks.....	4-22
4.6.2	Surrogate Recoveries.....	4-24
4.7	Database.....	4-25
4.7.1	Checks on Laboratory Reports.....	4-25
4.7.2	Database Checks.....	4-25
5.	Results and Discussion: VOC Concentration Temporal Trends and Relationship to HVAC and Mitigation.....	5-1
5.1	VOC Seasonal Trends Based on Weekly, Biweekly, and Monthly Measurements for 100+ Weeks.....	5-1
5.1.1	Indoor Air.....	5-1
5.1.2	Subslab Soil Gas.....	5-5
5.1.3	Shallow and Deep Soil Gas.....	5-9
5.2	Radon Seasonal Trends (based on Weekly Measurements).....	5-23

5.3	VOC Sampling with the FROG 4000 Unit and TO-17 and Passive Samplers.....	5-23
5.3.1	Indoor Air Test of FROG 4000 Against Passive VOC Samplers.....	5-24
5.3.2	Subsurface Soil Gas Data by the FROG and TO-17	5-26
5.3.3	Water Sampling by FROG and EPA Laboratory	5-31
5.4	Radon Short-Term Variability (Based on Daily and More Frequent Measurements).....	5-32
5.4.1	AlphaGUARD Radon Measurements	5-32
5.4.2	SIRAD Radon Measurements	5-34
5.5	Outdoor Climate/Weather Data	5-36
5.5.1	Weather Parameters.....	5-36
5.5.2	Weather Related to VOCs and Radon.....	5-40
6.	Results and Discussion: Further Analysis of 2010–Early 2013 Data Sets as a Basis for Vapor Intrusion Predictions.....	6-1
6.1	Summary of 2013 Report Regarding Multiple Lines of Evidence Analysis	6-1
6.2	Updated Time Series Analysis	6-1
6.2.1	Categorical Predictor Variables for Wind Direction, Snow, Ice, and Thunder Events.....	6-3
6.2.2	Derived Predictor Variables Based on Barometric Pressure Measurements.....	6-3
6.2.3	Derived Predictor Variables Based on Differential Pressure and Temperature Measurements.....	6-4
6.2.4	Measures of Goodness of Fit between Predictor Variables and Outcome Variable (Indoor Air Concentration).....	6-6
6.2.5	Updated Time Series Analysis Results.....	6-6
6.2.6	Time Series Analysis of Hartman Online GC Data at Daily Resolution.....	6-25
6.3	Influence of Meteorological Conditions on Indoor VOC Concentration: Overall Analysis.....	6-43
6.3.1	Temperature Effect on VOCs.....	6-43
6.3.2	Barometric Pressure Effect on VOCs.....	6-46
6.3.3	Precipitation Effects on VOCs	6-47
6.3.4	Effect of Wind on VOC Concentrations	6-47
6.3.5	Humidity and Soil Moisture Correlation with VOC Concentrations	6-48
	Attachment 6A. Aggregation of Predictor Variables across Multiple Time Intervals	6-54
	Attachment 6B. Chloroform Time Series Results—January 2011 through February 2012.....	6-61
	Attachment 6C. PCE Time Series Results—January 2011 through February 2012	6-73
	Attachment 6D. Chloroform Time Series Results—September 2012 through April 2013	6-85
	Attachment 6E. PCE Time Series Results—September 2012 through April 2013.....	6-99
	Attachment 6F. Time Series Analysis Results—Hartman Online GC Data, Daily Resolution	6-113
7.	Vapor Intrusion Forecasting Performance.....	7-1
7.1	Forecasting Approach.....	7-1
7.2	Assessment of Accuracy of Vapor Intrusion Predictions	7-3
7.3	Potential Explanations of Differences between Forecast and Observations.....	7-9
7.3.1	Correlations to Change in Stack Effect Strength (as Opposed to Predicted Stack Effect Strength)	7-10
7.3.2	Effects of Annual or Rarer Flooding Events (and high water table).....	7-10
7.3.3	Winter to Winter Soil Gas Comparison.....	7-13
7.4	Summary and Implications of Forecasting Results	7-19
8.	Groundwater Results	8-1
8.1	Groundwater Level (Water Table) Changes beneath the Duplex.....	8-1
8.2	Groundwater VOC Concentration Trends.....	8-2
8.3	Groundwater VOC Concentration, Well Depth, and Water Level.....	8-4

8.4	Spatial Variability of Groundwater Samples	8-6
8.5	Systematic Variability Due to Groundwater Sampling Method	8-7
8.6	Comparing Groundwater Samples with Soil Gas Samples	8-10
8.6.1	Pairing of Groundwater Samples with Soil Gas Samples	8-10
8.6.2	Pairing Depth with Groundwater Measurements to Soil Gas and Groundwater Samples	8-11
8.6.3	Pairing Temperature Measurements with Groundwater Samples	8-11
8.6.4	Henry's Law Calculations	8-12
8.6.5	Results and Discussion	8-13
8.7	The Relationship of Groundwater Concentration to Soil Gas and Indoor Air Concentrations	8-18
8.8	Chapter Summary	8-19
	Attachment 8A. Cluster Analysis for Evaluating Spatio-Temporal Variability	8-21
9.	Conclusions and Practical Implications	9-1
9.1	Conclusions	9-1
9.1.1	Vapor Intrusion Prediction	9-1
9.1.2	Additional Analysis: Vapor Intrusion Mechanisms and Driving Forces	9-1
9.1.3	Groundwater as a Vapor Intrusion Source	9-2
9.2	Considerations for Practitioners	9-3
9.3	Potential for Improvements in the Analysis and Prediction of Vapor Intrusion Temporal Variability	9-4
10.	References	10-1

List of Figures

Figure 1-1. Temporal coverage of data sets collected (red line indicates the cutoff date for this report, yellow indicates cutoff for last report [U.S. EPA, 2013]).	1-3
Figure 3-1. Lithological fence diagram beneath the 422/420 house, toward N from street (top) and toward S from backyard (bottom). Basement is unshaded with silt and clay (brown) until 6 to 8 ft bls and sand and gravel (burnt orange) and sand (orange) below.	3-2
Figure 3-2. Aerial view of duplex, 420/422 East 28th Street, showing nearby sanitary and storm sewers.	3-3
Figure 3-3. East side of house (on right) and adjoining commercial quadraplex visible (left).	3-4
Figure 3-4. Roof of adjacent commercial quadraplex.	3-4
Figure 3-5. Looking toward southeast corner of adjacent commercial quadraplex.	3-5
Figure 3-6. Visual evidence of historic dry cleaners in area.	3-6
Figure 3-7. Front view of house during summer 2011 sampling, with fan testing and weather station.	3-7
Figure 3-8. Front view of duplex under winter conditions showing designation of sides and HVAC setup.	3-7
Figure 3-9. 422 (left) and 420 East 28th Street in January 2011.	3-8
Figure 3-10. Map view of the 422-side basement showing mitigation system legs, subslab soil gas extraction pits (red circles), and the position of the passive “sampling racks.”	3-14
Figure 3-11. Map view of the 420-side basement showing the mitigation system legs, subslab soil gas extraction pits (red circles), and the passive “sampling racks.”	3-15
Figure 3-12. Photos of mitigation system: (left) SSD blower and stack on northeast corner of duplex; (right) SSD extraction point showing valve and U-tube manometer.	3-16
Figure 3-13. Showing the general layout of the 422/420 north and central basements with the positioning of the extraction legs, exterior blower, and exhaust stack.	3-17
Figure 3-14. Sampling port and monitoring well locations: subsurface soil gas monitoring ports (SGP), subslab sampling ports (SSP), groundwater monitoring wells (MW), on-site gas chromatography (GC), and other monitoring locations. Probes/ports in red were sampled by the on-site GC. Soil temperature and moisture probes were installed in the 422 basement between SGP 8 and MW 3 and in the backyard to the north of MW 2.	3-18
Figure 3-15. Front view of 420/422 duplex with location of weather station sensors indicated with red arrow.	3-23
Figure 4-1. Comparison between FROG 4000 and TO-17 sampling of bag standards.	4-12
Figure 4-2. Correlation between radon measured using the electret and charcoal methods.	4-13
Figure 4-3. Aerial view of study house, showing potential influences on wind velocity; red arrow indicates study house.	4-20
Figure 4-4. Comparison of National Weather Service Indianapolis temperature data to a weather station at 422 East 28th Street.	4-21
Figure 4-5. Comparison of National Weather Service Indianapolis relative humidity to a weather station at 422 East 28th Street.	4-21
Figure 4-6. Comparison of National Weather Service wind speed data to a weather station at 422 East 28th Street.	4-22
Figure 5-1. PCE in indoor and outdoor (ambient) air over time (7-day Radiello samples).	5-2
Figure 5-2. Chloroform in indoor and outdoor (ambient) air over time (7-day Radiello samples).	5-3
Figure 5-3. Benzene in indoor and outdoor (ambient) air over time.	5-4
Figure 5-4. Toluene in indoor and outdoor (ambient) air over time.	5-5
Figure 5-5. Interior and exterior sampling port locations.	5-6
Figure 5-6. Plot of subslab chloroform concentrations over time (TO-17 data).	5-7
Figure 5-7. Plot of subslab PCE concentrations over time (TO-17 data).	5-8
Figure 5-8. Plot of wall port chloroform concentrations over time (TO-17 data).	5-9

Figure 5-9. Plot of wall port PCE concentrations over time (TO-17 data).	5-10
Figure 5-10. Chloroform at SGP11 on the 420 side of duplex.	5-11
Figure 5-11. PCE at SGP11 on the 420 side of the duplex.	5-11
Figure 5-12. Chloroform at SGP12 on the 420 side of duplex.	5-12
Figure 5-13. PCE at SGP12 on the 420 side of the duplex.	5-12
Figure 5-14. Chloroform at SGP8 on the 422 side of duplex.	5-13
Figure 5-15. PCE at SGP8 on the 422 side of the duplex.	5-13
Figure 5-16. Chloroform at SGP9 on the 422 side of duplex.	5-14
Figure 5-17. PCE at SGP9 on the 422 side of the duplex.	5-14
Figure 5-18. Chloroform at SGP10 on the 422 side of duplex.	5-15
Figure 5-19. PCE at SGP10 on the 422 side of the duplex.	5-15
Figure 5-20. Chloroform at SGP1 on the exterior of the duplex.	5-16
Figure 5-21. PCE at SGP1 on the exterior of the duplex.	5-16
Figure 5-22. Chloroform at SGP2 on the exterior of the duplex.	5-17
Figure 5-23. PCE at SGP2 on the exterior of the duplex.	5-17
Figure 5-24. Chloroform at SGP3 on the exterior of the duplex.	5-18
Figure 5-25. PCE at SGP3 on the exterior of the duplex.	5-18
Figure 5-26. Chloroform at SGP4 on the exterior of the duplex.	5-19
Figure 5-27. PCE at SGP4 on the exterior of the duplex.	5-19
Figure 5-28. Chloroform at SGP5 on the exterior of the duplex.	5-20
Figure 5-29. PCE at SGP5 on the exterior of the duplex.	5-20
Figure 5-30. Chloroform at SGP6 on the exterior of the duplex.	5-21
Figure 5-31. PCE at SGP6 on the exterior of the duplex.	5-21
Figure 5-32. Chloroform at SGP7 on the exterior of the duplex.	5-22
Figure 5-33. PCE at SGP7 on the exterior of the duplex.	5-22
Figure 5-34. Radon: Weekly time integrated samples (electret).	5-24
Figure 5-35. Radiello indoor air PCE data versus FROG indoor air PCE data.	5-25
Figure 5-36. SKC badge indoor air PCE data versus FROG indoor air PCE data.	5-26
Figure 5-37. FROG 4000 and TO-17 PCE data at SGP8-9.	5-27
Figure 5-38. FROG 4000 and TO-17 PCE data at SGP9-9.	5-28
Figure 5-39. FROG 4000 and TO-17 PCE data at SGP10-9.	5-28
Figure 5-40. FROG 4000 and TO-17 PCE data at SGP11-9.	5-29
Figure 5-41. FROG 4000 and TO-17 PCE data at SGP12-9.	5-29
Figure 5-42. FROG 4000 and TO-17 PCE data at SSP-1.	5-30
Figure 5-43. FROG 4000 and TO-17 PCE data at SSP-4.	5-30
Figure 5-44. FROG 4000 and TO-17 PCE data at SSP-5.	5-31
Figure 5-45. Comparison between water samples: FROG 4000 and EPA laboratory PCE data.	5-32
Figure 5-46. Real-time radon (422 basement) 2011–2014. Note: basement AlphaGUARD moved during the week of 10/24/13.	5-33
Figure 5-47. Real-time radon (422, second floor office), 2011–2014.	5-34
Figure 5-48. Real-time radon (422 south basement) AlphaGUARD vs. SIRAD.	5-35
Figure 5-49. Real-time radon (422, second floor office) AlphaGUARD vs. SIRAD.	5-36
Figure 5-50. Temperature plots from HOBO data loggers and the 422 house weather station.	5-37
Figure 5-51. Weather variables measured inside 422 office (second floor) and on roof (top to bottom): (list based on revised figure in figure folder).	5-39
Figure 5-52. Comparison graph plotting FROG PCE concentrations, wall port differential pressure, outdoor pressure, wind speed, and wind direction.	5-40
Figure 5-53. Comparison graph plotting AlphaGUARD radon, FROG VOCs, and snow events.	5-41
Figure 6-1. XY plot of first difference in snow depth vs. first difference in chloroform concentration (includes locally weighted scatterplot smoothing [LOESS] line [blue], with a 95% confidence interval [shaded]).	6-13

Figure 6-2a. XY plot of shallow external soil temperature at 1 ft vs. 422 basement south chloroform concentration (includes LOESS line [blue], with a 95% confidence interval [shaded]).	6-14
Figure 6-2b. XY plot of first difference of shallow external soil temperature at 1 foot vs. first difference of 422 basement south chloroform concentration (includes LOESS line [blue], with a 95% confidence interval [shaded]).	6-14
Figure 6-3. XY plot of first difference in barometric pressure standard deviation “pump speed” vs. PCE concentration.	6-15
Figure 6-4. XY plot of the first difference in snowdepth vs. PCE concentration.	6-16
Figure 6-5. XY plot of the first difference in shallow exterior soil temperature vs. PCE concentration.	6-17
Figure 6-6a. XY plot of barometric pressure (inches of mercury) and chloroform concentration (422 basement south) in September 2012 to April 2013 data set.	6-18
Figure 6-6b. XY plot of barometric pressure (inches of mercury) and chloroform concentration (422 basement south) in September 2012 to April 2013 data set; segregated by mitigation status.	6-18
Figure 6-7a. XY plot of barometric pressure vs. chloroform January 2011 to February 2012.	6-19
Figure 6-7b. XY plot of first difference in barometric pressure vs. first difference chloroform January 2011 to February 2012.	6-19
Figure 6-8. XY plot of radon (pCi/L) vs. chloroform ($\mu\text{g}/\text{m}^3$), 422 basement south, January 2011 to February 2012 data set.	6-20
Figure 6-9. XY plot barometric pressure vs. first difference in PCE concentration.	6-21
Figure 6-10. XY plot of first difference of radon vs. first difference in PCE.	6-22
Figure 6-11. XY plot of first difference of the 420 subslab to basement differential pressure vs. first difference in PCE concentration.	6-23
Figure 6-12. XY plot of first difference of 422 subslab to basement differential pressure vs. first difference of 422 basement south PCE concentration.	6-24
Figure 6-13. Time series plot, ADF and PACF for daily measurements of X422baseS_GC3_PCE. Location X422 base south. Time period: December 2012 to March 2013.	6-26
Figure 6-14. Time series plot, ADF and PACF for first difference of daily measurements of X422baseS_GC3_PCE. Location X422 base south. Time period: December 2012 to March 2013.	6-27
Figure 6-15. XY plot of barometric pressure rate of change in inches of mercury per hour vs. first difference in 422 base south PCE, online GC December 2012 to March 2013.	6-28
Figure 6-16. XY plot of barometric pressure net change vs. first difference in PCE concentration, online GC Data December 2012 to March 2013.	6-29
Figure 6-17a. XY plot of mean daily barometric pressure (inches of mercury) vs. first difference in PCE concentration, online GC data, December 2012 to March 2013.	6-30
Figure 6-17b. XY plot of first difference in average daily barometric pressure vs. first difference in PCE concentration, online GC data, December 2012 to March 2013.	6-31
Figure 6-18. XY plot of barometric pressure standard deviation “pump speed” vs. first difference in PCE concentration, online GC data, December 2012 to March 2013.	6-32
Figure 6-19. XY plot of the first difference in heating degree days vs. the first difference in indoor PCE concentration, online GC data, December 2012–March 2013.	6-34
Figure 6-20. XY plot of the first difference in temperature at the 422 base south location to the first difference in indoor PCE concentration at the same location; online GC data, December 2012 to March 2013.	6-35
Figure 6-21. XY plot of first difference in subslab port SSP-4 PCE vs. first difference in 422 basement south PCE, online GC data December 2012 to March 2013.	6-36
Figure 6-22. First difference in subslab port 7 PCE vs. first difference in indoor air PCE at 422 basement south; online GC data, December 2012 to March 2013.	6-37

Figure 6-23. XY plot of first difference in PCE concentration at soil gas point 8-9 vs. first difference in indoor concentration at 422 basement south; online GC data; December 2012 to March 2013.	6-38
Figure 6-24. XY plot of first difference (day to day) of differential pressure between basement and upstairs vs. first difference in PCE concentration; online GC data, December 2012 to March 2013.	6-39
Figure 6-25. XY plot of first difference (day to day) in basement to outdoor differential pressure vs. first difference in PCE concentration.	6-40
Figure 6-26. XY graph of first difference in indoor humidity (measured in the 422 2 nd floor office) vs. first difference in indoor concentration of PCE; online GC data, December 2012 to February 2013.	6-41
Figure 6-27. XY graph of first difference in outdoor humidity vs. first difference in indoor concentration of PCE; online GC data, December 2012 to February 2013.	6-42
Figure 6-28. XY plot of temperature in 422 at basement north location vs. indoor concentration of PCE at 422 basement south location, radiello passive samples, January 2011 to February 2012 (includes locally weighted scatterplot smoothing [LOESS] line [blue], with a 95% confidence interval [shaded]).	6-44
Figure 6-29. XY Plot of basement temperature in 422 basement north vs. indoor concentration in 422 basement south, December 2011 to February 2012, on-site GC, daily aggregated data (includes locally weighted scatterplot smoothing [LOESS] line [blue], with a 95% confidence interval [shaded]).	6-44
Figure 6-30. XY plot of basement temperature in 422 basement north vs. indoor concentration in 422 basement south, December 2012 to March 2013, on-site GC, daily aggregated data (includes locally weighted scatterplot smoothing [LOESS] line [blue], with a 95% confidence interval [shaded]).	6-45
Figure 6-31. XY plot of temperature at 422 basement south vs. PCE, 3 hour aggregated data, December 2012 to March 2013 on-site GC (includes locally weighted scatterplot smoothing [LOESS] line [blue], with a 95% confidence interval [shaded]).	6-45
Figure 6-32. XY plot of barometric pressure vs. PCE, online GC data, 3-hour aggregation, August 2011 to October 2011 (includes locally weighted scatterplot smoothing [LOESS] line [blue], with a 95% confidence interval [shaded]).	6-46
Figure 6-33. XY plot of barometric pressure vs. PCE, online GC data, 3-hour aggregation; December 2012 to March 2013 (includes locally weighted scatterplot smoothing [LOESS] line [blue], with a 95% confidence interval [shaded]).	6-47
Figure 6-34. XY plot of indoor humidity (422 office) vs. PCE concentration in 422 basement south; January 2011 to February 2012, Radiello passive sampler data (includes locally weighted scatterplot smoothing [LOESS] line [blue], with a 95% confidence interval [shaded]).	6-48
Figure 6-35. XY plot of indoor humidity (422 office) vs. PCE concentration in 422 basement south; August 2011 to October 2011, online GC data, 3-hour aggregation (includes locally weighted scatterplot smoothing [LOESS] line [blue], with a 95% confidence interval [shaded]).	6-49
Figure 6-36. XY plot of indoor humidity (422 office) vs. PCE concentration in 422 basement south, December 2011 to February 2012, online GC data, daily aggregation (includes locally weighted scatterplot smoothing [LOESS] line [blue], with a 95% confidence interval [shaded]).	6-49
Figure 6-37. XY plot of indoor humidity (422 office) vs. PCE concentration in 422 basement south; December 2012 to March 2013, online GC data, daily aggregation (includes locally weighted scatterplot smoothing [LOESS] line [blue], with a 95% confidence interval [shaded]).	6-50

Figure 6-38. XY plot of indoor humidity (422 office) vs. PCE concentration in 422 basement south; December 2012 to March 2013, online GC data, 3-hour aggregation (includes locally weighted scatterplot smoothing [LOESS] line [blue], with a 95% confidence interval [shaded]).	6-50
Figure 6-39. XY plot of soil moisture at 6 ft bls (immediately below floor) vs. PCE concentration, Radiello samples, January 2011 to February 2012 (includes locally weighted scatterplot smoothing [LOESS] line [blue], with a 95% confidence interval [shaded]).	6-51
Figure 6-40. XY plot of soil moisture at 6 ft bls (immediately below floor) vs. chloroform concentration, Radiello samples, January 2011 to February 2012 (includes locally weighted scatterplot smoothing [LOESS] line [blue], with a 95% confidence interval [shaded]).	6-52
Figure 6-41. XY plot of first difference of soil moisture at 6 ft bls (immediately below floor) vs. first difference of PCE concentration, online GC measurements, daily aggregation, December 2011 to February 2012 (includes locally weighted scatterplot smoothing [LOESS] line [blue], with a 95% confidence interval [shaded]).	6-52
Figure 6-42. XY plot of first difference of soil moisture at 6 ft bls (immediately below floor) vs. first difference of PCE concentration, online GC measurements, daily aggregation, December 2012 to March 2013.	6-53
Figure 7-1. Comparison of predicted indoor air concentration to actual observed concentration, PCE.	7-5
Figure 7-2. Comparison of predicted concentration to actual observed concentration, chloroform.	7-6
Figure 7-3. Comparison of predicted concentration to actual observed concentration, radon.	7-7
Figure 7-4. Subslab port PCE also showing flood periods (staggered dark blue lines below the light blue lines).	7-8
Figure 7-5. Subslab port chloroform also showing flood periods (staggered dark blue lines below the light blue lines).	7-9
Figure 7-6. Depth to groundwater as measured by the 422 well water-level logger (2012–2014).	7-11
Figure 7-7. Depth to groundwater at duplex, including actual water-level logger and manual depth to water measurements and a predicted model based on Fall Creek stream gage data.	7-12
Figure 7-8. Indoor and ambient temperatures observed during project period (January 2011 through March 2014).	7-13
Figure 7-9. Comparison of monthly temperatures—extremes and means for January in 6 successive years.	7-14
Figure 7-10. Comparison of monthly snowfall—extremes and means for January in 6 successive years.	7-14
Figure 7-11. Box and whisker plot for PCE comparing four heating seasons (October to March) interior locations. ^a For each location, five depths are plotted from subslab to 16.5'.	7-17
Figure 7-12. Box and whisker plot for chloroform comparing four heating seasons interior locations (October to March) for each location five depths are plotted from subslab to 16.5'.	7-18
Figure 7-13. Box and whisker plot for PCE comparing four heating seasons (October to March) exterior locations; for each location five depths are plotted 3.5 to 16.5'.	7-20
Figure 7-14. Box and whisker plot for chloroform comparing four heating seasons (October to March) exterior locations; for each location five depths are plotted 3.5 to 16.5'.	7-21
Figure 8-1. Depth to groundwater at duplex, including water-level logger data and manual depth to water measurements (red) and a predicted model based on Fall Creek stream gage data (blue).	8-2
Figure 8-2. Groundwater VOC concentrations over time for Indianapolis duplex (open symbols represent nondetects plotted at one-half the detection limit).	8-4
Figure 8-3. Plot of groundwater PCE and chloroform concentrations against well screen (or soil gas port) depth (well depth measured to top of screen; open symbols are nondetects	

plotted at one-half the detection limit) (data set over full study period discussed in this report).....	8-5
Figure 8-4. Plot of groundwater PCE and chloroform concentrations against groundwater depth (open symbols are nondetects plotted at one-half the detection limit) (data set over full study period discussed in this report).....	8-5
Figure 8-5. Spatial variability in groundwater PCE (tetrachloroethene) concentration, April 2013.	8-6
Figure 8-6. Spatial variability in groundwater chloroform concentration, April 2013.	8-7
Figure 8-7. Distribution of concentration differences by sampling method—PCE.	8-10
Figure 8-8. Groundwater level measurements used for depth-to-water. “X” indicates where groundwater sample and soil gas sample depth-to-water differ by more than 12 inches.	8-12
Figure 8-9. Measured VOC concentrations in groundwater by time and sampling method (vertical lines indicate nondetects plotted from zero to one-half the detection limit).	8-13
Figure 8-10. Box and whiskers plots of VOC concentrations in measured in groundwater, organized by sampling method. Boxes outline 25th and 75th percentiles with heavy bar representing the median (50th percentile) concentration. Number of measurements is given below bars along with the count of nondetects in parentheses.	8-14
Figure 8-11. Expected and observed VOC concentrations in deep soil gas.	8-15
Figure 8-12. Expected vs observed VOC concentration.	8-16
Figure 8-13. Measured VOC concentrations in groundwater, with the total number of soil gas measurements and number of nondetects below each set of boxes. Each box spans the 25th percentile to 75th percentile range with the median plotted as the bold line.	8-17
Figure 8-14. Change in water depth (ft/day) vs. deviation from Henry’s law prediction.	8-18
Figure 8A-1. Choosing k: How many clusters should the data be grouped into? Within group sum of squares by number of clusters for the Indianapolis groundwater data.....	8-22
Figure 8A-2. Groundwater measurement clusters 1 – 4.	8-23
Figure 8A-3. X-Y distance (difference in location) does not explain difference in concentration.	8-24
Figure 8A-4. Z distance (difference depth) does not explain difference in concentration.....	8-24
Figure 8A-5. Euclidean distance does not explain difference in concentration.....	8-25
Figure 8A-6. Distance in time does not explain difference in concentration.....	8-25

List of Tables

Table 2-1. VOC Indoor Air Sampling Method Options	2-15
Table 2-2. Status of Original and Continuing Objectives from Earlier Phases of this Project	2-18
Table 2-3. Factors Causing Temporal Change in Vapor Intrusion and How They are Observed and Measured	2-21
Table 3-1. Data Aggregation Applied to Predictor Variables	3-26
Table 4-1. Indoor Air Passive Field Blank Summary—Radiello 130	4-2
Table 4-2. Indoor Air Passive Trip Blank Summary—Radiello 130	4-2
Table 4-3. Indoor Air Passive Laboratory Blank Summary—Radiello 130	4-2
Table 4-4. Indoor Air Passive Surrogate Summary—Radiello 130	4-3
Table 4-5. Indoor Air Passive LCS Summary—Radiello 130	4-4
Table 4-6. Indoor Air Passive Laboratory Precision (LCS/LCSD) Summary—Radiello 130	4-4
Table 4-7. Subslab and Soil Gas—EPA Field Blank Summary—TO-17	4-5
Table 4-8. Subslab and Soil Gas—EPA Trip Blank Summary—TO-17	4-6
Table 4-9. Subslab and Soil Gas—EPA Laboratory Blank Summary—TO-17	4-6
Table 4-10. Subslab and Soil Gas—EPA Fridge Blank Summary—TO-17	4-7
Table 4-11. EPA TO-17 Calibration Verification (CV) Summary	4-7
Table 4-12. EPA TO-17 Internal Standard (IS) Summary	4-8
Table 4-13. EPA TO-17 Surrogate Recovery Summary	4-8
Table 4-14. EPA TO-17 Laboratory Control Sample (LCS) Summary	4-9
Table 4-15. EPA TO-17 Field Duplicate Summary	4-9
Table 4-16. Comparison of Nominal and Measured FROG Performance Standard Concentrations.....	4-11
Table 4-17. Comparison between Electrets and Charcoal Canisters at the 422/420 EPA House from January 19 to 26, 2011	4-14
Table 4-18. Comparison of Electret and Charcoal Canister Data, April 27 to May 4, 2011	4-14
Table 4-19. Comparison of Charcoal and Electret Radon, December 28, 2011, to January 4, 2012.....	4-15
Table 4-20. Comparison of Charcoal and Electret Radon, June 19, 2013, to June 26, 2013.....	4-15
Table 4-21. Comparison between 422 Basement N AlphaGUARDS and Electrets, March 30, 2011, to May 18, 2011	4-16
Table 4-22. Comparison of Real-Time AlphaGUARD to Integrated Electret, August through October, 2011.....	4-16
Table 4-23. Comparison of Real-Time AlphaGUARDS to Integrated Electret Measurements, from December 28, 2011, to January 4, 2012.....	4-17
Table 4-24. Comparison of Real-Time AlphaGUARDS to Integrated Electret Measurements, January through March 2012	4-17
Table 4-25. Comparison of Real-Time AlphaGUARDS to Integrated Electret Measurements, January through March 2013	4-18
Table 4-26. Comparison of Real-Time AlphaGUARDS to Integrated Electret Measurements, January through March 2014	4-19
Table 4-27. Groundwater (5 mL)—EPA Field Blank Summary	4-23
Table 4-28. Groundwater (5 mL)—EPA Laboratory Blank Summary.....	4-23
Table 4-29. Groundwater (25 mL)—EPA Field Blank Summary	4-24
Table 4-30. Groundwater (25 mL)—EPA Laboratory Blank Summary.....	4-24
Table 4-31. EPA Groundwater (5 mL)—Surrogate Recovery Summary	4-25
Table 4-32. EPA Groundwater (25 mL)—Surrogate Recovery Summary	4-25
Table 5-1. Table of Temperature, Precipitation, and Change from Normal	5-38
Table 6-1. Summary of Lines of Evidence for Meteorological Factors Influencing Vapor Intrusion (U.S. EPA 2012a, 2013).....	6-2

Table 6-2. Derived Barometric Pressure Variables Used in U.S. EPA (2013) and Retained in this Analysis	6-4
Table 6-3. Derived Pressure Variables Added for this Analysis	6-4
Table 6-4. Additional Derived Variables Based on Differential Pressure and Temperatures	6-5
Table 6-5. Significant Lags for Radiello Models.....	6-9
Table 6-6. Analysis for Outcome First Difference of X422baseS_GC3_PCE. Variables Needing Lag-1 and Lag-2 Week Terms. Period December 2012 to March 2013	6-43
Table 6A-1. Data Aggregation Applied to Predictor Variables.....	6-55
Table 6B-1. Time Series Analysis for 422 Basement South Chloroform, Predictor Variables Not Requiring Lag Terms, Period January 2011 to February 2012.....	6-62
Table 6B-2. Time Series Analysis for 422 Basement South Chloroform: Predictor Variables Requiring One Lag Term, Period January 2011 to February 2012.....	6-63
Table 6B-3. Time Series Analysis for 422 Basement South Chloroform: Predictor Variables Requiring Two Lag Terms, Period January 2011 to February 2012.....	6-69
Table 6B-4. Time Series Analysis for 422 Basement South Chloroform: Categorical Predictor Variables, Period January 2011 to February 2012	6-71
Table 6C-1. Time Series Analysis for 422 Basement South PCE: Predictor Variables Requiring No Lag Terms, Period January 2011 to February 2012	6-74
Table 6C-2. Time Series Analysis for 422 Basement South PCE: Predictor Variables Requiring One Lag Term, Period January 2011 to February 2012.....	6-75
Table 6C-3. Time Series Analysis for 422 Basement South PCE: Predictor Variables Requiring Two Lag Terms, Period January 2011 to February 2012.....	6-80
Table 6D-1. Time Series Analysis for 422 Basement South Chloroform: Predictor Variables Requiring No Lag Terms, Period September 2012 to April 2013	6-86
Table 6D-2. Time Series Analysis for 422 Basement South Chloroform: Predictor Variables Requiring One Lag Term, Period September 2012 to April 2013	6-90
Table 6D-3. Time Series Analysis for 422 Basement South Chloroform: Categorical Predictor Variables, Period September 2012 to April 2013	6-97
Table 6E-1. Time Series Analysis for 422 Basement South PCE: Predictor Variables Requiring No Lag Terms, Period September 2012 to April 2013	6-100
Table 6E-2. Time Series Analysis for 422 Basement South PCE: Predictor Variables Requiring One Lag Term, Period September 2012 to April 2013	6-104
Table 6E-3. Time Series Analysis for 422 Basement South PCE: Categorical Predictor Variables, Period September 2012 to April 2013.....	6-111
Table 6F-1. Time Series Analysis for First Difference of 422 Basement South PCE Concentration (GC) Variables That Did Not Need Lag Terms. Period December 2012 to March 2013.....	6-114
Table 6F-2. Time Series Analysis for 422 Basement South PCE Concentration (GC). Variables that Needed a Lag-1 Day Term. Period December 2012 to March 2013	6-115
Table 7-1. Meteorological Predictor Variables Used to Guide Prediction	7-2
Table 7-2. Ability to Forecast Weather of Major Providers in Indianapolis, IN	7-3
Table 7-3. Flooding Events During Project Period (stream discharge greater than 2,000 cfs in Fall Creek).....	7-11
Table 7-4. Comparison of Indoor Air Concentrations in Four Successive Januaries	7-15
Table 7-5. Comparison of Average Subslab Concentrations in Four Successive Decembers—422 Side of Duplex ($\mu\text{g}/\text{m}^3$).....	7-15
Table 7-6. Comparison of Average Subslab Concentrations in Four Successive Januarys—422 Side of Duplex ($\mu\text{g}/\text{m}^3$).....	7-16
Table 8-1. Groundwater Monitoring Locations	8-3
Table 8-2. Four Clusters Defined for Indianapolis Groundwater Data.....	8-7
Table 8-3. Mean Difference in Concentration (Observed Mean – Group Mean) by Sampling Method.....	8-8

Table 8-4. Percent Nondetects by Compound and Cluster8-8
Table 8-5. Summary of Groundwater Measurements ($\mu\text{g/L}$)8-14
Table 8A-1. Four Clusters Defined for Indianapolis Groundwater Data8-22
Table 8A-2. Concentration Variability within Each Indianapolis Groundwater VOC Measurement
Cluster8-23

Notice

The information in this document has been funded wholly by the United States Environmental Protection Agency under contract number EP-C-11-036 to the Research Triangle Institute. It has been subjected to external peer review as well as the Agency's peer and administrative review and has been approved for publication as an EPA document. Mention of trade names or commercial products does not constitute endorsement or recommendation for use.

Acknowledgments

This project was conceived, directed, and managed by Brian Schumacher and John Zimmerman of U.S. EPA NERL. Robert Truesdale (RTI International) and Chris Lutes (ARCADIS) led the project, with report input by Brian Cosky, Nadine Weinberg, and Margaret Bartee (ARCADIS), Breda Munoz and Robert Norberg (RTI), and Heidi Hayes (Eurofins Air Toxics). The authors would also like to thank the following for their valuable input to the project:

- Alan Williams and Jade Morgan, U.S. EPA NERL, TO-17 analytical support
- Leigh Riley Evans, Executive Director of Mapleton-Fall Creek Development Corporation, the not for profit that provided the house used for this work
- Patrick Lewis, Defiant Technologies, who provided and supported the FROG GC analyses without cost
- Ausha Scott, analytical support, Air Toxics Ltd.
- Robert Uppencamp ARCADIS – field and site selection support; Sara Jonker, ARCADIS, field support
- Rebecca Forbort, ARCADIS data management
- Sharon Barrell, RTI report editing and document preparation.

Preface

This report entitled, “Simple, Efficient, and Rapid Methods to Determine the Potential for Vapor Intrusion into the Home: Temporal Trends, Vapor Intrusion Forecasting, Sampling Strategies, and Contaminant Migration Routes” is the third in a series of reports based on research performed to look at vapor intrusion into a historical duplex in Indianapolis, Indiana. The research is being conducted to look at the general principles of how vapors enter into this single residence.

The study was initiated in 2011 with the primary initial goal to investigate distributional changes in VOC and radon concentrations in the indoor air, slab, and subsurface soil gas from an underground source (groundwater source and/or vadose zone source) proximal to a residence. Currently, the study has extended more than 3.5 years in order to evaluate the effects due to seasonal variations on radon and VOC vapor intrusion. As a result, a significant dataset has been generated that can be used to advance and inform the understanding of vapor intrusion.

A series of at least four (4) reports are anticipated from the currently generated data.

- The initial report entitled, “Fluctuation of Indoor Radon and VOC Concentrations Due to Seasonal Variations” (EPA/600/R-12/673) examined the distributional changes in VOC and radon concentrations in the indoor air, slab, and subsurface from the ground water source into a residence.

- This second report entitled, “Assessment of Mitigation Systems on Vapor Intrusion: Temporal Trends, Attenuation Factors, and Contaminant Migration Routes under Mitigated and Non-mitigated Conditions” (EPA/600/R-13/241) examined: (a) subsurface conditions that influence the movement of VOCs and radon into the home; (b) effects of an installed mitigation system on VOC and radon concentration into the residence; and (c) the influence of a winter capping event on vapor movement into the home.
- This third report examines the use radon and other variables; such as weather data changes in temperature and differential pressure between indoors and outdoors, as potential low-cost, easily monitored indicators of when to sample for vapor intrusion events and when to turn on the mitigation system to reduce vapor intrusion exposure to the residents. Select data trends through the years of study at this site are also presented.
- The fourth report will provide information regarding the effectiveness of a soil vapor extraction system in preventing vapor intrusion into the residence.

In general, because this work was conducted at a single residential duplex, it cannot be representative of all sites and site conditions subject to vapor intrusion. However, it should be useful to compare the results of this study of an older building in a temperate Midwest climate with other ongoing detailed studies, such as the one conducted in a newer home in Layton, Utah for common threads that can be applied across all vapor intrusion sites.

A separate research report will be looking at the performance of passive samplers for the monitoring of vapor intrusion at multiples sites, including the Indianapolis duplex. It is anticipated that this report will be released in late 2015.

It is anticipated that research will continue (e.g., see fourth report) as new areas of scientific concern are identified and build on the research that has been conducted to date. The publication of peer-reviewed journal articles on select topics is also anticipated.

1. Executive Summary

1.1 Context in Overall Research Program

Current practice for evaluating the vapor intrusion pathway involves a multiple line of evidence approach based on direct measurements of volatile organic compound (VOC) concentrations in groundwater, external soil gas, subslab soil gas, and/or indoor air. No single line of evidence is considered definitive, and direct measurements of vapor intrusion can be costly, especially where significant spatial and temporal variability require repeated measurements at multiple locations to accurately assess the chronic risks of long-term exposure to VOCs like chloroform, perchloroethylene (PCE), and trichloroethylene (TCE).

The main goal of this project is to better characterize temporal and spatial variability by collecting a detailed long-term data set of weekly measurements of subslab soil gas, external soil gas, and indoor air on a single residential building that is affected by vapor intrusion of both radon and VOCs. This report is the third in a series reporting on this study. The first project report (U.S. Environmental Protection Agency [U.S. EPA], 2012a) provided information on how to best take and evaluate measurements to estimate long-term, chronic risk for VOCs by examining:

- both short-term (hourly, daily) and long-term (average annual) VOC and radon concentrations;
- passive sorbent performance over various sampling durations;
- the usefulness of soil gas samples taken externally to the building;
- the effects of heating, ventilation, and air conditioning (HVAC) system cycles;
- the comparative performance of temporary vs. permanent subslab ports; and
- induced depressurization within a building as a vapor intrusion evaluation strategy (fan testing).

Based on observations during the first year of the project, special attention was later paid to snow/ice events and flooding events as potential causes of dramatic temporal variability. We also implemented a common mitigation technology—subslab depressurization—to evaluate the effectiveness of this approach as a tool for reducing indoor concentrations and the temporal variability. Results regarding mitigation performance and the effects of weather factors on vapor intrusion were covered in a second report (U.S. EPA, 2013) based on a retrospective analysis of observed chemical concentration and weather measurements. This work led to the question of whether the level of understanding achieved was sufficient to allow a prospective forecasting of vapor intrusion potential on a building-specific basis based on forecasted weather conditions.

Radon concentration fluctuations have been studied all along in this project because if radon can be shown to indicate when there is a potential for chemical (i.e., VOC) vapor intrusion, radon, which is much cheaper to measure than VOCs, could be an important tool in improving the investigation and mitigation of chemical vapor intrusion (Schuver and Mosley, 2009; U.S. EPA 2012a, 2013). In addition, there is an extensive research literature and practical field experience base from radon intrusion into indoor air that could provide valuable lessons for chemical vapor intrusion (Steck, 2012).

1.2 Purpose and Objectives

In this, the third report of the series, we focus on:

- additional analyses of the independent variables (such as weather, building operations, water changes, and source concentrations) that can potentially influence vapor intrusion's variation over time;
- reporting of the results of the first experiment of which we are aware that attempts to forecast vapor intrusion's temporal variations; and
- continued interpretation of a multiyear detailed record of indoor air, groundwater, and soil gas data for a single building in terms of year-to-year variations in weather patterns and vapor intrusion.

The authors plan a later report to be released in 2015 regarding additional tests of long-term passive sampler performance and long-term mitigation system operation.

The main objectives for this phase of the study included:

- Use radon, determined using a simple in-home radon monitor, as an indicator of when to collect air samples to confirm vapor intrusion is occurring and when to turn on mitigation systems, as well as looking at correlations between radon and VOCs before and after the mitigation system is turned on (either manually or under computer control). For this report, we focus on work with the mitigation system primarily off. Longer term testing with the mitigation system on is in progress and will be reported on in 2015.
- In conjunction with the radon monitoring, investigate other variables, such as weather data and large changes in temperature and differential pressure between the indoors and outdoors, as potential low-cost, easily monitored indicators of when to sample and when to turn on the mitigation system.
- Continue evaluating the groundwater, soil gas, and indoor air VOC and radon concentrations in the home with respect to spatial and temporal trends and their relationship to vapor intrusion.

This work included additional data analyses to refine our understanding of the causes of higher amounts of vapor intrusion in this structure (both for radon and VOCs). We also tested our ability to apply that knowledge to forecast VOC vapor intrusion being measured in the duplex. The results of this experiment, along with the additional year of vapor intrusion monitoring, were also used to further our understanding of vapor intrusion processes and mechanisms at this house and elsewhere.

1.3 Methods

This study was conducted at a highly instrumented, pre-1920 residential duplex. The house was devoid of potential indoor VOC sources, but one half of the structure (the 422 side) was operated as if occupied with the provision of a central heating system and window air conditioner units. To characterize the basement and first floor of this residential duplex, radon and VOC sampling devices were installed at several locations: radon electrets and passive VOC samplers at four to seven stations, seven conventional subslab sampling ports, four basement wall ports similar to conventional subslab ports, seven exterior nested soil-gas probes with five sampling depths per probe, and five nested soil gas probes below the basement with four depths per probe. This arrangement of sampling devices provides for collection of an unusually comprehensive data set to formulate three-dimensional visualizations of seasonal VOC concentrations. Details of methods used and data collected from January 2011 to March 2013 have been previously reported in U.S. EPA (2012a, 2013) and are summarized in **Section 3** of this report.

Figure 1-1 shows the various types of samples and sampling frequency employed for each across this study. The more continuous variables (shown with black lines) were used in time series analysis. For

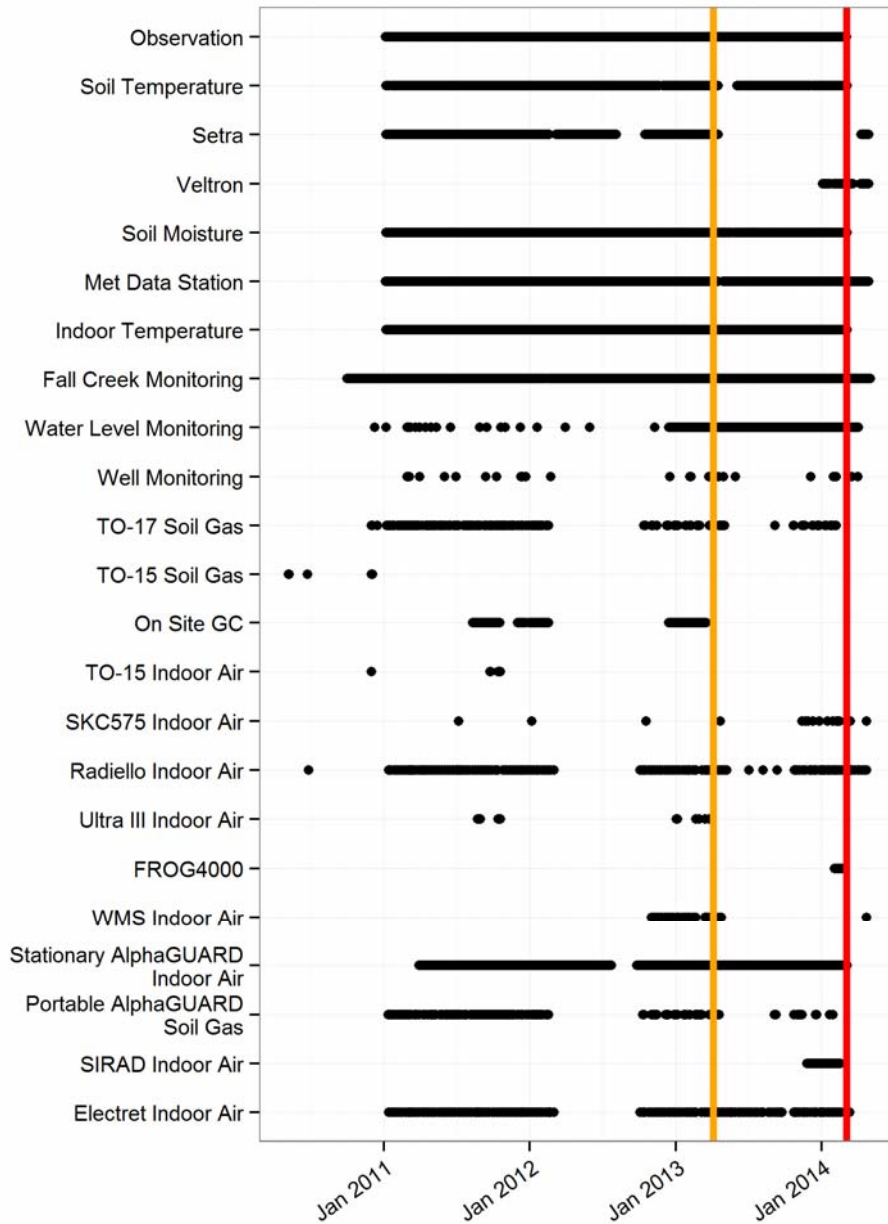


Figure 1-1. Temporal coverage of data sets collected (red line indicates the cutoff date for this report, yellow indicates cutoff for last report [U.S. EPA, 2013]).

Dots represent discrete sampling events. Bars represent continuous sampling methods. TO-15 is a summa canister sampler; TO-17 is an active (pumped) sorbent tube sampler; SKC 575 and Ultra III are badge-style passive sorbent samplers; Setra and Veltron are differential pressure measurement devices; GC = SRI 8610 gas chromatograph; FROG 4000 = porGC; WMS = Waterloo Membrane Sampler; Electret, AlphaGUARD, and SIRAD are radon measurement devices;. See Section 3 for additional information on measurements and methods.

radon, continuous measurements (weeklong electrets or continuous AlphaGUARD data) were taken for indoor air, while short-term grab samples were used to characterize soil gas. Similarly, the primary VOC

measurements were weeklong Radiello passive samples (for the entire project), daily SKC badge samples, continuous measurements of soil gas and indoor air VOC levels with an onsite gas chromatograph (GC) during critical project phases, and TO-17 grab samples to characterize soil gas on a weekly basis. Groundwater well samples were collected approximately monthly. Meteorological, observational, and pressure differential (Setra, Veltron) data were collected essentially continuously during the entire project.

In our overall study design, we used sequential week-long passive samplers and electrets to continuously observe our dependent variables—indoor air concentrations of VOCs and radon. We expected the indoor air concentration to depend on the flux from vapor intrusion from soil gas. Our dependent variables (indoor air VOC and radon concentrations) are therefore controlled by a series of independent variables with different time cycles that have been demonstrated or postulated to affect the vapor intrusion process: air temperature; barometric pressure; wind; soil moisture; soil temperature; groundwater level; and heating, ventilation, and air conditioning (HVAC) operation.

This project used indoor AlphaGUARD real-time radon instruments and Setra and Veltron differential pressure monitoring devices to observe possible indicators that chemical (VOC) vapor intrusion is or will occur at this particular house with high-time resolution. Standard National Weather Service forecasts were interpreted in terms of previous time series analysis results to predict the relative expected degree of vapor intrusion up to 7 days in advance. Stream gauge information, previously shown to correlate with shallow groundwater levels at this site, was also obtained real time from the U.S. Geological Survey (USGS) along with data from a continuous water-level logger installed in one of the groundwater monitoring wells at the duplex. During the times of predicted high vapor intrusion events and during control times, intensive periods of sampling were performed. These sampling events included additional TO-17 tubes for sampling soil gas, short-term (daily) passive samplers, AlphaGUARD soil-gas radon measurements, and groundwater sampling using passive diffusion bag (PDB) samplers and peristaltic pumps.

We attempted to predict vapor intrusion up to 1 week into the future and then compared our predictions to observed indoor air concentrations. Testing our ability to predict peak vapor intrusion events in this duplex (as indicated by indoor air concentrations) required several steps:

- A prediction approach based on meteorological variables was developed based on several years of intensive indoor air sampling to guide human judgment. An understanding was also developed of the relationship between radon concentrations and VOC concentrations in this duplex as well as the predictive value of differential pressure measurements.
- Forecasts of indoor air VOC concentrations were made using meteorological variables given by the National Weather Service. The meteorological-based forecasts of vapor intrusion were modified in some cases based on real-time observations of radon and differential pressure on the day the forecast was prepared. Adjectival indoor air forecasts were made approximately 1 week in advance of sampling from November 8, 2013, to March 4, 2014¹.
- Actual indoor air concentration data for VOCs and radon and actual weather data were reviewed and compared with the forecast.

Data analysis methods applied emphasized the use of statistical time series analyses supplemented with graphical visualization of the changes in predictor variables against changes in indoor air concentrations. We calculated and presented measures of the strength of the correlation between the predictor and

¹ We believe that it is unlikely that we will be able to forecast vapor intrusion conditions with more accuracy or lead time than is currently possible for weather forecasts, which are typically limited to 5 days or less. Weather forecast accuracy is not perfect even for less than 3 days in the United States; city-specific performance data can be obtained at <http://www.forecastadvisor.com/>.

outcome variables such as r^2 , Akaike information criteria (AIC), and the Bayesian information criteria (BIC).

The prediction approach was based on the following:

- Previous analysis of data from this duplex was available that related indoor air concentrations to predictor variables, including exterior temperature, snowfall, and wind direction provided in local weather forecasts. Because interior temperature was being maintained at a relatively constant point by a thermostatically controlled heating system, exterior temperature would control the indoor/outdoor temperature differential and thus was expected to control the strength of the stack effect moving soil gas into the duplex.
- Human expert interpretation of “rules of thumb” derived from the previous studies in light of the next week’s weather forecast to predict vapor intrusion strength on an adjectival scale.
- The use of real-time observations of indoor radon concentrations and differential pressure on a weekly basis as an additional line of evidence for the vapor intrusion forecasts.
- An implicit mental model that the subsurface source term was relatively constant and, therefore, indoor air concentrations were primarily controlled by the current strength of the driving forces across the building envelope. Given the measured air exchange rates for the duplex are generally between 0.5 and 1.5 air exchanges per hour (U.S. EPA, 2012a, 2013), the indoor air concentration would be expected to respond to changes in the rate of infiltration of soil gas within several hours if the source strength and subslab VOC concentrations remained relatively constant.

1.4 Results and Conclusions

1.4.1 Performance of the Prediction Methods

Although some aspects of the observed trends in indoor air concentrations during the test period in winter 2013–2014 were similar to those predicted, other aspects were not accurately predicted. Notably, an unpredicted decline in indoor air concentrations of VOCs was observed to begin in December 2013 despite sustained and even intensifying cold weather. Meanwhile, radon concentrations in indoor air stayed relatively high throughout the winter, suggesting that somewhat different mechanisms control VOC than radon vapor intrusion at this house. In our forecasting approach, the sustained cold weather was expected to lead to a continuing strong stack effect and consistently high indoor VOC concentrations. This discrepancy led us to conduct a more in-depth analysis of the driving forces and mechanisms of vapor intrusion in this duplex, which indicated the following:

- Notable differences between the range of indoor concentrations experienced in one winter and the indoor concentrations experienced in the next winter reemphasized that year-to-year meteorological and/or hydrogeological variations can be an important factor in vapor intrusion.
- The week-to-week change in the differential temperature, and thus stack effect, was more important than the absolute value of the differential temperature. In other words, indoor air concentrations of VOCs are expected to be high when the weather is getting colder but would not necessarily be expected to be as high during a period of sustained cold weather. This would appear to largely explain a repeatable trend in the duplex indoor air data set when indoor air VOC concentrations peaked early in winter (e.g., in mid- to late December 2011 and 2013).
- For example, the increase of the calculated stack effect strength was statistically associated with higher chloroform indoor air concentrations but not high stack effect strength values in and of themselves. This result may suggest why chloroform concentrations in our data sets tended to peak in late fall/early winter because that is the time of year when cooling temperatures would be expected to result in an increasing stack effect. A physical explanation of this result may be that

the stronger stack effects encourage advective chloroform migration but that sustained migration may temporarily deplete the source term (such as the concentration of chloroform at the interface between groundwater and soil gas). This behavior has been previously observed in the chamber-scale vapor intrusion experiments of Illangasekare and Petri (2013).

- Underlying, repeatable gradual seasonal trends in subslab soil gas concentrations appear to be present in the data set that were not well predicted based on our 7-day forecasts. These trends in subslab soil gas concentration generally correlate with trends in indoor concentrations. Although these trends repeated over several years, they did not have the same effect on two different subslab ports beneath the same side of the same duplex. Several mechanisms, such as temporary depletion of soil gas concentrations and periodic flood events affecting groundwater levels, could potentially explain such seasonal-scale variations.
- The relationships between several predictor variables and indoor air concentrations were nonlinear. For example, an inflection point was noted in the temperature data at approximately 52 to 55 °F. A U-shaped relationship between indoor air humidity and indoor PCE concentrations was noted with minimal PCE concentrations reached at intermediate humidities. A similar U-shaped relationship was noted between indoor air concentrations and continuous measurements of soil moisture directly beneath the basement floor. The relationships among the predictor variables may also be additive synergistic. This requires further analysis.
- In this report, we show that the most consistent relationship for barometric pressure is that an elevated (greater than 30 inches) and/or rising barometric pressure is associated with increasing vapor intrusion.
- In the time series analysis presented in **Section 6** of this report, we show a strong statistical relationship between increases in radon concentration and VOC concentrations in indoor air. In some data sets, increases in radon as a predictor was found to be statistically significant at the 1% level and to predict 40 to 60% of the variability in indoor air VOC concentrations (see specifically **Sections 6.2.5.4** and **6.2.5.5**).

The radon literature points to as many as 10 variables that continuously interact to control indoor radon concentrations. In this study, we found that the proportion of the VOC variability predicted by any one statistically significant predictor variables alone was modest (<30%). The ability of human experts to effectively predict such a complex multivariable process is expected to be limited. For example, despite more than a century of study, access to computerized forecasting tools, and a large data set of previous observations, weather forecasts are still frequently inaccurate.

1.4.2 Groundwater as a Vapor Intrusion Source

The most important groundwater finding was the reasonable agreement between the observed deep soil gas PCE concentrations and those predicted by Henry's law from groundwater concentrations and, in contrast, that chloroform is generally more concentrated in the deep soil gas than in groundwater. This is consistent with a conceptual site model in which (1) PCE is migrating to the immediate vicinity of the house in groundwater and vapor intrusion is driven by transport from groundwater and (2) chloroform is arriving at the immediate vicinity of the house at least in part from other sources, such as a buried storm sewer or sewer main. Additional conclusions from the study of groundwater concentrations include the following:

- Observations and statistical tests of groundwater PCE and chloroform data indicate that groundwater VOC concentrations remains consistent at the Indianapolis site, especially for PCE.
- Although groundwater remains the most likely source of PCE vapors, the variability of groundwater PCE concentrations is not sufficient to drive the variability observed in indoor air levels of PCE.

- Chloroform also generally shows less than an order of magnitude variability in groundwater, but groundwater concentrations did consistently increase by almost an order of magnitude in the latter part of this study during the winter of 2013–2014 without an obvious corresponding increase in indoor air. This suggests different sources for chloroform and PCE, which is consistent with other lines of evidence in this study.
- No correlation was observed or measured between groundwater sample depths, groundwater (water table) levels, and VOC levels in groundwater.

These findings supplement the results of tracer tests reported in Sections 12.2 and 13.1.3 of our previous report (U.S. EPA, 2013). Those tracer tests showed lateral migration of up to 20 ft in a few days. Tracer tests also showed vertical migration in a few days from 13 ft bls (just above the water table) to 6 ft. bls (the approximate elevation of the basement floor). In our first report on this project, we showed that the deep vs. shallow differential pressure responded strongly to the use of a box fan in the house to cause depressurization in the subsurface (U.S. EPA, 2012a, Section 12.2). These previous findings suggest that migration of soil gas to the house is primarily advective out to the horizontal and vertical limits of the soil gas and groundwater monitoring well network installed on the duplex lot for this project.

1.5 Considerations for Practitioners

Vapor intrusion strength appears to be a function of multiple independent weather and hydrological variables interacting in complex ways. There is no assurance that the most important variables in this single case study will be the most important variables at all residences in the United States. Most analyses of VOC vapor intrusion to date have attempted to correlate indoor concentrations directly to the current value of single variables. However, the evidence from the radon literature and from this vapor intrusion study, it is clear that multiple variables—perhaps as many as 10—interact to control vapor intrusion. This complexity suggests that a more completely automated forecasting approach to vapor intrusion may perform better than a human expert’s judgment informed by “rules of thumb” derived from quantitative analysis of previous indoor air concentrations. This complex behavior also suggests that current attempts by practitioners to select near-worst-case sampling conditions on the basis of guidance documents, “rules of thumb,” and experience at other sites are likely to be ineffective.

The following ideas are presented for consideration by vapor intrusion practitioners based on the research performed at the Indianapolis duplex site:

- Current indoor air sampling guidance that implicitly considers a sample collected at any time in any winter as a reasonable prediction of near-worst-case vapor intrusion should be reconsidered, especially when actual VOC concentrations are close (i.e., $\pm 30\%$) to the target exposure threshold values. Similarly, approaches that base an expectation for near-worst-case conditions on a single variable, such as indoor/outdoor temperature differential, are unlikely to lead to accurate predictions. One possible interim approach, based on our research site findings, would be to collect two samples in a winter, one in early to mid-winter and another later in the winter months. Prediction approaches that emphasize the week-to-week change in the values of the predictor variables, such as temperature differential and radon concentration, should be further tested.
- Should it be necessary to establish the worst-case short-term indoor air concentrations (with an exposure averaging period ranging from 1 week to 1 month), it will be necessary to consider year-to-year variations in meteorological conditions because it is possible to observe indoor air concentrations continuously for several months during one winter but miss by a factor of approximately 5 peak concentrations observed in prior and subsequent winters. Thus, to accurately measure the peak short-term concentrations expected over a long exposure period (e.g., years), one would likely have to sample various times during multiple years to capture the

effect of extreme weather effects. Alternatively, an appropriate factor of safety could be applied to the available measurements.

- We continue to see no evidence of a statistically significant rain effect in our data set.
- Rather than expecting high radon concentrations at any given time to be predictive of high VOC concentrations, practitioners should consider *increasing* values of radon concentrations in indoor air as a strong predictor of *increasing* VOC vapor intrusion. Similarly, the rapid decrease in outdoor temperature appears to be a better predictor of vapor intrusion than cold temperature alone.

2. Introduction

Vapor intrusion is the migration of subsurface vapors, including radon and VOCs, in soil gas from the subsurface to indoor air. Vapor intrusion happens because there are pressure and concentration differentials between indoor air and soil gas. Indoor environments are often negatively pressurized with respect to outdoor air and soil gas, for example, from exhaust fans or the stack effect,² and this pressure difference allows soil gas containing subsurface vapors to flow into indoor air through advection. In addition, concentration differentials cause VOCs and radon to migrate from areas of higher to lower concentrations through diffusion, which is another cause of vapor intrusion.

For VOCs, the vapor intrusion exposure pathway extends from the contaminant source, which can be free product (nonaqueous phase liquids [NAPLs]), VOCs sorbed to the geologic matrix (soil or aquifer material), or VOCs dissolved in groundwater, to indoor air exposure points. Contaminated matrices may include groundwater, soil, soil gas, and indoor air. VOC contaminants of concern typically include halogenated solvents such as TCE, PCE, chloroform, and the degradation products of TCE and PCE, including dichloroethylenes and vinyl chloride. These halogenated VOCs were widely used as solvents and cleaning agents, are toxic, and often degrade slowly in the subsurface, making them priority contaminants of concern through the vapor intrusion exposure pathway at many hazardous waste sites nationwide. Petroleum hydrocarbons, such as the aromatic VOCs of benzene, toluene, ethylbenzene, and xylenes (BTEX), are also contaminants of potential concern for vapor intrusion, but because they degrade much more readily in the subsurface, they are much less likely to lead to a vapor intrusion problem (U.S. EPA, 2012f).

Radon is a colorless radioactive gas that is released by radioactive decay of naturally occurring radionuclides in soil, where it migrates into homes through vapor intrusion in a similar fashion to VOCs. Radon is high in areas where the radioactive precursors to radon occur at relatively high concentrations in soil (as with the subject house of this investigation) and affects many more homes across the United States than halogenated VOCs. Low-cost testing and effective mitigation methods are available for radon, and the vapor intrusion of radon has been studied extensively by EPA and other organizations, thus contributing to our current conceptual understanding of the vapor intrusion process.

This project focused on halogenated VOCs with at least three chlorines per molecule, which are relatively recalcitrant (resistant) to biodegradation in aerobic soils and groundwater (with typical half-lives of a year or more; Howard et al., 1991), and radon, which has a radioactive half-life of about 3.8 days (Cohen, 1971). Of the two primary VOCs subject to investigation under this project (chloroform and PCE), PCE is generally considered quite recalcitrant, with an aerobic half-life in groundwater of 1 to 2 years (Howard et al., 1991). Studies of chloroform biodegradation under aerobic conditions are mixed, with some showing recalcitrance (e.g., a 0.2- to 5-year half-life in Howard et al., 1991) and others showing moderate cometabolic biodegradation with methylene chloride and chloromethane as sequential degradation products (Air Force Center for Environmental Excellence [AFCEE], 2004; Agency for Toxic Substances and Disease Registry [ATSDR], 1997). However, the much higher degradation rate for radon versus either of the halogenated VOCs studied under this project is perhaps the most significant differentiator to consider during interpretation of this study's results.

Current practice for evaluating the vapor intrusion pathway involves a multiple line of evidence approach based on direct measurements in groundwater, external soil gas, subslab soil gas, and/or indoor air.

² The stack effect is the overall upward movement of air inside a building that results from heated air rising and escaping through openings in the building super structure, thus causing an indoor pressure level lower than that in the soil gas beneath or surrounding the building foundation (<http://www.epa.gov/iaq/glossary.html>). This can result from heating for comfort in winter or solar heating of indoor air in summer.

Modeling approaches ranging from simple constructs, such as attenuation factors, to one- to three-dimensional models are frequently used as an aid to data interpretation and predictive tool. No single line of evidence is considered definitive, and direct measurements of vapor intrusion can be costly, especially where significant spatial and temporal variability require repeated measurements at multiple locations to assess the chronic risks of long-term VOC exposure accurately.

The main focus of this project is to better characterize this variability by collecting a detailed long-term data set of measurements of subslab soil gas, external soil gas, and indoor air on a single building that is affected by vapor intrusion of radon and VOCs. By examining both short-term and long-term (average annual) concentrations, the project provides valuable information on how to best take and evaluate measurements to estimate long-term, chronic risk for VOCs. In its first report (U.S. EPA, 2012a), the study examined

- passive sorbent performance over various timescales;
- the usefulness of soil gas samples taken externally to the building;
- the effects of heating, ventilation, and air conditioning (HVAC) system cycles;
- the use of temporary vs. permanent subslab ports; and
- induced depressurization within a building (fan testing) as a vapor intrusion evaluation strategy.

Based on observations during the first year of the project, subsequent research has paid special attention to snow/ice events and flooding events as potential causes of dramatic temporal variability. During the second year of the project, we implemented a common mitigation technology—subslab depressurization—to evaluate the effectiveness of this approach as a tool for reducing indoor concentrations and the temporal variability. Results regarding mitigation performance and the effects of weather factors on vapor intrusion were covered in a second report (U.S. EPA, 2013) based on a retrospective analysis of observed chemical concentration and weather data. This report addresses whether the level of understanding achieved in the first part of the study was sufficient to predict vapor intrusion potential based on forecasted weather conditions at the Indianapolis duplex.

Radon concentration fluctuations were also studied in this project because if radon can be shown to indicate when there is a potential for chemical (i.e., VOC) vapor intrusion, radon, which is much cheaper to measure than VOCs, could be an important tool in improving the investigation and mitigation of chemical vapor intrusion (Schuver and Mosley, 2009; U.S. EPA 2012a, 2013). In addition, extensive past research and practical field experience with radon intrusion could provide valuable lessons for chemical vapor intrusion.

This third report of the series focuses on:

- interpreting a multiyear record of indoor air, groundwater, and soil gas data for a single building in terms of year-to-year variations in weather patterns;
- additional analyses of how independent variables (e.g., weather, building operations, water fluctuations) can potentially influence vapor intrusion variation over time;
- reporting the results of the first attempt we are aware of to forecast the temporal variations of vapor intrusion; furthering development of conceptual site model with regard to VOC sources and the relationships between shallow groundwater and deep soil gas concentrations; and
- statistically evaluating how well typical vapor intrusion sampling plans would function when applied to the observed temporal variability in this duplex.

Data through April 2013 were reviewed and interpreted in the first and second reports. For relevant topics where significant new data were obtained after April 2013 but before March 5, 2014, we interpreted the new evidence in conjunction with that reported previously. We anticipate a later report to be released in 2015 regarding additional tests of long-term passive sampler performance and long-term mitigation system operation.

2.1 Background

An overview of the VOC vapor intrusion pathway is shown in **Figure 2-1**; the building in which exposure occurs is shown in the center. Three main routes of VOC migration have been defined:

1. movement of VOC vapors from shallow soil sources through unsaturated soil (the vadose zone)
2. transport of VOCs through groundwater, followed by volatilization of VOCs from the most shallow layer of groundwater into vadose zone soil gas
3. vapor movement through preferential pathways, such as storm drains or utility corridors, from soil or groundwater sources

Advection dominates transport through parts of these three routes, while diffusion dominates in others.

The final step of vapor intrusion typically involves soil gas moving from immediately below a building slab into the indoor air. This occurs through advection for most slabs,³ although diffusion also may be important when the slab is very well sealed. The subslab space is often significantly more permeable than the bulk vadose zone soil, either because a gravel drainage layer has been installed or because the soils have shrunk back from the slab in places. In such cases, the subslab space may serve as a plenum where VOCs can mix and reach the building through multiple points of entry. In cases where the subslab space is not so interconnected, subslab VOC concentrations can differ at different locations across the slab.

Others (e.g., Robinson and Sextro, 1997; Robinson et al., 2007a; DeVaul, 2012, 2013) have argued that in addition to the average advective force, the fluctuating element of the pressure field, which, like diffusion, contributes to the movement of mass from high to low concentration zones, can play an important and even dominant role in transport under some conditions (such as high permeability).

Vapor and liquid transport processes interact with various meteorological, geologic, and physical site conditions to control migration through the vapor intrusion pathway. Variations in building design, construction, use, and maintenance; site-specific stratigraphy; subslab composition; temporal variation in atmospheric pressure, temperature, precipitation, infiltration, soil moisture, and water elevation; and other factors combine to create a complex and dynamic system. As summarized by NJ DEP (2013), important factors controlling vapor intrusion at many sites include

- biodegradation of VOCs as they migrate in the vadose zone,
- site stratigraphy,
- soil moisture and groundwater recharge,
- fluctuations in water elevation, and
- temporal and interbuilding variations in the operation of ventilation systems in commercial/industrial buildings.

³ Here the term “slab” should be read to include the concept of “basement floor.”

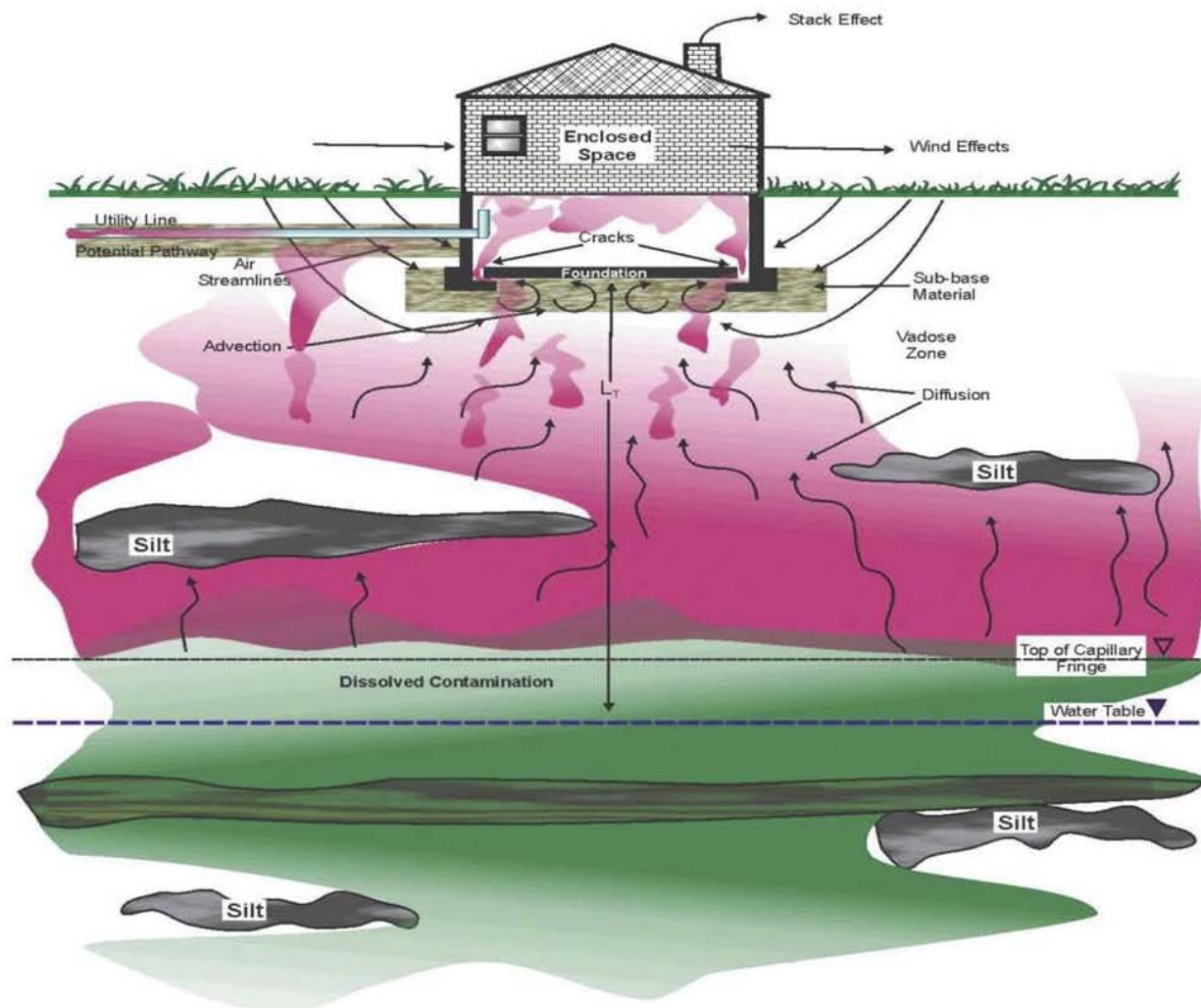


Figure 2-1. An overview of important vapor intrusion pathways (U.S. EPA graphic).

Utility corridors, such as the backfill around water lines or partially full sanitary or combined sewers, can provide routes of preferential migration through the vadose zone. This can occur on a site scale of hundreds of feet to a mile (Distler and Mazierski, 2010) or on the scale of an individual residential lot (Johnson et al., 2014). Advective flow into a building can occur more locally through cracks in the floor, below grade walls, or at incompletely sealed utility penetrations in the building foundation.

This project explored and further developed several promising cost-effective techniques to evaluate the vapor intrusion pathway and improve data quality. Two primary tools were investigated: (1) using passive sorbent-based measurement techniques for time-integrated measurements of indoor air VOCs and (2) using radon measurements for assessing VOC vapor intrusion. The project also investigated measurements of pressure differentials (subslab vs. indoor), meteorological conditions, and air exchange rates in the context of the chemical-specific measurements described above. These physical measurements are not stand-alone tools nor are they the emphases of the current research program, but they are valuable supporting tools for developing a better understanding of temporal and spatial variability, seasonal effects, and contaminant mass balances around a building subject to vapor intrusion.

This report cannot provide a complete review of the rapidly growing vapor intrusion literature. The reader may wish to consult reviews by Provoost (2010), ITRC (2007), and Tillman and Weaver (2005) for more comprehensive reviews. Useful literature and modeling-based discussions of the effect of numerous variables on vapor intrusion is also provided in U.S. EPA (2012d).

2.1.1 Variability in Vapor Intrusion Studies

This project observed changes in vapor intrusion over a >3-year period both with and without mitigation. In order to express quantitatively our goals for this project, it is necessary to understand the causes and typical ranges of spatial and temporal variation in various matrices studied for vapor intrusion assessment.

Through measurements of radon and VOC vapor intrusion under various conditions, several studies have provided insight into the complex temporal variability in indoor air concentrations attributable to vapor intrusion—the primary focus of this work. Nazaroff et al. (1987) studied how induced-pressure variations can influence radon transport from soil into buildings with roughly hourly resolution. In a more recent study, Mosley (2007) presented the results of experiments, showing that induced building-pressure variations influence both the temporal and spatial variability of both radon and chlorinated VOCs (CVOCs) in subslab samples and in indoor air (hourly sampling for radon). Schuver and Mosley (2009) have also reviewed numerous studies of radon indoor concentrations, in which multiple repeated indoor air samples were collected with hourly, daily, weekly, monthly, 3-month, and annual sample durations for study periods of up to 3 years; however, detailed soil gas radon data sets are much rarer.

Several radon studies have demonstrated that barometric pressure fluctuations can affect the transport of soil gas into buildings (Robinson and Sextro, 1997; Robinson et al., 1997). The impact of barometric pressure fluctuations on indoor air is influenced by the interaction of the building structures and conditions, as well as other concurrent factors, such as wind (Luo et al., 2006, 2009). Mechanisms of wind effects on vapor intrusion as they may apply to this duplex are discussed in Section 9.2.4 of U.S. EPA (2012). Changes in atmospheric conditions (e.g., pressure, wind) and building conditions (e.g., open doors and windows) may temporarily over- or under-pressurize a building. Based on long-term pressure differential data sets acquired by ARCADIS and EPA’s National Risk Management Research Laboratory (NRMRL) at a different Indianapolis study site at which both radon and VOCs are being measured in both subslab and indoor air, other factors that may cause temporal and spatial variability in soil vapor and indoor air concentrations include

- fluctuation in building air exchange rates due to resident behavior/HVAC operations,
- fluctuations in outdoor/indoor temperature difference, and
- rainfall events and resultant infiltration and fluctuations in the water elevation.

The pressure difference between a house-sized building and the surrounding soil is usually most significant within 1 to 2 m of the structure, but measurable effects have been reported up to 5 m from the structure (Nazaroff et al., 1987). Temperature differences or unbalanced mechanical ventilation is likely to induce a symmetrical pressure distribution in the subsurface, but the wind load on a building adds an asymmetrical component to the pressure and distribution of contaminants in soil gas.

Folkes et al. (2009) summarized several large groundwater, subslab, and indoor air data sets collected with sampling frequencies ranging from quarterly to annually during investigations of vapor intrusion from CVOC plumes beneath hundreds of homes in Colorado and New York. They analyzed these data sets to illustrate the temporal and spatial distributions in the concentration of VOCs. Their analysis demonstrated that although the areal extent of structures affected by vapor intrusion mirrored the plume of chlorinated VOCs in groundwater, not all structures above the plume were affected. In addition, they found that measured concentrations of VOCs in indoor air and subslab soil gas can vary considerably

from month to month and season to season and that sampling results from a single location or point in time cannot be expected to represent the range of conditions that may exist spatially or at other times.

In a study of the vapor intrusion pathway at the Raymark Superfund site, DiGuilio et al. (2006) showed that measured concentrations of CVOCs in subslab exhibited spatial and temporal variability between neighboring houses and within individual houses. Similar variability in subslab CVOC concentrations within and between houses has been observed during vapor intrusion evaluations of several sites in New York State (Wertz and Festa, 2007).

In scenarios with coarser soils (e.g., sands, gravels), the soil gas permeability is high, and changes in building pressurization may affect the airflow field and the resultant soil vapor concentration profiles near buildings. In scenarios with fine-grained soils (e.g., silts, clays), the soil gas permeability is low and soil gas flow rates (Q_s) may be negligible and not affect the subsurface concentration. Nevertheless, in both soil-type scenarios, overpressurization of the building may still significantly reduce the indoor air concentration because of the reversal of soil gas flow direction from the building into the soil (Abreu and Johnson, 2005, 2006).

A wind-induced, nonuniform pressure distribution on the ground surface on either side of a house may cause spatial and temporal variability in the subslab soil vapor concentration distribution if the wind is strong and the soil gas permeability is high (Luo et al., 2006, 2009; U.S. EPA, 2012d). In addition, during or after a rainfall event, the subsurface beneath the building may have a lower moisture content than the adjacent areas because of water infiltration.

2.1.1.1 Spatial Variability

Spatially, reports of several orders of magnitude variability without apparent patterns between indoor air and subslab concentrations for adjacent structures in a neighborhood are very common (see, for example, U.S. EPA, 2012c). Six orders of magnitude in subslab concentration variability were reported by Eklund and Burrows (2009) for one building of 8,290 sq ft. As shown in **Figure 2-2**, Schumacher et al. (2010) observed more than three orders of magnitude concentration variability in shallow soil gas below a slab over a span of 50 lateral feet, suggesting a strong effect of impervious surfaces both in limiting soil gas exchange with the atmosphere and in maintaining relatively high concentrations of VOCs in shallow groundwater. They also observed two orders of magnitude concentration variability with a depth change of 10 ft in the unsaturated zone within one borehole.

Lee et al. (2010) observed two orders of magnitude variability in subslab concentration within a small townhouse. Studies by McHugh et al. (2007) have generally found markedly less variability in indoor air concentrations than in subslab concentrations, probably due to the greater degree of mixing in the indoor environment.



Measured Soil Gas Profile for TCE – Phase 2

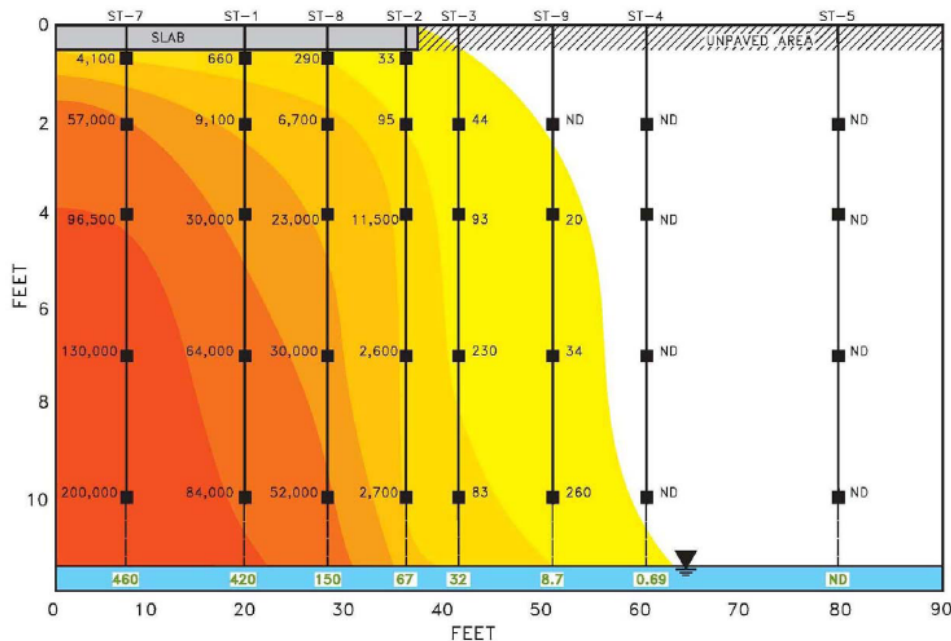


Figure 2-2. Soil gas and groundwater concentrations below a slab (Schumacher et al., 2010).

2.1.1.2 Temporal Variability

The current understanding of temporal variability has been summarized by ITRC (2007), which states that temporal variability in VOC concentrations in soil gas is primarily a result of the variability of temperature, precipitation, and activities within the structure of concern. They also note that variability increases close to the surface and decreases with depth. As of 2006, available data indicated that short-term variations in soil gas concentrations at depths 4 ft or deeper are less than a factor of 2 and that seasonal variations in colder climates are less than a factor of 5 (Hartman, 2006). Larger variations may be expected by current practitioners in areas of greater temperature variation and during heavy periods of precipitation, as described in ITRC (2007):

IBM, Endicott, New York

Recent data from a large site in Endicott, New York, collected over a 15-month period showed soil gas concentration variations of less than a factor of 2 at depths greater than 5 ft bls.

- Temperature. Effects on soil gas concentrations due to actual changes in the vadose zone temperature are minimal. The bigger effect is due to changes in an overlying heating or HVAC system and the ventilation of the structure due to open doors and windows. In colder climates, worse-case scenarios are most likely in the winter season. The radon literature suggests that temporal variations in soil gas are typically less than a factor of 2 and that seasonal effects are less than a factor of 5. If soil gas values are more than a factor of 5 below acceptable levels, repeated sampling is likely not necessary regardless of the season. If the measured values are within a factor of 5 of allowable risk levels, then repeated sampling may be appropriate.*

- *Precipitation. Infiltration from rainfall can potentially impact soil gas concentrations by displacing the soil gas, dissolving VOCs, and by creating a “cap” above the soil gas. In many settings, infiltration from large storms penetrates into only the uppermost vadose zone. In general, soil gas samples collected at depths greater than about 3–5 feet bgs⁴ or under foundations or areas with surface cover are unlikely to be significantly affected. Soil gas samples collected closer to the surface (<3 feet) with no surface cover may be affected. If the moisture has penetrated to the sampling zone, it typically can be recognized by difficulty in collecting soil gas samples. If high vacuum readings are encountered when collecting a sample or drops of moisture are evident in the sampling system or sample, measured values should be considered as minimum values.*
- *Barometric Pressure. Barometric pressure variations are unlikely to have a significant effect on soil gas concentrations at depths exceeding 3–5 feet bgs unless a major storm front is passing by. A recent study in Wyoming (Luo et al. 2006) has shown little to no relationship between barometric pressure and soil gas oxygen concentrations for a site with a water at ~15 feet bgs.*

In summary, temporal variations in soil gas concentrations, even for northern climates, are minor compared with the conservative nature of the risk-based screening levels. If soil gas values are a factor of 5–10 times below the risk-based screening levels, there likely is no need to do repeated sampling unless a major change in conditions occurs at the site (e.g., elevated water table, significant seasonal change in rainfall)...

And in Section D.8 of the same document, ITRC notes:

Short-term temporal variability in subsurface vapor intrusion occurs in response to changes in weather conditions (temperature, wind, barometric pressure, etc.), and the variability in indoor air samples generally decreases as the duration of the sample increases because the influences tend to average out over longer intervals. Published information on temporal variability in indoor air quality shows concentrations with a range of a factor of 2–5 for 24-hour samples (Kuehster, Folkes, and Wannamaker 2004; McAlary et al. 2002). If grab samples are used to assess indoor air quality, a factor of safety (at least a factor of 5) should be used to adjust for short-term fluctuations before comparing the results to risk-based target concentrations. Long-term integrated average samples (up to several days) are technically feasible, using a slower flow rate this is the USEPA recommended approach for radon monitoring). Indoor air sampling during unusual weather conditions should generally be avoided.

In Section D.11.8, ITRC goes on to discuss the effect of meteorological changes on vapor intrusion:

A variety of weather conditions can influence soil gas or indoor air concentrations. The radon literature suggests that temporal variations in the soil gas are typically less than a factor of 2 during a season and less than a factor of 5 from season to season). Recent soil gas data from Endicott, New York and Casper, Wyoming are in agreement with the radon results. For soil gas, the importance of

⁴ below ground surface

these variables will be greater the closer the samples are to the surface and are unlikely to be important at depths greater than 3–5 feet below the surface or structure foundation.

The most frequent time interval of observation in routine vapor intrusion practice has been 8- to 24-hour integrated samples. In this project, multiple durations of observation of indoor air concentrations were compared, including automated discrete samples collected on 3-hour intervals and passive samples with varying integration times: 24–48 hours, 7 days, 14 days, 28 days, 91 days, 182 days, and 364 days.

A team led by Paul Johnson (Johnson et al., 2012; Holton et al., 2013a,b; Johnson et al., 2014) recently reported more than 4 years of high-frequency observation of a home overlying a chlorinated solvent groundwater plume in Layton, Utah. The key observations at that site with regard to temporal variability include the following:

- Indoor air variability in TCE of about 3 orders of magnitude was observed. But vapor intrusion essentially ceased when a land drain lateral connecting the house to the sewer was experimentally shut off with a valve that was not a normal part of the system as constructed.
- The near-source data, such as deep soil gas, were more consistent in time than the near-surface data sets such as subslab air or indoor air.
- The temporal trend was characterized by “long periods of relative VI inactivity with sporadic VI activity” and “long periods of relative VI activity with sporadic VI inactivity” (Johnson et al., 2012).
- “24-h samples are not a very practicable option at the resolution required for robust VI pathway assessment” (Holton et al., 2013a,b).

The average long-term exposure can be potentially influenced by short, high-concentration events occurring at brief periods during the year, although this effect may not be large enough to change the risk management decision (Holton et al., 2013a,b; Lutes et al., 2013; Weinberg et al., 2014). Regulatory concerns have also been raised regarding the potential for health effects to be related to exposure periods as short as 24 hours over 21 days for TCE (Inside EPA, 2013).

2.1.1.3 Measurement Variability

Beyond spatial and temporal variability, the underlying uncertainty of the measurements used to assess vapor intrusion must also be considered. Many measurements of vapor intrusion, both in indoor air and subslab soil gas, have traditionally relied on Summa canister samples analyzed by Methods TO-14/TO-15. (U.S. EPA, 1999a, 1999b). Method TO-15 specifies an audit accuracy of 30% and a replicate precision of 25% as performance criteria. But even those figures do not fully convey the interlaboratory variability observed for these methods when applied to the low concentrations typical of indoor air studies. As Lutes et al. (2010) report:

- “In two recent TO-15 or 8260 interlaboratory comparisons administered by the company ERA for gas phase samples the acceptance range for tetrachloroethylene results were:
4.31–22.3 ppbv (July–Sept 2009 study)
31.6–74.1 µg/L (October–November 2007 study)
- For comparison in a 2007 TO-14/TO-15 study conducted by Scott Specialty Gasses the reported values for toluene reported by 12 labs varied from 3.1 to 18.6 ppb.”

These two examples show that at concentrations near detection limits actual TO-15 results can exhibit lower precision and accuracy than is specified in the method. Moreover, measurement variability is a combination of both sampling and analysis variability, and these interlaboratory studies essentially only examine analytical variability.

2.1.2 Vapor Attenuation Factors

One common way of evaluating the impact of subsurface vapors on indoor air quality is to compute the ratio of indoor air concentration to subslab soil vapor concentration. EPA has defined the resulting “attenuation factor” as follows: “The attenuation factor, α , is a proportionality constant relating indoor air concentrations ($C_{\text{indoor air}}$) to the concentrations of vapors in soil gas ($C_{\text{soil gas}}$) or groundwater ($C_{\text{groundwater}}$) concentrations.” For soil gas to indoor air, the equation is as follows:

$$C_{\text{indoor air}} = \alpha_{\text{SG}} \times C_{\text{soil gas}}$$

For groundwater, a similar equation is used except that the dimensionless Henry’s Law Constant (H) is used to convert the dissolved VOC concentration in groundwater to the corresponding equilibrium vapor concentration:

$$C_{\text{indoor air}} = \alpha_{\text{GW}} \times C_{\text{groundwater}} \times H$$

A larger α indicates less attenuation, and a smaller value indicates more attenuation. The greater the attenuation factor, the greater the indoor concentration.

Within any one given site, the attenuation factors

- between groundwater and indoor air typically vary 2 to 3 orders of magnitude and
- between external soil gas and indoor air typically vary 2 to 4 orders of magnitude.

Subslab soil gas and indoor air typically vary 2 to 4 orders of magnitude (Dawson and Schuver, 2010). EPA recently published a compilation of attenuation factor data (U.S. EPA, 2012c) that analyzes spatial and temporal variability. Because six is the maximum number of data rounds at a site in this compilation, the reports from this project (U.S. EPA, 2012a, 2013) are expected to provide a valuable addition to the literature regarding the temporal variability of attenuation factors.

U.S. EPA (2012c) also splits up the attenuation factor into processes occurring across the building envelope and within the soil as follows:

$$\alpha_{\text{building}} = \text{indoor air concentration/subslab concentration}$$

$$\alpha_{\text{soil}} = \text{subslab concentration/groundwater vapor concentration.}$$

2.1.3 Potential for Use of Radon as a Surrogate for VOC Vapor Intrusion

Radon, a naturally occurring radioactive gas, is a potentially useful surrogate for assessing VOC vapor intrusion because the physics of radon intrusion into indoor air is similar to VOC vapor intrusion. Radon is ubiquitous in the soil and present at measurable quantities in soil gas throughout the United States. Indeed, much of the research in VOC vapor intrusion is an expansion of earlier work on radon intrusion. Applications of radon as a VOC surrogate have been proposed for the following (Lutes et al., 2009; McHugh et al., 2008; Mosley, 2007; Mosley et al., 2008; Schuver and Mosley, 2009):

- estimating attenuation factors, with the measured radon attenuation factor serving as a surrogate for the attenuation that may be occurring for VOCs
- screening large populations of housing units/buildings, with the presence of radon above ambient levels in indoor air serving as evidence of soil gas influence

- using radon as a line of evidence to help distinguish indoor sources of VOCs where VOC indoor concentrations are higher than would be inferred based on the radon attenuation factor. Also, differing responses of radon and VOCs to building pressurization/depressurization tests could be used to assess the potential for indoor sources
- locating soil gas entry points where higher radon readings are observed
- verifying mitigation system performance based on the reduction of indoor air radon concentrations during mitigation system operation

Radon provides a nearly unique surrogate for VOC vapor intrusion because its presence in the indoor environment is usually a result of radon in the soil gas immediately surrounding a building. In theory, the entry mechanisms are believed to be the same for VOCs and radon in soil gas. Thus, measured radon entry rates should be a good predictor of relative entry rates for VOCs. The advantages of using radon as a surrogate measure for VOC vapor intrusion characterization include the following:

- Measurements of radon are easier, more accurate and precise, and much less expensive than canister (TO-15) measurements of VOCs, with radon measurement costs typically less than 10% of VOC analysis cost. Passive indoor sampling for radon costs approximately \$5 to \$20 per sample. Active radon sampling (indoor air and subslab) uses some of the same equipment and setup as for VOCs. This minimizes sampling times and cost. Continuous measurement devices for radon are also available ranging from consumer grade devices costing under \$150 to professional grade instruments costing up to \$10,000.
- High levels of indoor radon identify buildings that are vulnerable to soil gas entry.
- Because of the low sampling/analytical costs for radon, it is possible to conduct more field measurements than with VOCs. This, in turn, can increase confidence in the field evaluation.
- Because mitigation systems are the same for radon and VOCs and behave similarly in the vicinity of the building, radon measurements before and after installation of vapor intrusion mitigation systems may be useful for assessing mitigation system performance for VOCs.

In summary, the limited data gathered to date suggest that radon measurement may be an inexpensive, semiquantitative surrogate for VOC measurement when characterizing vapor intrusion and may significantly enhance vapor intrusion characterization and decision making, particularly when used in conjunction with subslab sampling. However, several key aspects and assumptions of this approach need to be verified before it can be put into widespread use. For radon to be a valuable surrogate for VOCs:

- Radon detection in building interiors should be quantitatively possible across the wide range of subslab concentrations encountered in the United States. Ideally, these measurements can be made with inexpensive passive methods (i.e., charcoal or electrets).
- The radon mechanism and route of entry should be similar to that of the VOCs of interest, and both species should be present in the subslab soil gas. This would imply that the subslab attenuation factors for radon and VOCs are similar.
- Variability in the natural soil radon concentration across a given building footprint should not be high enough to interfere with the use of radon as an indicator.
- Concentrations of radon and VOCs of concern should be well correlated in subslab soil gas, although this would not necessarily be expected because radon and VOCs have different sources.
- Interior sources of radon should be negligible.
- The loss rates to indoor radon sinks should be similar or negligible for both radon and VOCs so that the air exchange rate is the primary control on the radon or VOC indoor air concentration from vapor intrusion.

To our knowledge, the concept of radon as a surrogate for VOC vapor intrusion was first applied in a relatively small study (Cody et al., 2003) at the Raymark Superfund Site in Connecticut. The study compared the vapor intrusion behavior of radon and individual VOCs by determining attenuation factors between the subslab and indoor (basement) air in 11 houses. The results indicated that the use of radon measurements in the subslab and basement areas was promising as a conservative predictor of indoor VOC concentrations when the subslab VOC concentrations were known. Further work at the Raymark site (U.S. EPA, 2005b) statistically compared basement and subslab concentration ratios for radon and VOCs associated with vapor intrusion. Of six test locations, three showed that basement/subslab concentration ratios for radon and VOCs associated with subsurface contamination were similar. Three had statistically different ratios, suggesting that further research was needed to evaluate the usefulness of radon in evaluating vapor intrusion. Conservative VOCs (i.e., those believed to be associated only with subsurface contamination) were a better predictor of other individual volatile compounds associated with vapor intrusion than was radon.

A three-building complex, commercial case study of the radon tracer approach was published by Wisbeck et al. (2006). Radon and indoor air attenuation factors were calculated for five sampling points and were generally well correlated. Subslab radon concentrations varied by approximately a factor of 10 across the five sampling points.

Results of an earlier test program at Orion Park Housing units at Moffett Field have been preliminarily reported (Mosley, 2007). Results showed the following:

- Low levels of radon can be measured with sufficient accuracy to be used in analysis of vapor intrusion problems.
- Radon is a promising, low-cost surrogate for soil gas contaminants; however, as with VOCs themselves, the complete distribution under the slab must be known in order to properly interpret its impact on indoor measurements.
- Unexpectedly, the subslab areas under each unit were segmented. The four subslab sampling points installed in one unit were not in good communication with one another. An introduced tracer, SF₆, moved very slowly and not very uniformly under the slab.
- Results showed that for soils like these with poor communication, a subslab measurement at a single point is not very reliable for estimating potential vapor intrusion problems. The average value of subslab measurements at several locations also may not yield a reliable estimate of indoor concentrations. When subslab communication is poor, one must identify a connection between subslab contaminants and a viable entry path.

The potential usefulness of the radon tracer was studied in 2007 to 2010 by EPA NRMRL at Moffett Field in California and in the Wheeler building in Indianapolis. These studies are summarized in three draft peer-reviewed papers that have been submitted for EPA internal review:

- *Vapor Intrusion Evaluation Using Radon as a Naturally Occurring Tracer*: This paper compiles data from five study sites where radon has been used in VOC vapor intrusion investigations and attenuation factors were calculated. A total of 17 buildings are included in the data set, a mix of commercial and residential, in a wide variety of geographical areas within the United States. Attenuation factors were roughly correlated between radon and VOCs.
- *Randomized Experiment on Radon Tracer Screening for Vapor Intrusion in a Renovated Historical Building Complex*: This study focused on a renovated former industrial facility now being reused as residential, public, and office space. Fifty locations within the complex were originally screened for radon using passive sampling techniques. Then two subsets of these sample locations were selected for passive VOC sampling, one randomly and the other based on

the radon information. The upstairs radon-guided samples were significantly higher in TCE than the randomly selected locations. The portions of the building complex where the radon guidance appeared to provide predictive power were understandable in terms of the building design and the concept of the open basement serving as a common plenum.

- *Case Study: Using Multiple Lines of Evidence to Distinguish Indoor and Vapor Intrusion Sources in a Historic Building:* This paper uses data sets developed at the Southeast Neighborhood Development Corporation (SEND) Wheeler Arts Building site in Indianapolis, Indiana, to demonstrate the use of multiple lines of evidence⁵ in distinguishing indoor from subsurface sources in a complex multiuse, multiunit building. The paper demonstrates the use of radon as a quantitative tracer to discriminate vapor intrusion sources as well as the use of differential pressure data as an additional line of evidence. Box and whisker plots of the distribution of indoor air pollutants on multiple floors are used to distinguish pollutants with predominant subslab sources from those with predominant indoor sources. Those pollutants that the box and whisker analysis suggest have indoor sources are also corroborated from the literature as having very common indoor sources expected in this building, including arts and crafts activities, human exhalation, consumer products, and tobacco smoking.

A recent review presentation by Schuver (2013) summarizes the usefulness of radon as a “qualitative/semi-quantitative indicator of building specific susceptibility to near-surface soil-gas/vapor intrusion” and “a signature of the building-specific responses to environmental changes” and a “key (3rd strike) evidence basis for demonstrated-potential for chem-VI.” Steck (2012) summarizes an EPA document currently under development that describes lessons learned from radon that can be applied in vapor intrusion research and practices.

2.1.4 Passive VOC Sampling

Sorbent-based methods are an emerging technology for vapor intrusion assessment. Current standard practices for indoor air VOC monitoring in the United States include the use of negatively pressurized, ultra-clean, passivated, stainless steel canisters for sample collection. Practitioners frequently use 8- to 48-hour integrated samples with Summa canisters in an attempt to average over an exposure period. This is the U.S. “gold standard” for indoor air analysis, but it is expensive to implement. Professional experience shows that the flow controllers currently used in commercial practice are subject to substantial flow rate and final pressure errors when set for integration times in excess of 24 hours (Hayes, 2008).

Active and passive sorbent sampling techniques are already in use in the United States for personal air monitoring for industrial workers and are outlined in both the Occupational Safety and Health Administration (OSHA) Sampling and Analytical Methods (<http://www.osha.gov/dts/sltc/methods/toc.html>) and National Institute for Occupational Safety and Health (NIOSH) *Manual of Analytical Methods* (<http://www.cdc.gov/niosh/nmam/>). Typical sampling scenarios involve collecting active or passive samples to monitor a single chemical used in the workplace over a period of up to 10 hours. These methods are designed to meet OSHA permissible exposure limits (PELs), which are typically in the ppm range and consequently several orders of magnitude higher than risk-based indoor air screening levels and not suitable for ambient air measurements without modification.

Active sorbent methods (i.e., TO-17) have also been published by EPA for VOC measurements in ambient air (U.S. EPA, 1999c). However, in those methods, air samples are normally actively collected over 1 hour, using a sample pump with a sampling rate of 16.7 mL/min to 66.7 mL/min, yielding total sample volumes between 1 and 4 liters. Sampling intervals can be extended beyond 1 hour; however, care

⁵ The concept of multiple lines of evidence in vapor intrusion studies is described in ITRC (2007).

must be taken to ensure breakthrough volumes are not exceeded in order to quantitatively retain the compounds of interest on the sorbent tube. Given the minimum pump flow rate cited in TO-17 of 10 mL/min, the practical upper limit for chlorinated VOCs using a multibed thermal desorption sorbent tube is on the order of 10 liters up to 20 L for select VOCs yielding a corresponding maximum collection period of 8 to 24 hours (Marotta et al., 2012).

One way to lower the detection limits and control day-to-day variability is to sample over a longer period of time. Recent studies have shown that it may be feasible to use passive sorbent samplers to collect a continuous indoor air sample over several weeks. This approach would provide a lower detection limit, be cost-effective, and result in a time-integrated composite sample. Laboratory and field evaluations of such an approach for ambient and indoor air applications have been published and showed promising results for sampling durations of up to 14 days. Exposure of badge-type charcoal passive samplers to controlled atmospheres of 10 to 200 ppb benzene, toluene, and m-xylene showed good performance when deployed for 14 days (Oury et al., 2006). A field study published by Begerow et al. (1999) showed comparability between two charcoal-based passive sampler geometries, badge and tube-style for 4-week indoor and outdoor air samples. Field evaluations were also conducted using radial charcoal and thermal desorption Radiello® samplers to determine performance over a 14-day period. Ambient BTEX measurements using the Radiello samplers compared well to active sorbent sampling results (Cocheo et al., 2009).

Testing at Orion Park, Moffett Field in California by EPA NRMRL Air Pollution Prevention and Control Division (APPCD), EPA Region IX, and ARCADIS compared measurements of VOCs by Method TO-15 to three different radial and axial tube-type sorbent systems:⁶

1. Radial: activated charcoal (with carbon disulfide [CS₂] extraction: gas chromatography–mass spectrometry [GC/MS])
2. Radial: carbograph 4 (TO-17: thermal desorption [TD] GC/MS)
3. Axial: chromosorb 106 thermal desorption tube (TO-17: TD GC/MS)

Performance for the two radial methods was superior to the axial method (Lutes et al., 2010a,b,c). Testing was also performed at the Wheeler site in Indianapolis comparing Summa canisters to Radiello radial solvent-extracted samplers. Across the two sites, the Radiello solvent extracted showed good agreement to TO-15 and precision at both sites for chlorinated compounds. Agreement was poor for polar compounds: ethanol, methyl ethyl ketone (MEK), methyl isobutyl ketone (MIBK), and acetone. Radiello TD correlated well with Summa TO-15 but gave noticeably lower concentrations, suggesting that 2 weeks is too long an integration time for these samplers. The agreement of the axial (tube) method was inferior (Mosley et al., 2008; Lutes et al., 2010a,b,c).

Table 2-1 compares the characteristics of commercially available passive sampler geometries and available sorbent configurations. The geometry of the sampler (radial, badge, or axial tube) largely determines the sampling rate or uptake rate with the radial design resulting in the highest sampling rate and the tube-style the lowest sampling rate. The permeation sampler relies on permeation of the vapor-phase compound through the polydimethylsiloxane (PDMS) membrane and adsorption to the sorbent bed behind the membrane. The greater the sampling rate, the greater the mass of VOCs adsorbed onto the

⁶ Radial samplers are sorbent-containing tubes where diffusion from the surrounding air occurs radially along the entire length of the tube. Axial samplers are tubes containing sorbent where diffusion occurs axially through one open end of the tube. Because of the higher surface area exposed for diffusion, radial samplers have higher uptake rates than axial tube-type samplers.

Table 2-1. VOC Indoor Air Sampling Method Options

Parameter Compared	Whole Air Sample	Active Sorbent	Passive Sorbent						
			Radial: Charcoal (Radiello 130)	Radial: TD sorbent (Radiello 145)	Badge: Charcoal type (SKC 575, 3M OVM3500)	Badge: TD sorbents selected by deployment time: (SKC Ultra I, II, III)	Tube: TD sorbents (e.g., Chromosorb 106)	Permeation: Charcoal type (WMS™)	Permeation: TD sorbent (WMS™)
<i>Collection media</i>	Summa canister (TO-15)	Multibed ATD sorbent tubes (TO-17)	Radial: Charcoal (Radiello 130)	Radial: TD sorbent (Radiello 145)	Badge: Charcoal type (SKC 575, 3M OVM3500)	Badge: TD sorbents selected by deployment time: (SKC Ultra I, II, III)	Tube: TD sorbents (e.g., Chromosorb 106)	Permeation: Charcoal type (WMS™)	Permeation: TD sorbent (WMS™)
<i>Ease of deployment</i>	Good	Good	Excellent	Excellent	Excellent	Excellent	Excellent	Excellent	Excellent
<i>Estimated media & shipping cost</i>	\$\$\$	\$\$	\$	\$\$	\$	\$\$	\$\$	\$	\$
<i>Method and analysis</i>	TO-15 GC/MS	TO-17 GC/MS	Solvent extraction GC/MS or GC/FID	TO-17 GC/MS	Solvent extraction GC/MS or GC/FID	TO-17 GC/MS	TO-17 GC/MS	Solvent extraction GC/MS	TO-17 GC/MS
<i>Estimated analytical reporting limit</i>	0.05–0.1 µg/m ³	1–10 ng	100–200 ng	1–10 ng	75–200 ng	1–10 ng	1–10 ng	50–200 ng	1–10 ng
<i>Expected sampling rate</i>	0.5–3.5 mL/min	10–200 mL/min	~60 mL/min	~25 mL/min	~10 mL/min SKC ~30 mL/min 3M	~10 mL/min	~0.5 mL/min	~0.5–5 mL/min	~0.5–5 mL/min
<i>Recommended sampling duration</i>	Typically 24 hours	8–24 hours	Up to 30 days	Up to 7 days for chlorinated solvents	Up to 4 weeks	1–7 days	In general, up to 4 weeks)	Up to 30 days	Up to 30 days
<i>Estimated sample reporting limits^a</i>	~0.05 (SIM)–0.1 µg/m ³	~0.1–1 µg/m ³	~0.1–0.4 µg/m ³	~0.005–0.05 µg/m ³	~0.25–2 µg/m ³	~0.01–0.1 µg/m ³	~0.2–2 µg/m ³	~1–40 µg/m ³	~1–40 µg/m ³
<i>Applicable range of chlorinated solvents (based on available sampling rates)</i>	TCE/PCE and all breakdown products including vinyl chloride (VC)	TCE/PCE and all breakdown products including VC	TCE, PCE, 111-TCA, chloroform	TCE, PCE, 111-TCA	Validated for a wide range of chlorinated solvents for 8 hours, several for up to 30 days	TCE, PCE, DCE, 111-TCA, chloroform, 12-DCA, cis-12-DCE, trans-12-DCE, 11-DCA	TCE, PCE, 111-TCA	TCE, PCE and most breakdown products	TCE, PCE and most breakdown products

^a Normalized to a 7-day period for diffusive samplers.

sorbent bed. In addition to the passive geometries available, sorbent pairings fall into two main categories—charcoal based and thermally desorbable. Charcoal-based materials are characterized as very strong sorbents with a large surface area and a corresponding high adsorption capacity. To efficiently extract adsorbed compounds for measurement in the laboratory, an aggressive solvent extraction is required. The thermally desorbable sorbents are generally much weaker than charcoal with a smaller surface area, allowing for analysis of the adsorbed compounds through thermal extraction. As **Table 2-1** shows, when comparing the same passive geometry, the thermally desorbed model provides the lowest detection limits, while the charcoal-based solvent-extracted system allows for longer sampling times as well as a greater dynamic range because the high capacity of the charcoal minimizes sorbent saturation under conditions of high analyte or background matrix.

European agencies have developed standard methods for passive sampling for VOCs that are applicable to the range of concentrations and durations to be tested in this project:

- Methods for the Determination of Hazardous Substances (MDHS) 88: *Volatile Organic Compounds in Air: Laboratory Method Using Diffusive Samplers, Solvent Desorption and Gas Chromatography*, December 1997. Published by the Health and Safety Executive of the United Kingdom: <http://www.hse.gov.uk/index.htm>.
- MDHS 80: *Volatile Organic Compounds in Air: Laboratory Method Using Diffusive Solid Sorbent Tubes, Thermal Desorption and Gas Chromatography*, August 1995. Published by the Health and Safety Executive of the United Kingdom: <http://www.hse.gov.uk/index.htm>.
- Ambient air quality: *Standard Method for Measurement of Benzene Concentrations—Part 4: Diffusive Sampling Followed by Thermal Desorption and Gas Chromatography*, EN 14662-4:2005. Published by the European Committee of Standardization.
- Ambient air quality: *Standard Method for Measurement of Benzene Concentrations—Part 5: Diffusive Sampling Followed by Solvent Desorption and Gas Chromatography*, EN 14662-5:2005. Published by the European Committee of Standardization. (Also published as the British Standard BS EN 14662-5:2005).
- Indoor air quality: *Diffusive Samplers for Determination of Concentrations of Gases and Vapors: Guide for Selection, Use, and Maintenance*, EN 14412:2004. Published by the European Committee of Standardization.

Given the wide range of sampling durations required for this project, several diffusive sampler configurations are recommended to meet anticipated project objectives for indoor air measurements. For short-term samples (less than 7 days), the sampler must have sufficient sensitivity to measure the low VOC concentrations that are expected in the indoor air. Thermally desorbable sorbents paired with a badge or radial-style geometry can be used effectively for the 24-hour samples and yield low reporting limits. The badge style is recommended over the radial style given the larger number of chlorinated compounds for which sampling rates have been generated and validated. For durations of greater than 7 days, stronger sorbents with higher adsorptive capacity are recommended, which require solvent extraction. Although the solvent extraction is less sensitive than thermal desorption, the high sampling rate of the radial sampler geometry over durations of 7 to 30 days will result in sample reporting limits essentially equivalent to or lower than those generated using the thermal desorption technique.

Very few studies have evaluated VOC measurements using diffusive samplers beyond 30 days, and determining if this is possible is one objective of this study. The sorbent selection, the sampler geometry, and the target chemical's volatility all may have a significant impact on the successful application of diffusive samplers to extended deployment periods. The few published studies evaluating sampling intervals greater than 30 days are largely focused on measuring BTEX (Bertoni et al., 2001; Brown and Crump, 1993), and the stability of chlorinated compounds on sorbents in the presence of humidity and the

variability of the sampling rate past 30 days are not well understood for any of the diffusive samplers under consideration for this study.

Given the previous studies discussed above and the existence of standard methods for this application in Europe, the 1- and 2-week Radiello passive samplers for VOCs are considered sufficiently accurate and precise to be the primary VOC measurement tool in this project and are used as a basis of comparison for longer duration samples.

Results from our first report on studies of this house (U.S. EPA, 2012a) led to these conclusions regarding the performance of the solvent extracted radial style charcoal passive sampler:

- Excellent agreement was observed between numerical averages of successive 7-day exposure samples with the results of single passive samplers exposed for 14 days (almost always within $\pm 30\%$) for all compounds despite dramatic temporal variability. This suggests uniform uptake rates for these time periods.
- PCE, benzene, hexane, and toluene work well for 28 days.
- PCE and toluene performed well at 91, 182, and 364 days.
- Temporal variability is substantial and for certain compounds passive samplers allow cost-effective acquisition of long-term average concentration data.
- Vapor pressure predicted well the relative performance of different compounds with the passive samplers.

2.2 Research Program Objectives

2.2.1 Continuing Objectives

The overall goal of this project was to investigate distributional changes in VOC and radon concentrations in the indoor air, subslab, and subsurface soil gas of a residential building from an underground (groundwater or vadose zone) source adjacent to the residence and then to use this information to improve and better inform vapor intrusion investigation methods. By employing a time frame greater than 3 years, we were able to evaluate the effects due to seasonal and year-to-year variations on radon and VOC vapor intrusion. This report describes the third phase of this project, with the first and second phases described in U.S. EPA (2012a, 2013). Several objectives from the previous two phases were continued in this study:

1. Identify seasonal fluxes in radon and VOC concentrations as they relate to a typical use of HVAC in the building.
2. Establish relationship between subslab/subsurface soil gas and indoor air concentrations of VOCs and radon.
3. Determine the relationship of radon to VOC concentrations in, around, and underneath the building (This objective is not discussed extensively in this report but was discussed extensively in Chapters 7 and 8 of U.S. EPA (2013); further information about radon is likely to be presented in the forthcoming fourth report in the series.)
4. Characterize the near-building environment sufficiently to explain the observed variation of VOCs and radon in indoor air.
5. Determine whether the observed changes in indoor air concentration of VOCs of interest can be mechanistically attributable to changes in vapor intrusion.
6. Evaluate the extent to which groundwater and/or vadose zone sources control soil gas and indoor air VOC concentrations at this site.

Table 2-2 provides additional information on the objective statements continued from previous phases of this project.

Table 2-2. Status of Original and Continuing Objectives from Earlier Phases of this Project

Original Statement of Objective	Current/Ongoing Status
Determine relationship of radon to VOC concentrations at a given site.	<p>Extensively discussed in U.S. EPA (2012a) based primarily on statistical analysis of correlations. Results showed that radon was somewhat less variable with time than VOCs but that radon could be used as a semiquantitative indicator of vapor intrusion.</p> <p>Discussed in U.S. EPA (2013) as well, primarily with regard to behavior of radon and VOCs during mitigation on-off cycles. Results showed that radon mitigation was more consistent and efficient than VOC mitigation, primarily because VOCs were redistributed by the action of the mitigation system—including increases in the subslab area. The experimental design that included approximately 3-week on/off cycles for mitigation left open questions about whether the VOC mitigation performance would be better long term.</p> <p>A comparison of attenuation factors was also presented in U.S. EPA (2013) that showed that radon provided a reasonable estimate of the attenuation factor between subslab and indoor air (that portion of the attenuation factor dealing only with transport across the building envelope).</p>
Establish relationship between subslab/subsurface soil gas and indoor air concentrations of VOCs and possibly radon.	Results presented in U.S. EPA (2012, 2013) show that the subslab source of radon is relatively consistent and the source of VOCs is highly variable. Results suggest that subslab VOC concentrations increase when air is drawn upward toward the structure—whether that occurs through a long period of cold weather/strong stack effect or operation of a mitigation system. Results also point to a role for ground water levels in controlling subslab VOC concentrations.
Examine if near-building external samples could be used as a surrogate sampling location.	<p>The results of data analysis published in U.S. EPA (2012a) show clearly that shallow external soil gas is not a good surrogate location. Differences between deep external and deep internal soil gas are less definitive.</p> <p>Additional analysis of this topic was not pursued in U.S. EPA (2013).</p>
Identify any seasonal fluxes in radon and VOCs concentrations as they relate to a typical use of HVAC in the building.	<p>Although the U.S. EPA (2012a) report addressed this objective, it left unexplained why the relationship between stack effect driving force and indoor concentration appears to be nonlinear. Time series analyses and other lines of evidence discussed in U.S. EPA (2013) concluded that a variety of meteorological factors enhanced vapor intrusion, including low temperatures, snowfall events; snow/ice ground cover, winds from a specific direction, and barometric pressure. These factors likely interact in complex ways. Although there are repeating seasonal trends in these meteorological factors that influence vapor intrusion, observations over three winters point also to an important role for year-to-year variability in climate. In this new report, we are refining our time series analysis to facilitate testing of the prediction of vapor intrusion. Specifically, we are analyzing additional predictor variables not included in the U.S. EPA (2013) report, including standard deviation of differential pressure, interpolated water levels based on U.S. Geological Survey (USGS) data, a stack effect predictor, and snow/ice event information based on a newly processed weather service data set. We are also revising the wind direction analysis treating it as a categorical variable.</p>
Determine if observed changes in indoor air concentration of volatile organics of interest are mechanistically attributable to changes in vapor intrusion.	As discussed above, U.S. EPA (2013) highlighted the role of mitigation systems in altering subsurface mass transport processes; thus, setting the conditions for vapor intrusion. Time series analyses in U.S. EPA (2013) examined the role of subslab to indoor differential pressure (at center of slab) and several other differential pressure measurements as a mechanistic indication of vapor intrusion. U.S. EPA (2013) also included a review of “Extreme” differential pressure events and their meteorological causes.

(continued)

Table 2-2. Status of Original and Continuing Objectives from Earlier Phases of this Project (continued)

Original Statement of Objective	Current/Ongoing Status
<p>Characterize the near-building environment sufficiently to allow future 3D modeling of this site.</p> <p>Better define the particular subsurface conditions that influence the movement of VOCs and radon into this home and determine the effects of utility corridors on subsurface movements of VOCs and radon.</p>	<p>Soil gas sampling, boring logs, tracer tests, water level monitoring, and geophysical work included in U.S. EPA (2012a, 2013) address this goal with a spatial resolution likely to be much greater than is likely to be available for most actual vapor intrusion sites encountered by practitioners. It would be informative in a future effort to attempt 3D modeling to determine if it can accurately simulate the observed indoor air concentrations. Simulation of concentrations at individual subslab points is likely to require a finer spatial scale of resolution.</p> <p>The characterization done here is of the near-building environment. It would also be useful in future efforts to expand the size of the domain to encompass other parts of the site/plume. Testing to date has been limited to the lot on which this duplex sits.</p>
<p>Evaluate the extent to which groundwater concentrations control soil gas concentrations at this site and; thus, indoor air concentrations (as distinguished from vadose zone sources).</p>	<p>Previous work (U.S. EPA, 2012a) established that soil gas concentrations of both chloroform and PCE peak just above the water table. PCE groundwater concentrations measured correlated well with deep soil gas (U.S. EPA, 2012a, 2013). Chloroform had been observed in deep groundwater but not in concentrations that account for the soil gas concentrations (U.S. EPA, 2013). This suggests that there may be other sources of chloroform, such as combined sewers⁷ or drinking water mains,⁸ that leak below grade, higher groundwater concentrations at some locations near the site, or chloroform mass stored in the vadose zone from a historic release. For PCE, the results suggest a groundwater source, but the narrow range of variability in PCE concentrations and stability of this variability over time make it unlikely that variability in groundwater concentrations is the only source of the observed changes in soil gas or indoor air concentrations observed in this study. The variability in indoor air PCE concentrations is also influenced by subsurface, building-related, and meteorological variables (U.S. EPA, 2013).</p> <p>In this third phase of the report, we continued to gather data on deep soil gas concentrations, groundwater concentrations, and water levels; we will have an additional basis for understanding how the groundwater and deep soil gas concentrations relate over time.</p>
<p>Collect additional data to evaluate the possibility of a “capping” effect from snow and ice cover.</p>	<p>Data analysis presented in U.S. EPA (2013) suggests that both snow fall events and snow/ice covers have an effect. Additional National Weather Service data on hourly snowfall observations have been acquired, and in this report we will use that information as part of refined time series analysis.</p>
<p>Evaluate the ability of a widely available low cost (\$129) consumer grade radon detector based on an ionization chamber to provide a continuous indication of soil gas entry into the structure. (Safety Siren Pro Series 3 manufactured by Family Safety Products Inc.).</p>	<p>Results in U.S. EPA (2012a) and U.S. EPA (2013) describe the operational performance of the Safety Siren adequately. The response time for the Safety Siren is 1 week, so we will not emphasize testing of that device during this third phase of the project. In this third phase, we tested the SIRAD-106Ns in this project (\$379 radon detectors that can be computer interfaced/remote read and have 4-hour response time).</p>

⁷ Chloroform can form in sewers that receive bleach-containing products.

⁸ Groundwater chloroform concentrations at this duplex are lower than the mean and peak drinking water concentrations for Indianapolis (19 ppb and 82 ppb).

2.2.2 New Objectives

This study had the following new objectives:

1. Use radon, measured using a simple in-home radon monitor, to determine when to collect air samples for VOCs to confirm vapor intrusion is occurring, and when to turn on mitigation systems, as well as to look for correlations between radon and VOCs before and after the mitigation system is turned on. This report primarily focuses on work with the mitigation system off.
2. In conjunction with the radon monitoring, investigate other variables, such as large changes in temperature and differential pressure between the indoors and outdoors, as potential low-cost, easily monitored indicators of when to sample and when to turn on the mitigation system.

The overall approach to this work began with refining our understanding of the causes of higher amounts of vapor intrusion in this structure (both for radon and VOCs). Then we tested our ability to apply that knowledge to forecast VOC vapor intrusion.

For devising sampling approaches to estimate the reasonable maximum exposure, it would be ideal for the practitioner to determine the likelihood of a near-future increase in vapor intrusion. The average long-term exposure can be potentially influenced by short, high-concentration events occurring at brief periods during the year, although this effect may not be large enough to change the risk management decision (Holton et al., 2013a,b; Lutes et al., 2013, Weinberg et al., 2014). Thus, it would be beneficial to the practitioner to be able to deploy a small number of short-term samplers during occasions when there is likely to be a sharp increase in vapor intrusion or when vapor intrusion is at its worst. Current state guidance documents generally call for sampling at times of the year believed to be associated with the highest vapor intrusion potential (e.g., winter) and for timing sampling events with respect to rain events. For example, California requires that soil gas sampling be delayed for 5 days after any rain of more than 1/2 inch (California EPA, 2012).

Radon can potentially be used as a semiquantitative tracer of vapor intrusion across the building envelope, although it is less useful as a tracer for VOC migration through soil gas. In using radon as a potential predictor variable, it should be noted that radon is normally managed based on chronic risk (cancer). Based on a limited number of studies, TCE is currently being managed in some EPA regions based on risk screening levels that are similar for both chronic cancer risk and shorter-term reproductive effects, with exposure periods of 1 month or less.

Characteristics of the experimental design and data quality objectives developed to meet these objectives are described below.

2.2.3 Time Scale and Measurement of Independent and Dependent Variables

In our overall study design, we used weekly measurements to observe our dependent variable—indoor air concentration. We expected the indoor air concentration to depend on the flux from vapor intrusion from soil gas. Our dependent variable is thus controlled by a series of independent variables with different time cycles that affect the vapor intrusion process, including air temperature, barometric pressure, wind, soil moisture, soil temperature, groundwater level and VOC concentrations, and HVAC operation.

In the course of this study, we monitored or measured most of these independent variables or their surrogates and different frequencies balancing on the general desire for continuous measurements against logistic considerations. **Table 2-3** was prepared to consider these time-scale issues and the implications they may have for our test matrix. Figures in Nazaroff and Nero (1988) show examples of how such independent variables controlled indoor radon concentrations in previous studies.

Table 2-3. Factors Causing Temporal Change in Vapor Intrusion and How They are Observed and Measured

Independent Variables/ Causes of Variability	Expected Time Cycle	Indoor VOC & Soil Gas Measurement Intervals Available to Observe at these Time Scales	Measurements of Independent Variables Available
HVAC system on/off	<ul style="list-style-type: none"> ▪ 10 min–1 hour 	The influence of the HVAC system in general was observed on a scale of days and weeks by comparing sides of the duplex and periods of “on” and “off” for AC units. Although the individual cycles of the forced air heating system are not visible in measurements taken over a 24-hour or longer time scale or even in the 2-hour on-site GC data, the cumulative impact of heating system “on” and “off” over exposure periods of weeks was relevant. In addition, data were gathered with a higher time resolution for comparison to the high time resolution on-site GC measurements.	Measurement with data logger was planned with a frequency as great as every 5 minutes within heating season.
Diurnal temperature/ wind (night/day)	<ul style="list-style-type: none"> ▪ 24 hours 	Measurements with the on-site GC and continuous radon instruments have sufficient time resolution on the scale of hours to observe this.	Weather station: one data point per 30 minutes at a minimum.
Barometric pumping from weather fronts	<ul style="list-style-type: none"> ▪ 2–3 days typical 	Weekly, except for daily samples and continuous measurements during intensive sampling events.	Weather station: ambient pressure logging with at least one data point per 30 minutes.
Water fluctuations	<ul style="list-style-type: none"> ▪ Barometric pressure: 2–3 days ▪ Rain events: irregular ▪ Seasonal climate: monthly ▪ Surface water level: hours 	Weekly and monthly integrated indoor air samples. Measurements with the continuous radon and onsite GC instruments have time resolution on the scale of minutes to hours.	Monthly water-level measurements; supplemented beginning in fall 2012 with real-time data logger at one station on site with one data point per 30 minutes; strong correlation of USGS Fall Creek gauge height (recorded every 15 minutes) and groundwater level enabled hindcasting of groundwater levels for entire project (U.S. EPA, 2013).
Soil and groundwater temperature change	<ul style="list-style-type: none"> ▪ Annual/ seasonal 	Weekly, biweekly, and quarterly samples of indoor air and soil gas.	Soil temperature logging with thermocouples: one or more points per hour. Groundwater temperature monthly during sampling.
Vadose zone moisture change	<ul style="list-style-type: none"> ▪ Seasonal major rain events? 	Weekly samples of indoor air and soil gas. Measurements with the on-site GC and continuous radon instruments have time resolution on the scale of hours.	Once per hour at five depths.

(continued)

Table 2-3. Factors Causing Temporal Change in Vapor Intrusion and How They are Observed and Measured (continued)

Independent Variables/ Causes of Variability	Expected Time Cycle	Indoor VOC & Soil Gas Measurement Intervals Available to Observe at these Time Scales	Measurements of Independent Variables Available
Stack effect, heating vs. cooling season	<ul style="list-style-type: none"> ▪ Daily and seasonal 	Weekly samples of indoor air and soil gas. Measurements with the on-site GC and continuous radon instruments have time resolution on the scale of hours.	Differential pressures, indoor temperatures: 15-minute rolling average.

3. Methods

This chapter describes the Indianapolis duplex, its location and environment, and the sampling locations and methods used to monitor radon and VOC vapor intrusion in the duplex. Material in this chapter is repeated, summarized, and/or updated from the previous two reports on this study (U.S. EPA, 2012a, 2013), to which the reader is referred for more detailed information.

3.1 Site Description

The test house is a vacant residential duplex at 420/422 East 28th Street in the Mapleton Fall Creek neighborhood of Indianapolis. This area of Indianapolis was initially a farming settlement known as Mapleton founded in the 1840s. The primary residential development in this area occurred in the late 1800s and early 1900s, with the test duplex being built before 1915. Commercial development on the immediate cross street, Central Avenue, began in the 1920s.

3.1.1 Area Geology/Hydrogeology

Several soil borings were advanced in the area immediately surrounding the house, during monitoring well (MW) construction and soil gas port installation between April and September 2010. Soil gas ports and MW-3 located beneath the house itself were installed in September 2010. 3-D visualizations of subsurface lithology are presented in **Figure 3-1**. Boring logs are included in Appendix A to an earlier report (U.S. EPA, 2013), which also includes detailed lithological descriptions. The general stratigraphy is about 1–3 ft of topsoil and fill, 3 to 7 ft of silty/sandy clay, and 7 to 16 ft of coarse gravelly sand with cobbles, which serves as the surficial aquifer underlying the house. More detailed stratigraphic descriptions taken from the boring logs are as follows.

- *Southern side*: topsoil to 0.5 to 1 ft; fill (sand/silt with cinders, coal fragments, ash) to about 1.5 ft; silt or silty sand with varying clay, to 5–6 ft; trace gravels from 7 ft, with sands and gravels to 16 ft or deeper.
- *East side*: topsoil or concrete sidewalk to 1 ft; sand or clayey sand (with some gravel and coal) from 1–3 ft; 3–7 ft, predominantly clay with some sand or silt; 7 to 12–14 ft, sand with some clay and gravel; 13–16.5 ft sand and gravel.
- *North side*: fill, sand, and gravel to 1 ft; 1 to 3.5 ft, brick with sand and weathered brick; 3.5–6 ft, silty, sandy clay; 6–8 ft, sand; 6–12 ft, sand, gravel, and some clay; 12–16 ft, sand.
- *West side*: concrete sidewalk to 0.5 ft; 0.5–1 ft fill, cinders, gravel; 1–7 ft, silty, sandy clay with trace gravel; 7–16.5 ft, sand and gravel with some clay, sand.

See Section 6.1 in U.S. EPA (2013) for additional details on on-site soils.

3.1.2 Area Potential Sources

The site is bounded to the north by 29th St., to the west by N New Jersey St., and to the east by Central Avenue (**Figure 3-2**). Groundwater flow generally trends toward Fall Creek, which is approximately 300 ft to the south of the site and flows to the west southwest. Across the street south, between the duplex and Fall Creek, there is a parking lot and to the east there is an open field. Across an alley to the west of the site, there is an open lot with a grassy area and a paved parking lot. To the north, the site borders on the backyard of the first residential building on Central Avenue.

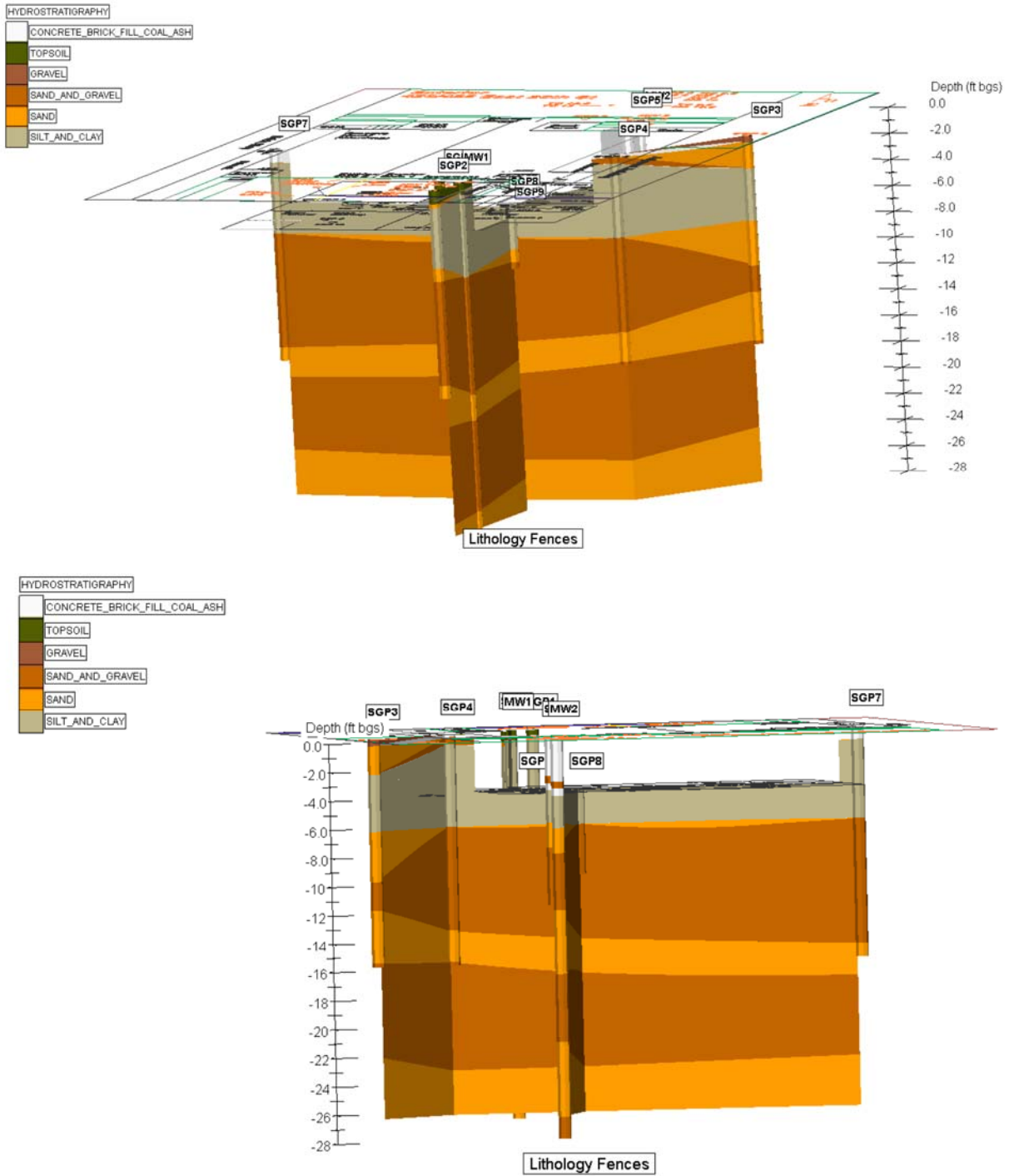


Figure 3-1. Lithological fence diagram beneath the 422/420 house, toward N from street (top) and toward S from backyard (bottom). Basement is unshaded with silt and clay (brown) until 6 to 8 ft bls and sand and gravel (burnt orange) and sand (orange) below.

420 E. 28th St, Indianapolis, IN

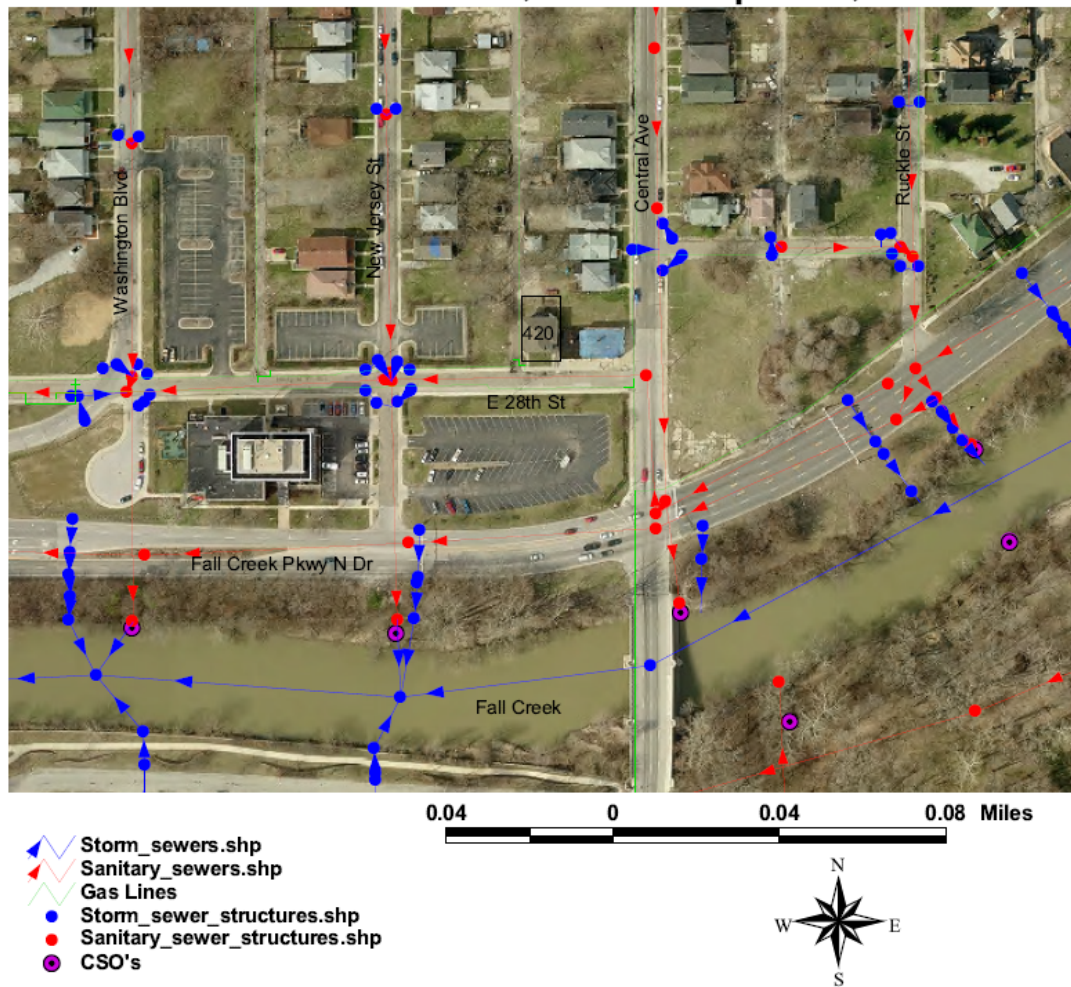


Figure 3-2. Aerial view of duplex, 420/422 East 28th Street, showing nearby sanitary and storm sewers.

Immediately adjacent to the studied duplex (approximately 10 ft east) lies a small commercial/residential quadruplex (**Figures 3-3, 3-4, and 3-5**) with a diverse, primarily commercial history dating back to 1930. The four portions of the building are numbered as 424 East 28th Street, 426 East 28th Street, 2802 Central Avenue, and 2804 Central Avenue. Among the historic uses of parts of that building were an Italian restaurant, pharmacy, beauty supply, radio shop, fur store, and detector company. Regarding most of the businesses that occupied that space, only their name is currently known, and those names do not match any businesses with a current local or Internet presence. Thus, chemical uses, though probable, are not documented. The back part of the adjacent building at 2804 Central Avenue has historically been occupied by “Wolf Fur Co.” Later in 1954, the same location was occupied by the “Avideo Detectors Telaveta.” In 1930, it was occupied by “Gould & Schildmoler ENEN and Home Radio Co.” The records for the adjacent buildings (424 to 428 East 28th Street and 2802 to 2804 Central Avenue) show a number of drug store and beauty shop uses. There are substantial gaps in the records for these properties, and there seems to be little or nothing reported about what was occupying these locations between 1970 and 2000.

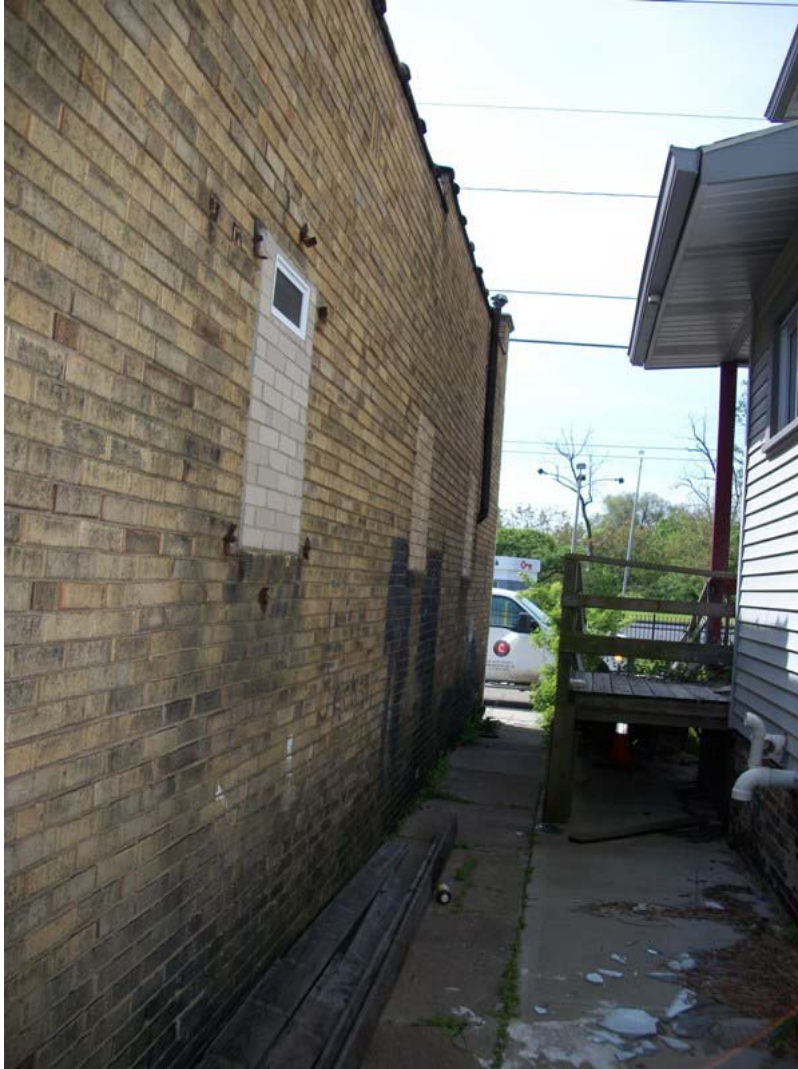


Figure 3-3. East side of house (on right) and adjoining commercial quadraplex visible (left).



Figure 3-4. Roof of adjacent commercial quadraplex.



Figure 3-5. Looking toward southeast corner of adjacent commercial quadraplex.

There were 9 to 10 historic laundry cleaners located less than a quarter of a mile to the north of the 422/420 house, and one was a quarter of a mile to the west (**Figure 3-6**). These were listed as hand and steam laundries, pressers, and driers. The most recent laundry was present in 1970 (EDR Radius Map, June 15, 2010). In the fall of 2010, we observed Mapleton/Fall Creek Development Corporation (MFCDC) staff excavating an underground storage tank that appeared to contain product at a dry cleaners several blocks upgradient from the house.

There were three historic gas stations or auto service and repair shops within a quarter of a mile to the north as well. The most recent auto repair shop was present in 1990 (EDR Radius Map, June 15, 2010). The property southwest of the intersection of East 28th and Central Avenue was historically mildly impacted with petroleum hydrocarbons and managed as a brownfield named “Mapleton-Fall Creek Site” or “Fall Creek Central Project.” This site was closed after tank and soil removal. One round of VOC groundwater data was acquired at that location that showed chloroform at 8.9 to 22.1 $\mu\text{g/L}$ in a June 2005 sampling event. These previous studies showed that the study area has sand and gravel geology from approximately 7 to 25 ft below land surface (bls) and groundwater at approximately at 16 ft bls. The upper 7 ft of the stratigraphy is heterogeneous, variously described as including fill materials, loam, and silty and moist sandy clay.

Based on the general topography of the area and professional experience in this portion of Indianapolis, groundwater is thought to flow from the north of the 422/420 house south of the house to Fall Creek. Thus, many of the historic laundries or auto shops that are potential contaminant sources are generally upgradient of the study house.



Figure 3-6. Visual evidence of historic dry cleaners in area.

3.1.3 Building Description

3.1.3.1 Building Age, Condition, and HVAC

The tested house located at 422/420 East 28th Street, Indianapolis, IN, (**Figure 3-7**) is an early twentieth century duplex, dating from before 1915 because it is present on the 1915 Sanborn map of the area. Based on the mirrored floor plans of the two sides, it is likely that the house was always a duplex. Construction is wood frame on a brick foundation with a poured concrete basement floor. Interior floor materials include tile, carpet, and wood flooring.

The duplex at 422/420 was abandoned and is now owned by MFCDC in Indianapolis. Before our involvement, the house had been vandalized and stripped of all valuable metals and fixtures. A staff member from the Indianapolis ARCADIS office acquired the use of the house for the duration of the project through the generosity of the MFCDC. To cover taxes and other basic operating expenses, a small rent was paid to MFCDC for use of the house for this study.

Historical (preproject) vandalism and theft of household items included the following: all copper wiring and tubing, most plumbing fixtures, and many outlets. Vandals destroyed the previous HVAC unit, probably in an attempt to salvage valuable metals. Power was restored to the house in September 2010. A gas-fired forced air HVAC unit was installed on the 422 side in October 2010 by Edwards Electric and Mechanical for use in this project (**Figure 3-8**). The house had no air conditioning (AC) system, and we



Figure 3-7. Front view of house during summer 2011 sampling, with fan testing and weather station.



Figure 3-8. Front view of duplex under winter conditions showing designation of sides and HVAC setup.

chose to install window-mounted units, which would have been the likely type used by any tenants in this house.

There are internal and external visual clues indicating (**Figure 3-9**) the house has been updated several times. For example, visual clues suggest that a previous HVAC unit had been installed that was not native to the house's original construction. In the basement, there is evidence of former coal chutes (possibly) and cisterns on both the 420 and 422 sides. The probable coal chutes and old windows had been blocked by cinder blocks before ARCADIS occupancy. The cisterns had also been cemented over. Evidence in the basement suggests that at one time the house had been heated by an old style furnace, indicated by cemented-over holes in the walls, but that it had been gone for some time.



Figure 3-9. 422 (left) and 420 East 28th Street in January 2011.

3.1.3.2 Building Utilities/Potential Entry Points

The electric lines connect to the house at the northwest corner of the 420 side. Because all original wiring native to the house had been removed by vandals before the project, the junction box was rewired to the city electrical line and new lines were run within the house to new outlets at designated points. The gas line was connected only to the furnace from an access point in the south wall of the 422 side. Both the electrical lines and the gas line were replaced during furnace installation and enter the house at the original entry points for each utility.

Sanitary sewer lines run immediately south of the house along East 28th Street. Sanitary and combined sewer lines run less than one block east and west of the house along Central Avenue and New Jersey Street (see previous **Figure 3-2**). There is a sewer lateral running beneath the basement floor along the length of the 422 side from north to south that was buried and cemented over sometime after the floor's original construction. PVC drain lines join this lateral from the plumbing on both sides of the duplex. The

HVAC unit drains condensation into a floor grill leading to the lateral. A nonfunctional water line enters the house from the south. Large, cinder-blocked portions of the north interior basement walls of both sides of the duplex along with brick strata in borings have been observed. We interpret these to be vestigial entranceways to the basement from a time when the basement was accessed from the back yard, rather than from an interior basement door.

3.1.4 Building Occupancy During Sampling

The initial concept for the 422/420 house was to create an environment free from lifestyle-related indoor air sources, but operated as though the space were occupied, to simulate a residential environment free from indoor sources. The 422/420 house was borrowed (and is now rented) from MFCDC that owns the property. It was thought that the house would eventually be torn down because it had been previously abandoned and vandalized. The house was ideal for this study because it had no occupants, was in limited use beyond the project, and was at an ideal location and price range, and vapor intrusion was present.

Because the house was in poor condition and the house had no occupants, alterations could be made to the house necessary to set up ports, wells, and sensors for observations without disturbing any occupants. Changes to the house were made considering how to best simulate a living environment. For example, a field scientist worked on site regularly for several months before sampling began. During most normal work weeks during the periods of active VOC sampling, the field scientist was at the house at least 4 days per week. During the down times between VOC sampling efforts (such as April to September 2012), visits to the house were less frequent. The intent during VOC sampling periods was to have an individual who would open doors and windows, move through the environment, and make temperature adjustments to the 422 side of the duplex when the seasons dictated, similar to the way a homeowner would. The constant close proximity of the worker to the work zone also allowed for quick observation and response to environmental changes. A second floor bedroom on the heated 422 side of the duplex was minimally modified and used as an office for the sampling staff member.

3.1.5 Investigation History

The selection and screening of this duplex was conducted in April to June 2010 as described in the first report on this series of projects (U.S. EPA, 2012a). That report also describes the design and results of an extensive 14-month soil gas, groundwater, and indoor air sampling program conducted from December 2010 to March 2012. The second report (U.S. EPA, 2013) covered VOC and radon samples taken after March 2012, including prior to and after the October 2012 installation of a mitigation system, and until May 2013. This report covers monitoring from May 2013 through March 5, 2014, during which the mitigation system was not operating, with an emphasis on using the detailed knowledge assembled under the previous project phases to try and predict vapor intrusion into the duplex.

In many cases, the results and analysis in this report build on the results presented in U.S. EPA (2012a, 2013). This report also describes the effects of the subslab depressurization mitigation system on radon and VOC levels in the duplex and investigates the factors that influence VOC and radon levels in and under the duplex. Where sampling locations and techniques are relevant to the third stage of the investigation, the descriptions from U.S. EPA (2012a and/or 2013) are repeated here.

3.2 Evolution of Conceptual Site Model

This report provides a further opportunity to document how a conceptual site model can evolve through intensive study of the vapor intrusion situation surrounding a single building.

3.2.1 Prior to 2011–2012 Investigations

During site selection, the initial conceptual site model for this structure was that a vapor intrusion source was most likely present in shallow and subslab soil gas due to historical dry cleaning facilities and adjacent commercial uses. Radon impacts were suspected because Marion County, Indiana, is in EPA's Zone 1—highest risk for radon. Concentrations of chlorinated hydrocarbons were detected during initial site screening and responded to depressurization of the structure by fans (U.S. EPA, 2012a).

The source of the primary VOCs (PCE and chloroform) observed at this duplex was initially suspected to be transport of contaminants either

- through a groundwater pathway from upgradient dry cleaners or
- released into the shallow vadose zone during the operations of the adjacent commercial quadraplex.

Later observations and discussions suggested that disinfection byproducts in city drinking water could be an additional potential source for chloroform detected in soil gas.

3.2.2 After 2011–2012 Investigations (U.S. EPA, 2012a)

The detailed 2011–2012 site investigation and monitoring work described in U.S. EPA (2012a) added the following details to our conceptual site model of this duplex and the vapor intrusion exposure pathway:

- The groundwater and nearby Fall Creek are intimately connected. The groundwater level beneath the house is subject to rapid swings of up to 5 ft over the course of a few days during seasonal flooding in the creek. There also could be connections to the combined sewers that discharge into Fall Creek.
- The stack effect caused by indoor/outdoor temperature differentials operates not only during the heating season, but also during the summer as well, due to the “solar stack effect” and the storage of heat in the building during cool late summer/fall nights. Differential pressure measurements indicate that changes in building differential pressure are reflected in a measureable advective driving force between the 13-ft depth near the water and the 6-ft depth directly beneath the basement. Therefore, in this case, advection may be the primary cause of VOC migration through the deeper portions of the vadose zone.
- The heterogeneity of the subslab concentrations and geophysical result suggests the absence of an engineered gravel layer beneath the duplex. Thus, the subslab does not behave here as a well-mixed plenum.
- PCE is apparently widely spatially distributed in site groundwater at concentrations well below the current 5 µg/L MCL (U.S. EPA, 2012a). These shallow groundwater concentrations are sand apparently control deep soil gas concentrations. Only a moderate degree of attenuation occurs in those deep soil concentrations as they are drawn toward the basement of the structure. Substantial attenuation occurs in the upper 6 ft of the site external soil gas, which is finer grained materials than the sandy deeper materials. It is currently unclear whether this is due to gas permeability contrasts, sorption processes, or most likely barometric pumping dilution. Substantial attenuation also occurs across the building envelope between subslab and indoor air.
- Chloroform is present in highest concentration in deep soil gas. Substantial chloroform has been historically been detected in groundwater on a site 200 ft to the southwest. Chloroform also was detected in groundwater at this house in preliminary sampling and at low levels (< 0.6 µ/L) in the spring of 2013. Studies were conducted that determined that the lack of detections in 2012 to early 2013 groundwater samples on site was not from losses in the sampling and analysis process. U.S. EPA (2012a) noted that chloroform attenuation in soil gas was substantial between the area

just above the water and the 6-ft depth below the structure, and that chloroform also appeared to be attenuated between subslab air and indoor air.

- The relative importance of the potential sources of PCE and chloroform was unclear. These sources include a historic dry cleaners, historical activities in the adjacent commercial/industrial quadraplex, and leaking storm sewers/drinking water lines.
- Sewer lines and laterals appeared to play some role in contaminant fate and transport in this system. Elevated concentrations of PCE and chloroform were present in the headspace of sewer gas. Their role as a direct entry pathway were minimized through plumbing trap and vent maintenance. Their role in lateral transport through the vadose zone and into the subslab of the duplex were elucidated through the geotechnical studies described in U.S. EPA (2013).
- There appears to be a strong seasonal component to the PCE and chloroform indoor air concentrations (see Section 11, Figure 11-12 of U.S. EPA, 2012a). The seasonal component is partially but not completely correlated to the strength of the stack effect (see Section 10, Figures 10-10 and 10-11, U.S. EPA, 2012a).
- Concentrations of benzene, hexane, and toluene in indoor air are quite similar to ambient levels and appear to move in lockstep with ambient air, although there are some traces of benzene in soil gas (Section 11, Figure 11-12, U.S. EPA, 2012a). TCE in indoor air also tracks ambient concentrations when TCE is low, but are very similar to the PCE plots when concentrations were high at the beginning of the study, suggesting a contribution of subsurface sources to TCE indoor air concentrations, either through a TCE source or as a PCE degradation product.

3.2.3 Refinements in Conceptual Site Model during the 2012–2013 Study (U.S. EPA, 2013)

The quality assurance project plan (QAPP) for the 2012–2013 work defined several goals related to improving the conceptual site model.

- Better define the particular subsurface conditions that influence the movement of VOCs and radon into this home. These conditions are expected to include differences in air permeability on a spatial scale of 1 to 20 ft in the vadose zone beneath and immediately adjacent to the structure.
- Better define the particular entry routes of soil gas into the building envelope. Define the degree to which utility corridors function as preferential transport pathways—either through the vadose zone or through the building envelope.
- Determine how the structure of the foundation may subdivide the subslab air space.
- Capture a winter capping event to monitor its influence on vapor movement into the home.

U.S. EPA (2013) expressed a remaining uncertainty about the relative importance of groundwater as the source of the VOCs detected in soil gas and indoor air within the duplex. Henry's law calculations determined that the PCE concentrations detected in groundwater were sufficient to serve as a source for the highest deep soil gas concentrations, but chloroform soil gas concentrations were 12 times higher than the vapor concentrations calculated using Henry's Law off of a groundwater source. In U.S. EPA (2013), the highest soil gas concentrations were reported to be on the downgradient (southeast) side of the house and the highest concentrations observed in soil gas were generally just above the water table (see Figure 8-25 in our previous report (U.S. EPA, 2013). This is consistent with observations during this study, along with the large and rapid responses of the groundwater level (water table) to rainfall, perhaps related to the coarseness of the aquifer material between the house and nearby Fall Creek. Also, at a site 200 ft to the southeast, substantial chloroform was previously detected in groundwater (U.S. EPA, 2012a, Section 11 and Section 13.1.6).

U.S. EPA (2103) proposed that the following hypotheses could explain these observations:

- The primary stored VOC mass may be in the deep vadose zone either sorbed to soil particles, present in soil moisture, or present as soil gas in the least permeable portions of the soils, with vadose zone soils retaining VOC mass for a substantial time period after an associated groundwater plume naturally attenuates.
- The primary source for PCE is impacted groundwater adjacent to the duplex on a location not observed by our monitoring wells, as suggested by prior off-site detections. The primary source of chloroform may be from water that is periodically transported along deep combined sewers and leaked water from those sewers percolating downward toward the water table. This might manifest in higher chloroform concentrations in soil moisture in the vadose zone or in the capillary fringe than in the sampled shallowest portion of the saturated zone.

General support for the importance of these hypotheses at other sites can be found in the literature (Carr et al., 2011; Christ, 2010). Particularly relevant is this statement from Carr (2010): “*The common perception that VI potential is largely a function of contemporaneous groundwater quality is flawed.*”

3.2.4 Refinements in Conceptual Site Model During This Study (May 2013–March 2014)

For chloroform, generally the highest concentrations observed in soil gas are just above the water table. There is a large and rapid response of the potentiometric surface to rainfall, perhaps related to the presence of combined sewers and surface water bodies in the vicinity of the study duplex. There is a correlation between chloroform trends and changes in hydrogeology.

Although chloroform has been found in groundwater at significantly higher concentrations than in U.S. EPA (2013), concentrations are still too low to entirely account for the peak chloroform concentrations in soil gas, which is consistent with several alternate conceptual models:

1. Chloroform is primarily transported to the site through combined sewers and/or water mains⁹ that leak well below ground surface. Chloroform is stripped from these waters as they infiltrate down to the water table. Higher chloroform concentrations in soil moisture in the vadose zone than at the water table.
2. Chloroform may be present in higher concentration in groundwater at some locations near the site that have not yet been delineated by the three existing groundwater well clusters close to the structure. Thus, the primary source is affected groundwater lateral to the duplex location not observed by our monitoring wells, as may be suggested by prior off-site detections reported in U.S. EPA (2012a, 2013).
3. Groundwater chloroform concentrations at the site may have been higher in the past and the observed soil gas concentrations are a legacy of that period.
4. The primary stored mass is in the deep vadose zone either sorbed to soil particles, present in soil moisture, or present as soil gas in the least permeable portions of the soils. Others (e.g., Carr et al., 2011; Christ, 2010) have hypothesized that vadose zone soils will retain mass for a substantial time period after an associated groundwater plume naturally attenuates.)

Our previous results (U.S. EPA, 2013) suggested a groundwater source for PCE, and the work described in **Section 8** of this report confirms this hypothesis with additional groundwater measurements and a

⁹ It should be noted that the concentrations observed in groundwater at this duplex are lower than the mean drinking water concentration for Indianapolis (19 ppb) and are far below the peak reported drinking water concentration (82 ppb) (New York Times, 2012). Additional chloroform formation is possible in combined sewers that receive chlorine bleach containing products.

positive correlation between shallow groundwater and soil gas PCE concentrations. However, the narrow range of variability in PCE concentrations (below an order of magnitude) and stability of this variability over time observed in this report and Section 11 of the previous report make it unlikely that variability in groundwater concentrations is strongly related to the changes in soil gas or indoor air concentrations over the time scales observed in this study. As has been shown in this and other studies, the variability in indoor air PCE concentrations at the Indianapolis duplex is also influenced by subsurface, building-related, and meteorological variables that affect the concentration of PCE as it migrates from the water table, enters the building, and mixes with indoor air. However, other sources of PCE vapors in soil gas that may also exist in the vadose zone or combined sewer lines cannot be ruled out, and variability in those sources could also influence the PCE concentrations in indoor air.

3.3 Building Renovation and Mitigation

Details of the original building renovations were presented in U.S. EPA (2012a). Generally, the house was rewired, a heating system was installed on the 422 side of the duplex, window air conditions were installed along with locks and a security system. The primary renovation for the second phase of the project was the design and installation of a radon mitigation system, which is described in detail in U.S. EPA (2013). The initial plan for the installation planned for two extraction pits to be installed at the northern basement sections on the 422 and 420 sides of the house. After installation of the two legs the project team decided that pressures were insufficient and that two additional legs were needed. The full system, then consisting of four extraction legs total (**Figures 3-10** and **3-11**), was turned on at 17:20 on October 17, 2012.

The system included sampling ports on the positive side of the mitigation system stack (i.e., above the blower) that were drilled for Waterloo Membrane Samplers (WMS), AlphaGUARD sampling, and a port for insertion of an airfoil velocity measurement attachment for the micromanometer that was used to test the system after installation but prior to monitoring. **Figure 3-12** shows external and internal photographs of the system, and **Figure 3-13** is a cross-section diagram showing the general layout of the 422/420 north and central basements with the positioning of the extraction legs, exterior blower, and exhaust stack. Additional system photographs and details on system testing can be found in Appendix A of U.S. EPA (2013).

After installation and testing, the system was operated and monitored for three on periods, two passive periods, and one fully off period. The three on periods ran from October 17, 2012, to November 14, 2012; December 12, 2012, to December 29, 2012; and February 6, 2013, to April 24, 2013. The two passive periods ran from November 14, 2012, to December 12, 2012, and from December 29, 2012, to January 16, 2013. The fully off period ran from January 16, 2013 to February 6, 2013. The most recent mitigation on period began on March 5, 2014, and has been running to the current phase.

3.4 VOC Monitoring, Sampling, and Analysis

Section 3 in the previous project reports (U.S. EPA, 2012a, 2013) provided details on the design and installation of the monitoring infrastructure used in this project including wells, soil gas monitoring ports, soil temperature and moisture sensors, differential pressure sensors, weather data, and indoor and outdoor monitoring for VOCs and radon. This report updates the previous reports, with this section summarizing and updating the previous reports text on the VOC sampling configurations used for soil gas, air, and groundwater monitoring. **Section 3.5** describes radon sampling, and **Section 3.6** describes monitoring of physical parameters like weather, indoor temperature, and differential pressures. **Figure 3-14** shows the location of subsurface monitoring points including soil gas sampling ports and groundwater monitoring wells.

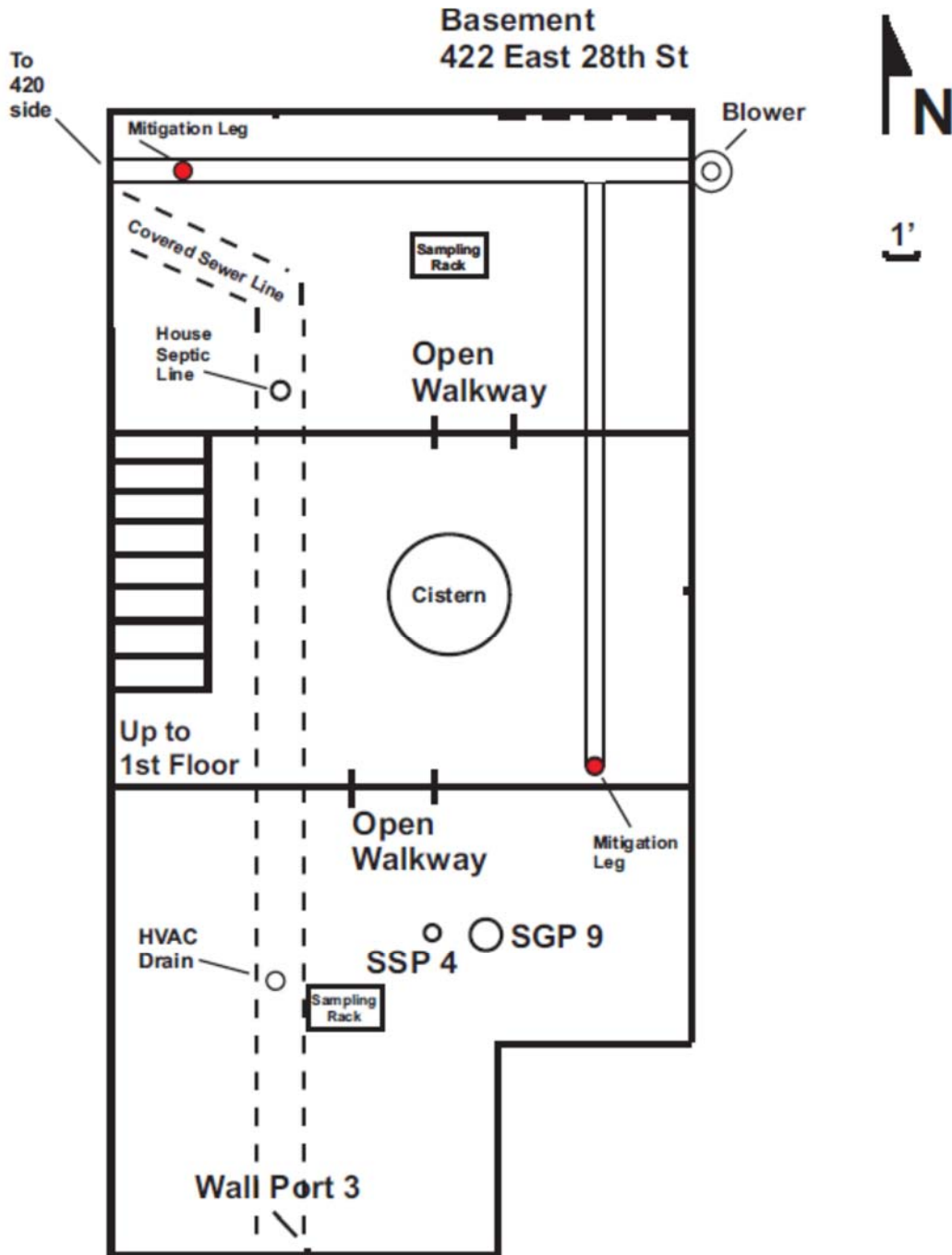


Figure 3-10. Map view of the 422-side basement showing mitigation system legs, subslab soil gas extraction pits (red circles), and the position of the passive “sampling racks.”

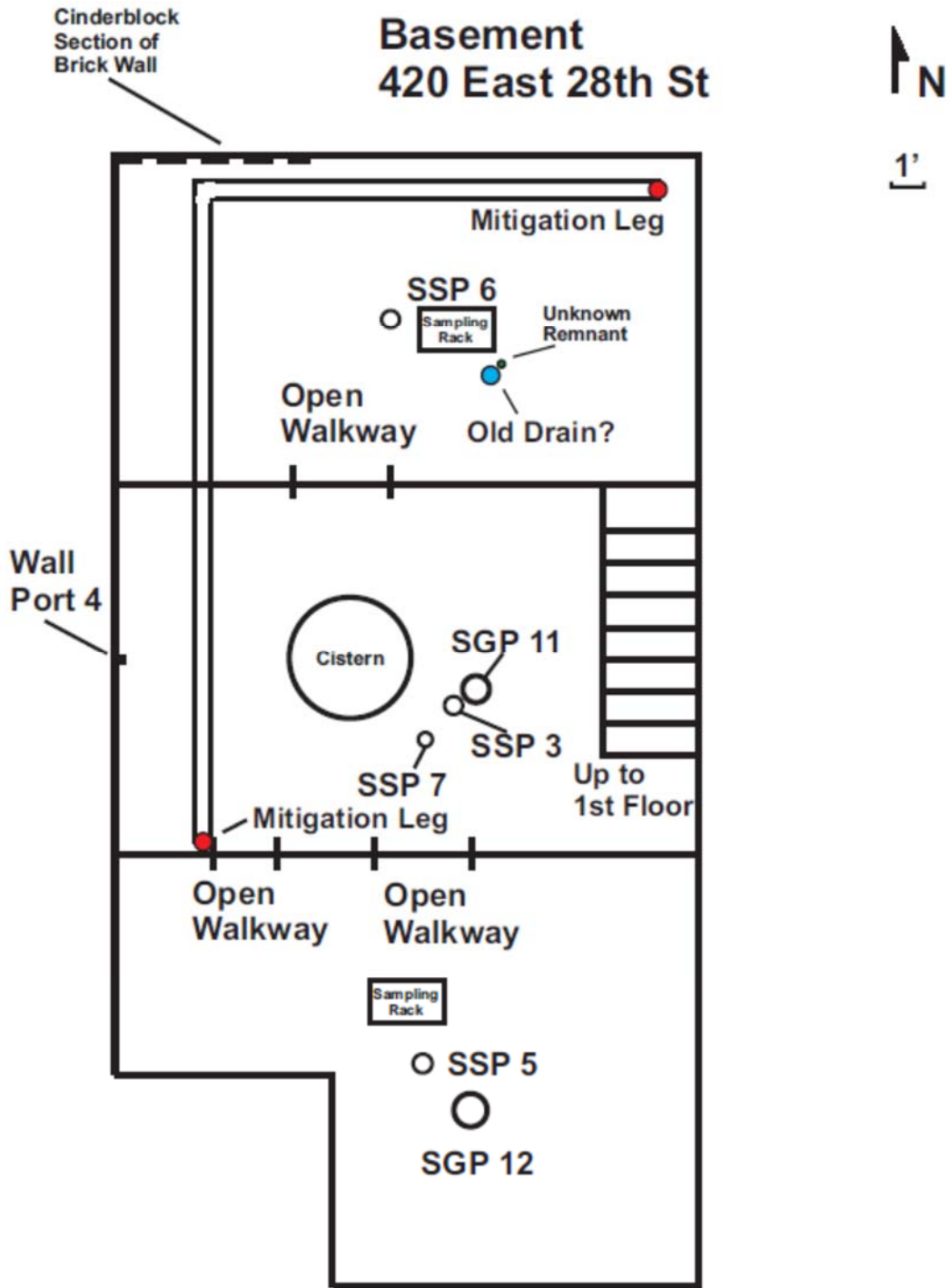


Figure 3-11. Map view of the 420-side basement showing the mitigation system legs, subslab soil gas extraction pits (red circles), and the passive “sampling racks.”



Figure 3-12. Photos of mitigation system: (left) SSD blower and stack on northeast corner of duplex; (right) SSD extraction point showing valve and U-tube manometer.

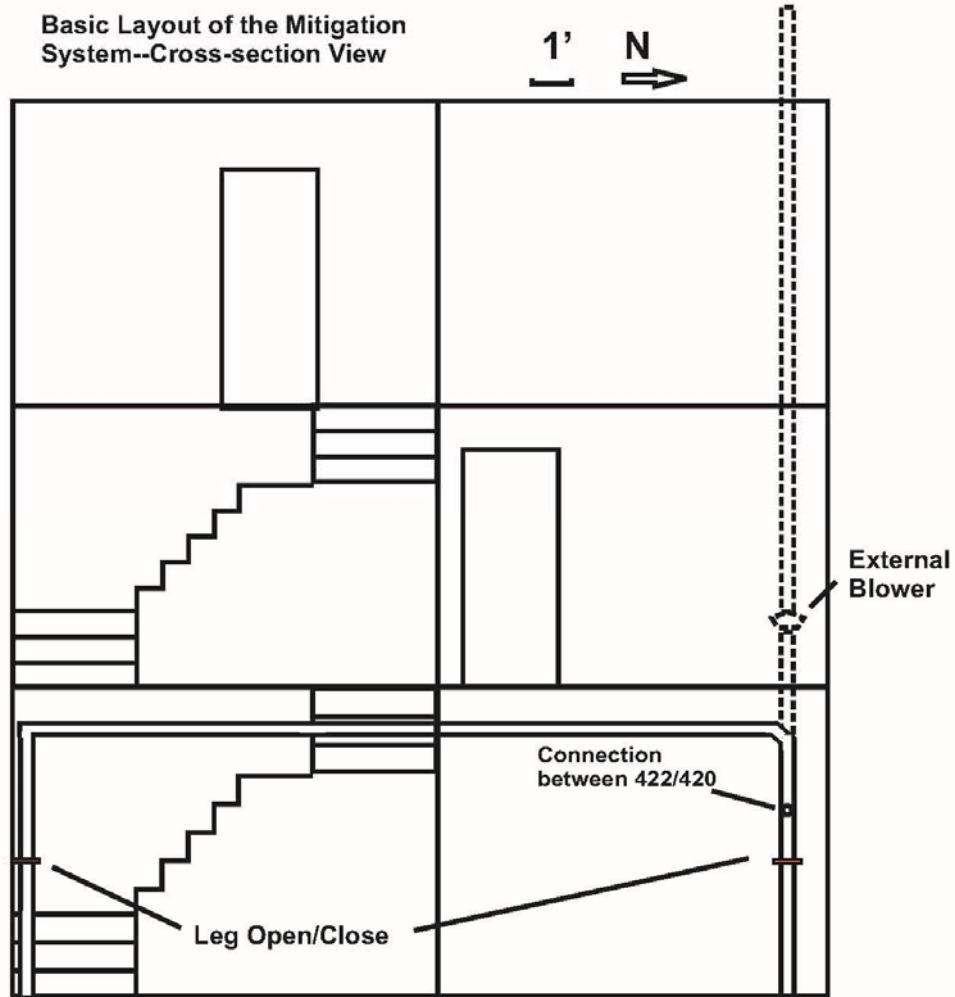


Figure 3-13. Showing the general layout of the 422/420 north and central basements with the positioning of the extraction legs, exterior blower, and exhaust stack.

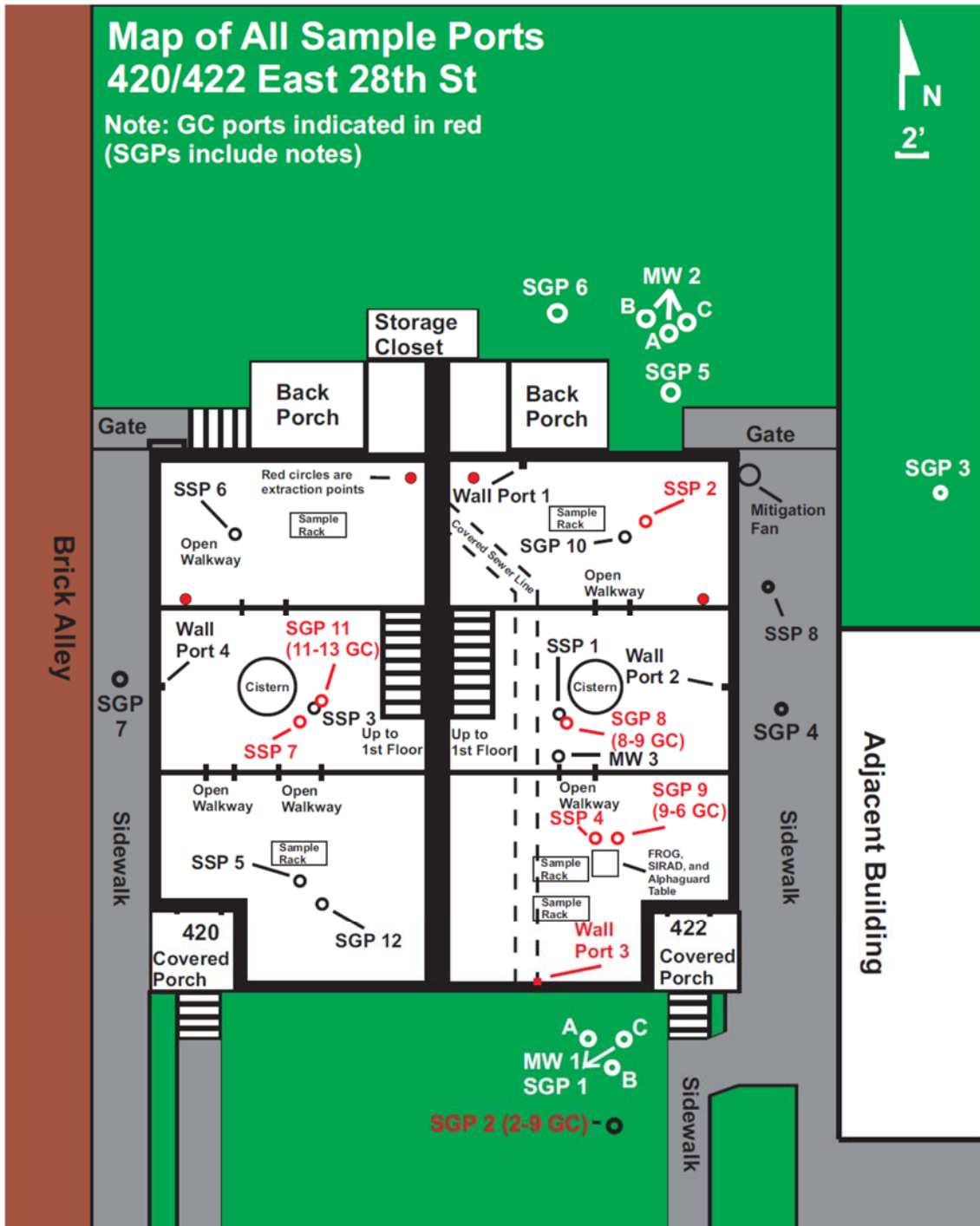


Figure 3-14. Sampling port and monitoring well locations: subsurface soil gas monitoring ports (SGP), subslab sampling ports (SSP), groundwater monitoring wells (MW), on-site gas chromatography (GC), and other monitoring locations. Probes/ports in red were sampled by the on-site GC. Soil temperature and moisture probes were installed in the 422 basement between SGP 8 and MW 3 and in the backyard to the north of MW 2.

3.4.1 Indoor and Outdoor Air VOC Monitoring (Passive Samplers)

The overwhelming majority of the indoor passive sampling was done with Radiello 130 samplers supplied by and analyzed by Air Toxics Ltd. For comparison, two different types of SKC badges were also used that were specifically adapted to use at very short or long sampling durations.

For passive sampling, several racks were set up to facilitate arranging groups of samplers in consistent locations for different durations during the run of the project. One rack was placed in the first floor center room of 420 and 422 and in the northern and southern areas of each basement. In addition to these indoor racks, a hooded outdoor (ambient) location was made to accommodate the passive samplers on a telephone pole near the house.

At each rack, passive samplers were placed for durations of 7, 14, 28, 91, 182, and 364 days from January 2011 to March 2012. From October 2012 through May 2013, the primary emphasis of the passive sampling was to study the effects of the mitigation system and snow/ice effects on VOC and radon levels using weekly and quarterly sampling durations. To extend the sampling record under existing resources, sampling locations were reduced initially on October 30, 2013, and then further on November, 20, 2013. Since November 2013 the following passive sampling locations have been in use: 422 first floor, 422 basement south, 420 basement south, and the ambient location. For the 2013–2014 period of the project, different passive samplers were deployed to compare their efficiencies between sampler types over periods of 6 months and 1 year. The sampler types compared were Radiello 130 samplers with yellow diffusive bodies, SKC 575 Ultra III badges, and the WMS. These were each hung from free spaces on sampler racks at the following locations: 422 first floor, 422 basement south (an additional rack was set up in this section of the basement to accommodate duplicates), 420 basement south, and some at the ambient location.

3.4.2 Subslab and Soil Gas (TO-17)

The primary method of subslab and soil gas sampling for VOCs during the current phase of the project was by TO-17 using Tenax TA ATD tubes. In this method, a thermal desorption tube, with a female Swagelok end, was connected to each sampling port in turn. Each port had its own male union connected to a valve. Before sampling, the port was purged with an SKC Universal XR pump set to 1L/min. Five well volumes were then purged via an exhaust line that ran away from the operator for exterior ports or out of a basement window in the case of the interior ports. The fittings were attached with wrenches, and an air tight syringe was mounted onto the other end of the TO-17 tube. Once this was done, the port's valve was opened, and the syringe was used to draw 200 mL of air through the TO-17 tube over a period of a minute. After this, the port valve was closed, and the TO-17 tube was removed and sealed for shipping.

A round of TO-17 sampling occurred about once per month, except during the FROG study, when sampling occurred more frequently at certain ports. The regular sampling began in September 2013 and has continued through the current phase. Initially, the preferred depths to sample were 3.5, 9, and 16.5 ft bls exterior and 6, 9, and 16.5 ft bls interior. However, a higher than expected water prevented the sampling of the 16.5 ft depths for most of the duration of the project. Unusually high water tables or perched/infiltrating water occasionally made other soil gas ports inoperative. In addition, all wall ports were sampled during most sampling rounds, as well as a subset of the subslab ports.

The majority of the TO-17 tubes collected were prepared by and analyzed by the EPA National Exposure Research Laboratory (NERL) in Las Vegas, NV. For the extensive sampling of the intensive rounds conducted in 2011 to 2012, additional TO-17 tubes were prepared by and analyzed by Air Toxics. An intercomparison study of the two TO-17 laboratories was conducted in the previous project and showed agreement between the two laboratories (see Section 4.2.4 of U.S. EPA [2012a]). During the intensive

rounds, all functioning ports (not made inoperative by water) were sampled at least once each day of the round. For a few days of each round, several locations were sampled multiple times of the day with the intention of comparing hourly and daily variability to the normal weekly variability. Field duplicates were also analyzed, as discussed in Section 4.2.6.

3.4.3 Groundwater

Groundwater samples were taken approximately monthly with permeable diffusion bags (PDBs) from EON Products Inc. However, because of difficulties sampling the indoor 1-inch well (MW-3) by PDB, samples were taken by bailers from February 6, 2013, onward. The 422/420 duplex has six exterior MWs (two clusters of three) and one single-depth interior well installed in the basement and completed on the first floor. The exterior wells are arranged in groups of three in the front and the back yards. Each group of three is divided into depths of 16–21 ft, 21–24 ft, and 24–26 ft bls. The interior well (MW-3) is about 18 ft bls, but the casing extends up to the first floor for ease of access, so it is about 24 ft deep at its access point. The exterior wells are 2 inches in diameter, and the internal well is 1 inch in diameter. PDBs for the exterior wells are 12 by 1.75 inches, and the interior is 18 by 0.75 inches. PDBs were deployed for at least 2 weeks, and a new set of PDBs was cycled through almost monthly. PDBs were filled initially with deionized water provided by the EPA NERL laboratory. Most groundwater samples were shipped to EPA NERL-Las Vegas for VOC analysis by Method 8260. A few samples were analyzed by Pace laboratories in Indianapolis as a quality control check.

Groundwater samples were also collected from soil gas points when they were temporarily flooded using a peristaltic pump. Peristaltic pump samples were also collected from the monitoring wells for comparison purposes.

3.4.4 SSD System Stack Gas Sampling

Passive sampling from the SSD stack for VOCs was conducted using a passive sampler, the WMS. The WMS was selected for sampling the SSD stack because its design makes it resistant to changes in air velocity and because of its small size. The sampler and its validation are described at <http://www.sirem-lab.com/images/PDF/wms.pdf> (last accessed 10/9/2012). Radon readings in the stack were taken using the portable AlphaGUARD instrument used for soil gas. Stack velocity readings were taken with a Shortridge AND-870C Multimeter with the Airfoil Velocity measurement probe.

3.4.5 FROG Portable GC

In early 2014, the FROG 4000 portable GC unit from Defiant technologies was tested at the site. Initially designed to analyze water and soil samples for VOCs in the field, the FROG 4000 was later adapted to perform on-site VOC analyses on indoor and outdoor air samples as well as soil gas. This project compared FROG 4000 results against Radiello samplers and SKC 575 Ultra III badges for indoor air and TO-17 for soil gas. A water sampling comparison was also made between on-site measurements made by the FROG 4000 and groundwater samples sent to the EPA lab.

Most of the FROG 4000 sampling events occurred from February 3 through February 7, 2014. One FROG unit monitored indoor air continuously from February 3, 2014, until its return to Defiant on March 6, 2014. However, the unit did not run consistently. A software problem resulted in periodic, random shutdown times. After a shutdown, the unit would be restarted by on-site personnel.

3.5 Radon Sampling and Analysis

The primary radon sampling method was electret ion chambers collecting radon samples passively in indoor air for the same 7-day intervals as Radiello-collected VOCs (Section 3.5.1). Several additional methods were used for radon in indoor air:

- real-time AlphaGUARD instruments for both subslab and deeper soil gas measurements from the soil gas monitoring ports (Section 3.5.2) and stationary radon measurements in indoor air (Section 3.5.3)
- a consumer grade ionization chamber-based detector (Safety Siren Pro Series 3 manufactured by Family Safety Products Inc.) (Section 3.5.4)
- the SIRAD MR-106N professional grade radon detector (Section 3.5.5)

3.5.1 Indoor and Outdoor Air Radon Sampling and Analysis (Electrets)

We used Rad Elec, E-Perm, ST-type (short-term) electrets according to U.S. EPA (1992). To sample, electrets were opened within their chambers at their assigned locations for a week. After a week, the chambers were closed, all electrets were allowed to equilibrate for an hour to the room temperature where they would be read, and then their voltages were read on a Rad Elec electret voltage reader. Start and stop times, as well as voltages, were recorded and the electrets redeployed. The voltages, configurations (e.g., ST electrets in s-chambers), dates, and times were then used in a formula to convert voltage to pico Curies per liter (pCi/L), with background gamma correction.

The electret reader was calibrated weekly with three standards. In addition, an electret blank test was run weekly to test for effects of the chamber on the electrets. In this test, an electret not used during the sampling was inserted into one of the used electret chambers (closed) and then read to determine whether there had been any voltage drop from the previous week's reading.

Electrets were hung in mesh bags, one at each of the same locations used for sampling Radiello samplers, plus a duplicate at one location (three locations on the 422 side of the house and three on the 420 side). Only three locations have been in use since November 20, 2013: 422 first floor, 422 basement south, and 420 basement south. The ambient electret was kept in a permeable bag and hung from a wooden dowel about 2 ft from the house. Since December 28, 2011, a new electret was added in the 422 second floor office to be used in conjunction with the Safety Siren testing described in U.S. EPA (2013). This office electret was discontinued on November 14, 2013.

3.5.2 Subslab and Soil Gas Radon Sampling and Analysis (AlphaGUARD)

Radon readings were collected weekly in 2011–2012 and approximately monthly or as meteorological conditions required in 2012–2014 with a portable AlphaGUARD Professional Radon Monitor from Genitron Instruments. Operations were based on EPA guidelines for using continuous radon monitors (U.S. EPA, 1992). More information on the AlphaGUARD can be found at www.genitron.de/products/products.html. During routine sampling, this device was connected to subslab, soil gas, and wall ports with an SKC Universal XR pump set to 1 L/min. Tubes connected the sample port to the pump (with a moisture filter on the sampling end) and the pump to the AlphaGUARD. A purge line led away from the operator for exterior sampling and out of basement windows for interior sampling locations. The AlphaGUARD requires a 10-minute cycle of uninterrupted air flow from the sample location for an accurate reading. Because a certain amount of time was needed for movement between, one 10-minute cycle was spent relocating and then another to sample at the next location. Thus, each sample port required 20 minutes to sample.

Because radon has a short half-life (3.8 days) and the migration time from substantial depths for soil gas is estimated to be months to years (Kurtz and Folkes, 2008; Carr et al., 2011), radon sampling focused on the shallowest depths and, thus, differed from the VOC sampling strategy. Exterior sampling consisted of the shallowest ports available of the wells closest to the house. Usually, these were the 3.5- and 6-ft deep ports of SGPs 1, 7, 4, and 5. Periodically, these depths would not yield a sample, presumably because of moisture infiltration. In such cases, the next shallowest depths were chosen. Routine interior sampling

included all wall ports, five of the subslab ports, and the shallowest intervals of the nested interior soil gas ports.

For routine sampling, an ambient reading was taken outdoors and about 20 ft away from the 422/420 house. Lines to be sampled were purged with the SKC pump (five soil gas point volumes, calculated based on the depth). Finally, the pump would be connected to the AlphaGUARD to acquire a full 10-minute sample.

The AlphaGUARD has a readout screen that details the results of the analysis at the end of each 10-minute cycle. The data provided are radon concentration (Bq/m^3), relative humidity (%), pressure (mbar), and temperature ($^{\circ}\text{C}$). These data were recorded each week in a spreadsheet and the Bq/m^3 converted to pCi/L .

3.5.3 Continuous (Real-Time) Indoor Air Radon Sampling and Analysis (AlphaGUARD)

The real-time AlphaGUARDs are essentially the same as the handheld AlphaGUARD instrument used to sample from the soil gas ports, except they are not fitted with the same nozzle type, because they are not connected to external pumps. Rather, in this application they are operated in a diffusion mode. These AlphaGUARDs are intended to be placed to give readings in specific rooms. In the case of the 422/420 duplex, one unit was placed in the 422 second floor office, and the other was placed in the 422 north basement area. These units stayed in their locations, except for brief, periodic data downloadings. These units were first regularly deployed on March 31, 2011, and were in near-continuous operation until the present, except for a period of off-site recalibration in late July through late September 2012.

The data are produced by the instrument in the same units as the portable AlphaGUARD (requiring conversion to pCi/L), and data points are collected every 10 minutes. However, because these devices were not moved, all 10-minute cycles are usable. The real-time AlphaGUARDs are used in conjunction with Data Expert software, also from Genitron Instruments. Approximately once each week, the AlphaGUARDs were connected to the computer (the one in the basement required briefly moving the instrument to download), and the software downloaded the readings for the week. These readings were then saved as text files for later conversion to Excel spreadsheet files.

3.5.4 Consumer-Grade Radon Detector (Safety Siren)

Consumer-grade radon detector (Safety Siren) testing was a later addition to the project. Six Pro Series 3 Safety Siren radon gas detectors were deployed on December 23, 2011, and in use until March 1, 2012. They were tested again from October 2012 to May 2013 during a period of mitigation on/off testing. Each detector was installed at one of six locations: 422 second floor office, 422 first floor center room, 422 basement south, 422 basement north, 420 first floor center room (stolen October 11, 2012, not replaced), and 420 basement south. The intention of the test was to determine the agreement among the radon Safety Sirens, electrets, stationary AlphaGUARDs, and (for 1 week) charcoal canisters. The Safety Sirens can be read once each week, so their readings were taken when the other weekly data types were being acquired to facilitate comparison.

3.5.5 Professional Radon Detector (SIRAD)

Professional-grade radon detectors (the SIRAD MR-106N) were added to the project on November 25, 2013, in both the south basement of 422 and the first floor of 422. On December 23, 2013, the first floor SIRAD was moved to the second floor office of 422 to allow for comparison between that SIRAD and the AlphaGUARD present in the second floor office. Each SIRAD operated by taking a reading over a 4-hour period. The readings were then recorded by the units and could later be accessed by an operator through a series of menus. The original intent for using the SIRADs was not only to provide additional lines of

radon monitoring, but also because the SIRADs are capable of connecting to a computer. This computer connection could have allowed for remote access to data within the SIRAD units.

Both SIRAD units malfunctioned and ceased to operate on February 17, 2014, due to an unknown system error, so SIRAD data in this report are limited to measurements taken before that date.

3.6 Physical Parameters Monitoring

3.6.1 On-Site Weather Station

This project used a Davis Vantage Vue Weather Station on site with Weather Link data logger and software. The components consist of the outdoor monitoring unit, the indoor receiver, and the computer connection. The outdoor monitoring unit was mounted on an accessible portion of the 422/420 house roof. The unit was mounted on steel pipes, but 5 ft above the highest roof deck (that of the attic dormer) (Figure 3-15).



Figure 3-15. Front view of 420/422 duplex with location of weather station sensors indicated with red arrow.

The outdoor unit contains all the exterior monitoring equipment (e.g., wind speed cups, rain gauge) and has a solar panel/battery backup for power. The outdoor unit transmits a radio signal to the indoor receiver, which also records the data every half hour. The indoor unit is human readable and can also be used to set a variety of parameters. The indoor unit also records the house interior data at its location, in this case the 422 second floor office. Once each week, the data were downloaded from the indoor unit onto the computer containing the Weather Link software. These data were saved as a text file and later compiled in an Excel spreadsheet file. Many parameters are recorded; the key ones required for this project are temperature (degrees F, interior and exterior), relative humidity (%), wind speed (mph), and wind direction (16 points [22.5°] on compass rose).

Initially, and at least every 6 months, the results from this on-site system were compared with other nearby weather stations in Indianapolis using at least 1 day's observations. The National Weather Service (NWS) Indianapolis International Airport (KIND) is approximately 15 miles southwest from the site. The Indianapolis NWS station at Eagle Creek Airpark (KEYE) is approximately 9 miles west of the site. There is also a private weather station available online closer to the site in Indianapolis, IN (KININDIA33).

In the late fall of 2013, the problem of the periodic data dropouts experienced in the second phase of the project began again. As before, a tree service was called to change the exterior weather station battery. This seemed to stop the data outages for a while, but they then reoccurred sporadically or during periods of extreme cold. The manufacturer thought the cause was a faulty capacitor in the exterior weather station. The manufacturer thought that the station battery became less efficient during times of extreme cold, causing the station to draw on the charge stored by its capacitor. If the capacitor were faulty, it would not be able to power the station through the whole night until the solar cell could once again power the station in daylight. The data outages ceased as temperatures rose during the spring of 2014.

3.6.2 Indoor Temperature

Although the indoor weather station unit can record temperature, it only does this in the 422 second floor office where it is located. Because temperature readings were required at all sample locations to allow adjustment of the passive sampler data for uptake rate variation due to temperature, another form of data collection was necessary. HOBOS data loggers, made by Onset (<http://www.onsetcomp.com/>), were placed—one at each of the six passive sampler racks in the house (three since November 20, 2013). HOBOS record temperature (degrees F) and relative humidity (%) every 30 minutes. Once a week, these data were recorded by taking them to the computer with the Hoboware reading software and later importing those data to the project database. Special spreadsheets were created to provide this information for the different Radiello time durations to the passive sampler analytical laboratory for temperature correction of passive sampler results.

3.6.3 Soil Temperature

Soil temperature was recorded by thermocouples from Omega (Type T, hermetically sealed tip insulated thermocouples, HSTC-TT-T-24S-120). During the initial house set up, holes were drilled beneath the 422 basement slab and back yard soils of the duplex (see **Figure 3-14**) to accommodate thermocouple probes with end points set at different depths corresponding to the depths of the soil gas ports: inside at 6, 9, 13, and 16.5 ft bls and outside at 1, 3.5, 6, and 13 ft bls. Wires were run from the probe to the PDAQ 56 data acquisition system, with a reading taken about every 15 minutes.

3.6.4 Soil Moisture

Soil moisture was recorded by implanted Watermark moisture sensors. As explained by Smajstrla and Harrison (2002), water potential is commonly measured in units of bars and centibars (English system) or kilopascals (metric), with 1 bar is approximately equal to one atmosphere (14.7 lbs/in²) of pressure. One

centibar is equal to one kilopascal. “Because water is held by capillary forces within unsaturated soil pore spaces, its water potential is negative, indicating that the water is under tension and that work must be done to extract water from the soil. A water potential reading of 0 indicates that the soil is saturated, and plant roots may suffer from lack of oxygen. As the soil dries, water becomes less available and the water potential becomes more negative. The negative sign is usually omitted for convenience when soil water potentials are measured.”

Soil moisture sensors were installed in the holes drilled during the house set up. Soil moisture probes were installed near the soil temperature probes in the 422 basement and backyard (see **Figure 3-14**). As with soil temperature, soil moisture sensors were installed to approximately correspond to the soil gas port depths: inside at 6, 13, and 16.5 ft bls and outside at 3.5, 6, 9, 13, and 16.5 ft bls. The sensors were wired to a Watermark 900M monitor, which reads and records the data every 30 minutes. Data were downloaded to the project database once each week and were recorded in centibars.

3.6.5 Groundwater and Surface Water Levels

Initially groundwater levels in the seven wells (three clusters) on site were taken monthly with a Solinst water-level meter. Because water levels seemed to be varying greatly (fluctuating by 8–10 ft or more) and quickly, a Solinst water Levelogger Model 3001 was installed on November 12, 2012, to obtain higher resolution (i.e., every 30 minutes) data. The data logger was installed in the deepest well (1A, ~26 ft) of the south yard monitoring well cluster (MW1), and data are downloaded monthly from the logger and transferred to the project database.

As described in U.S. EPA (2013), when the water-level results from the data logger were compared against USGS stream gauge data for Fall Creek at Millersville (USGS site 03352500), about 300 ft south of the house a very strong relationship was observed. This enabled us to develop a mathematical relationship between the stream level and groundwater level beneath the house. This relationship was then used to extend the groundwater level record to the beginning of the project so fluctuations in groundwater level could be considered against VOC levels indoors and in soil gas (see **Section 8**).

3.6.6 Differential Pressure

As described in U.S. EPA (2012a, 2013), differential pressure readings were monitored by Setra Model 264 low differential pressure transducers and Veltron pressure transducers. These units contain a pressure-sensitive diaphragm that measures pressure changes from high/low poles, with some connected with tubing from the areas to be measured and some left open as an interior reference points.

The Setra pole configurations on the 422 side were as follows: two subslab versus basement (SSP1, SSP2), basement versus upstairs, deep soil gas versus shallow soil gas, and basement versus exterior (out of the basement window), and Wall Port3 versus basement. Only subslab versus basement was measured on the 420 side. Three lines were connected to soil gas ports: 422 deep soil gas versus shallow soil gas (SGP8-6 versus SGP8-13), 422 subslab versus basement (SSP-1 versus 422 basement) and 420 subslab versus basement (SGP11-9 versus 420 basement). The four Setras on the 422 side of the house take instantaneous readings every 5 to 15 minutes depending on setting. The one Setra on the 420 side also takes an instantaneous reading every 5 or 15 minutes, but not necessarily the same interval as the 422 Setras.

After the PMD-1208LS stopped working in early 2014, it was replaced with an Arduino configured with two Veltrons and the 420 Setra. This system came fully on line on April 9, 2014, and has run until the present.

3.7 Data Aggregation Methods

In order to conduct statistical time series analysis in Sections 9 and 10, data had to be arranged into files that contained one value for each predictor (independent) variable for each value of an outcome (dependent) variable. Because of methodological constraints, not all data sets were acquired with exactly the same time intervals. Therefore, data were aggregated at the level of individual days and weeks for data analysis. Professional judgment was used to determine the most appropriate method of aggregation for a given parameter (e.g., mean, sum, mode, maximum) ; in most cases the mean or mode was used as a central tendency estimate to avoid any bias in the aggregated variable. The methods of aggregation for each variable are provided in **Table 3-1**.

Table 3-1. Data Aggregation Applied to Predictor Variables

Variable Name (Plain Language)	Variable Code	Method of Aggregation
<i>Building Variables</i>		
420 air conditioning status (on/on briefly/off)	AC_on-off_420_daily	Mode
422 air conditioning status (on/on briefly/off)	AC_on-off_422_daily	Mode
422 fan status (on/off) (Note: fan was never used on 420)	Fan_on-off_422_daily	Mode
420 side heating status (on/off)	Heat_on-off_420_daily	Mode
422 heating status (on/off)	Heat_on-off_422_daily	Mode
House mitigation status (not yet installed/on/passive/off)	Mitigation_Status_Daily	Mode
<i>Building Environment Variables</i>		
Air density interior	AirDens_422	Mean
Dew point, interior, Fahrenheit	Dew_pt_422_F	Mean
Humidity interior	Hum_422_%.	Mean
Interior heating index	Indoor_Heat_Index	Mean
420, slab vs. basement differential pressure	Setra_420ss.base_Pa	Mean
422 basement vs. exterior differential pressure, Pascals	Setra_422base.out_Pa	Mean
422, basement vs. upstairs differential pressure, Pascals	Setra_422base.upst_Pa	Mean
422, deep vs. shallow soil gas differential pressure, Pascals	Setra_422SGdp.ss_Pa	Mean
422, slab vs. basement differential pressure, Pascals	Setra_422ss.base_Pa	Mean
Temperature at 420 basement north sampling location from HOBO	T_420baseN_C	Mean
Temperature at 420 basement south sampling location from HOBO	T_420baseS_C	Mean
Temperature at 420 first floor sampling location from HOBO	T_420first_C	Mean
Temperature, 422 first floor from weather station	T_422_F	Mean
Temperature 422 basement north from HOBO	T_422baseN_C	Mean
Temperature 422 first floor from HOBO	T_422baseS_C	Mean
Temperature on first floor of 422 of duplex from HOBO	T_422first_C	Mean
<i>Subsurface and Stream Variables</i>		
Water height measured at Fall Creek stream gauge, feet	Fall_Crk_Gage_ht_ft	Mean
Depth to groundwater (MW-3), feet	DepthToWater	Mean
Soil moisture, 13 ft bls beneath structure, cbar	Soil_H2O_In13._cbar	Mean
Soil moisture 16.5 ft bls beneath structure, cbar	Soil_H2O_In16.5._cbar	Mean

(continued)

Table 3-1. Data Aggregation Applied to Predictor Variables (continued)

Variable Name (Plain Language)	Variable Code	Method of Aggregation
Soil moisture 6 ft bls beneath structure, cbar	Soil_H2O_In6._cbar	Mean
Soil moisture 13 ft bls exterior, cbar	Soil_H2O_Out13._cbar	Mean
Soil moisture, 3.5 ft bls exterior, cbar	Soil_H2O_Out3.5._cbar	Mean
Soil moisture 6 ft bls exterior, cbar	Soil_H2O_Out6._cbar	Mean
Soil temperature 13 ft bls beneath structure	Soil_T_C_MW3.13	Mean
Soil temperature 16.4 ft bls beneath structure	Soil_T_C_MW3.16.5	Mean
Soil temperature 6 ft bls beneath structure, degrees C	Soil_T_C_MW3.6	Mean
Soil temperature 9 ft bls beneath structure, degrees C	Soil_T_C_MW3.9	Mean
Soil temperature 1 ft bls exterior, degrees C	Soil_T_C_OTC.1	Mean
Soil temperature 13 ft bls exterior, degrees C	Soil_T_C_OTC.13	Mean
Soil temperature 16.5 ft bls exterior, degrees C	Soil_T_C_OTC.16.5	Mean
Soil temperature 6 ft bls exterior, degrees C	Soil_T_C_OTC.6	Mean
<i>Weather Variables</i>		
Barometric pressure rate of change in inches of mercury per hour	Bar_drop_.Hg.hr	Mean
Barometric pressure in inches of mercury	Bar_in_Hg	Mean
Net barometric pressure change over measurement period in inches of mercury	BP_Net_Change	First-last, by date/time
Standard deviation of barometric pressure change over measurement period in inches of mercury	BP_Pump_Speed	Standard deviation
Largest barometric pressure change over measurement period ("stroke length" of barometric pumping) in inches of mercury	BP_Stroke_Length	Maximum-minimum
Cooling degree day	Cool_Degree_Day	Sum
Dew point, exterior	Dew_pt_out_F	Mean
Heating degree days	Heat_Degree_Day	Sum
Exterior Heating Index—calculated based on temperature and humidity	Heat_Index_F	Mean
Humidity exterior, percent relative	Hum_out_%.	Mean
Rain (inches) totaled during observation period	Rain_In_met	Sum
Rain highest rate during observation period in inches/hour	Rain_IPH	Maximum
Depth of snow on the ground, inches	Snowdepth_daily	Mean
Temperature exterior from HOBO	T_out_C	Mean
Exterior temperature from weather station (°F)	T_out_F	Mean
Temperature exterior, high during data collection period	T_out_Hi_F	Maximum
Lowest exterior temperature, Fahrenheit	T_out_Lo_F	Minimum
Temperature, humidity and wind index	THW_F	Mean
Wind chill	Wind_Chill_F	Mean
Average Wind direction in degrees	Wind_Dir	Trigonometric mean
Wind direction of high speed during measurement period in Degrees	Wind_Dir_Hi	Direction paired to high speed
Wind run is a function of wind speed and duration, miles	Wind_Run_mi	Sum

(continued)

Table 3-1. Data Aggregation Applied to Predictor Variables (continued)

Variable Name (Plain Language)	Variable Code	Method of Aggregation
High wind speed during measurement period, miles per hour	Wind_Speed_Hi_MPH	Maximum
Average wind speed during measurement period, miles per hour	Wind_Speed_MPH	Mean
<i>Chemical Concentration Measurements</i>		
Chloroform concentration at 420 basement north sampling location, in $\mu\text{g}/\text{m}^3$, as measured by Radiello sample	420BaseN_Radiello_Weekly_CHCl3	Randomly choose (when more than one per week)
Chloroform concentration at 420 basement south sampling location, in $\mu\text{g}/\text{m}^3$, as measured by Radiello sample	420BaseS_Radiello_Weekly_CHCl3	Randomly choose (when more than one per week)
Chloroform concentration at 422 basement north sampling location, in $\mu\text{g}/\text{m}^3$, as measured by Radiello sample	422BaseN_Radiello_Weekly_CHCl3	Randomly choose (when more than one per week)
Chloroform concentration at 422 basement south sampling location, in $\mu\text{g}/\text{m}^3$, as measured by Radiello sample	422BaseS_Radiello_Weekly_CHCl3	Randomly choose (when more than one per week)
Chloroform concentration at 422 first floor sampling location, in $\mu\text{g}/\text{m}^3$, as measured by Radiello sample	420First_Radiello_Weekly_CHCl3	Randomly choose (when more than one per week)
Chloroform concentration at 422 first floor sampling location, in $\mu\text{g}/\text{m}^3$, as measured by Radiello sample	422First_Radiello_Weekly_CHCl3	Randomly choose (when more than one per week)
Chloroform concentration at Outside sampling location, in $\mu\text{g}/\text{m}^3$, as measured by Radiello sample	Out_Radiello_Weekly_CHCl3	Randomly choose (when more than one per week)
Tetrachloroethylene concentration at 420 basement north sampling location, in $\mu\text{g}/\text{m}^3$, as measured by Radiello sample	420BaseN_Radiello_Weekly_PCE	Randomly choose (when more than one per week)
Tetrachloroethylene concentration at 420 basement south sampling location, in $\mu\text{g}/\text{m}^3$, as measured by Radiello sample	420BaseS_Radiello_Weekly_PCE	Randomly choose (when more than one per week)
Tetrachloroethylene concentration at 422 basement north sampling location, in $\mu\text{g}/\text{m}^3$, as measured by Radiello sample	422BaseN_Radiello_Weekly_PCE	Randomly choose (when more than one per week)
Tetrachloroethylene concentration at 422 basement south sampling location, in $\mu\text{g}/\text{m}^3$, as measured by Radiello sample	422BaseS_Radiello_Weekly_PCE	Randomly choose (when more than one per week)
Tetrachloroethylene concentration at 422 first floor sampling location, in $\mu\text{g}/\text{m}^3$, as measured by Radiello sample	420First_Radiello_Weekly_PCE	Randomly choose (when more than one per week)
Tetrachloroethylene concentration at 422 first floor sampling location, in $\mu\text{g}/\text{m}^3$, as measured by Radiello sample	422First_Radiello_Weekly_PCE	Randomly choose (when more than one per week)
Tetrachloroethylene concentration at outside sampling location, in $\mu\text{g}/\text{m}^3$, as measured by Radiello sample	Out_Radiello_Weekly_PCE	Randomly choose (when more than one per week)
Radon concentration at 422 basement north sampling location, in pCi/L, as measured by AlphaGUARD sample	422baseN_AG_radon	Mean

(continued)

Table 3-1. Data Aggregation Applied to Predictor Variables (continued)

Variable Name (Plain Language)	Variable Code	Method of Aggregation
Radon concentration at 422 office sampling location, in pCi/L, as measured by AlphaGUARD sample	422office_2nd_AG_radon	Mean
Tetrachloroethylene concentration at 420 basement south sampling location, in $\mu\text{g}/\text{m}^3$, as measured by GC sample during the first period of GC sampling	420baseS_GC1_PCE	Mean
Tetrachloroethylene concentration at 422 basement south sampling location, in $\mu\text{g}/\text{m}^3$, as measured by GC sample during the first period of GC sampling	422baseS_GC1_PCE	Mean
Tetrachloroethylene concentration at 420 first sampling location, in $\mu\text{g}/\text{m}^3$, as measured by GC sample during the first period of GC sampling	420first_GC1_PCE	Mean
Tetrachloroethylene concentration at 422 first sampling location, in $\mu\text{g}/\text{m}^3$, as measured by GC sample during the first period of GC sampling	422first_GC1_PCE	Mean
Tetrachloroethylene concentration at Wall Port 3 sampling location, in $\mu\text{g}/\text{m}^3$, as measured by GC sample during the first period of GC sampling	WP3_GC1_PCE	Mean
Tetrachloroethylene concentration at Subslab Port 2 sampling location, in $\mu\text{g}/\text{m}^3$, as measured by GC sample during the first period of GC sampling	SSP2_GC1_PCE	Mean
Tetrachloroethylene concentration at Subslab Port 4 sampling location, in $\mu\text{g}/\text{m}^3$, as measured by GC sample during the first period of GC sampling	SSP4_GC1_PCE	Mean
Tetrachloroethylene concentration at Subslab Port 7 sampling location, in $\mu\text{g}/\text{m}^3$, as measured by GC sample during the first period of GC sampling	SSP7_GC1_PCE	Mean
Tetrachloroethylene concentration at Soil Gas Port 11 sampling location at a depth of 13 feet, in $\mu\text{g}/\text{m}^3$, as measured by GC sample during the first period of GC sampling	SGP11-13_GC1_PCE	Mean
Tetrachloroethylene concentration at Soil Gas Port 2 sampling location at a depth of 9 feet, in $\mu\text{g}/\text{m}^3$, as measured by GC sample during the first period of GC sampling	SGP2-9_GC1_PCE	Mean
Tetrachloroethylene concentration at Soil Gas Port 8 sampling location at a depth of 9 feet, in $\mu\text{g}/\text{m}^3$, as measured by GC sample during the first period of GC sampling	SGP8-9_GC1_PCE	Mean
Tetrachloroethylene concentration at Soil Gas Port 9 sampling location at a depth of 6 feet, in $\mu\text{g}/\text{m}^3$, as measured by GC sample during the first period of GC sampling	SGP9-6_GC1_PCE	Mean
Tetrachloroethylene concentration at 420 basement south sampling location, in $\mu\text{g}/\text{m}^3$, as measured by GC sample during the second period of GC sampling	420baseS_GC2_PCE	Mean
Tetrachloroethylene concentration at 422 basement south sampling location, in $\mu\text{g}/\text{m}^3$, as measured by GC sample during the second period of GC sampling	422baseS_GC2_PCE	Mean
Tetrachloroethylene concentration at 420 first sampling location, in $\mu\text{g}/\text{m}^3$, as measured by GC sample during the second period of GC sampling	420first_GC2_PCE	Mean

(continued)

Table 3-1. Data Aggregation Applied to Predictor Variables (continued)

Variable Name (Plain Language)	Variable Code	Method of Aggregation
Tetrachloroethylene concentration at 422 first sampling location, in $\mu\text{g}/\text{m}^3$, as measured by GC sample during the second period of GC sampling	422first_GC2_PCE	Mean
Tetrachloroethylene concentration at Wall Port 3 sampling location, in $\mu\text{g}/\text{m}^3$, as measured by GC sample during the second period of GC sampling	WP3_GC2_PCE	Mean
Tetrachloroethylene concentration at Subslab Port 2 sampling location, in $\mu\text{g}/\text{m}^3$, as measured by GC sample during the second period of GC sampling	SSP2_GC2_PCE	Mean
Tetrachloroethylene concentration at Subslab Port 4 sampling location, in $\mu\text{g}/\text{m}^3$, as measured by GC sample during the second period of GC sampling	SSP4_GC2_PCE	Mean
Tetrachloroethylene concentration at Subslab Port 7 sampling location, in $\mu\text{g}/\text{m}^3$, as measured by GC sample during the second period of GC sampling	SSP7_GC2_PCE	Mean
Tetrachloroethylene concentration at Soil Gas Port 11 sampling location at a depth of 13 feet, in $\mu\text{g}/\text{m}^3$, as measured by GC sample during the second period of GC sampling	SGP11-13_GC2_PCE	Mean
Tetrachloroethylene concentration at Soil Gas Port 2 sampling location at a depth of 9 feet, in $\mu\text{g}/\text{m}^3$, as measured by GC sample during the second period of GC sampling	SGP2-9_GC2_PCE	Mean
Tetrachloroethylene concentration at Soil Gas Port 8 sampling location at a depth of 9 feet, in $\mu\text{g}/\text{m}^3$, as measured by GC sample during the second period of GC sampling	SGP8-9_GC2_PCE	Mean
Tetrachloroethylene concentration at Soil Gas Port 9 sampling location at a depth of 6 feet, in $\mu\text{g}/\text{m}^3$, as measured by GC sample during the second period of GC sampling	SGP9-6_GC2_PCE	Mean
Tetrachloroethylene concentration at 420 basement south sampling location, in $\mu\text{g}/\text{m}^3$, as measured by GC sample during the third period of GC sampling	420baseS_GC3_PCE	Mean
Tetrachloroethylene concentration at 422 basement south sampling location, in $\mu\text{g}/\text{m}^3$, as measured by GC sample during the third period of GC sampling	422baseS_GC3_PCE	Mean
Tetrachloroethylene concentration at 420 first sampling location, in $\mu\text{g}/\text{m}^3$, as measured by GC sample during the third period of GC sampling	420first_GC3_PCE	Mean
Tetrachloroethylene concentration at 422 first sampling location, in $\mu\text{g}/\text{m}^3$, as measured by GC sample during the third period of GC sampling	422first_GC3_PCE	Mean
Tetrachloroethylene concentration at Wall Port 3 sampling location, in $\mu\text{g}/\text{m}^3$, as measured by GC sample during the third period of GC sampling	WP3_GC3_PCE	Mean
Tetrachloroethylene concentration at Subslab Port 2 sampling location, in $\mu\text{g}/\text{m}^3$, as measured by GC sample during the third period of GC sampling	SSP2_GC3_PCE	Mean
Tetrachloroethylene concentration at Subslab Port 4 sampling location, in $\mu\text{g}/\text{m}^3$, as measured by GC sample during the third period of GC sampling	SSP4_GC3_PCE	Mean

(continued)

Table 3-1. Data Aggregation Applied to Predictor Variables (continued)

Variable Name (Plain Language)	Variable Code	Method of Aggregation
Tetrachloroethylene concentration at Subslab Port 7 sampling location, in $\mu\text{g}/\text{m}^3$, as measured by GC sample during the third period of GC sampling	SSP7_GC3_PCE	Mean
Tetrachloroethylene concentration at Soil Gas Port 11 sampling location at a depth of 13 feet, in $\mu\text{g}/\text{m}^3$, as measured by GC sample during the third period of GC sampling	SGP11-13_GC3_PCE	Mean
Tetrachloroethylene concentration at Soil Gas Port 2 sampling location at a depth of 9 feet, in $\mu\text{g}/\text{m}^3$, as measured by GC sample during the third period of GC sampling	SGP2-9_GC3_PCE	Mean
Tetrachloroethylene concentration at Soil Gas Port 8 sampling location at a depth of 9 feet, in $\mu\text{g}/\text{m}^3$, as measured by GC sample during the third period of GC sampling	SGP8-9_GC3_PCE	Mean
Tetrachloroethylene concentration at Soil Gas Port 9 sampling location at a depth of 6 feet, in $\mu\text{g}/\text{m}^3$, as measured by GC sample during the third period of GC sampling	SGP9-6_GC3_PCE	Mean

4. Results and Discussion: Quality Assurance Checks of Individual Data Sets

This section describes the sampling and analytical quality assurance/quality control (QA/QC) checks conducted for passive VOC sampling using Radiello samplers (4.1), active sorbent tube VOC sampling using Method TO-17 for soil gas samples (4.2), an on-site gas chromatograph (GC) used for short-term (less than 2 months) continuous monitoring of VOCs in indoor air and soil gas (4.3), radon measurements by AlphaGUARD and electret instruments (4.4), weather station measurements (4.5), groundwater sampling and analysis (4.6 and 4.7), and entry of the compiled data into the project databases (4–8). Additional details on each of the sampling methods can be found in Section 3. All measurements except the on-site GC tested during the first quarter of 2013 are addressed as critical measurements in the quality assurance project plan (QAPP).

4.1 VOC Sampling—Indoor Air, Passive Radiello—Eurofins Air Toxics, Ltd.

QA/QC checks for the passive Radiello 130 samplers used for indoor and outdoor air sampling are described in the following sections for blanks (4.1.1), surrogate recoveries (4.1.2), and laboratory control surrogate (LCS) recoveries (4.1.3). For blanks, chloroform showed no detections, whereas PCE showed an acceptably small percentage (2%–9%) of detectable concentrations between the detection and reporting limits. All surrogate recoveries met the laboratory control acceptance criteria. Chloroform failed to meet the LCS recovery limits once, whereas all PCE LCS recoveries met the control limits.

4.1.1 Blanks

Field blanks, trip blanks, and laboratory blanks were used to evaluate false positives and/or high bias due to transport, storage, sample handling, and sorbent contamination.

- **Field blanks** were collected using a blank Radiello 130 cartridge from the media sample batch sent to the field from the laboratory. The cartridge was removed from the sealed storage vial and transferred to the diffusive housing in a manner similar to sample deployment. The cartridge was then immediately removed from the housing, returned to the storage vial, and sealed for shipment back to the laboratory with the field samples. In general, a field blank was collected with each shipment to the laboratory. A total of 80 field blanks were submitted over the duration of the project.
- **Trip blanks** were also assigned as blank Radiello cartridges from the media batches. The cartridge was not opened or removed from the storage vial but was sent back to the laboratory along with the field samples. There were 23 trip blanks submitted for analysis.
- For the **laboratory blanks**, a Radiello 130 cartridge was extracted with each analytical batch to measure background from the sorbent and the extraction process. A total of 115 unique laboratory blanks were analyzed and reported over the duration of the project.

To assist in data interpretation, all blank samples and all field sample results were evaluated down to the method detection limit (MDL). The results of the field, trip, and laboratory blanks are summarized in **Tables 4-1, 4-2, and 4-3**. The number of blanks with detections above the reporting limit (RL) and MDL are tabulated. Summary statistics were then calculated on this subset of positive detections.

Benzene was detected above the MDL but below the RL in a majority of the field, trip, and laboratory blanks at similar background levels. The average of the positive detections was 0.14, 0.10, and 0.14 μg for the field, trip, and laboratory blanks, respectively. The benzene blank levels are largely due to benzene

Table 4-1. Indoor Air Passive Field Blank Summary—Radiello 130

	RL (µg)	FBs Analyzed (#)	FB Conc. > RL	RL > FB Conc. > MDL	FBs with Detections (%)	Mean Blank Mass (µg)	Std. Dev. (µg)	Min. (µg)	Max. (µg)
Benzene	0.4	80	0	70	89	0.14	0.056	0.040	0.29
Chloroform	0.1	80	0	0	0	NA	NA	NA	NA
cis-1,2-DCE	0.1	80	0	0	0	NA	NA	NA	NA
Hexane	0.1	80	4	9	16	0.099	0.091	0.033	0.35
PCE	0.1	80	0	4	5	0.032	0.020	0.0067	0.049
Toluene	0.1	80	1	24	31	0.044	0.037	0.014	0.17
TCE	0.1	80	0	5	6	0.015	0.0093	0.0064	0.031

NA = not applicable. cis-1,2-DCE = cis-1,2-dichloroethylene; TCE = trichloroethylene

Table 4-2. Indoor Air Passive Trip Blank Summary—Radiello 130

	RL (µg)	TBs Analyzed (#)	TB Conc. > RL	RL > TB Conc. > MDL	TBs with Detections (%)	Mean Blank Mass (µg)	Std. Dev. (µg)	Min. (µg)	Max. (µg)
Benzene	0.4	23	0	21	91	0.10	0.039	0.042	0.16
Chloroform	0.1	23	0	0	0	NA	NA	NA	NA
cis-1,2-DCE	0.1	23	0	0	0	NA	NA	NA	NA
Hexane	0.1	23	0	10	43	0.049	0.012	0.036	0.069
PCE	0.1	23	0	2	9	0.015	0.0094	0.0087	0.022
Toluene	0.1	23	0	18	78	0.020	0.0083	0.012	0.041
TCE	0.1	23	0	4	17	0.024	0.016	0.0094	0.043

NA = not applicable.

Table 4-3. Indoor Air Passive Laboratory Blank Summary—Radiello 130

	RL (µg)	LBs Analyzed (#)	LB Conc. > RL	RL > LB Conc. > MDL	LBs with Detections (%)	Mean Blank Mass (µg)	Std. Dev. (µg)	Min. (µg)	Max. (µg)
Benzene	0.4	115	0	109	95	0.14	0.070	0.039	0.34
Chloroform	0.1	115	0	0	0	NA	NA	NA	NA
cis-1,2-DCE	0.1	115	0	0	0	NA	NA	NA	NA
Hexane	0.1	115	1	23	21	0.061	0.024	0.034	0.14
PCE	0.1	115	0	2	2	0.0081	0.0004	0.0078	0.0084
Toluene	0.1	115	0	64	56	0.027	0.018	0.0084	0.081
TCE	0.1	115	0	4	3	0.022	0.0068	0.013	0.027

NA = not applicable.

contamination present in the carbon disulfide extraction solvent. Although the laboratory used high-purity (99.99%) carbon disulfide reagent, benzene is present as a common contaminant in this solvent (White, 1964).

Although the benzene background levels were below the RL, a positive bias is expected for the daily Radiello and a large subset of the weekly indoor air samples. Longer-duration samples would normally collect more mass and thus would not be significantly affected.

Hexane and toluene were also commonly detected in the field, trip, and laboratory blanks above the MDL. Some field and laboratory blanks had concentrations above the RL for hexane and toluene. All detections in the trip blanks were below the RL but above the MDL. Similar to benzene, a positive bias for hexane and toluene is anticipated for the daily Radiello samples because of the blank levels.

Because benzene, hexane, and toluene have a relatively constant low-level blank contribution from the media, the blank problems are more significant for the shortest duration samples (i.e., daily and to a lesser extent weekly). See Section 4.1.1 of U.S. EPA (2012a) for a full discussion of these issues.

No detections of chloroform or cis-1,2-dichloroethene (cis-1,2-DCE) were measured in any of the blanks. For a small percentage of the blanks, low concentration detections above the MDL were measured for PCE and TCE.

In summary, the contaminants of most concern in this study showed either no blank detections (for chloroform) or an acceptably small percentage (2%–9%) of low concentrations between the detection and reporting limits (for PCE). The contaminants with highest blank detections (benzene, toluene, and hexane) were not a primary focus for this study in that they were attributed to ambient outdoor air sources and did not come from vapor intrusion.

4.1.2 Surrogate Recoveries

To monitor extraction efficiency, 5.0 µg of toluene-d8 was spiked into each field sample and QC sample Radiello 130 cartridge immediately before extraction. The recoveries were evaluated against laboratory limits of 70%–130%. All surrogate recoveries met the laboratory criterion, and summary statistics are presented in **Table 4-4**.

Table 4-4. Indoor Air Passive Surrogate Summary—Radiello 130

Parameter	Result
Number of surrogate recoveries measures	1,735
Average recovery (%R)	103
Standard deviation (%R)	5.3
Minimum recovery (%R)	86
Maximum recovery (%R)	122

4.1.3 Laboratory Control Sample Recoveries

Accuracy of the extraction and analysis step for the target compounds was evaluated by analyzing an LCS. An unused Radiello cartridge was spiked with a standard containing 5.0 µg of each compound of interest. The laboratory acceptance criterion for LCS recovery was 70%–130%. One of the 117 LCS spikes demonstrated anomalously high recovery for benzene (147%), chloroform (206%), cis-1,2-DCE (192%), hexane (219%), and TCE (148%). The remaining LCS spikes met the recovery criterion of 70%–

130% with the exception of one additional exceedance for benzene (137%) and two additional exceedances for hexane (135% each). No recoveries below 70% were measured in the LCS spikes. Summary statistics are presented in **Table 4-5**.

Table 4-5. Indoor Air Passive LCS Summary—Radiello 130

	LCSs Analyzed (#)	Mean LCS Recovery (%)	LCS Std. Dev. (%R)	Min. (%R)	Max. (%R)	Exceedances (#)
Benzene	117	96	14	70	147	2
Chloroform	117	100	16	70	206	1
cis-1,2-DCE	117	99	13	72	192	1
Hexane	117	102	19	71	219	3
PCE	117	101	10	80	130	0
Toluene	117	97	11	76	131	1
TCE	117	101	11	78	148	1

4.1.4 Duplicates

Sample precision was evaluated by collecting field duplicates and by analyzing laboratory control sample duplicates (LCSDs). Field duplicates were collected for approximately every 10 field samples, and an LCSD was prepared and analyzed with each sample preparation batch. Because the LCSD was a second cartridge prepared and extracted in the same manner as the LCS, the relative percentage difference (%RPD) represents the precision of the analytical method from extraction through analysis. The method precision is summarized in **Table 4-6**. The laboratory acceptance criterion of %RPD \leq 25% was met by PCE, toluene, and TCE but exceeded in 2 batches for benzene and chloroform, 1 batch for cis-1,2-DCE, and 11 batches for hexane.

Table 4-6. Indoor Air Passive Laboratory Precision (LCS/LCSD) Summary—Radiello 130

	LCSDs Analyzed (#)	Mean (%RPD)	Std. Dev. (%RPD)	Min. (%RPD)	Max. (%RPD)	Exceedances (#)
Benzene	117	9.2	7.4	0	29	2
Chloroform	117	9.6	7.3	0	35	2
cis-1,2-DCE	117	5.5	4.5	0	31	1
Hexane	117	13.0	10.0	0	47	11
PCE	117	4.5	4.2	0	19	0
Toluene	117	4.9	4.4	0	19	0
TCE	117	4.7	4.0	0	20	0

4.2 VOC Sampling—Subslab and Soil Gas (TO-17)—U.S. EPA

4.2.1 Blanks

Field, trip, refrigerator, and laboratory blanks were used to evaluate false positives and/or high bias due to transport, storage, sample handling, and sorbent contamination. Field blanks were collected using a blank

Tenax TA TO-17 sorbent tube from the media sample batch sent to the field from the laboratory. The Swagelok end caps were removed as if to prepare for sample collection; however, no soil vapor was pulled through the tube. The end caps were immediately replaced, and the tube was sent back to the laboratory with the field samples. Typically, a field blank was collected with each shipment to the laboratory. A total of 127 field blanks were submitted over the duration of the project.

Blank Tenax TA TO-17 sorbent tubes from the media batches were also assigned as trip blanks. The tube remained capped and wrapped in aluminum foil and was sent from the laboratory to the field and back to the laboratory along with the field samples. There were 120 trip blanks submitted for analysis.

In the case of the laboratory blank, a Tenax TA TO-17 tube was analyzed with each analytical batch to measure background from the sorbent tubes and instrumentation. A total of 462 lab blanks were analyzed and reported over the duration of the project.

For a refrigerator (fridge) blank, a Tenax TA TO-17 tube was stored and analyzed with each sample batch to measure background from the sample storage refrigerator. The tubes were stored in the refrigerator capped and sealed in a zip lock bag on top of the jars containing the samples that were received as a batch. The fridge blanks were placed in the refrigerator with a sample batch and remained in the refrigerator with the batch until all the samples from that batch had been analyzed. So, the fridge blanks were in the refrigerator longer than some of the samples within a batch. A total of 69 fridge blanks were analyzed and reported over the duration of the project.

To assist in data interpretation, all blank samples and all field sample results were evaluated down to the MDL. The results of the field, trip, laboratory, and fridge blanks are summarized in **Tables 4-7, 4-8, 4-9, and 4-10**. The number of blanks with detections above the RL and MDL are tabulated. Summary statistics were then calculated on this subset of positive detections.

Table 4-7. Subslab and Soil Gas—EPA Field Blank Summary—TO-17

	RL (ng)	Number of Field Blanks			% of Field Blanks with Detections	Mean Blank Conc. (ng)	Std. Dev. (ng)	Min (ng)	Max (ng)
		Analyzed	Conc. > RL	RL > Conc. > MDL					
Benzene	5.0	127	0	53	42	1.4	0.5	0.81	3.0
Carbon disulfide	5.0	127	0	9	7	3.4	1.4	1.7	6.4
Chloroform	2.0	127	5	0	4	72	110	3.0	260
cis-1,2-DCE	2.0	127	0	1	1	1.5	N/A	1.5	1.5
Hexane	10	127	0	2	2	1.6	1.5	2.2	4.4
Methylene chloride	50	127	0	9	7	8.7	5.2	2.5	19
PCE	2.0	127	9	0	7	9.6	4.3	2.1	10
Toluene	5.0	127	0	18	14	2.2	2.0	1.1	7.7
TCE	2.0	127	1	0	1	2.8	N/A	2.8	2.8

N/A = not applicable

Table 4-8. Subslab and Soil Gas—EPA Trip Blank Summary—TO-17

	RL (ng)	Number of Trip Blanks			% of Trip Blanks with Detections	Mean Blank Conc. (ng)	Std. Dev. (ng)	Min (ng)	Max (ng)
		Analyzed	Conc. > RL	RL > Conc. > MDL					
Benzene	5.0	120	0	38	32	1.3	0.5	0.81	2.6
Carbon disulfide	5.0	120	0	9	8	2.6	0.8	1.6	4.0
Chloroform	2.0	120	6	1	6	32	41	2.0	120
cis-1,2-DCE	2.0	120	0	0	0	0	0	0	0
Hexane	10	120	0	2	2	2.0	1.5	1.0	3.0
Methylene chloride	50	120	0	5	4	3.1	0.4	2.2	4.0
PCE	2.0	120	4	0	3	18	11	2.3	27
Toluene	5.0	120	3	20	19	3.1	4.1	1.0	19
TCE	2.0	120	2	0	2	3.7	2.0	2.3	5.2

Table 4-9. Subslab and Soil Gas—EPA Laboratory Blank Summary—TO-17

	RL (ng)	Number of Lab Blanks			% of Lab Blanks with Detections	Mean Blank Conc. (ng)	Std. Dev. (ng)	Min (ng)	Max (ng)
		Analyzed	Conc. > RL	RL > Conc. > MDL					
Benzene	5.0	462	11	99	24	1.8	1.9	0.80	12
Carbon disulfide	5.0	462	4	63	16	14	12	0.87	52
Chloroform	2.0	462	17	2	4	2.3	1.7	1.3	5.8
cis-1,2-DCE	2.0	462	0	4	1	4.1	0.7	4.9	3.4
Hexane	10	462	1	10	2	4.9	5.6	1.5	21
Methylene chloride	50	462	0	8	2	3.2	1.2	2.4	5.6
PCE	2.0	462	7	8	3	1.6	1.0	0.7	4.1
Toluene	5.0	462	22	47	15	2.2	3.0	1.0	16
TCE	2.0	462	4	3	2	5.6	5.3	1.4	16

N/A = not applicable

Benzene was detected above the MDL in 42%, 32%, 24%, and 32% of the field, trip, laboratory, and fridge blanks, respectively. The average of the positive detections was 1.4, 1.3, 1.8, and 1.2 nanogram (ng) for the field, trip, lab, and fridge blanks, respectively. Seven laboratory blanks had benzene concentrations above the RL of 5.0 ng. The benzene blank levels are largely due to background contribution from the Tenax TA polymer, which can break down during the heating step to generate low levels of benzene (Middleditch, 1989).

The concentrations of benzene in the TO-17 soil vapor samples were similar in magnitude to those measured in the field blanks. Of the 3,088 TO-17 soil vapor samples analyzed by EPA, 55% of the samples had a positive detection of benzene. Of the samples that had a positive detection for benzene, only 2% had a detected concentration above the RL of 5.0 ng. The second most common contaminant in these blank samples was toluene, which has also been reported as a Tenax breakdown product (MacLeod and Ames, 1986; Cao and Hewitt, 1994).

Table 4-10. Subslab and Soil Gas—EPA Fridge Blank Summary—TO-17

	RL (ng)	Number of Fridge Blanks			% of Fridge Blanks with Detections	Mean Blank Conc. (ng)	Std. Dev. (ng)	Min (ng)	Max (ng)
		Analyzed	Conc. > RL	RL > Conc. > MDL					
Benzene	5.0	69	0	22	32	1.2	0.40	0.81	1.8
Carbon disulfide	5.0	69	0	2	3	2.3	0.69	1.8	2.8
Chloroform	2.0	69	2	0	3	2.3	0.29	2.1	2.5
cis-1,2-DCE	2.0	69	0	0	0	0	0	0	0
Hexane	10	69	0	3	4	1.0	0.08	0.88	1.0
Methylene chloride	50	69	0	7	10	6.1	7.5	1.8	17
PCE	2.0	69	6	4	14	3.2	1.7	0.8	3.5
Toluene	5.0	69	5	12	25	7.6	20	0.96	82
TCE	2.0	69	8	1	13	7.4	4.6	1.5	17

Detections of the key compounds that form the focus of this work—PCE, chloroform, and TCE—occurred in 3% or less of the hundreds of samples and field, trip, and lab blanks analyzed. However, the percentage of refrigerator blanks with PCE and TCE contamination was considerably higher—16%.

4.2.2 Calibration Verification

The calibration relationship established during the initial calibration was verified at the beginning of each 24-hour analytical shift using a calibration verification standard concentration equal to the mid-point of the initial calibration range. If the analyte concentration was within $\pm 30\%$ (40% for carbon disulfide and methylene chloride) of the expected concentration of the calibration verification standard, then the initial calibration was considered valid, and the analysis of samples was continued. Most analyte calibration verification standard recoveries met the QAPP established criterion, and summary statistics are presented in **Table 4-11**.

Table 4-11. EPA TO-17 Calibration Verification (CV) Summary

	Number of CV Analyzed	Mean CV % Recovery	CV Std Dev (%R)	Min (%R)	Max (%R)	CV Recovery Limits	Number of Sample Exceedances
Benzene	742	98	16	2	276	70–130%	22
Carbon disulfide	742	81	52	0	664	60–140%	274
Chloroform	742	92	17	0	298	70–130%	54
cis-1,2-DCE	742	95	28	0	268	70–130%	47
Hexane	742	91	17	0	262	70–130%	53
Methylene chloride	742	92	62	0	818	60–140%	304
PCE	742	87	15	0	262	70–130%	75
Toluene	742	97	16	0	286	70–130%	23
TCE	742	95	15	0	276	70–130%	19

4.2.3 Internal Standard Recoveries

Two internal standards were utilized in the calibration of the TO-17 analytical instrumentation, 1,4-difluorobenzene and chlorobenzene-d5. 4.7 ng of 1,4-difluorobenzene and 4.8 ng of chlorobenzene-d5 in a gas phase standard were automatically introduced into the sample flow path by the instrumentation during the initial tube desorption of all samples. The internal standard calibration was used to account for routine variation in the response of the chromatographic system as well as variations in the exact volume of sample introduced into the chromatographic system. The recoveries were evaluated against the QAPP established criteria of 60 to 140% recovery. Most internal standard recoveries met the QAPP established criterion, and summary statistics are presented in **Table 4-12**.

Table 4-12. EPA TO-17 Internal Standard (IS) Summary

	Number of IS Analyzed	Mean IS % Recovery	IS Std Dev (%R)	Min (%R)	Max (%R)	IS Recovery Limits	Number of Sample Exceedances
1,4-Difluorobenzene	5,152	100	30	15	373	60–140%	993
Chlorobenzene-d5	5,152	100	33	18	358	60–140%	847

4.2.4 Surrogate Recoveries

To monitor analytical efficiency, 5.3 ng of bromochloromethane were loaded onto each QC and field sample sorbent tube along with the vapor phase internal standard mix during sample analysis. Field surrogates were not included in the scope of this project. The recoveries were evaluated against laboratory limits of 70 to 130%. Most surrogate recoveries met the QAPP established criterion, and summary statistics are presented in **Table 4-13**.

Table 4-13. EPA TO-17 Surrogate Recovery Summary

Parameter	Result
Number of surrogate recoveries measured	5,152
Average recovery (%R)	105
Standard deviation (%R)	12
Minimum recovery (%R)	22
Maximum recovery (%R)	360

4.2.5 Laboratory Control Sample Recoveries

Analytical accuracy was evaluated by analyzing an LCS. Two clean Tenax TA TO-17 sorbent tubes were spiked with a calibration standard from a source independent from the primary calibration standard and analyzed after each initial calibration. The spike contained approximately 100 nanograms of each target compound. The performance of the EPA TO-17 LCS spikes is summarized in **Table 4-14**. A total of 10 LCS samples were evaluated, and all met the laboratory RLs with the exceptions of five outliers for carbon disulfide, four outliers for methylene chloride, and one outlier for cis-1,2-DCE.

Table 4-14. EPA TO-17 Laboratory Control Sample (LCS) Summary

	Number of LCS Analyzed	Mean LCS % Recovery	LCS Std Dev (%R)	Min (%R)	Max (%R)	LCS Recovery Limits	Number of Sample Exceedances
Benzene	11	101	25	86	118	70–130%	0
Carbon disulfide	11	120	172	24	272	70–130%	7
Chloroform	11	97	33	82	122	70–130%	0
cis-1,2-DCE	11	105	37	96	133	70–130%	2
Hexane	11	97	18	72	120	70–130%	0
Methylene chloride	11	112	128	29	291	70–130%	6
PCE	11	86	11	71	97	70–130%	0
Toluene	11	102	20	80	128	70–130%	0
TCE	11	100	20	80	120	70–130%	0

4.2.6 Field Duplicates

Sample precision was evaluated by collecting field duplicates. Field duplicates were collected for approximately every 10 field samples. The sample precision is summarized in **Table 4-15**. The laboratory acceptance criterion of %RPD < 50% was met by toluene but exceeded in 1 batch by PCE, 2 by TCE, 2 by benzene, 6 by chloroform, 1 by cis-1, 2-DCE, and 11 by hexane.

Table 4-15. EPA TO-17 Field Duplicate Summary

	Number Analyzed	Mean %RPD	Std Dev. (%RPD)	Min (%RPD)	Max (%RPD)	Number of Sample Exceedances
Benzene	181	40	36	0	163	35
Chloroform	181	39	38	0	197	27
cis-1,2-DCE	181	21	32	1	106	2
Hexane	181	45	34	13	119	5
PCE	181	22	58	0	197	21
Toluene	181	27	23	0	91	8
TCE	181	40	59	0	180	10

4.3 Field Portable Gas Chromatograph (Soil Gas and Indoor Air)

An opportunity arose to use a FROG-4000, a miniaturized, handheld GC made by Defiant Technologies, in the Indianapolis duplex. The FROG-4000 has a photoionization detector (PID), and its portability and rapid analysis times made it an attractive tool for making high-resolution measurements of the temporal variability of VOC levels in indoor air and soil gas. Although previous soil gas testing showed a general pattern of gradual change predominating in subslab and deeper ports, some anomalous rapid-change events were seen with another on-site GC, and verification of those events with a different instrument would provide a useful check. The instrument as configured was able to measure TCE and PCE but not chloroform because the lamp used has an ionization energy of 10.6 eV, and the ionization potential of chloroform is 11.4 eV.

The FROG-4000 instrument was operated in general accordance with EPA SW-846 Method 8021 and 8000 (U.S. EPA, 1996a,b) with a purge-and-trap option available for groundwater samples under SW-846 Method 5030C (U.S. EPA, 2003b). The method's options for external standardization were used. The method refers to the type of analysis performed here as tentative detection because it is based on retention time for only one column and the response of one detector. (The dual column or dual detector confirmation approaches were not implemented in this project.) Defiant Technologies refers to this level of QA/QC as "screening with meaning." Detailed operational procedures are provided in the FROG-4000 User's Manual, Volume 3, 2012 (Defiant Technologies, 2012).

In brief, most air samples are introduced into the instrument directly with an inlet volume of 30 mL. The analysis cycle time is approximately 6 minutes. The air sampler collects for only 30 seconds, then its valve is closed, so no more air will be collected for that cycle. A port on the side of the instrument takes in ambient air and scrubs it through activated carbon and molecular sieves before use as the carrier gas. The study used 1.2 mL/min of this filtered ambient air for the carrier gas.

Two identically designed FROG instruments were taken to the field for the first week of testing. One (FROG-21) was dedicated to routine/continuous monitoring of indoor air at 422 basement south. The second (FROG-22) was used in a portable mode for analysis of soil gas and groundwater samples.

Defiant Technologies staff set the retention time windows based on a multiple of the standard deviation of retention times from the calibration files. Defiant staff were responsible for reviewing the raw data produced and submitting them to ARCADIS/RTI. On the basis of Defiant staff input, three to four samples collected after each instrument startup were deleted as anomalous. In the experience of Defiant staff, when the instrument sites idle in the presence of an analyte, the preconcentrator gradually loads the analyte diffusively.

4.3.1 Blanks

Blanks were created on site by sampling ambient air.

One ambient air blank was performed on the FROG-21 on February 3, 2014. Thereafter, the instrument was left in continuous service in the 422 basement south.

Ambient air blanks were run on FROG-22, the instrument used for soil gas and groundwater analysis, on five occasions during the February 3 and February 4 analyses. Three of the five blanks were not detectable for PCE. One blank gave a concentration of 1 ppbv = $6.9 \mu\text{g}/\text{m}^3$, and one blank gave a concentration of 0.18 ppbv = $1.2 \mu\text{g}/\text{m}^3$. Although ambient air blanks were not performed on February 5, four samples of indoor air were taken near potential points of soil gas entry on February 5 and PCE was not detected by the soil gas instrument, indicating that instrument carryover was minimal during that day. Similarly, although no ambient air blanks were performed on the February 6 samples, four samples from WP-2 and WP-4 showed no detectable PCE that day. That result is consistent with the historical TO-17 results for those wall ports and also indicates a lack of analytical carryover. On February 7, three analyses of blinded blank Tedlar bags provided by Air Toxics Ltd. yielded PCE concentrations of 0.05, 0.07, and 0.09 ppbv, indicating minimal instrument carryover.

4.3.2 Initial Calibration

Initial calibration of the instruments was performed by Defiant Technologies in Albuquerque and Indianapolis before bringing the instruments on site in Indianapolis. Use of gas phase calibration standards within the test duplex was avoided.

FROG-21

- The initial FROG calibration for the instrument used for indoor air included six standards ranging from 0.1 to 50 ppbv preceded by a blank. Each standard was prepared in a Tedlar bag, allowed to equilibrate, and analyzed in order of increasing concentration. The calibration curve linearity was 0.99768.

FROG-22

- The initial FROG calibration for the instrument used for soil gas and groundwater included five standards ranging from 0.5 to 50 ppbv preceded by a blank. Each standard was prepared in a Tedlar bag, allowed to equilibrate, and analyzed in order of increasing concentration. The calibration curve linearity was 0.99772.

4.3.3 Continuing Calibration

After the field effort, it was discovered that the stability of the instrument used to monitor indoor air in 422 basement south was adversely affected by an inadvertent setting of the preconcentrator voltage. Because of operator error, the preconcentrator voltage was set at 14.5 V when it should have been 10.5 V, which unnecessarily fatigued the membrane. This error is believed to have caused the postoperation continuing calibration to record a response of 14 ppbv when a 20 ppbv PCE standard was introduced (i.e., 35 %RPD for a parameter with a QAPP-set goal of < 30 %RPD). Thus, the concentrations reported in indoor air are likely underestimated especially during the latter portions of the run. This missetting did not apply to the FROG-22, which was used for soil gas and groundwater analysis. The FROG-22 gave a response of 18.3 ppbv with a 20 ppbv standard in the postoperation continuing calibration check (i.e., 8.8 %RPD, which is well within the acceptable range of <30%).

4.3.4 Calibration Check via Comparison to Fixed Laboratory (TO-17 versus Field PorGC)

A series of four Tedlar bags of known concentrations were provided by Eurofins Air Toxics and shipped to the 422/420 house for a comparison study between the FROG GC and the USEPA TO-17 method. Two bags contained only blank air, and two contained known concentrations of PCE. Eurofins Air Toxics reported two values:

- The nominal value that the chemist who prepared the standards by serial dilution from neat liquids was targeting.
- The measured value prior to shipment.

As shown in **Table 4-16**, the measured values were substantially below the nominal values.

Table 4-16. Comparison of Nominal and Measured FROG Performance Standard Concentrations

Sample ID:	Concentrations (µg/m ³)			
	PT1		PT2	
Standard ID:	1402049-B		1402049-C	
Chemical	Nominal	Measured	Nominal	Measured
PCE	162	68	162	85
TCE	148	85	148	96
Chloroform	148	89	148	96

In the field in Indianapolis, each bag was tested one at a time, first by the FROG in the field and then by collecting a sample for Method TO-17 analysis by EPA NERL. **Figure 4-1** plots the FROG results (circles), TO-17 results (squares), and actual concentrations within the bags (lines). TO-17 results agree much more closely to the Air Toxics limited measured concentrations of the Tedlar bags, and the FROG results indicate much higher concentrations for Tedlar bags A and C, which however are close to the nominal values that the Air Toxics Limited chemist was targeting. These results were reviewed by the Air Toxics Ltd technical director and an ARCADIS chemist and no obvious reason for the discrepancy could be discerned.

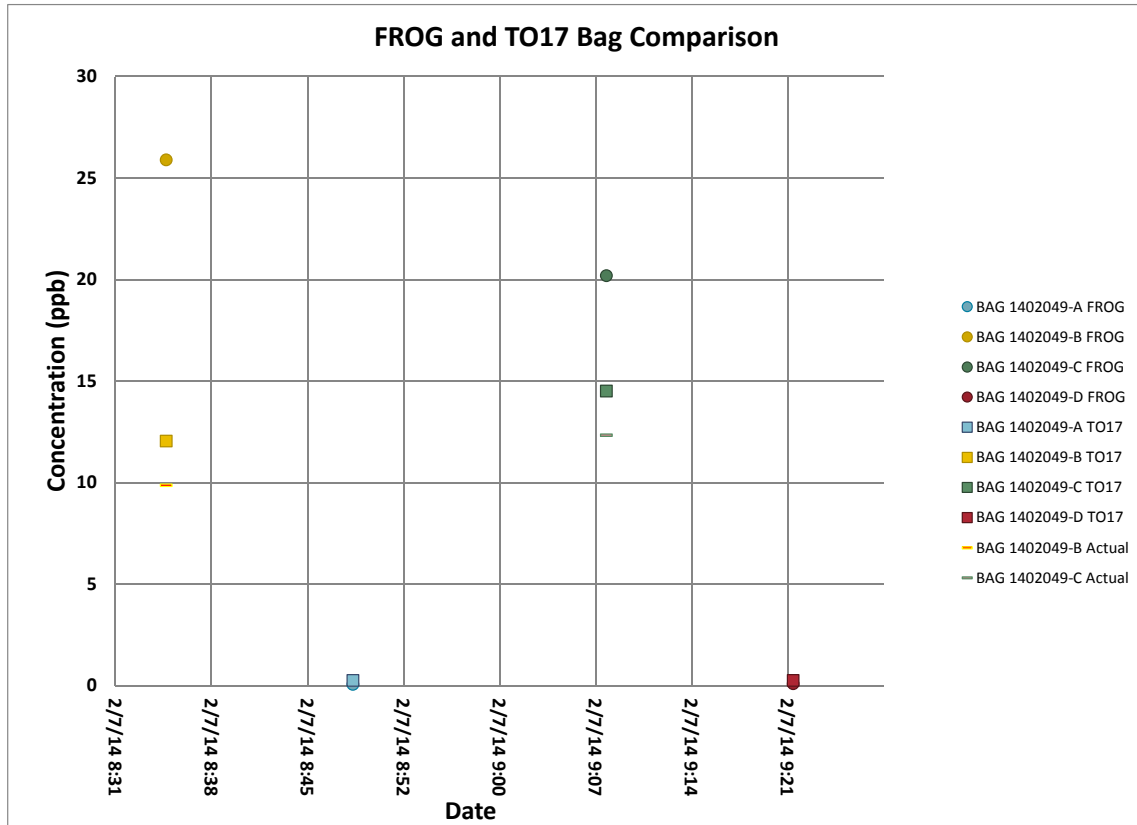


Figure 4-1. Comparison between FROG 4000 and TO-17 sampling of bag standards.

4.4 Radon

4.4.1 Indoor Air: Comparison of Electrets to Charcoal Canisters Analyzed by EPA Radiation and Indoor Environments National Laboratory

Four comparisons were made between electrets and charcoal canisters. See **Figure 4-2** for graphical representation of the data from 2011 through 2013. Charcoal canisters were provided and analyzed by EPA’s Radiation and Indoor Environments National Laboratory Center for Indoor Environments in Las Vegas, Nevada. ARCADIS collected charcoal canister samples and electret samples. Electrets were obtained from Rad Elec (Frederick, Maryland) and read by ARCADIS on site before and after deployment. The charcoal canisters were used as a QC check on four separate occasions: January 19, 2011, to January 26, 2011; April 27, 2011, to May 4, 2011; December 28, 2011, to January 4, 2012; and June 19, 2013 to June 26, 2013. Charcoal canisters (plus duplicates) were placed at indoor locations and the ambient location that were routinely being used for electret monitoring. When the results were received, the sample and its duplicate were averaged to obtain a result for the location. This result was then compared with the electret result for that location and period.

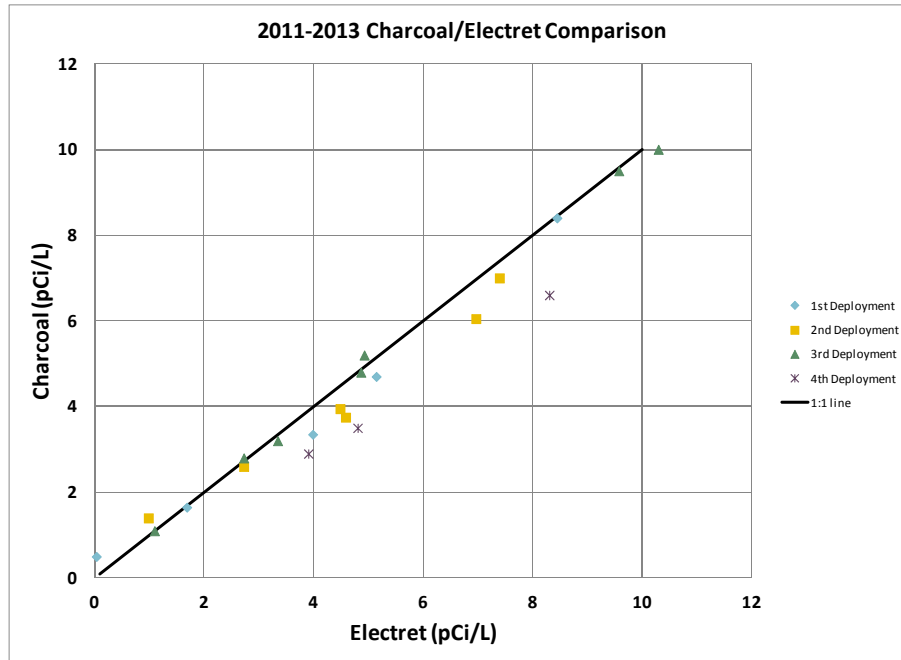


Figure 4-2. Correlation between radon measured using the electret and charcoal methods.

For the first occasion, the RPD between the two methods was 20% or less (**Table 4-17**). The maximum absolute difference was 0.63 pCi. An RPD could not be calculated for the ambient, which was below the detection limit (BDL) with the charcoal method.

On the second occasion, five of six comparisons showed an RPD of 20% or less, and three of the six comparisons were within 0.5 pCi/L of each other (**Table 4-18**).

The exceptions were 422 basement north and 420 basement south, which were within 0.8–0.9 pCi/L of each other. The ambient was again BDL by the charcoal method, as would have been predicted from the electret data.

For the third occasion, December 28, 2011, to January 4, 2012, the absolute difference between the methods is at or below 0.3 pCi/L, and RPD is < 6% for all samples (**Table 4-19**). The ambient charcoal sample was BDL, and that detection limit was equal to the ambient value reported by the electret method.

For the fourth occasion, June 19, 2013, to June 26, 2013, the absolute difference between the methods is –1.7, and the maximum RPD is –31.33% (**Table 4-20**).

Figure 4-2 shows the correlations from **Tables 4-17** through **4-19** in graphical form. As can be seen by the clustering of points around the 1:1 line, there was an excellent correlation between the electret and charcoal radon measurements regardless of radon level.

Table 4-17. Comparison between Electrets and Charcoal Canisters at the 422/420 EPA House from January 19 to 26, 2011

Sample Location	Electret Radon (pCi/L)	Charcoal Radon (pCi/L)	Charcoal Average	Absolute Difference (pCi/L)	RPD (%)
422 First	5.14	4.8	4.7	0.44	8.94
422 First	—	4.6	—	—	—
422 Base N	8.44	8	8.4	0.04	0.48
422 Base N	—	8.88	—	—	—
420 First	1.68	1.7	1.65	0.03	1.80
420 First	—	1.6	—	—	—
420 Base N	3.98	3.3	3.35	0.63	17.19
420 Base N	—	3.4	—	—	—
Ambient	0.03	<0.5	<0.5	—	—
Ambient	—	<0.5	—	—	—

— = no data

Table 4-18. Comparison of Electret and Charcoal Canister Data, April 27 to May 4, 2011

Location	Electret Data (pCi/L)	Charcoal Canister Radon Activity (pCi/L)	Charcoal Canister Average Radon Activity (pCi/L)	Absolute Difference (pCi/L)	RPD (%)
Ambient	0.47	<0.5	—	—	—
Ambient Dup	—	<0.5	—	—	—
422 First	2.72	2.8	2.6	0.12	4.51
422 First Dup	—	2.4	—	—	—
422 Base S	7.39	7.3	7	0.39	5.42
422 Base S Dup	—	6.7	—	—	—
422 Base N	7.14	6.3	6.05	0.905	13.92
422 Base N Dup	6.77	5.8	—	—	—
420 First	0.98	1.3	1.4	-0.42	-35.29
420 First Dup	—	1.5	—	—	—
420 Base S	4.58	3.8	3.75	0.83	19.93
420 Base S Dup	—	3.7	—	—	—
420 Base N	4.48	4.2	3.95	0.53	12.57
420 Base N Dup	—	3.7	—	—	—
Field blank	NA	<0.5	—	—	—
Field blank	NA	<0.5	—	—	—

NA = not available; — = no data.

Table 4-19. Comparison of Charcoal and Electret Radon, December 28, 2011, to January 4, 2012

Canister ID	Radon Activity (pCi/L)	Charcoal Average (pCi/L)	Location	Electrets (pCi/L)	Absolute Difference (pCi/L)	RPD (%)
877138	3.1	3.2	420 Base N	3.34	-0.2	-5.86
877113	3.2	—	420 Base N Dup	—	—	—
877137	2.8	2.8	420 Base S	2.72	0.0	1.10
877115	2.7	—	420 Base S Dup	—	—	—
877133	1.1	1.1	420 First	1.09	0.0	-3.74
877107	1.0	—	420 First Dup	—	—	—
877139	10.0	10.0	422 Base N	10.22	-0.3	-2.67
877136	9.9	—	422 Base N Dup	10.35	—	—
877128	9.6	9.5	422 Base S	9.57	-0.1	-0.73
877111	9.4	—	422 Base S Dup	—	—	—
877108	4.8	4.8	422 First	4.86	-0.1	-2.29
877140	4.7	—	422 First Dup	—	—	—
877110	5.0	5.2	422 Office	4.92	0.2	4.57
877131	5.3	—	422 Office Dup	—	—	—
877130	<0.5	—	Ambient	0.5	NA	NA

NA = not available; — = no data.

Table 4-20. Comparison of Charcoal and Electret Radon, June 19, 2013, to June 26, 2013

Canister ID	Radon Activity (pCi/L)	Charcoal Average (pCi/L)	Location	Electrets (pCi/L)	Absolute Difference (pCi/L)	RPD (%)
880610	2.9	—	422 First	3.9	-1.0	-29.41
880609	6.8	6.6	422 Base N	8.3	-1.7	-22.82
880611	6.4	—	422 Base N Dup	—	—	—
880614	3.5	—	420 Base S	4.8	-1.3	-31.33

— = no data.

4.4.2 Comparison of Average of Real-Time AlphaGUARD to Electrets and Charcoal Canisters

Stationary AlphaGUARD units provided by EPA were used for real-time monitoring of indoor air radon at two locations (422 basement north and 422 office [second floor]). Several comparisons were made between the stationary AlphaGUARD data and electrets nearby (at 422 basement north at first and both 422 basement north and 422 office later).

The first comparison took place over several weeks between March 30, 2011, and May 18, 2011 (**Table 4-21**). The absolute difference ranged from -0.04 pCi/L to 1.44 pCi/L. The RPD ranged from 0.50% to 26.04%.

Table 4-21. Comparison between 422 Basement N AlphaGUARDs and Electrets, March 30, 2011, to May 18, 2011

Date Range	AlphaGUARD Reading (pCi/L)	Electret (pCi/L)	Electret Dup(pCi/L)	Electret Ave (pCi/L)	Absolute Difference (pCi/L)	RPD (%)
03/30–04/07	6.18	6.30	4.98	5.64	0.54	9.14
04/07–04/13	5.90	4.94	5.87	5.41	0.50	8.76
04/13–04/20	8.41	6.97	7.83	7.40	1.01	12.78
04/20–04/27	6.25	4.04	5.58	4.81	1.44	26.04
04/27–05/04	6.92	7.14	6.77	6.96	-0.04	-0.50
05/04–05/11	4.66	2.93	4.50	3.72	0.95	22.57
05/11–05/18	6.15	5.81	6.01	5.91	0.24	3.98

For the second comparison, which occurred from August 3, 2011, to October 6, 2011, in the 422 basement north location, the absolute difference ranged from -1.11 pCi/L to 2.42 pCi/L. Although the RPD ranged from -40.18% to 30.76% (Table 4-22), most (8 out of 10) were within the acceptable range of +/- 30%.

Table 4-22. Comparison of Real-Time AlphaGUARD to Integrated Electret, August through October, 2011

End Date/ Time	Radon (pCi/L) A GUARD (averaged over a week)	Radon (pCi/L) Electrets 422 Base N	Radon (pCi/L) Electrets 422 Base N Dup	Average of Duplicate Electrets (pCi/L)	Absolute Difference (pCi/L)	RPD (%)
8/3/2011	6.85	6.85	5.14	6.00	0.85	13.26
8/10/2011	7.24	7.25	6.79	7.02	0.22	3.09
8/17/2011	8.38	7.53	7.20	7.37	1.02	12.91
8/24/2011	3.84	3.48	3.00	3.24	0.60	16.93
8/31/2011	2.21	2.17	4.46	3.32	-1.11	-40.18
9/7/2011	4.34	4.52	1.84	3.18	1.16	30.76
9/14/2011	6.09	5.68	5.44	5.56	0.53	9.16
9/21/2011	8.69	8.03	7.84	7.94	0.75	9.05
9/28/2011	12.51	11.67	11.44	11.56	0.96	7.97
10/6/2011	10.33	7.83	7.99	7.91	2.42	26.53

During the third comparison, electrets, the AlphaGUARD, and the charcoal canisters were compared from December 28, 2011, to January 4, 2012. Only the 422 office and 422 basement north were compared by all three methods during this time. The absolute difference between the canisters and AlphaGUARD ranged from -0.05 pCi/L to 0.15 pCi/L, and the absolute difference between the electrets and AlphaGUARD ranged from -0.08 pCi/L to 0.29 pCi/L. The RPD between canisters and AlphaGUARD ranged from -0.50% to 2.96%, and the RPD between electrets and AlphaGUARD ranged from -1.61% to 2.81% (Table 4-23).

Table 4-23. Comparison of Real-Time AlphaGUARDS to Integrated Electret Measurements, from December 28, 2011, to January 4, 2012

Location	Canister Radon Activity (pCi/L)	Dup Canister Radon Activity (pCi/L)	Canister Average (pCi/L)	Electret (pCi/L)	Electret Dup (pCi/L)	Electret Average (pCi/L)	422 Base N AlphaGUARD Approximation (pCi/L)	Absolute Difference between Canisters and AlphaGUARDS (pCi/L)	Absolute Difference between Electrets and AlphaGUARDS (pCi/L)	RPD between Canisters and AlphaGUARD (%)	RPD between Electrets and AlphaGUARD (%)
422 Base N	10.00	9.90	9.95	10.22	10.35	10.29	10.00	-0.05	0.29	-0.50	2.81
422 Office	5.00	5.30	5.15	4.92	—	—	5.00	0.15	-0.08	2.96	-1.61

— = no data.

The fourth comparison occurred between January 4, 2012, and March 1, 2012, for both the 422 office and 422 basement north. The absolute difference between 422 basement north AlphaGUARDS and electrets ranged from -0.52 pCi/L to 1.79 pCi/L, and the absolute difference between 422 office AlphaGUARDS and electrets ranged from 0.05 pCi/L to 0.77 pCi/L. The RPD for 422 basement north ranged from -5.95% to 26.15%, and the RPD for the 422 office ranged from 1.05% to 17.68% (Table 4-24).

Table 4-24. Comparison of Real-Time AlphaGUARDS to Integrated Electret Measurements, January through March 2012

Date Range	422 Base N AlphaGUARD Reading (pCi/L)	Office AlphaGUARD Reading (pCi/L)	422 Base N Electret (pCi/L)	422 Base N Dup Electret (pCi/L)	422 Base N Electret Average (pCi/L)	Office Electret (pCi/L)	Absolute Difference between 422 Base N AlphaGUARDS and Electrets (pCi/L)	Absolute Difference between Office AlphaGUARDS and Electrets (pCi/L)	422 Base N RPD (%)	Office RPD (%)
12/28/11-1/04/12	10	5	10.22	10.35	10.29	4.92	-0.29	0.08	-2.81	1.61
01/04/12-01/11/12	8.78	4.69	9.05	9.11	9.08	4.56	0.30	0.13	-3.36	2.81
01/11/12-01/18/12	9.73	5.09	9.34	9.73	9.54	4.88	0.19	0.21	2.02	4.21
01/18/12-01/25/12	8.52	4.79	7.83	7.98	7.91	4.74	0.61	0.05	7.49	1.05
01/25/12-02/01/12	7.71	4.46	8.24	8.03	8.14	4.15	-0.43	0.31	-5.36	7.20
02/01/12-02/08/12	8.68	4.78	8.60	8.62	8.61	4.58	0.06	0.20	0.81	4.27
02/08/12-02/15/12	8.44	4.80	8.28	7.47	7.88	4.41	0.56	0.39	6.93	8.47
02/15/12-02/22/12	7.74	4.3	6.08	5.82	5.95	3.68	1.79	0.62	26.15	15.54
02/22/12-03/01/12	8.48	4.74	9.00	9.00	9.00	3.97	-0.52	0.77	-5.95	17.68

The fifth comparison covers the period from the week of January 2, 2013, through March 6, 2013 (Table 4-25). It compares the stationary AlphaGUARDS and electrets at both the 422 basement north and the 422 office. The normal and duplicate electrets at the 422 basement north location are averaged. The agreement was within 12 RPD when the mitigation system was in a passive mode and the radon concentrations were above the EPA action level. The portion of the comparison that corresponded with the period when the mitigation system was on (February 6 through April 24, 2013) showed much greater RPDs. However, the paired results during these weeks are within +/- 0.7 pCi/L. The high RPDs are due to the small concentrations of the radon present in the mitigated structure that was measured by both methods. This suggests that results below 1.5 pCi/L may have a higher percentage uncertainty with these instruments.

Table 4-25. Comparison of Real-Time AlphaGUARDs to Integrated Electret Measurements, January through March 2013

Week Start Date	422 Basement North Alpha-GUARD (pCi/L)	422 Basement North Ave Electret (pCi/L)	422 Office Alpha-GUARD (pCi/L)	422 Office Electret (pCi/L)	Absolute Difference 422 Basement North Alpha-GUARD and Electrets (pCi.L)	Absolute Difference 422 Office Alpha-GUARD and Electrets (pCi.L)	RPD 422 Basement North Alpha-GUARD and Electrets (%)	RPD 422 Office Alpha-GUARD and Electrets (%)
01/02/13	8.0	8.7	4.3	4.5	-0.7	-0.2	-8.50	-3.88
01/09/13	8.4	9.4	4.4	4.7	-1.0	-0.3	-11.02	-6.59
01/16/13	8.8	9.5	4.6	4.6	-0.7	0.0	-7.65	0.65
01/23/13	8.3	8.2	3.9	4.0	0.2	-0.1	1.82	-2.28
01/30/13	9.4	9.2	5.0	4.7	0.3	0.3	2.70	5.76
02/06/13	1.3	0.6	0.8	0.2	0.7	0.6	68.04	116.83
02/13/13	0.4	0.5	0.3	0.1	-0.1	0.2	-26.09	100.00
02/20/13	0.4	0.5	0.3	0.1	-0.1	0.3	-22.22	142.86
03/06/13	0.3	0.5	0.2	0.0	-0.2	0.2	-44.16	147.83

All three AlphaGUARDs (two stationary and one portable) were returned to EPA on July 7, 2012, for recalibration and were returned to the 422 test house for redeployment on September 25, 2012. This recalibration was conducted at Saphymo in Frankfurt, Germany.

Additionally, when the number of electret locations was reduced on October 24, 2013, the basement AlphaGUARD location was simultaneously changed from the 422 north basement to the 422 south basement, in order to match with the only basement electret. Use of the 422 office electret was also discontinued at this time.

The sixth comparison between AlphaGUARD and electret occurs from January 2, 2014, through March 5, 2014 (**Table 4-26**). It compares the stationary AlphaGUARD and electrets at only the 422 basement south location because the office electret had been discontinued by this time. The normal and duplicate electrets at the 422 basement north location are averaged. The portion of the comparison that corresponded with the period the mitigation system was on (after the March 5, 2014, mitigation on date) showed much greater RPDs. However, the paired results during these weeks are within ± 0.6 pCi/L. The high RPDs are due to the tiny absolute value of the radon present as indicated by both methods. This suggests that results below 1.5 pCi/L may have a higher percentage uncertainty. In this range, however, the radon levels are close to background concentrations in outside air and may not be indicating a significant amount of vapor intrusion.

Table 4-26. Comparison of Real-Time AlphaGUARDs to Integrated Electret Measurements, January through March 2014

Week Start Date	422 Base S AlphaGUARD (pCi/L)	422 Base S Ave Electret (pCi/L)	Absolute Difference 422 Base S AlphaGUARD and Electrets (pCi/L)	RPD 422 Base S AlphaGUARD and Electrets (%)
01/02/14	9.3	9.6	-0.3	-3.17
01/08/14	9.6	9.0	0.6	6.45
01/15/14	10.1	9.5	0.6	6.12
01/22/14	10.4	10.1	0.3	2.93
01/29/14	9.0	8.3	0.7	8.09
02/05/14	8.6	8.4	0.2	2.35
02/12/14	8.2	6.6	1.6	21.62
02/19/14	11.1	10.4	0.7	6.51
02/26/14	8.9	8.1	0.8	9.41
03/05/14	1.0	0.4	0.6	85.71

4.4.3 Quality Assurance Checks of Electrets

QC was performed on the electret reader and on the chambers holding the electrets. The QC check on the reader was performed by placing reference electrets within the reader each week to measure any deviation from the standard. The standard reference electrets were 0 V, 245 V, and 250 V. Over the duration of the project, the readings on the 0 V electret fluctuated but stayed within 4 V of the nominal value. The 245 V electret, with only two exceptions, stayed within 20 V of its stated value. It steadily declined over the duration of the project, hitting a low before slowly rising toward the end of the project. The 250 V electret stayed within 6 V of its nominal value, showing a slight decline toward the end of the project.

To check for drift within the electret chambers, a normal electret was placed in a closed electret chamber each week and then read on the voltage meter to measure any change in the voltage from the previous week's readings. This change would indicate any deviation caused by the chambers. Near the beginning of the project, this electret dropped an average of 5 V per 4 weeks or 1.25 V per week. The rate was even lower in the second half of the project, to a drop of 5 V per 30 weeks or 0.16 V per week. These rates of drift are insignificant because the actual observed voltage change at the indoor sampling locations was typically 25 V per week or more.

From September 26, 2012, until October 3, 2012, the electret reader was at the manufacturer (Rad Elec, Inc.) for recalibration and replacement of the motherboard. During this week, a rental unit was in use. When the original reader was returned, it included three new standards: 0 V, 223 V, and 243 V. This reader, combined with its new standards, has remained in use until the current time. Between October 3, 2012, and March 5, 2014, the reader was tested weekly with all three standards, and an electret was used to test the electret chambers in the same way as before the recalibration (as described in the first two paragraphs of this section).

The 0 V electret mostly read 0 +/- 1V and as high as 2 V on rare occasions. The 223 V reference electret read from 223 V to 225 V. The 243 V reference electret read from 243 V to 245 V. One reading on the week of November 21, 2012, read as low as 0 V, 173 V, and 218 V for the three standards but is likely due to reader error as the readings occurred within the normal range on all successive weeks. In the test for checking the drift of the electret chambers, the electrets used dropped an average of 2.8 V per month. This rate of drift is insignificant because the actual observed voltage change at the indoor sampling locations was typically 25 V per week or more.

4.5 On-Site Weather Station versus National Weather Service

A Vantage Vue weather station from Davis Instruments was installed at the 422/420 house. Because it was not safe to mount the station directly on the peak of the roof, it was mounted on vertical rods raised to the approximate peak elevation from the edge of the second-story roof. The trees near the house, especially to the north, are quite tall, equal to or higher than the weather station. Branches extend close to the house on the northwest corner. The house is much taller than the neighboring building to the east. There is also a neighboring two-story residential structure to the northeast, approximately 30 ft–40 ft away. A seven-story commercial structure is approximately 150 ft southwest of the studied duplex. Essentially, the only side completely free from all air current obstructions is the southern side, which borders 28th Street (**Figure 4-3**).

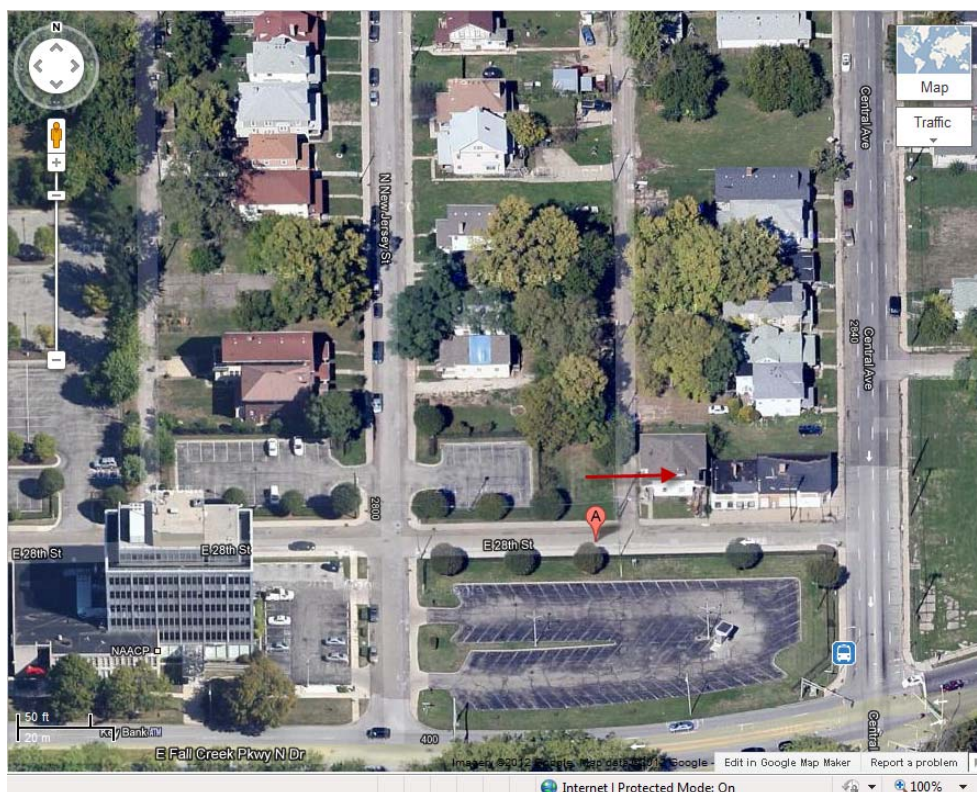


Figure 4-3. Aerial view of study house, showing potential influences on wind velocity; red arrow indicates study house.

A 3-month comparison between the house weather station data and National Weather Service (NWS) data was made from January 1, 2013, to March 31, 2013, as a QC check. Three parameters were compared: temperature, relative humidity, and wind speed. For temperature, the data from the two weather stations match well, only differing by an average of 2° F (**Figure 4-4**). Relative humidity at both weather stations differed by an average of ~4% (**Figure 4-5**). House wind speed and that of the NWS differed by an average of ~6 mph; the airport weather station was generally higher. This difference is likely due to the local NWS station being at the Indianapolis International Airport. The KIND weather station is located in the middle of the runways at the Indianapolis airport approximately 500 meters from the nearest building. Thus, the readings obtained at the house are probably a better representation of the wind speeds that directly impinge on the house (**Figure 4-6**).

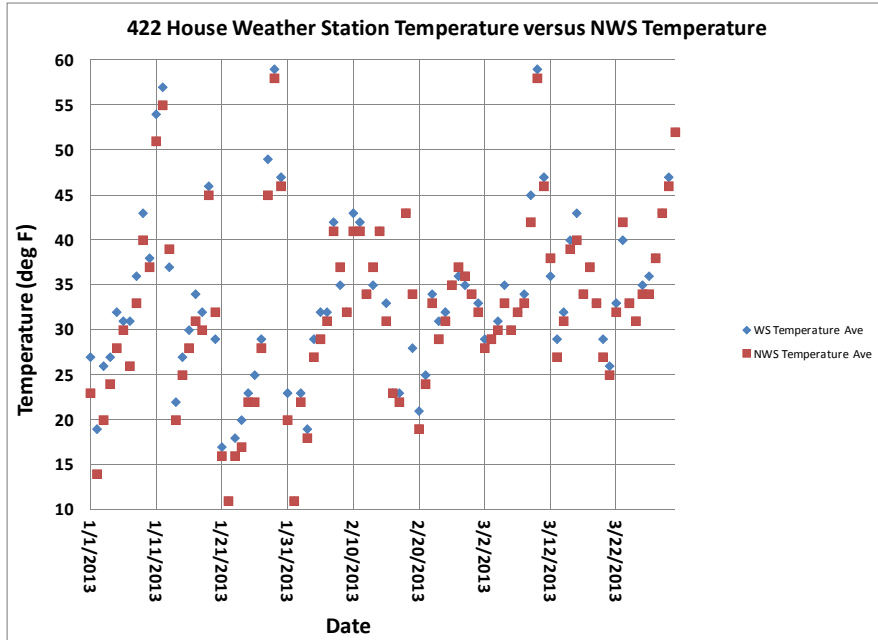


Figure 4-4. Comparison of National Weather Service Indianapolis temperature data to a weather station at 422 East 28th Street.

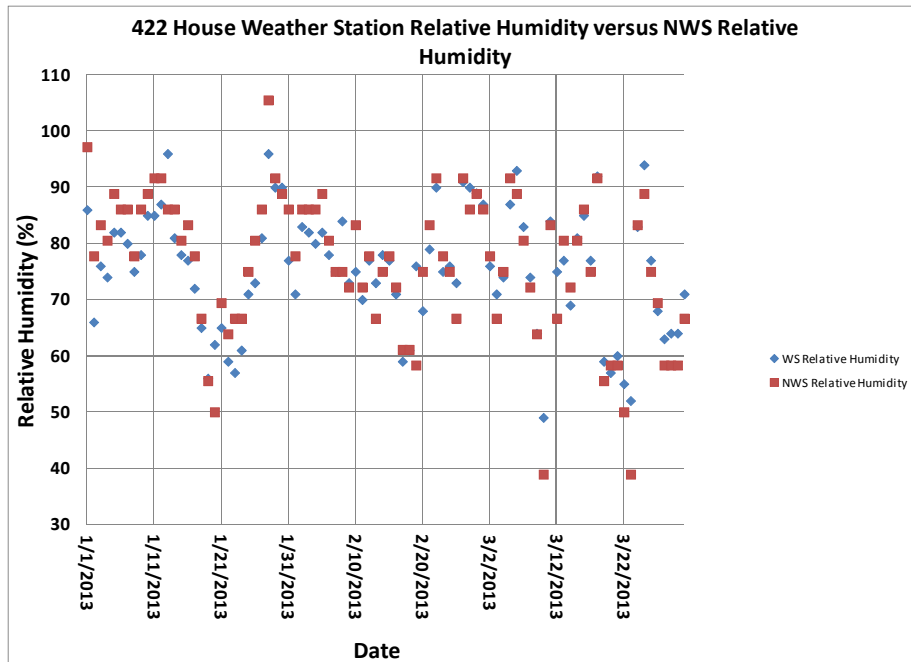


Figure 4-5. Comparison of National Weather Service Indianapolis relative humidity to a weather station at 422 East 28th Street.

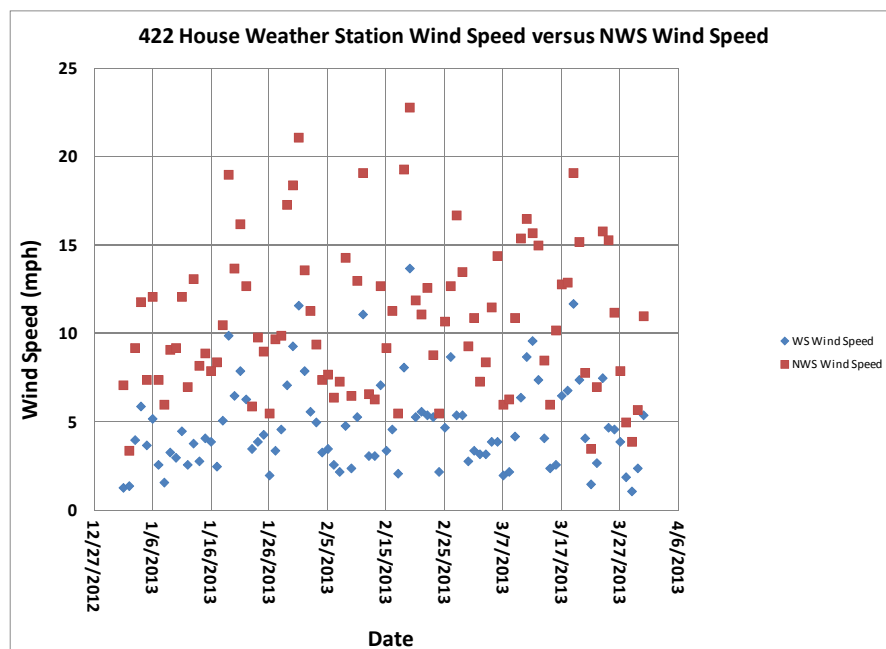


Figure 4-6. Comparison of National Weather Service wind speed data to a weather station at 422 East 28th Street.

From roughly mid-October of 2012 through mid-January of 2013, the 422 house weather station would periodically stop reporting data in the early morning hours, for roughly 15 minutes to 2 hours, and then restart. Eventually, it was determined that this error was attributable to a weakness in the solar-recharged battery in the exterior weather sensor. When weather conditions were safe enough, Ping’s Tree Service was called in on January 15, 2013, to use a bucket truck to change the sensor’s battery. This addressed the problem.

In late fall 2013, the periodic data dropouts began again. Ping’s Tree Service was again called to the 422 house to change the exterior weather station battery. The problem discontinued, but then reoccurred sporadically or during periods of extreme cold. The manufacturer believed the cause to be a faulty capacitor in the exterior weather station. The manufacturer thought that the station battery became less efficient during times of extreme cold, causing the station to draw on the charge stored by its capacitor. If the capacitor were faulty, it would not be able to power the station through the whole night until the solar cell could once again power the station in daylight. The problem discontinued as temperatures rose during the warmer weather. Although this problem only affected a small portion of the data for each day, the project team has been cognizant of the potential for it to systematically bias the exterior temperature measurements because the battery failure would frequently coincide with the lowest temperatures for the 24-hour cycle. Thus, conclusions based on ambient temperature are also being checked using the NWS data for the Indianapolis airport, which is not subject to this battery problem.

4.6 Groundwater Analysis—EPA NERL

4.6.1 Blanks

Field and laboratory blanks were used to evaluate false positives and/or high bias due to transport, storage, and sample handling. Field blanks were collected by filling a volatile organic analysis (VOA) vial with deionized (DI) water (provided by the laboratory) at the field site, then sealing and including the

vial with the samples sent to the laboratory for analysis. Typically, a field blank was collected with each shipment to the laboratory. A total of 17 field blanks were submitted over the 3-year duration of the project.

In the case of the laboratory blank, a VOA vial of laboratory DI water was analyzed with each analytical batch to measure background from the instrumentation. A total of 27 laboratory blanks were analyzed and reported over the duration of the project.

To assist in data interpretation, all blank samples and all field sample results were evaluated down to the MDL. During the first phase of this project, the volume of sample analyzed was 5 mL, and during the second phase, the volume of sample analyzed was increased to 25 mL to lower the detection limits. The results of the field and laboratory blanks for the 5 mL sample size are summarized in **Tables 4-27** and **4-28**. The results of the field and laboratory blanks for the 25 mL sample size are summarized in **Tables 4-29** and **4-30**. The number of blanks with detections above the RL and MDL are tabulated. Summary statistics were then calculated on this subset of positive detections.

Table 4-27. Groundwater (5 mL)—EPA Field Blank Summary

	RL (ng)	MDL (ng)	Number of Field Blanks			Field Blanks with Detections (%)	Mean Blank Conc. (ng)	Std. Dev. (ng)	Min. (ng)	Max. (ng)
			Analyzed	Conc. > RL	RL > Conc. > MDL					
Benzene	25	1.4	11	0	5	45	1.8	0.9	1.4	4.6
Chloroform	25	10	11	0	0	0	10	NA	10	10
cis-1,2-DCE	25	13	11	0	0	0	13	NA	13	13
PCE	25	14	11	0	0	0	13	NA	17	17
Toluene	25	14	11	0	0	0	10	NA	10	10
TCE	25	17	11	0	0	0	13	NA	13	13

NA = not applicable.

Table 4-28. Groundwater (5 mL)—EPA Laboratory Blank Summary

	RL (ng)	MDL (ng)	Number of Lab Blanks			Lab Blanks with Detections (%)	Mean Blank Conc. (ng)	Std. Dev. (ng)	Min. (ng)	Max. (ng)
			Analyzed	Conc. > RL	RL > Conc. > MDL					
Benzene	25	1.4	17	0	8	47	1.6	0.7	1.4	3.5
Chloroform	25	10	17	0	3	18	11	1.9	10	14
cis-1,2-DCE	25	13	17	0	0	0	13	NA	13	13
PCE	25	14	17	0	0	0	14	NA	14	14
Toluene	25	14	17	0	0	0	14	NA	14	14
TCE	25	17	17	0	0	0	17	NA	17	17

NA = not applicable.

Table 4-29. Groundwater (25 mL)—EPA Field Blank Summary

	RL (ng)	MDL (ng)	Number of Field Blanks			Field Blanks with Detections (%)	Mean Blank Conc. (ng)	Std. Dev. (ng)	Min. (ng)	Max. (ng)
			Analyzed	Conc. > RL	RL > Conc. > MDL					
Benzene	13	1.2	6	0	0	0	1.2	NA	1.2	1.2
Chloroform	13	1.3	6	0	0	0	1.3	NA	1.3	1.3
cis-1,2-DCE	13	1.7	6	0	0	0	1.7	NA	1.7	1.7
PCE	13	1.2	6	0	1	17	7.1	NA	1.2	7.1
Toluene	13	1.1	6	0	2	33	1.7	0.04	1.1	1.8
TCE	13	1.6	6	0	0	0	1.6	NA	1.6	1.6

NA = not applicable.

Table 4-30. Groundwater (25 mL)—EPA Laboratory Blank Summary

	RL (ng)	MDL (ng)	Number of Lab Blanks			Lab Blanks with Detections (%)	Mean Blank Conc. (ng)	Std. Dev. (ng)	Min. (ng)	Max. (ng)
			Analyzed	Conc. > RL	RL > Conc. > MDL					
Benzene	13	1.2	16	0	1	10	1.6	0.7	1.2	3.5
Chloroform	13	1.3	16	1	0	10	14	NA	1.3	14
cis-1,2-DCE	13	1.7	16	0	5	50	3.0	2.2	1.7	7.0
PCE	13	1.2	16	0	0	0	1.2	NA	1.2	1.2
Toluene	13	1.1	16	0	3	19	1.6	0.4	1.1	2.1
TCE	13	1.6	16	0	1	10	5.5	NA	1.6	5.5

NA = not applicable.

4.6.2 Surrogate Recoveries

To monitor analytical efficiency, 200 ng of dibromofluoromethane, 1,4-dichloroethane-d4, and toluene-d8 were added into each QC and field sample with the vapor phase internal standard mix during sample analysis. Field surrogates were not included in the scope of this project. The recoveries were evaluated against laboratory limits of 70%–130%. Most surrogate recoveries met the laboratory criterion, and summary statistics are presented in **Tables 4-31** and **4-32**.

Table 4-31. EPA Groundwater (5 mL)—Surrogate Recovery Summary

Parameter	Dibromofluoromethane Results	1,4-dichloroethane-d4 Results	Toluene-d8 Results
Number of surrogate recoveries measured	111	111	111
Average recovery (%R)	105	95	98
Standard deviation (%R)	10	4	8
Minimum recovery (%R)	79	85	83
Maximum recovery (%R)	131	106	117

Table 4-32. EPA Groundwater (25 mL)—Surrogate Recovery Summary

Parameter	Dibromofluoromethane Results	1,4-dichloroethane-d4 Results	Toluene-d8 Results
Number of surrogate recoveries measured	163	163	163
Average recovery (%R)	100	98	98
Standard deviation (%R)	7	6	6
Minimum recovery (%R)	77	82	86
Maximum recovery (%R)	116	115	108

4.7 Database

4.7.1 Checks on Laboratory Reports

Throughout the project, the ARCADIS project manager briefly reviewed laboratory reports as they were received from the VOC analytical laboratories. The primary focus of these checks was on blanks and ambient samples as a sampling performance indicator, as well as the general consistency and reasonableness of the trends in reported concentrations for the primary analytes: PCE and chloroform.

The ARCADIS project manager also performed a manual review of the electrets' radon computations in the spreadsheet used for those calculations. He also reviewed that data set regularly and interacted with the field scientist collecting these data when any anomalous results were observed.

The lead analyst (from Hartman Environmental Geoscience), the ARCADIS principal scientist, and an RTI data specialist were all involved in reviewing the online GC calculations. For suspect values, QC checks performed included calibration checks and chromatogram reviews.

4.7.2 Database Checks

A Microsoft Access database was developed and used to compile results for VOCs (TO-17, TO-15, and passive indoor air) and radon in indoor air and soil gas (electret and AlphaGUARD).

The following QC checks were performed on this database:

- The ARCADIS field scientist responsible for the majority of the field sampling performed a check of the reports received from laboratories against his own records. He checked for the

following: approximate number of each sample type (to determine what reports were still pending) and a line-by-line check of the sample times, dates, and sample numbers of each sample type. The assignment of sample locations was also reviewed. Notes of any discrepancies and corrections were sent to the ARCADIS database manager.

- During the initial portions of the project, the Eurofins ATL technical director manually prepared a Microsoft Excel spreadsheet from laboratory reports comparing the results of passive samplers exposed at the same location for multiple durations and calculating percentage bias. The ARCADIS project manager then used that spreadsheet to spot-check the calculations of percentage bias performed in the database. After correcting for slight differences in the percentage bias formula used, excellent agreement was found. This finding indicates that, at least for the calculations spot-checked, both the calculation and the importation of the underlying concentration data from electronic deliverable files into the database are being performed correctly.
- During the initial portions of the project, the ATL technical director manually prepared an Excel spreadsheet of indoor air VOC results from laboratory reports. The Excel spreadsheet was used to prepare temporal trend plots of indoor concentrations for key analytes for the first 18 weeks of the project before the Access database was fully implemented. The ARCADIS project manager then confirmed that the essential features of these temporal trend plots (such as range of concentrations and overall temporal trends) were consistent between these plots and similar plots generated from the Access database. For this period, this finding indicates that the importation of the underlying concentration data from electronic deliverable files into the database is being performed correctly.
- The ARCADIS project manager provided to the database manager a design document for the reports to be generated, including definitions of key formulas and variables. The design document was prepared based on the project objectives in the QAPP. As database reports were prepared, the ARCADIS project manager reviewed their format and content and requested changes as necessary.
- The ARCADIS project manager and database manager both spot-checked the transfer of the NERL results for groundwater into the database.
- The ARCADIS project manager and RTI statistical intern both reviewed the data sets for outliers, queried them, and addressed any problems identified.
- Database reports were run to identify samples that were collected but for which data were not received. These samples were investigated and often determined to be due to problems that occurred in the analytical laboratory. These lost samples were notated in the project database.

5. Results and Discussion: VOC Concentration Temporal Trends and Relationship to HVAC and Mitigation

This chapter provides an update from the previous two reports (U.S. EPA, 2012a, U.S. EPA, 2013) of the temporal trends in VOC and radon concentrations in the various indoor air, subslab, and soil gas sampling locations installed in the Indianapolis duplex during the course of the study (see **Section 3** for sampling locations). As described in U.S. EPA (2012a), a central heating system was installed in the 422 side of the duplex before testing in 2011 while the 420 side remained unheated during the entire study. As described in U.S. EPA (2013), a conventional subslab depressurization radon mitigation system was installed under the entire duplex in October 2012 and was operated and tested during the winter and early spring 2012/2013. The mitigation system was off for the 2013-2014 sampling period discussed in this report.

The contents of the first two reports and the focus areas for this report are described in greater detail in **Section 2**. The initial report for this study (U.S. EPA, 2012a) covered site screening data collected in 2010 and explored temporal trends from a continuous sampling program conducted from January 2011 through February 2012. The second report interpreted the full data set up to May 2013 with special attention to time series analysis and mitigation testing. This report extends testing and analysis until March 5, 2014, and includes a complete record of the 109 weekly VOC measurements from the start of the project until that date.

5.1 VOC Seasonal Trends Based on Weekly, Biweekly, and Monthly Measurements for 100+ Weeks

5.1.1 Indoor Air

Figures 5-1 and **5-2** show PCE and chloroform versus time, respectively, at all six indoor air monitoring locations, in addition to the ambient outdoor location (see **Section 3** for maps of the placement of the indoor air, subslab, and soil gas sampling locations included in this section). All sampling locations in these figures operated from the start of the project until October 24, 2013, but only 422 first floor, 422 south basement, 420 south basement, and outdoor (ambient) locations were sampled since that date, for a total of 109 weekly measurements at those locations.

As shown in **Figure 5-1**, PCE levels at all six indoor locations follow the same general trend of starting higher at the beginning of the project (January 2011), dropping to a low in spring 2011, and rising slightly and leveling out through the end of the premitigation period in October 2012. (Note that indoor air sampling was discontinued from February 2012 to October 2012 because of funding limitations, which resulted in the data gap that can be seen in these and subsequent figures in this chapter.) Interestingly, fall/winter of 2013 did not repeat this trend. Instead, the data show a rising trend toward December 2013/January 2014, followed by a downward trend just before the mitigation system was turned back on in the beginning of March 2014. The concentrations in October 2012 before the mitigation system was installed were very similar to those observed in October 2011. The timing of the spring minimum differed substantially for the unheated side of the duplex (when it occurred in late March) from the heated side of the duplex (where the minimum was reached in July). The highest readings were generally found at 422 south basement except during brief periods when first floor concentrations were higher, which occurred mostly during operation of a basement depressurization fan on the 422 side of the duplex (see U.S. EPA, 2012a, Section 12.2).

Surprisingly, indoor air PCE concentrations during the first period of active mitigation rose to levels not seen in the duplex since February 2011. The concentrations continued to rise after the active mitigation system was switched off, reaching a maximum of 5.7 $\mu\text{g}/\text{m}^3$ in November 2012. Indoor air concentrations

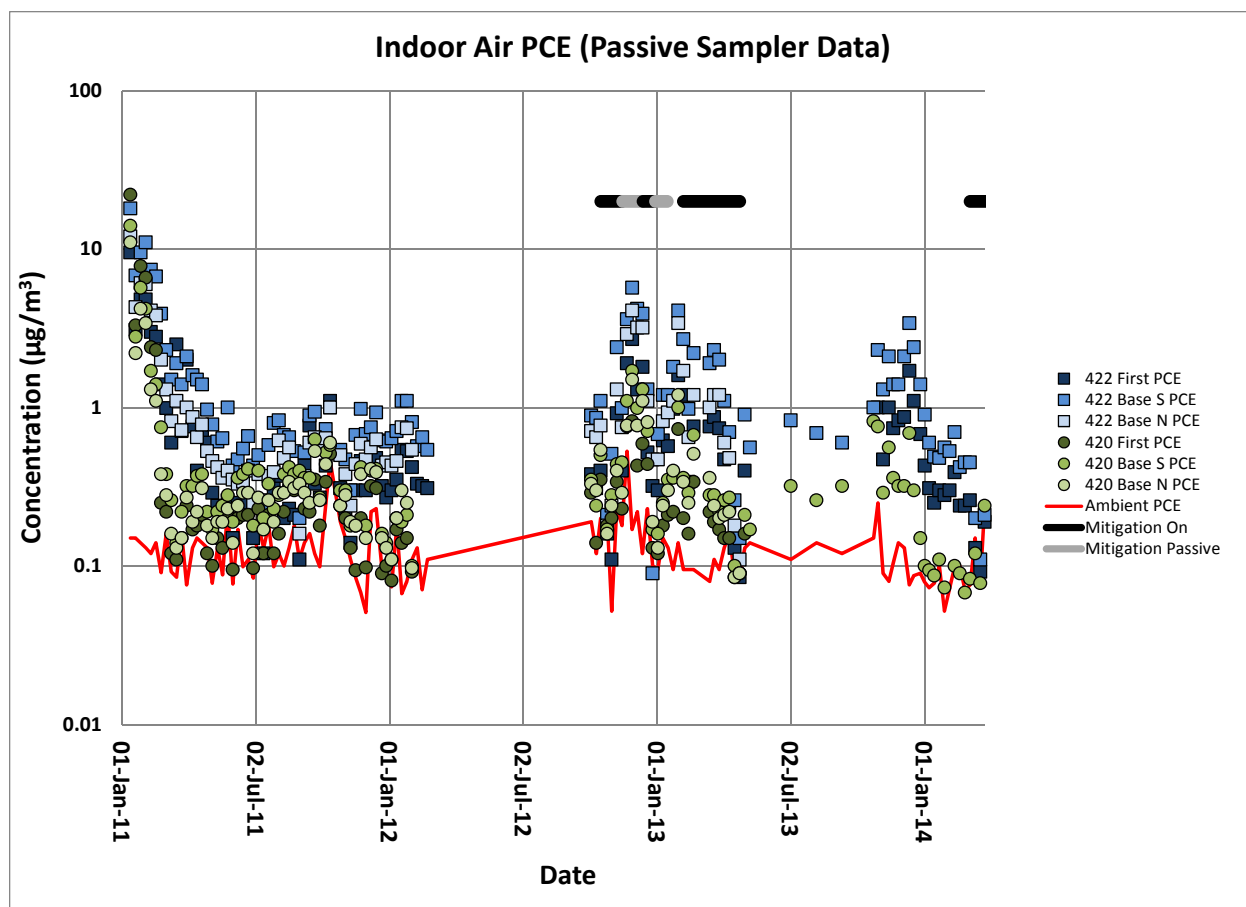


Figure 5-1. PCE in indoor and outdoor (ambient) air over time (7-day Radiello samples).

higher than $5.7 \mu\text{g}/\text{m}^3$ had not been observed at the duplex since January and February 2011. PCE concentrations reached a high of $3.4 \mu\text{g}/\text{m}^3$ on December 12, 2013, prior to turning on the mitigation system. PCE concentrations observed in late fall/early winter 2013 also substantially exceeded those observed in the winter of 2011-2012.

In discussions and comments during conference presentations (Schumacher et al., 2013; Lutes et al., 2012a, 2012b, 2012c, 2012d) on the PCE data set through February 2012, questions were raised about whether the highest PCE concentrations observed in January and February 2011 were artifacts. At the time, the authors offered other lines of evidence (such as the lack of indoor sources, preparation of the house prior to sampling) as support for the observed levels. The observation of higher PCE after mitigation during the winter of 2012 to 2013 does confirm that the subsurface can yield enough vapor intrusion-derived PCE to account for the January 2011 concentrations. The differences between the fall of 2011 and fall of 2013 show that year to year variations can be significant. To explain these results, we postulate that VOCs may have been moved close to the structure either by a cumulative stack effect during the severe winter of 2011 or during the initial operation of the SSD system in the winter of 2012-2013. How VOC levels will change over time as the mitigation system is operated continuously for many months remains to be seen. This topic will be covered in a forthcoming report.

Chloroform concentration patterns (Figure 5-2) were generally similar to PCE and can be summarized as follows:

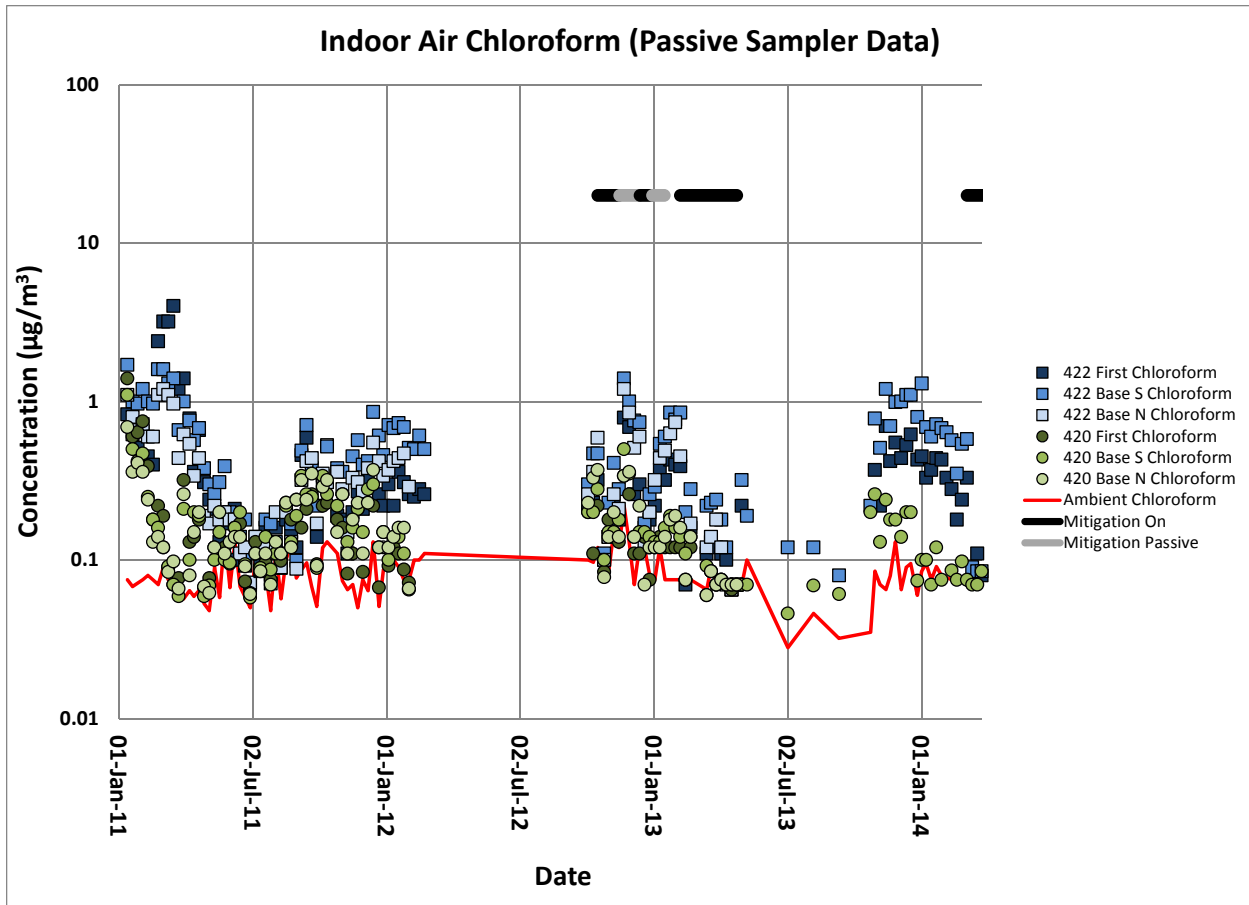


Figure 5-2. Chloroform in indoor and outdoor (ambient) air over time (7-day Radiello samples).

- Broadly, the six indoor locations show a general concentration decline from a localized maximum at the beginning of the sampling interval (January 2011). The minimum was reached in early July on the 422 side of the house, as with PCE. Also similar to PCE’s behavior, the chloroform minimum concentration on the 420 side of the house occurred much earlier in the year (March).
- The levels at the 422 first floor sampling location rose abruptly to a maximum in March 2011 immediately after a brief drop in January. During this maximum, the first floor concentrations exceeded those of even the basement stations. The 422 basement sampling stations showed a less dramatic rise in this period.
- Chloroform concentrations reached a minimum in July 2011 and began steadily increasing thereafter, forming a generally U-shaped curve. The post-mitigation winter 2012 levels more closely approached their 2011 highs than do the corresponding PCE results.
- The second maximum concentration for chloroform occurred in October 2011 for the 420 (unheated) locations and was followed by a considerable decline through the winter months. A second peak occurred later (December 2012) on the 422 (heated) side of the duplex and concentrations stayed near that maximum until February 2012.
- The concentrations of chloroform in October 2012 (after the February to October break in sampling) were similar to those observed in October 2011.
- Chloroform concentrations during the fall/winter period of 2013/2014 show similar trends to those seen in the previous year’s fall/winter period.

- With the exception of the elevated chloroform from late February to late March 2011, the highest chloroform levels were found at 422 basement south, the same station that was generally highest for PCE (**Figures 5-1 and 5-2**).
- In general many of the seasonal cycles show that chloroform concentrations peak in late fall/early winter; before the coldest temperatures of the year are normally experienced in January.

Figures 5-3 and 5-4 show benzene and toluene at 422 basement south versus time, along with ambient outdoor air levels of benzene and toluene. Although both benzene and toluene are above their indoor air screening levels (benzene = $0.31\mu\text{g}/\text{m}^3$; toluene = $0.0052\mu\text{g}/\text{m}^3$; U.S. EPA Regional Screening Level Summary Table, November 2011), each tends to trend similarly to its respective outdoor sample; this is not the case with PCE or chloroform indoor air levels, which are almost always considerably higher than outdoor air. This finding suggests that benzene and toluene indoor air levels are controlled by outdoor air levels, not vapor intrusion.

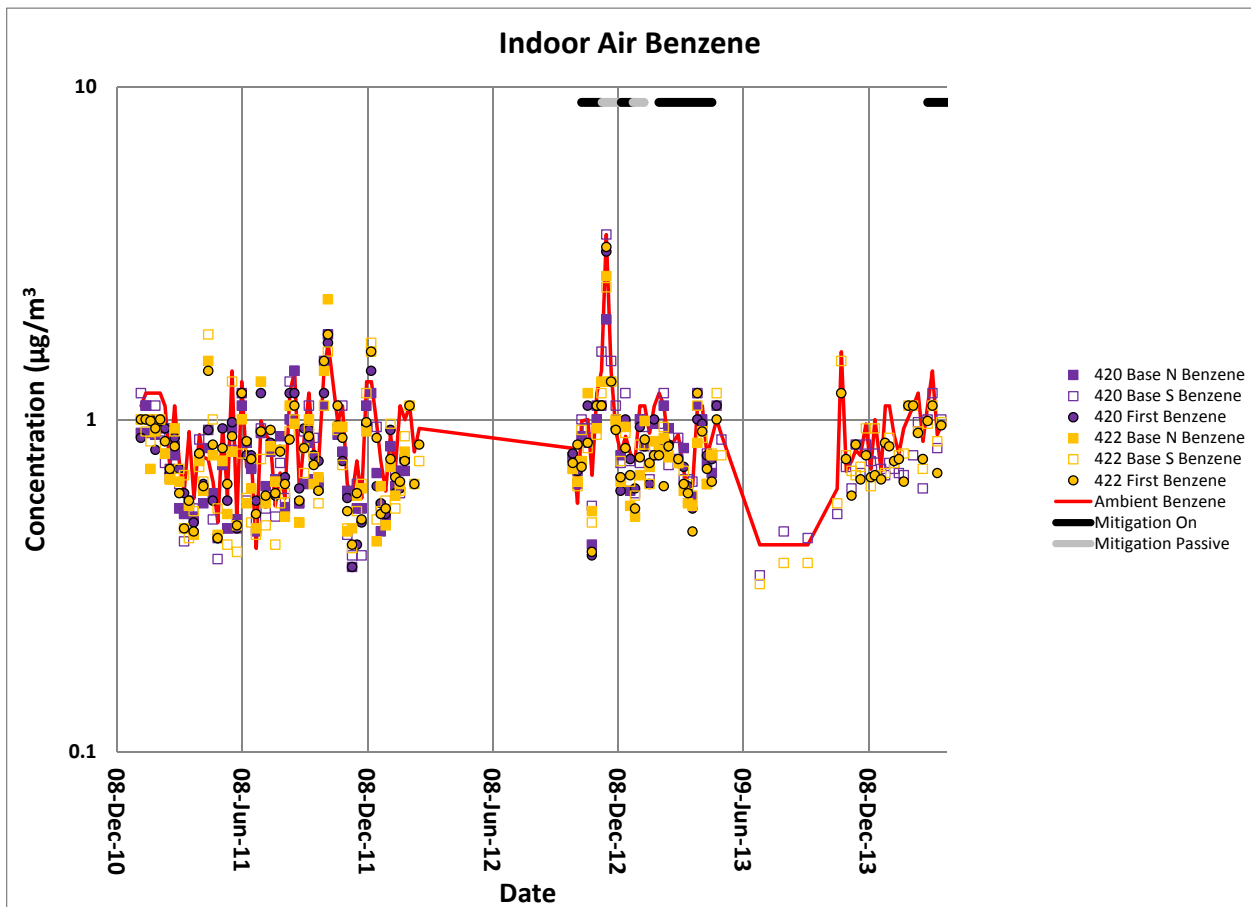


Figure 5-3. Benzene in indoor and outdoor (ambient) air over time.

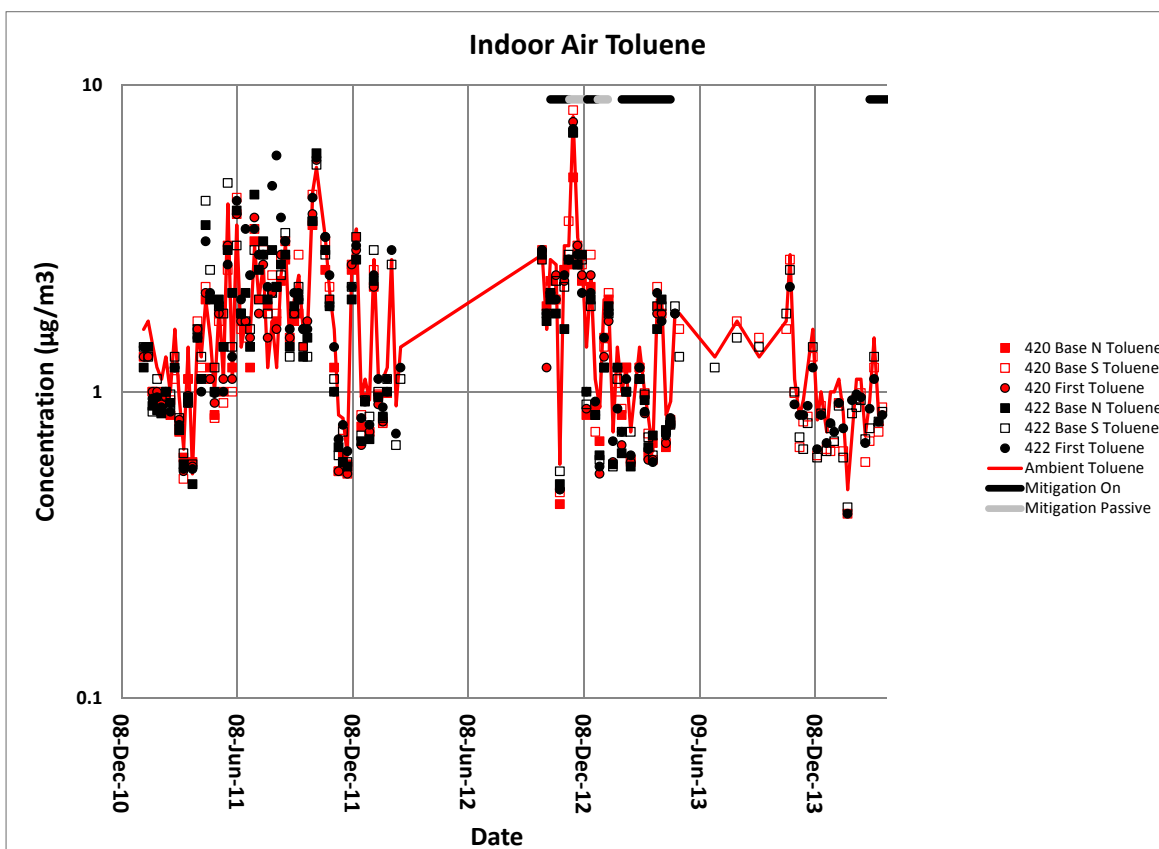


Figure 5-4. Toluene in indoor and outdoor (ambient) air over time.

5.1.2 Subslab Soil Gas

Subslab soil gas was monitored with a set of seven points covering both sides of the duplex. Given the low initial concentration of subslab probe SSP-2 and its proximity to soil gas probe SGP10-6, SSP-2 was sampled relatively infrequently. As described in **Section 3**, sampling probes on the 420 side of the house included SSP-3 and SSP-5 through SSP-7 and wall port WP-4. The basements of both sides of the duplex are each divided into thirds by interior walls. There is generally one subslab port per basement division; with one section on the 420 side has two. The wall ports are located on the exterior walls of the duplex. WP-1 and WP-3 are each located in the centers of the north and south ends of the 422 basement, and WP-2 is in the center of the east side of the 422 basement. WP-4 is located in the center of the west wall of the 420 basement. Additionally, during the 2013 year, 55-gallon drums containing soil cuttings from well and soil gas port installation were removed from the site. Upon their removal, an additional external subsidewalk port was rediscovered, likely from the initial days of testing for vapor intrusion at the 422/420 house. This port was labeled SSP-8 and periodically brought into the sampling rotation. SSP-8 is located in the breezeway on the eastern side of the house between the 422/420 house and the adjacent building. **Figure 5-5** shows the locations of the subslab, soil gas, and wall port probes sampled in the course of this study.

Figures 5-6 and **5-7** plot subslab TO-17 chloroform and PCE concentrations versus time. For chloroform, **Figure 5-6** shows that some subslab ports, such as SSP-4 and SSP-7, reached new high concentrations after mitigation began during the fall of 2012. However, there were no clear visible trends during the mitigation testing period. In the winter of 2013–2014, with the mitigation system off, previous highs in SSP-1 and SSP-4 were equaled or exceeded, with a general decline in chloroform levels in SSP-1 but a general increase in SSP-4 occurring as the 2013–2014 winter progressed.

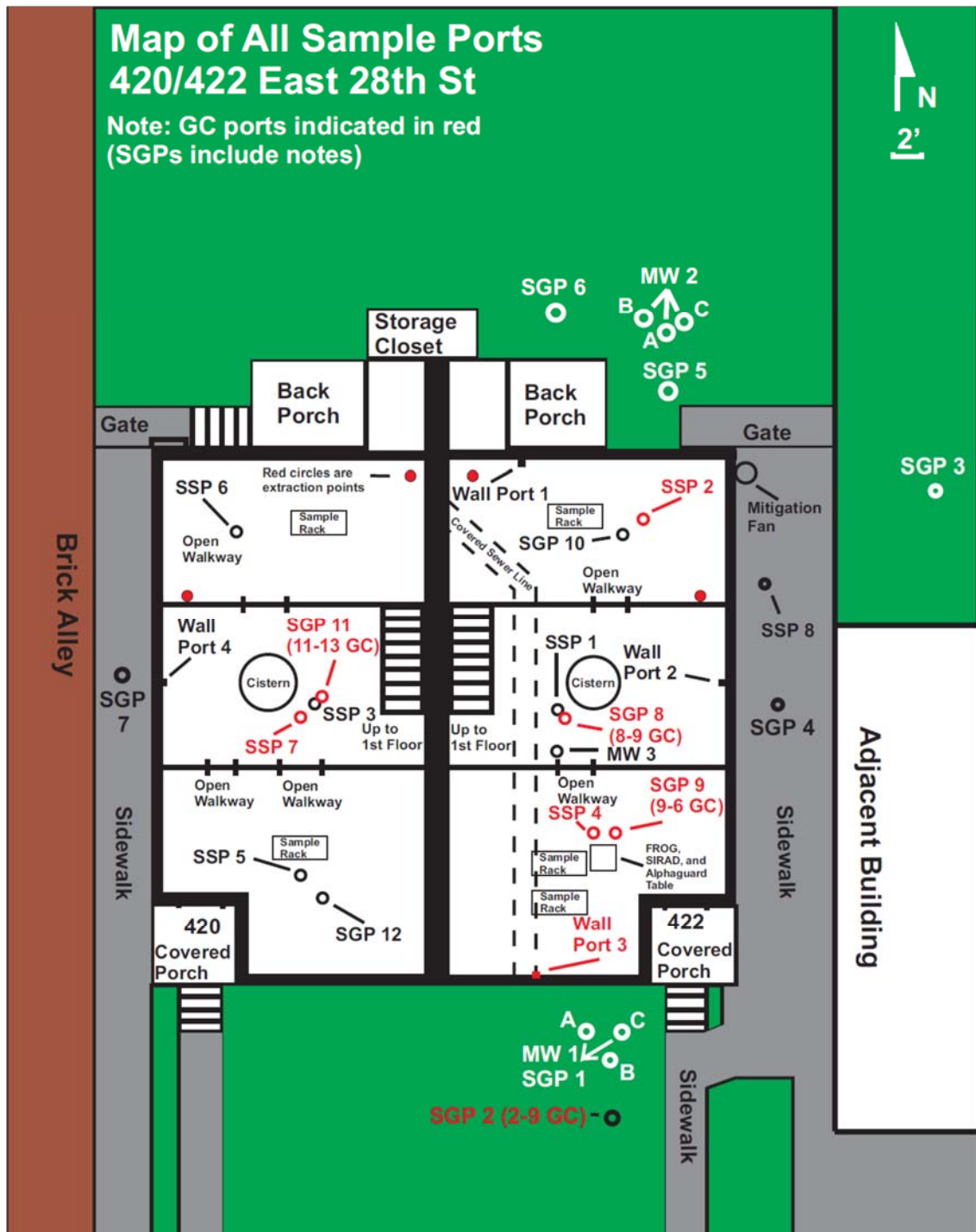


Figure 5-5. Interior and exterior sampling port locations.

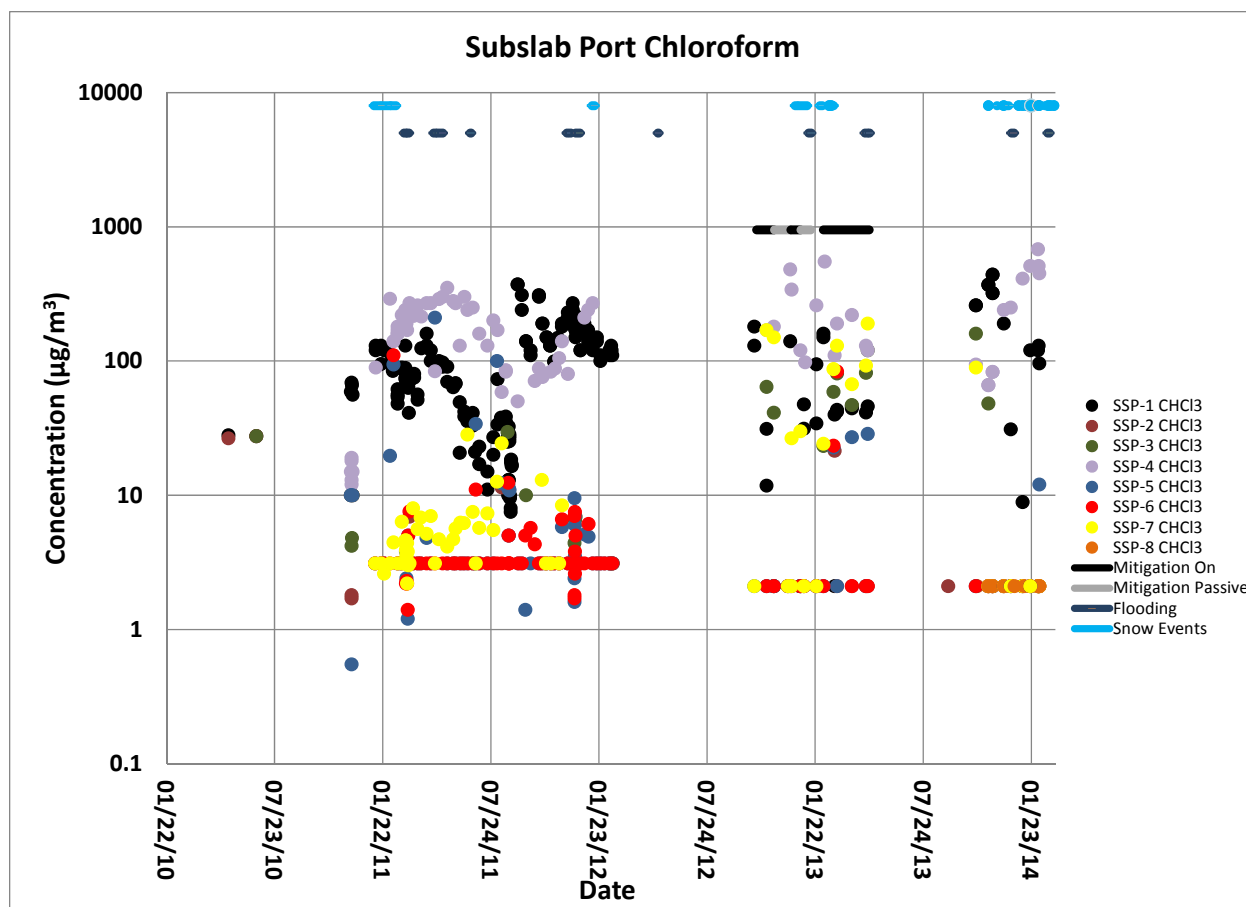


Figure 5-6. Plot of subslab chloroform concentrations over time (TO-17 data).

Chloroform on the 422 side (shown in **Figure 5-6** as the black, burgundy, and light purple circles) showed a rough sinusoidal trend over months in 2011, although the different ports are somewhat out of phase. These data generally show lows during the warmer months (SSP-1 and SSP-4 seem to both reach a minimum in August/September 2011) and highs during cooler months. It is also notable that the concentration increases abruptly two orders of magnitude between August 27 and September 8, 2011, a period of time during which a series of fan tests (coded B and F) intended to simulate the stack effect expected under winter conditions were conducted (as discussed in Section 12.2 of EPA [2012a]). Another smaller rise occurs from September 30 to October 14, 2011. Fan test “I” was conducted from October 6 to October 14, 2011. These sinusoidal trends are not apparent during the mitigation on/off cycles or during the winter of 2013–2014.

The subslab ports on the heated 422 side of the duplex (SSP-1, SSP-2, SSP-4, and SSP-8) generally have higher concentrations of PCE and chloroform than those on the unheated 420 side of the structure (SSP-3, SSP-5, SSP-6, and SSP-7). In **Figure 5-7**, the SSP-5, SSP-6, and SSP-7 ports on the 420 side of the duplex showed PCE highs during the warmer months and PCE lows during the cooler months. On the 422 side, SSP-1 shows the opposite trend, while SSP-2 and SSP-4 are more stable across the seasons, perhaps with a slight increase during the summer months. In general, it appears that there is more spatial variability in PCE concentrations between the subslab ports in winter than in summer.

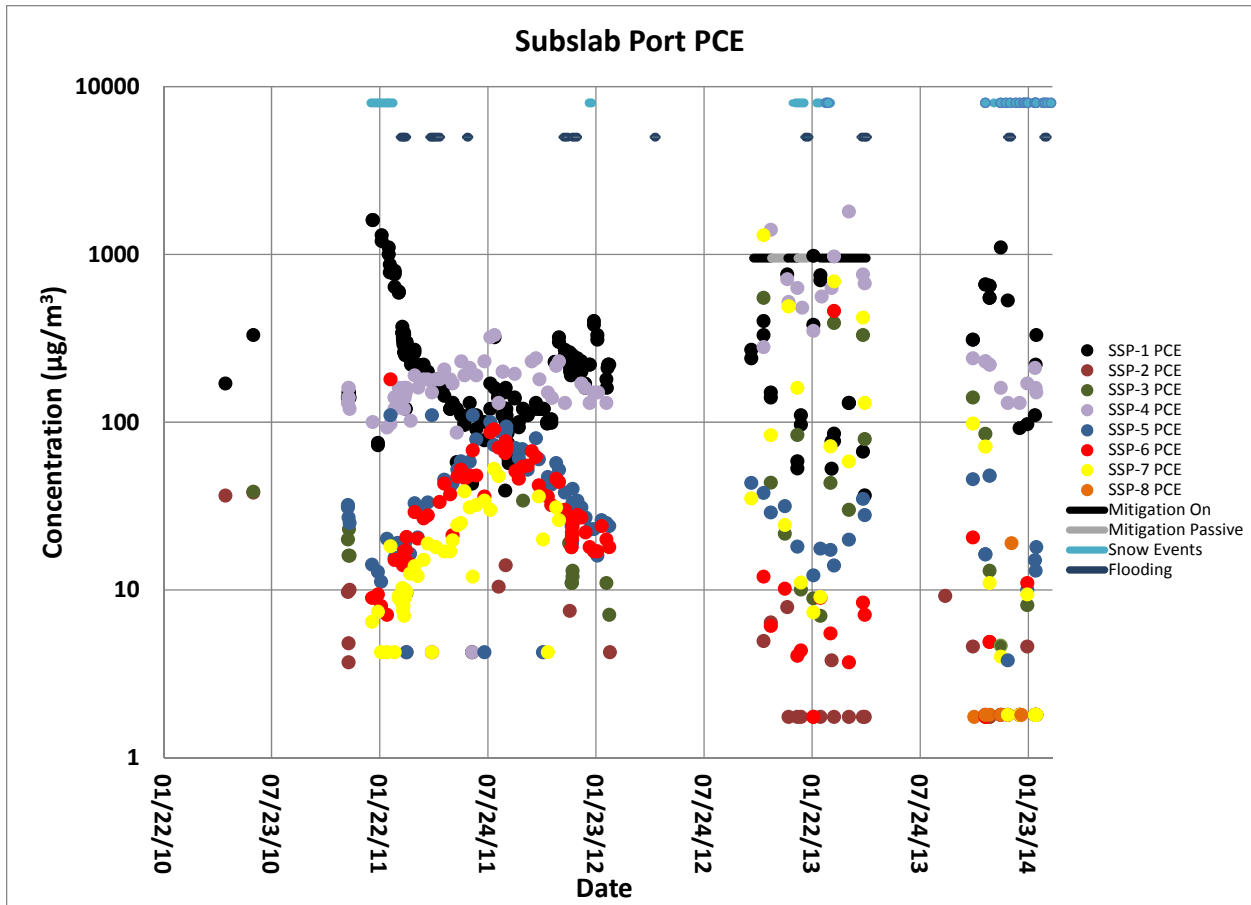


Figure 5-7. Plot of subslab PCE concentrations over time (TO-17 data).

As occurred with chloroform concentrations, some ports—SSP-3, SSP-4, SSP-6, and SSP-7—reached new high PCE values after mitigation began (Figure 5-7). As discussed in the descriptive statistical analysis in Section 5.3 of U.S. EPA (2013), within the mitigation testing period, higher subslab PCE concentrations were clearly associated with the mitigation system being on.

When graphed for the wall ports (Figures 5-8 and Figure 5-9), neither chloroform or PCE shows the same patterns of seasonal highs and lows found in the subslab (Figures 5-6 and 5-7). Chloroform highs for WP-3 in January through February and September through October 2011 (Figure 5-8) could suggest the influence of the snow and ice and fan testing, respectively. The somewhat greater variability of the wall ports as compared with the subslab ports may be attributed to their more shallow depths (approximately 1.5 ft bls) and greater atmospheric influence.

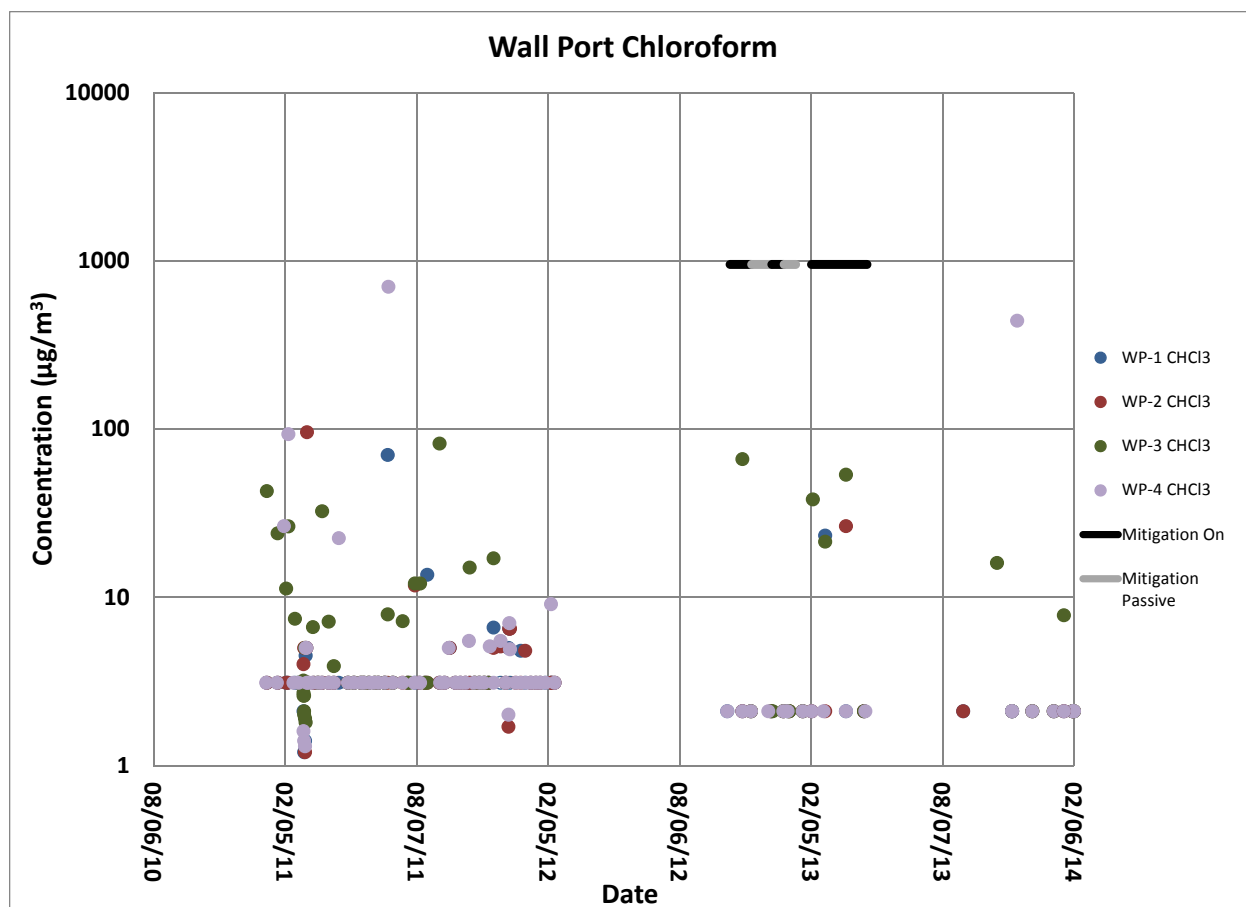


Figure 5-8. Plot of wall port chloroform concentrations over time (TO-17 data).

Wall port PCE concentrations over time (Figure 5-9), although generally modest, appear to show greater variability than the subslab ports, possibly reflecting a greater influence of outdoor air along the basement walls compared to under the house (see also Figures 8-25 and 8-27 of the second report [U.S. EPA, 2013]). The high concentrations of PCE in WP-3 at the beginning of the project could be due to the snow and ice capping event during the severe winter of January and February 2011; a similarly high level was observed in January 2014 when frozen ground also prevailed. Wall port PCE highs in September and October 2011 might be attributed to the fan testing during that time. Relatively high VOC concentrations at WP-3 were also reached during mitigation testing, which suggests that the SSD system may be drawing VOCs closer to the building envelope.

5.1.3 Shallow and Deep Soil Gas

A series of 12 nested soil gas ports surround the 420/422 house or originate in the basements of either side of the duplex (see Figure 5-5). The five depths at each of the external nested locations are as follows: 3.5 feet below land surface (ft bls), 6 ft bls, 9 ft bls, 13 ft bls, and 16.5 ft bls. Internal to the house are the nested locations notated SGP8 through 12. Each individual port is notated based on its location and its depth (e.g., SGP1-3.5 for the 3.5-ft depth at the SGP1 location). At the internal nested locations, there are only four depths; the 3.5-ft depth is omitted because the basement floor is at ~5 ft bls. The internal soil gas data are graphed in Figures 5-10 through 5-13 for the 420 side of the duplex and Figures 5-14 to 5-19 for the 422 side of the duplex. External to the house are seven nested locations, labeled SGP1 through 7 and graphed as Figures 5-20 to 5-33. Groundwater levels varied throughout the project but remained high enough most of the time to render the 16.5 ft bls depths inaccessible for soil gas sampling

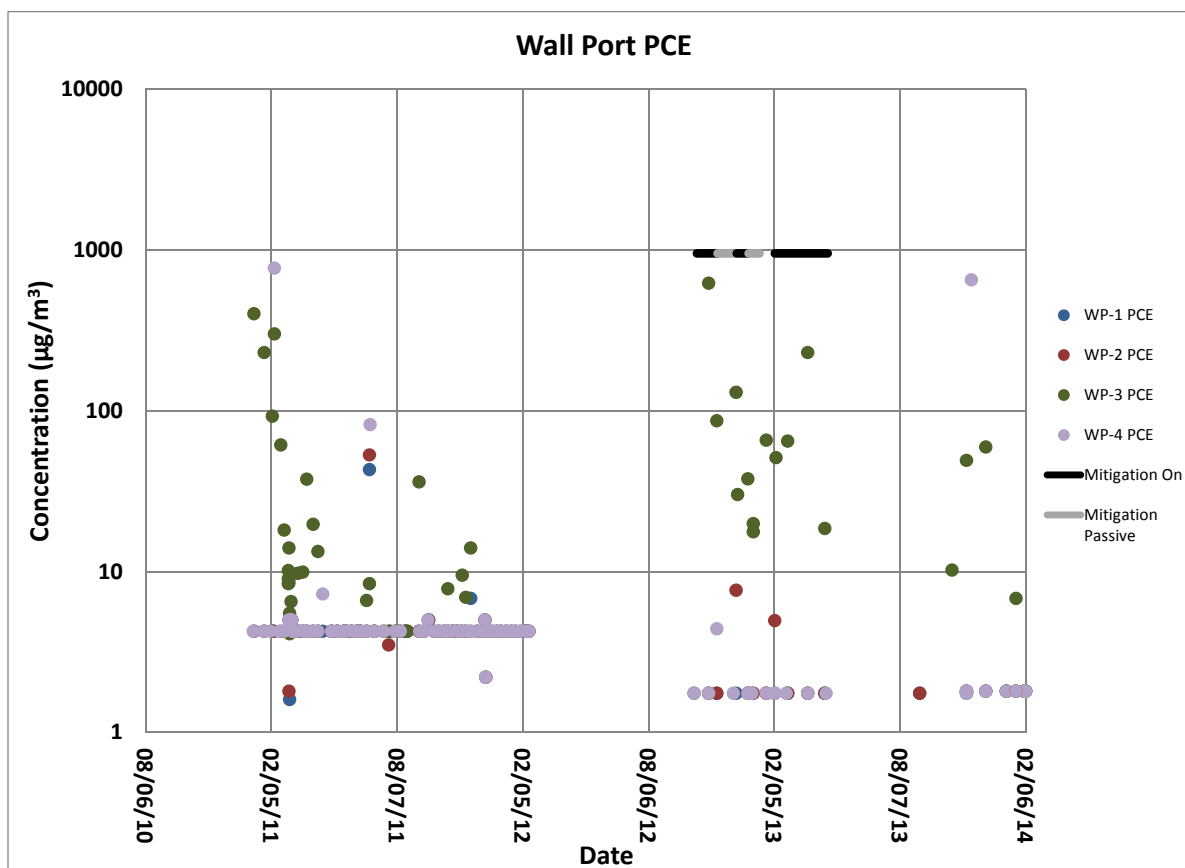


Figure 5-9. Plot of wall port PCE concentrations over time (TO-17 data).

for much of the project. Because of this lack of data, the limited 16.5 ft bls results are not shown in **Figures 5-10** through **5-33**. Measurements with data quality flags (including nondetects) are plotted by their letter symbols in these figures, with below detection values plotted at one-half the detection limit.

Except for when the mitigation system was on, soil gas concentrations were generally highest in the deepest ports of each cluster and decreased at shallower depths. This pattern is consistent with expectations for attenuation of vapor intrusion of VOCs originating from a deep source (whether in the vadose zone or groundwater). This attenuation pattern appears to be more pronounced for chloroform (frequently two to three orders of magnitude) than for PCE (generally one order of magnitude).

Chloroform on the duplex exterior is most consistently detectable at high soil gas concentrations at 9 and 13 ft in the area south of the duplex (SGP-1 and SGP-2 [**Figures 5-20 and 5-22**]). Detections at 13 ft are also relatively frequent north (SGP-5 [**Figure 5-28**]) and west (SGP-6, SGP-7 [**Figure 5-30 and Figure 5-32**]) of the duplex. Although some seasonal variability is observed, there is not a dominant multiyear trend. Chloroform is almost entirely absent or low at the exterior 3.5 ft and 6 ft depths, suggesting that it is rapidly lost to volatilization to the surface.

On the 422 side of the duplex chloroform is consistently detectable in the central (SGP-8 [**Figure 5-14**]) and southern soil gas ports (SGP-9 [**Figure 5-16**]) at all three depths that are frequently sampled beneath the house—6, 9, and 13 ft. The appearance at 6 ft beneath the duplex contrasts with the rare appearance at 6 ft exterior to the duplex, suggesting a capping effect of the structure. Chloroform detections are less frequent at the northern end of 422 (SGP-10 [**Figure 5-18**]). Although some seasonal variability is observed, there is not a dominant multiyear trend.

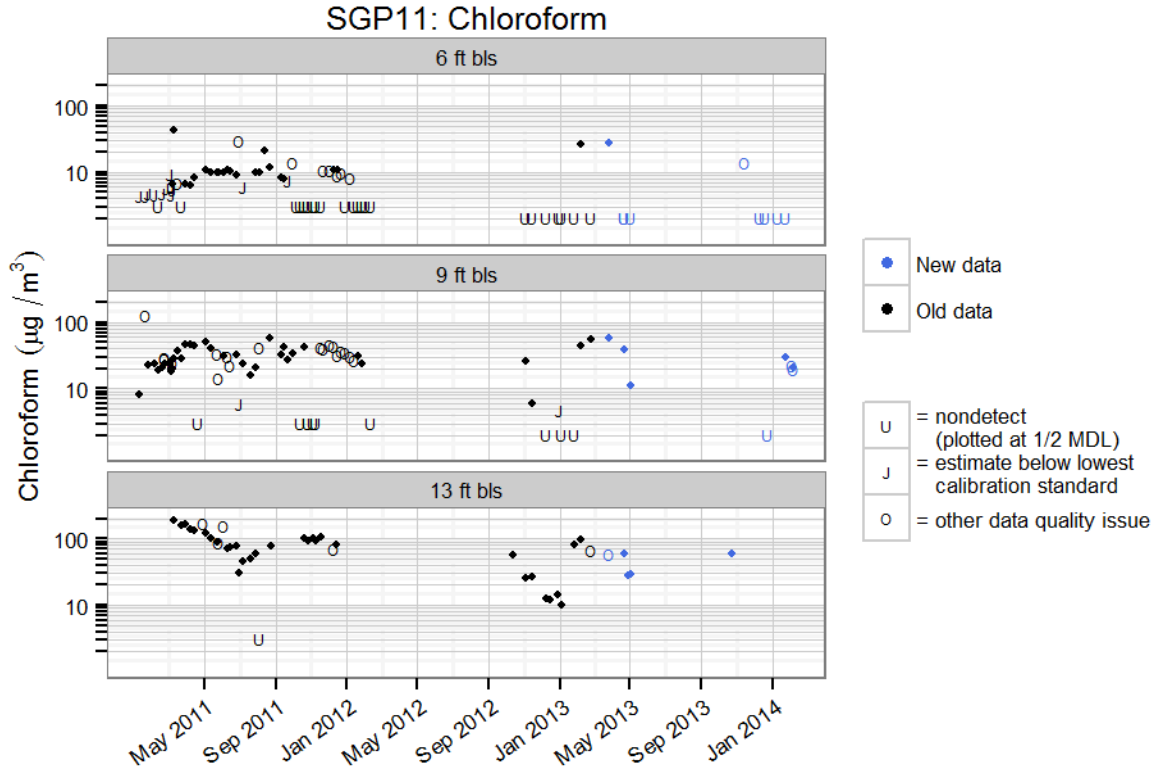


Figure 5-10. Chloroform at SGP11 on the 420 side of duplex.

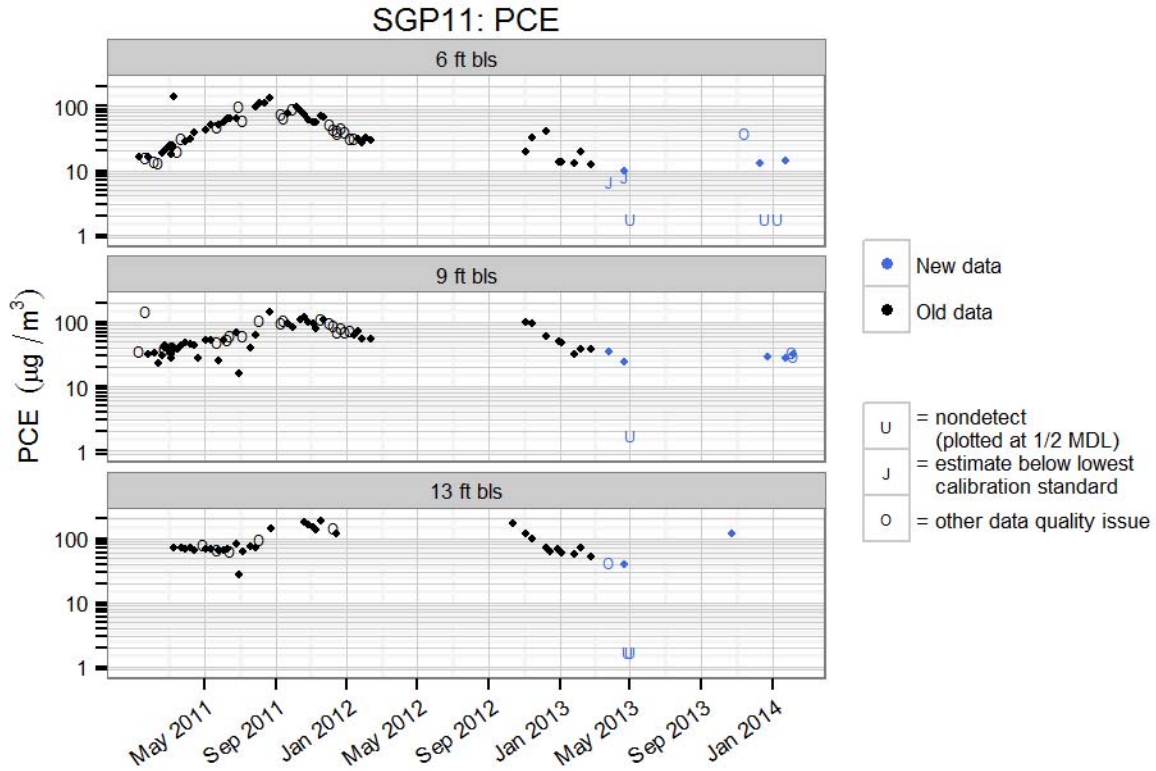


Figure 5-11. PCE at SGP11 on the 420 side of the duplex.

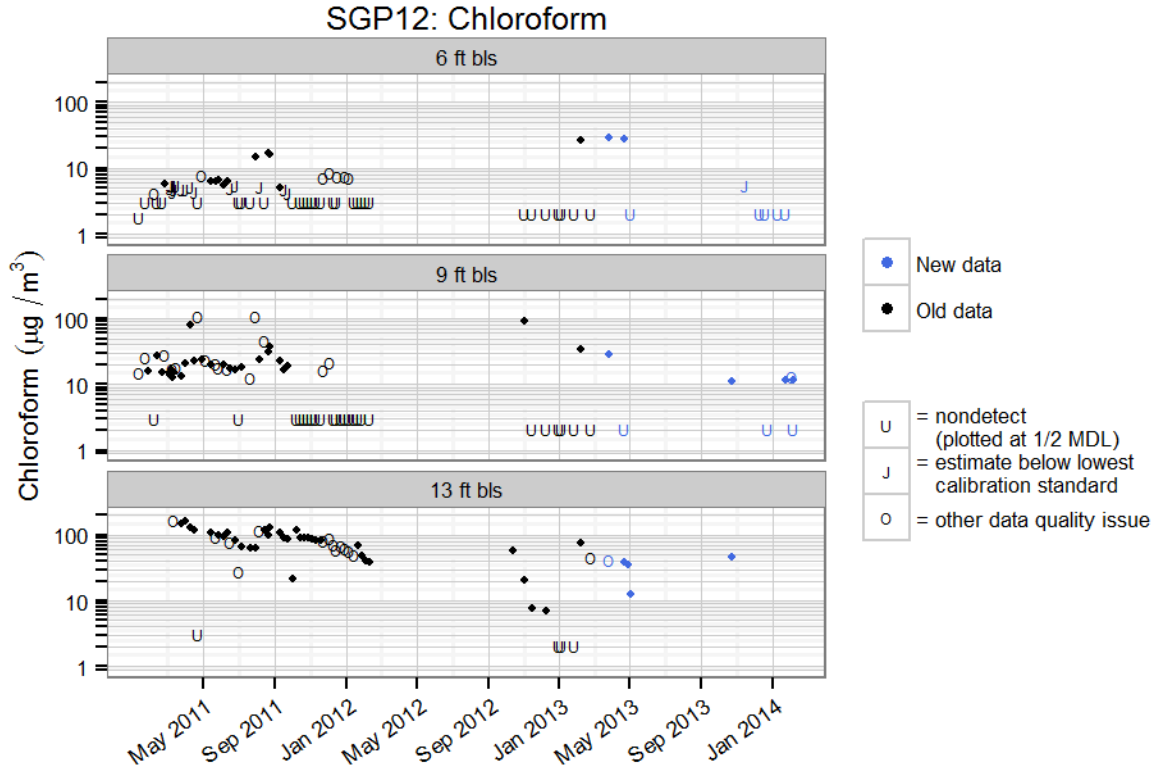


Figure 5-12. Chloroform at SGP12 on the 420 side of duplex.

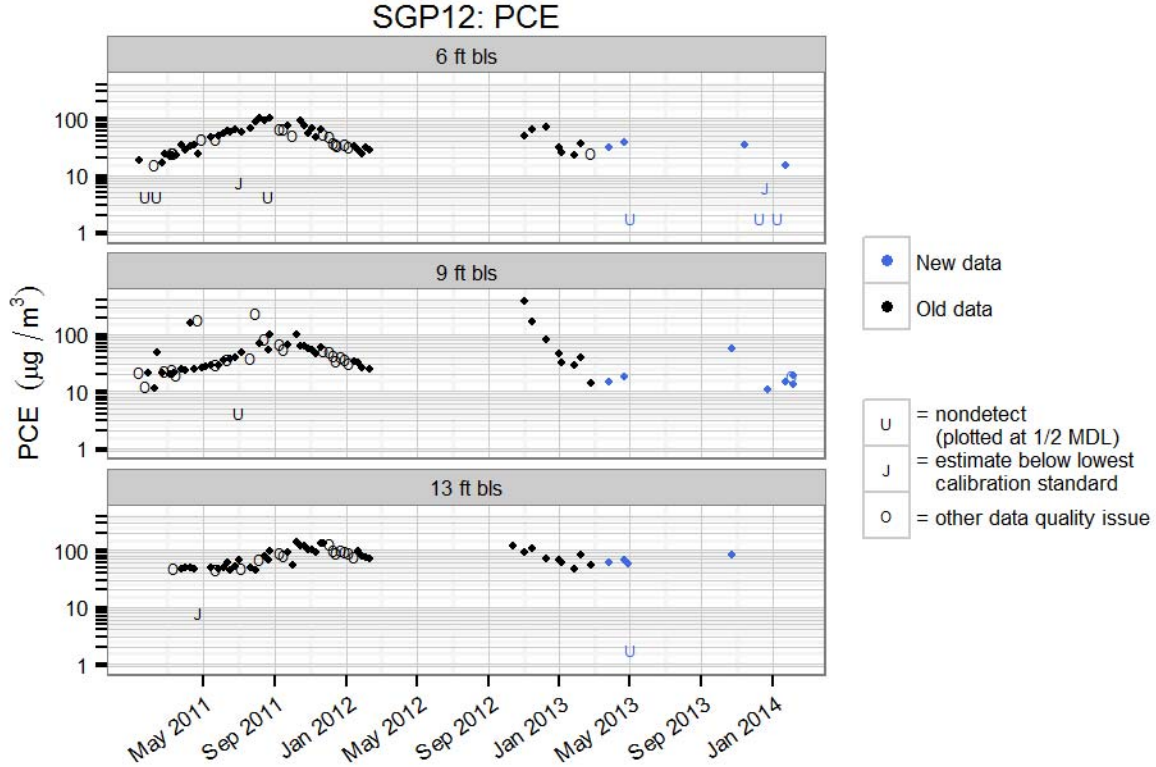


Figure 5-13. PCE at SGP12 on the 420 side of the duplex.

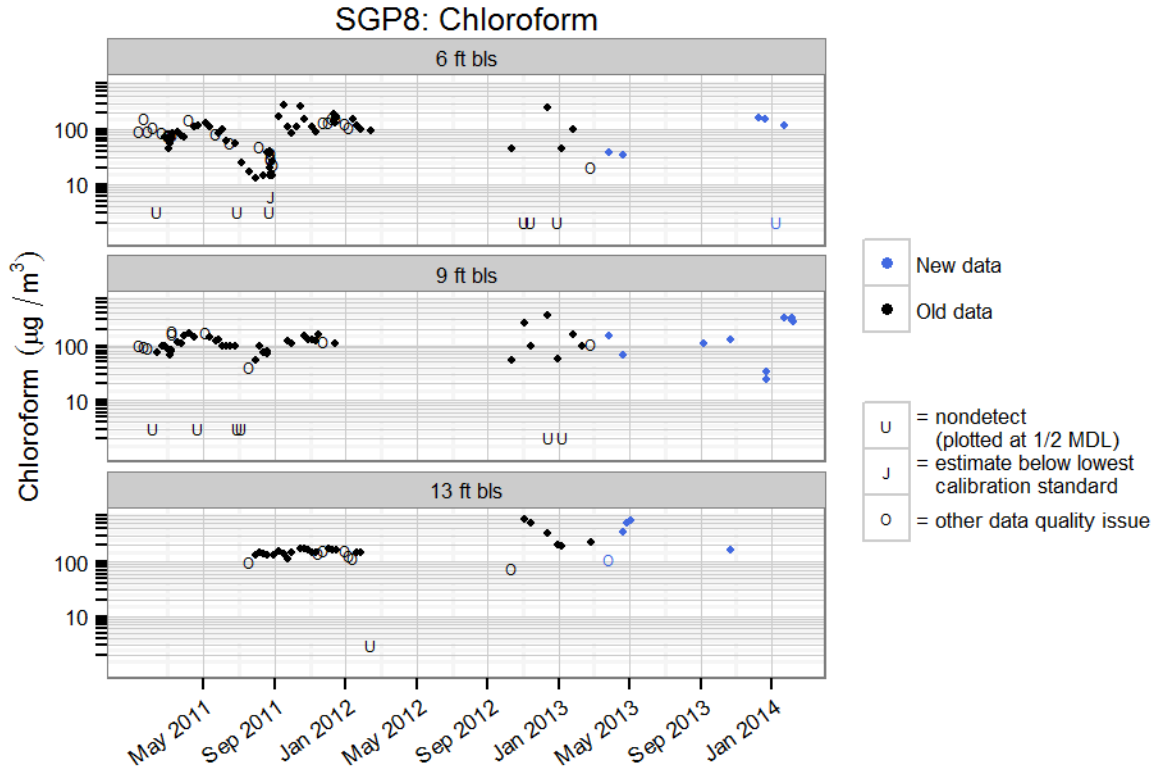


Figure 5-14. Chloroform at SGP8 on the 422 side of duplex.

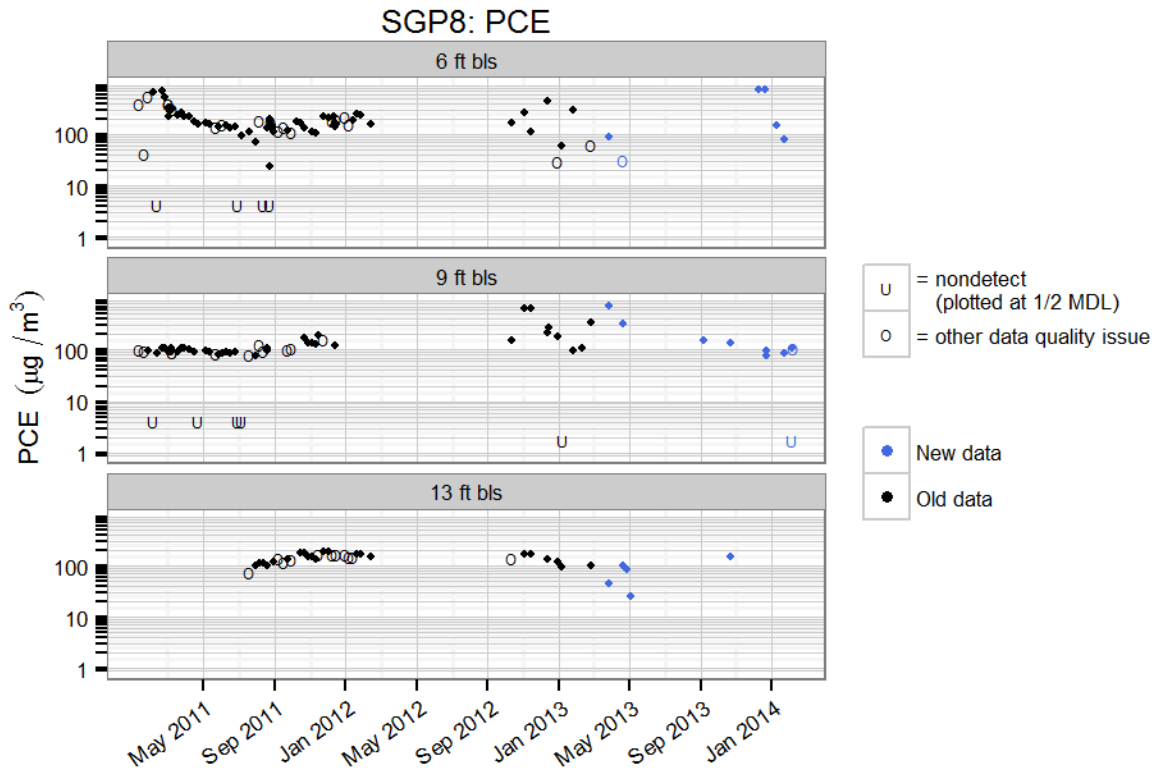


Figure 5-15. PCE at SGP8 on the 422 side of the duplex.

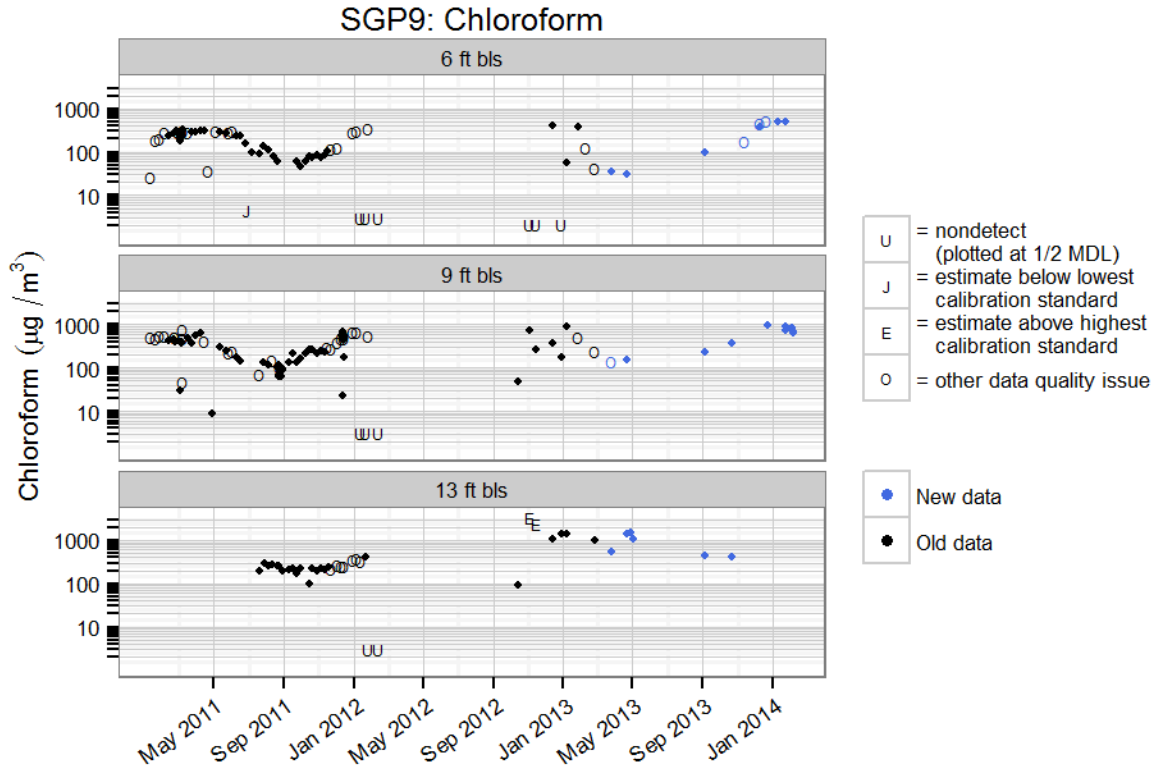


Figure 5-16. Chloroform at SGP9 on the 422 side of duplex.

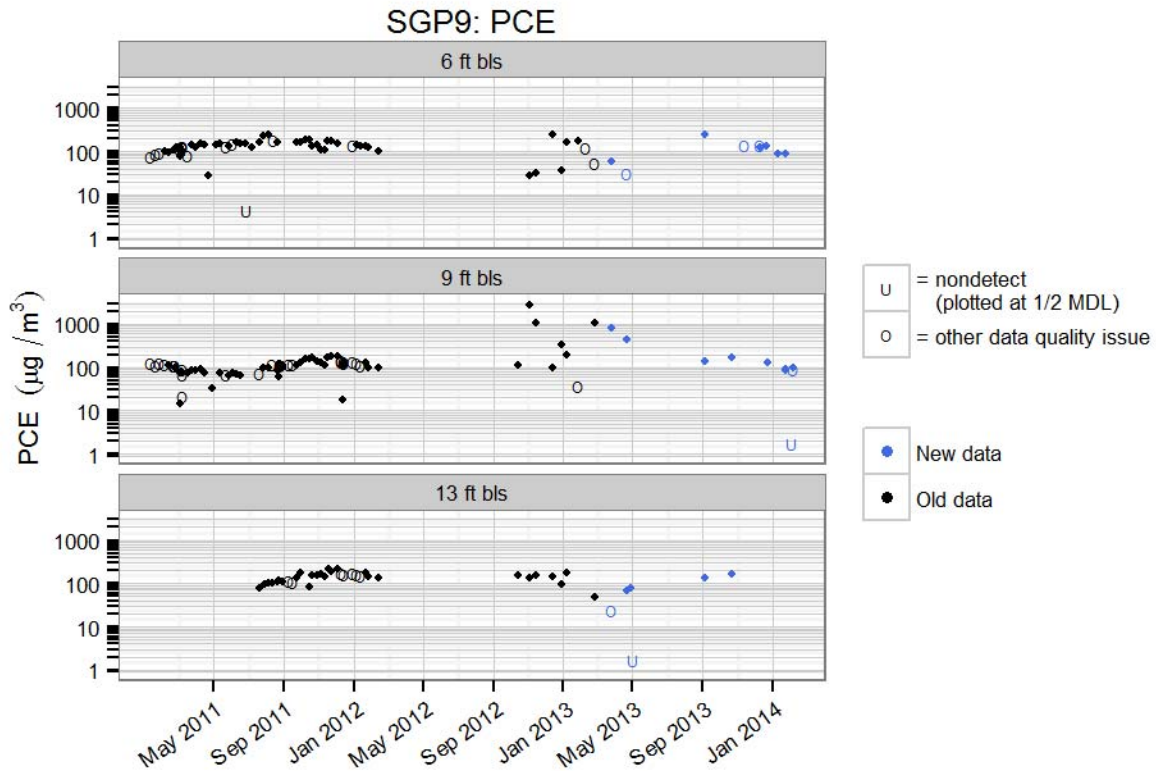


Figure 5-17. PCE at SGP9 on the 422 side of the duplex.

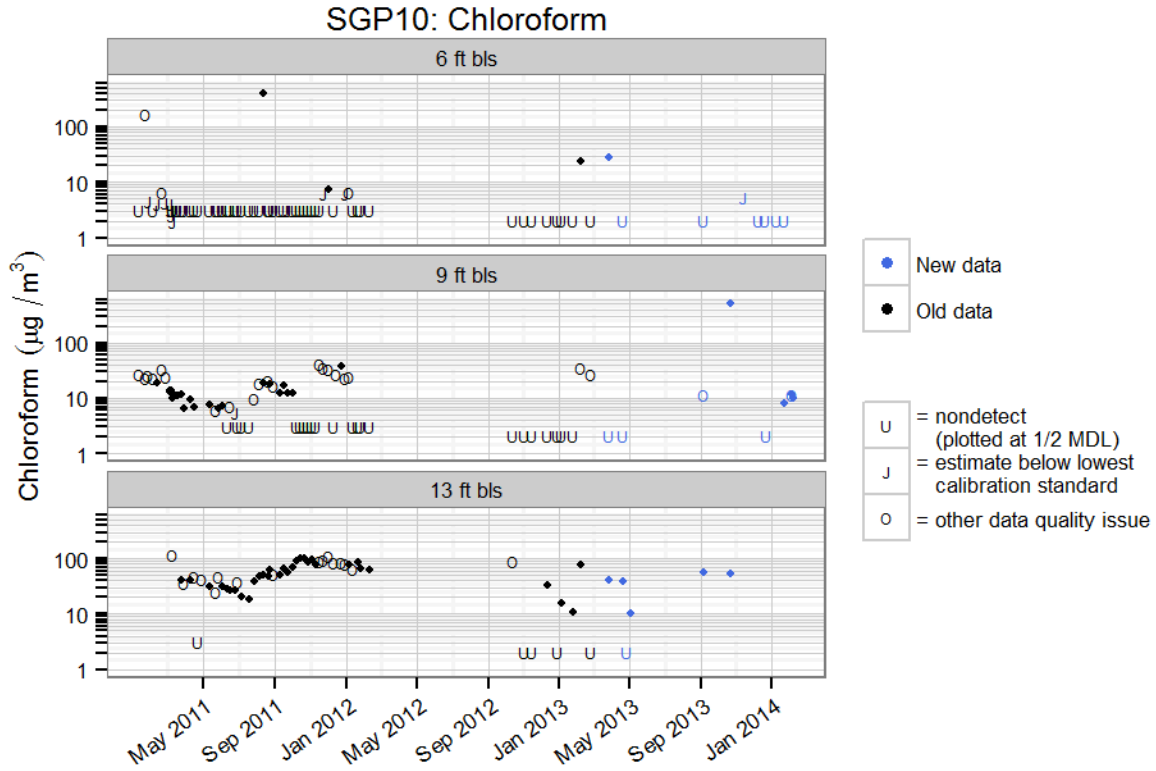


Figure 5-18. Chloroform at SGP10 on the 422 side of duplex.

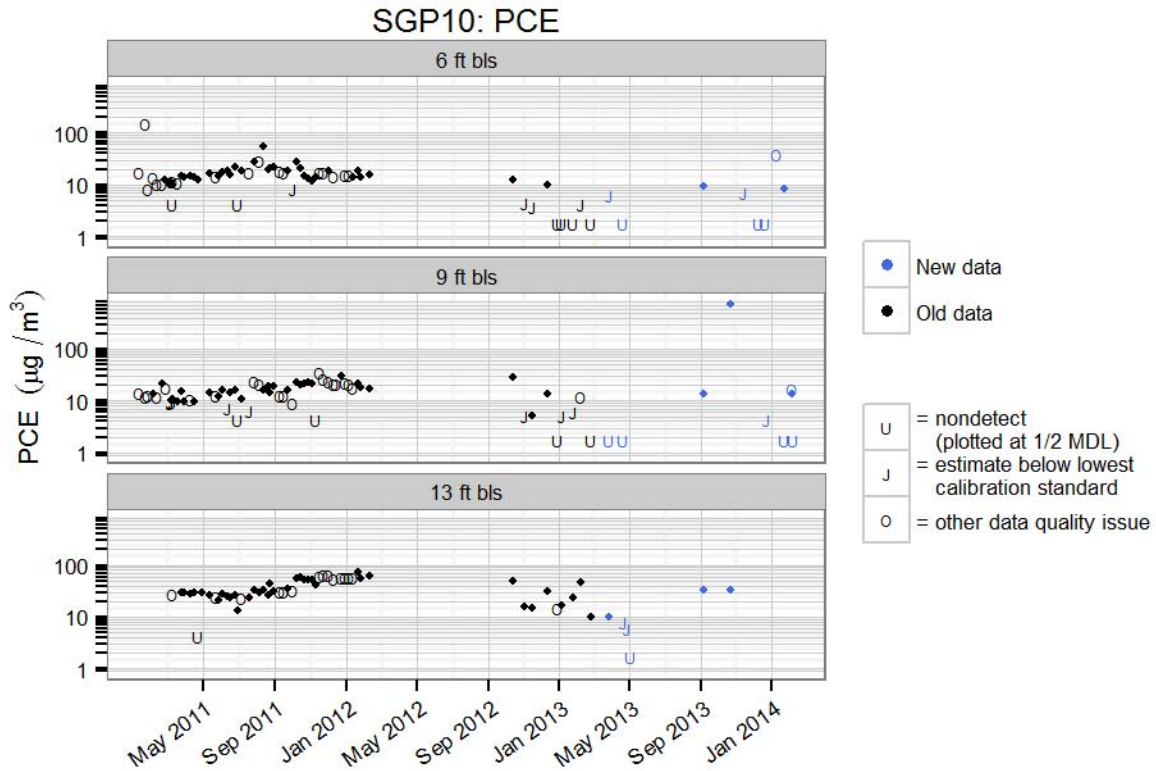


Figure 5-19. PCE at SGP10 on the 422 side of the duplex.

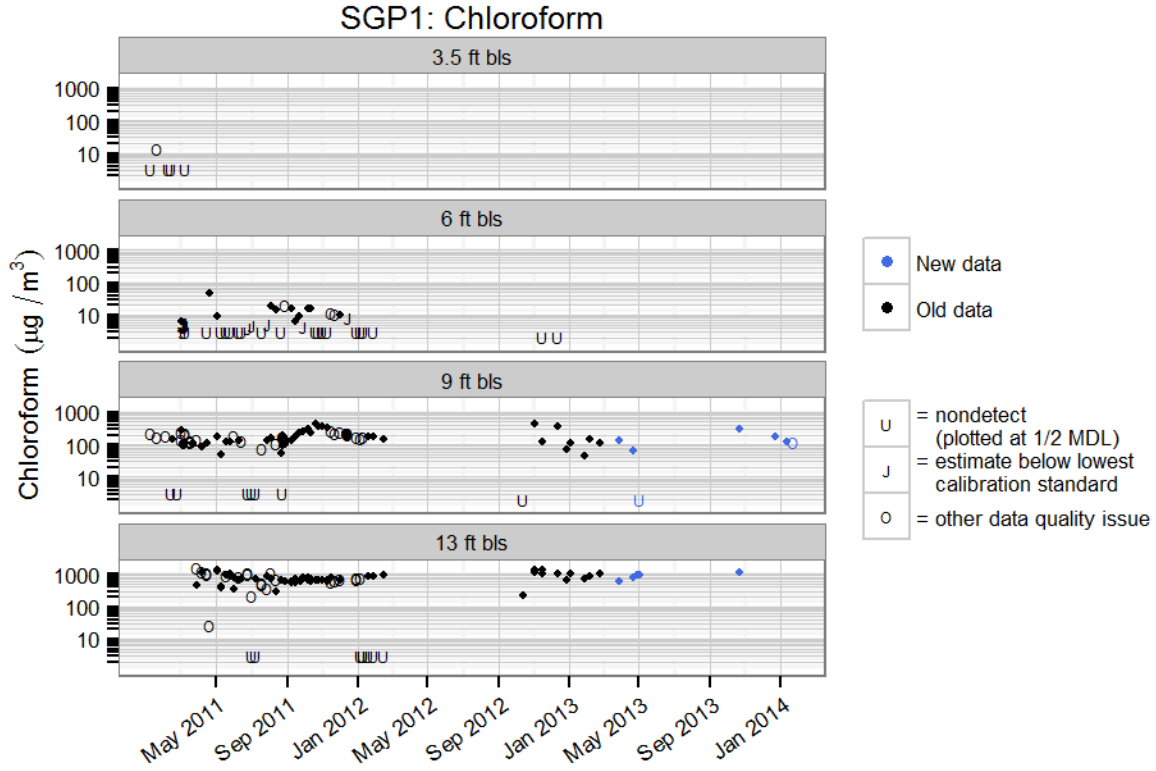


Figure 5-20. Chloroform at SGP1 on the exterior of the duplex.

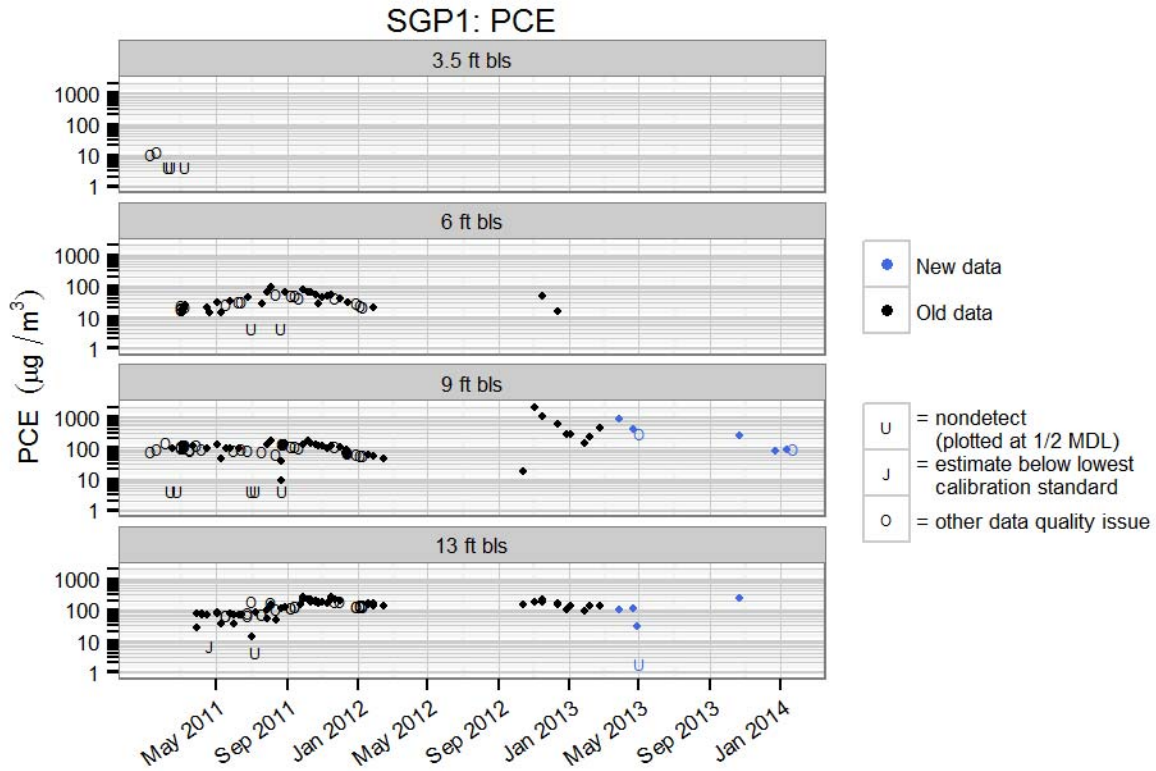


Figure 5-21. PCE at SGP1 on the exterior of the duplex.

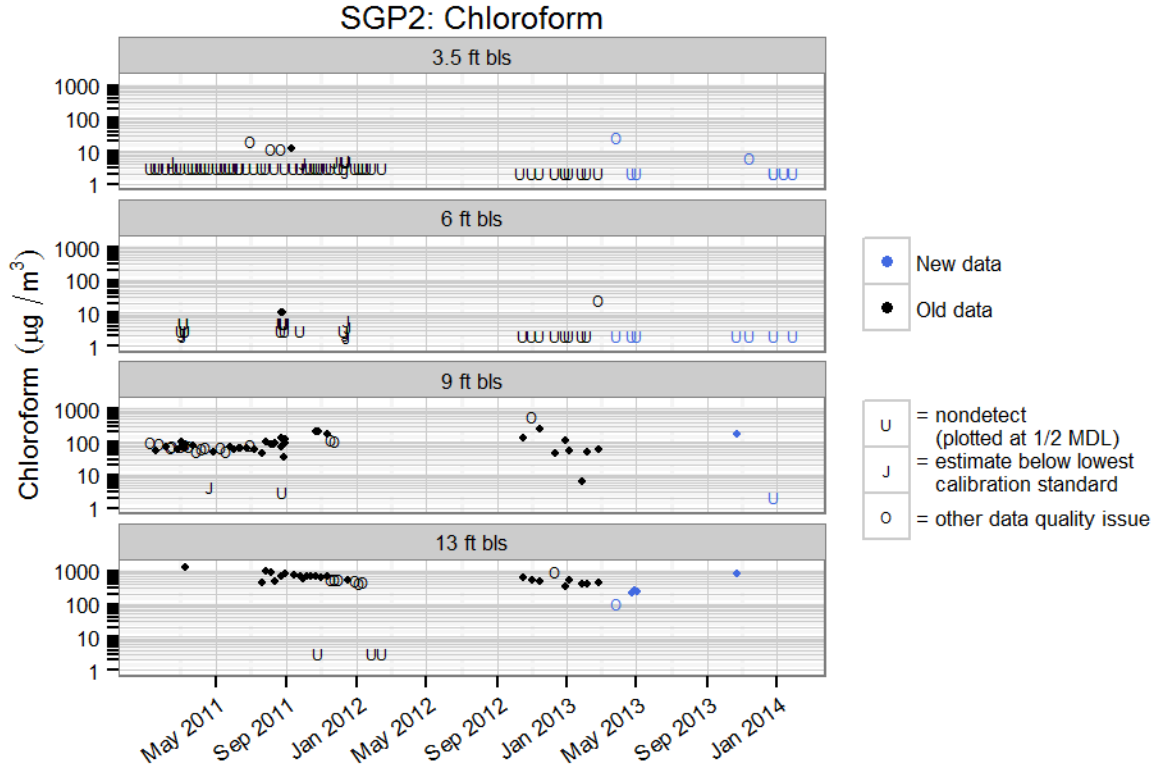


Figure 5-22. Chloroform at SGP2 on the exterior of the duplex.

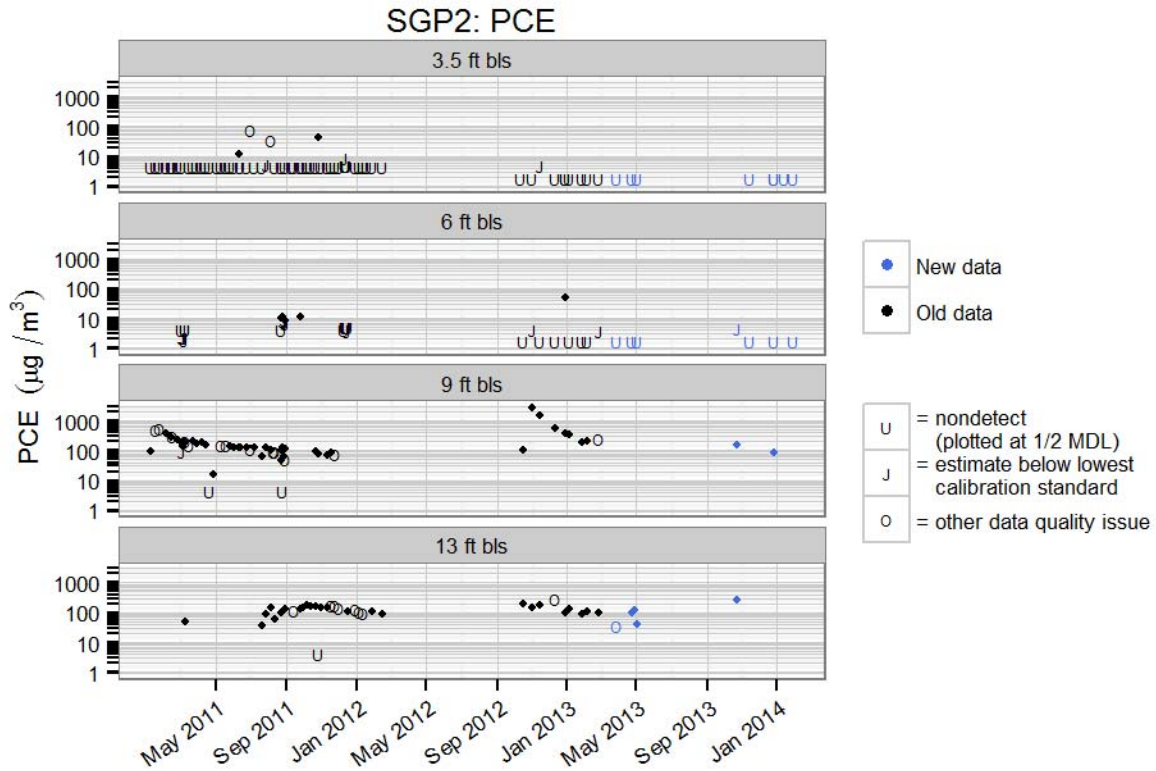


Figure 5-23. PCE at SGP2 on the exterior of the duplex.

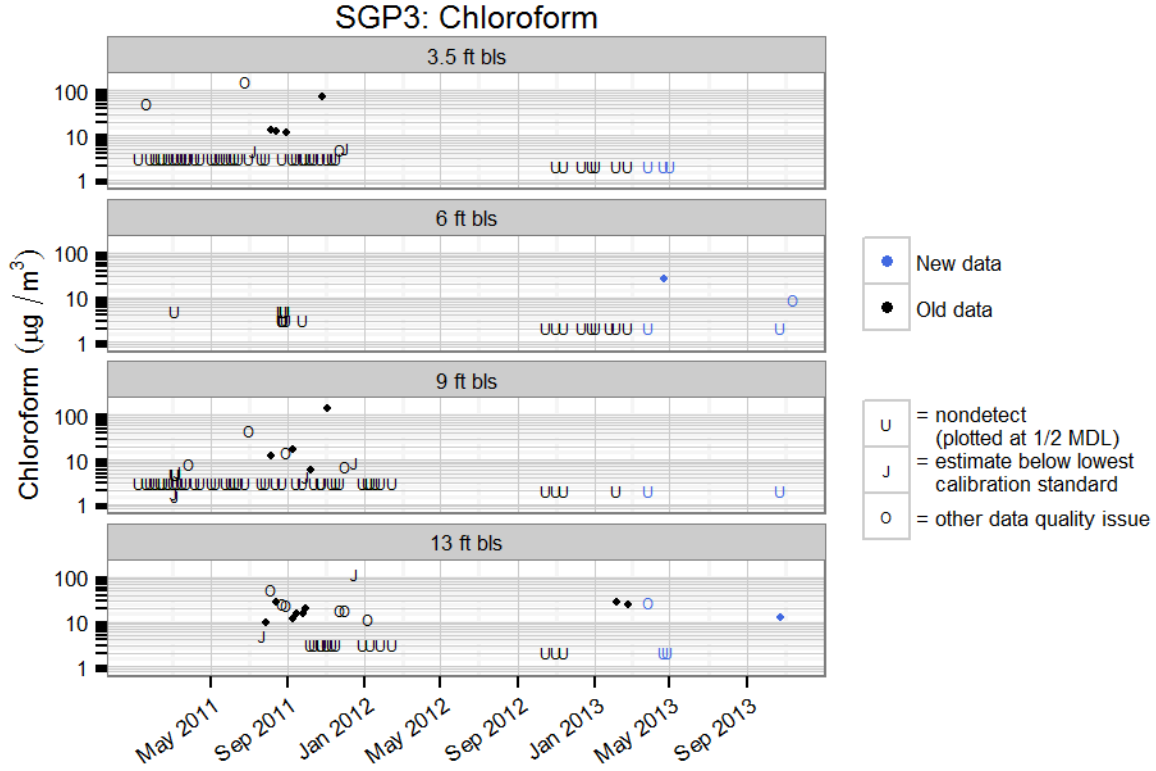


Figure 5-24. Chloroform at SGP3 on the exterior of the duplex.

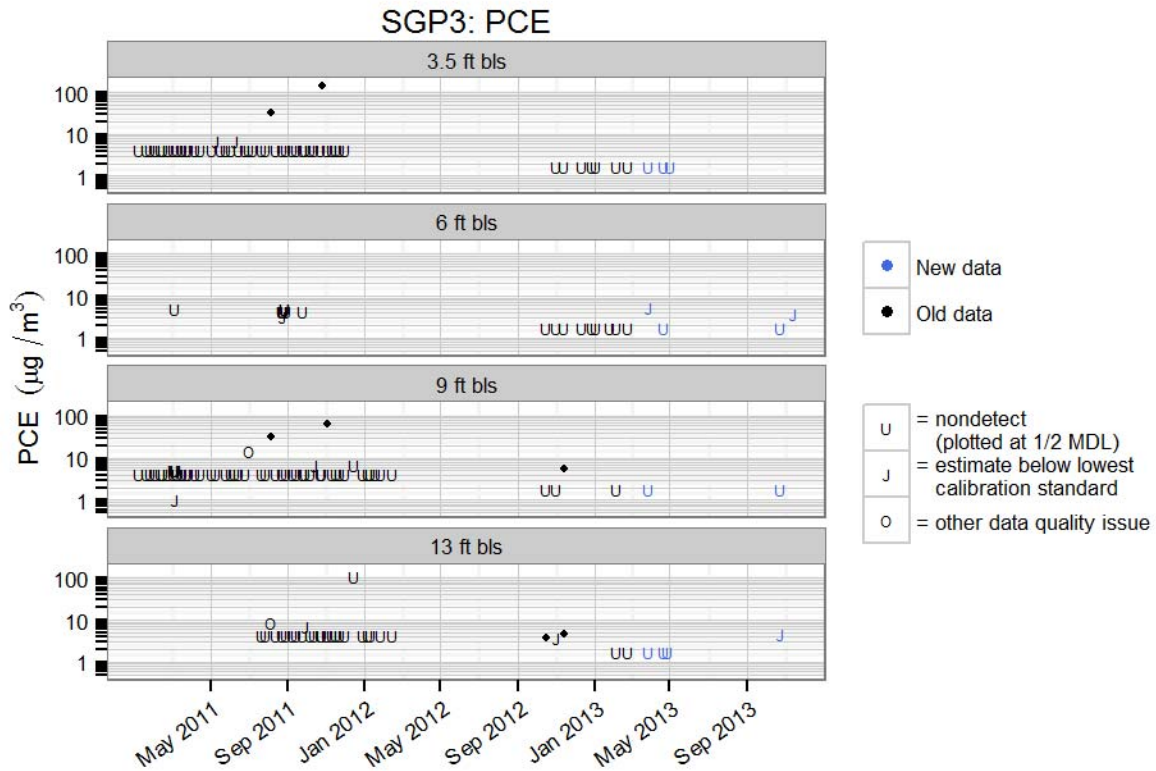


Figure 5-25. PCE at SGP3 on the exterior of the duplex.

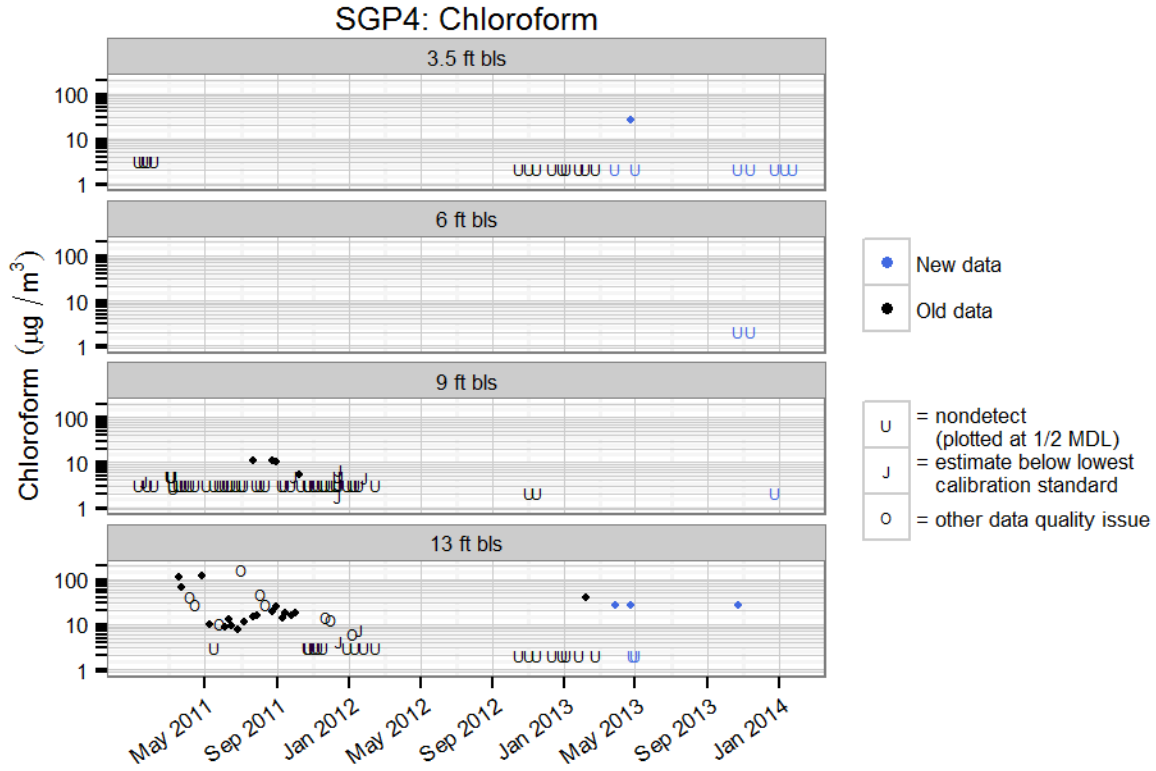


Figure 5-26. Chloroform at SGP4 on the exterior of the duplex.

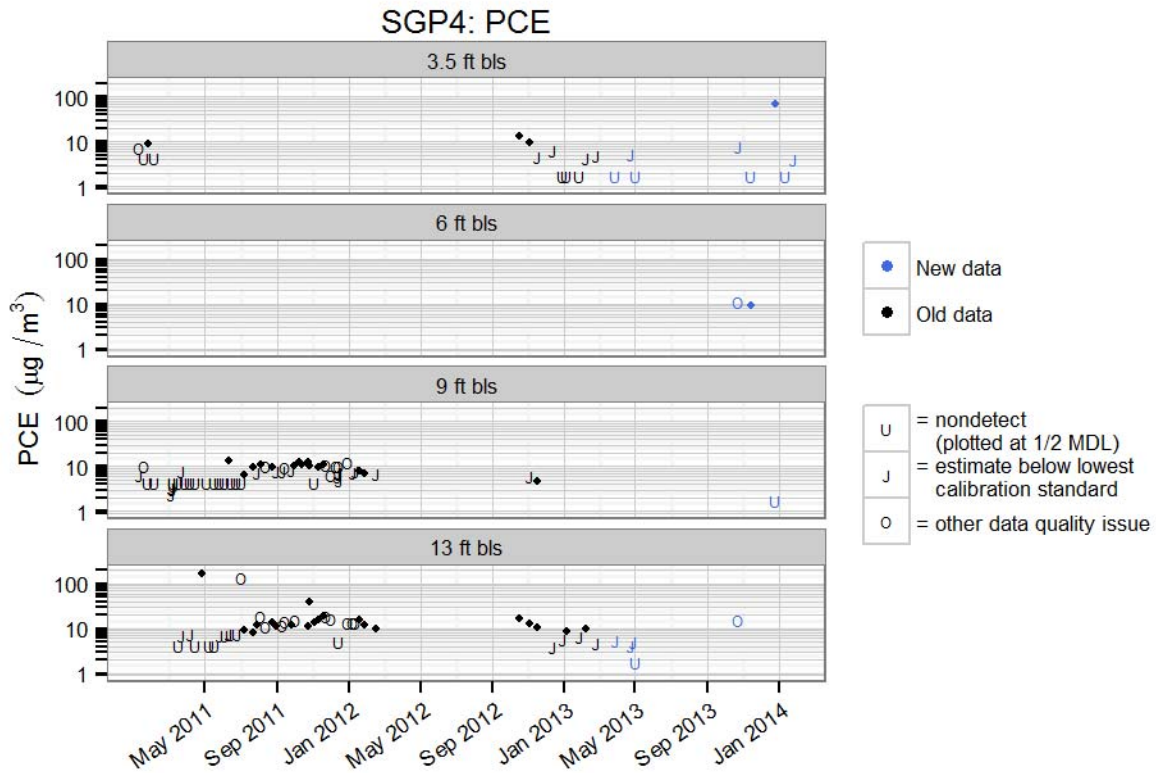


Figure 5-27. PCE at SGP4 on the exterior of the duplex.

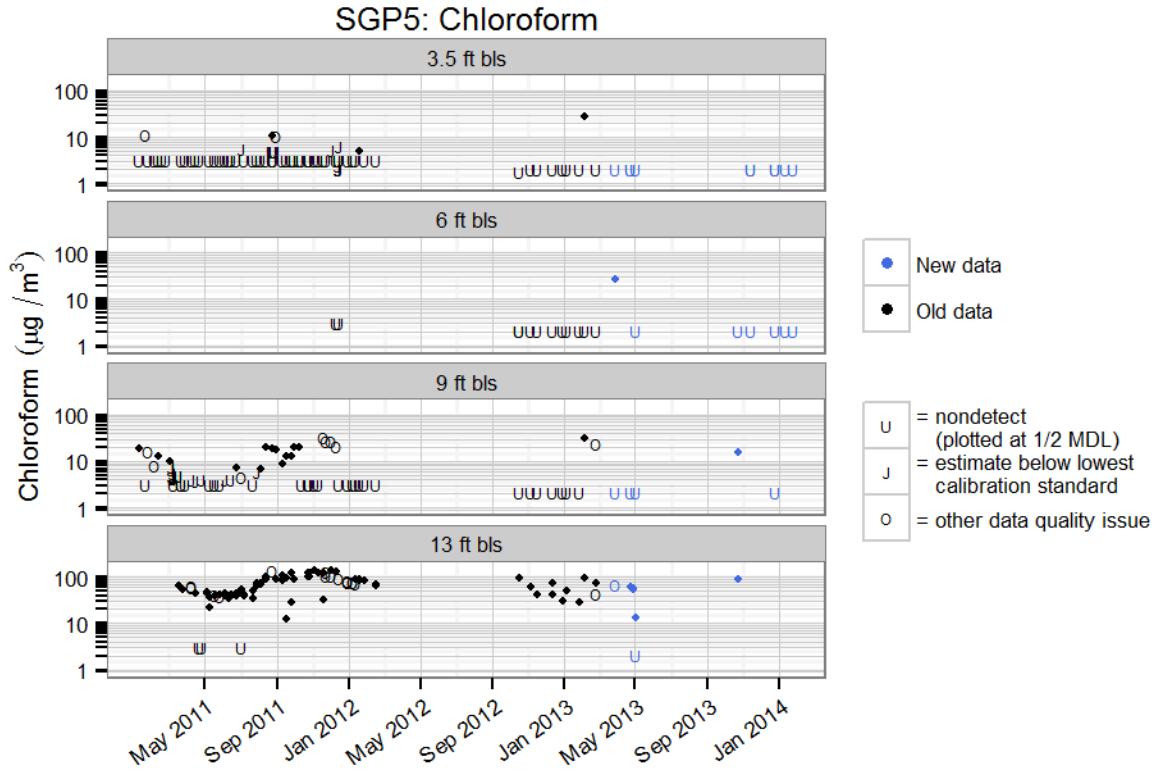


Figure 5-28. Chloroform at SGP5 on the exterior of the duplex.

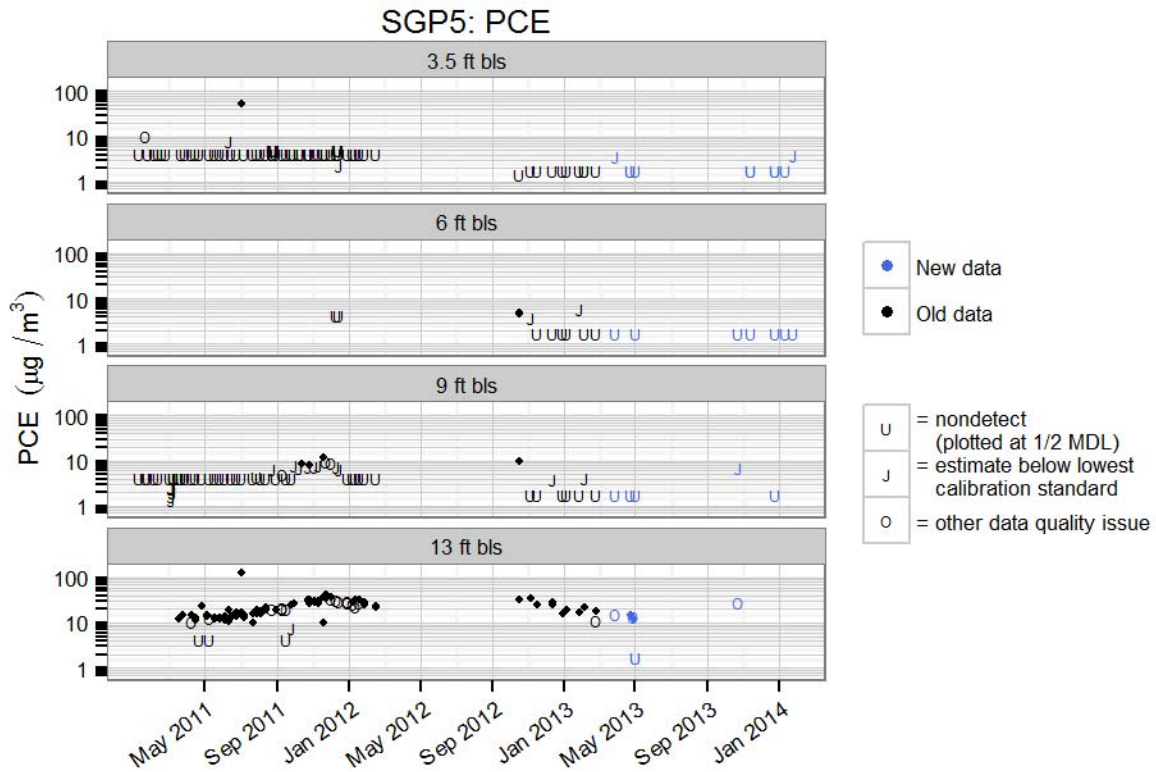


Figure 5-29. PCE at SGP5 on the exterior of the duplex.

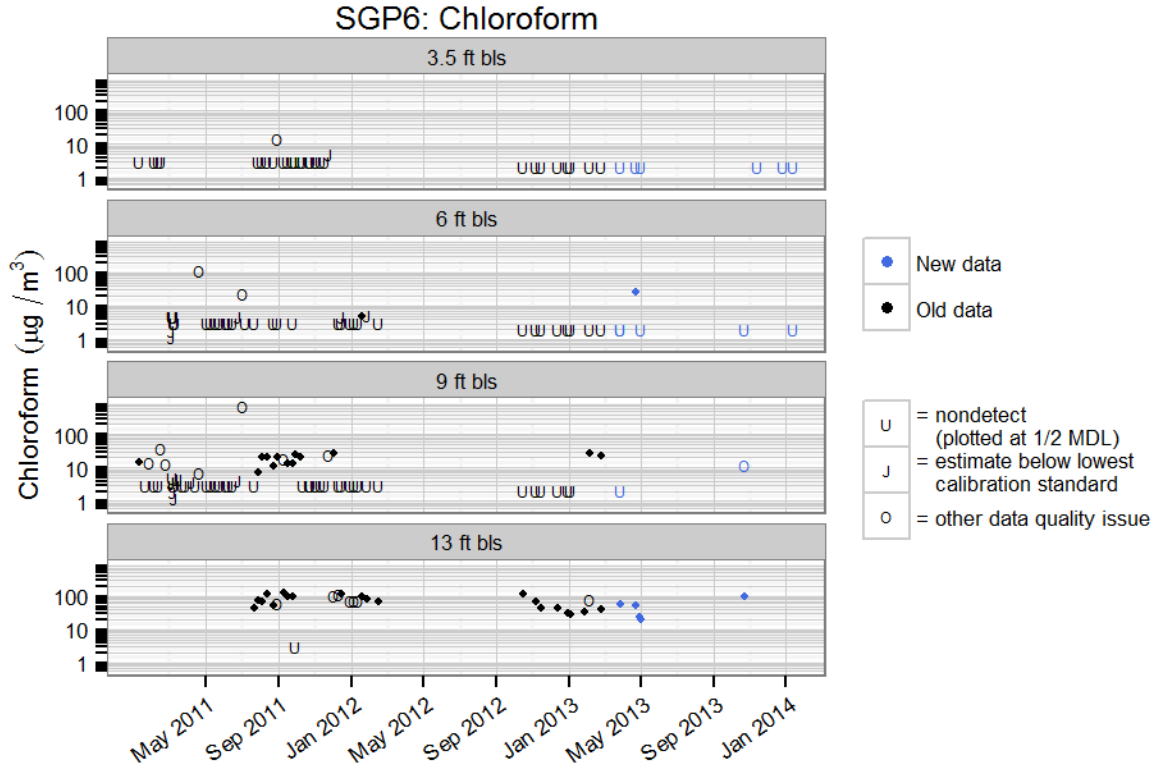


Figure 5-30. Chloroform at SGP6 on the exterior of the duplex.

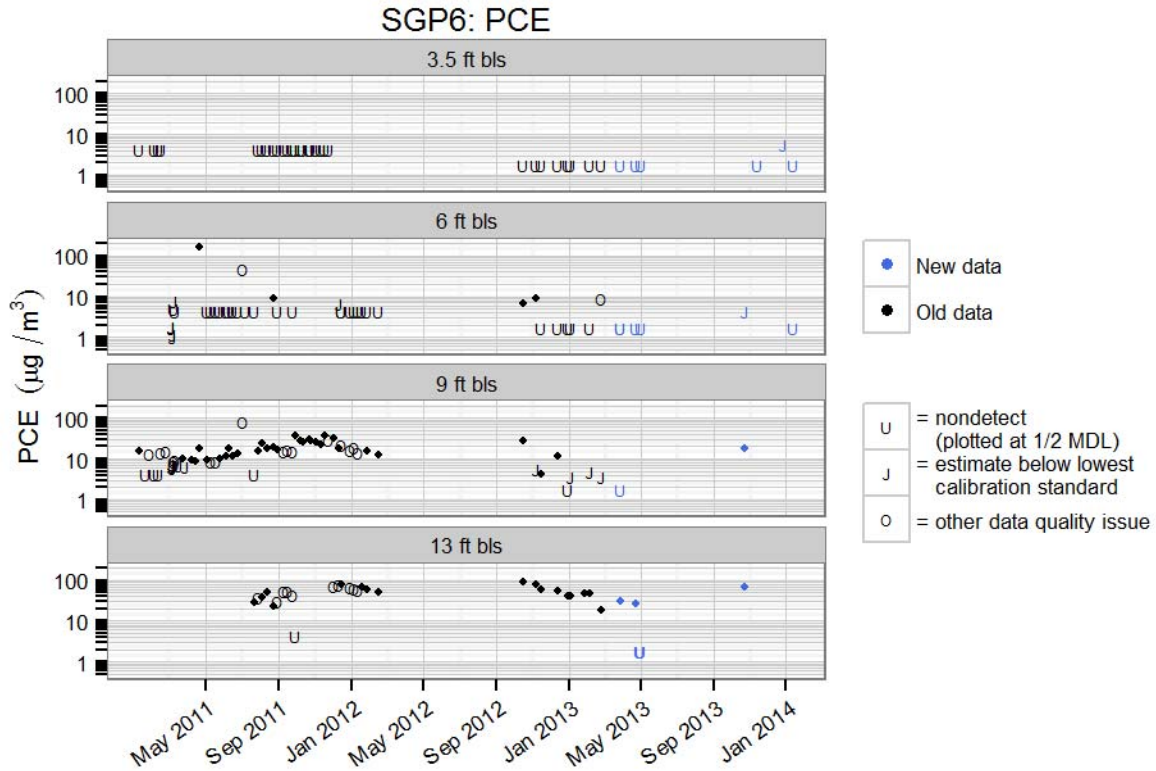


Figure 5-31. PCE at SGP6 on the exterior of the duplex.

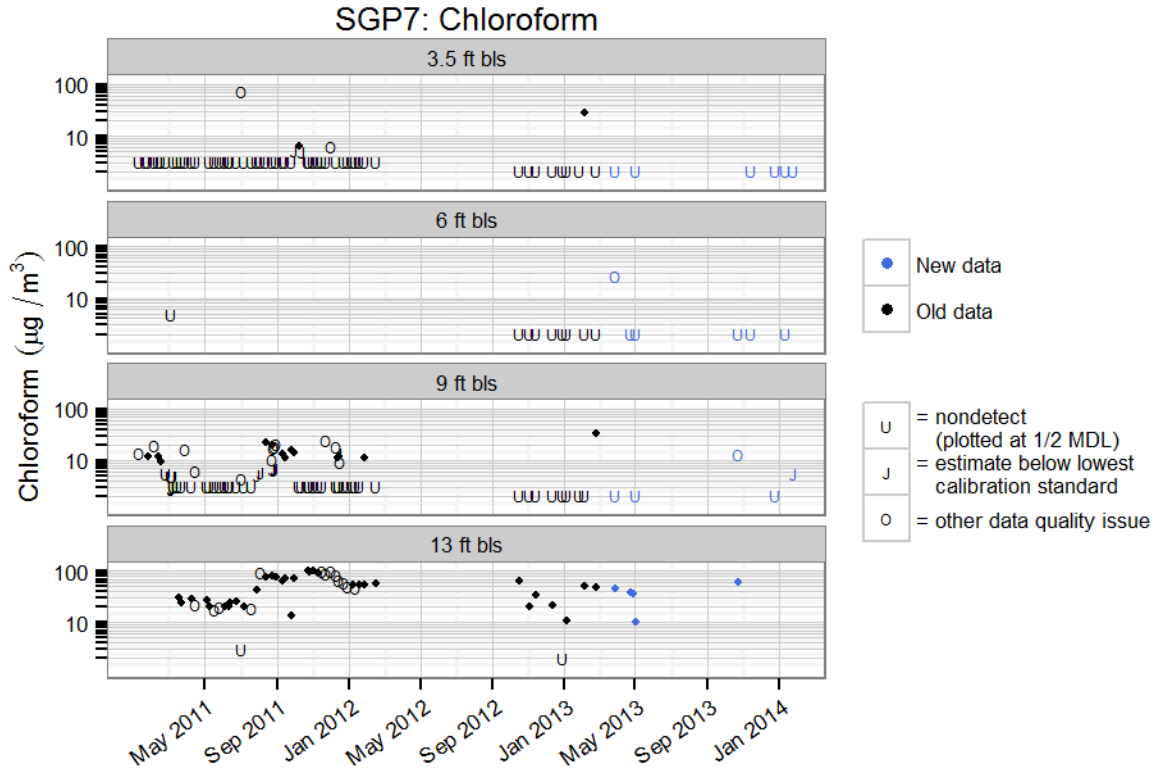


Figure 5-32. Chloroform at SGP7 on the exterior of the duplex.

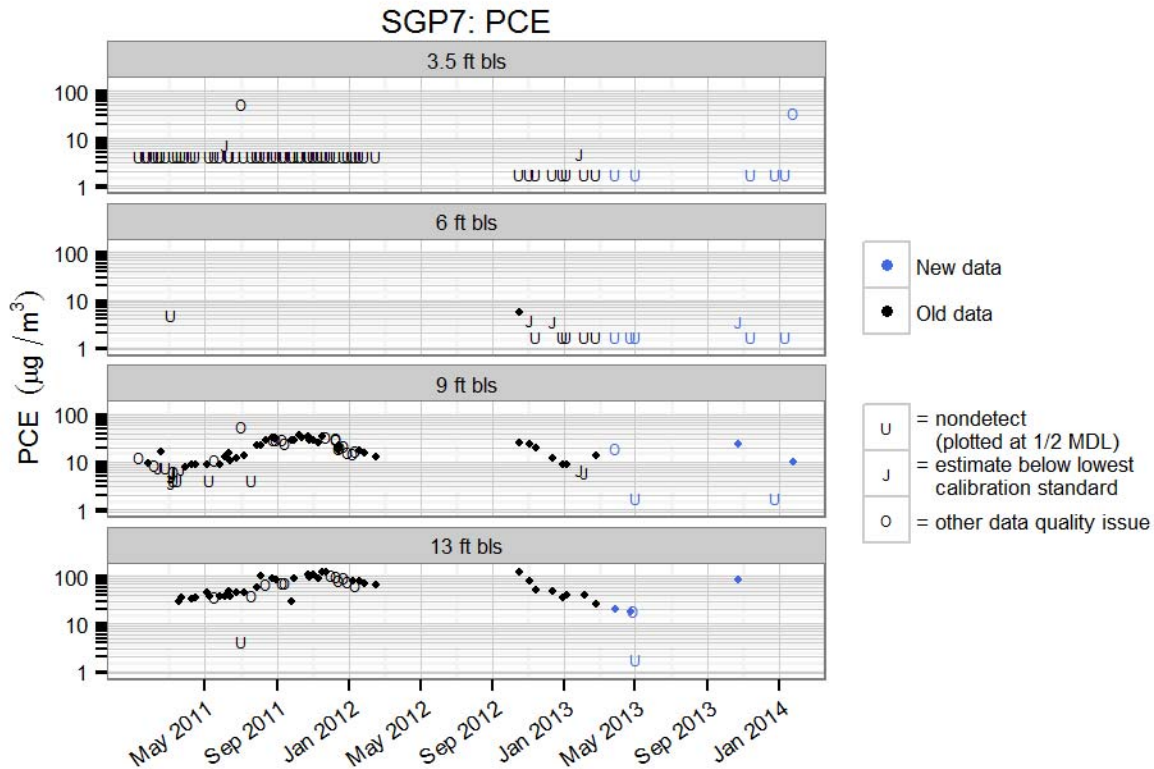


Figure 5-33. PCE at SGP7 on the exterior of the duplex.

Chloroform detections in the central portion of the 420 side of the duplex (SGP-11 [Figure 5-10]) are reasonably frequent at 9 and 13 ft and occur sporadically at 6 ft. SGP-12 (Figure 5-12) on the south side of 420 shows frequent detections at 13 ft and sporadic detections at 6 and 9 ft depths.

PCE detections in soil gas sampled outside of the duplex are most frequent and high in concentration south of the duplex at SGP-1 and SGP-2 (Figures 5-21 and 5-23) with the highest levels at 9 and 13 ft. Detections are rarer at 6 ft and almost nonexistent at 3.5 ft, suggesting the influence of volatilization. The highest concentrations at these locations at 9 ft occurred near the end of 2012, contemporaneous with initial SSD operation. Concentrations observed in the winter of 2013-2014 are similar to those observed in 2011 and early 2012, suggesting a relatively consistent deep source strength at these locations. Cluster SGP-7 (Figure 5-33) west of the duplex shows a similar pattern to clusters south of the duplex. PCE was rarely detected east of the duplex at any depth. North of the duplex (SGP-5 and SGP-6) detections are generally confined to the 13 ft depth with detections at 9 ft occurring frequently in SGP-6 but not SGP-5.

PCE on the 422 side of the duplex is generally detectable in the central (SGP-8; Figure 5-15) and southern (SGP-9; Figure 5-15) soil gas ports at all three depths sampled beneath the house (6, 9, and 13 ft). The relatively high PCE soil gas concentration at 6 ft in SGP-8 beneath the central portion of the duplex contrasts with the rare detections in the 6 ft soil gas probes exterior to the duplex¹⁰ suggesting a capping effect of the structure. The high peak concentration at SGP-8—6 ft observed in early 2011—was not replicated until the winter of 2013–2014 (Figure 5-15). This suggests that year-to-year differences in soil gas concentrations can be substantial. The 2013–2014 observations also support our contention that the high concentrations observed in early 2011 were not artifacts. Concentrations are substantially lower and less frequently detectable at SGP-10 on the northern side of 422 (Figures 5-18 and 5-19).

PCE in soil gas on the 420 side of the duplex (SGP-11 [Figure 5-11] and SGP-12 [Figure 5-13]) has a moderate frequency of detection at three depths (6 ft, 9 ft, and 13 ft). A regular seasonal pattern is suggested in these clusters with peak concentrations in late fall/early winter.

5.2 Radon Seasonal Trends (based on Weekly Measurements)

Please see Section 5.2 of U.S. EPA (2012a) for a complete discussion of radon trends in the duplex, based on the 2011–2012 data, and Section 5.2 of U.S. EPA (2013) for a discussion of the effects of the mitigation system on radon concentrations. The periodic operations of the mitigation system, while having dramatic short-term effects in reducing radon, appear to have not changed the long-term concentrations observed in periods when the system was not on. Figure 5-34 shows the complete record of weekly electret radon measurements from the start of the study through March 5, 2014. Except for very low concentrations during the periods when the mitigation system was on, radon concentrations remain fairly consistent at indoor electret locations sampled during the entire study period, although the radon levels observed following mitigation system shutdown in May 2013 were a little higher than those measured prior to mitigation system installation.

5.3 VOC Sampling with the FROG 4000 Unit and TO-17 and Passive Samplers

From February 3, 2014 through March 6, 2014, a series of comparisons were performed to evaluate the performance of the FROG 4000 porGC unit manufactured by Defiant Technologies (Defiant). These units were originally designed for field analysis of VOCs in water and soil samples but were later modified to analyze air samples as well.

¹⁰ Exterior soil gas probes include SGP-1 (Figure 5-21), SGP-2 (Figure 5-23), SGP-3 (Figure 5-25), SGP-5, Figure 5-29), SGP-6 (Figure 5-31), and SGP-7 (Figure 5-33).

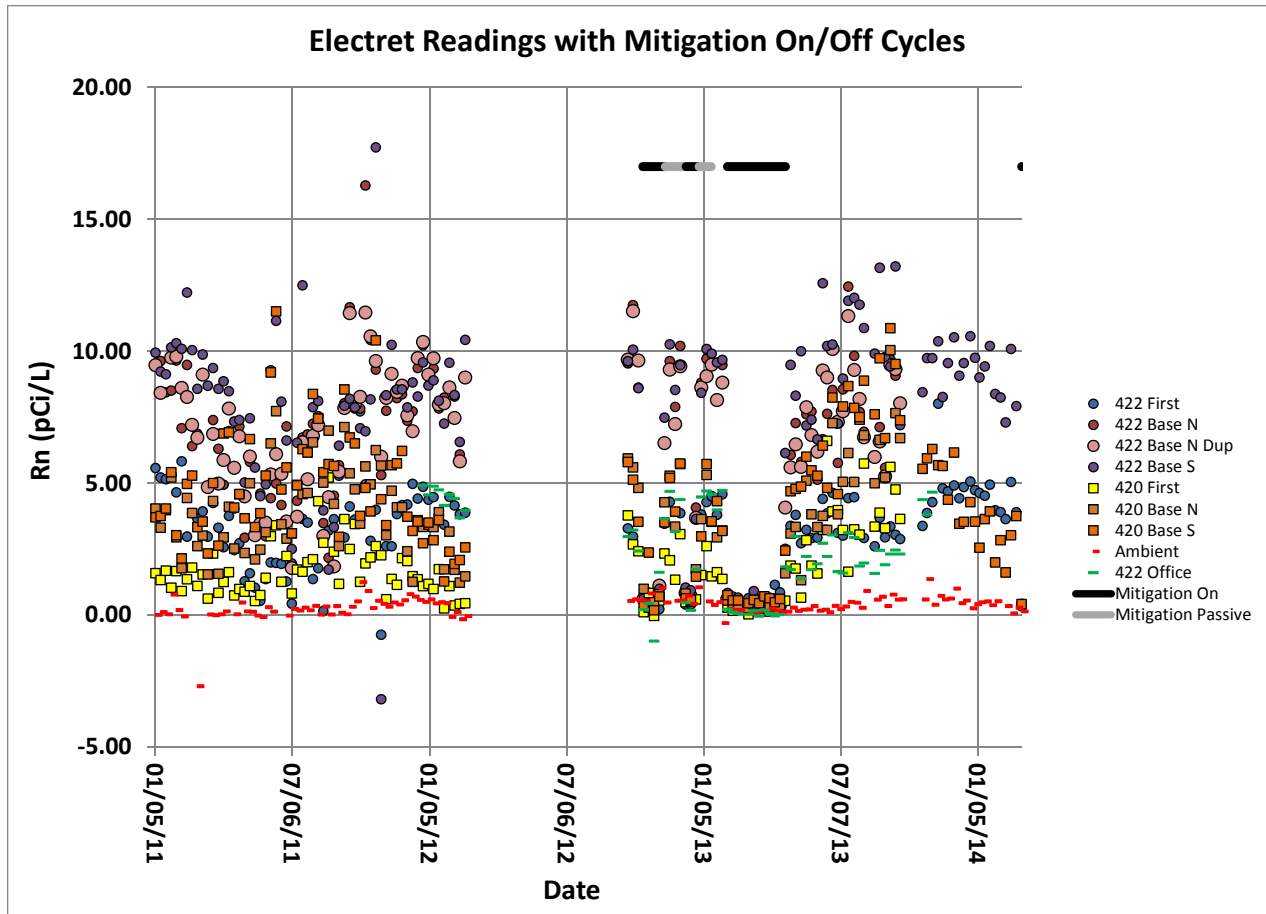


Figure 5-34. Radon: Weekly time integrated samples (electret).

Two units were used in the performance evaluation. One was set up to be an indoor air sampler in 422 basement south, next to the passive sampler rack and AlphaGUARD for that basement section (FROG unit #21). This unit ran nearly continuously from February 3, 2014, through March 6, 2014. Several SKC 575 Ultra III badges and Radiello passive samplers were set out for comparison to this FROG unit’s results. The other GC (FROG unit #22) was used to sample a series of indoor soil gas locations, which were also sampled and measured by the TO-17 method. Additionally, a comparison was made between the FROG and the TO-17 method by sampling Tedlar bags with PCE of predetermined concentrations provided by Eurofins Air Toxics. Water samples were taken at some of the 422 house monitoring wells. A comparison of the FROG’s water sampling capabilities was made by testing samples from the wells with the FROG in addition to sending samples to the EPA lab. PCE was the primary VOC measured in these studies, because the FROG 4000 does not analyze for chloroform.

5.3.1 Indoor Air Test of FROG 4000 Against Passive VOC Samplers

The indoor air test between the FROG 4000 unit and passive VOC samplers occurred from February 3–March 6, 2014. During this time, passive Radiello samplers were changed four times on their regular weekly schedule, with stop dates of February 12, February 19, February 26, and March 5, 2014. SKC Ultra III badges, were only deployed during brief periods, either as an additional comparison or to supplement testing during a weather event. The SKC Ultra III badges ran from February 3–7, February 4–7, February 7–10, and February 12–14, 2014.

Due to malfunctions in the FROG software, the program that recorded data from the stationary FROG periodically shut down resulting in a loss of data until the program was restarted by the onsite operator. This issue required a software upgrade that was completed on February 26, 2014, and the issue did not reoccur after that. However, the PID lamp in the stationary FROG malfunctioned on March 2, 2014, resulting in a loss of data until March 6 when the unit was returned to Defiant. Because of these periodic stoppages, the stationary FROG only ran for only a portion of the times it was in place against the Radiellos or SKC badges. For the four Radiello sampler periods, the FROG recorded data for 58%, 62%, 84%, and 49% of the Radiello sample periods. For the four SKC badge periods, the FROG recorded data for 87%, 100%, 0%, and 86%, respectively.

Because the FROG only ran continuously for one of the passive sampler periods tested, we did not have a full FROG record to compare to passive sampler results. Not surprisingly, Radiello and FROG results show better agreement the longer the FROG ran continuously during the passive sample period (**Figure 5-35**). However, this better agreement was not exhibited in the SKC badge comparisons, with the period during which the FROG and the SKC badges were in place 100% of the time having the greatest difference in concentrations (**Figure 5-36**). The passive indoor air samplers and the FROG compared generally well, with the FROG consistently underestimating the passive sampler results. In spite of the FROG not running for the full passive sampler time, agreement was good between the FROG and Radiello results, with the FROG being a factor of 1.1 to 2.2 below the Radiello. For the SKC badge samplers, the SKC badges were 2.2 to 4.4 times higher than the FROG results over the same period.

A generally downward VOC concentration trend over time was present in both the passive sampler and FROG results for indoor air. Also, SKC badge and Radiello passive samples were always higher than the FROG measurements. One possible explanation for this observation is that the continuous passive sample measurements could have captured short high concentration peaks that may have been missed by the intermittent short duration FROG point samples.

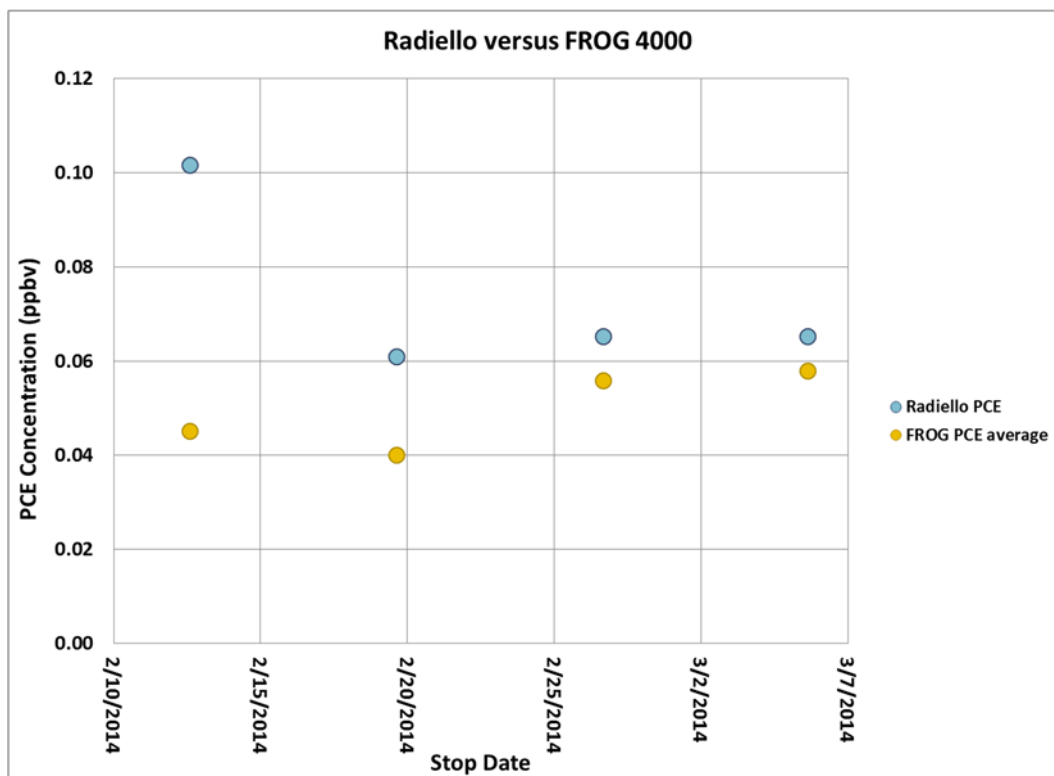


Figure 5-35. Radiello indoor air PCE data versus FROG indoor air PCE data.

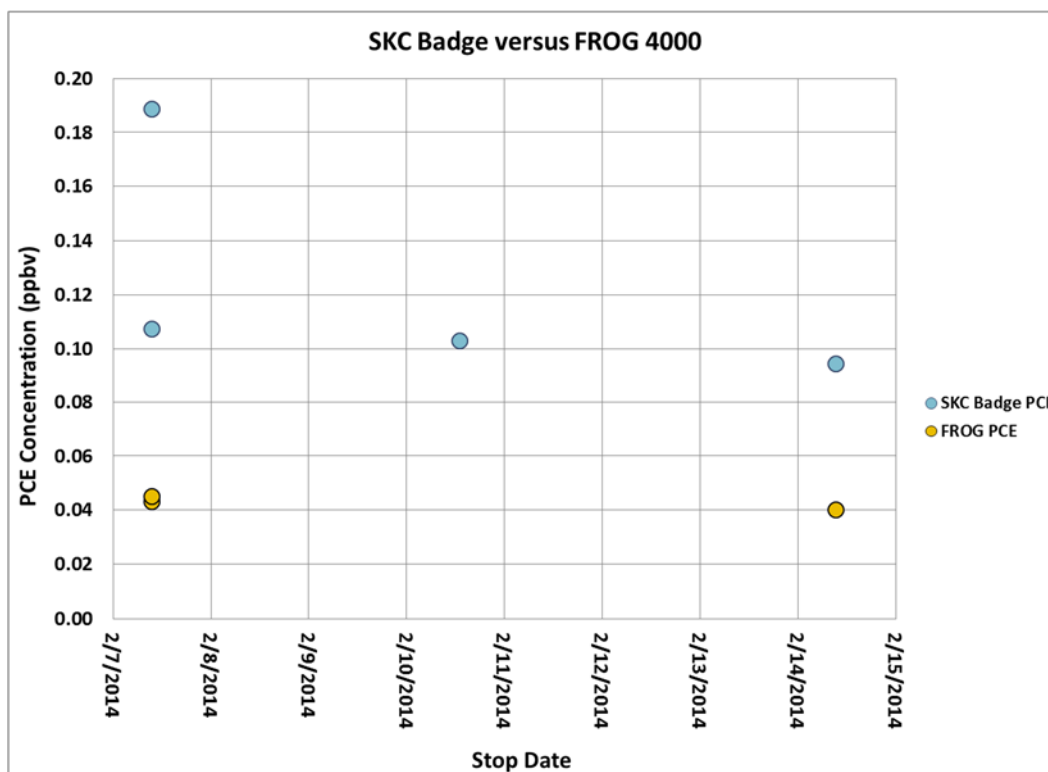


Figure 5-36. SKC badge indoor air PCE data versus FROG indoor air PCE data.

5.3.2 Subsurface Soil Gas Data by the FROG and TO-17

Between February 3 and 7, 2014, subsurface soil gas was sampled by the FROG 4000 and the conventional (TO-17) method at the several subslab ports (SSP-1, SSP-2, SSP-3, SSP-4, SSP-5, SSP-6, SSP-7, and SSP-8), wall ports (WP-1, WP-2, WP-3, and WP-4), and 9-ft bls soil gas probes (SGP8-9, SGP9-9, SGP10-9, SGP11-9, SGP12-9) in the basement of the 422 side of the duplex.¹¹ During this “mini-intensive” period, samples were taken two to three times a day from the locations listed above, with sample times roughly corresponding to morning, early afternoon, and late evening. FROG and TO-17 samples were taken simultaneously during each morning, afternoon, and evening period for at least three of the days. Simultaneous samples were taken with the FROG and the TO-17 tube connected to the ends of a double-ended sampling train.

Data from the FROG 4000 versus TO-17 sampling rounds are plotted in **Figures 5-37** through **5-44**, with simultaneous sampling events plotting above and/or below each other. The difference between the FROG and TO-17 results ranged from 0.87 ppb to 22 ppb, but in general the results agreed within a factor of 2. Unlike the indoor air comparisons, the FROG was not consistently higher or lower than the TO-17 measurements, although the reason for this difference in bias consistency is not known. Both FROG and TO-17 soil gas results show a slight downward trend in **Figures 5-40** (SGP11-9) and **5-41** (SGP12-9) and an upward trend in **Figure 5-42** (SSP1) but otherwise do not appear to exhibit consistent trends over time. Looking across the repeated FROG PCE measurements shown in **Figures 5-37** through **5-44**, short-term (1-week) temporal variability in the subslab and 9 ft bls soil gas ports from the repeated FROG measurements is generally within a factor of 5. Spatially the FROG 9 ft soil gas measurements vary from a low of less than 1 ppbv in SGP10-9 (**Figure 5-39**) to a high of 24 ppbv in SGP8-9 (**Figure 5-37**). The

¹¹ Note that several locations with VOC nondetects for the TO-17 samples are not included in this comparison.

subslab FROG measurements vary from a minimum of less than 1 ppbv in **Figure 5-44** to a maximum over 50 ppbv in SSP-1 (**Figure 5-42**).

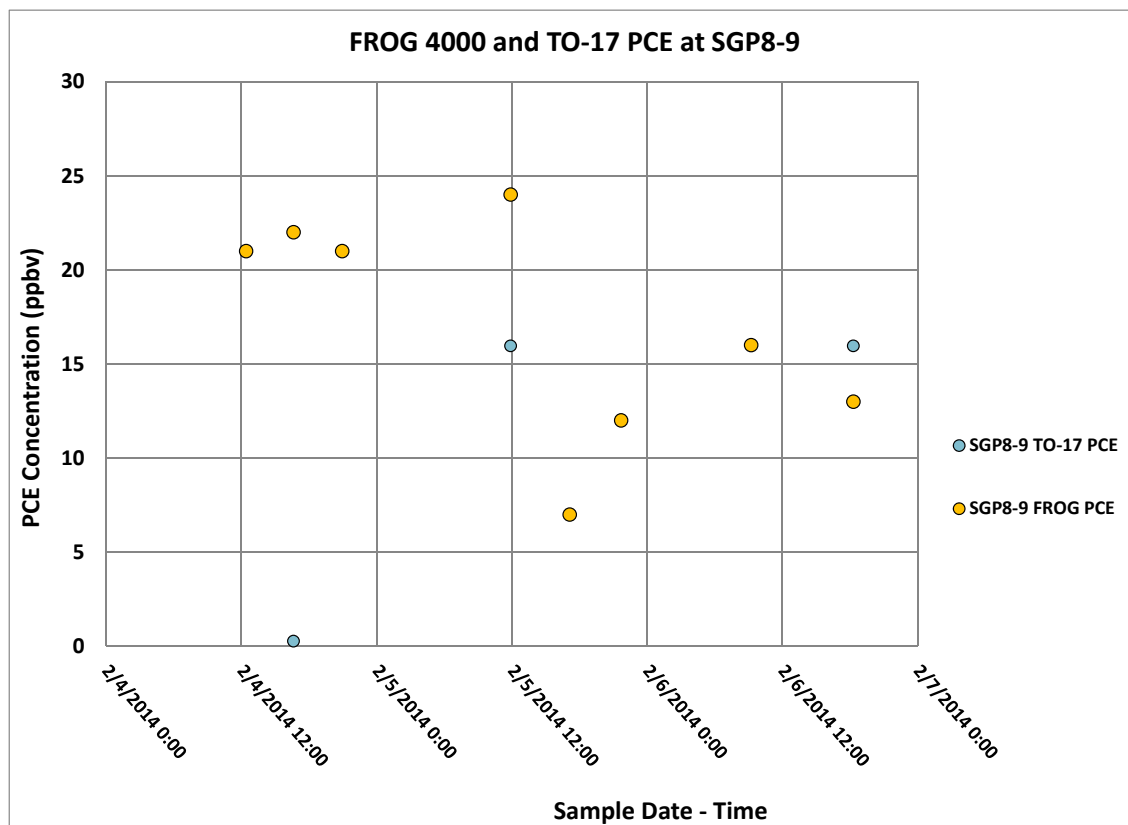


Figure 5-37. FROG 4000 and TO-17 PCE data at SGP8-9.

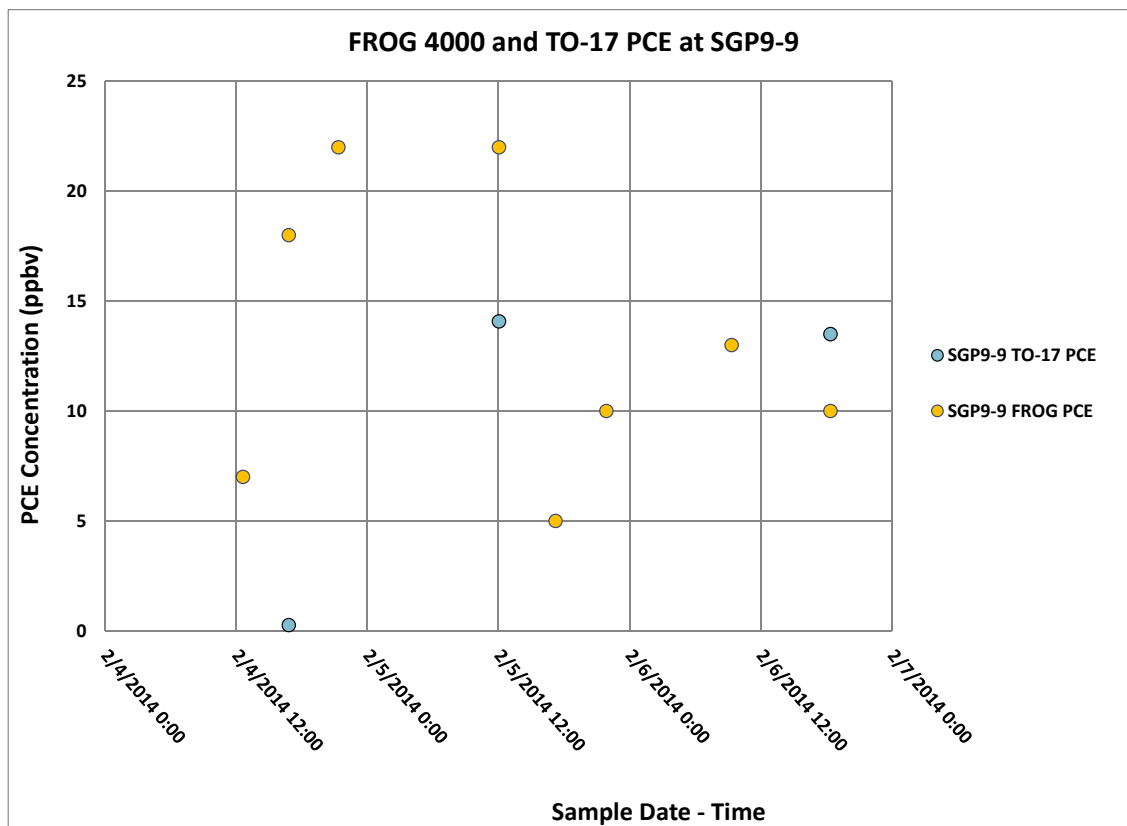


Figure 5-38. FROG 4000 and TO-17 PCE data at SGP9-9.

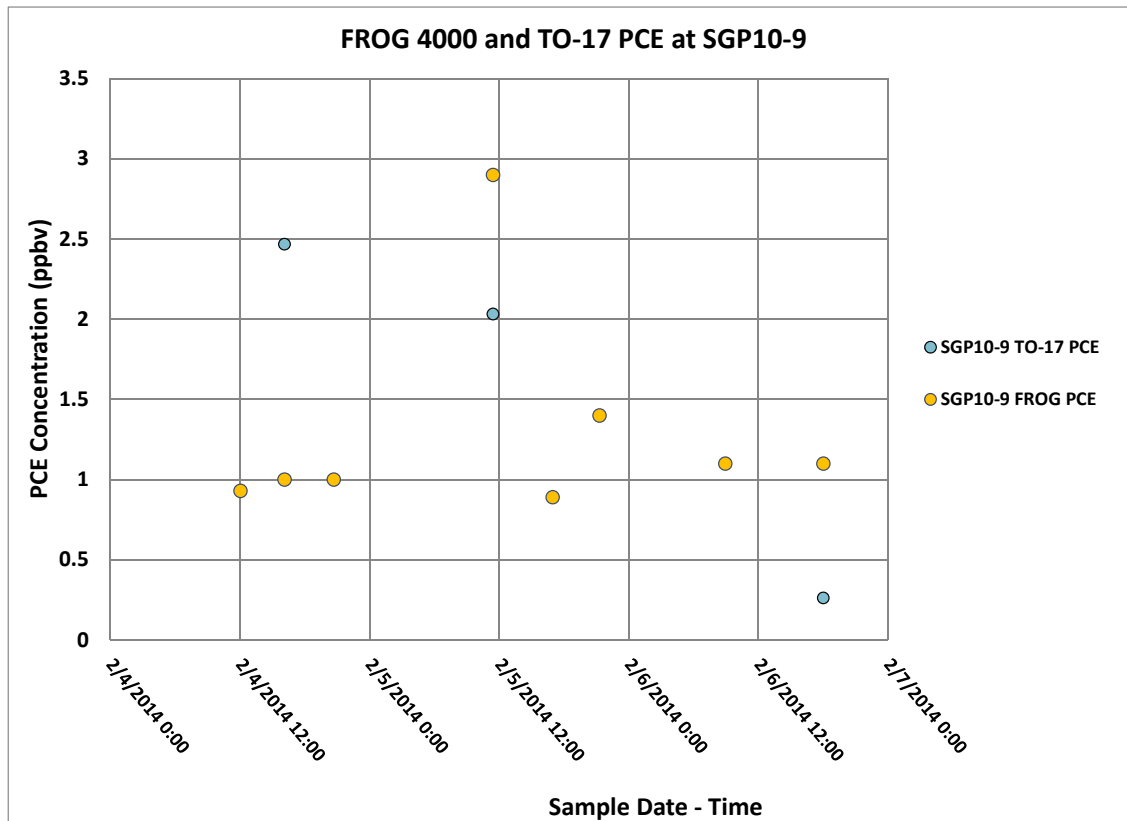


Figure 5-39. FROG 4000 and TO-17 PCE data at SGP10-9.

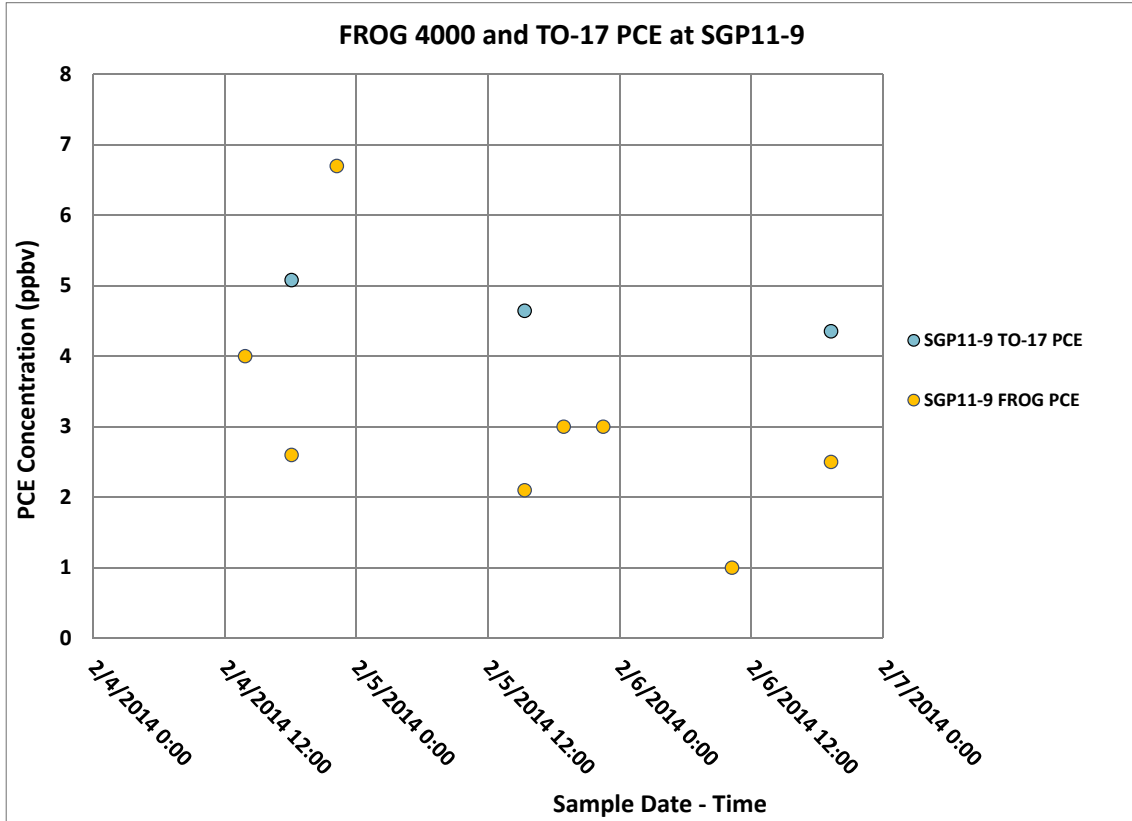


Figure 5-40. FROG 4000 and TO-17 PCE data at SGP11-9.

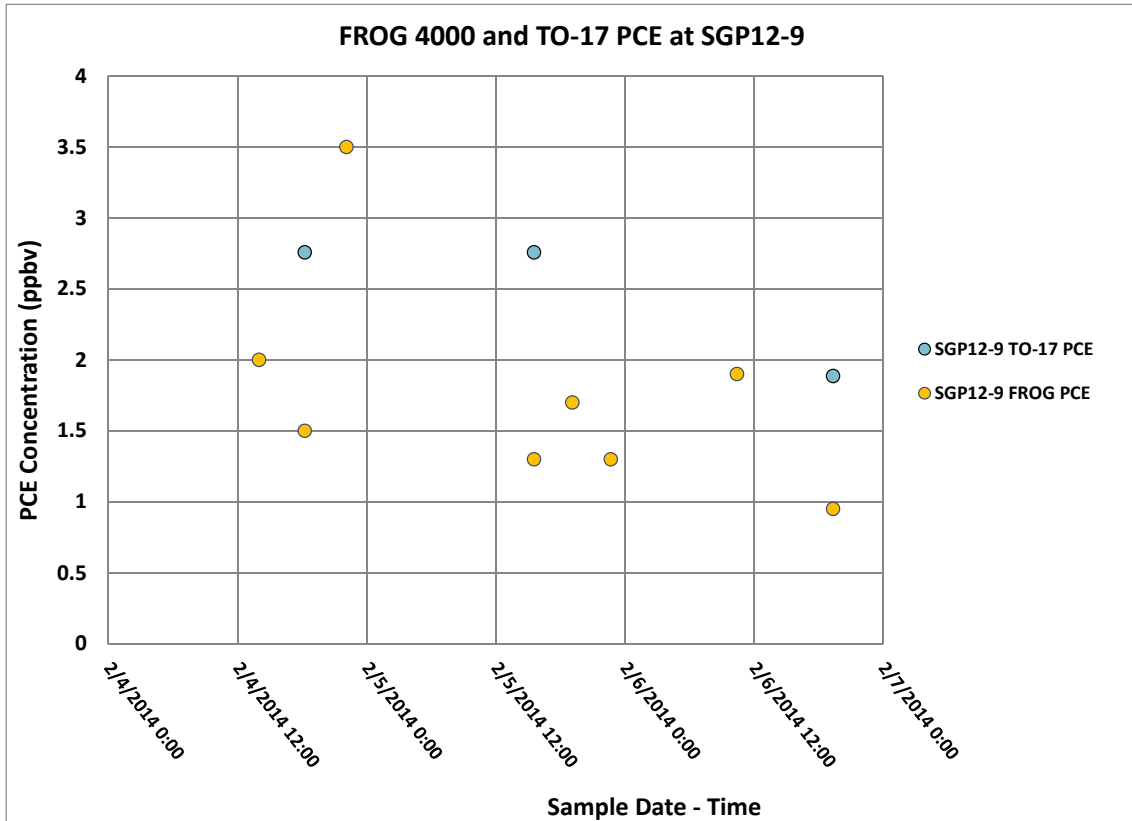


Figure 5-41. FROG 4000 and TO-17 PCE data at SGP12-9.

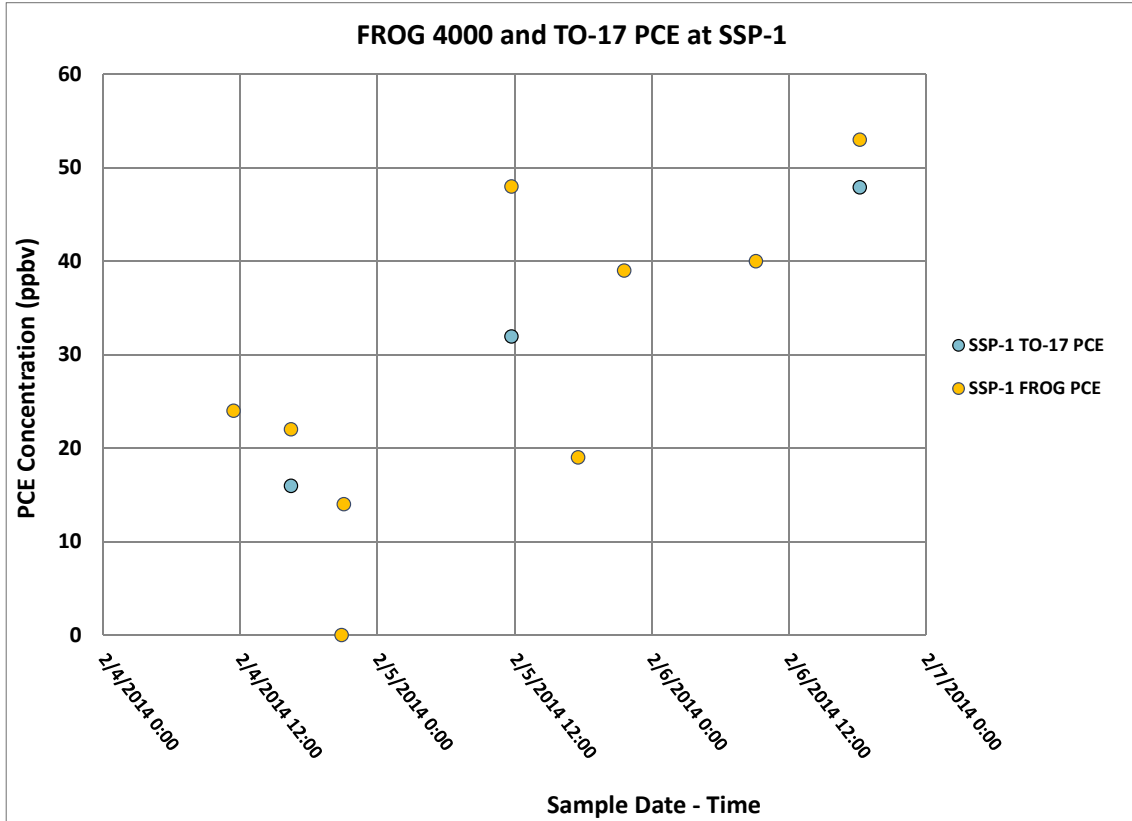


Figure 5-42. FROG 4000 and TO-17 PCE data at SSP-1.

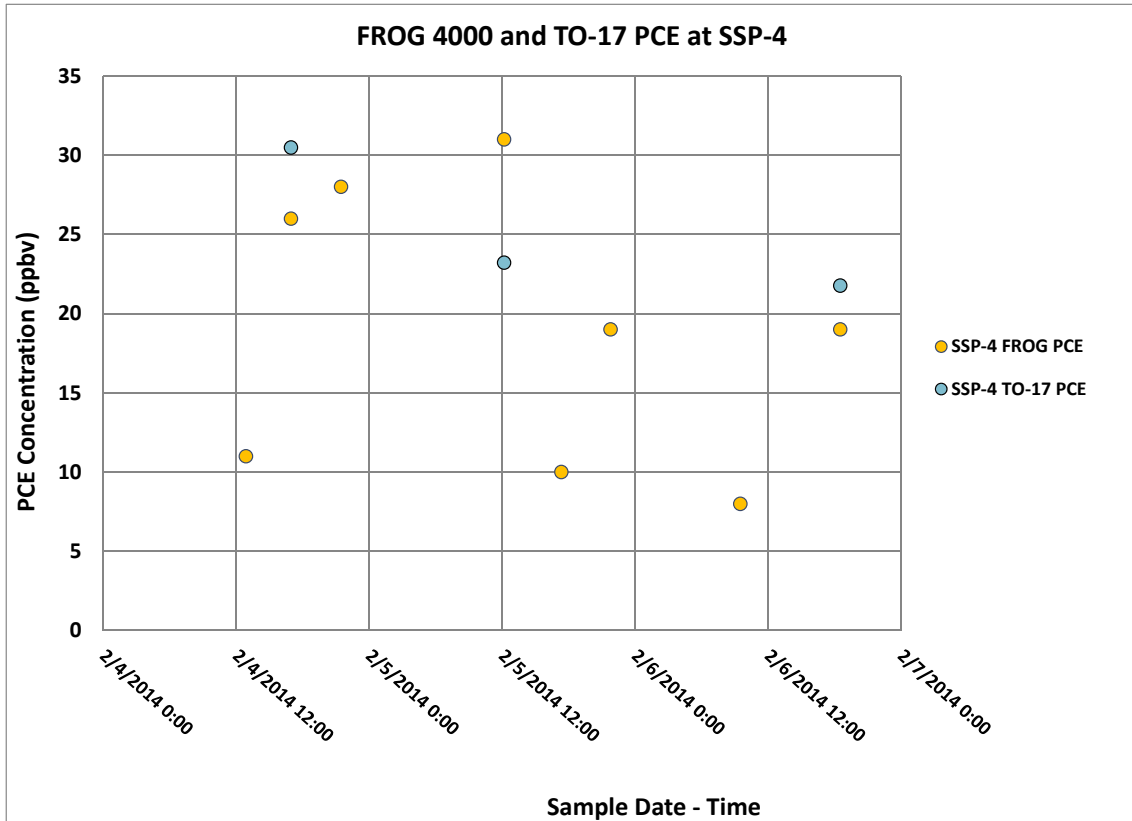


Figure 5-43. FROG 4000 and TO-17 PCE data at SSP-4.

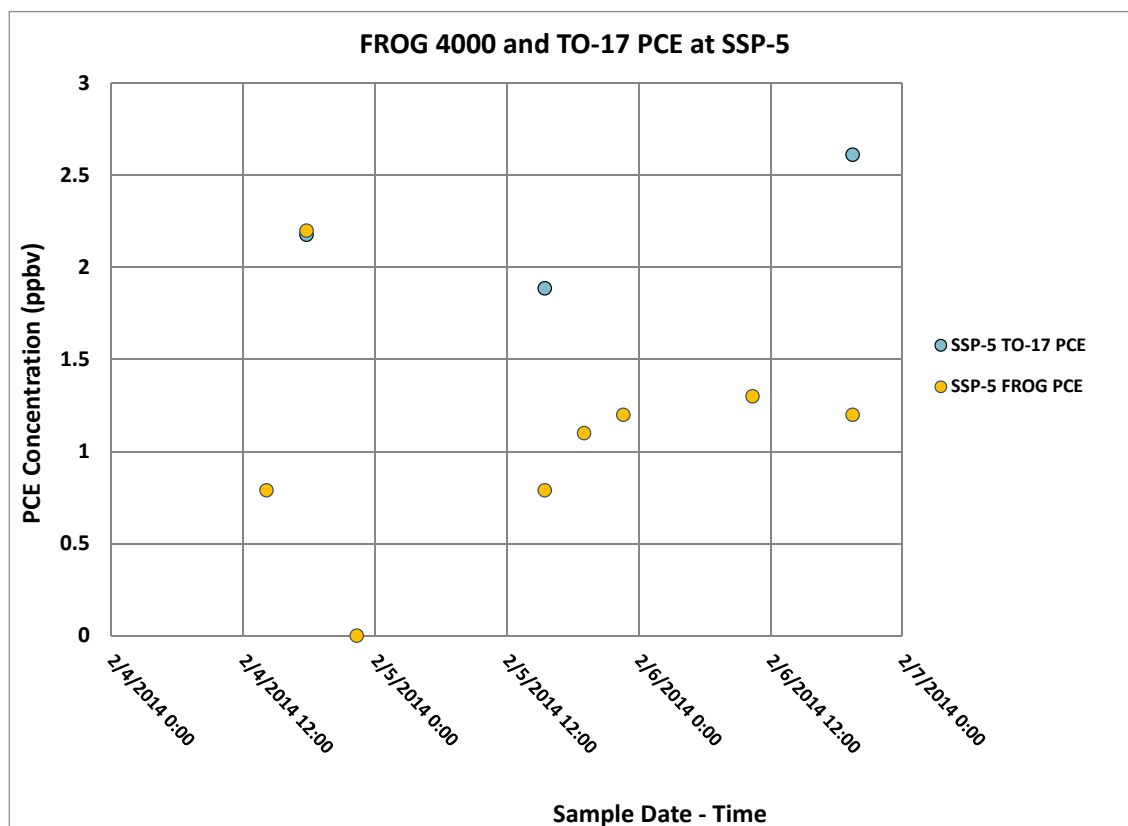


Figure 5-44. FROG 4000 and TO-17 PCE data at SSP-5.

5.3.3 Water Sampling by FROG and EPA Laboratory.

The FROG can also test for VOCs in water samples using purge and trap GC. A comparison test was made between water samples analyzed by the FROG and water samples sent to the EPA laboratory. Three wells on the 422/420 property were chosen for their similar depths: MW1-B, MW2-B, and MW3, each between ~23.5' and 24.5'. At each well, bailers were used to obtain water samples that were (1) immediate analyzed by the FROG and (2) sealed in VOA vials and sent to the EPA laboratory for analysis. The FROG field measurements were consistently about an order of magnitude higher than EPA data (Figure 5-45). Possible explanations for this different could include volatile loss from the VOA vials sent to the laboratory (which is viewed as unlikely) or miscalibration of the FROG device for the water VOC analyses.

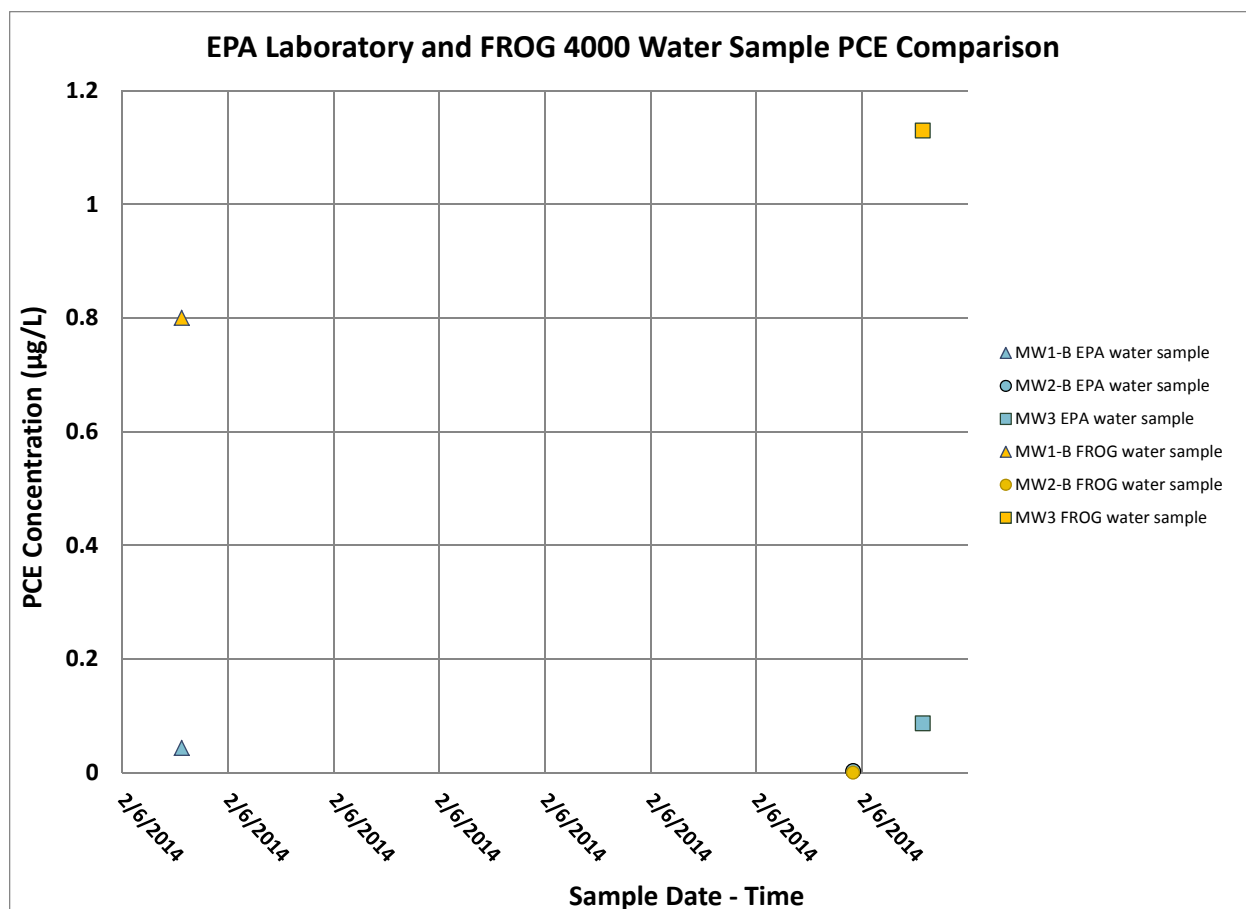


Figure 5-45. Comparison between water samples: FROG 4000 and EPA laboratory PCE data.

5.4 Radon Short-Term Variability (Based on Daily and More Frequent Measurements)

Please see the discussion in Section 5.4 of U.S. EPA (2012a) regarding the 2011–2012 data and Section 5.2 of U.S. EPA (2013), which discussed the effect of the mitigation system on radon concentrations in the duplex. Section 5.4 of U.S. EPA (2012a) discussed electret radon in indoor air and a breakdown of electret and stationary AlphaGUARD data during intensive periods. With respect to the post-mitigation radon levels unique to this report, when the radon system was shut off, indoor radon concentrations returned to levels slightly higher than observed before (Figure 4-46), with a peak over 35 pCi/L in July 2013 and another peak over 30 pCi/L in March 2014.

5.4.1 AlphaGUARD Radon Measurements

The stationary AlphaGUARD data set now includes more than 140,000 measurements taken from two locations (basement and office) over a 3-year period, at approximately 10-minute intervals (Figure 5-46). The levels and short-term variability in radon concentration observed when the mitigation system is installed but not on is quite similar to the long-term trend prior to mitigation, indicating that the mitigation system was not effective in a passive (fan-off) mode. After the mitigation system was shut down, dramatic variations of as much as 15 pCi/L within a few days continued to be common in the basement AlphaGUARD data set (Figure 5-46).

During the active mitigation (“mitigation on”) periods (black bars in Figure 5-46), the vast majority of the data is confined to a narrower and much lower absolute range from –0.5 to 2.3 pCi/L (note that

negative readings are not physically realistic, but likely reflect a small offset error), indicating that the active mitigation system was very effective in reducing radon concentrations in the duplex.

The office data set (422 side second floor) has a somewhat smaller range of short-term variation (about 8 pCi/L is typical) but shows a similar response to mitigation (**Figure 5-47**). As with the basement AlphaGUARD, during the period of active mitigation, the variation in indoor radon concentrations is confined to a much smaller absolute range (approximately 0 to 2.5 pCi/L) than observed before the mitigation system was installed or was not active (fan off) after installation.

The 422 north basement electret sampling was discontinued during the week of October 24, 2013. The 422 north basement AlphaGUARD was also moved at that time to the 422 south basement where it has remained. No significant change in radon levels measured was observed with this move.

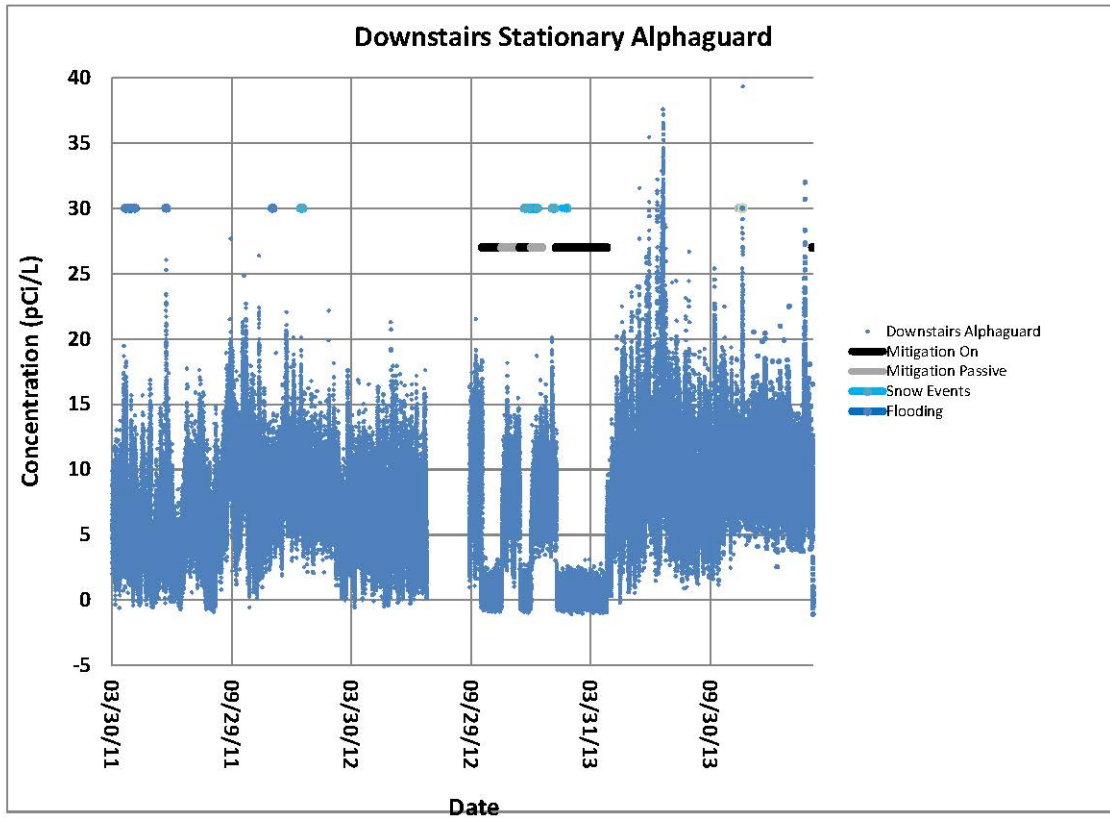


Figure 5-46. Real-time radon (422 basement) 2011–2014. Note: basement AlphaGUARD moved during the week of 10/24/13.

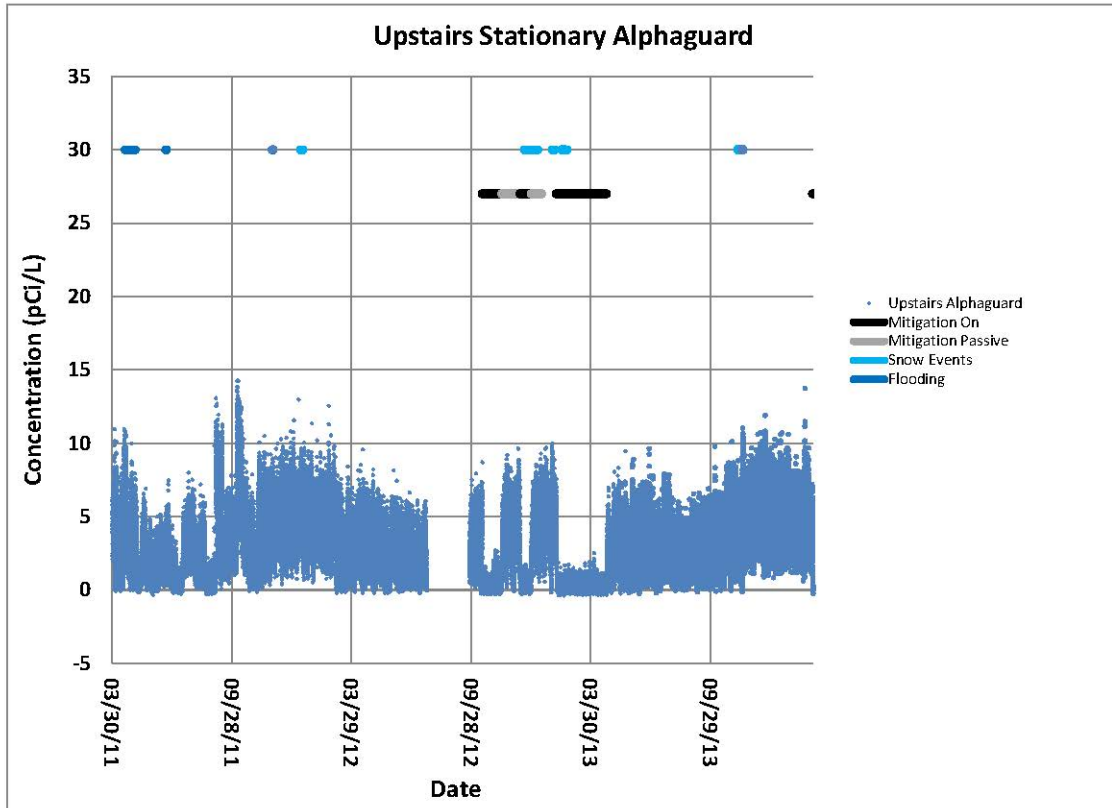


Figure 5-47. Real-time radon (422, second floor office), 2011–2014.

5.4.2 SIRAD Radon Measurements

A commercially available low cost radon detector was also tested during this project. These units were made by a Russian company called SIRAD, and the units were called the SIRAD MR-106N. Initially, two SIRADs were added to the project because they are capable of connecting to a computer for remote data monitoring. However, these devices have yet to be used in this manner. The units also have a more manual system to allow periodic data downloads that was used in the study. At first, one device was placed near the 422 south basement AlphaGUARD unit and the other on the 422 first floor. The basement unit ran from November 25, 2013, until February 17, 2014. The 422 first floor unit ran from November 25, 2013, until December 23, 2013. The SIRAD unit was then moved to the 422 second floor office so its data could be compared to that of the 422 second floor AlphaGUARD. The 422 second floor SIRAD ran from December 23, 2013, until February 17, 2014. On February 17, 2014, both units stopped functioning due to an unidentified fault.

Figure 5-48 plots radon concentrations versus time for both the 422 basement south SIRAD and AlphaGUARD in the same location. SIRAD data are generally lower than those of the AlphaGUARD. Although there is some correspondence between the higher peaks of the different instruments, the highest concentrations detected by the AlphaGUARD are not matched by the highest concentrations detected by the SIRAD, with the SIRAD radon levels always being lower than the SIRAD radon levels. As a result, the average AlphaGUARD radon level (9.6 pCi/L) was 1.7 times higher than the average SIRAD radon level (5.8 pCi/L).

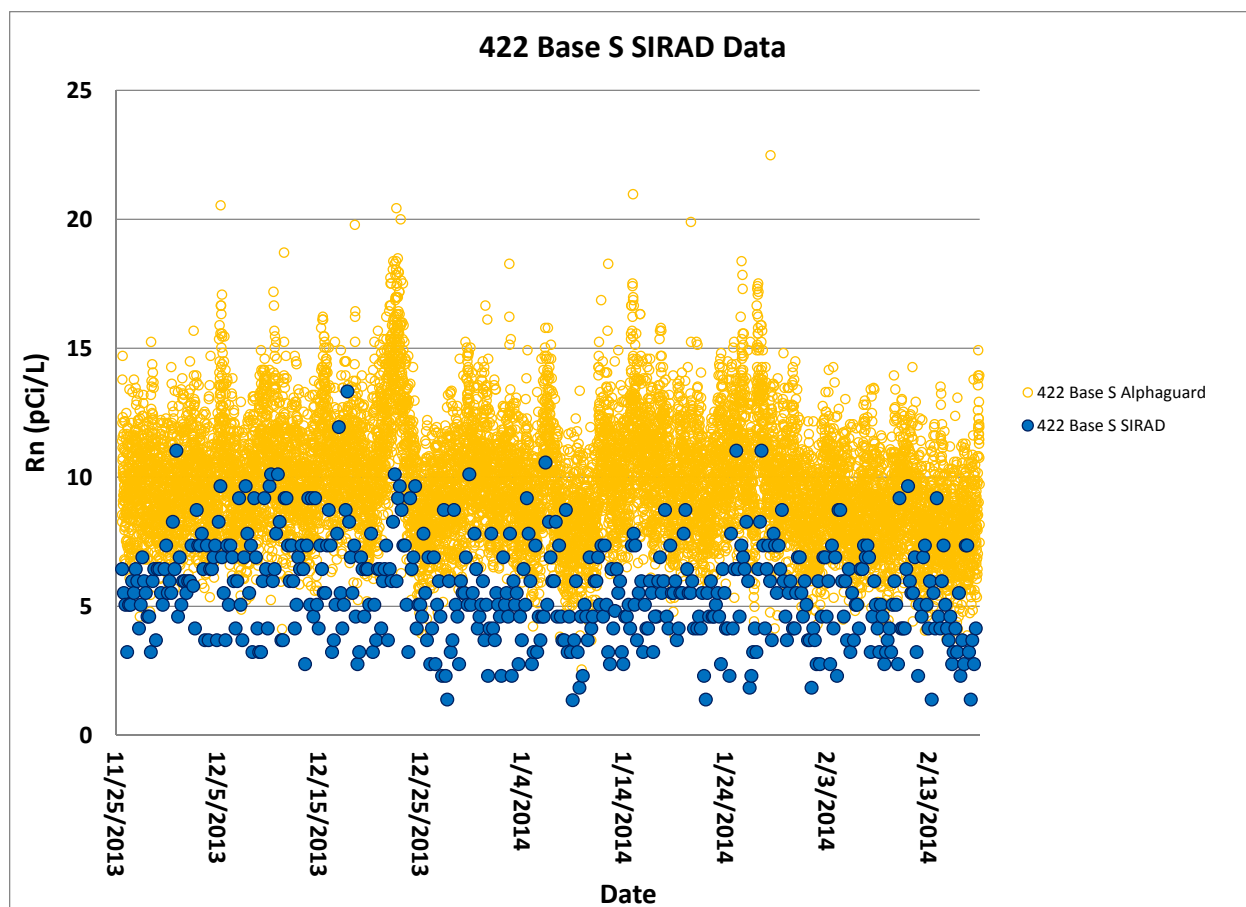


Figure 5-48. Real-time radon (422 south basement) AlphaGUARD vs. SIRAD.

Figure 5-49 plots radon level versus time for the 422 second floor office SIRAD and AlphaGUARD. The maximum radon levels are much lower in the 422 second floor office than in 422 south basement (10.7 pCi/L as opposed to 22.5 pCi/L). At the lower radon levels observed in the office, which span the 4 pCi/L regulatory level, there is better agreement between the range of the two devices as well as better agreement during the peak times recorded by both instruments.

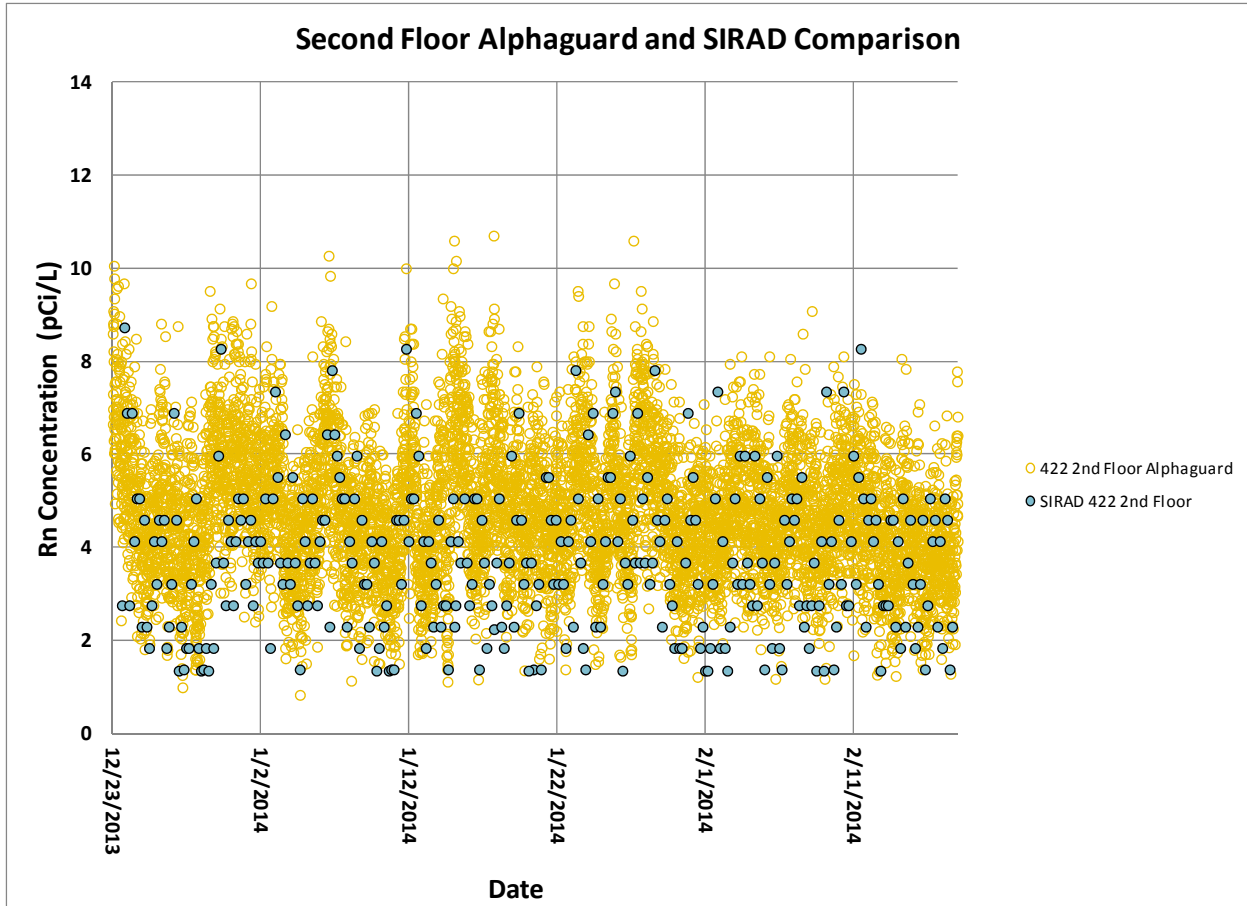


Figure 5-49. Real-time radon (422, second floor office) AlphaGUARD vs. SIRAD.

5.5 Outdoor Climate/Weather Data

External and internal weather parameters were measured at the 422/420 house on a Vantage Vue weather monitor. Internal temperatures were recorded by HOBO data loggers. Barometric pressure readings were taken about every 15 minutes by Setra pressure sensors. Data were downloaded from these sources approximately once per week. Well water levels were measured approximately once per month during the first portion of the study but then continuously in late 2012 early 2013. The 2011 through 2012 weather data were presented and analyzed in Section 5.5 of U.S. EPA (2012a) and 2012 through 2013 in Section 6.5 of U.S. EPA (2013).

5.5.1 Weather Parameters

All winters at the 422/420 test house have not been the same. The ambient trend in **Figure 5-50** shows the difference between maximum and minimum temperatures for each of the four winters of the study. The winter of 2013–2014 had by far the coldest temperatures. Temperatures stayed consistently cold as well, with many days staying well below the freezing point. From the date when temperatures began to stay consistently cold (approximately October 24, 2013) until March 5, 2014, the maximum temperature was 66°F, the minimum was -11°F, and the average was 30°F.

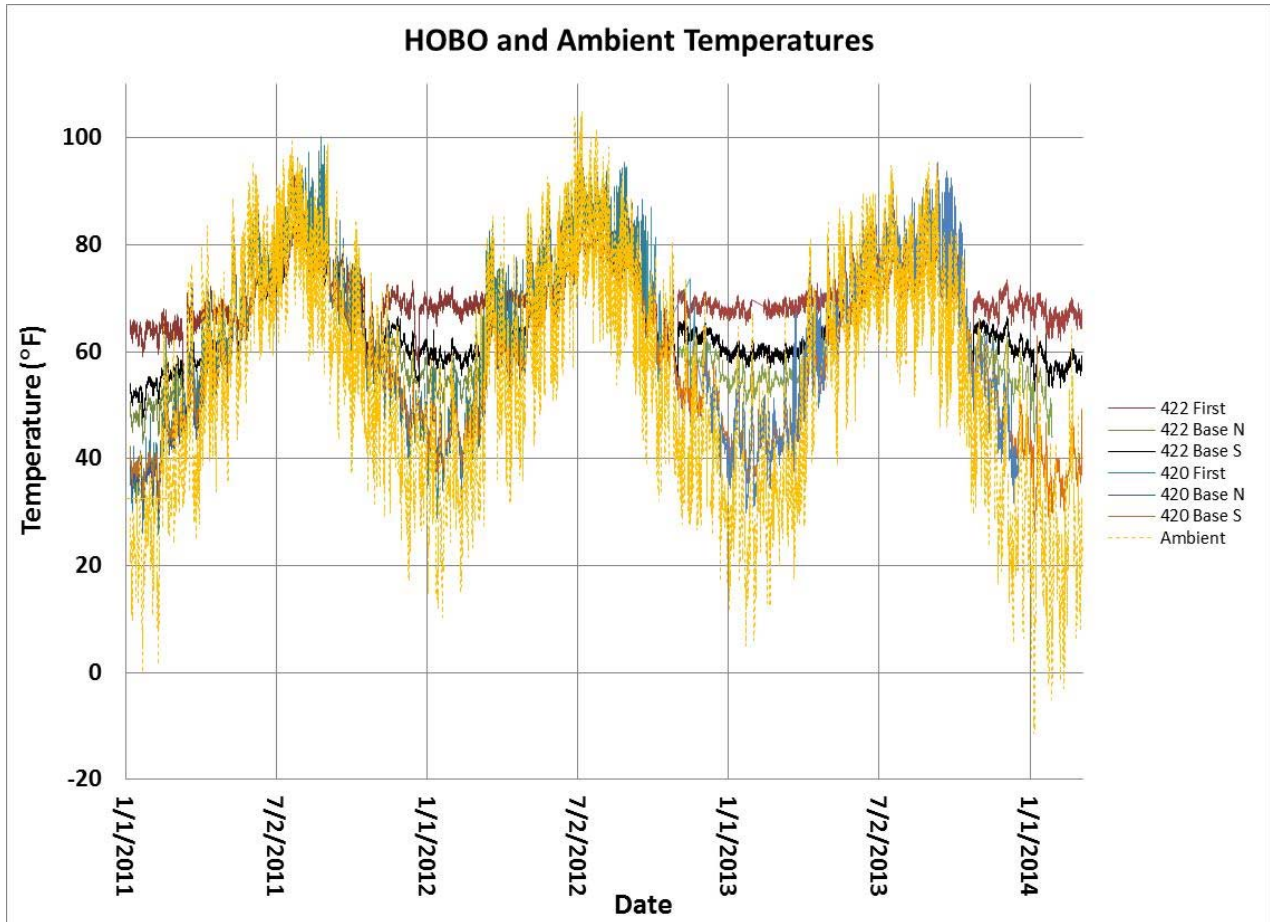


Figure 5-50. Temperature plots from HOBO data loggers and the 422 house weather station.

Table 5-1 shows state average temperatures for Indiana, state and central average precipitation, special characteristics, and weekly deviations from normal. For September 2013 through March 2014, weather patterns across Indiana deviated substantially from normal. State average temperatures dropped by as much as 8.7 °F below normal in February. Average precipitation was 160% of normal during December. Many weeks during the winter were 13–15 °F below normal. All of these characteristics combined to produce extended periods of frigid cold with more snow than any other recent years. Additionally, there were some periods of thawing that produced some flooding, especially in December and February.

Table 5-1. Table of Temperature, Precipitation, and Change from Normal

Month/ Year	State Avg. T (°F)	State Avg. Precipitation (in)	Central Avg. Precipitation (in)	Notes on Central IN	Week 1 T avg. (°F)	Week 2 T avg. (°F)	Week 3 T avg. (°F)	Week 4 T avg. (°F)
Sep-13	67.1; 1.5 [^]	2.98; 0.11 _v		Dry start of month, then heavy rain	1 _v	4 [^]	Normal	1 [^]
Oct-13	54.4; 0.4 [^]	3.97; 1.07 [^]	140% of normal	Warm 1 st half of month, cold 2 nd	9 [^]	4 [^]	1 _v	Normal
Nov-13	39.2; 3.2 _v	3.20; 0.39 _v		Alt. warm and cold, 28 tornadoes	1 _v	3 _v	10 _v	1 _v
Dec-13	29.2; 1.9 _v	4.50; 1.47 [^]	160% of normal	Snowfall, rainfall, flooding	15 _v	13 _v	3 [^]	Normal
Jan-14	19.1; 6.9 _v	2.34; 0.09 _v	125% of normal	Frigid cold, regular snowfall	14 _v	6 [^]	3 _v	14 _v
Feb-14	21.7; 8.7 _v	2.74; 0.47 [^]	125% of normal	Frigid cold, flooding	7 _v	15 _v	Normal	14 _v
Mar-14	34.1; 6.6 _v	2.01; 1.39 _v	65% of normal	5 th month in a row w/<normal temps	13 _v	2 [^]	1 _v	9 _v

Note that the symbols “[^]” and “_v” mean “above” and “below” normal, respectively, and that the weekly averages differ from normal (from Scheeringa and Price, 2013 and 2014)

Various weather measurements collected with the weather station at the house are shown in **Figure 5-51**. Summer is a period of higher temperatures, lower wind speeds, and lower barometric pressure variations at this house. Indoor humidity is less variable over short time scales than outdoor (exterior) humidity in this record. The temperature record is consistent with the airport observations, with the coldest winter weather experienced in late December 2013 to early January 2014.

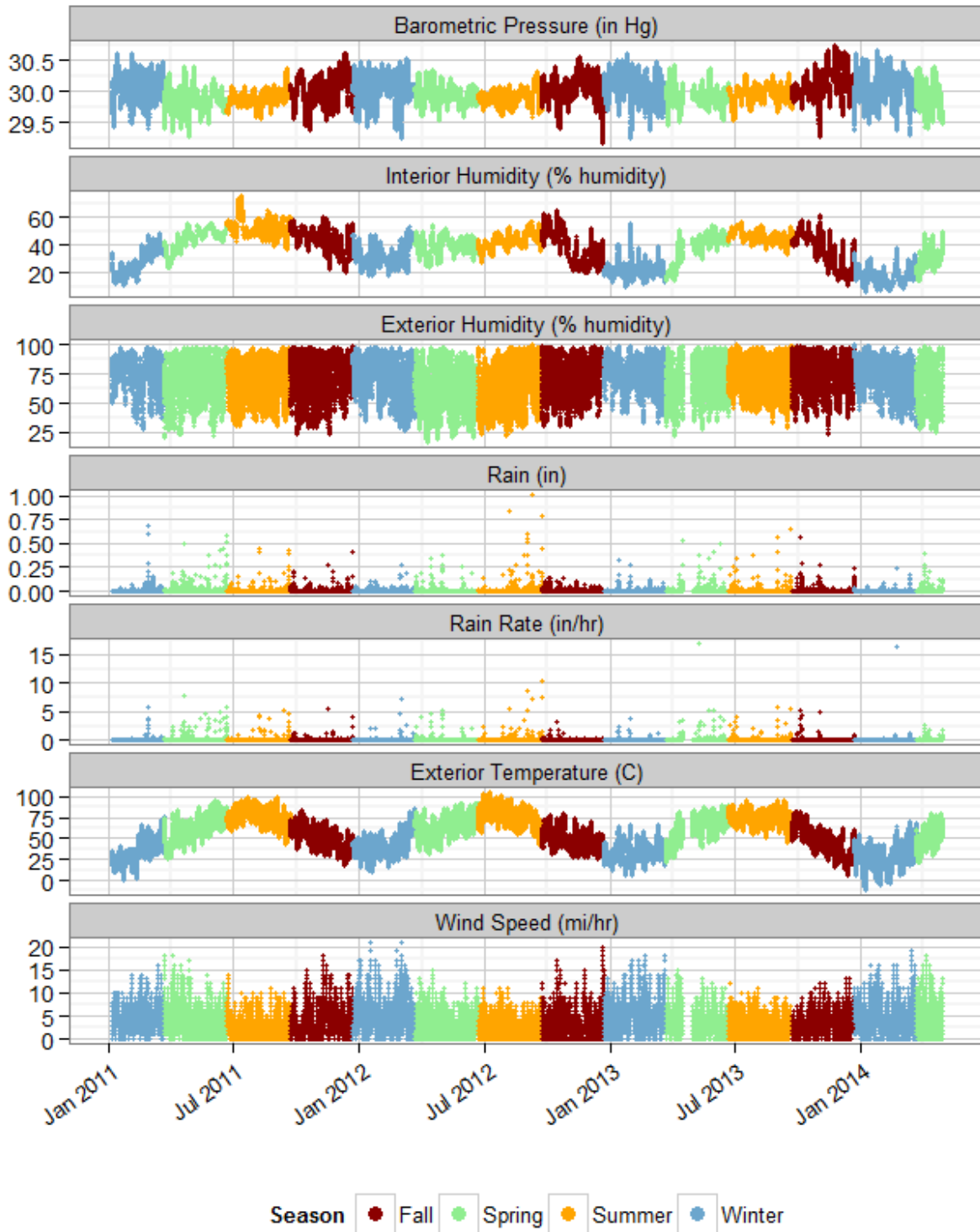


Figure 5-51. Weather variables measured inside 422 office (second floor) and on roof (top to bottom): (list based on revised figure in figure folder).

5.5.2 Weather Related to VOCs and Radon

Figure 5-52 plots stationary FROG PCE concentrations versus time along with differential pressure at wall port 3, pressure changes outside the 422/420 house, wind speed (in miles per hour), and wind direction (in degrees). Differential pressure changes at wall port 3 are sensitive to exterior weather changes, reflected well by the similarity between several of the peaks and troughs in exterior pressure and wind speed graphs and the peaks and troughs found in the wall port 3 graph. The fluctuations of the FROG PCE concentrations are also very similar to the graph for wall port 3. The most noticeable points of similarity between the graphs are found on February 4–5, 2014, February 17–18, 2014, February 20–21, 2014, and February 27, 2014–March 1, 2014. Commonly, each of these date ranges shows increases in PCE concentration, greater differential pressure, a drop in external pressure, and usually higher wind speeds. The relationships between these variables and indoor VOC concentrations have been addressed more quantitatively in Chapter 6, although time series analysis of the FROG data set has not yet been performed.

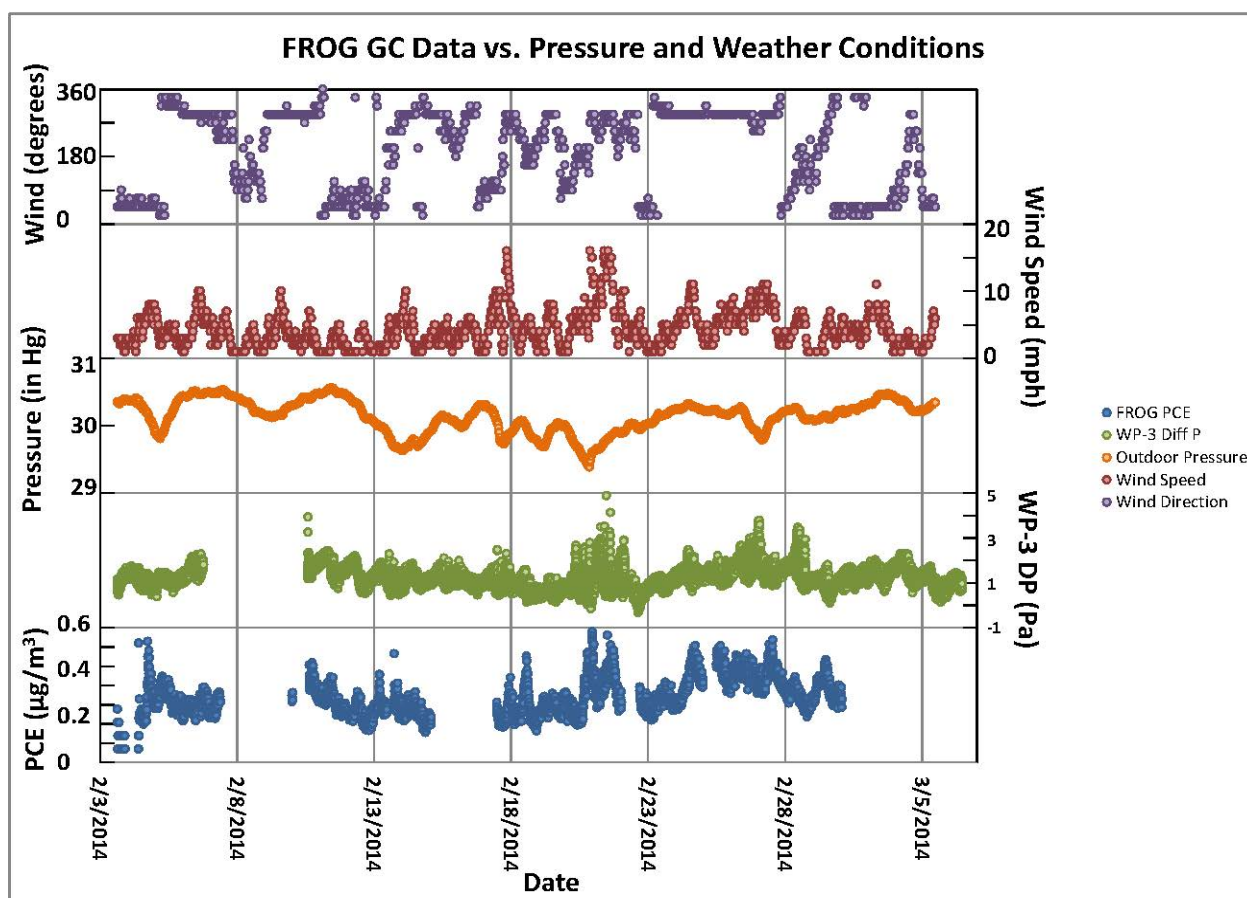


Figure 5-52. Comparison graph plotting FROG PCE concentrations, wall port differential pressure, outdoor pressure, wind speed, and wind direction.

Cold and warm fronts possess the following characteristics¹²: “Cold fronts are characterized by gusty winds, shifting of wind direction, steadily falling pressure before, a sharp rise during passage of the front,

¹² From: <http://www.infoplease.com/cig/weather/frontal-attack.html>

and a steady rise after. Warm fronts are characterized by variable wind speeds with changes in direction, falling pressures before the front's passage, a leveling during, and a slight rise and fall after.”

Based on these descriptions, the data described above from early February through early March 2014 (Figure 5-52) seem to indicate the passage of several cold fronts in the mid-February time period. This could be consistent with the weather becoming cold and staying cold during the 2014 winter (Figure 5-50) as well as the higher wall port differential pressures and indoor air PCE concentrations observed in February.

Figure 5-53 plots AlphaGUARD radon at both 422 south basement and the 422 second floor office, as well as PCE data from the FROG data set. Note that both radon levels and VOC concentrations show a prominent mid- to late-February peak following the passage of several cold fronts earlier in the month (shown in Figure 5-52). Additionally, snow events that occurred during this time period are also included as light blue circles along the top of the graph. There does not appear to be a direct correspondence between the mere presence of snow on the ground (regardless of the quantity) and increases in radon or VOC concentrations. However, other weather phenomena related to the snow events, such as temperature drops, cold fronts, and wind shifts, may contribute to concentration increases.

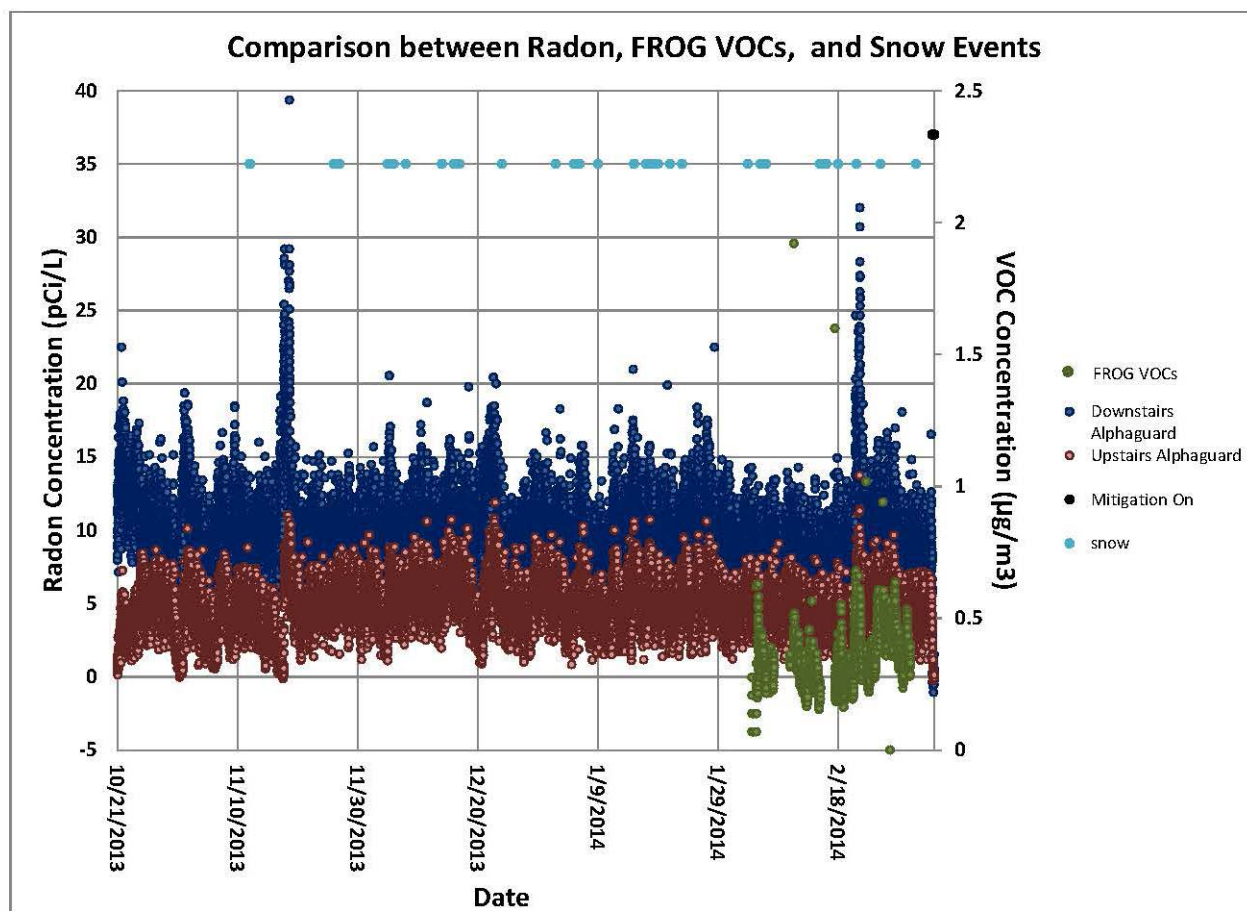


Figure 5-53. Comparison graph plotting AlphaGUARD radon, FROG VOCs, and snow events.

6. Results and Discussion: Further Analysis of 2010–Early 2013 Data Sets as a Basis for Vapor Intrusion Predictions

6.1 Summary of 2013 Report Regarding Multiple Lines of Evidence Analysis

This section extends the work described in our previous report (U.S. EPA, 2013), where we used multiple analytical tools to assess the relationship between meteorological parameters and vapor intrusion. These analyses included (U.S. EPA, 2013):

- exploratory data analysis through visual examination of the shape of temporal trends in stacked plots of indoor air and certain soil gas ports over the full project period (Section 6),
- detailed examination of temporal trends on stacked plots during unusual differential pressure events (Section 9.1)
- visual examination of XY graphs (Section 9.2), and
- quantitative time series methods (Section 10).

Because of the complexity of these analyses, not all analysis methods were completed for all possible meteorological variables. The lines of evidence that were investigated for the meteorological variables are summarized with results in **Table 6-1**. The evidence was considered overwhelming that cold temperatures contribute to greater vapor intrusion in this duplex. This was expected from knowledge of the stack effect mechanism. Other correlations were not so clear, but wind speed and direction and snow/ice cover seemed to show some effects.

6.2 Updated Time Series Analysis

Section 10 of U.S. EPA (2013) presents a formal statistical time series analysis for radon and VOCs using as outcome variables the available uninterrupted indoor air data sets for daily radon observations (AlphaGUARD daily averages) and weekly VOC data (Radiello). Predictor variables in those analyses included meteorological, hydrological, and building operation factors. Each predictor variable was analyzed for each outcome variable individually assuming a linear relationship. An updated list of predictor variables and how they were aggregated across multiple time intervals is provided in **Attachment 6A** to this section.

In this report we extend that data analysis in the following ways:

- Repeating the weekly VOC data analysis using a revised set of predictor variables that improves the parameterization of categorical variables for wind direction, snow events, ice events, and thunder storms.
- Revision of the derived variables for barometric pressure.
- Calculation and presentation of measures of the strength of the correlation between the predictor and outcome variables such as r^2 , Akaike Information Criteria (AIC), and the Bayesian Information Criteria (BIC). This allows us to describe statistically which of the meteorological predictor variables is most closely correlated to the indoor air concentrations.
- Presenting time series analysis of daily resolution VOC data drawn from the online GC.

Table 6-1. Summary of Lines of Evidence for Meteorological Factors Influencing Vapor Intrusion (U.S. EPA 2012a, 2013)

(Blank cells reflect types of analysis not completed for a given parameter; section numbers refer to U.S. EPA [2013])

	Snowfall	Snow or Ice Accumulation on Ground	Cold Exterior Temperatures (or substantial change in temperatures)	Rain Events/Rainfall Amount	Barometric Pressure Changes	West to NW Winds	High Wind Velocity
Apparent temporal association with VOC concentrations in indoor Air (Chapter 6; also U.S. EPA, 2012a)	Yes	Yes	Yes	Possibly for chloroform			
Apparent temporal association with VOC concentrations in wall ports or subslab ports (Chapter 6)	Yes	Yes			Weak		Some
Apparent temporal association with large subslab to indoor differential pressure events (Section 9.1)	Yes in some cases		Yes in some cases		Yes in some cases	Yes in a few cases	Yes in a few cases
Apparent trend in XY graph of meteorological parameter vs. subslab/indoor differential pressure (Section 9.1 and U.S. EPA, 2012a)			Yes	No		Yes	No
Apparent trend in XY graph of meteorological parameter versus VOC concentration (Section 9.2)	No	Yes for PCE, not definitive for chloroform	Yes	No clear relationship	Not definitive	Yes for PCE, No for chloroform	No for PCE, Yes for chloroform
Correlation with radon in quantitative time series analysis (Sections 10.1 to 10.4); 422 basement and office		No	Yes in most analyses	Yes in some analyses	Yes in most analyses		Yes in some analyses
Correlation with chloroform in quantitative time series analysis (Sections 10.5 and 10.7); 422 basement		Yes in one of two cases with opposite signs for the coefficients of the current and past weeks.	Yes	No	Yes in some analyses		
Correlation with PCE in quantitative time series analysis (Sections 10.6 and 10.8), 422 basement		Yes in one of two cases but with an unexpectedly negative coefficient for the current week.	Yes, although coefficients sometimes have an unexpected sign	No	Yes	No	No

6.2.1 Categorical Predictor Variables for Wind Direction, Snow, Ice, and Thunder Events

In the analyses reported in U.S. EPA (2013), wind direction was treated as a continuous, scalar predictor variable (input as 0 to 360 degrees). That was not ideal for two reasons:

- It does not correctly show the similarity between a wind blowing from 1° to one blowing from 359°. Note that these winds are only 2° apart when we recall that the wind rose is circular.
- It does not recognize the directionality of wind. For example a North wind of 359° cannot be properly thought of as an intensification of a west wind of 270°.

Thus, in the current analysis wind direction (average) and wind direction (high for the period) are treated as categorical variables assigned to one of the categories.

The only snow variable in U.S. EPA (2013) was depth in inches on the ground. We have now obtained and parsed the Automated Surface Observing System (ASOS) measurements made by the National Weather Service for the Indianapolis Airport (station identification KIND). The data reported in the remarks element of the Meteorological Aviation Report (METAR) format include observations made by the precipitation identification sensor, which differentiates precipitation types such as rain, freezing rain, and snow based on an optical sensor and structured algorithm (NOAA, 1998). At stations with a trained human observer, the human observer interacts with the system to back up or augment the automated observations, and these observations are also incorporated into the METAR format, which is generally the case at station KIND. Thus, we were able to populate a binary variable “yes” if there was any observation of snow in the METAR reports during the period of data aggregation. Similarly, we coded a binary variable for “icy precipitation event” yes if there were any mentions of “hail,” “ice,” or “freezing” in the METAR report for the period of data aggregation. We coded “thunder event” yes if there was any mention of “thunder” in the METAR records. Thunderstorms are coded by ASOS based on the observation of nearly simultaneous optical flash and electrical field change (from radio signals) (NOAA, 1998).

6.2.2 Derived Predictor Variables Based on Barometric Pressure Measurements

Barometric pumping is believed to be important in the movement of contaminants in the soil gas system. Our weather station measured barometric pressure generally on 30-minute intervals. Barometric pressure fluctuates within a known range with daily and longer cycles related to the passage of weather fronts. Barometric pumping is generally believed to result from changes in barometric pressure, but there is no consensus, however, as to what mathematical function based on barometric pressure best predicts barometric pumping relevant to vapor intrusion. Therefore, we have explored a number of derived variables based on the barometric pressure record. The derived variables related to barometric pressure included in the U.S. EPA (2013) analysis are listed in **Table 6-2**. The derived variables added for the current analysis are listed in **Table 6-3**.

Table 6-2. Derived Barometric Pressure Variables Used in U.S. EPA (2013) and Retained in this Analysis

Variable Description	Variable Code	Method of Aggregation
Barometric pressure rate of change in, inches of mercury per hour	Bar_drop_Hg.hr	Mean
Barometric pressure, inches of mercury	Bar_in_Hg	Mean
Net barometric pressure change over measurement period, inches of mercury	BP_Net_Change	First-last, by date/time
Standard deviation of barometric pressure change over measurement period, inches of mercury	BP_Pump_Speed	Standard deviation
Largest barometric Pressure Change over measurement period (“stroke length” of barometric pumping), inches of mercury	BP_Stroke_Length	Maximum-minimum

Table 6-3. Derived Pressure Variables Added for this Analysis

Variable Description	Variable Code	Method of Aggregation
Largest barometric pressure rate of change, inches of mercury per hour	Max_Change_dPdt	Maximum absolute value, keeping sign
Absolute value of largest barometric pressure rate of change, inches of mercury per hour	Abs_Max_Change_dPdt	Maximum absolute value, not keeping sign

6.2.3 Derived Predictor Variables Based on Differential Pressure and Temperature Measurements

In order to further explore the potential predictors of vapor intrusion, we added predictor variables for the standard deviation of each measured differential pressure. To better understand the influence of temperature differential, temperatures between each indoor monitoring station and the outside ambient temperature sensor on the building roof were calculated. These differential temperatures were also used to calculate estimates of the strength of the stack effect using the formula presented in Section 10.3 of U.S. EPA (2012a). These new predictor variables are summarized in **Table 6-4**.

Because we added these additional derived predictor variables to the time series analysis, we dropped some variables that had been included in U.S. EPA (2013) to keep the analysis tractable. The dropped variables were judged to be essentially duplicative or unlikely to yield significant correlations. Examples of dropped variables include the temperature, humidity, and wind (THW) index, which is a derived variable based on temperature, humidity, and wind speed that is designed to predict the human perception of temperature. Another example of a dropped variable was the Fall Creek stream gage height, which was dropped because of its tight correlation to the on-site depth to groundwater.

Table 6-4. Additional Derived Variables Based on Differential Pressure and Temperatures

Variable Name (Plain Language)	Variable Code	Method of Aggregation
420 side, subslab vs. basement Standard Deviation of Differential Pressure over measurement period, Pascals	StdDev_Setra_420ss.base_Pa	Standard deviation
422 side basement vs. exterior Standard Deviation of Differential Pressure over measurement period, Pascals	StdDev_Setra_422base.out_Pa	Standard deviation
422 side, basement vs. upstairs Standard Deviation of Differential Pressure over measurement period, Pascals	StdDev_Setra_422base.upst_Pa	Standard deviation
422 side, deep vs. shallow soil gas Standard Deviation of Differential Pressure over measurement period, Pascals	StdDev_Setra_422SGdp.ss_Pa	Standard deviation
422 side, subslab vs. basement Standard Deviation of Differential Pressure over measurement period, Pascals	StdDev_Setra_422ss.base_Pa	Standard Deviation
Temperature at 420 basement north (HOBO) minus outside temperature (weather station), °F	Diff_T_420baseN-Out_F	Temp in–temp out
Temperature at 420 first floor (HOBO) minus outside temperature (weather station), °F	Diff_T_420first-Out_F	Temp in–temp out
Temperature at 422 basement south (HOBO) minus outside temperature (weather station), °F	Diff_T_422baseS-Out_F	Temp in–temp out
Temperature at 420 basement south (HOBO) minus outside temperature (weather station), °F	Diff_T_420baseS-Out_F	Temp in–temp out
Temperature at 422 basement north (HOBO) minus outside temperature (weather station), °F	Diff_T_422baseN-Out_F	Temp in–temp out
Temperature at 422 first floor (HOBO) minus outside temperature (weather station), °F	Diff_T_422first-Out_F	Temp in–temp out
Stack effect between 420 basement north and outside (Rankine)	StackEffect_420baseN	If Temp In is higher than Temp Out: $\sqrt{(T_{in}-T_{out})/abs(T_{in})}$, if Temp Out is higher than Temp In: $\sqrt{(T_{out}-T_{in})/abs(T_{out})}$
Stack effect between 420 basement south and outside (Rankine)	StackEffect_420baseS	If Temp In is higher than Temp Out: $\sqrt{(T_{in}-T_{out})/abs(T_{in})}$, if Temp Out is higher than Temp In: $\sqrt{(T_{out}-T_{in})/abs(T_{out})}$
Stack effect between 420 first floor and outside (Rankine)	StackEffect_420first	If Temp In is higher than Temp Out: $\sqrt{(T_{in}-T_{out})/abs(T_{in})}$, if Temp Out is higher than Temp In: $\sqrt{(T_{out}-T_{in})/abs(T_{out})}$
Stack effect between 422 basement north and outside (Rankine)	StackEffect_422baseN	If Temp In is higher than Temp Out: $\sqrt{(T_{in}-T_{out})/abs(T_{in})}$, if Temp Out is higher than Temp In: $\sqrt{(T_{out}-T_{in})/abs(T_{out})}$
Stack effect between 422 basement south and outside (Rankine)	StackEffect_422baseS	If Temp In is higher than Temp Out: $\sqrt{(T_{in}-T_{out})/abs(T_{in})}$, if Temp Out is higher than Temp In: $\sqrt{(T_{out}-T_{in})/abs(T_{out})}$
Stack effect between 422 first floor and outside (Rankine)	StackEffect_422first	If Temp In is higher than Temp Out: $\sqrt{(T_{in}-T_{out})/abs(T_{in})}$, if Temp Out is higher than Temp In: $\sqrt{(T_{out}-T_{in})/abs(T_{out})}$

6.2.4 Measures of Goodness of Fit between Predictor Variables and Outcome Variable (Indoor Air Concentration)

We used a variety of statistics to evaluate which linear models best predict the indoor air concentration.

- **“R-squared**, often called the coefficient of determination, is defined as the ratio of the sum of squares explained by a regression model and the “total” sum of squares around the mean

$$R^2 = 1 - \text{SSE}/\text{SST}$$

in the usual ANOVA notation. Most people refer to it as the proportion of variation explained by the model.” (Henry, 2001). Thus, R-squared is equal to one minus the sum of the squares due to error (SSE) divided by the total sum of the squares (SST). Larger R-squared values closer to 1 are considered to indicate a stronger correlation. However, “A small R-squared does not imply you haven’t got something interesting” (Jones, no date).

- **“The Akaike information criterion (AIC)** is defined as

$$\text{AIC} = -2 \ln \mathcal{L} + 2k, \tag{1}$$

where \mathcal{L} is the maximum likelihood and k the number of parameters of the model (Akaike, 1974). The best model is the model which minimizes the AIC, and there is no requirement for the models to be nested. Typically, models with too few parameters give a poor fit to the data and hence have a low log-likelihood, while those with too many are penalized by the second term. The form of the AIC comes from minimizing the Kullback-Leibler information entropy, which measures the difference between the true distribution and the model distribution” (Liddle, 2004).

- **“The Bayesian information criterion (BIC)** was introduced by Schwarz (1978), and can be defined as

$$\text{BIC} = -2 \ln \mathcal{L} + k \ln N, \tag{2}$$

where N is the number of datapoints used in the fit ... It comes from approximating the Bayes factor ... which gives the posterior odds of one model against another presuming that the models are equally favoured prior to the data fitting” (Liddle, 2004).

The use of these information criteria is described by Mazerolle (2004): “In itself, the value of the AIC for a given data set has no meaning. It becomes interesting when it is compared to the AIC of a series of models specified a priori, the model with the lowest AIC being the « best » model among all models specified for the data at hand. If only poor models are considered, the AIC will select the best of the poor models. This highlights the importance of spending time to determine the set of candidate models based on previous investigations, as well as judgement and a knowledge of the system under study.” When using both the AIC and BIC, it is best to select the model giving the lowest value for the criteria. The BIC and AIC are related with the BIC using a more complex formulation of the “penalty term,” which discourages adding to the number of independent variables modeled.

6.2.5 Updated Time Series Analysis Results

Observations in time series are, in general, time correlated and, thus, not independent of each other. Modeling time series data using standard modeling approaches (e.g., usual regression analysis) will produce standard errors estimates that can be wrong, and the results of the statistical tests used in hypothesis testing might be biased, which can affect the conclusions derived from them. We considered in this analysis only consecutive, evenly spaced observations (i.e., daily or weekly observations). Having

missing and nonevenly spaced data introduces technical complications and would have required modifications to the approaches adopted here.

The differences between standard linear regression and time series analysis are described by Saint-Germain (1997): *“Linear regression is useful for exploring the relationship of an independent variable that marks the passage of time to a dependent variable when the relationship is linear; that is, when there is an obvious downward, or upward, trend in the data over time. However, if the trend of the dependent variable over time is not linear, then linear regression will not capture the relationship. Linear regression fails to capture seasonal, cyclical, and counter-cyclical trends in time series data. Neither does linear regression capture the effects of changes in direction of time series data, nor changes in the rate of change over time. For time series regression, it is important to obtain a plot of the data over time and inspect it for possible non-linear trends. There is also a problem if the values at one point in the time series are determined or strongly influenced by values at a previous time. This is called auto-correlation. This occurs when the values of the dependent variable over time are not randomly distributed.”*

Thus, we analyzed four time series using the weekly (7-day duration) Radiello 422 basement south indoor air concentrations as the outcome variable:

- X422BaseS Radiello CHCl₃-1, chloroform from Jan. 5, 2011–Feb. 15, 2012
- X422BaseS Radiello PCE-1, PCE from Jan. 5, 2011–Feb. 15, 2012
- X422BaseS Radiello CHCl₃-2, chloroform from Sept. 26, 2012–April 10, 2013
- X422BaseS Radiello PCE-2, PCE from Sept. 26, 2012–April 10, 2013

Note that by conducting the time series analysis in this way (using available continuous data sets, which were 13 months or less in duration), the analysis would be expected to provide information about causes of change in indoor air concentration from week to week and season to season (summer to immediately following fall for example). The analysis would not capture any factors that varied from one winter season to successive winter seasons because the continuous data set did not span a multiyear period (due to resource constraints). Note also that a time series based on individual data points collected over 7 days would not be expected to illuminate any regular patterns of diurnal change repetitively occurring within each day.

Given the expected correlation between consecutive observations, a time series regression model usually includes past and present observations of the outcome of interest (e.g., PCE or chloroform concentration) as well as other predictors. In statistics, the term “predictor” refers to a variable that is possibly a predictor of the outcome under study, also known as the independent variable. Models that include past observations of the time series are called autoregressive models. Previous values of a time-ordered variable are referred as lagged terms. The order of the lag of the outcome (aka dependent), or y-variable, in a model determines the order of the time-series model. For example, if the model only includes the previous observation (denoted as $y(t-1)$) and predictors, it will be termed autoregressive model of order 1, first order autoregressive model or AR(1). A model can include lag terms of the predictors as well.

We conducted a statistical analysis to determine if any of the predictors available were good predictors of the variability of the outcome (e.g., VOC concentrations). The analysis included the evaluation of the stationarity of the time series, determination of which autoregressive model to use, and determination of the lags for the predictor functions. Full and reduced model¹³ approaches were used to evaluate the significance of the reduced models.

¹³ The reduced models are ones from which the lag terms have been successively removed to simplify the equation.

A time series is termed “stationary” if the mean, variance, autocorrelation, etc. are all constant over time. The Augmented Dickey–Fuller test (ADF) (Said and Dickey, 1984) and the Phillips–Perron Unit Root Test (PP) (Perron, 1988) test for stationarity were also calculated to formally evaluate stationarity of the time series. The null hypothesis for the two tests is that the data is nonstationary. Small p-values (p-values < 0.05) suggest evidence favoring stationarity. It is desirable for a time series to be stationary—it does not necessarily mean that it is boring—only amenable to analysis. As Nau (2005a) states:

Most statistical forecasting methods are based on the assumption that the time series can be rendered approximately stationary (i.e., “stationarized”) through the use of mathematical transformations. A stationarized series is relatively easy to predict: you simply predict that its statistical properties will be the same in the future as they have been in the past!The predictions for the stationarized series can then be “untransformed,” by reversing whatever mathematical transformations were previously used, to obtain predictions for the original series.Thus, finding the sequence of transformations needed to stationarize a time series often provides important clues in the search for an appropriate forecasting model.

Another reason for trying to stationarize a time series is to be able to obtain meaningful sample statistics such as means, variances, and correlations with other variables. Such statistics are useful as descriptors of future behavior only if the series is stationary. For example, if the series is consistently increasing over time, the sample mean and variance will grow with the size of the sample, and they will always underestimate the mean and variance in future periods. And if the mean and variance of a series are not well-defined, then neither are its correlations with other variables. For this reason you should be cautious about trying to extrapolate regression models fitted to nonstationary data.

Predictor variables that are significantly associated with the transformed outcome variable are also associated with the original outcome variable. We presented an analysis of what transformations were required to make the chloroform and PCE outcome variable time series adequately stationary in Section 10.7.1 of U.S. EPA (2013); in general, the first difference was used.

6.2.5.1 Introduction to Results—Format of Presentation

Table 6-5 lists a set of variables considered potential predictors for the VOC concentrations. We investigated the serial correlation within each predictor variable’s time series (significant lags). Thus, we determined the transformation (e.g., no transformation, include a lag variable (e.g., lag 1 or past observation = $x(t - 1)$) needed for the inclusion of each predictor in the model. Variables with 0 significant lags did not show significant serial correlation among consecutive measurements and, therefore, did not need any lag transformation. Variables with 1 significant lag necessitated two terms in the model, the variable ($x(t)$) and the previous observation ($x(t - 1)$). Variables with 2 significant lags required a model with three terms: the variable ($x(t)$), the previous observation ($x(t - 1)$), and the second previous observation ($x(t - 2)$).

A control variable is a variable that can affect the association between the dependent variable and other predictors in the model. In this analysis, the variable `Mitigation_status_daily` was considered a control variable because it was expected to have a dramatic effect on the behavior of the vapor intrusion process.

Table 6-5. Significant Lags for Radiello Models

Variable Name	Jan 5, 2011–Feb 15, 2012		Sep 26, 2012–April 10, 2013	
	Significant lags	AR model for	Significant lags	AR model for
Column 1	Column 2	Column 3	Column 4	Column 5
Abs_AMax_Change_dPdt	1	AR(1)	0	0
Bar_drop_Hg.hr	0	0	0	0
Bar_in_Hg	1	AR(1)	0	0
BP_Net_Change	0	0	0	0
BP_Pump_Speed	1	AR(1)	0	0
BP_Stroke_Length	1	AR(1)	0	0
Cool_Degree_Day	1	AR(1)	0	0
DepthToWater	1	AR(1)	0	0
Diff_T_420baseN.Out_F	2	AR(2)	0	0
Diff_T_420baseS.Out_F	2	AR(2)	0	0
Fall_Crk_Gage_ht_ft	1	AR(1)	0	0
Hum_out_.	1	AR(1)	0	0
Max_Change_dPdt	0	0	0	0
Rain_In_met	1	AR(1)	0	0
Rain_IPH	1	AR(1)	0	0
StackEffect_420baseN	1	AR(1)	0	0
StackEffect_420baseS	2	AR(2)	0	0
StdDev_Setra_420ss.base_Pa	1	AR(1)	0	0
StdDev_Setra_422base.out_Pa	1	AR(1)	0	0
StdDev_Setra_422ss.base_Pa	1	AR(1)	0	0
T_422first_C	1	AR(1)	0	0
Wind_Run_mi	0	0	0	0
Wind_Speed_Hi_MPH	0	0	0	0
Wind_Speed_MPH	2	AR(2)	0	0
Soil_H2O_Out13._cbar	1	AR(1)		
Soil_T_C_MW3.6	1	AR(1)		
Soil_T_C_OTC.16.5	1	AR(1)		
StackEffect_420first	2	AR(2)		
T_420baseS_C	1	AR(1)		
T_420first_C	1	AR(1)		
Dew_pt_422_F	1	AR(1)	1	AR(1)
Heat_Degree_Day	2	AR(2)	1	AR(1)
Hum_422_%	1	AR(1)	1	AR(1)

(continued)

Table 6-5. Significant Lags for Radiello Models (continued)

Variable Name	Jan 5, 2011–Feb 15, 2012		Sep 26, 2012–April 10, 2013	
	Significant lags dat1	AR model for dat1	Significant lags dat2	AR model for dat2
Column 1	Column 2	Column 3	Column 4	Column 5
Out_Wkly_Elect_radon	1	AR(1)	1	AR(1)
Setra_420ss.base_Pa	1	AR(1)	1	AR(1)
Setra_422base.out_Pa	1	AR(1)	1	AR(1)
Setra_422base.upst_Pa	1	AR(1)	1	AR(1)
Setra_422SGdp.ss_Pa	1	AR(1)	1	AR(1)
Setra_422ss.base_Pa	1	AR(1)	1	AR(1)
Snowdepth_daily	1	AR(1)	1	AR(1)
Soil_H2O_In6._cbar	1	AR(1)	1	AR(1)
Soil_H2O_Out3.5._cbar	1	AR(1)	1	AR(1)
Soil_H2O_Out6._cbar	1	AR(1)	1	AR(1)
Soil_T_C_MW3.9	1	AR(1)	1	AR(1)
Soil_T_C_OTC.1	1	AR(1)	1	AR(1)
Soil_T_C_OTC.3.5			1	AR(1)
Soil_T_C_OTC.6	1	AR(1)	1	AR(1)
StackEffect_422baseN	2	AR(2)	1	AR(1)
StackEffect_422baseS	2	AR(2)	1	AR(1)
StackEffect_422first	1	AR(1)	1	AR(1)
StdDev_Setra_422base.upst_Pa	1	AR(1)	1	AR(1)
StdDev_Setra_422SGdp.ss_Pa	1	AR(1)	1	AR(1)
T_422_F	1	AR(1)	1	AR(1)
T_422baseN_C	1	AR(1)	1	AR(1)
T_422baseS_C	1	AR(1)	1	AR(1)
T_out_F	1	AR(1)	1	AR(1)
T_out_Hi_F	1	AR(1)	1	AR(1)
T_out_Lo_F	2	AR(2)	1	AR(1)
Wind_Chill_F	1	AR(1)	1	AR(1)
X422baseN_Wkly_Elect_radon	1	AR(1)	1	AR(1)
X422baseS_Wkly_Elect_radon	0	0	1	AR(1)
X422office2nd_Wkly_Elect_radon			1	AR(1)

It was included in the model to account for the testing of subslab depressurization. Because mitigation was not installed in the period 2011 to 2012, none of the models using the 2011 to 2012 data set included mitigation as a control variable. Mitigation was included as a control variable only in models using data from 2012 and 2013. Thus, for the 2012 to 2013 data, the change in VOC concentration was modeled

separately for each predictor variable, but mitigation was always included in the equation. The mitigation was coded with on =1 and off = 0.

The results of the time series analysis that was performed as discussed in U.S. EPA (2013) (Section 10) with the modifications discussed in the previous subsection are reported in the tables in **Attachments 6B** through **6E**. In these and subsequent tables, an * by the coefficient means that the term is significantly correlated with VOC concentration at the 5% significance level. A ** denotes significance at the more stringent 1% significance level.

Note that some of our predictor variables could be described only with a limited number of values; that is, they are categorical variables. Categorical variables included the status of the air conditioning, fan used in fan testing, and central heating. In each case, these were either “on” or “off.” On was coded as a 1 and off as a 0. Other categorical variables included icy precipitation, snow event, and thunder event. In interpreting outputs note that the reference state for these events is no (no events). The reference state for wind direction is East.

For an example of how to read these tables for a continuous variable with a lag term, refer to **Attachment 6B, Table 6B-2** where the outcome is 422 Base south chloroform in units of $\mu\text{g}/\text{m}^3$ and the predictor variable is the second set of rows in the table, barometric pressure in inches of mercury: Bar_in_Hg.

Outcome is $y(t) - y(t - 1)$

Model1: Outcome = intercept + $x(t) + x(t - 1)$

Model1: Change in concentration of chloroform between one week and the previous = -1.35
+Barometric pressure in current week* $-.0115$ + barometric pressure in the previous week* 0.055

Model2: Outcome = intercept + $x(t)$

Model2 (reduced model) Change in concentration of chloroform between one week
and the previous = -0.51 +Barometric pressure in current week* $.0165$

Then in **Attachment B, Table 6B-2** the left-hand set of results columns [estimate, standard error (SE1) r^2 and relative r^2 (rel r^2)] is for the full model. The right-hand set of columns is for the reduced model [estimate (est2), standard error (SE2) and r^2].

For an example of how to read these tables for categorical variables, refer to **Attachment 6B, Table 6B-4**. Referring to the first two rows of results for Predictor: AC_on.off_420_daily; Outcome is 422 Base South Chloroform in units of $\mu\text{g}/\text{m}^3$:

Outcome is $y(t) - y(t - 1)$

Model: Outcome = intercept + $x(t)$

So when AC is OFF, then $y(t) - y(t - 1) = -0.021$

When AC is ON, then $y(t) - y(t - 1) = -0.021 + 0.009$; i.e.:

Change in concentration of chloroform between one week and the previous = -0.012 when the AC is on.
If the AC is off, then the outcome is -0.021 .

The data were compiled and analyzed based on a “passive sampling week,” generally Wednesday to Wednesday. For example, if a sample was taken from July 15 to July 22, it would have an associated “current” week air temperature or rainfall, etc., for July 15 to July 22. Then the 1-week lag would refer to the concentration, temperature, or rainfall from July 8 to July 15. The first difference would be, for example, the (average temperature July 15–July 22) (average temperature July 8–July 15). The 2-week lag would refer to the concentration, temperature, or rainfall from July 1 to July 8.

In U.S. EPA (2013; Section 10), we discussed all of the significant relationships found in the earlier version of this time series analysis. In this discussion, we are more selective, focusing on the relationships that have the most predictive power or that suggest novel insights. We do not discuss cases where only the intercept is significant but slope is not found to be significant.

6.2.5.2 Chloroform Time Series Results January 2011 through February 2012

These results are presented in **Attachment 6B, Tables 6B-1** through **6B-4**. One outcome that is immediately apparent is that no one variable controls vapor intrusion—most individual predictors explain less than 15% of the variation in the indoor air concentration and most individual predictors were not judged to be significant at the 5% significance level. This can be understood as a mathematical demonstration of the observation that multiple factors operate together to control the extent of vapor intrusion—recall the listing of 13 factors for radon vapor intrusion listed by Lewis and Houle (1985; see Section 6.1).

The strength of the stack effect predicted by the temperature differential between the 422 basement south was significant at the 1% level (with r^2 of 0.20) (**Attachment 6B, Table 6B-3**; see also the XY plots of stack effect strength in Section 10.2 of U.S. EPA [2012a]). A stronger stack effect in the current week was associated with higher concentrations of chloroform. Note, however, that the coefficient of the lagged term for the previous week is negative. Results of this type (when the coefficients of the predictor variable in the current period and the lagged period are similar in magnitude but opposite in sign generally) indicate that the change in the predictor variable is the factor related to the outcome variable. So in this case, increasing values of the stack effect are associated with higher chloroform concentrations. This result may suggest why chloroform concentrations in our data sets tend to peak in late fall/early winter because that is the time of year when cooling temperatures outside would be expected to be increasing the strength of the stack effect week over week. A physical explanation of this result may be that the stronger stack effects encourage advective chloroform migration but sustained migration may temporarily deplete the source term (such as the concentration of chloroform at the interface between groundwater and soil gas). This behavior has been previously observed in chamber-scale vapor intrusion experiments (Illangasekare and Petri, 2013). The practical implication of this behavior is that maximum concentrations in indoor air may be more likely to be observed with sampling in early winter. Current guidance in most jurisdictions considers any time within winter to be equivalent.

Snow depth was determined to be significant at the 1% level and had a r^2 of 0.15 for the equation with one lag term (**Attachment 6B, Table 6B-2**). A worked example can help us understand the interpretation of the equation fit to this data. For example, if the average snow depth was 4 inches this week and 0 inches last week, the model predicts that the chloroform concentration would be $0.80 \mu\text{g}/\text{m}^3$ lower this week than the week before. Conversely, if the average snow depth was 0 inches this week and 4 inches last week, the model predicts that the concentration of chloroform this week will be $0.67 \mu\text{g}/\text{m}^3$ higher this week than the week before. A graphical representation of this relationship between the difference in snow depth week to week and the difference in chloroform is shown in **Figure 6-1**. For comparison, note that the “snow event” categorical variable was not statistically significant. One possible physical explanation of this observation is that decreasing snow depth is often associated with flood events and rising water tables, which could bring affected groundwater closer to the structure.

Another term that was significant at the 1% level and had an r^2 of 0.26 was the soil temperature at 1 ft below surface (**Attachment 6B, Table 6B-2**). A worked example can help us understand the interpretation of this equation. For example, if the soil temperature is 0°C this week and was 2°C last week, then the model predicts that this week’s chloroform will be $0.062 \mu\text{g}/\text{m}^3$ higher than the prior week. Conversely, if the soil temperature is 2°C this week and was 0°C last week, then the model predicts that this week’s chloroform concentration will be $-0.179 \mu\text{g}/\text{m}^3$ and thus lower than the week before. The

association of colder shallow soil temperatures with higher chloroform concentrations can also be observed in a simple XY plot (**Figure 6-2a**). Although this simple visualization of the data is subject to the weaknesses of using linear regression on a time series, it may be a more familiar way of thinking about the data to the reader. **Figure 6-2b** shows the first difference of the soil temperature plotted against the first difference of the chloroform concentration—a better representation of what the time series equation is describing. This plot shows that decreasing soil temperatures are associated with increasing chloroform concentrations. The physical mechanism behind this observed trend could be that chloroform is less likely to partition to the gas phase with lower temperatures or that frozen soils create a cap.

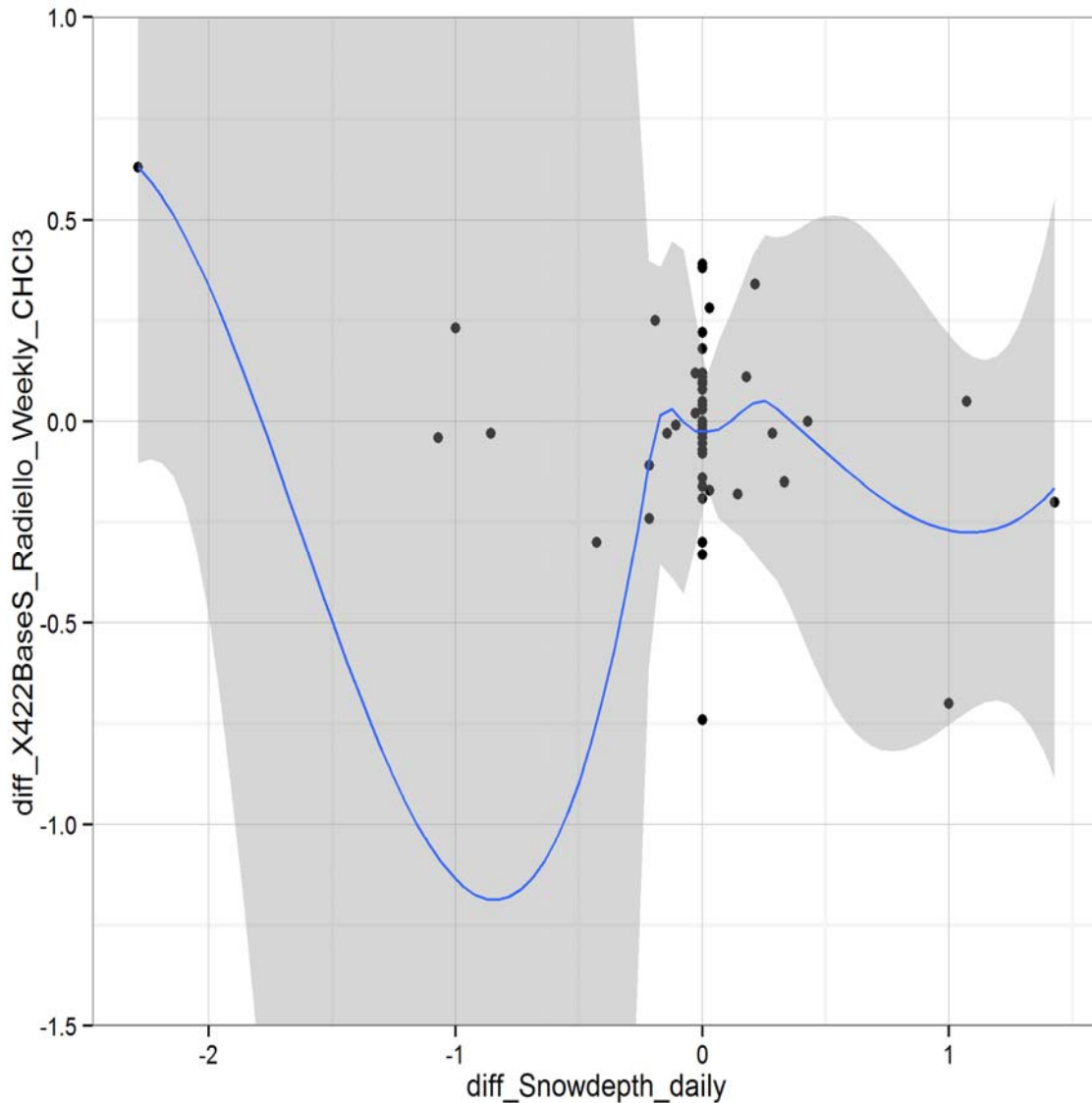


Figure 6-1. XY plot of first difference in snow depth vs. first difference in chloroform concentration (includes locally weighted scatterplot smoothing [LOESS] line [blue], with a 95% confidence interval [shaded]).

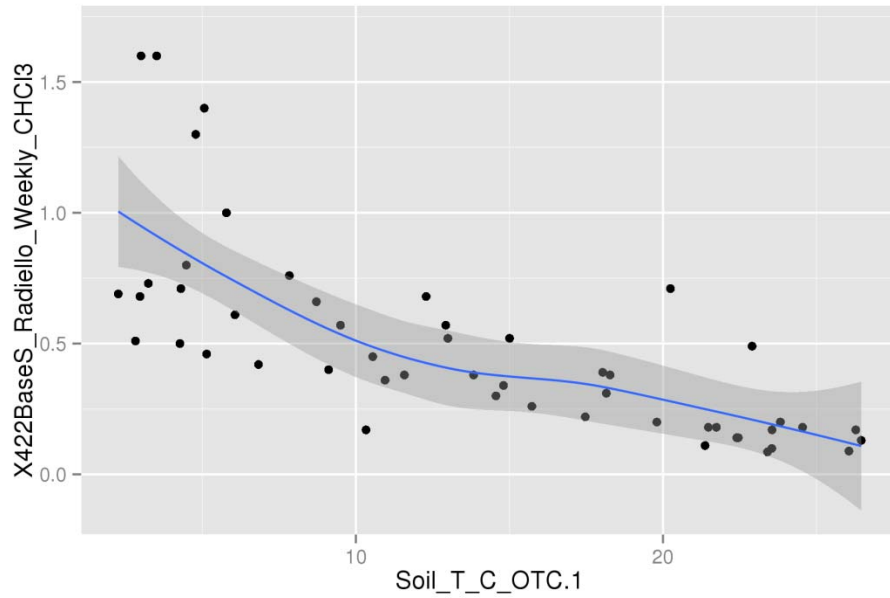


Figure 6-2a. XY plot of shallow external soil temperature at 1 ft vs. 422 basement south chloroform concentration (includes LOESS line [blue], with a 95% confidence interval [shaded]).

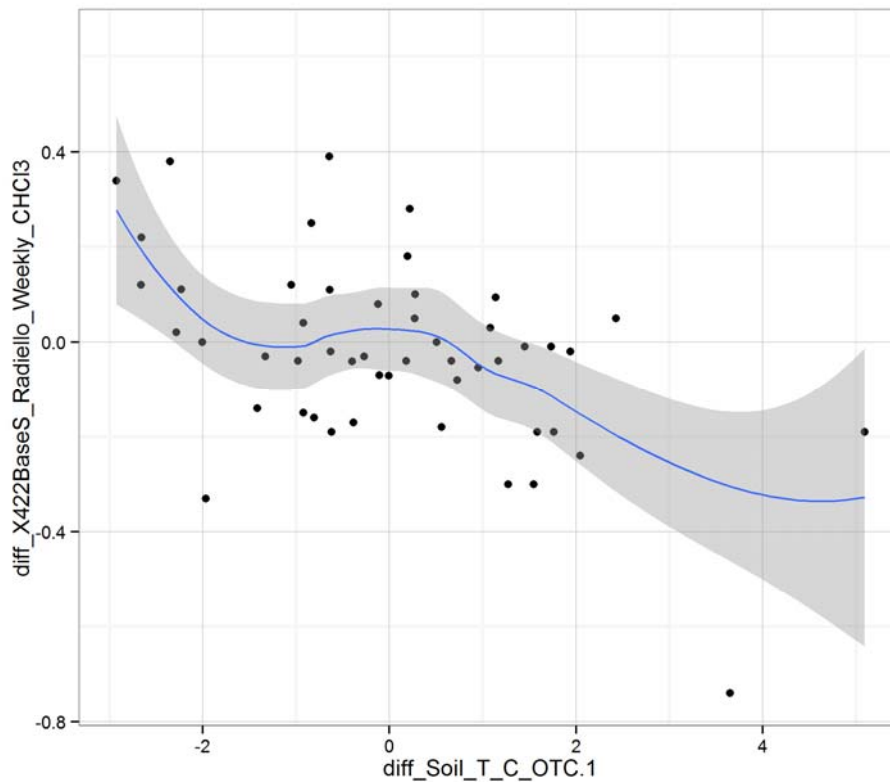


Figure 6-2b. XY plot of first difference of shallow external soil temperature at 1 foot vs. first difference of 422 basement south chloroform concentration (includes LOESS line [blue], with a 95% confidence interval [shaded]).

6.2.5.3 PCE Time Series Results January 2011 through February 2012

The results of this time series are reported in **Attachment 6C, Tables 6C-1 through 6C-4**.

The barometric pressure standard deviation, what we called pump speed of the barometric pumping, was significant at the 5% level but had an R^2 in the reduced model of 0.19 (**Attachment 6C, Table 6C-2**). However, the negative coefficient is surprising, because it would indicate that steadier pressures were associated with greater PCE. An examination of the difference plot suggests that the effect may be nonlinear and, thus, not well captured by the way the analysis was performed. The graphical analysis (**Figure 6-3**) suggests that a substantial change in pump speed week to week, either negatively or positively, increases PCE concentrations and/or the variability of the PCE concentrations. The fact that the full model was significant only for the lag term and the lag coefficient was higher than the $X(t)$ coefficient also suggests the time series modeling may be imperfectly describing the phenomenon.

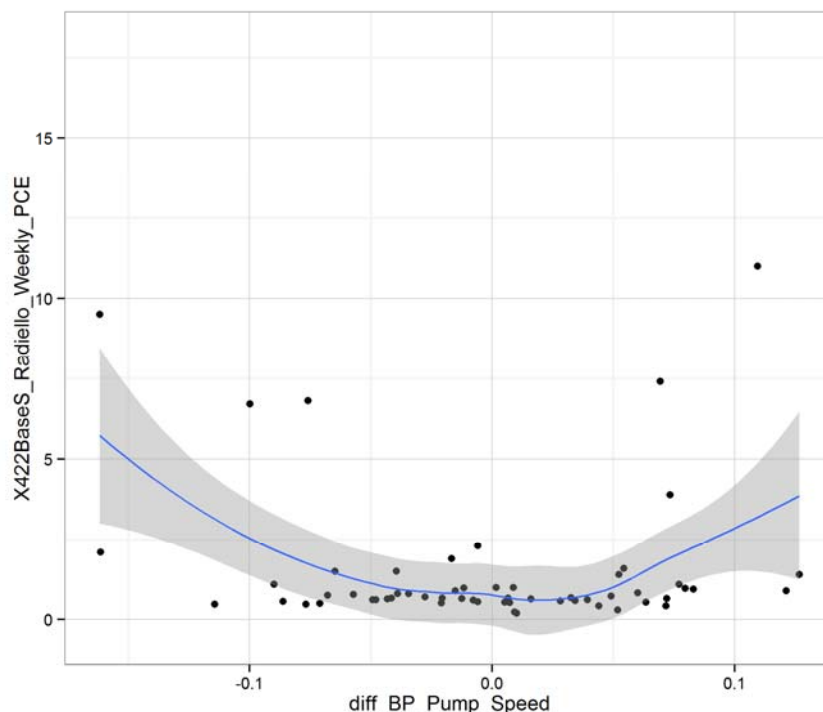


Figure 6-3. XY plot of first difference in barometric pressure standard deviation “pump speed” vs. PCE concentration.

A negative association between snow depth and PCE was noted to be significant at the 1% level in the reduced model, although with only a small R^2 of 0.039 (**Attachment 6C, Table 6C-2**). This is similar to the directionality of the effect for chloroform. A possible physical mechanism would be that snow melt decreases the air permeability of certain surface soils or is contemporaneous with rising water driven by the regional melting. A negative correlation with snow events was also noted (**Attachment 6C, Table 6C-4**) to be significant at the 5% level. However, the difference plot suggests that this is a nonlinear effect (**Figure 6-4**). Although the data set is small, it suggests that either substantial decreases in snow pack or increases in snow pack are associated with higher weekly PCE concentration and/or more changes in PCE concentrations.

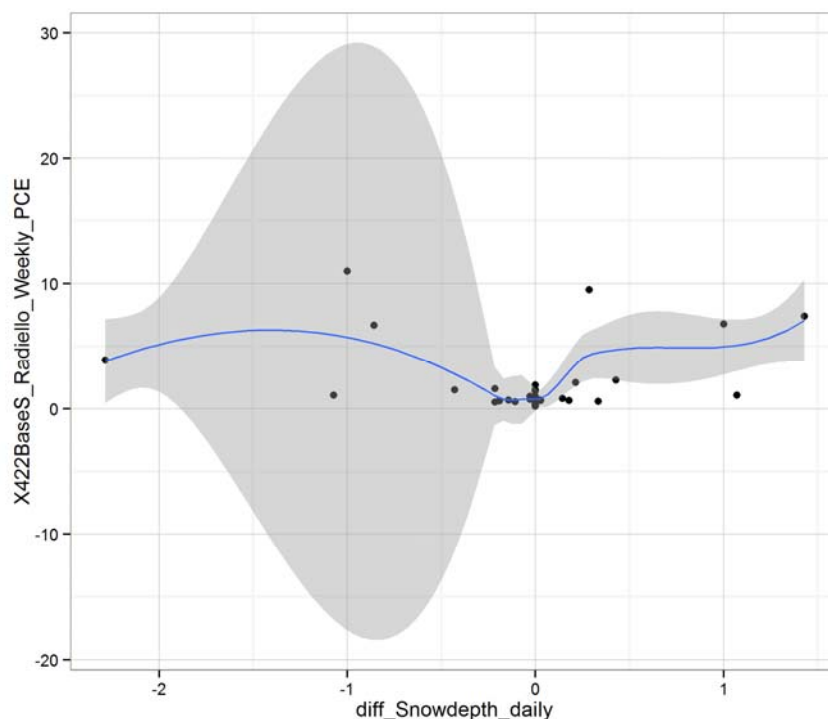


Figure 6-4. XY plot of the first difference in snowdepth vs. PCE concentration.

A positive association between soil temperature directly beneath the building Soil_T_C_MW3.6 and PCE indoor concentration was noted to be significant at the 1% level in the reduced model but with only a small R^2 of 0.044 (**Attachment 6C, Table 6C-2**). This is a physically reasonable result because higher temperatures in the soil would be associated with more partitioning to the gas phase. The same relationship was also noted at the 9 ft depth with a 1% significance and a somewhat larger R^2 of 0.089. The same direction of relationship but with a shallower slope coefficient was also noted at the 6 ft exterior thermocouple with a significance level of 1% and R^2 of 0.089. These results all appear to be physically consistent, because the soil temperatures should run together and the external soil temperature at 6 ft is likely to be more variable than the interior soil temperature at the same depth.

Note that the outside thermocouple at 1 ft was best fitted by the full model, in which the coefficients of the $X(t)$ and $x(t - 1)$ terms were opposite in sign but similar in magnitude, pointing to the importance of the change of the shallow temperature (**Figure 6-5**). One possible physical mechanism for this observation is that cooler surface soil temperatures inhibit the transmission of VOCs to the atmosphere. However, as shown, although there is relatively little scatter in this plot, the r^2 is high and the AIC is low, and the effect is not particularly dramatic (**Attachment 6C, Table 6C-2**).

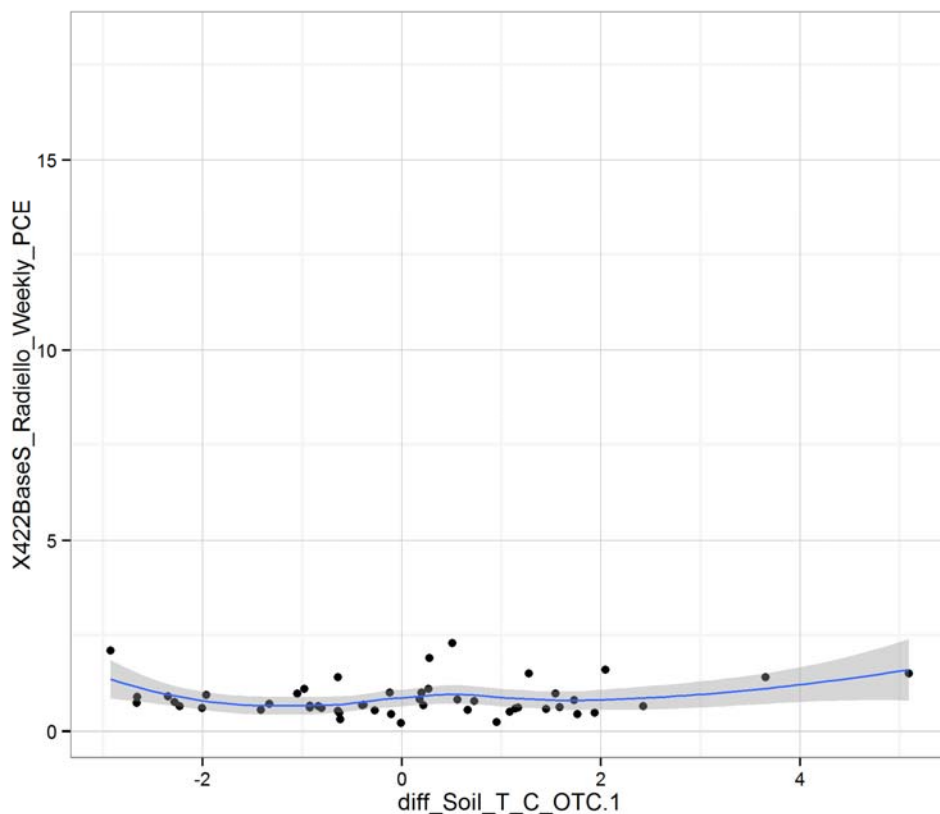


Figure 6-5. XY plot of the first difference in shallow exterior soil temperature vs. PCE concentration.

The stack effect results shown in **Attachment 6C, Table 6C-3** for PCE have to be carefully interpreted (see rows labeled `stack effect_422BaseS` and `stack effect_422BaseN`). Although the coefficient for the highly reduced model for $x(t)$ is shown to be negative and statistically significant, the coefficient for $x(t)$ in the full model is positive. The full model has a significantly superior r^2 and AIC (recall that superior r^2 is a higher value and the superior AIC is a lower value). The positive coefficient for $x(t)$ is consistent with the physical model of stack effect-driven vapor intrusion. Note that in the full model, the coefficient of the $x(t)$ and $x(t - 1)$ terms are similar in magnitude but opposite in sign, suggesting that the change in stack effect may be the important factor in indoor air concentrations as opposed to the absolute stack effect magnitude.

A significant negative effect of wind speed is shown at the 1% level (**Attachment 6C, Table 6C-3**) but with a small $r^2 = 0.03$ and an AIC indicative of a relatively weak correlation. Physically, this could be attributed to enhanced ventilation/air exchange at higher wind speeds.

6.2.5.4 Chloroform Time Series Results September 2012 through April 2013

The results for this time series are presented in **Attachment 6D, Tables 6D-1** through **6D-3**. One of the most interesting results is the relationship to barometric pressure in inches of mercury, which is significant at the 5% level with an r^2 of 0.22 (**Attachment 6D, Table 6D-1**). This shows an association between higher barometric pressures during the current week and increasing chloroform concentrations. The relationship can also be seen in a simple XY plot (**Figure 6-6a**), which, though familiar, may be deceptive for time series data. Thus, we have also plotted the first difference of the barometric pressure against the first difference of the chloroform concentration (**Figure 6-6b**), segregating the data by mitigation status, which was used as a control variable in the time series analysis.

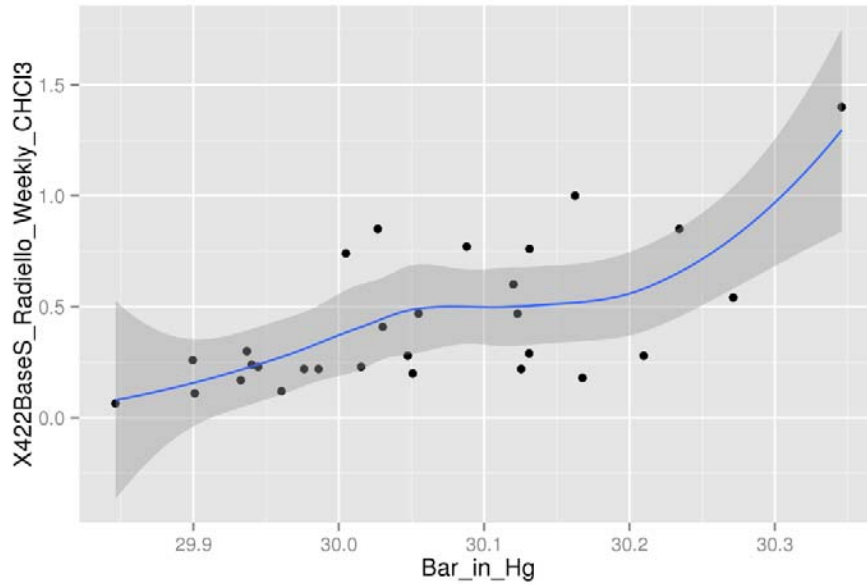


Figure 6-6a. XY plot of barometric pressure (inches of mercury) and chloroform concentration (422 basement south) in September 2012 to April 2013 data set.

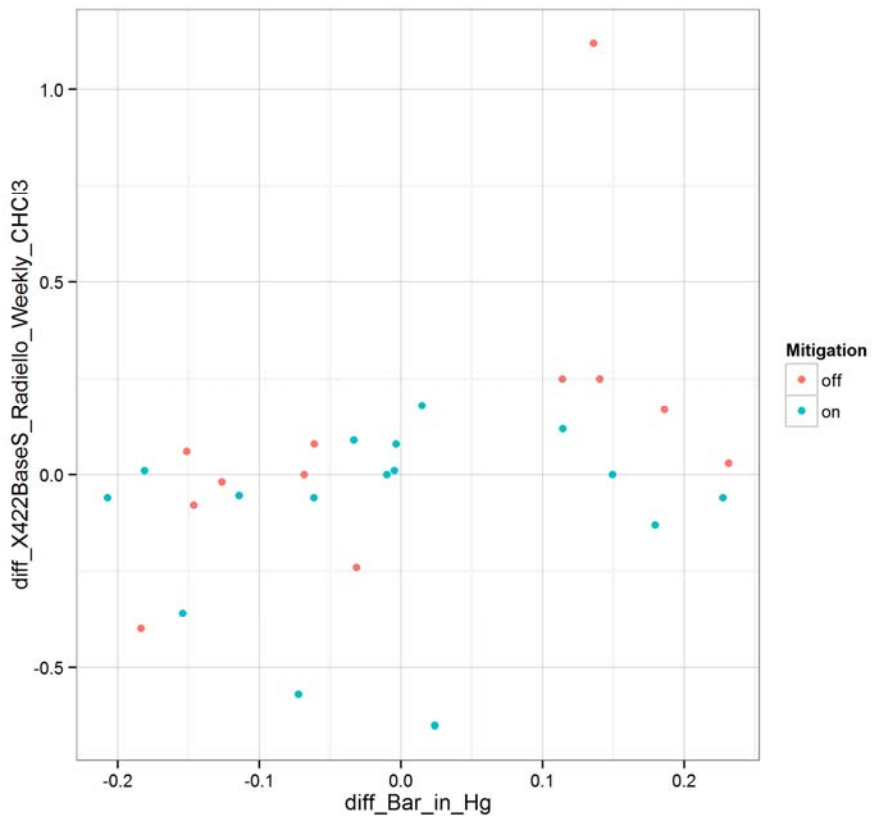


Figure 6-6b. XY plot of barometric pressure (inches of mercury) and chloroform concentration (422 basement south) in September 2012 to April 2013 data set; segregated by mitigation status.

Although in the January 2011 to February 2012 data set the relationship did not reach statistical significance in the time series analysis, it is notable in the XY plot (**Figure 6-7a**) that there does appear to be an association between high chloroform concentrations and higher barometric pressures. Note that the 11 highest chloroform concentrations in this plot all occur during weeks with average barometric pressures between 30.0 and 30.2 inches (**Figure 6-7a**). However, a plot of the first difference of barometric pressure vs. the first difference of chloroform concentration does not show a clear trend (**Figure 6-7b**). Overall, however, considering both data sets and all of these approaches to data analysis, there appears to be a relationship between higher barometric pressure and higher VOC vapor intrusion.

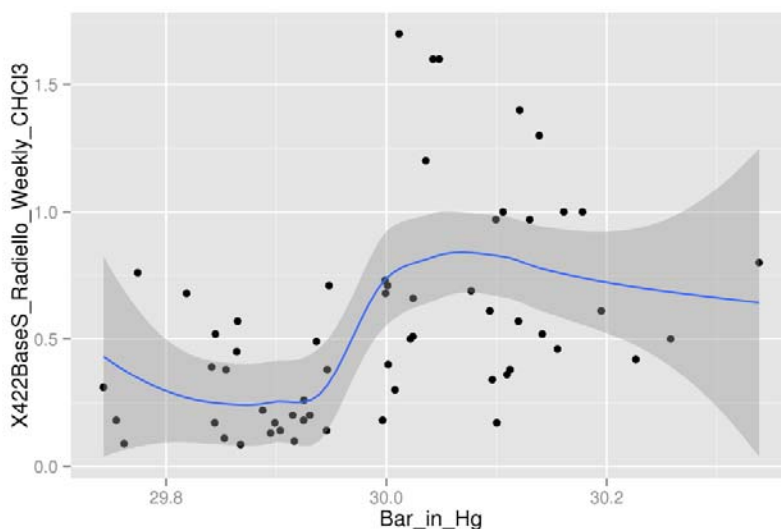


Figure 6-7a. XY plot of barometric pressure vs. chloroform January 2011 to February 2012.

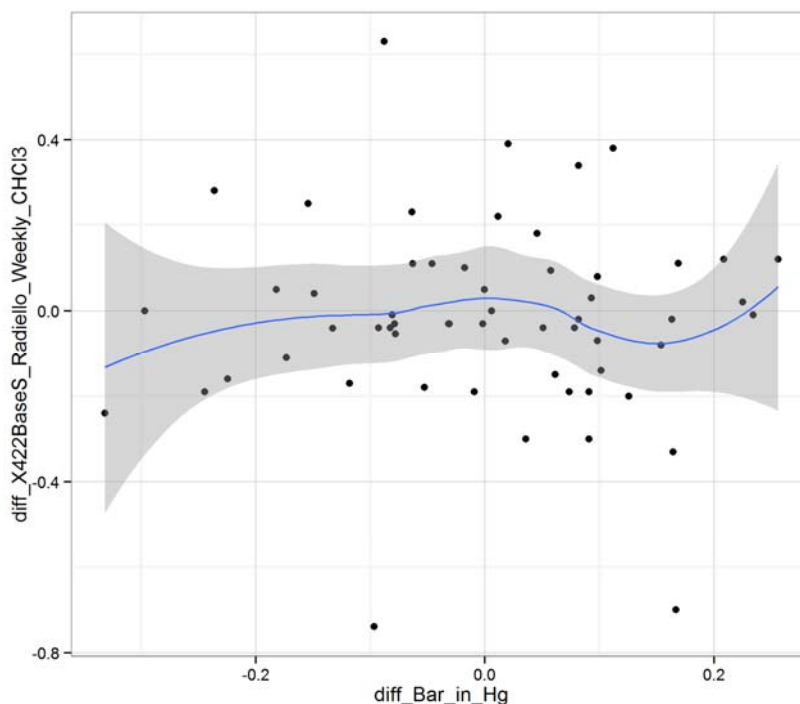


Figure 6-7b. XY plot of first difference in barometric pressure vs. first difference chloroform January 2011 to February 2012.

Although in the radon literature there is generally an association between drops in barometric pressure and increased vapor intrusion (Lewis and Houle, 1985), some insight to the mechanism of this barometric pressure effect may be visible from an analysis of the standard deviation of the basement interior to outside (ambient) differential pressure (StdDev_Setra_422base.out_Pa). That variable is significant at the 5% level in the January 2011 to February 2012 data set (**Attachment 6B, Table 6B-2**) and at the 1% level in the September 2012 to April 2013 data set (**Attachment 6D, Table 6D-1**). The coefficients of $X(t)$ are also similar: 0.046 in the earlier data set and 0.057 in the later data set. Physically, high standard deviations of the barometric pressure between the basement and the ground surface would indicate a greater degree of barometric pumping.

Another interesting correlation found to be significant at the 1% level is the relationship with radon concentration (**Attachment 6D, Table 6D-2**). The r^2 of 0.63 and the very small (actually negative) AIC show this is one of the strongest relationships observed. The same level of significance was found for the weekly electrets in the 422 basement and 422 second floor office. Also very interesting is the observation that the coefficients for $X(t)$ are always positive and those for $x(t - 1)$ are negative and similar in magnitude. This suggests that increasing radon concentrations may be a better indicator of chloroform vapor intrusion than the radon concentration itself. However, this relationship was not statistically significant in the earlier data set. Yet in the earlier data set there does seem to be a relationship, albeit not linear, between radon and chloroform in the XY plot (**Figure 6-8**). High chloroform concentrations are expected to correlate with high radon concentrations if both are due to vapor intrusion, and this is indeed seen with the “high” radon concentrations around 10 pCi/L. However, mechanistically, it is not clear why the highest radon concentrations (two data points with > 15 pCi/L) concentrations are not associated with similarly high chloroform concentrations.

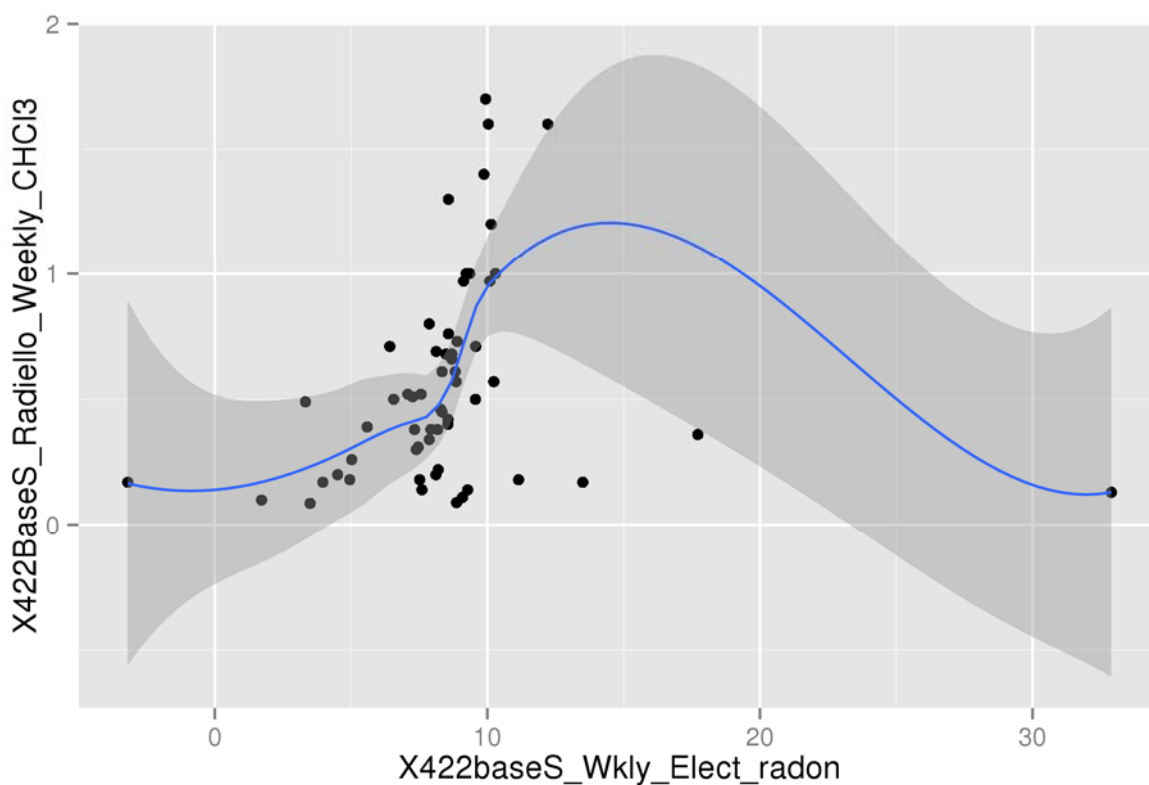


Figure 6-8. XY plot of radon (pCi/L) vs. chloroform ($\mu\text{g}/\text{m}^3$), 422 basement south, January 2011 to February 2012 data set.

A positive correlation with northeast wind direction was noted at the 1% significance level (**Attachment 6D, Table 6D-3**). (Note that northeast winds are a relatively infrequent occurrence [EPA 2013, Chapter 9]). Note that the control variable of mitigation is not found to be statistically significant, but the coefficient is generally negative, suggesting that the mitigation system being turned on provides some benefits but not to a statistically significant degree.

6.2.5.5 PCE Time Series Results September 2012 through April 2013

A positive correlation between PCE and barometric pressure was found, significant at the 5% level and a $r^2 = 0.19$ (**Attachment 6E, Table 6E-1**). This relationship did not require a lag term and is shown in **Figure 6-9**. It is interesting that the same positive relationship was also found for chloroform.

The correlation with radon was found to be significant at the 1% level and a $r^2 = 0.41$. Note that the correlation is opposite in sign and similar in magnitude for the $X(t)$ and $X(t - 1)$ terms (**Attachment 6E, Table 6E-2**). The relationship is shown in **Figure 6-10**. The physical meaning of this result is that week-to-week increases in radon are significantly correlated with increases in PCE.

A correlation between the differential pressure measured between 420 subslab and indoor air was found to be correlated with the 422 basement south indoor air (**Figure 6-11**) at the 5% significance level (**Attachment 6E, Table 6E-2**) and a $r^2 = 0.286$. The coefficients for the $x(t)$ and $x(t - 1)$ were opposite in sign and similar in magnitude indicating that the most important relationship is with the change in differential pressure to the change in indoor concentration. A worked example can help illustrate this equation. If the subslab to indoor differential pressure was +2 Pa this week (into structure), -1 Pa last week (out of structure) and the mitigation system was off the model predicts an increase in PCE week over week of $0.87 \mu\text{g}/\text{m}^3$. If on the other hand pressure was steady both weeks at +2 Pa and the mitigation system was off, the model predicts an increase of only $0.52 \mu\text{g}/\text{m}^3$. If the pressure was steady at -5 Pa both weeks with the mitigation system on, the model predicts essentially unchanged PCE between the two weeks.

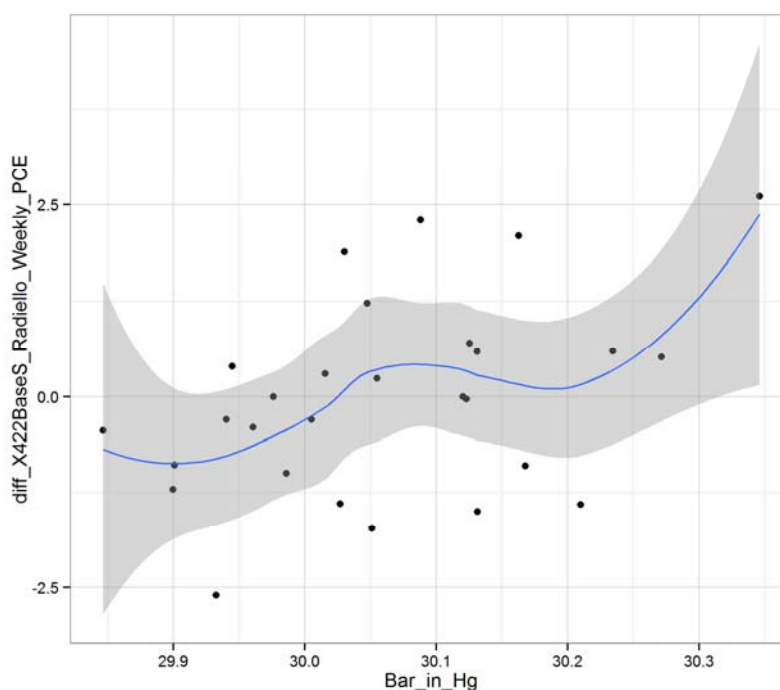


Figure 6-9. XY plot barometric pressure vs. first difference in PCE concentration.

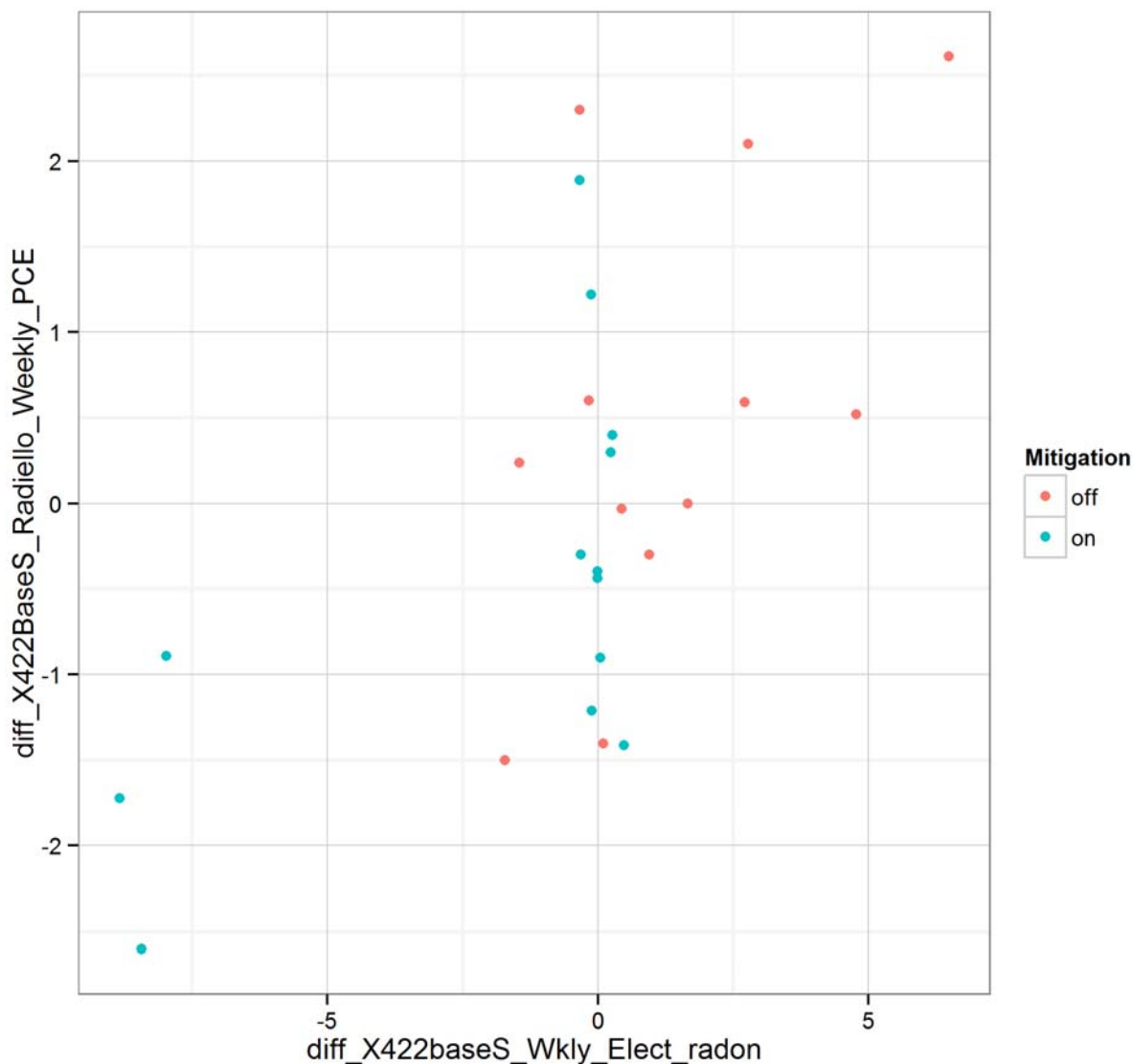


Figure 6-10. XY plot of first difference of radon vs. first difference in PCE.

The physical explanation of this correlation is clear—a differential pressure toward the building supplies a driving force for soil gas to enter the structure. Although this differential pressure monitoring point is on the other side of the demising wall, it is possible that it is correlated with the differential pressure for portions of the 422 side of the basement. The corresponding relationship with the pressure monitoring point on the 422 side of the duplex was found to be significant only in the lag term coefficient. However, the signs of the various terms were the same for the 420 and 422 differential pressure equations. The XY plots of the first difference of the differential pressures vs. concentration are similar for the 420 and 422 sensors (**Figures 6-11 and 6-12**).

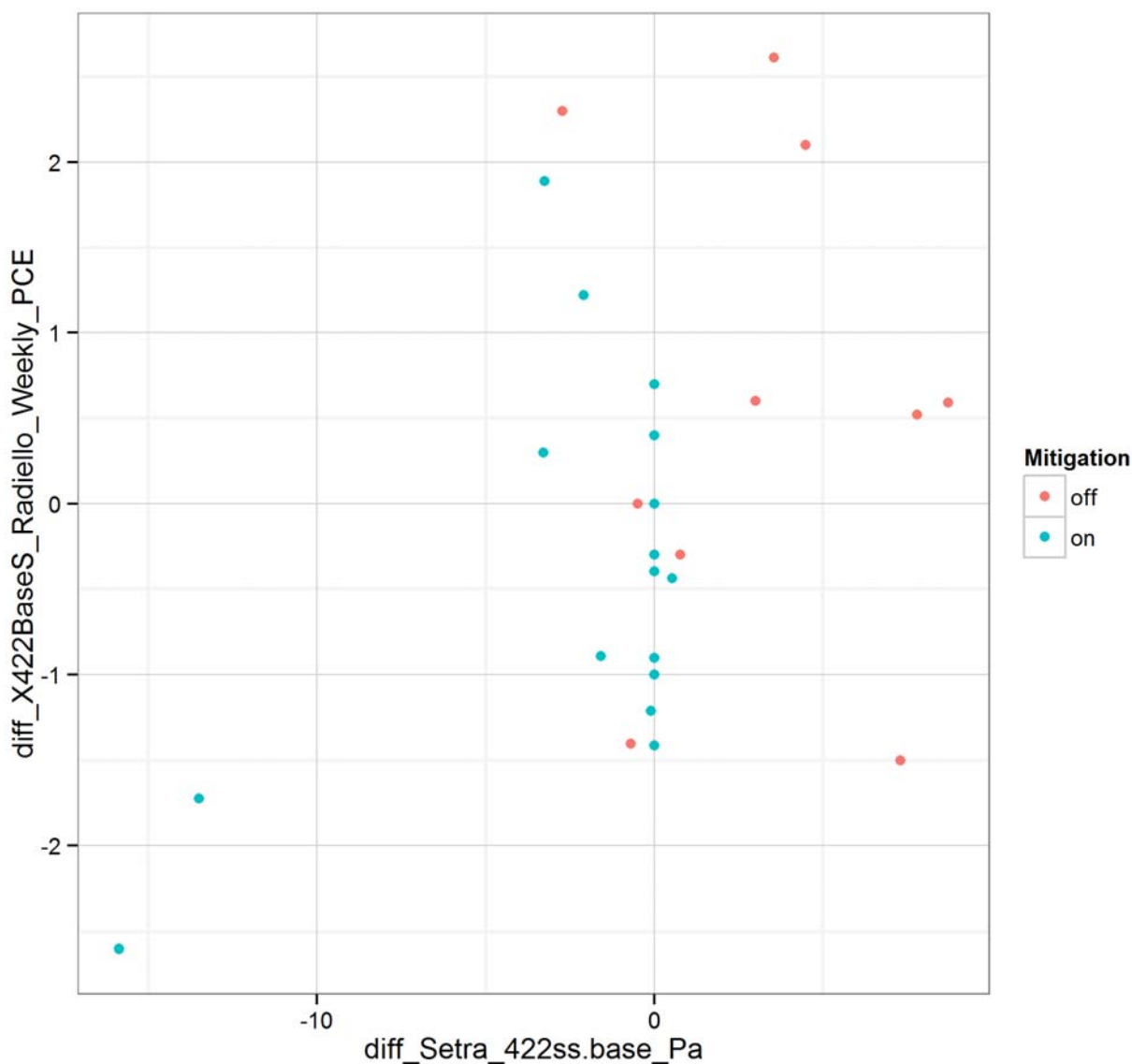


Figure 6-12. XY plot of first difference of 422 subslab to basement differential pressure vs. first difference of 422 basement south PCE concentration.

The only predictor variables among the categorical variables that are statistically significant are wind directions (**Attachment 6E, 6E-3**). However, the signs of those terms that are significant disagree with our previous analysis on this subject (U.S. EPA, 2013, Chapters 9 and 10), so we will need to conduct further analysis/gather more data before reaching any firm conclusions.

It is notable that the mitigation term (control variable) never rises to statistical significance although almost all of the analyses show a coefficient of between -0.3 and -0.9 , suggesting that the mitigation system being on provides a benefit on the order of -0.3 and $-0.9 \mu\text{g}/\text{m}^3$.

6.2.6 Time Series Analysis of Hartman Online GC Data at Daily Resolution

An analysis of the online GC data had been performed using the procedures and variables discussed in U.S. EPA (2013) but was not available in time for the finalization of that document and so is presented here. Aggregation at the daily level of these more frequent measurements was done to facilitate analysis and would serve to deemphasize diurnal effects and focus attention on weather phenomena on the time scale of frontal passage and seasonal change. These data will allow analysis of phenomena on shorter time scales than the weekly Radiello time series discussed earlier in this chapter.

Figures 6-13 and **6-14** show the results of the stationary analysis for the PCE results for the online GC collected at the 422 basement south location for the period from Dec 2012 to March 2013 during which mitigation on-off cycle testing was performed (this data set is referred to as the Hartman 3 period in EPA 2013). The time series analysis was performed using data aggregated to 1-day time resolution (aggregation methods are provided in **Attachment 6A**). Transforming the data with a first difference method was necessary. The first difference solved the stationarity issue observed in the untransformed data in **Figure 6-13**, but a serial correlation was still present. A model for the error term was incorporated in the regression model to account for the remaining serial correlation. See Section 10.7 of U.S. EPA (2013) for a discussion of this procedure. A regression model with an autoregressive 2-day term was fitted to the data sets to account for the remaining serial correlation. Mitigation was used as a control variable.

Among the predictor variables not needing a lag term in their model, three predictors calculated from barometric pressure data (Bar_drop_Hg.hr, BP_Net_Change and BP_Pump_Speed) were found to be significantly associated with PCE (**Attachment 6F, Table 6F-1**) at the 1% level. The sign of the coefficient for the variable “BP-drop,” the mean rate of change in the barometric pressure for the day, was positive. The graphical interpretation suggests that a steady barometer is associated with no change in PCE, a falling barometer with a decrease in PCE, and a rising barometer with increasing PCE (**Figure 6-15**). The barometric pressure net change is defined as the first measurement minus the last measurement for the day. Thus, a positive value for net change is what is commonly referred to as a “falling barometer” and is associated with a decrease in PCE (**Figure 6-16**). These two results from the daily resolution time series based on the online GC data are in agreement with the weekly time series analyses from passive samples discussed earlier that showed associated higher PCE with higher barometric pressures. The association of a rising barometer in the daily data set with higher PCE is also consistent with the analysis of the daily data for mean barometric pressure (**Attachment 6F, Table 6F-2**) that shows in the reduced model that higher barometric pressures are associated with increasing PCE concentrations (**Figure 6-17a** and **6-17b**).

A statistically significant link between PCE concentration and barometric pressure was detected (Table 6F-1). As noted in Table 6F-1 (and as was previously discussed in Section 10.7 of U.S. EPA [2013]), the sign of the coefficient for barometric pressure “pump speed” (the standard deviation of the barometric pressure) was surprising, suggesting that vapor intrusion was associated with steady barometric pressure. However, a visual examination of the data set suggests that this trend is pronounced only for the mitigation system on data (**Figure 6-18**).

The rate of rainfall and two variables relating to wind direction (Wind_Dir and Wind_Dir_Hi) were not found to be significant.

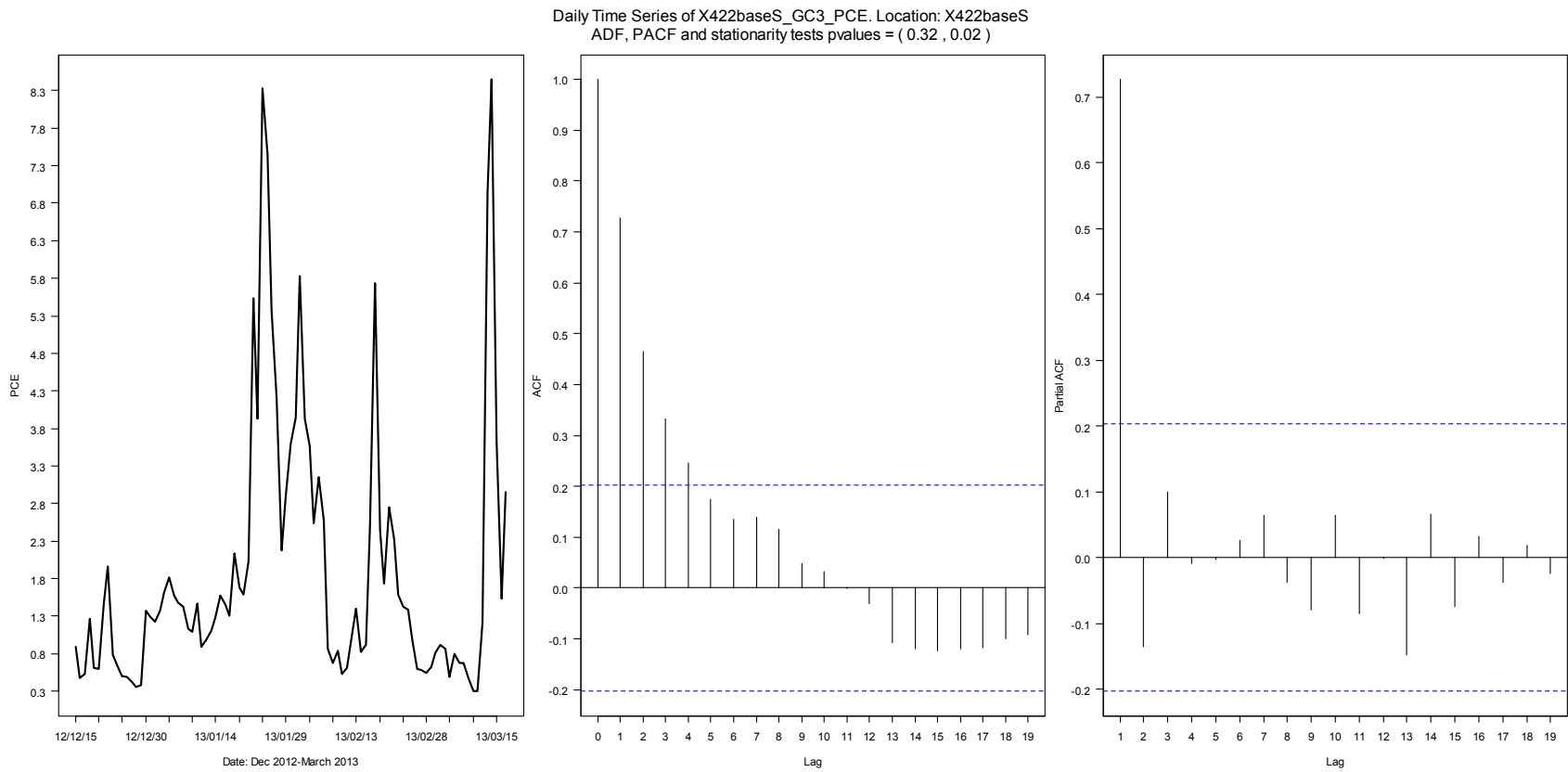


Figure 6-13. Time series plot, ADF and PACF for daily measurements of X422baseS_GC3_PCE. Location X422 base south. Time period: December 2012 to March 2013.

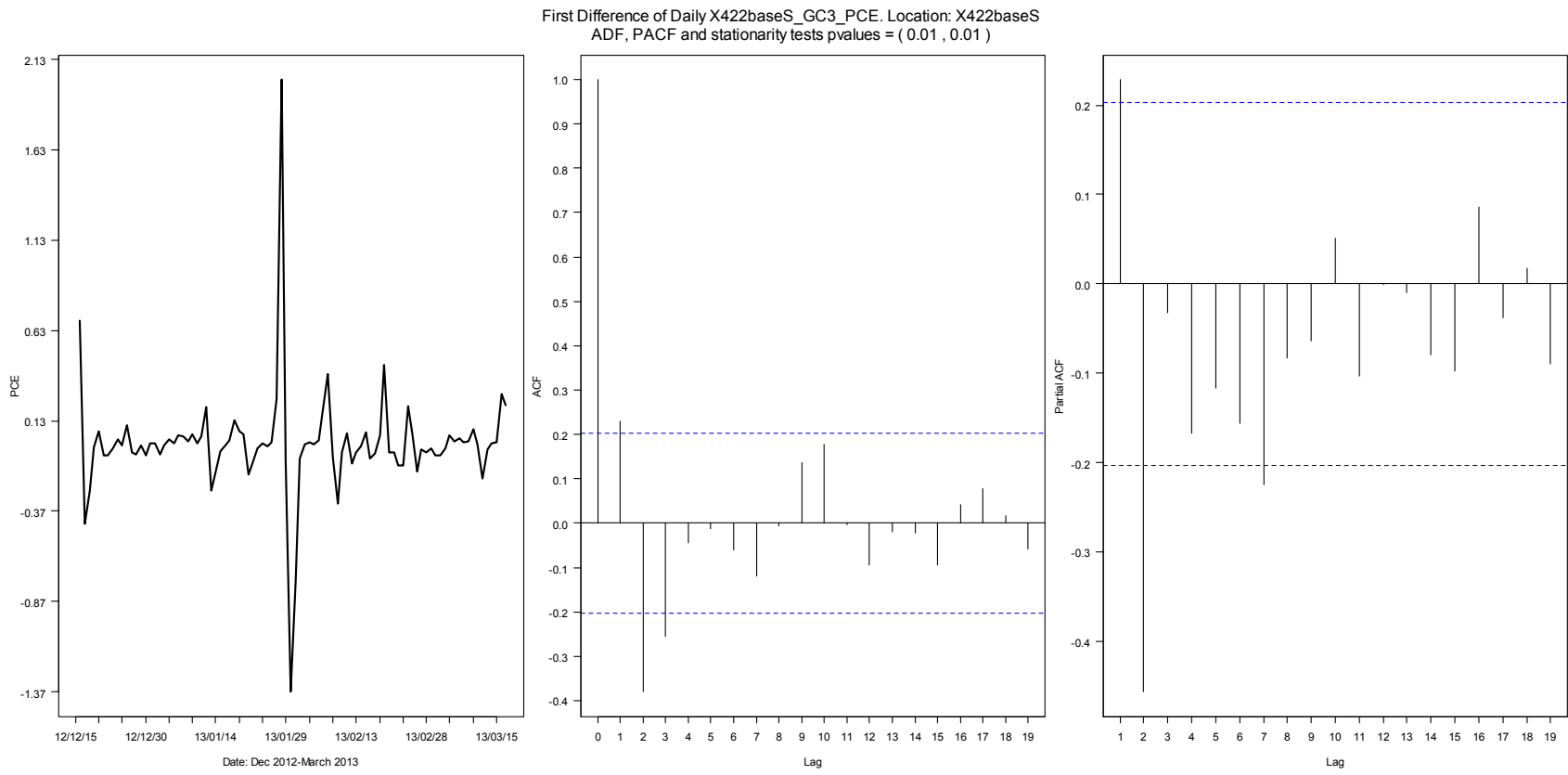


Figure 6-14. Time series plot, ADF and PACF for first difference of daily measurements of X422baseS_GC3_PCE. Location X422 base south. Time period: December 2012 to March 2013.

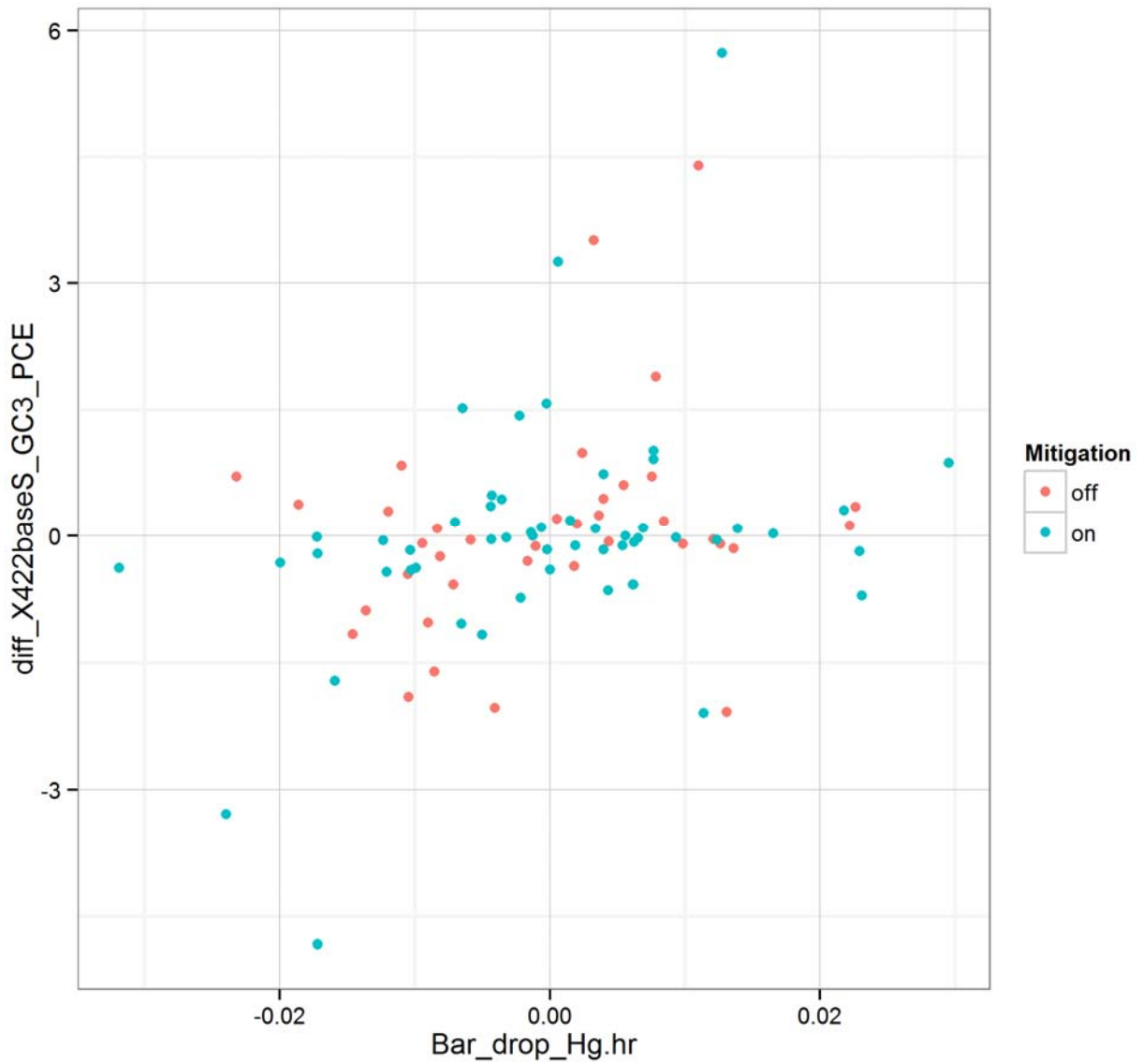


Figure 6-15. XY plot of barometric pressure rate of change in inches of mercury per hour vs. first difference in 422 base south PCE, online GC December 2012 to March 2013.

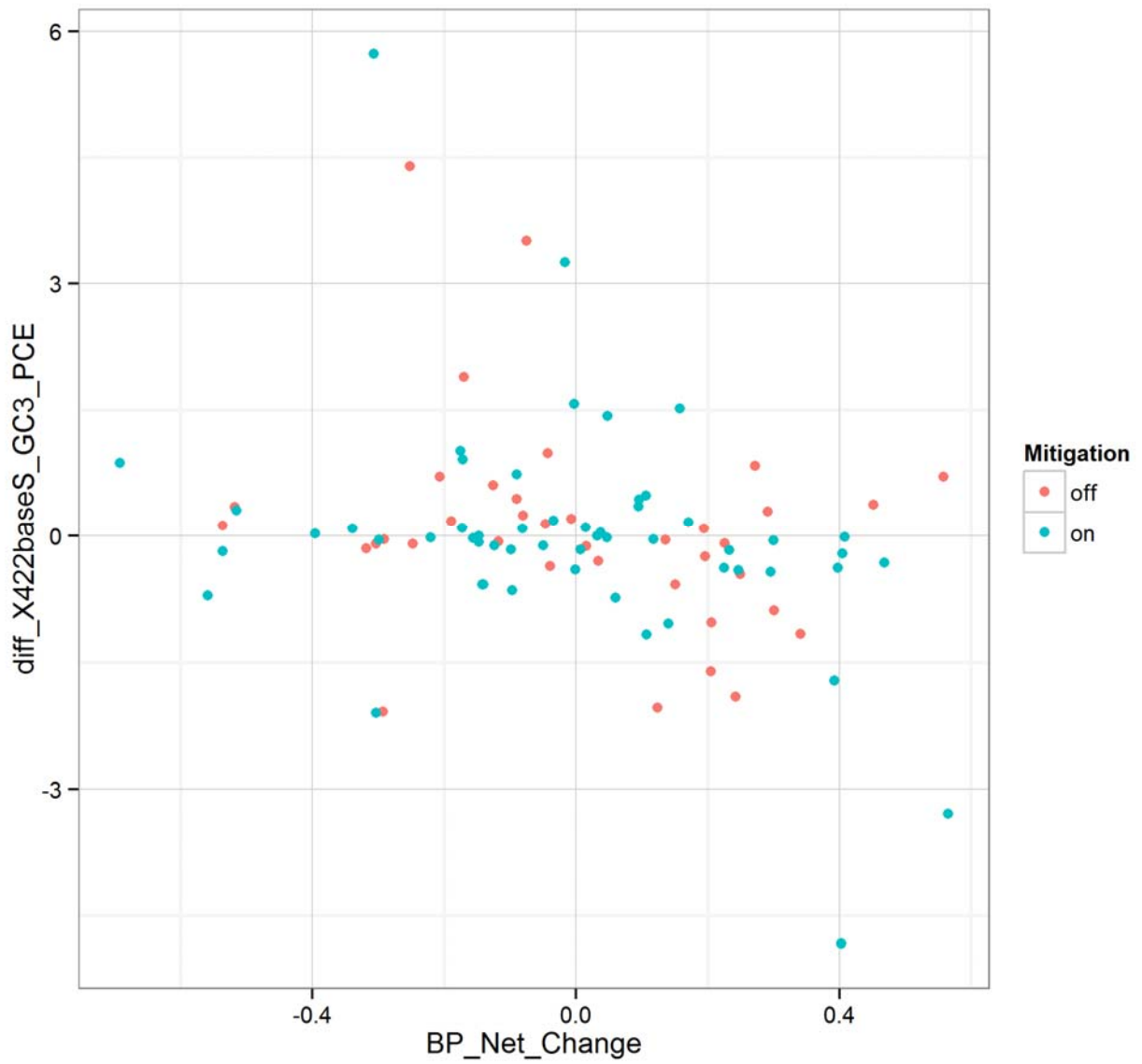


Figure 6-16. XY plot of barometric pressure net change vs. first difference in PCE concentration, online GC Data December 2012 to March 2013.

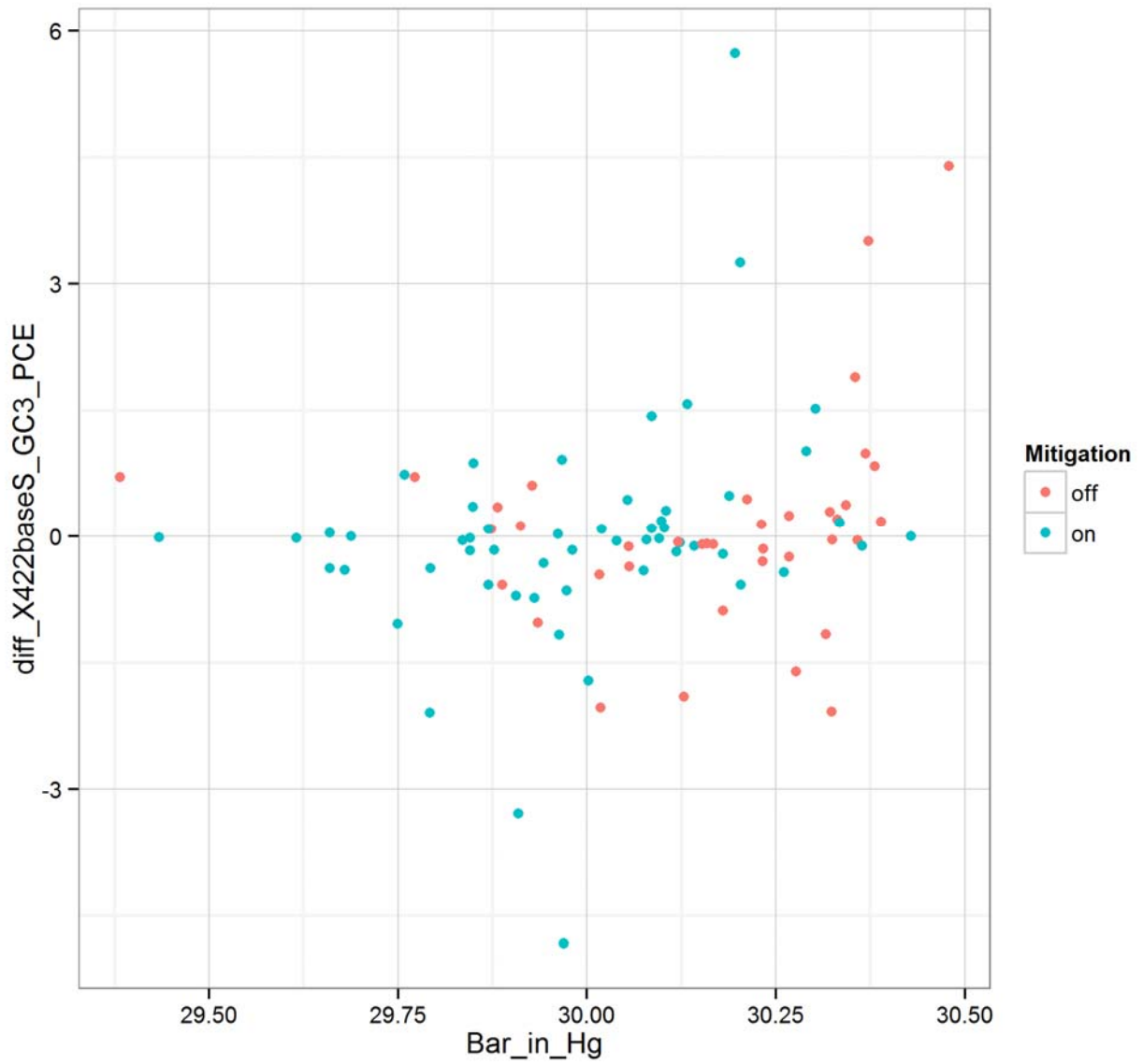


Figure 6-17a. XY plot of mean daily barometric pressure (inches of mercury) vs. first difference in PCE concentration, online GC data, December 2012 to March 2013.

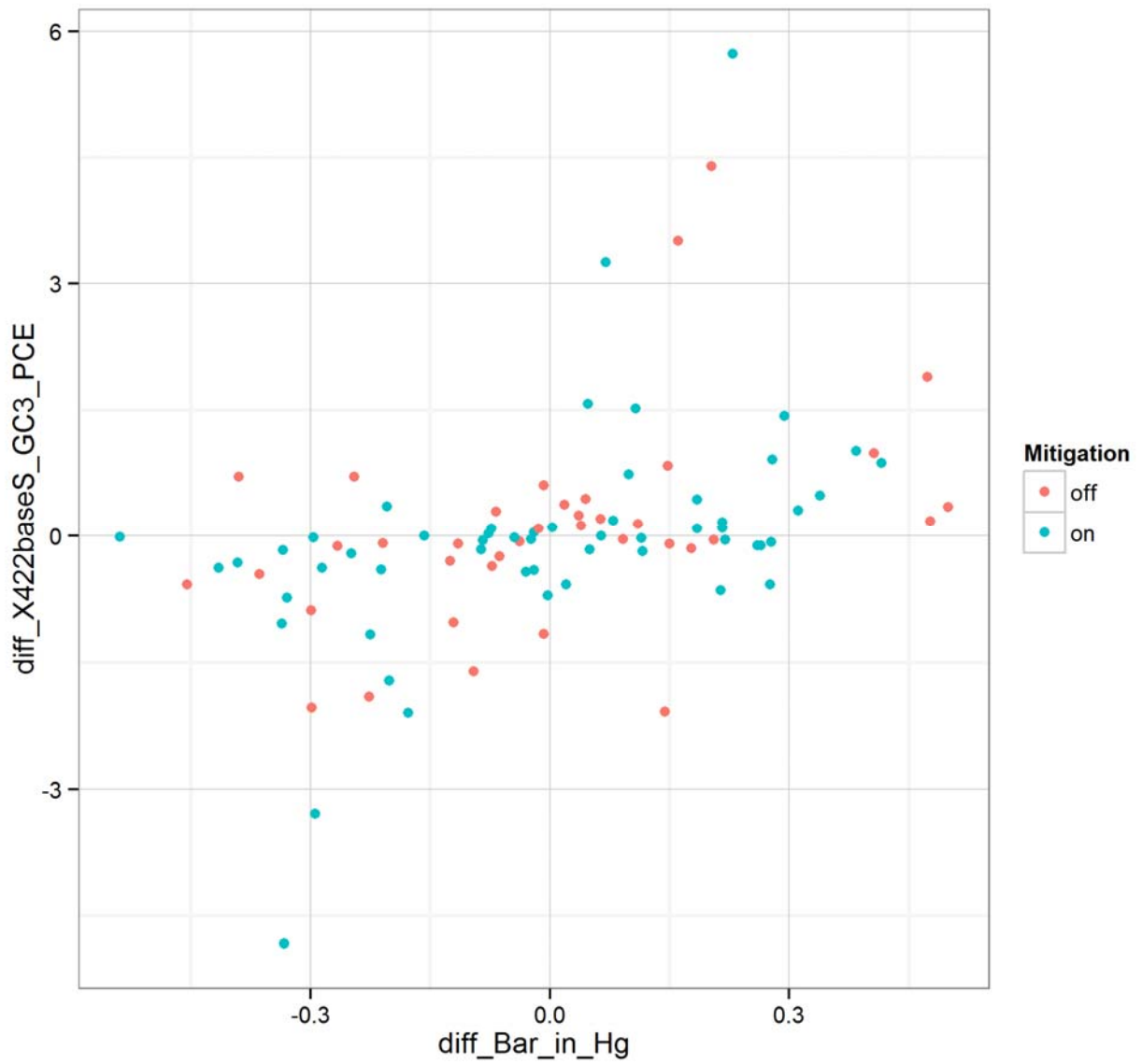


Figure 6-17b. XY plot of first difference in average daily barometric pressure vs. first difference in PCE concentration, online GC data, December 2012 to March 2013.

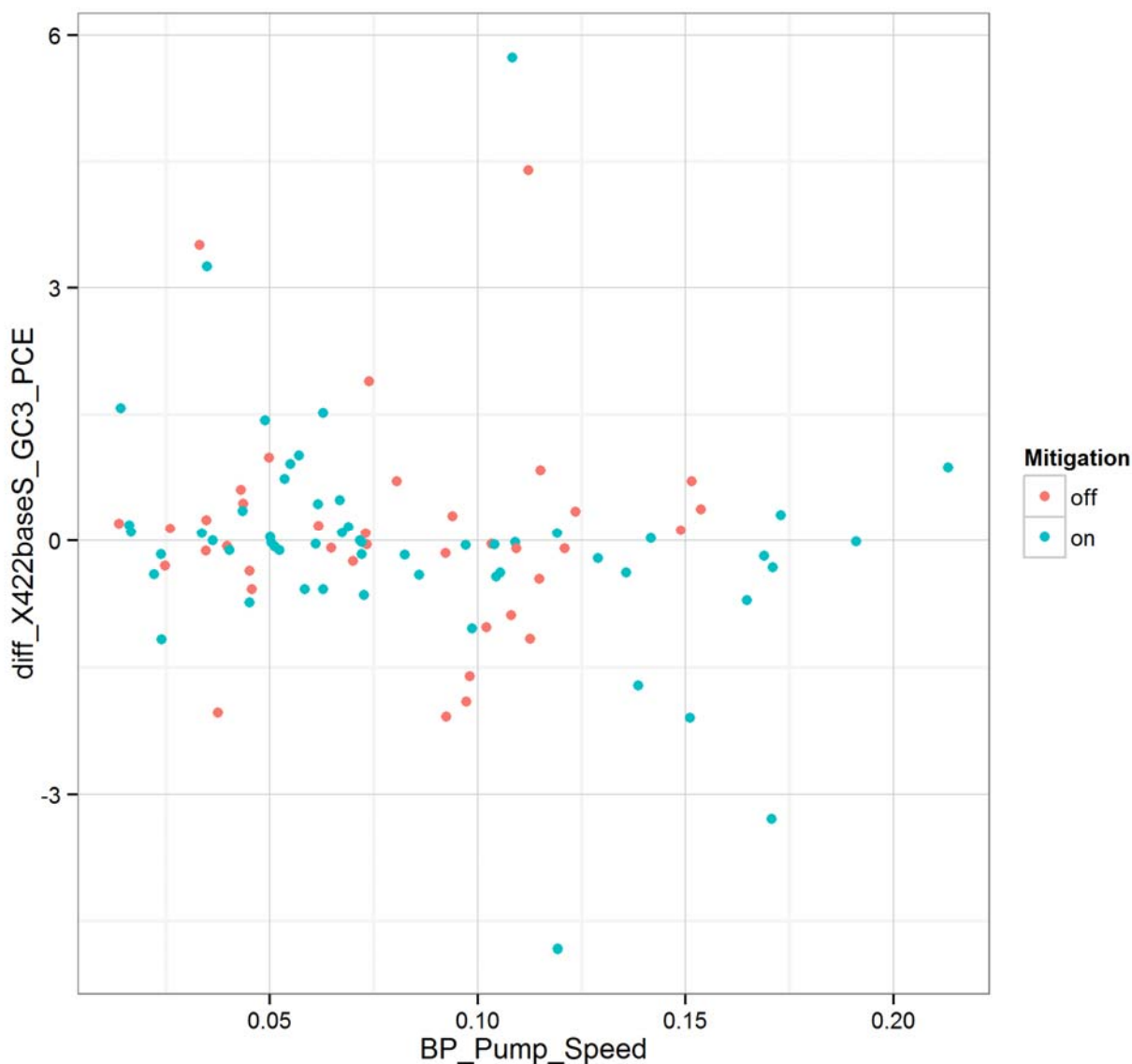


Figure 6-18. XY plot of barometric pressure standard deviation “pump speed” vs. first difference in PCE concentration, online GC data, December 2012 to March 2013.

Attachment 6F, Table 6F-2 summarizes the results for predictor variables requiring a lag-1 day term. Predictors with present and past observations correlated with PCE concentration were:

- six exterior temperature-related variables: mean exterior temperature, the high and low temperatures of the day, heating degree days, heat index, and wind chill;
- five of six interior temperature variables—all of those in the basement and the first floor on the 420 side;
- two differential pressures—between basement and upstairs and basement vs. exterior;
- PCE concentrations at four soil gas locations: SSP4, SSP7, SGP2-9, and SGP8-9;
- one exterior soil thermocouple at 6 ft; and
- the indoor and outdoor humidity.

Some worked examples of the models in **Attachment 6F, Table 6F-2** can help us understand the implications of these exterior temperature results:

- Using the reduced model for the mean outdoor temperature, with the mitigation system off, if today's temperature is 20° F, then the indoor concentration is predicted to be 0.57 $\mu\text{g}/\text{m}^3$ higher than the previous day's concentration. If, in contrast, today's temperature is 50°F, then the concentration is predicted to be $-0.8 \mu\text{g}/\text{m}^3$ lower than that the day before. This relationship agrees with expectations from the stack effect. The break point where the indoor concentration is expected to not change is interestingly at 32° F with the mitigation off.
- Using the full model, if the mean outdoor temperature has fallen to 20° F today and was 40° F yesterday, indoor concentrations are projected to have increased by 1.5 $\mu\text{g}/\text{m}^3$. If temperature is steady at 20° F both today and yesterday, then indoor concentration is predicted to be 0.3 $\mu\text{g}/\text{m}^3$ higher than the day before. If temperatures, however, are rising with 20° F today and 10° F yesterday, indoor concentrations are projected to have decreased by 0.2 $\mu\text{g}/\text{m}^3$.
- Note that in both the reduced and full model of mean outdoor temperature, the mitigation term is not statistically significant and is small in magnitude so that the difference of the mitigation being on or off is equivalent to 2° F of temperature.
- Examining the reduced model of heating degree days we notice that a high number of heating degree days (colder weather) is required for the indoor air concentration to increase over the previous days. The “break even” point is reached at 30 heating degree days = 35° F average daily temperature with the mitigation off. At temperatures below 35° F, the indoor concentration is projected to increase. This agrees quite closely with the model for mean outdoor temperature as would be expected.
- Using the full model of heating degree days (**Figure 6-19**) with mitigation off if the mean outdoor temperature has fallen to 20° F today (45 HDD) and was 40° F yesterday (25 HDD), indoor concentrations are projected to have increased by 1.5 $\mu\text{g}/\text{m}^3$, essentially the same prediction as we saw with the full model of outdoor temperature for the same circumstances.

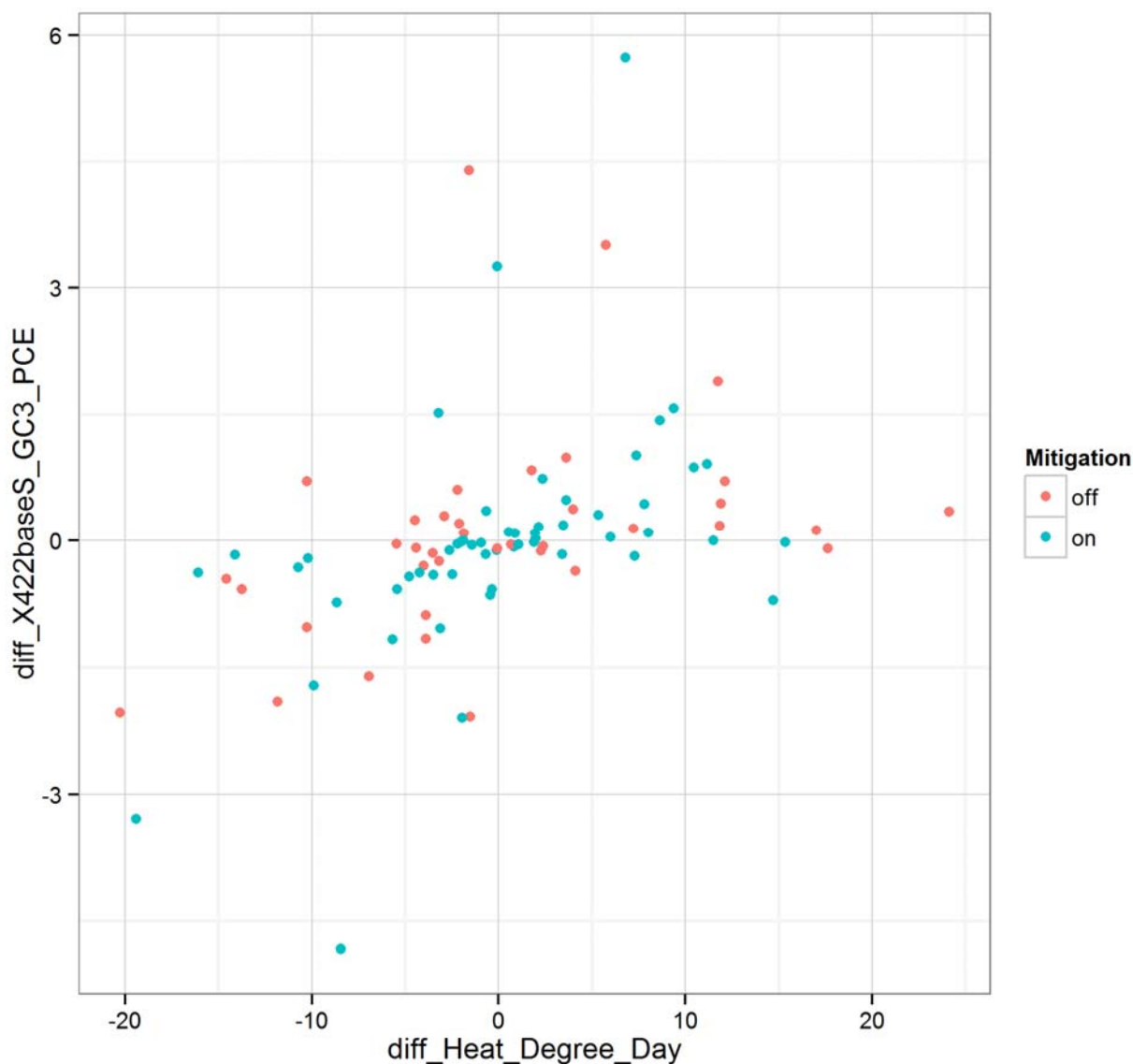


Figure 6-19. XY plot of the first difference in heating degree days vs. the first difference in indoor PCE concentration, online GC data, December 2012–March 2013.

The interior temperature results in **Attachment 6F, Table 6F-2** show a pattern where the coefficients for $x(t)$ and $x(t - 1)$ are opposite in sign and similar in magnitude, indicating that they are most sensitive to changes in temperature from day to day. The large coefficients for the 422 basement temperatures suggest that the 422 basement interior concentrations are most sensitive to changes at that location, which is expected. For example, if the temperature at the 422 basement south location is 58° F today and 60° F yesterday, PCE is predicted to have increased by approximately 2.0 $\mu\text{g}/\text{m}^3$ (**Figure 6-20**). The lack of significance for the 422 first floor temperature is rational, but the statistically significant, rather weak dependence on the 420 first floor temperature is an unexpected result.

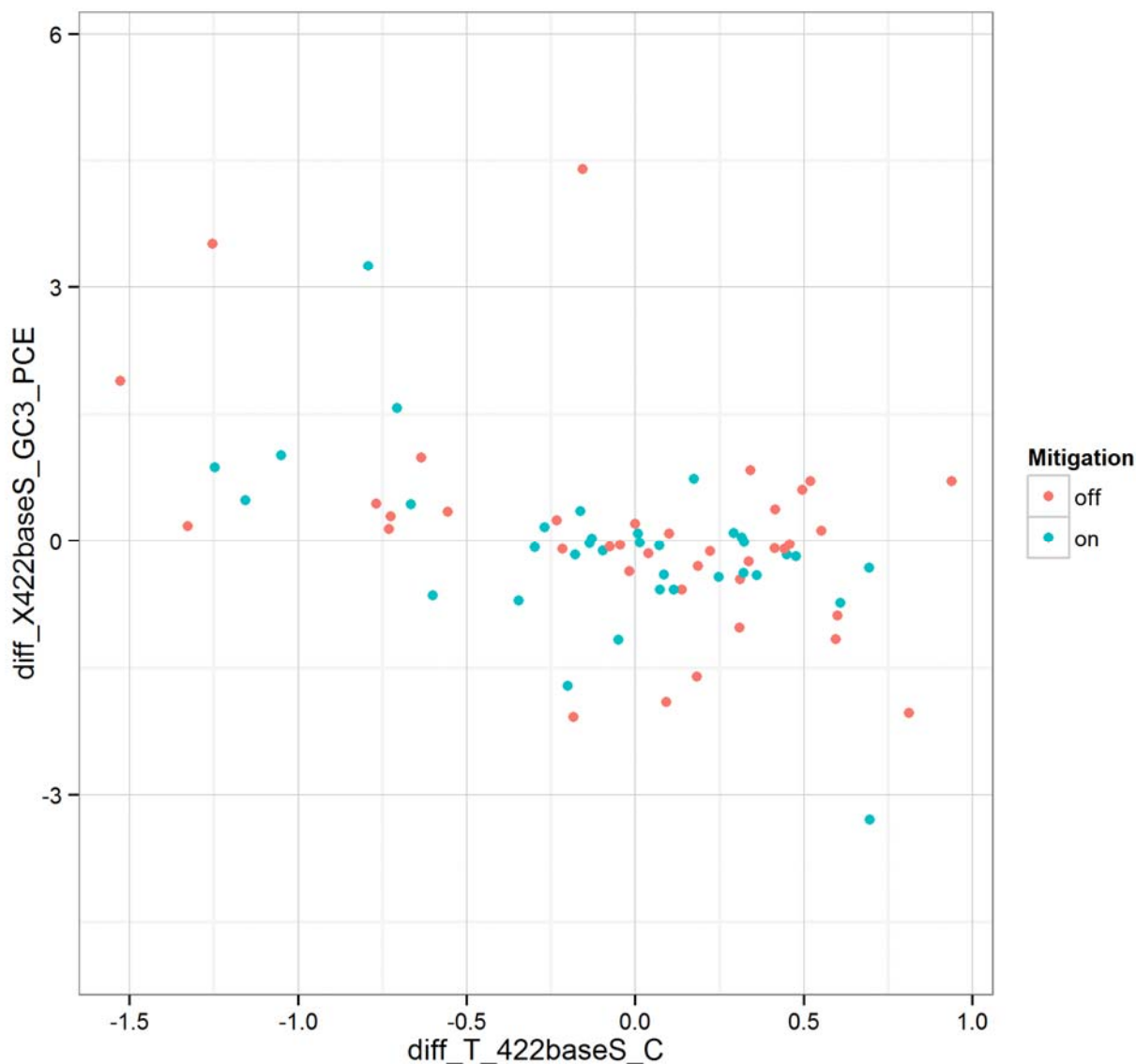


Figure 6-20. XY plot of the first difference in temperature at the 422 base south location to the first difference in indoor PCE concentration at the same location; online GC data, December 2012 to March 2013.

The subslab ports also show a pattern of opposite coefficients and similar magnitude for today's and yesterday's concentrations, indicating that the relationship to indoor air is strongest to the changes in subslab concentrations. Using example concentrations similar to some of those observed at this port (800 and 1000 $\mu\text{g}/\text{m}^3$), worked examples show that increasing concentrations at SSP-4 are associated with decreasing indoor concentration (**Figure 6-21**). The observed concentrations at SSP-7 were much lower, so the worked examples were tested with concentrations of 4 and 18 $\mu\text{g}/\text{m}^3$. Those calculations showed that increasing concentrations at SSP-7 were associated with increasing indoor air concentrations in the 422 basement (**Figure 6-22**). The quality of the fit at SSP-7 with the mitigation off is remarkably good. One possible interpretation of these results is that increases at SSP-7 are indicative of VOC mass moving toward the center of the building along a north-south axis.

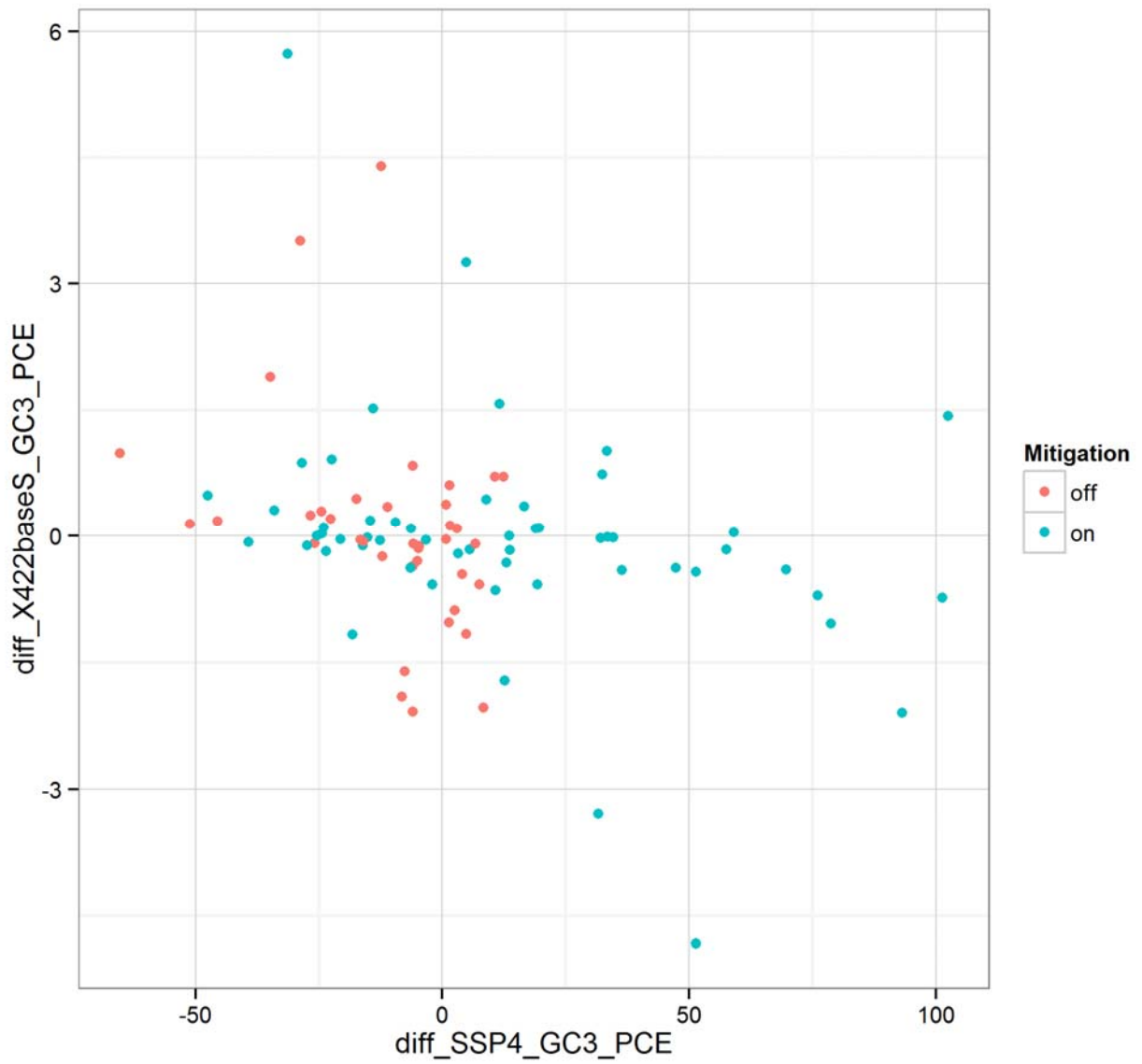


Figure 6-21. XY plot of first difference in subslab port SSP-4 PCE vs. first difference in 422 basement south PCE, online GC data December 2012 to March 2013.

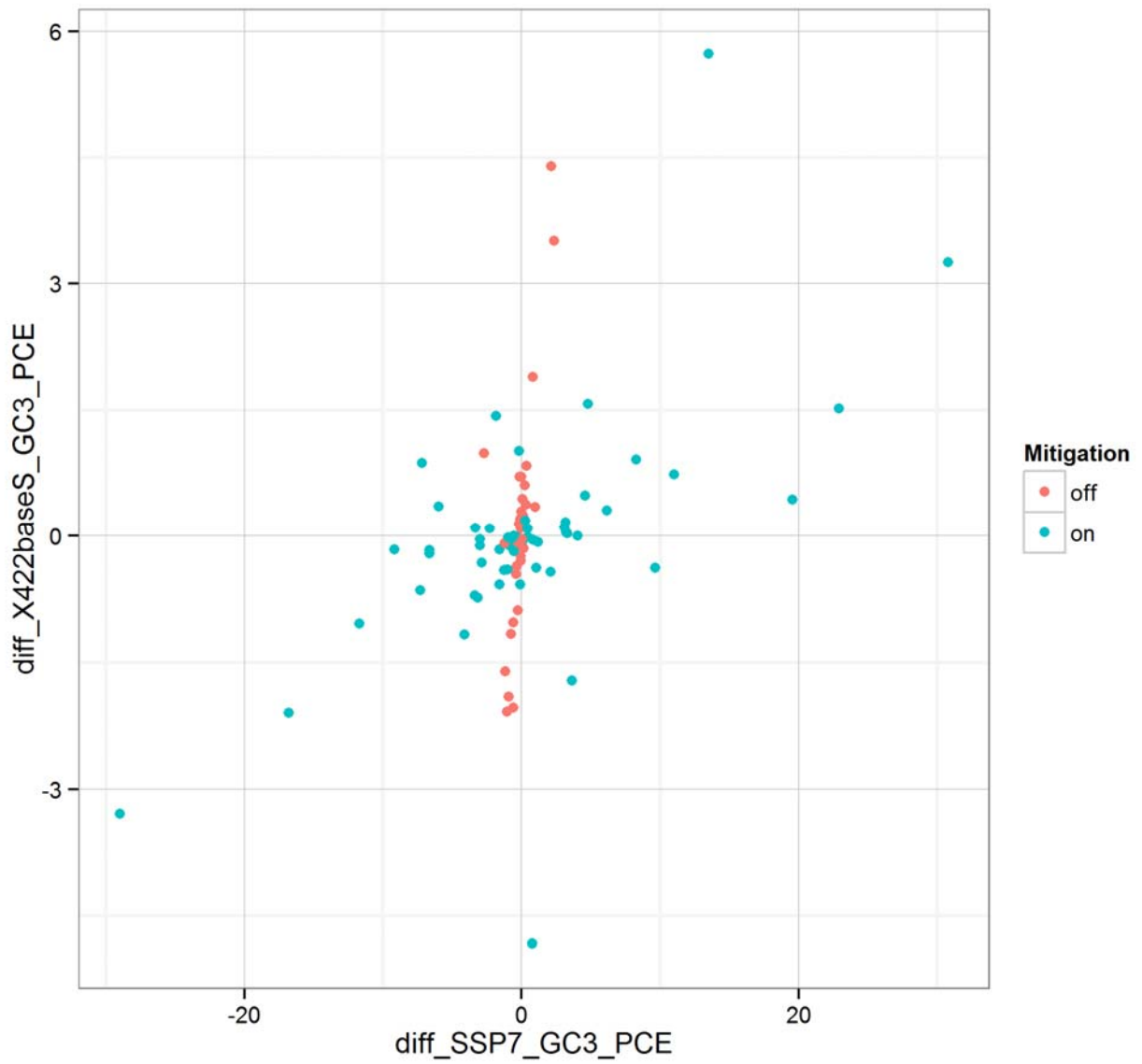


Figure 6-22. First difference in subslab port 7 PCE vs. first difference in indoor air PCE at 422 basement south; online GC data, December 2012 to March 2013.

Similarly, in **Figure 6-23** with the mitigation system on, there appears to be a pattern where decreasing concentrations at a deeper level (9 ft) are associated with increasing indoor basement concentrations.

The differential pressures that were statistically significant in the time series analysis are those that were essentially unaffected by the mitigation system (see Figures 5-4 and 5-5 in U.S. EPA, 2012a). It is possible that the fact that other differential pressures “pegged” off scale means that the data analysis for those differential pressures was harmed by the off-scale behavior. The positive correlation in the reduced model of basement vs. upstairs differential pressure with basement VOC concentration may be indicating that higher flows up through the house are associated with greater vapor intrusion (**Figure 6-24**). The negative coefficient for the basement vs. exterior differential pressure implies that as the basement pressure increases, the VOC concentration decreases, which is a physically reasonable result because an outward driving force would be expected to reduce vapor intrusion (**Figure 6-25**).

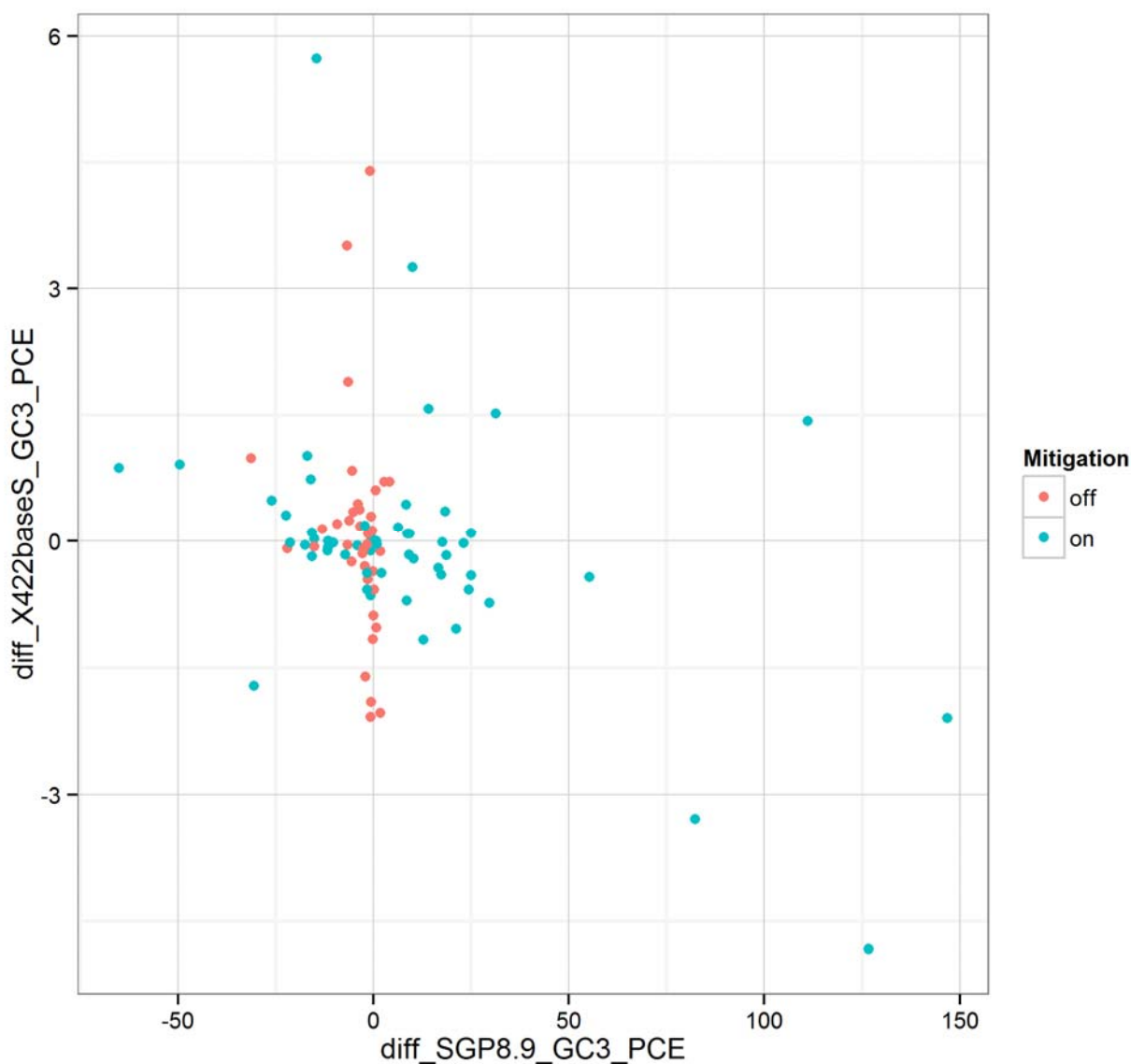


Figure 6-23. XY plot of first difference in PCE concentration at soil gas point 8-9 vs. first difference in indoor concentration at 422 basement south; online GC data; December 2012 to March 2013.

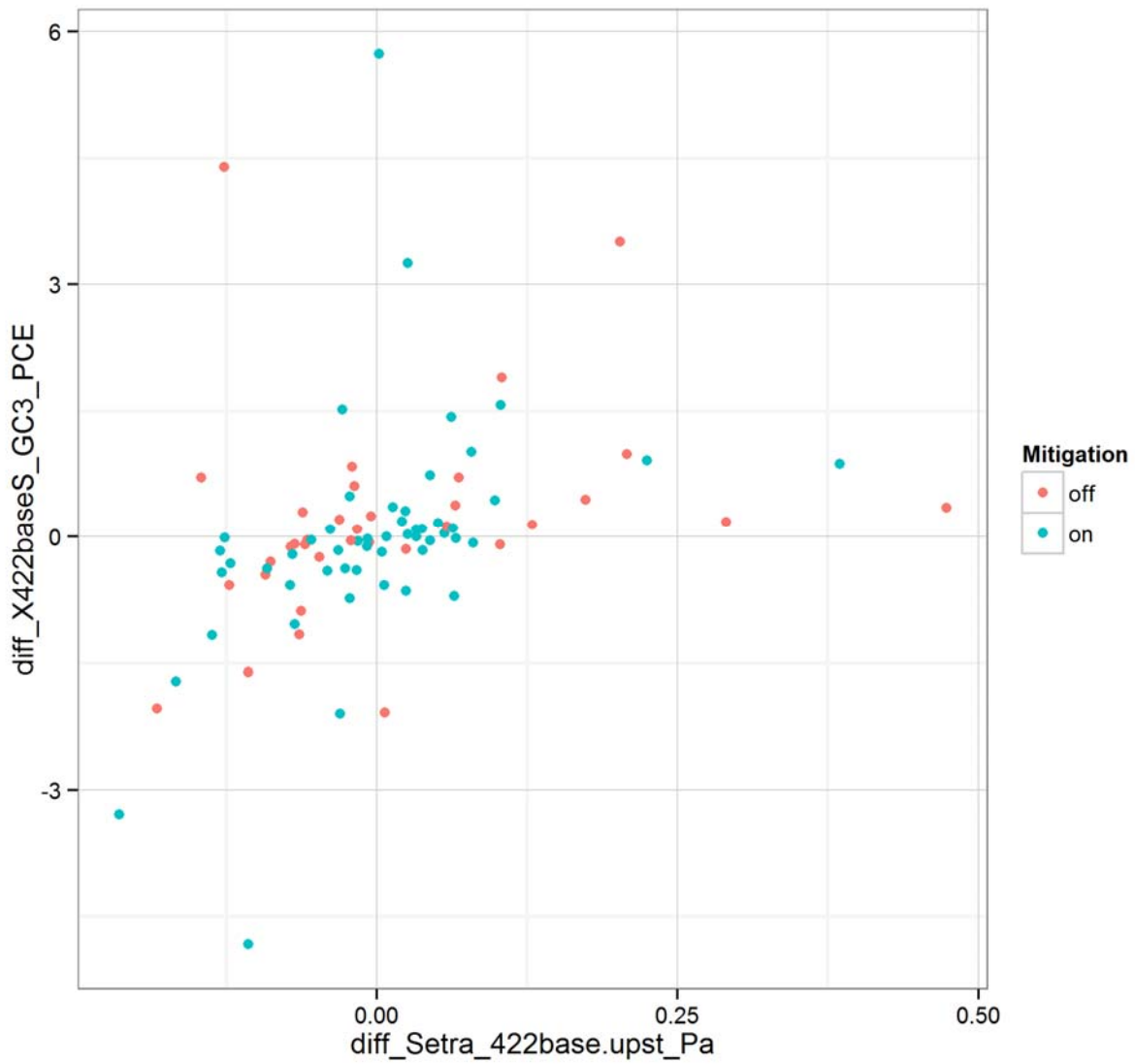


Figure 6-24. XY plot of first difference (day to day) of differential pressure between basement and upstairs vs. first difference in PCE concentration; online GC data, December 2012 to March 2013.

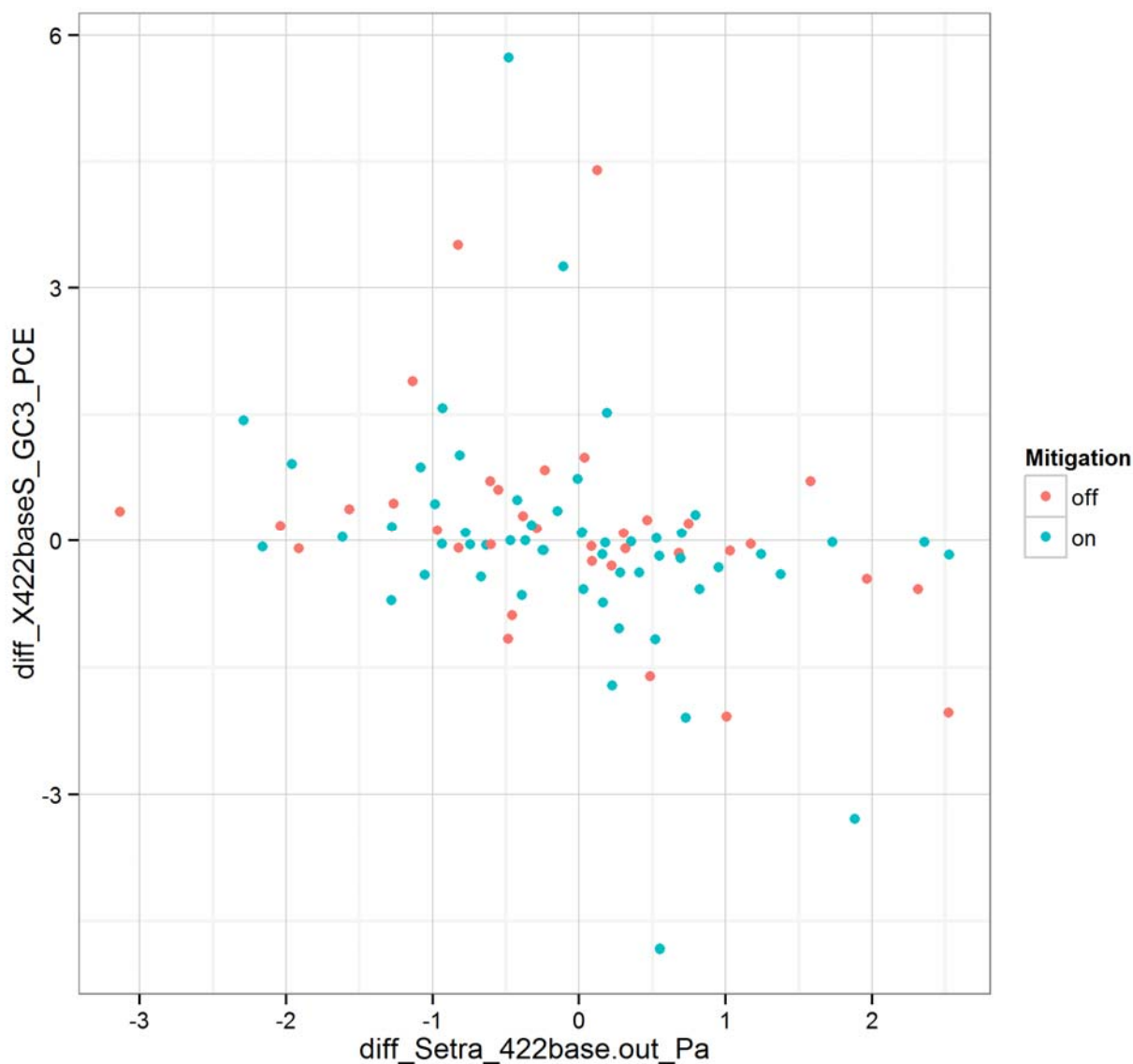


Figure 6-25. XY plot of first difference (day to day) in basement to outdoor differential pressure vs. first difference in PCE concentration.

Both the indoor and outdoor humidity values were significant at the 1% confidence level in the analysis of the GC data set. In the example calculations we performed using 25% and 35% indoor relative humidity values, air becoming drier on the second floor was associated with increasing indoor concentrations of PCE in the basement (**Figures 6-26** and **6-27**). Air becoming drier in the outdoors (using 75% and 85% outdoor relative humidity values) was also associated with increasing indoor concentrations in the basement.

The statistically significant observed relationships between humidity and vapor intrusion could have multiple physical mechanisms; thus, this analysis is complex:

- When the indoor air is dry suggests the soils around the basement are drying out, which would make them more air permeable and lead to an increase in vapor intrusion.

- Increasing humidity in soil gas decreases the adsorption capacity of a variety of soil minerals for VOCs (Ruiz et al., 1998). Thus, high humidity in soil gas may increase vapor intrusion.
- Because soil gas is typically very humid, high indoor humidity could also be a marker (as opposed to cause) of vapor intrusion.
- This analysis could be confounded. Colder weather outside means the atmospheric air can hold less moisture, and when that air gets inside the duplex, it is warmed up by a dry gas heating system and RH decreases. In this case, low indoor humidity would thus be a surrogate for cold outside temperatures, which are known to be correlated to vapor intrusion.
- Dry air is denser than humid air (because water vapor is a relatively light gas compared with oxygen and nitrogen).¹⁴ Based on density alone, dry basement air would be expected to decrease vapor intrusion, so this mechanism is apparently not predominant in our system.

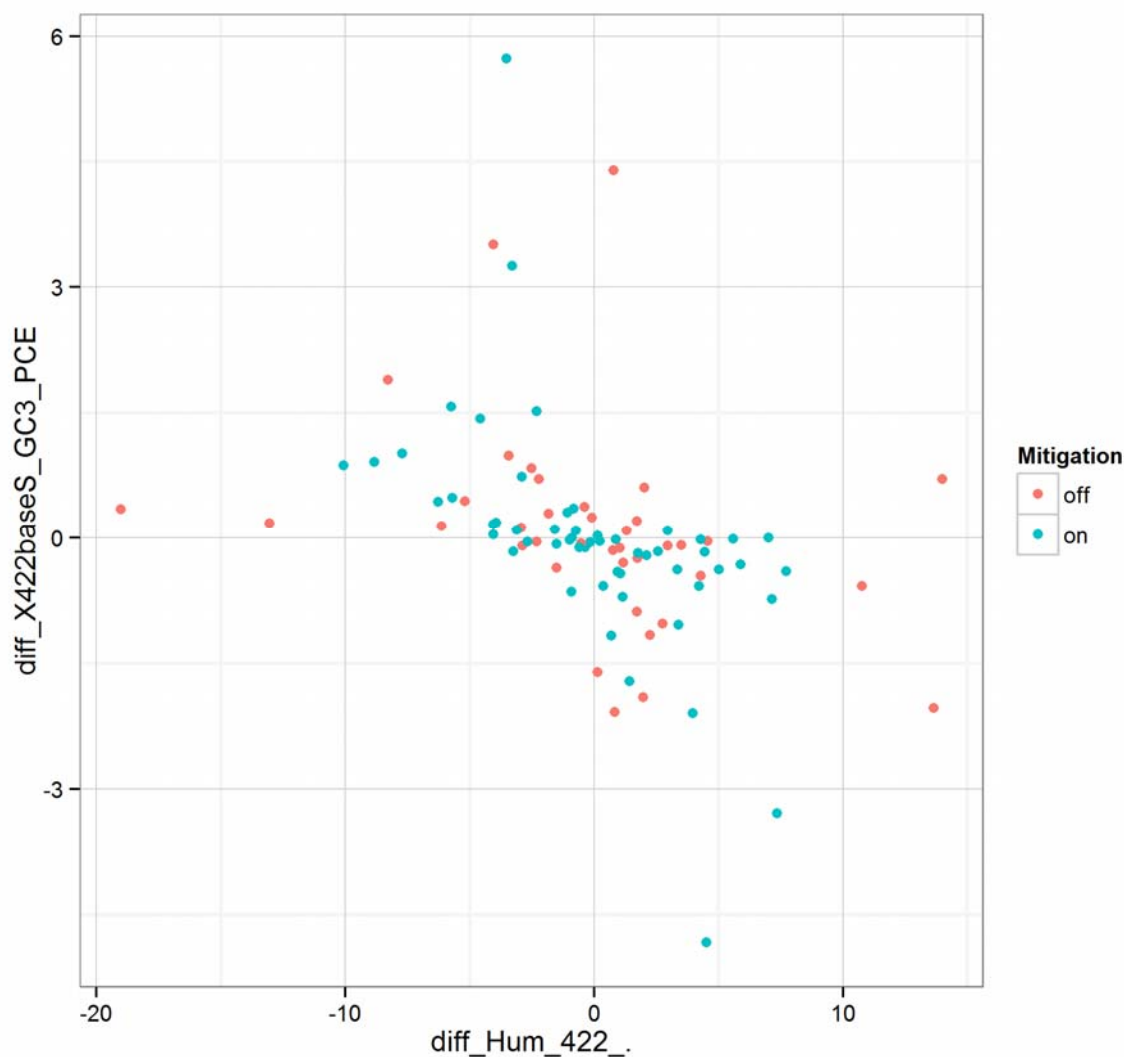


Figure 6-26. XY graph of first difference in indoor humidity (measured in the 422 2nd floor office) vs. first difference in indoor concentration of PCE; online GC data, December 2012 to February 2013.

¹⁴ http://www.engineeringtoolbox.com/density-air-d_680.html

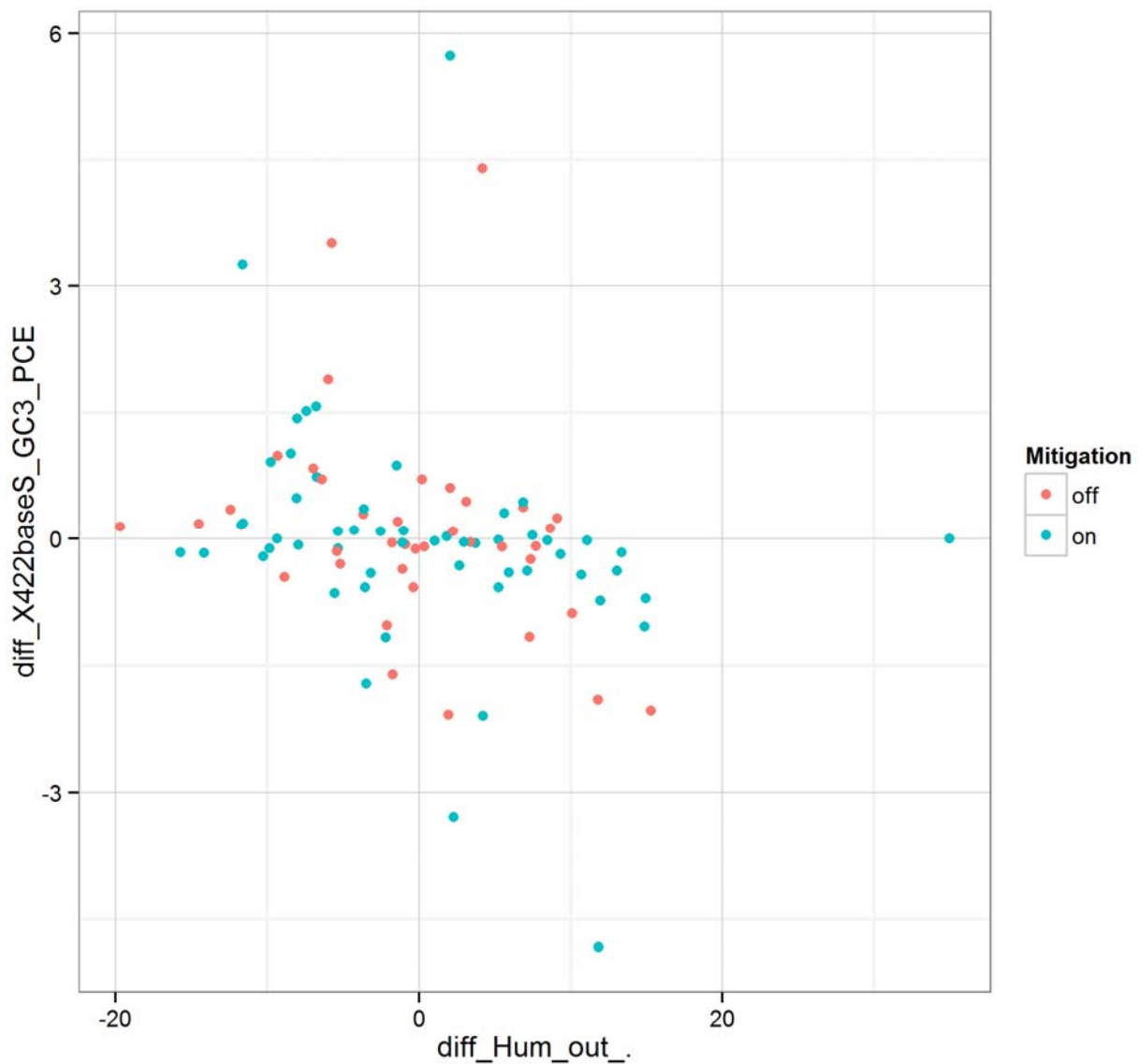


Figure 6-27. XY graph of first difference in outdoor humidity vs. first difference in indoor concentration of PCE; online GC data, December 2012 to February 2013.

The variable for subslab to basement differential pressure on the 420 side of the duplex needed lag-1 and lag-2 terms in the model (**Table 6-6**). Results indicated that its past and present measurements are significantly correlated with the 422 side basement PCE. The results are physically realistic because they indicate that increasing pressure toward the structure is correlated with increasing indoor air concentrations. This same relationship was discussed for the PCE data from the week-long passive samplers in **Section 6.2.5.5**.

Table 6-6. Analysis for Outcome First Difference of X422baseS_GC3_PCE. Variables Needing Lag-1 and Lag-2 Week Terms. Period December 2012 to March 2013

Predictor Name (x(t))	Model Term	$y(t) - y(t - 1) = \beta_0 + \beta_1x(t) + \beta_2x(t - 1) + \beta_3x(t - 2) + u(t)$		$y(t) - y(t - 1) = \beta_0 + \beta_1x(t) + \beta_2x(t - 1) + u(t)$		$y(t) - y(t - 1) = \beta_0 + \beta_1x(t) + u(t)$	
		Coefficient	SE	Coefficient	SE	Coefficient t	SE
Setra_420ss. base_Pa	intercept	0.081	0.200	0.080	0.197	0.081	0.207
	Mitigation	-0.087	0.262	-0.086	0.257	-0.097	0.270
	x(t)	44.163**	12.130	41.448**	11.363	33.592**	11.506
	x(t-1)	35.921**	12.088	33.225**	11.229		
	x(t-2)	7.785	12.044				

6.3 Influence of Meteorological Conditions on Indoor VOC Concentration: Overall Analysis

In the proceeding sections and in Section 10 of U.S. EPA (2013), we have presented time series analyses for the data sets collected during this project. In this section, we attempt to synthesize that information across data sets. The authors recognize that although the statistical time series analyses tabulated in this document and in U.S. EPA (2013) represent the mathematically correct way to understand the relationships between predictor and outcome variables, they can be difficult for some readers to follow; thus, in the section in some cases simple XY plots with local regression (LOESS) fits are presented as an aid to qualitative understanding.

6.3.1 Temperature Effect on VOCs

We have previously shown that vapor intrusion is generally increased with decreasing outdoor temperatures (Sections 9.2.1 and 10 of U.S. EPA [2013]). We have also shown that the direction of this effect is consistent with the stack effect mechanism (section 10.3 of U.S. EPA [2013]) but that the fit was imperfect and appeared to be nonlinear. In this report we report a statistically significant relationship to the stack effect for both chloroform and PCE. We also note that the correlation to indoor air concentrations may be better described by the change in the strength of the stack effect from week to week than by the instantaneous strength of the stack effect.

We can also view indoor concentrations as a function of indoor temperature in the basement (which is heated by one ventilation duct but may not always be maintained at normal room temperature). It appears that once the temperature gets below 52–55° F in the basement, the VOC concentration rises sharply. All of the data sets examined seem consistent with this finding, although some have different shaped graphs because they include narrower temperature ranges. The result was observable both with the passive samplers and the on-site GC whether aggregated to daily or 3-hour resolution (**Figures 6-28, 6-29, 6-30, and 6-31**). Note that because the time series analyses assumed a linear relationship between predictor and outcome variables, it may not have ideally analyzed this relationship.

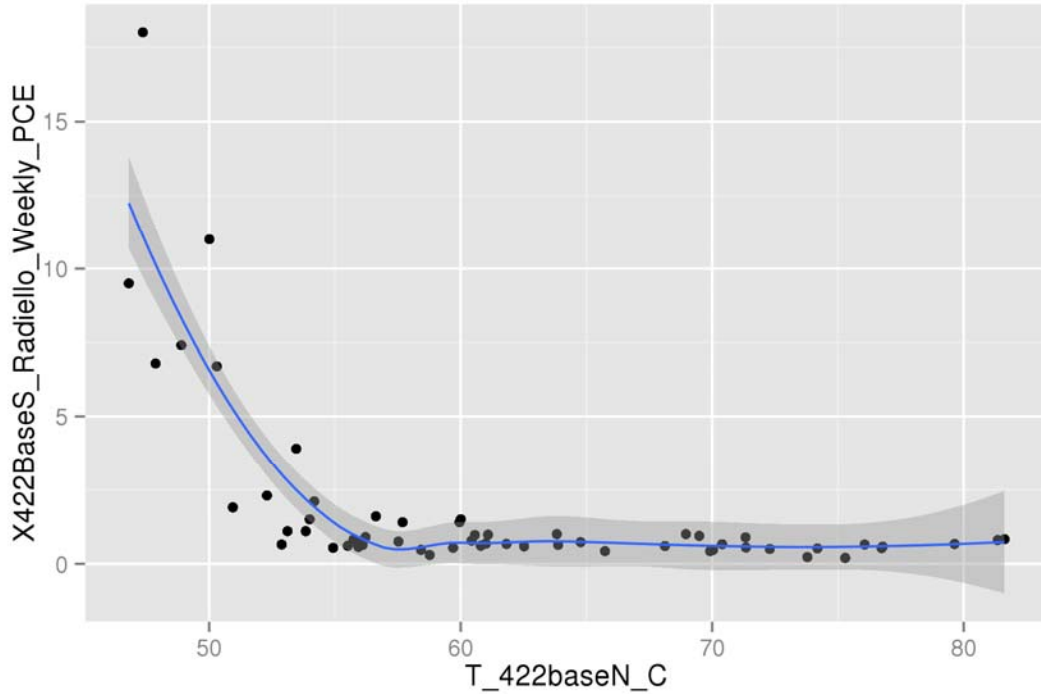


Figure 6-28. XY plot of temperature in 422 at basement north location vs. indoor concentration of PCE at 422 basement south location, radiello passive samples, January 2011 to February 2012 (includes locally weighted scatterplot smoothing [LOESS] line [blue], with a 95% confidence interval [shaded]).

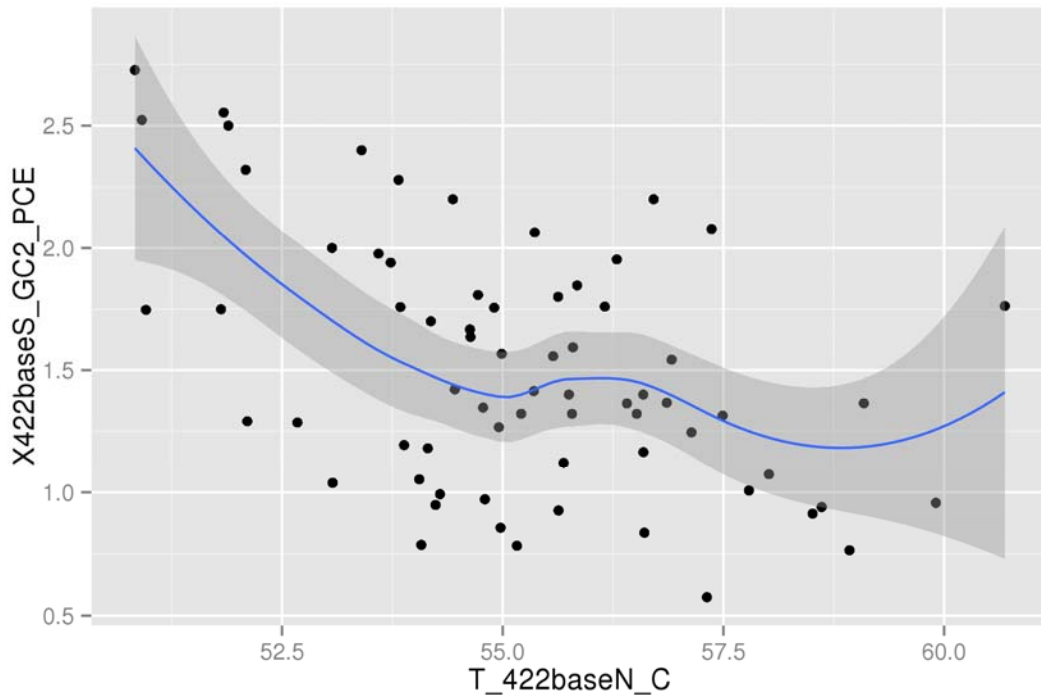


Figure 6-29. XY Plot of basement temperature in 422 basement north vs. indoor concentration in 422 basement south, December 2011 to February 2012, on-site GC, daily aggregated data (includes locally weighted scatterplot smoothing [LOESS] line [blue], with a 95% confidence interval [shaded]).

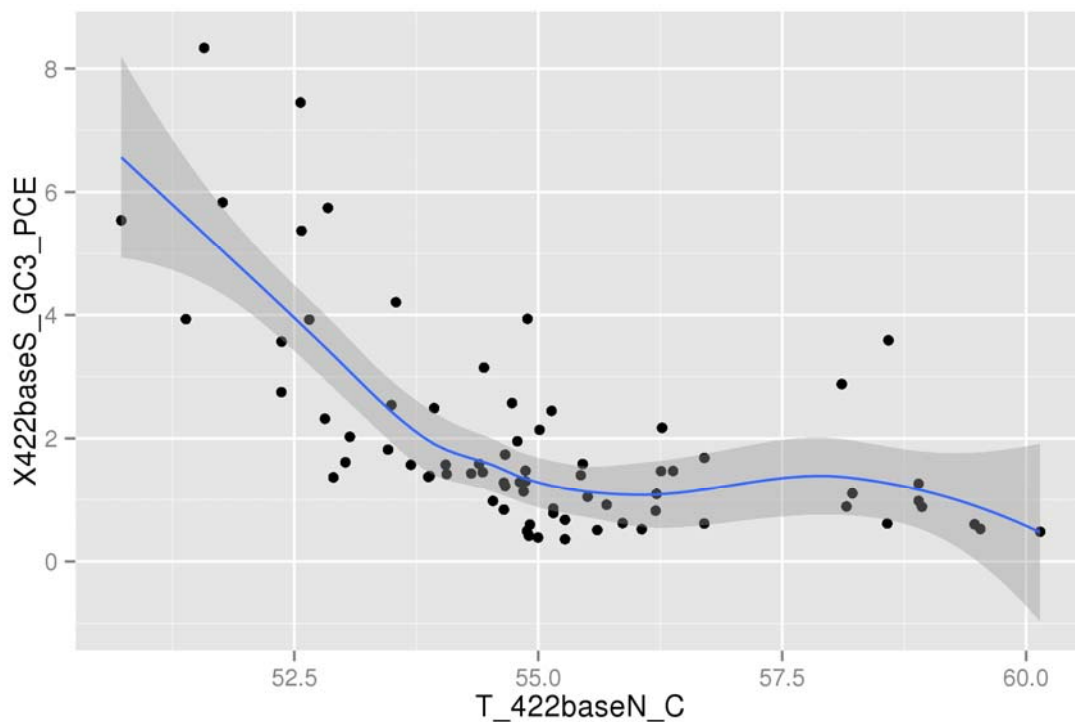


Figure 6-30. XY plot of basement temperature in 422 basement north vs. indoor concentration in 422 basement south, December 2012 to March 2013, on-site GC, daily aggregated data (includes locally weighted scatterplot smoothing [LOESS] line [blue], with a 95% confidence interval [shaded]).

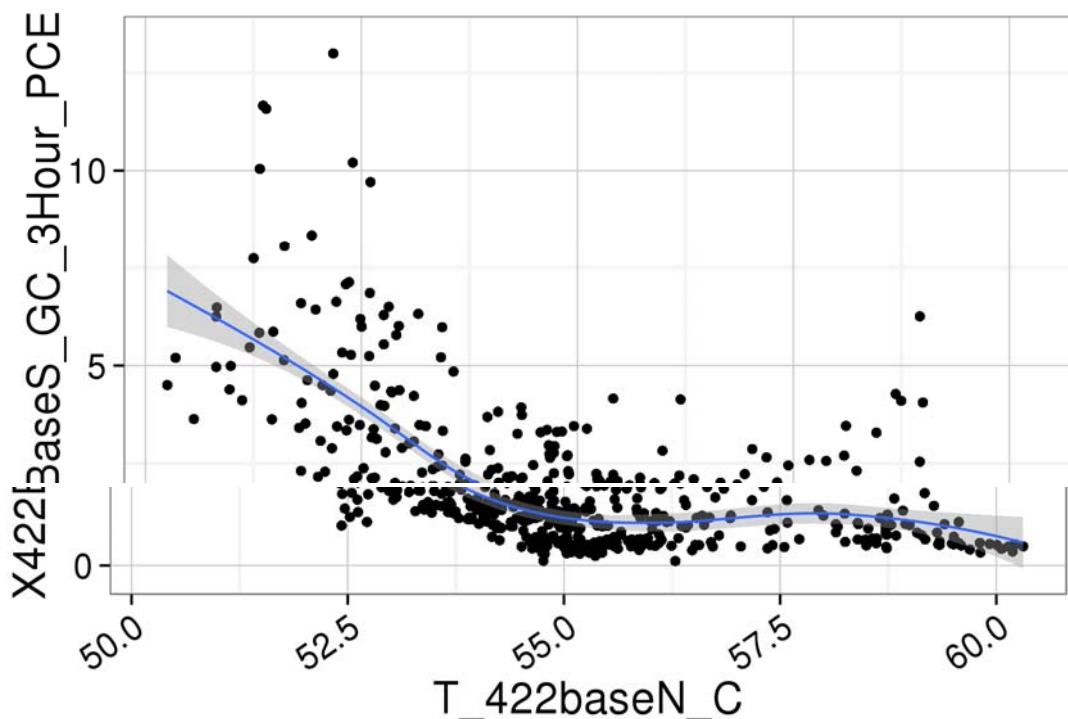


Figure 6-31. XY plot of temperature at 422 basement south vs. PCE, 3 hour aggregated data, December 2012 to March 2013 on-site GC (includes locally weighted scatterplot smoothing [LOESS] line [blue], with a 95% confidence interval [shaded]).

6.3.2 Barometric Pressure Effect on VOCs

We noted in Section 9.2.2 of U.S. EPA (2013) that “The 11 weeks with the highest PCE concentrations were all characterized by average barometric pressures in a relatively narrow range from 30.01 to 30.18 inches of mercury. There is no readily apparent direct physical mechanism to explain why these midrange barometric pressures may be associated with the highest PCE concentrations. Chloroform did not show the same relationship.” In this report, we show that the most consistent relationship for barometric pressure is that an elevated (greater than 30 inches) and/or rising barometric pressure is associated with increasing vapor intrusion. This relationship was seen for both chloroform and PCE. This trend was also seen in both Radiello and daily aggregated online GC data time series analyses. Although a time series analysis with the 3- hour aggregated data set has not been completed, an XY plot of that data set does suggest a relationship (**Figures 6-31, 6-32, and 6-33**).

Current state vapor intrusion guidance documents mention barometric pressure as an influence on vapor intrusion but do not forecast the results of specific types of barometric pressure changes. In the radon literature and in our studies, drops in barometric pressure are associated with increased radon emanation and increased indoor air concentrations (U.S. EPA, 2013, Section 10). We noted in Section 10 of U.S. EPA (2013) a relationship between higher pressures and decreasing wind speeds in our data set and attributed that to the well-known association of falling barometric pressures and storms. Thus, it is possible that higher barometric pressures are associated with higher indoor VOC concentrations because lower wind speeds under those conditions provide less air exchange within the 100-year-old duplex tested in this study.

Although a number of other barometric pressure variables were examined, some have inconclusive results across data sets (for example, the standard deviation of barometric pressure or “pump speed”).

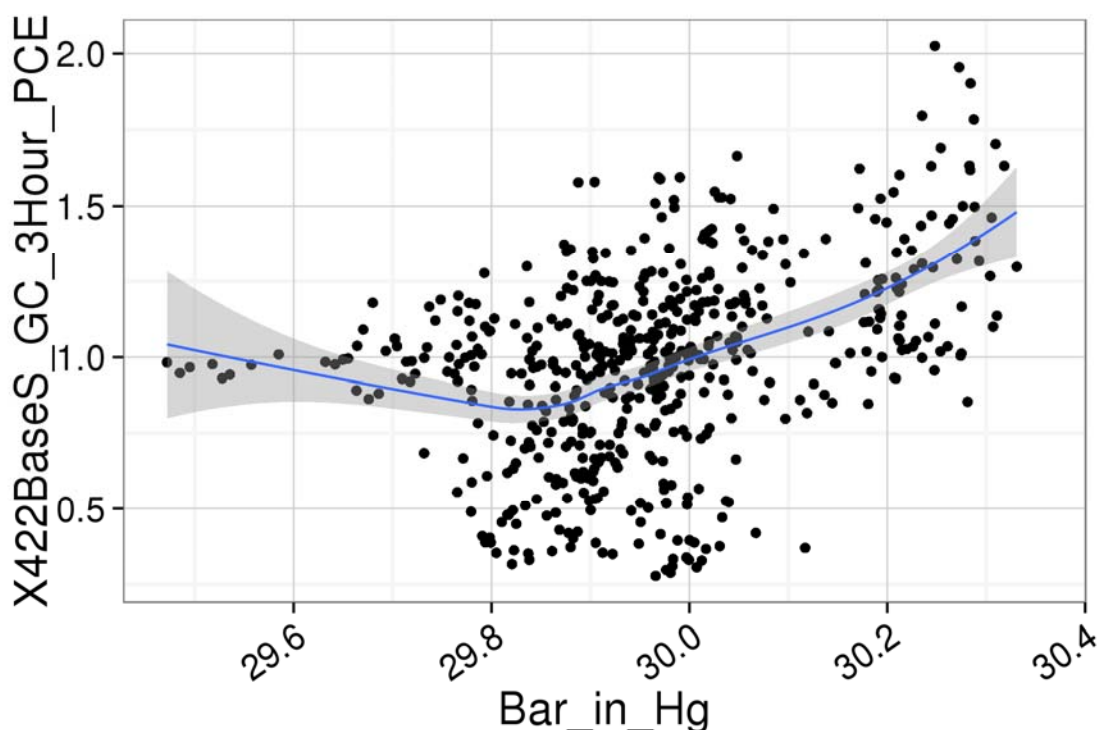


Figure 6-32. XY plot of barometric pressure vs. PCE, online GC data, 3-hour aggregation, August 2011 to October 2011 (includes locally weighted scatterplot smoothing [LOESS] line [blue], with a 95% confidence interval [shaded]).

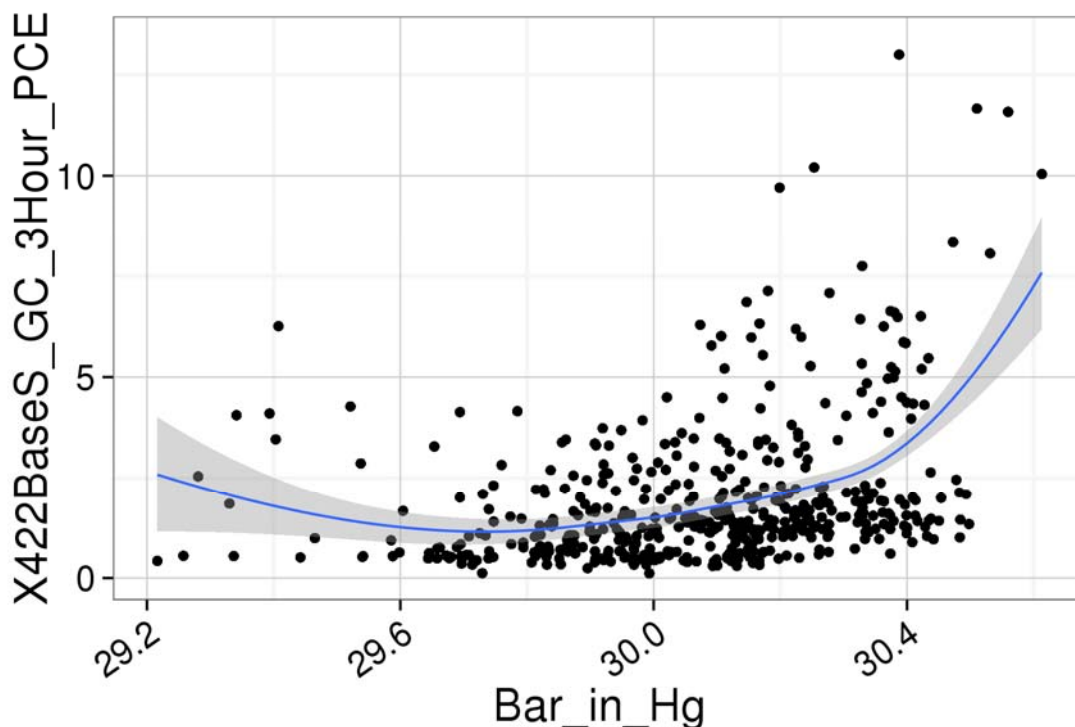


Figure 6-33. XY plot of barometric pressure vs. PCE, online GC data, 3-hour aggregation; December 2012 to March 2013 (includes locally weighted scatterplot smoothing [LOESS] line [blue], with a 95% confidence interval [shaded]).

6.3.3 Precipitation Effects on VOCs

Our previous analyses of the effects of snow and rain on vapor intrusion are reported in Sections 9.2.3 and 13.1.2 of U.S. EPA (2013). We noted that the snow effects were expected to be complex because not all snows are the same (in terms for example of water content and air permeability). In this current work, we have noted increasing chloroform and PCE in indoor air with melting snow packs. We attributed this potentially to effects on air permeability or water levels. With PCE, there is apparently also an effect of increasing indoor concentration with increasing snow pack depth. Thus, it appears that at least for PCE this effect is nonlinear and thus would not have been well represented by a linear time series analysis.

We continue to see no evidence of a statistically significant rain effect in this data set.

6.3.4 Effect of Wind on VOC Concentrations

The qualitatively observed correlation between west winds and increased PCE concentrations (Section 9.2.4 of U.S. EPA, 2013) was not judged to be statistically significant in our current analysis. Northwest and southwest winds were significantly associated with PCE in the Sept. 2012 to April 2013 data set but had a negative coefficient, indicating that they decreased concentration. In one data set, northeast winds were positively associated with increased chloroform concentrations.

Weak evidence was noted in this current analysis for a negative correlation between indoor PCE concentration and wind speed.

6.3.5 Humidity and Soil Moisture Correlation with VOC Concentrations

A correlation between indoor humidity in the 422 duplex and vapor intrusion is suggested by the online GC data, which was not extensively explored in either our 2012 or 2013 report. A significant humidity effect is also seen in **Attachment 6D, 6D-2** for chloroform in the Sept. 2012 to Aug. 2013 data set. As we discuss in Section 6.2.6:

- There are multiple physical mechanisms by which humidity changes could increase or decrease vapor intrusion.
- It is unclear whether humidity is a cause of the observed changes in vapor intrusion or is being affected by the same independent variable that controls vapor intrusion, such as temperature.

Note that many of the XY plots of humidity vs. PCE concentration suggest a U-shaped curve with the minimum PCE concentration at intermediate humidities (**Figures 6-34 through 6-38**). A similar pattern is seen using the Radiello 7-day passive data as well as the online GC data with either 3-hour or 1-day aggregation. The potential for nonlinear and parabolic relationships shown here suggests that the assumption of a linear relationship in the time series analysis performed to date may be imperfect for this variable.

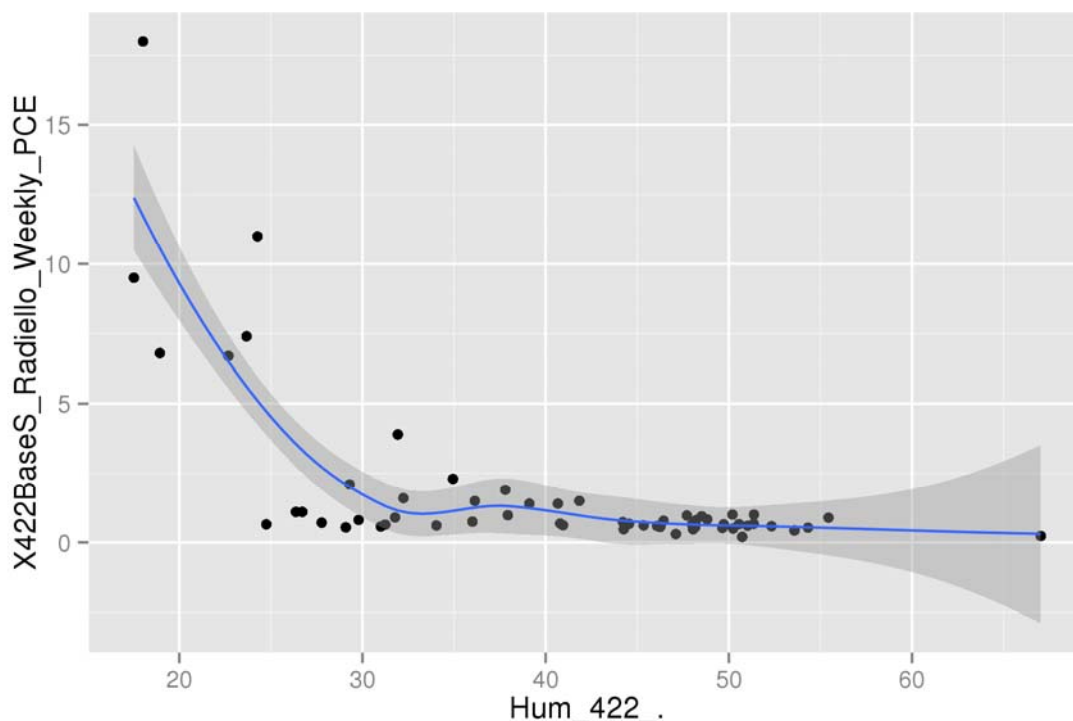


Figure 6-34. XY plot of indoor humidity (422 office) vs. PCE concentration in 422 basement south; January 2011 to February 2012, Radiello passive sampler data (includes locally weighted scatterplot smoothing [LOESS] line [blue], with a 95% confidence interval [shaded]).

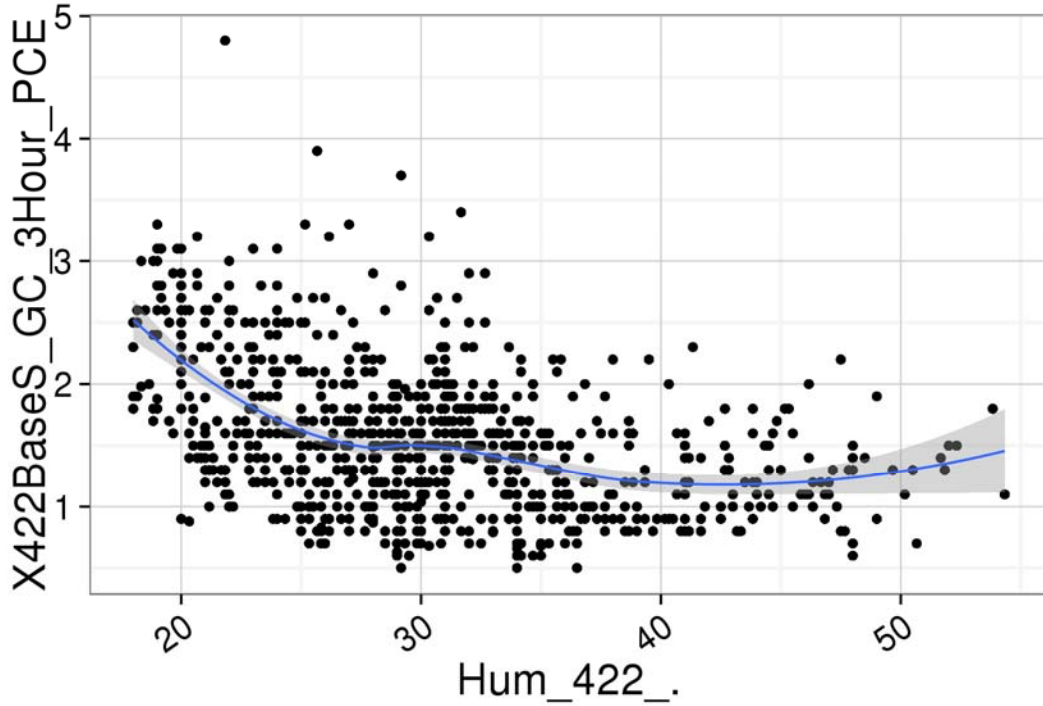


Figure 6-35. XY plot of indoor humidity (422 office) vs. PCE concentration in 422 basement south; August 2011 to October 2011, online GC data, 3-hour aggregation (includes locally weighted scatterplot smoothing [LOESS] line [blue], with a 95% confidence interval [shaded]).

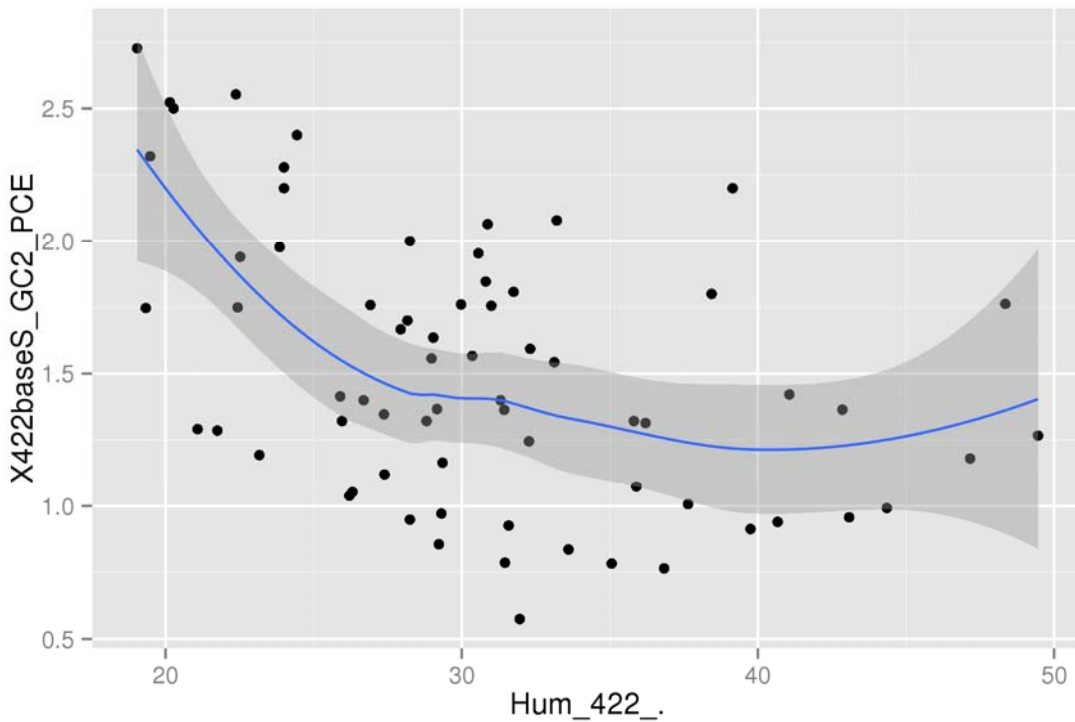


Figure 6-36. XY plot of indoor humidity (422 office) vs. PCE concentration in 422 basement south, December 2011 to February 2012, online GC data, daily aggregation (includes locally weighted scatterplot smoothing [LOESS] line [blue], with a 95% confidence interval [shaded]).

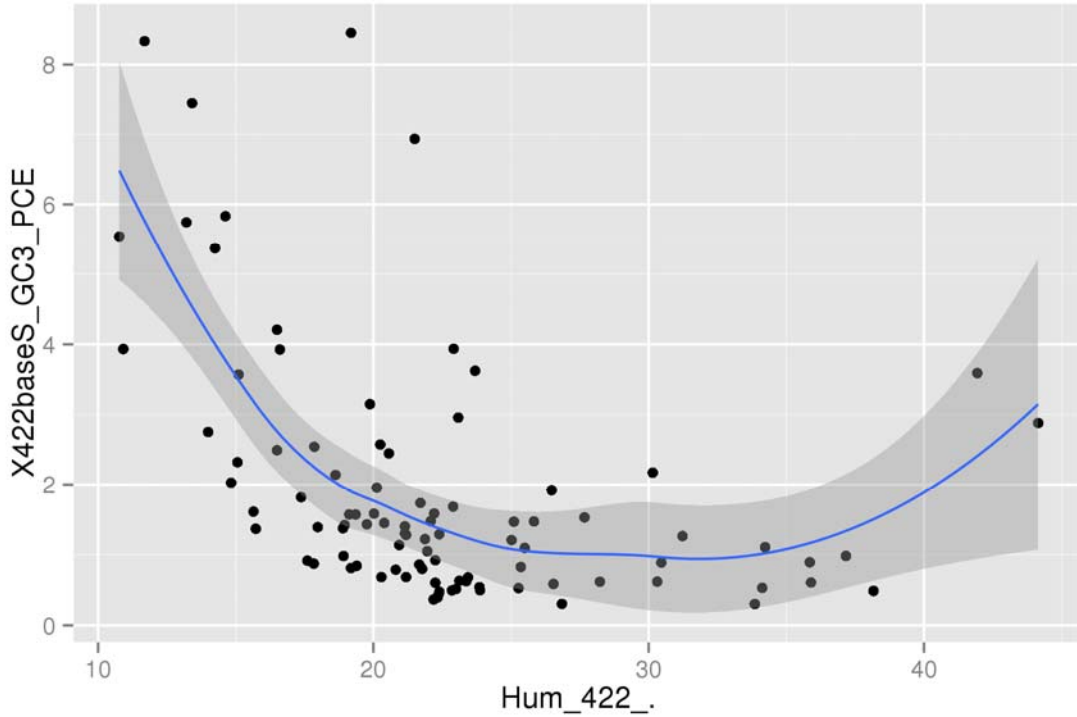


Figure 6-37. XY plot of indoor humidity (422 office) vs. PCE concentration in 422 basement south; December 2012 to March 2013, online GC data, daily aggregation (includes locally weighted scatterplot smoothing [LOESS] line [blue], with a 95% confidence interval [shaded]).

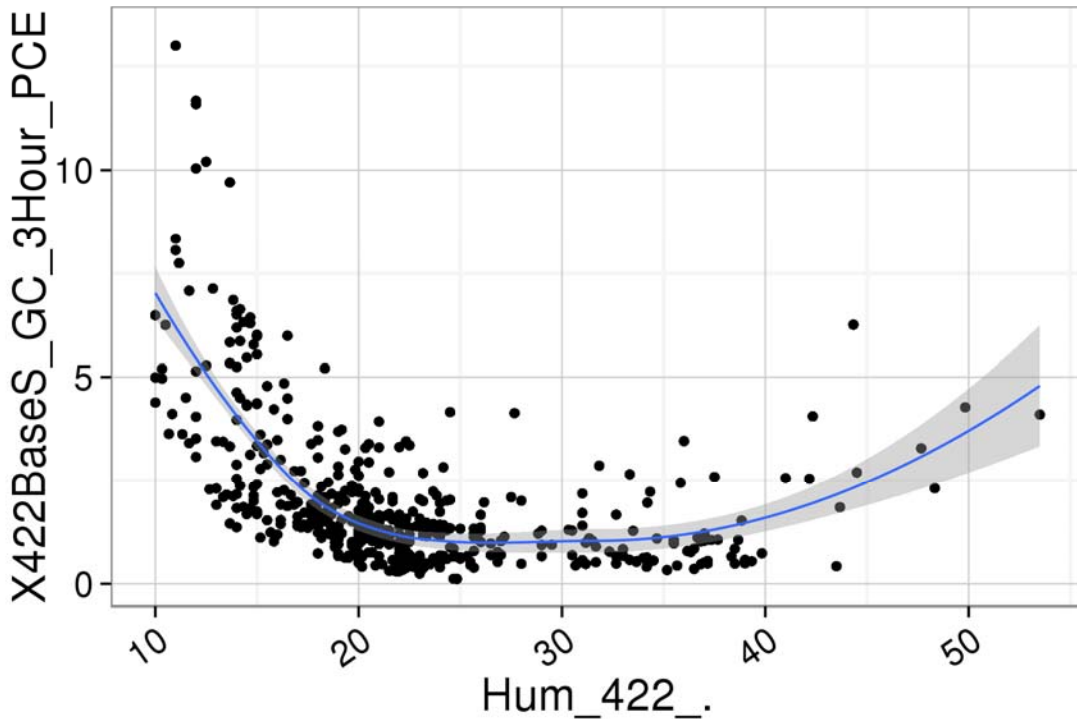


Figure 6-38. XY plot of indoor humidity (422 office) vs. PCE concentration in 422 basement south; December 2012 to March 2013, online GC data, 3-hour aggregation (includes locally weighted scatterplot smoothing [LOESS] line [blue], with a 95% confidence interval [shaded]).

A similar U-shaped relationship with the minimum indoor air concentration associated with median moisture was observed in some cases using the data from an implanted moisture sensor just below the basement floor (Soil_H2O_in6_cbar). The lower centibar (cbar) readings are wetter conditions. Evidence for this was seen both in Radiello and GC measurements and for both chloroform and PCE (**Figures 6-39** through **6-42**). This suggests that the following mechanisms may be operative:

- Drying soils around the basement are more air permeable, thus increasing vapor intrusion.
- Increasing humidity in soil gas decreases the adsorption capacity of a variety of soil minerals for VOCs (Ruiz, 1998). Thus, high humidity in soil gas may increase vapor intrusion.

The potential for nonlinear and parabolic effects here suggests that the assumption of a linear relationship in the time series analysis done to date may be imperfect for this variable.

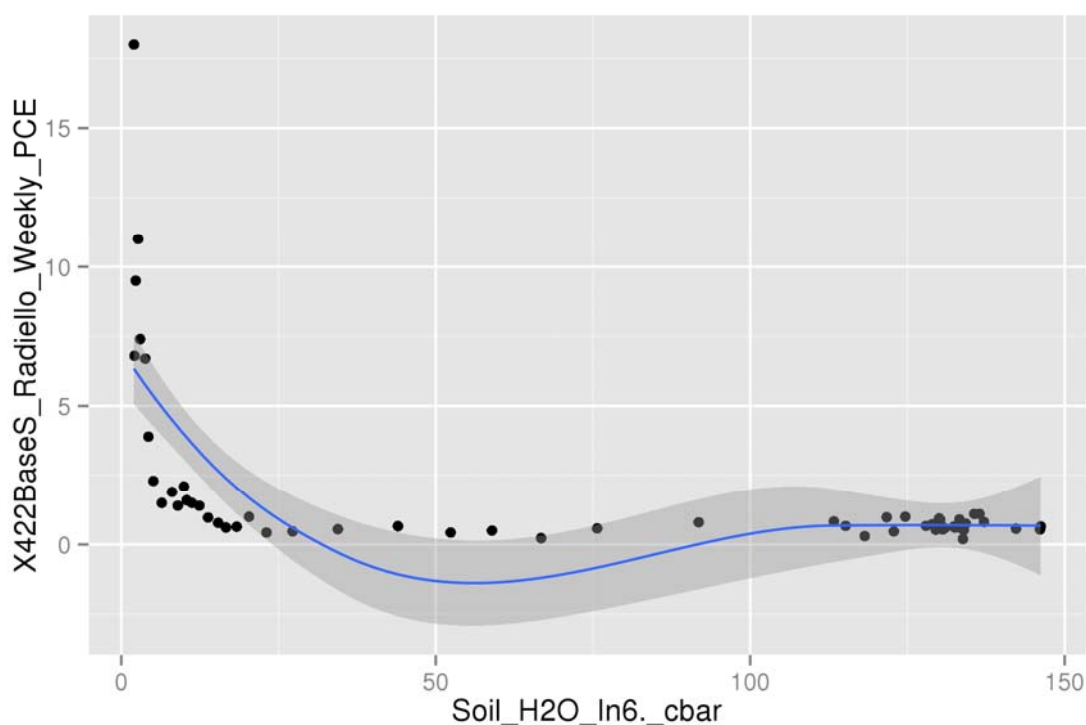


Figure 6-39. XY plot of soil moisture at 6 ft bls (immediately below floor) vs. PCE concentration, Radiello samples, January 2011 to February 2012 (includes locally weighted scatterplot smoothing [LOESS] line [blue], with a 95% confidence interval [shaded]).

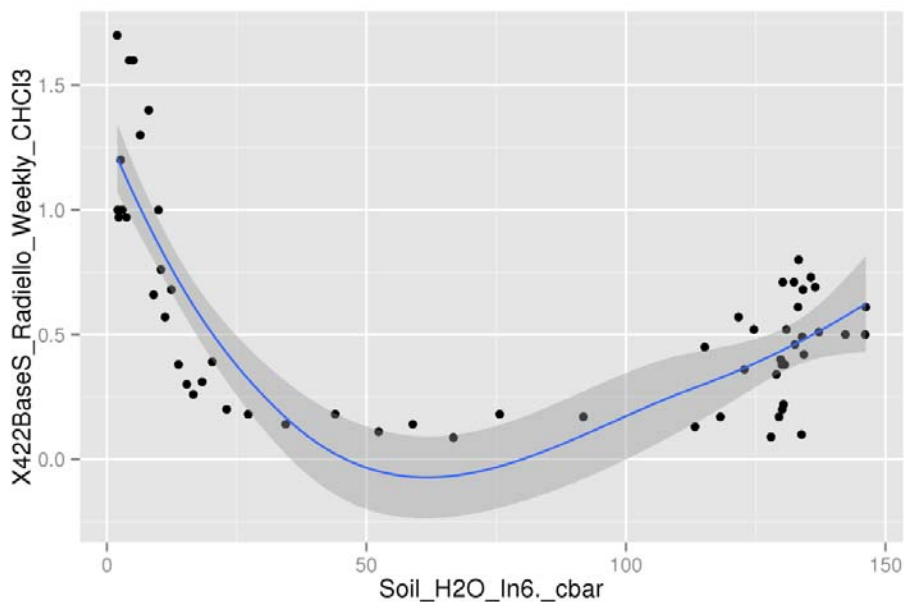


Figure 6-40. XY plot of soil moisture at 6 ft bls (immediately below floor) vs. chloroform concentration, Radiello samples, January 2011 to February 2012 (includes locally weighted scatterplot smoothing [LOESS] line [blue], with a 95% confidence interval [shaded]).

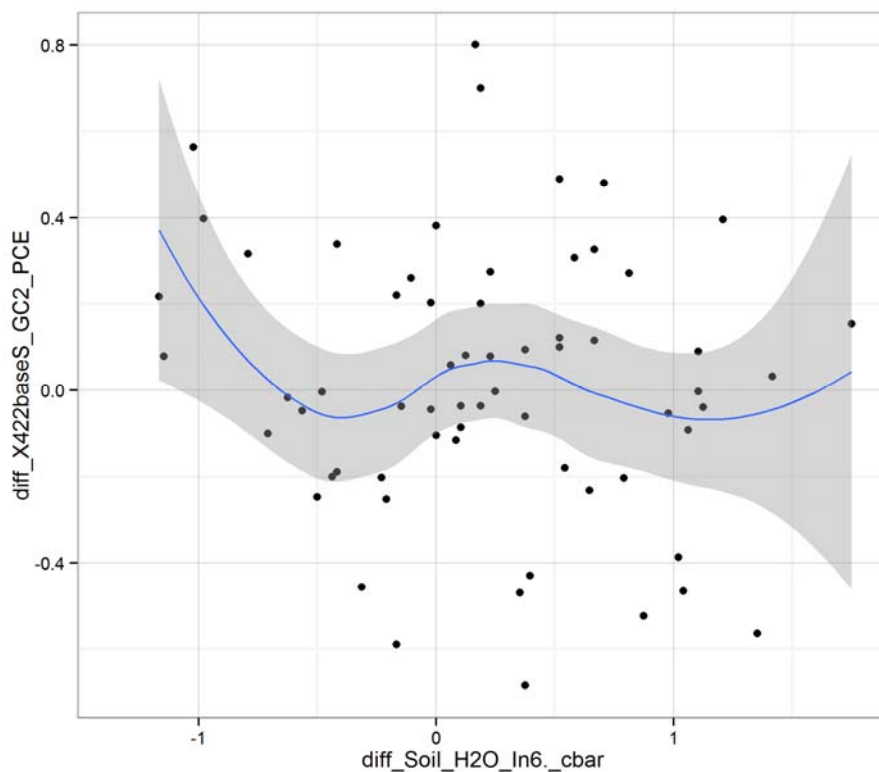


Figure 6-41. XY plot of first difference of soil moisture at 6 ft bls (immediately below floor) vs. first difference of PCE concentration, online GC measurements, daily aggregation, December 2011 to February 2012 (includes locally weighted scatterplot smoothing [LOESS] line [blue], with a 95% confidence interval [shaded]).

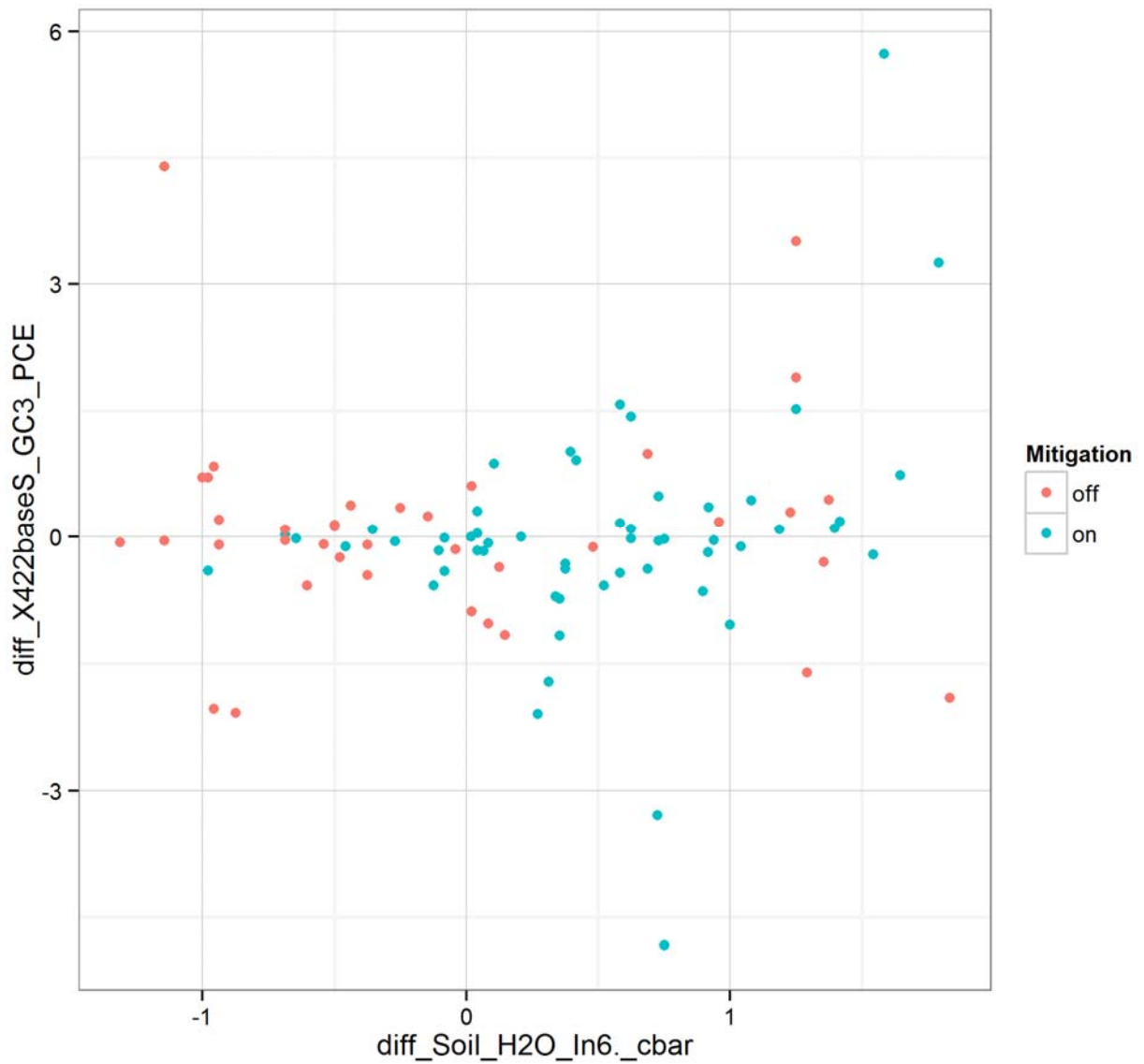


Figure 6-42. XY plot of first difference of soil moisture at 6 ft bls (immediately below floor) vs. first difference of PCE concentration, online GC measurements, daily aggregation, December 2012 to March 2013.

Attachment 6A. Aggregation of Predictor Variables across Multiple Time Intervals

Table 6A-1. Data Aggregation Applied to Predictor Variables

Predictor Description	Predictor Code	Method of Aggregation
Building Variables		
420 air conditioning status (On/On briefly/Off)	AC_on-off_420_daily	Mode
422 air conditioning status (On/On briefly/Off)	AC_on-off_422_daily	Mode
422 fan status (On/Off)	Fan_on-off_422_daily	Mode
420 heating status (On/Off)	Heat_on-off_420_daily	Mode
422 heating status (On/Off)	Heat_on-off_422_daily	Mode
House mitigation status (not yet installed/on/passive/off)	Mitigation_Status_Daily	Mode
Building Environment Variables		
Air density interior	AirDens_422	Mean
Dew point, Interior, °F	Dew_pt_422_F	Mean
Humidity interior 422 side, percent	Hum_422_%.	Mean
420 side, subslab vs. basement differential pressure, Pascals	Setra_420ss.base_Pa	Mean
422 side basement vs. exterior differential pressure, Pascals	Setra_422base.out_Pa	Mean
422 side, basement vs. upstairs differential pressure, Pascals	Setra_422base.upst_Pa	Mean
422 side, subslab vs. basement differential pressure, Pascals	Setra_422ss.base_Pa	Mean
420 side, subslab vs. basement standard deviation of differential pressure over measurement period, Pascals	StdDev_Setra_420ss.base_Pa	Standard deviation
422 side basement vs. exterior standard deviation of differential pressure over measurement period, Pascals	StdDev_Setra_422base.out_Pa	Standard deviation
422 side, basement vs. upstairs standard deviation of differential pressure over measurement period, Pascals	StdDev_Setra_422base.upst_Pa	Standard deviation
422 side, deep vs. shallow soil gas standard deviation of differential pressure over measurement period, Pascals	StdDev_Setra_422SGdp.ss_Pa	Standard deviation
Temperature at 420 basement north sampling location (HOBO), °C	T_420baseN_C	Mean
Temperature at 420 basement south sampling location (HOBO), °C	T_420baseS_C	Mean
Temperature at 420 first floor sampling location (HOBO), °C	T_420first_C	Mean
Temperature, 422 first floor (weather station), °C	T_422_F	Mean
Temperature 422 basement north (HOBO), °C	T_422baseN_C	Mean
Temperature 422 first floor (HOBO), °C	T_422baseS_C	Mean
Temperature on first floor of 422 side of duplex (HOBO), °C	T_422first_C	Mean
Temperature at 420 basement north (HOBO) minus outside temperature (weather station), °F	Diff_T_420baseN-Out_F	Temp In–Temp Out
Temperature at 420 first floor (HOBO) minus outside temperature (weather station), °F	Diff_T_420first-Out_F	Temp In–Temp Out

(continued)

Table 6A-1. Data Aggregation Applied to Predictor Variables (continued)

Predictor Description	Predictor Code	Method of Aggregation
Building Environment Variables (continued)		
Temperature at 422 basement south (HOBO) minus outside temperature (weather station), °F	Diff_T_422baseS-Out_F	Temp In–Temp Out
Temperature at 420 basement south (HOBO) minus outside temperature (weather station), °F	Diff_T_420baseS-Out_F	Temp In–Temp Out
Temperature at 422 basement north (HOBO) minus outside temperature (weather station), °F	Diff_T_422baseN-Out_F	Temp In–Temp Out
Temperature at 422 first floor (HOBO) minus outside temperature (weather station), °F	Diff_T_422first-Out_F	Temp In–Temp Out
Stack effect between 420 basement north and outside, Rankine	StackEffect_420baseN	If Temp In is higher than Temp Out: $\sqrt{(T_{in}-T_{out})/abs(T_{in})}$, if Temp Out is higher than Temp In: $\sqrt{(T_{out}-T_{in})/abs(T_{out})}$
Stack effect between 420 basement south and outside, Rankine	StackEffect_420baseS	If Temp In is higher than Temp Out: $\sqrt{(T_{in}-T_{out})/abs(T_{in})}$, if Temp Out is higher than Temp In: $\sqrt{(T_{out}-T_{in})/abs(T_{out})}$
Stack effect between 420 first floor and outside, Rankine	StackEffect_420first	If Temp In is higher than Temp Out: $\sqrt{(T_{in}-T_{out})/abs(T_{in})}$, if Temp Out is higher than Temp In: $\sqrt{(T_{out}-T_{in})/abs(T_{out})}$
Stack effect between 422 basement north and outside, Rankine	StackEffect_422baseN	If Temp In is higher than Temp Out: $\sqrt{(T_{in}-T_{out})/abs(T_{in})}$, if Temp Out is higher than Temp In: $\sqrt{(T_{out}-T_{in})/abs(T_{out})}$
Stack effect between 422 basement south and outside, Rankine	StackEffect_422baseS	If Temp In is higher than Temp Out: $\sqrt{(T_{in}-T_{out})/abs(T_{in})}$, if Temp Out is higher than Temp In: $\sqrt{(T_{out}-T_{in})/abs(T_{out})}$
Stack effect between 422 first floor and outside, Rankine	StackEffect_422first	If Temp In is higher than Temp Out: $\sqrt{(T_{in}-T_{out})/abs(T_{in})}$, if Temp Out is higher than Temp In: $\sqrt{(T_{out}-T_{in})/abs(T_{out})}$
Subsurface Variables		
Depth to groundwater, ft	DepthToWater	Mean
422 side, deep vs. shallow soil gas differential pressure, Pascals	Setra_422SGdp.ss_Pa	Mean
422 side, slab vs. basement standard deviation of differential pressure over measurement period, Pascals	StdDev_Setra_422ss.base_Pa	Standard deviation
Soil moisture, 13 ft bls, interior, cbar	Soil_H2O_In13._cbar	Mean
Soil moisture 16.5 ft bls, interior, cbar	Soil_H2O_In16.5._cbar	Mean
Soil moisture 6 ft bls, interior, cbar	Soil_H2O_In6._cbar	Mean
Soil moisture 13 ft bls, exterior, cbar	Soil_H2O_Out13._cbar	Mean
Soil moisture, 3.5 ft bls, exterior, cbar	Soil_H2O_Out3.5._cbar	Mean
Soil moisture 6 ft bls, exterior, cbar	Soil_H2O_Out6._cbar	Mean
Soil temperature 13 ft bls, interior, °C	Soil_T_C_MW3.13	Mean
Soil temperature 16.4 ft bls, interior, °C	Soil_T_C_MW3.16.5	Mean

(continued)

Table 6A-1. Data Aggregation Applied to Predictor Variables (continued)

Predictor Description	Predictor Code	Method of Aggregation
Subsurface Variables (continued)		
Soil temperature 6 ft bls, interior, °C	Soil_T_C_MW3.6	Mean
Soil temperature 9 ft bls, interior, °C	Soil_T_C_MW3.9	Mean
Soil temperature 1 ft bls, exterior, °C	Soil_T_C_OTC.1	Mean
Soil temperature 13 ft bls, exterior, °C	Soil_T_C_OTC.13	Mean
Soil temperature 16.5 ft bls, exterior, °C	Soil_T_C_OTC.16.5	Mean
Soil temperature 6 ft bls, exterior, °C	Soil_T_C_OTC.6	Mean
Surface Water Variables		
Height Measured at Fall Creek Stream Gauge in feet	Fall_Crk_Gage_ht_ft	Mean
Weather Variables		
Barometric pressure rate of change, inches of mercury per hour	Bar_drop_.Hg.hr	Mean
Largest barometric pressure rate of change, inches of mercury per hour	Max_Change_dPdt	Maximum absolute value, keeping sign
Absolute value of largest barometric pressure rate of change, inches of mercury per hour	Abs_Max_Change_dPdt	Maximum absolute value, not keeping sign
Barometric pressure, inches of mercury	Bar_in_Hg	Mean
Net pressure change over measurement period, inches of mercury	BP_Net_Change	First-last, by date/time
Standard deviation of pressure change over measurement period, inches of mercury	BP_Pump_Speed	Standard deviation
Largest pressure change over measurement period (barometric pumping "stroke length"), inches of mercury	BP_Stroke_Length	Maximum-minimum
Cooling degree days	Cool_Degree_Day	Sum
Dew point, exterior, °F	Dew_pt_out_F	Mean
Heating degree days	Heat_Degree_Day	Sum
Exterior heating index (based on temperature and humidity), °F	Heat_Index_F	Mean
Humidity exterior, percent	Hum_out_%.	Mean
Interior heating index	Indoor_Heat_Index	Mean
Rain total during observation period., inches	Rain_In_met	Sum
Rain total during observation period., inches	Rain_In_met	Sum
Rain, highest rate during observation period, inches per hour	Rain_IPH	Maximum
Depth of snow on the ground, inches	Snowdepth_daily	Mean
Icy precipitation event during the time period of aggregation? (METAR), Yes/No	METAR_IcyPrecip_YorN	If any "yes" in the METAR data during the time period of aggregation, has value of "Yes," otherwise has a value of "No"
Thunder event during the time period of aggregation? (METAR data), Y/N	METAR_ThunderEvent_YorN	If any "yes" in the METAR data during the time period of aggregation, has value of "Yes," otherwise has a value of "No"

(continued)

Table 6A-1. Data Aggregation Applied to Predictor Variables (continued)

Predictor Description	Predictor Code	Method of Aggregation
Weather Variables (continued)		
Snow event during the time period of aggregation? (METAR data), Yes/No	METAR_SnowEvent_YorN	If any “yes” in the METAR data during the time period of aggregation, has value of “Yes,” otherwise has a value of “No”
Exterior temperature (HOBO), °C	T_out_C	Mean
Exterior temperature (weather station), °F	T_out_F	Mean
Temperature exterior, high during data collection period, °F	T_out_Hi_F	Maximum
Lowest exterior temperature, °F	T_out_Lo_F	Minimum
Temperature, humidity, and wind index, °F	THW_F	Mean
Wind chill, °F	Wind_Chill_F	Mean
Average wind direction, degrees	Wind_Dir	Trigonometric mean, converted to categorical (one of N, NE, E, SE, S, SW, W, NW)
Wind direction of high speed during measurement period, degrees	Wind_Dir_Hi	Direction paired to high speed, converted to categorical (one of N, NE, E, SE, S, SW, W, NW)
Wind run (function of wind speed and duration), miles	Wind_Run_mi	Sum
High wind speed during measurement period, miles per hour	Wind_Speed_Hi_MPH	Maximum
Average wind speed during measurement period, miles per hour	Wind_Speed_MPH	Mean
VOC Measurements		
Weekly chloroform concentration—420 basement north Radiello sample (µg/m ³)	420BaseN_Radiello_Weekly_CHCl3	Randomly choose one (where there is more than one sample for that week)
Weekly chloroform concentration—422 basement south Radiello sample (µg/m ³)	420BaseS_Radiello_Weekly_CHCl3	Randomly choose one (where there is more than one sample for that week)
Weekly chloroform concentration—422 basement north Radiello sample (µg/m ³)	422BaseN_Radiello_Weekly_CHCl3	Randomly choose one (where there is more than one sample for that week)
Weekly chloroform concentration—422 basement south Radiello sample (µg/m ³)	422BaseS_Radiello_Weekly_CHCl3	Randomly choose one (where there is more than one sample for that week)
Weekly chloroform concentration—420 first floor Radiello sample (µg/m ³)	420First_Radiello_Weekly_CHCl3	Randomly choose one (where there is more than one sample for that week)
Weekly chloroform concentration—422 first floor Radiello sample (µg/m ³)	422First_Radiello_Weekly_CHCl3	Randomly choose one (where there is more than one sample for that week)
Weekly chloroform concentration—422 outside Radiello sample (µg/m ³)	Out_Radiello_Weekly_CHCl3	Randomly choose one (where there is more than one sample for that week)
Weekly PCE concentration—420 basement north Radiello sample (µg/m ³)	420BaseN_Radiello_Weekly_PCE	Randomly choose one (where there is more than one sample for that week)
Weekly PCE concentration—422 basement south Radiello sample (µg/m ³)	420BaseS_Radiello_Weekly_PCE	Randomly choose one (where there is more than one sample for that week)
Weekly PCE concentration—422 basement south Radiello sample (µg/m ³)	422BaseN_Radiello_Weekly_PCE	Randomly choose one (where there is more than one sample for that week)
Weekly PCE concentration—422 basement south Radiello sample (µg/m ³)	422BaseS_Radiello_Weekly_PCE	Randomly choose one (where there is more than one sample for that week)

(continued)

Table 6A-1. Data Aggregation Applied to Predictor Variables (continued)

Predictor Description	Predictor Code	Method of Aggregation
VOC Measurements (continued)		
Weekly PCE concentration—420 first floor Radiello sample ($\mu\text{g}/\text{m}^3$)	420First_Radiello_Weekly_PCE	Randomly choose one (where there is more than one sample for that week)
Weekly PCE concentration—422 first floor Radiello sample ($\mu\text{g}/\text{m}^3$)	422First_Radiello_Weekly_PCE	Randomly choose one (where there is more than one sample for that week)
Weekly PCE concentration—422 outside Radiello sample ($\mu\text{g}/\text{m}^3$)	Out_Radiello_Weekly_PCE	Randomly choose one (where there is more than one sample for that week)
First period GC PCE concentration at 420 basement south sampling location ($\mu\text{g}/\text{m}^3$)	420baseS_GC1_PCE	Mean
First period GC PCE concentration at 422 basement south sampling location ($\mu\text{g}/\text{m}^3$)	422baseS_GC1_PCE	Mean
First period GC PCE concentration at 420 first floor sampling location ($\mu\text{g}/\text{m}^3$)	420first_GC1_PCE	Mean
First period GC PCE concentration at 422 first floor sampling location ($\mu\text{g}/\text{m}^3$)	422first_GC1_PCE	Mean
First period GC PCE concentration at Wall Port 3 sampling location ($\mu\text{g}/\text{m}^3$)	WP3_GC1_PCE	Mean
First period GC PCE concentration at Subslab Port 2 sampling location ($\mu\text{g}/\text{m}^3$)	SSP2_GC1_PCE	Mean
First period GC PCE concentration at Subslab Port 4 sampling location ($\mu\text{g}/\text{m}^3$)	SSP4_GC1_PCE	Mean
First period GC PCE concentration at Subslab Port 7 sampling location ($\mu\text{g}/\text{m}^3$)	SSP7_GC1_PCE	Mean
First period GC PCE concentration at Soil Gas Port 11, 13 feet bls ($\mu\text{g}/\text{m}^3$)	SGP11-13_GC1_PCE	Mean
First period GC PCE concentration at Soil Gas Port 2, 9 feet bls ($\mu\text{g}/\text{m}^3$)	SGP2-9_GC1_PCE	Mean
First period GC PCE concentration at Soil Gas Port 8, 9 feet bls ($\mu\text{g}/\text{m}^3$)	SGP8-9_GC1_PCE	Mean
First period GC PCE concentration at Soil Gas Port 9, 6 feet bls ($\mu\text{g}/\text{m}^3$)	SGP9-6_GC1_PCE	Mean
Second period GC PCE concentration at 420 basement south sampling location ($\mu\text{g}/\text{m}^3$)	420baseS_GC2_PCE	Mean
Second period GC PCE concentration at 422 basement south sampling location ($\mu\text{g}/\text{m}^3$)	422baseS_GC2_PCE	Mean
Second period GC PCE concentration at 420 first floor sampling location ($\mu\text{g}/\text{m}^3$)	420first_GC2_PCE	Mean
Second period GC PCE concentration at 422 first floor sampling location ($\mu\text{g}/\text{m}^3$)	422first_GC2_PCE	Mean
Second period GC PCE concentration at Wall Port 3 sampling location ($\mu\text{g}/\text{m}^3$)	WP3_GC2_PCE	Mean
Second period GC concentration at Subslab Port 2 sampling location ($\mu\text{g}/\text{m}^3$)	SSP2_GC2_PCE	Mean
Second period GC concentration at Subslab Port 4 sampling location ($\mu\text{g}/\text{m}^3$)	SSP4_GC2_PCE	Mean
Second period GC concentration at Subslab Port 7 sampling location ($\mu\text{g}/\text{m}^3$)	SSP7_GC2_PCE	Mean

(continued)

Table 6A-1. Data Aggregation Applied to Predictor Variables (continued)

Predictor Description	Predictor Code	Method of Aggregation
VOC Measurements (continued)		
First period GC PCE concentration at Soil Gas Port 11, 13 feet bls ($\mu\text{g}/\text{m}^3$)	SGP11-13_GC2_PCE	Mean
Second period GC PCE concentration at Soil Gas Port 2, 9 feet bls ($\mu\text{g}/\text{m}^3$)	SGP2-9_GC2_PCE	Mean
Second period GC PCE concentration at Soil Gas Port 8, 9 feet bls ($\mu\text{g}/\text{m}^3$)	SGP8-9_GC2_PCE	Mean
Second period GC PCE concentration at Soil Gas Port 9, 6 feet bls ($\mu\text{g}/\text{m}^3$)	SGP9-6_GC2_PCE	Mean
Third period GC PCE concentration at 420 basement south sampling location ($\mu\text{g}/\text{m}^3$)	420baseS_GC3_PCE	Mean
Third period GC PCE concentration at 422 basement south sampling location ($\mu\text{g}/\text{m}^3$)	422baseS_GC3_PCE	Mean
Third period GC PCE concentration at 420 third floor sampling location ($\mu\text{g}/\text{m}^3$)	420first_GC3_PCE	Mean
Third period GC PCE concentration at 422 third floor sampling location ($\mu\text{g}/\text{m}^3$)	422first_GC3_PCE	Mean
Third period GC PCE concentration at Wall Port 3 sampling location ($\mu\text{g}/\text{m}^3$)	WP3_GC3_PCE	Mean
Third period GC PCE concentration at Subslab Port 2 sampling location ($\mu\text{g}/\text{m}^3$)	SSP2_GC3_PCE	Mean
Third period GC PCE concentration at Subslab Port 4 sampling location ($\mu\text{g}/\text{m}^3$)	SSP4_GC3_PCE	Mean
Third period GC PCE concentration at Subslab Port 7 sampling location ($\mu\text{g}/\text{m}^3$)	SSP7_GC3_PCE	Mean
Third period GC PCE concentration at Soil Gas Port 11, 13 feet bls ($\mu\text{g}/\text{m}^3$)	SGP11-13_GC3_PCE	Mean
Third period GC PCE concentration at Soil Gas Port 2, 9 feet bls ($\mu\text{g}/\text{m}^3$)	SGP2-9_GC3_PCE	Mean
Third period GC PCE concentration at Soil Gas Port 8, 9 feet bls ($\mu\text{g}/\text{m}^3$)	SGP8-9_GC3_PCE	Mean
Third period GC PCE concentration at Soil Gas Port 9, 6 feet bls ($\mu\text{g}/\text{m}^3$)	SGP9-6_GC3_PCE	Mean
Radon Measurements		
AlphaGUARD radon concentration at 422 basement north sampling location (pCi/L)	422baseN_AG_radon	Mean
AlphaGUARD radon concentration at 422 office sampling location (pCi/L)	422office_2nd_AG_radon	Mean

**Attachment 6B. Chloroform Time Series Results—January 2011 through
February 2012**

Table 6B-1. Time Series Analysis for 422 Basement South Chloroform, Predictor Variables Not Requiring Lag Terms, Period January 2011 to February 2012

Predictor Code ^a	Model Term	Coefficient	SE	R ²
Bar_drop_Hg.hr	intercept	-0.0193	0.02887	0.066847424
Bar_drop_Hg.hr	x(t)	28.65373	14.3061	0.066847424
BP_Net_Change	intercept	-0.01916	0.02861	0.083546524
BP_Net_Change	x(t)	-0.18906*	0.08367	0.083546524
Max_Change_dPdt	intercept	-0.02021	0.02981	0.00551378
Max_Change_dPdt	x(t)	0.1431	0.25682	0.00551378
Wind_Run_mi	intercept	-0.00082	0.08497	0.001112373
Wind_Run_mi	x(t)	-0.00003	0.00012	0.001112373
Wind_Speed_Hi_MPH	intercept	-0.02491	0.12557	2.13553E-05
Wind_Speed_Hi_MPH	x(t)	0.00014	0.00416	2.13553E-05
X422baseS_Wkly_Elect_radon	intercept	-0.04345	0.06601	0.00266163
X422baseS_Wkly_Elect_radon	x(t)	0.00268	0.00694	0.00266163

^a Descriptions of predictor codes can be found in Table 6A-1.

* = significant at 5%

** = significant at 1%

Full Model: $y(t) - y(t - 1) = \beta_0 + \beta_1x(t) + u(t)$

Table 6B-2. Time Series Analysis for 422 Basement South Chloroform: Predictor Variables Requiring One Lag Term, Period January 2011 to February 2012

Predictor Code ^a	Model Term	Full Model				First Reduced Model		
		Coefficient	SE	R ²	Rel R ²	Coefficient	SE	R ²
Abs_AMax_Change_dPdt	intercept	0.01747	0.08972	0.004293	0	-0.00259	0.074658	0.001248
Abs_AMax_Change_dPdt	x(t)	-0.08101	0.68357	0.004293	0.000751	-0.17018	0.64323	0.001248
Abs_AMax_Change_dPdt	x(t-1)	-0.27886	0.68003	0.004293	0.003541			
Bar_in_Hg	intercept	-1.35186	7.75973	0.000943	0	-0.51804	6.669049	9.93E-05
Bar_in_Hg	x(t)	-0.01156	0.25948	0.000943	6.77E-05	0.01658	0.222323	9.93E-05
Bar_in_Hg	x(t-1)	0.05594	0.25953	0.000943	0.000875			
BP_Pump_Speed	intercept	0.12302	0.08462	0.057294	0	0.10215	0.07625	0.051455
BP_Pump_Speed	x(t)	-0.6044	0.52883	0.057294	0.036922	-0.77112	0.442424	0.051455
BP_Pump_Speed	x(t-1)	-0.29423	0.50412	0.057294	0.020372			
BP_Stroke_Length	intercept	0.11727	0.08821	0.04962	0	0.101358	0.079458	0.046436
BP_Stroke_Length	x(t)	-0.15557	0.14536	0.04962	0.033114	-0.19239	0.116506	0.046436
BP_Stroke_Length	x(t-1)	-0.06173	0.14379	0.04962	0.016506			
Cool_Degree_Day	intercept	-0.03465	0.03642	0.014274	0	-0.03171	0.036019	0.005269
Cool_Degree_Day	x(t)	-0.00084	0.00192	0.014274	0.004364	0.000408	0.000749	0.005269
Cool_Degree_Day	x(t-1)	0.00136	0.00192	0.014274	0.00991			
DepthToWater	intercept	-0.52129	0.44463	0.02469	0	-0.49833	0.412495	0.023697
DepthToWater	x(t)	0.02626	0.04153	0.02469	0.01589	0.029725	0.025726	0.023697
DepthToWater	x(t-1)	0.005	0.0414	0.02469	0.0088			
Dew_pt_422_F	intercept	-0.06485	0.1051	0.044483	0	-0.04105	0.105426	0.000724
Dew_pt_422_F	x(t)	-0.00816	0.00585	0.044483	0.017246	0.000449	0.002228	0.000724
Dew_pt_422_F	x(t-1)	0.00916	0.00577	0.044483	0.027237			
Fall_Crk_Gage_ht_ft	intercept	0.05022	0.09262	0.014286	0	0.045639	0.084451	0.013567
Fall_Crk_Gage_ht_ft	x(t)	-0.01826	0.02971	0.014286	0.010646	-0.01846	0.021224	0.013567
Fall_Crk_Gage_ht_ft	x(t-1)	-0.00096	0.02956	0.014286	0.00364			

(continued)

Table 6B-2. Time Series Analysis for 422 Basement South Chloroform: Predictor Variables Requiring One Lag Term, Period January 2011 to February 2012 (continued)

Predictor Code ^a	Model Term	Full Model				First Reduced Model		
		Coefficient	SE	R ²	Rel R ²	Coefficient	SE	R ²
Hum_422_.	intercept	-0.07369	0.11926	0.021318	0	-0.05212	0.117637	0.001361
Hum_422_.	x(t)	-0.00481	0.00596	0.021318	0.006483	0.000769	0.002782	0.001361
Hum_422_.	x(t-1)	0.00613	0.00579	0.021318	0.014834			
Hum_out_.	intercept	0.47052	0.38021	0.033099	0	0.258291	0.324197	0.01316
Hum_out_.	x(t)	-0.00149	0.00493	0.033099	0.007386	-0.00382	0.00442	0.01316
Hum_out_.	x(t-1)	-0.00523	0.00491	0.033099	0.025712			
Out_Wkly_Elect_radon	intercept	-0.0242	0.03789	0.061681	0	-0.05434	0.031176	0.082422
Out_Wkly_Elect_radon	x(t)	0.12471	0.07511	0.061681	0.052059	0.09625195*	0.046354	0.082422
Out_Wkly_Elect_radon	x(t-1)	-0.07098	0.07666	0.061681	0.009622			
Rain_In_met	intercept	0.0289	0.04549	0.036493	0	0.009939	0.040877	0.020596
Rain_In_met	x(t)	-0.02655	0.03688	0.036493	0.014839	-0.03786	0.034889	0.020596
Rain_In_met	x(t-1)	-0.03497	0.03671	0.036493	0.021654			
Rain_IPH	intercept	0.00255	0.04358	0.060669	0	-0.0327	0.039879	0.003663
Rain_IPH	x(t)	0.01498	0.01564	0.060669	0.009667	0.00695	0.015318	0.003663
Rain_IPH	x(t-1)	-0.02851	0.01561	0.060669	0.051002			
Setra_420ss.base_Pa	intercept	0.00124	0.07342	0.042839	0	-0.05414	0.062731	0.006581
Setra_420ss.base_Pa	x(t)	0.05663	0.05553	0.042839	0.012682	0.031811	0.053186	0.006581
Setra_420ss.base_Pa	x(t-1)	-0.07869	0.05553	0.042839	0.030157			
Setra_422base.out_Pa	intercept	-0.01792	0.03015	0.022484	0	-0.02056	0.030133	2.03E-05
Setra_422base.out_Pa	x(t)	-0.01908	0.027	0.022484	0.004445	0.000692	0.020542	2.03E-05
Setra_422base.out_Pa	x(t-1)	0.02983	0.02653	0.022484	0.018038			
Setra_422base.upst_Pa	intercept	-0.0204	0.02933	0.057104	0	-0.02208	0.029418	0.031767
Setra_422base.upst_Pa	x(t)	-0.05065	0.03109	0.057104	0.038641	-0.04088	0.030157	0.031767
Setra_422base.upst_Pa	x(t-1)	0.03778	0.03108	0.057104	0.018463			
Setra_422SGdp.ss_Pa	intercept	0.01465	0.04898	0.032175	0	-0.01963	0.044904	3.37E-05
Setra_422SGdp.ss_Pa	x(t)	0.02381	0.02962	0.032175	0.006096	-0.00093	0.021617	3.37E-05
Setra_422SGdp.ss_Pa	x(t-1)	-0.04651	0.03526	0.032175	0.026079			

(continued)

Table 6B-2. Time Series Analysis for 422 Basement South Chloroform: Predictor Variables Requiring One Lag Term, Period January 2011 to February 2012 (continued)

Predictor Code ^a	Model Term	Full Model				First Reduced Model		
		Coefficient	SE	R ²	Rel R ²	Coefficient	SE	R ²
Setra_422ss.base_Pa	intercept	-0.11005	0.11181	0.025711	0	-0.12812	0.09656	0.023802
Setra_422ss.base_Pa	x(t)	0.05122	0.04359	0.025711	0.024131	0.044379	0.037979	0.023802
Setra_422ss.base_Pa	x(t-1)	-0.0143	0.04356	0.025711	0.00158			
Snowdepth_daily	intercept	-0.01928	0.02985	0.155572	0	-0.00596	0.031267	0.032828
Snowdepth_daily	x(t)	-0.19513**	0.06254	0.155572	0.091154	-0.05725	0.041524	0.032828
Snowdepth_daily	x(t-1)	0.17307**	0.06121	0.155572	0.064418			
Soil_H2O_In6._cbar	intercept	-0.06832	0.05302	0.028445	0	-0.07212	0.050542	0.02725
Soil_H2O_In6._cbar	x(t)	-0.00093	0.00609	0.028445	0.013829	0.000652	0.000521	0.02725
Soil_H2O_In6._cbar	x(t-1)	0.00158	0.00607	0.028445	0.014616			
Soil_H2O_Out13._cbar	intercept	-0.06386	0.04534	0.028299	0	-0.06277	0.044774	0.02708
Soil_H2O_Out13._cbar	x(t)	0.00067	0.00145	0.028299	0.015441	0.000297	0.000238	0.02708
Soil_H2O_Out13._cbar	x(t-1)	-0.00038	0.00144	0.028299	0.012857			
Soil_H2O_Out3.5._cbar	intercept	-0.04118	0.03688	0.017185	0	-0.04097	0.036027	0.017166
Soil_H2O_Out3.5._cbar	x(t)	0.00047	0.00091	0.017185	0.010987	0.000495	5.01E-04	0.017166
Soil_H2O_Out3.5._cbar	x(t-1)	0.00003	0.00091	0.017185	0.006199			
Soil_H2O_Out6._cbar	intercept	-0.03738	0.03984	0.00903	0	-0.03807	0.039392	0.008032
Soil_H2O_Out6._cbar	x(t)	-0.0002	0.00158	0.00903	0.004154	0.000171	0.000254	0.008032
Soil_H2O_Out6._cbar	x(t-1)	0.00038	0.0016	0.00903	0.004876			
Soil_T_C_MW3.6	intercept	-0.24998	0.16054	0.038359	0	-0.20374	0.156614	0.025964
Soil_T_C_MW3.6	x(t)	0.00846	0.0507	0.038359	0.019362	0.010699	0.009002	0.025964
Soil_T_C_MW3.6	x(t-1)	0.00462	0.04997	0.038359	0.018997			
Soil_T_C_MW3.9	intercept	-0.33326	0.19393	0.058585	0	-0.26751	0.190441	0.031381
Soil_T_C_MW3.9	x(t)	0.08932	0.0843	0.058585	0.032978	0.015134	0.01155	0.031381
Soil_T_C_MW3.9	x(t-1)	-0.07067	0.08309	0.058585	0.025607			
Soil_T_C_OTC.1	intercept	-0.06129	0.05047	0.266508	0	-0.00212	0.061774	0.000355
Soil_T_C_OTC.1	x(t)	-0.05861**	0.01511	0.266508	0.120027	-0.00052	0.003933	0.000355
Soil_T_C_OTC.1	x(t-1)	0.06156**	0.01504	0.266508	0.146481			

(continued)

Table 6B-2. Time Series Analysis for 422 Basement South Chloroform: Predictor Variables Requiring One Lag Term, Period January 2011 to February 2012 (continued)

Predictor Code ^a	Model Term	Full Model				First Reduced Model		
		Coefficient	SE	R ²	Rel R ²	Coefficient	SE	R ²
Soil_T_C_OTC.16.5	intercept	-0.47979	0.31746	0.04172	0	-0.46196	0.310209	0.037637
Soil_T_C_OTC.16.5	x(t)	-0.01854	0.11261	0.04172	0.019197	0.032043	0.021848	0.037637
Soil_T_C_OTC.16.5	x(t-1)	0.05181	0.11279	0.04172	0.022523			
Soil_T_C_OTC.6	intercept	-0.09156	0.07029	0.038588	0	-0.06916	0.06889	0.011343
Soil_T_C_OTC.6	x(t)	-0.03029	0.03474	0.038588	0.016663	0.00368	0.00472	0.011343
Soil_T_C_OTC.6	x(t-1)	0.03531	0.03464	0.038588	0.021925			
StackEffect_420baseN	intercept	0.04934	0.10411	0.030054	0	-0.0166	0.091587	3.99E-05
StackEffect_420baseN	x(t)	0.5312	0.94528	0.030054	0.002804	-0.03984	0.843061	3.99E-05
StackEffect_420baseN	x(t-1)	-1.20078	0.92044	0.030054	0.02725			
StackEffect_422first	intercept	0.0012	0.0717	0.058695	0	-0.02807	0.07142	0.000231
StackEffect_422first	x(t)	1.30522	0.78516	0.058695	0.023763	0.04525	0.397866	0.000231
StackEffect_422first	x(t-1)	-1.43263	0.77513	0.058695	0.034932			
StdDev_Setra_420ss.base_Pa	intercept	-0.02524	0.03767	0.095766	0	-0.04971	0.036074	0.036971
StdDev_Setra_420ss.base_Pa	x(t)	0.08644*	0.04221	0.095766	0.054254	0.057861	0.040187	0.036971
StdDev_Setra_420ss.base_Pa	x(t-1)	-0.07841	0.04224	0.095766	0.041512			
StdDev_Setra_422base.out_Pa	intercept	-0.0365	0.05089	0.092159	0	-0.0774	0.045497	0.045051
StdDev_Setra_422base.out_Pa	x(t)	0.04599*	0.0216	0.092159	0.059925	0.033555	0.020644	0.045051
StdDev_Setra_422base.out_Pa	x(t-1)	-0.03655	0.02163	0.092159	0.032234			
StdDev_Setra_422base.upst_Pa	intercept	-0.04946	0.03544	0.107504	0	-0.06113	0.03303	0.093838
StdDev_Setra_422base.upst_Pa	x(t)	0.17391*	0.06777	0.107504	0.100343	0.1563364*	0.06492	0.093838
StdDev_Setra_422base.upst_Pa	x(t-1)	-0.06225	0.06783	0.107504	0.007161			
StdDev_Setra_422SGdp.ss_Pa	intercept	-0.00938	0.03838	0.001951	0	-0.01862	0.036345	0.000272
StdDev_Setra_422SGdp.ss_Pa	x(t)	-0.00036	0.01231	0.001951	0.000368	-0.00127	0.010367	0.000272
StdDev_Setra_422SGdp.ss_Pa	x(t-1)	-0.00328	0.01283	0.001951	0.001583			
StdDev_Setra_422ss.base_Pa	intercept	-0.01678	0.0363	0.00389	0	-0.01405	0.034065	0.002908
StdDev_Setra_422ss.base_Pa	x(t)	-0.00695	0.01532	0.00389	0.003319	-0.00582	0.014403	0.002908
StdDev_Setra_422ss.base_Pa	x(t-1)	0.00394	0.01694	0.00389	0.00057			

(continued)

Table 6B-2. Time Series Analysis for 422 Basement South Chloroform: Predictor Variables Requiring One Lag Term, Period January 2011 to February 2012 (continued)

Predictor Code ^a	Model Term	Full Model				First Reduced Model		
		Coefficient	SE	R ²	Rel R ²	Coefficient	SE	R ²
T_420baseS_C	intercept	-0.12447	0.13648	0.056629	0	-0.11032	0.138447	0.007786
T_420baseS_C	x(t)	-0.01379	0.00937	0.056629	0.02249	0.001537	0.002319	0.007786
T_420baseS_C	x(t-1)	0.01561	0.00925	0.056629	0.034139			
T_420first_C	intercept	-0.10384	0.12043	0.077053	0	-0.08073	0.123426	0.004467
T_420first_C	x(t)	-0.01145	0.00629	0.077053	0.030049	0.000997	0.001989	0.004467
T_420first_C	x(t-1)	0.01288*	0.00619	0.077053	0.047004			
T_422_F	intercept	-0.10263	0.27042	0.023879	0	-0.00946	0.25899	3.40E-05
T_422_F	x(t)	-0.00633	0.00642	0.023879	0.008628	-0.00016	0.003607	3.40E-05
T_422_F	x(t-1)	0.00747	0.00644	0.023879	0.015252			
T_422baseN_C	intercept	-0.20772	0.20328	0.053359	0	-0.18766	0.205405	0.011907
T_422baseN_C	x(t)	-0.01554	0.01219	0.053359	0.01995	0.002692	0.003277	0.011907
T_422baseN_C	x(t-1)	0.0186	0.01198	0.053359	0.033409			
T_422baseS_C	intercept	-0.29257	0.24304	0.031584	0	-0.27489	0.241382	0.019711
T_422baseS_C	x(t)	-0.00591	0.01259	0.031584	0.011796	0.003961	0.003733	0.019711
T_422baseS_C	x(t-1)	0.01017	0.01238	0.031584	0.019788			
T_422first_C	intercept	-0.32715	0.30477	0.037071	0	-0.24293	0.298641	0.00989
T_422first_C	x(t)	-0.00684	0.00905	0.037071	0.009954	0.003149	0.00421	0.00989
T_422first_C	x(t-1)	0.0112	0.00899	0.037071	0.027118			
T_out_F	intercept	-0.06658	0.09123	0.110941	0	-0.03519	0.095031	0.000461
T_out_F	x(t)	-0.00957*	0.00409	0.110941	0.044499	0.00027	0.00168	0.000461
T_out_F	x(t-1)	0.01048*	0.00401	0.110941	0.066442			
T_out_Hi_F	intercept	-0.1174	0.12366	0.087143	0	-0.07571	0.12659	0.003559
T_out_Hi_F	x(t)	-0.00619	0.0035	0.087143	0.027735	0.000757	0.001693	0.003559
T_out_Hi_F	x(t-1)	0.00757*	0.00337	0.087143	0.059408			
Wind_Chill_F	intercept	-0.0599	0.08146	0.126745	0	-0.03018	0.085653	0.00025
Wind_Chill_F	x(t)	-0.00912*	0.0036	0.126745	0.051016	0.000182	0.001542	0.00025
Wind_Chill_F	x(t-1)	0.00994**	0.00352	0.126745	0.075729			

(continued)

Table 6B-2. Time Series Analysis for 422 Basement South Chloroform: Predictor Variables Requiring One Lag Term, Period January 2011 to February 2012 (continued)

Predictor Code ^a	Model Term	Full Model				First Reduced Model		
		Coefficient	SE	R ²	Rel R ²	Coefficient	SE	R ²
X422baseN_Wkly_Elect_radon	intercept	0.03218	0.10647	0.087172	0	-0.07941	0.096687	0.007224
X422baseN_Wkly_Elect_radon	x(t)	0.02447	0.0145	0.087172	0.027228	0.008231	0.012894	0.007224
X422baseN_Wkly_Elect_radon	x(t-1)	-0.03162*	0.01441	0.087172	0.059944			

^a Descriptions of predictor codes can be found in Table 6A-1.

* = significant at 5%

** = significant at 1%

Note: Model with only intercept and x term does not have Relative R² since R² = Relative R²

Full Model: $y(t) - y(t - 1) = \beta_0 + \beta_1 x(t) + \beta_2 x(t - 1) + u(t)$

First Reduced Model: $y(t) - y(t - 1) = \beta_0 + \beta_1 x(t) + u(t)$

Table 6B-3. Time Series Analysis for 422 Basement South Chloroform: Predictor Variables Requiring Two Lag Terms, Period January 2011 to February 2012

Predictor Code ^a	Model Term	Full Model				First Reduced Model				Second Reduced Model		
		Coefficient	SE	R ²	Rel R ²	Coefficient	SE	R ²	Rel R ²	Coefficient	SE	R ²
Diff_T_420baseN.Out_F	intercept	-0.01959186	0.03223503	0.108617	0	-0.01817	0.034399	0.100398		-0.03668	0.034702	0.013894
Diff_T_420baseN.Out_F	x(t)	0.01422424*	0.00665654	0.108617	0.063623	0.01425572*	0.0064	0.100398	0.04753	0.004369	0.004919	0.013894
Diff_T_420baseN.Out_F	x(t-1)	-0.01217301	0.00640382	0.108617	0.036628	-0.01439116*	0.006258	0.100398	0.052868			
Diff_T_420baseN.Out_F	x(t-2)	0.0013039	0.00664277	0.108617	0.008366							
Diff_T_420baseS.Out_F	intercept	-0.02291876	0.03453393	0.114926	0	-0.01803	0.036771	0.10566		-0.04075	0.036924	0.014634
Diff_T_420baseS.Out_F	x(t)	0.01434685*	0.00646464	0.114926	0.068261	0.01423084*	0.006206	0.10566	0.050065	0.004358	0.004779	0.014634
Diff_T_420baseS.Out_F	x(t-1)	-0.01202284	0.00619435	0.114926	0.037924	-0.01432603*	0.006055	0.10566	0.055596			
Diff_T_420baseS.Out_F	x(t-2)	0.00110429	0.0064144	0.114926	0.008741							
Heat_Degree_Day	intercept	-0.01454303	0.04153997	0.117041	0	0.001435	0.043964	0.122176		-0.02147	0.045671	9.02E-06
Heat_Degree_Day	x(t)	0.00116796	0.0006426	0.117041	0.040604	0.00142932*	0.000598	0.122176	0.045585	7.27E-06	0.000323	9.02E-06
Heat_Degree_Day	x(t-1)	-0.00154546*	0.00062229	0.117041	0.062877	-0.00160784**	0.000581	0.122176	0.076591			
Heat_Degree_Day	x(t-2)	0.00044224	0.00063621	0.117041	0.013561							
StackEffect_420baseS	intercept	-0.0506789	0.0978561	0.046781	0	0.022223	0.098522	0.044272		-0.04739	0.089008	0.001808
StackEffect_420baseS	x(t)	1.0324079	0.89481769	0.046781	0.021338	0.996323	0.908975	0.044272	0.011342	0.249422	0.783178	0.001808
StackEffect_420baseS	x(t-1)	-1.15713981	0.89908124	0.046781	0.018194	-1.38309	0.88476	0.044272	0.032929			
StackEffect_420baseS	x(t-2)	0.52293159	0.88420384	0.046781	0.00725							
StackEffect_420first	intercept	-0.08080257	0.09669901	0.126469	0	-0.05036	0.100704	0.096345		-0.14439	0.089886	0.036468
StackEffect_420first	x(t)	2.45948804*	0.93265656	0.126469	0.098309	1.92779961*	0.87391	0.096345	0.05821	1.153088	0.792033	0.036468
StackEffect_420first	x(t-1)	-1.10691217	0.82516071	0.126469	0.019437	-1.64103	0.859626	0.096345	0.038134			
StackEffect_420first	x(t-2)	-0.66749047	0.92244355	0.126469	0.008723							

(continued)

Table 6B-3. Time Series Analysis for 422 Basement South Chloroform: Predictor Variables Requiring Two Lag Terms, Period January 2011 to February 2012 (continued)

Predictor Code ^a	Model Term	Full Model				First Reduced Model				Second Reduced Model		
		Coefficient	SE	R ²	Rel R ²	Coefficient	SE	R ²	Rel R ²	Coefficient	SE	R ²
StackEffect_422baseN	intercept	-0.04336728	0.06965698	0.17663	0	0.007669	0.073495	0.142661		-0.06566	0.073704	0.007881
StackEffect_422baseN	x(t)	1.66060496*	0.68938328	0.17663	0.068964	1.81532197*	0.699008	0.142661	0.056506	0.348071	0.521869	0.007881
StackEffect_422baseN	x(t-1)	-2.13341933**	0.70489559	0.17663	0.086138	-2.02238731**	0.687774	0.142661	0.086155			
StackEffect_422baseN	x(t-2)	0.7497326	0.68760459	0.17663	0.021527							
StackEffect_422baseS	intercept	-0.04463821	0.06779417	0.200263	0	-4.4E-05	0.071634	0.168372		-0.07548	0.073121	0.011865
StackEffect_422baseS	x(t)	1.82936866**	0.63866253	0.200263	0.091204	1.91636007**	0.64708	0.168372	0.072242	0.389713	0.475247	0.011865
StackEffect_422baseS	x(t-1)	-2.08386913**	0.65663949	0.200263	0.091919	-2.05226258**	0.637895	0.168372	0.09613			
StackEffect_422baseS	x(t-2)	0.51859524	0.63791085	0.200263	0.017139							
T_out_Lo_F	intercept	0.00042096	0.06611725	0.009424	0	-0.04307	0.068917	0.002521		-0.04331	0.067211	0.002514
T_out_Lo_F	x(t)	-0.00046306	0.00369732	0.009424	0.000987	0.000677	0.003608	0.002521	0.001576	0.000613	0.001631	0.002514
T_out_Lo_F	x(t-1)	-0.00211223	0.00384018	0.009424	0.004111	-7.1E-05	0.003563	0.002521	0.000945			
T_out_Lo_F	x(t-2)	0.00233508	0.00368435	0.009424	0.004326							
Wind_Speed_MPH	intercept	0.06238384	0.10418381	0.022903	0	0.073085	0.104345	0.037454		-0.00021	0.092036	0.000987
Wind_Speed_MPH	x(t)	0.00953657	0.02508932	0.022903	0.001513	0.012275	0.02539	0.037454	0.002539	-0.00529	0.022498	0.000987
Wind_Speed_MPH	x(t-1)	-0.025247	0.02529748	0.022903	0.019167	-0.03637	0.025194	0.037454	0.034915			
Wind_Speed_MPH	x(t-2)	-0.00272754	0.02496182	0.022903	0.002223							

^a Descriptions of predictor codes can be found in Table 6A-1.

* = significant at 5%

** = significant at 1%

Note: Model with only intercept and x term doesn't have Relative R² since R² = Relative R²

Full Model: $y(t) - y(t - 1) = \beta_0 + \beta_1x(t) + \beta_2x(t - 1) + \beta_3x(t - 2) + u(t)$

First Reduced Model: $y(t) - y(t - 1) = \beta_0 + \beta_1x(t) + \beta_2x(t - 1) + u(t)$

Second Reduced Model: $y(t) - y(t - 1) = \beta_0 + \beta_1x(t) + u(t)$

Table 6B-4. Time Series Analysis for 422 Basement South Chloroform: Categorical Predictor Variables, Period January 2011 to February 2012

Predictor Code ^a	Model Term	Coefficient	SE	R ²	AIC
AC_on.off_420_daily	intercept	-0.021	0.03040643	0.00005394	-3.167763289
AC_on.off_420_daily	ON	0.009	0.16374364	0.00005394	-3.167763289
AC_on.off_422_daily	intercept	-0.0268	0.03387683	0.00258522	-3.314771604
AC_on.off_422_daily	ON	0.02726154	0.07155585	0.00258522	-3.314771604
Fan_on.off_422_daily	intercept	-0.0362	0.02929774	0.08822303	-8.521506868
Fan_on.off_422_daily	ON	0.29986667*	0.12882125	0.08822303	-8.521506868
Heat_on.off_422_daily	intercept	-5.00E-04	0.05077177	0.00429143	-3.414072873
Heat_on.off_422_daily	ON	-0.03081579	0.06272555	0.00429143	-3.414072873
METAR_IcyPrecip_YorN	intercept	-0.0525	0.03319495	0.06361493	-6.976886447
METAR_IcyPrecip_YorN	Yes	0.13178571	0.06756504	0.06361493	-6.976886447
METAR_ThunderEvent_YorN	intercept	-0.01785714	0.04299913	0.00014979	-3.173322816
METAR_ThunderEvent_YorN	Yes	-0.00547619	0.05978786	0.00014979	-3.173322816
Wind_Dir_Hi	intercept	0.10025	0.11208904	0.11605331	-0.319428951
Wind_Dir_Hi	N	-0.15691667	0.17121883	0.11605331	-0.319428951
Wind_Dir_Hi	NE	-0.43025	0.2506387	0.11605331	-0.319428951
Wind_Dir_Hi	NW	0.01075	0.2506387	0.11605331	-0.319428951
Wind_Dir_Hi	S	-0.40025	0.2506387	0.11605331	-0.319428951
Wind_Dir_Hi	SW	-0.28025	0.17121883	0.11605331	-0.319428951
Wind_Dir_Hi	W	-0.10851667	0.11696473	0.11605331	-0.319428951
Wind_Dir	intercept	0.045	0.11177064	0.13830203	0.202039404
Wind_Dir	N	0.109	0.17073247	0.13830203	0.202039404
Wind_Dir	NE	-0.026875	0.13689051	0.13830203	0.202039404
Wind_Dir	NW	-0.06944444	0.13433159	0.13830203	0.202039404
Wind_Dir	S	-0.04033333	0.17073247	0.13830203	0.202039404

(continued)

Table 6B-4. Time Series Analysis for 422 Basement South Chloroform: Categorical Predictor Variables, Period January 2011 to February 2012 (continued)

Predictor Code ^a	Model Term	Coefficient	SE	R ²	AIC
Wind_Dir	SE	-0.29	0.19359242	0.13830203	0.202039404
Wind_Dir	SW	0.02155556	0.13433159	0.13830203	0.202039404
Wind_Dir	W	-0.1395	0.1224386	0.13830203	0.202039404

^a Descriptions of predictor codes can be found in Table 6A-1.

* = significant at 5%

** = significant at 1%

Reference AC = OFF

Reference AC = OFF

Reference Fan = OFF

Reference Heat = OFF

Reference IcyPrecip = No

Reference SnowEvent = No

Reference Win Dir Hi = E

$$y(t) - y(t - 1) = \beta_0 + \beta_1 x_{ON}(t) + u(t) \text{ where } x_{ON}(t) = \begin{cases} 1 & \text{if predictor}_{iS} \text{ ON} \\ 0 & \text{if predictor}_{iS} \text{ OFF} \end{cases}$$

If X(t) = ON/OFF, then Off is reference cell

$$y(t) - y(t - 1) = \beta_0 + \beta_1 Wind_Dir_N(t) + \beta_2 Wind_Dir_{NE}(t) + \beta_3 Wind_Dir_{NW}(t) + \beta_4 Wind_Dir_{SE}(t) + \beta_5 Wind_Dir_S(t) + \beta_6 Wind_Dir_{SW}(t) + \beta_7 Wind_Dir_W(t) + u(t)$$

$$\text{where } x_d(t) = \begin{cases} 1 & \text{if } wind_{iS} \text{ in direction } d \\ 0 & \text{if } wind_{iS} \text{ not in direction } d \end{cases}$$

$$y(t) - y(t - 1) = \beta_0 + \beta_1 Wind_Dir_Hi_N(t) + \beta_2 Wind_Dir_Hi_{NE}(t) + \beta_3 Wind_Dir_Hi_{NW}(t) + \beta_4 Wind_Dir_Hi_{SE}(t) + \beta_5 Wind_Dir_Hi_S(t) + \beta_6 Wind_Dir_Hi_{SW}(t) + \beta_7 Wind_Dir_Hi_W(t) + u(t)$$

$$\text{where } x_d(t) = \begin{cases} 1 & \text{if } wind_{iS} \text{ in direction } d \\ 0 & \text{if } wind_{iS} \text{ not in direction } d \end{cases}$$

Attachment 6C. PCE Time Series Results—January 2011 through February 2012

Table 6C-1. Time Series Analysis for 422 Basement South PCE: Predictor Variables Requiring No Lag Terms, Period January 2011 to February 2012

Predictor Code ^a	Model Term	Coefficient	SE	R ²	AIC	BIC
Bar_drop_Hg.hr	intercept	-0.23167	0.13406	4.08E-05	215.0309	223.1323
Bar_drop_Hg.hr	x(t)	96.99715	122.4368	4.08E-05	215.0309	223.1323
BP_Net_Change	intercept	-0.23204	0.13373	0.019176	224.6403	232.7417
BP_Net_Change	x(t)	-0.81911	0.72409	0.019176	224.6403	232.7417
Max_Change_dPdt	intercept	-0.23284	0.13572	0.010446	223.7698	231.8713
Max_Change_dPdt	x(t)	0.82464	1.94786	0.010446	223.7698	231.8713
Wind_Run_mi	intercept	-0.09135	0.4647	0.022018	239.7899	247.8913
Wind_Run_mi	x(t)	-0.00022	0.00067	0.022018	239.7899	247.8913
Wind_Speed_Hi_MPH	intercept	-0.41885	0.71994	0.030703	232.6842	240.7856
Wind_Speed_Hi_MPH	x(t)	0.00622	0.02406	0.030703	232.6842	240.7856
X422baseS_Wkly_Elect_radon	intercept	-0.04068	0.36589	0.013925	231.3897	239.4911
X422baseS_Wkly_Elect_radon	x(t)	-0.02288	0.04005	0.013925	231.3897	239.4911

^a Descriptions of predictor codes can be found in Table 6A-1.

* = significant at 5%

** = significant at 1%

For PCE Radiello 1, the R² is an approximation, Model has serial correlated errors, R² is not robust estimator.

$$y(t) - y(t - 1) = \beta_0 + \beta_1 x(t) + u(t)$$

Table 6C-2. Time Series Analysis for 422 Basement South PCE: Predictor Variables Requiring One Lag Term, Period January 2011 to February 2012

Predictor Code ^a	Model Term	Full Model					First Reduced Model				
		Coefficient	SE	R ²	AIC	BIC	Coefficient	SE	R ²	AIC	BIC
Abs_AMax_Change_dPdt	intercept	-0.21861	0.45878	0.043309403	219.9823	230.019	-0.20072	0.40255	0.028885	222.7555	230.8569
Abs_AMax_Change_dPdt	x(t)	-0.47899	4.38666	0.043309403	219.9823	230.019	-0.3304	3.54843	0.028885	222.7555	230.8569
Abs_AMax_Change_dPdt	x(t-1)	0.29833	4.36924	0.043309403	219.9823	230.019					
Bar_in_Hg	intercept	50.04388	36.23412	0.059621848	220.9814	231.0181	56.16439	33.30263	0.036475	222.2251	230.3265
Bar_in_Hg	x(t)	-2.62042	1.76156	0.059621848	220.9814	231.0181	-1.88022	1.11024	0.036475	222.2251	230.3265
Bar_in_Hg	x(t-1)	0.94419	1.76379	0.059621848	220.9814	231.0181					
BP_Pump_Speed	intercept	0.71046	0.36444	0.02734325	212.227	222.2637	0.59297	0.4046	0.196213	219.0306	227.132
BP_Pump_Speed	x(t)	1.50028	3.40423	0.02734325	212.227	222.2637	-5.27864*	2.39544	0.196213	219.0306	227.132
BP_Pump_Speed	x(t-1)	-7.35424*	3.24753	0.02734325	212.227	222.2637					
BP_Stroke_Length	intercept	0.57402	0.38768	0.005142225	220.3888	230.4255	0.38572	0.40386	0.097569	223.6667	231.7681
BP_Stroke_Length	x(t)	0.49767	0.91185	0.005142225	220.3888	230.4255	-0.98777	0.60277	0.097569	223.6667	231.7681
BP_Stroke_Length	x(t-1)	-1.76287	0.89555	0.005142225	220.3888	230.4255					
Cool_Degree_Day	intercept	-0.3578*	0.1672	0.040610649	244.0829	254.1195	-0.35023*	0.1624	0.019919	235.0812	243.1826
Cool_Degree_Day	x(t)	0.00079	0.01155	0.040610649	244.0829	254.1195	0.00425	0.0034	0.019919	235.0812	243.1826
Cool_Degree_Day	x(t-1)	0.00366	0.01155	0.040610649	244.0829	254.1195					
DepthToWater	intercept	-0.3213	1.99578	0.121782639	224.8071	234.6586	-1.05712	2.00324	0.000613	226.4295	234.4589
DepthToWater	x(t)	0.32471	0.22225	0.121782639	224.8071	234.6586	0.05108	0.12504	0.000613	226.4295	234.4589
DepthToWater	x(t-1)	-0.31893	0.22158	0.121782639	224.8071	234.6586					
Dew_pt_422_F	intercept	-1.23475**	0.46004	0.014508776	235.6859	245.7225	-1.20101*	0.45399	0.005871	229.7828	237.8842
Dew_pt_422_F	x(t)	-0.01184	0.03898	0.014508776	235.6859	245.7225	0.02129*	0.00957	0.005871	229.7828	237.8842
Dew_pt_422_F	x(t-1)	0.03393	0.03856	0.014508776	235.6859	245.7225					
Fall_Crk_Gage_ht_ft	intercept	-0.15145	0.41718	0.114194748	225.7242	235.5757	-0.00779	0.41121	0.020716	226.5999	234.6292
Fall_Crk_Gage_ht_ft	x(t)	-0.24973	0.17007	0.114194748	225.7242	235.5757	-0.06212	0.10398	0.020716	226.5999	234.6292
Fall_Crk_Gage_ht_ft	x(t-1)	0.22863	0.16895	0.114194748	225.7242	235.5757					
Hum_422_.	intercept	-1.49386**	0.49754	0.012713819	232.4943	242.531	-1.4725**	0.51189	0.020571	228.1049	236.2063
Hum_422_.	x(t)	-0.02764	0.03953	0.012713819	232.4943	242.531	0.0302*	0.01208	0.020571	228.1049	236.2063
Hum_422_.	x(t-1)	0.05863	0.0385	0.012713819	232.4943	242.531					
Hum_out_.	intercept	2.06947	1.9258	0.077755189	238.3611	248.3978	1.87596	1.72745	0.077332	231.3023	239.4037
Hum_out_.	x(t)	-0.02477	0.0315	0.077755189	238.3611	248.3978	-0.02896	0.0236	0.077332	231.3023	239.4037
Hum_out_.	x(t-1)	-0.00684	0.03122	0.077755189	238.3611	248.3978					

(continued)

Table 6C-2. Time Series Analysis for 422 Basement South PCE: Predictor Variables Requiring One Lag Term, Period January 2011 to February 2012 (continued)

Predictor Code ^a	Model Term	Full Model					First Reduced Model				
		Coefficient	SE	R ²	AIC	BIC	Coefficient	SE	R ²	AIC	BIC
Out_Wkly_Elect_radon	intercept	0.09187	0.2	0.848191068	110.315	119.0033	-0.26648	0.14743	1.092561	195.6801	203.1649
Out_Wkly_Elect_radon	x(t)	0.54761	0.34138	0.848191068	110.315	119.0033	0.32735	0.24633	1.092561	195.6801	203.1649
Out_Wkly_Elect_radon	x(t-1)	-0.75483*	0.3513	0.848191068	110.315	119.0033					
Rain_In_met	intercept	-0.27251	0.22984	0.051688212	230.9154	240.952	-0.19743	0.20905	0.023827	228.5156	236.617
Rain_In_met	x(t)	-0.14976	0.23367	0.051688212	230.9154	240.952	-0.04681	0.19381	0.023827	228.5156	236.617
Rain_In_met	x(t-1)	0.19319	0.23277	0.051688212	230.9154	240.952					
Rain_IPH	intercept	-0.39868	0.21856	0.04375501	233.8994	243.9361	-0.35238	0.20211	0.0378	229.6001	237.7015
Rain_IPH	x(t)	0.0302	0.10704	0.04375501	233.8994	243.9361	0.06668	0.08538	0.0378	229.6001	237.7015
Rain_IPH	x(t-1)	0.06252	0.10684	0.04375501	233.8994	243.9361					
Setra_420ss.base_Pa	intercept	-0.20795	0.3765	0.005514833	224.2361	234.0876	-0.24781	0.33511	0.000103	222.0917	230.0477
Setra_420ss.base_Pa	x(t)	0.04613	0.3638	0.005514833	224.2361	234.0876	0.00422	0.29519	0.000103	222.0917	230.0477
Setra_420ss.base_Pa	x(t-1)	-0.08128	0.36373	0.005514833	224.2361	234.0876					
Setra_422base.out_Pa	intercept	-0.23593	0.13919	0.071531793	231.4461	241.4828	-0.24407	0.13624	0.005686	229.5562	237.6577
Setra_422base.out_Pa	x(t)	-0.24792	0.17864	0.071531793	231.4461	241.4828	-0.05537	0.10153	0.005686	229.5562	237.6577
Setra_422base.out_Pa	x(t-1)	0.23446	0.17596	0.071531793	231.4461	241.4828					
Setra_422base.upst_Pa	intercept	-0.226	0.13736	0.030387171	230.9971	241.0338	-0.23077	0.13566	0.022834	228.2601	236.3615
Setra_422base.upst_Pa	x(t)	0.04006	0.20735	0.030387171	230.9971	241.0338	0.12747	0.17044	0.022834	228.2601	236.3615
Setra_422base.upst_Pa	x(t-1)	0.1572	0.20748	0.030387171	230.9971	241.0338					
Setra_422SGdp.ss_Pa	intercept	-0.07921	0.20983	0.305388542	219.5753	229.4267	-0.26782	0.19887	0.157934	224.3789	232.4082
Setra_422SGdp.ss_Pa	x(t)	0.3311	0.18341	0.305388542	219.5753	229.4267	0.04361	0.10308	0.157934	224.3789	232.4082
Setra_422SGdp.ss_Pa	x(t-1)	-0.432	0.23405	0.305388542	219.5753	229.4267					
Setra_422ss.base_Pa	intercept	0.24887	0.54167	0.07279259	227.6823	237.719	-0.15432	0.50646	0.032856	228.4709	236.5723
Setra_422ss.base_Pa	x(t)	0.34745	0.28573	0.07279259	227.6823	237.719	-0.03391	0.20196	0.032856	228.4709	236.5723
Setra_422ss.base_Pa	x(t-1)	-0.55216	0.29864	0.07279259	227.6823	237.719					
Snowdepth_daily	intercept	-0.05937	0.12266	0.075389574	216.3765	226.4132	-0.05739	0.11846	0.039274	214.3087	222.4101
Snowdepth_daily	x(t)	-0.74632	0.4059	0.075389574	216.3765	226.4132	-0.69181**	0.17048	0.039274	214.3087	222.4101
Snowdepth_daily	x(t-1)	0.05007	0.38721	0.075389574	216.3765	226.4132					
Soil_H2O_In6_cbar	intercept	-0.70526**	0.22515	0.003361042	238.6194	248.6561	-0.64807**	0.21092	0.03991	231.8489	239.9503
Soil_H2O_In6_cbar	x(t)	0.02657	0.02735	0.003361042	238.6194	248.6561	0.00531*	0.00218	0.03991	231.8489	239.9503
Soil_H2O_In6_cbar	x(t-1)	-0.02123	0.02727	0.003361042	238.6194	248.6561					

(continued)

Table 6C-2. Time Series Analysis for 422 Basement South PCE: Predictor Variables Requiring One Lag Term, Period January 2011 to February 2012 (continued)

Predictor Code ^a	Model Term	Full Model					First Reduced Model				
		Coefficient	SE	R ²	AIC	BIC	Coefficient	SE	R ²	AIC	BIC
Soil_H2O_Out13_cbar	intercept	-0.55317**	0.1972	0.012232981	244.551	254.5877	-0.53725**	0.19104	0.024265	234.6569	242.7583
Soil_H2O_Out13_cbar	x(t)	0.00559	0.00689	0.012232981	244.551	254.5877	0.00217*	0.00102	0.024265	234.6569	242.7583
Soil_H2O_Out13_cbar	x(t-1)	-0.00343	0.00687	0.012232981	244.551	254.5877					
Soil_H2O_Out3.5_cbar	intercept	-0.34198	0.17307	0.051659344	247.0648	257.1015	-0.33373*	0.16582	0.021233	236.3374	244.4388
Soil_H2O_Out3.5_cbar	x(t)	0.0016	0.00507	0.051659344	247.0648	257.1015	0.0024	0.00235	0.021233	236.3374	244.4388
Soil_H2O_Out3.5_cbar	x(t-1)	0.00094	0.00506	0.051659344	247.0648	257.1015					
Soil_H2O_Out6_cbar	intercept	-0.41418*	0.17999	0.043773988	246.0004	256.037	-0.39717*	0.17473	0.016492	236.8053	244.9067
Soil_H2O_Out6_cbar	x(t)	0.00726	0.00887	0.043773988	246.0004	256.037	0.00162	0.00113	0.016492	236.8053	244.9067
Soil_H2O_Out6_cbar	x(t-1)	-0.00574	0.00897	0.043773988	246.0004	256.037					
Soil_T_C_MW3.6	intercept	-7.20764	20418.63		184.7353	194.3944	-2.2443**	0.62263	0.043922	213.2257	221.1069
Soil_T_C_MW3.6	x(t)	-0.1753	0.3185		184.7353	194.3944	0.11434**	0.03569	0.043922	213.2257	221.1069
Soil_T_C_MW3.6	x(t-1)	0.29259	0.31879		184.7353	194.3944					
Soil_T_C_MW3.9	intercept	-2.54614	20354.19		181.7361	191.3952	-2.67697**	0.74646	0.088885	212.6388	220.52
Soil_T_C_MW3.9	x(t)	0.54341	0.683		181.7361	191.3952	0.14655**	0.04517	0.088885	212.6388	220.52
Soil_T_C_MW3.9	x(t-1)	-0.77537	0.68075		181.7361	191.3952					
Soil_T_C_OTC.1	intercept	-0.20483	0.11513	0.966280066	60.65157	69.90231	-0.43412	0.33169	0.891385	84.39034	91.95762
Soil_T_C_OTC.1	x(t)	-0.07583*	0.03112	0.966280066	60.65157	69.90231	0.01702	0.02126	0.891385	84.39034	91.95762
Soil_T_C_OTC.1	x(t-1)	0.08568**	0.03096	0.966280066	60.65157	69.90231					
Soil_T_C_OTC.16.5	intercept	-1.02705	1.09008	0.863246925	133.386	143.2374	-1.47865	1.61787	0.812168	146.9027	154.932
Soil_T_C_OTC.16.5	x(t)	0.8165*	0.38208	0.863246925	133.386	143.2374	0.09803	0.11396	0.812168	146.9027	154.932
Soil_T_C_OTC.16.5	x(t-1)	-0.75417	0.38271	0.863246925	133.386	143.2374					
Soil_T_C_OTC.6	intercept	-5.33316	17612.93		185.801	195.4601	-1.04792**	0.27099	0.089096	214.9733	222.8545
Soil_T_C_OTC.6	x(t)	0.16913	0.26617		185.801	195.4601	0.05796**	0.01846	0.089096	214.9733	222.8545
Soil_T_C_OTC.6	x(t-1)	-0.2502	0.26572		185.801	195.4601					
StackEffect_420baseN	intercept	0.33287	0.50413	0.066509469	216.6382	226.6749	0.14387	0.47815	0.053408	221.6143	229.7157
StackEffect_420baseN	x(t)	2.18334	6.73597	0.066509469	216.6382	226.6749	-3.71706	4.47306	0.053408	221.6143	229.7157
StackEffect_420baseN	x(t-1)	-7.7	6.55799	0.066509469	216.6382	226.6749					
StackEffect_422first	intercept	0.33189	0.3061	0.045657438	215.2579	225.2946	0.27628	0.31999	0.03125	221.0836	229.185
StackEffect_422first	x(t)	5.4845	5.49403	0.045657438	215.2579	225.2946	-3.14746	1.80379	0.03125	221.0836	229.185
StackEffect_422first	x(t-1)	-8.92336	5.44403	0.045657438	215.2579	225.2946					

(continued)

Table 6C-2. Time Series Analysis for 422 Basement South PCE: Predictor Variables Requiring One Lag Term, Period January 2011 to February 2012 (continued)

Predictor Code ^a	Model Term	Full Model					First Reduced Model				
		Coefficient	SE	R ²	AIC	BIC	Coefficient	SE	R ²	AIC	BIC
StdDev_Setra_420ss.base_Pa	intercept	-0.29955	0.18796	0.007475173	224.5552	234.4067	-0.325	0.1771	0.012597	222.0731	230.0291
StdDev_Setra_420ss.base_Pa	x(t)	0.25083	0.27945	0.007475173	224.5552	234.4067	0.1685	0.21989	0.012597	222.0731	230.0291
StdDev_Setra_420ss.base_Pa	x(t-1)	-0.13652	0.27937	0.007475173	224.5552	234.4067					
StdDev_Setra_422base.out_Pa	intercept	0.11432	0.231	0.230449968	230.5566	240.5932	0.11774	0.21033	0.284932	226.3816	234.483
StdDev_Setra_422base.out_Pa	x(t)	-0.19861	0.13557	0.230449968	230.5566	240.5932	-0.20067	0.10183	0.284932	226.3816	234.483
StdDev_Setra_422base.out_Pa	x(t-1)	-0.001	0.1358	0.230449968	230.5566	240.5932					
StdDev_Setra_422base.upst_Pa	intercept	-0.30006	0.17696	0.021169544	228.201	238.2376	-0.31384	0.1659	0.012406	226.576	234.6774
StdDev_Setra_422base.upst_Pa	x(t)	0.38329	0.4637	0.021169544	228.201	238.2376	0.3057	0.37305	0.012406	226.576	234.6774
StdDev_Setra_422base.upst_Pa	x(t-1)	-0.13506	0.46417	0.021169544	228.201	238.2376					
StdDev_Setra_422SGdp.ss_Pa	intercept	-0.24466	0.15776	0.279611449	226.3429	236.1943	-0.26474	0.15725	0.138648	225.5952	233.6245
StdDev_Setra_422SGdp.ss_Pa	x(t)	0.03488	0.07667	0.279611449	226.3429	236.1943	0.03258	0.04939	0.138648	225.5952	233.6245
StdDev_Setra_422SGdp.ss_Pa	x(t-1)	-0.00613	0.08057	0.279611449	226.3429	236.1943					
StdDev_Setra_422ss.base_Pa	intercept	-0.06014	0.15035	0.29011972	231.3963	241.4329	-0.13587	0.15785	0.017608	229.1184	237.2198
StdDev_Setra_422ss.base_Pa	x(t)	0.00831	0.09483	0.29011972	231.3963	241.4329	-0.08771	0.0788	0.017608	229.1184	237.2198
StdDev_Setra_422ss.base_Pa	x(t-1)	-0.17571	0.10913	0.29011972	231.3963	241.4329					
T_420baseS_C	intercept	-1.57339**	0.58688	0.012068119	234.162	244.1987	-1.56694*	0.58844	0.007411	229.3132	237.4146
T_420baseS_C	x(t)	-0.0351	0.05663	0.012068119	234.162	244.1987	0.02284*	0.00983	0.007411	229.3132	237.4146
T_420baseS_C	x(t-1)	0.05815	0.05601	0.012068119	234.162	244.1987					
T_420first_C	intercept	-1.37557*	0.52987	0.002451305	235.4165	245.4532	-1.36245*	0.53366	0.010243	230.1646	238.266
T_420first_C	x(t)	-0.02766	0.04137	0.002451305	235.4165	245.4532	0.01871*	0.00858	0.010243	230.1646	238.266
T_420first_C	x(t-1)	0.04671	0.04082	0.002451305	235.4165	245.4532					
T_422_F	intercept	-1.67969	1.24631	0.012364425	238.5482	248.5849	-1.66727	1.18509	0.008172	232.0011	240.1025
T_422_F	x(t)	0.01914	0.04125	0.012364425	238.5482	248.5849	0.0201	0.0165	0.008172	232.0011	240.1025
T_422_F	x(t-1)	0.00111	0.04145	0.012364425	238.5482	248.5849					
T_422baseN_C	intercept	-2.29722*	0.89383	0.022718983	233.7298	243.7664	-2.27412*	0.87093	0.010462	228.4261	236.5275
T_422baseN_C	x(t)	0.0093	0.07445	0.022718983	233.7298	243.7664	0.03289*	0.01387	0.010462	228.4261	236.5275
T_422baseN_C	x(t-1)	0.02397	0.07327	0.022718983	233.7298	243.7664					
T_422baseS_C	intercept	-2.67619*	1.0522	0.011268757	233.5105	243.5471	-2.65837*	1.02718	0.012873	228.1151	236.2165
T_422baseS_C	x(t)	0.04735	0.07439	0.011268757	233.5105	243.5471	0.03778*	0.01586	0.012873	228.1151	236.2165
T_422baseS_C	x(t-1)	-0.00934	0.07313	0.011268757	233.5105	243.5471					

(continued)

Table 6C-2. Time Series Analysis for 422 Basement South PCE: Predictor Variables Requiring One Lag Term, Period January 2011 to February 2012 (continued)

Predictor Code ^a	Model Term	Full Model					First Reduced Model				
		Coefficient	SE	R ²	AIC	BIC	Coefficient	SE	R ²	AIC	BIC
T_422first_C	intercept	-2.63092	1.34029	0.018601986	235.413	245.4497	-2.71992*	1.30932	0.021074	229.6942	237.7956
T_422first_C	x(t)	0.06105	0.05569	0.018601986	235.413	245.4497	0.03524	0.01845	0.021074	229.6942	237.7956
T_422first_C	x(t-1)	-0.02711	0.05529	0.018601986	235.413	245.4497					
T_out_F	intercept	-1.07676*	0.40667	0.006860644	236.0481	246.0847	-1.06327*	0.41561	0.01508	230.7951	238.8965
T_out_F	x(t)	-0.02553	0.02987	0.006860644	236.0481	246.0847	0.0154*	0.00733	0.01508	230.7951	238.8965
T_out_F	x(t-1)	0.04137	0.0294	0.006860644	236.0481	246.0847					
T_out_Hi_F	intercept	-1.37939*	0.53609	0.036226142	233.8847	243.9213	-1.34009*	0.57314	0.051037	231.162	239.2634
T_out_Hi_F	x(t)	-0.035	0.02287	0.036226142	233.8847	243.9213	0.01516	0.00765	0.051037	231.162	239.2634
T_out_Hi_F	x(t-1)	0.05095*	0.02223	0.036226142	233.8847	243.9213					
Wind_Chill_F	intercept	-0.97998**	0.3604	0.016885953	235.4662	245.5029	-0.97302*	0.37511	0.015666	230.966	239.0674
Wind_Chill_F	x(t)	-0.03082	0.02662	0.016885953	235.4662	245.5029	0.01416*	0.00674	0.015666	230.966	239.0674
Wind_Chill_F	x(t-1)	0.04537	0.02615	0.016885953	235.4662	245.5029					
X422baseN_Wkly_Elect_radon	intercept	0.42771	0.51559	0.019863046	233.3576	243.3943	0.28878	0.49804	0.065316	229.4991	237.6005
X422baseN_Wkly_Elect_radon	x(t)	0.00328	0.10568	0.019863046	233.3576	243.3943	-0.07378	0.0672	0.065316	229.4991	237.6005
X422baseN_Wkly_Elect_radon	x(t-1)	-0.09558	0.10445	0.019863046	233.3576	243.3943					

^a Descriptions of predictor codes can be found in Table 6A-1.

* = significant at 5%

** = significant at 1%

$$y(t) - y(t - 1) = \beta_0 + \beta_1 x(t) + \beta_2 x(t - 1) + u(t)$$

First Reduced Model: $y(t) - y(t - 1) = \beta_0 + \beta_1 x(t) + u(t)$

Table 6C-3. Time Series Analysis for 422 Basement South PCE: Predictor Variables Requiring Two Lag Terms, Period January 2011 to February 2012

Predictor Code ^a	Model Term	Full Model					First Reduced Model					Second Reduced Model				
		Coefficient	SE	R ²	AIC	BIC	Coefficient	SE	R ²	AIC	BIC	Coefficient	SE	R ²	AIC	BIC
Diff_T_420baseN.Out_F	intercept	-0.09564	0.16626	0.811334	165.0014	176.8232	-0.10676	0.15875	0.023433	235.6436	245.6803	-0.13862**	1	0.045461	231.4913	239.5927
Diff_T_420baseN.Out_F	x(t)	0.02523	0.0256	0.811334	165.0014	176.8232	0.03783	0.05131	0.023433	235.6436	245.6803	-0.02696**	2	0.045461	231.4913	239.5927
Diff_T_420baseN.Out_F	x(t-1)	0.00187	0.02325	0.811334	165.0014	176.8232	-0.07139	0.05039	0.023433	235.6436	245.6803					
Diff_T_420baseN.Out_F	x(t-2)	-0.02604	0.02551	0.811334	165.0014	176.8232										
Diff_T_420baseS.Out_F	intercept	-0.08897	0.17828	0.811373	165.1966	177.0184	-0.06229	0.1694	0.026038	235.2913	245.3279	-0.09992**	1	0.04261	231.1797	239.2811
Diff_T_420baseS.Out_F	x(t)	0.02443	0.02496	0.811373	165.1966	177.0184	0.03476	0.04979	0.026038	235.2913	245.3279	-0.02979**	2	0.04261	231.1797	239.2811
Diff_T_420baseS.Out_F	x(t-1)	0.00029	0.02257	0.811373	165.1966	177.0184	-0.07087	0.04874	0.026038	235.2913	245.3279					
Diff_T_420baseS.Out_F	x(t-2)	-0.02517	0.02473	0.811373	165.1966	177.0184										
Heat_Degree_Day	intercept	-0.01363	0.18836	0.82685	177.2644	189.0861	0.12108	0.19182	0.023055	241.617	251.6536	0.09073	1	0.004127	233.9053	242.0067
Heat_Degree_Day	x(t)	0.00428	0.00248	0.82685	177.2644	189.0861	0.00513	0.00475	0.023055	241.617	251.6536	-0.00305**	2	0.004127	233.9053	242.0067
Heat_Degree_Day	x(t-1)	-0.00043	0.00224	0.82685	177.2644	189.0861	-0.00837	0.00465	0.023055	241.617	251.6536					
Heat_Degree_Day	x(t-2)	-0.0046	0.00246	0.82685	177.2644	189.0861										
StackEffect_420baseS	intercept	-0.24281	0.48308	0.807344	136.044	147.8657	0.41606	0.4687	0.06174	216.1159	226.1525	0.2563	1	0.050064	221.1921	229.2935
StackEffect_420baseS	x(t)	2.45955	3.41162	0.807344	136.044	147.8657	1.89332	6.67055	0.06174	216.1159	226.1525	-4.61271**	2	0.050064	221.1921	229.2935
StackEffect_420baseS	x(t-1)	0.34697	3.25207	0.807344	136.044	147.8657	-7.95093	6.49484	0.06174	216.1159	226.1525					
StackEffect_420baseS	x(t-2)	-1.3999	3.37163	0.807344	136.044	147.8657										

(continued)

Table 6C-3. Time Series Analysis for 422 Basement South PCE: Predictor Variables Requiring Two Lag Terms, Period January 2011 to February 2012 (continued)

Predictor Code ^a	Model Term	Full Model					First Reduced Model					Second Reduced Model				
		Coefficient	SE	R ²	AIC	BIC	Coefficient	SE	R ²	AIC	BIC	Coefficient	SE	R ²	AIC	BIC
StackEffect_420first	intercept	0.05867	0.49402	0.810668	135.341	147.1628	0.51587	0.46718	0.011714	215.0553	225.0919	0.34975	1	0.021808	220.6982	228.7996
StackEffect_420first	x(t)	2.83157	3.64967	0.810668	135.341	147.1628	2.87632	7.24159	0.011714	215.0553	225.0919	-5.4593**	2	0.021808	220.6982	228.7996
StackEffect_420first	x(t-1)	-0.62221	3.16467	0.810668	135.341	147.1628	-9.82845	7.13029	0.011714	215.0553	225.0919					
StackEffect_420first	x(t-2)	-3.61935	3.60526	0.810668	135.341	147.1628										
StackEffect_422baseN	intercept	-0.00164	0.37242	0.810759	136.7165	148.5382	0.38976	0.34497	0.020708	215.5713	225.608	0.29478	1	0.024343	220.7272	228.8286
StackEffect_422baseN	x(t)	2.65325	2.7691	0.810759	136.7165	148.5382	2.68915	5.39694	0.020708	215.5713	225.608	-4.11199**	2	0.024343	220.7272	228.8286
StackEffect_422baseN	x(t-1)	-2.43091	2.63121	0.810759	136.7165	148.5382	-7.50615	5.331	0.020708	215.5713	225.608					
StackEffect_422baseN	x(t-2)	-0.92593	2.7648	0.810759	136.7165	148.5382										
StackEffect_422baseS	intercept	0.02012	0.36952	0.8115	136.792	148.6137	0.3979	0.33873	0.015856	215.612	225.6487	0.3054	1	0.016961	220.7262	228.8276
StackEffect_422baseS	x(t)	2.6157	2.58049	0.8115	136.792	148.6137	2.70787	5.05108	0.015856	215.612	225.6487	-3.85211**	2	0.016961	220.7262	228.8276
StackEffect_422baseS	x(t-1)	-2.7306	2.46879	0.8115	136.792	148.6137	-7.19455	5.00062	0.015856	215.612	225.6487					
StackEffect_422baseS	x(t-2)	-0.68499	2.57974	0.8115	136.792	148.6137										
T_out_Lo_F	intercept	-0.26912	0.31198	0.827031	164.3325	176.1543	-0.82648**	0.29469	0.01117	237.6099	247.6465	-0.80852**	1	0.049756	230.3993	238.5008
T_out_Lo_F	x(t)	-0.02169	0.01291	0.827031	164.3325	176.1543	0.00255	0.02624	0.01117	237.6099	247.6465	0.01559*	2	0.049756	230.3993	238.5008
T_out_Lo_F	x(t-1)	-0.00714	0.012	0.827031	164.3325	176.1543	0.01352	0.02599	0.01117	237.6099	247.6465					
T_out_Lo_F	x(t-2)	0.03368*	0.01293	0.827031	164.3325	176.1543										

(continued)

Table 6C-3. Time Series Analysis for 422 Basement South PCE: Predictor Variables Requiring Two Lag Terms, Period January 2011 to February 2012 (continued)

Predictor Code ^a	Model Term	Full Model					First Reduced Model					Second Reduced Model				
		Coefficient	SE	R ²	AIC	BIC	Coefficient	SE	R ²	AIC	BIC	Coefficient	SE	R ²	AIC	BIC
Wind_Speed_MPH	intercept	0.19546	0.51471	0.812725	155.1054	166.9271	0.31794	0.47862	0.031722	229.3604	239.3971	0.03419*	1	0.022201	229.2248	237.3262
Wind_Speed_MPH	x(t)	-0.00059	0.09279	0.812725	155.1054	166.9271	0.19629	0.18117	0.031722	229.3604	239.3971	-0.06971**	2	0.022201	229.2248	237.3262
Wind_Speed_MPH	x(t-1)	-0.14492	0.08903	0.812725	155.1054	166.9271	-0.33857	0.18067	0.031722	229.3604	239.3971					
Wind_Speed_MPH	x(t-2)	0.07118	0.09279	0.812725	155.1054	166.9271										

^a Descriptions of predictor codes can be found in Table 6A-1.

* = significant at 5%

** = significant at 1%

$$y(t) - y(t - 1) = \beta_0 + \beta_1x(t) + \beta_2x(t - 1) + \beta_3x(t - 2) + u(t)$$

First Reduced Model: $y(t) - y(t - 1) = \beta_0 + \beta_1x(t) + \beta_2x(t - 1) + u(t)$

Second Reduced Model: $y(t) - y(t - 1) = \beta_0 + \beta_1x(t) + u(t)$

Table 6C-4. Time Series Analysis for 422 Basement South PCE: Categorical Predictor Variables, Period January 2011 to February 2012

Predictor Code ^a	Model Term	Coefficient	SE	AIC	BIC
AC_on.off_420_daily	intercept	-0.2443	0.14056	225.5362	233.6376
AC_on.off_420_daily	ON	0.23349	0.85557	225.5362	233.6376
AC_on.off_422_daily	intercept	-0.29809	0.15729	226.7636	234.865
AC_on.off_422_daily	ON	0.27602	0.34907	226.7636	234.865
Fan_on.off_422_daily	intercept	-0.26852	0.13992	225.1078	233.2092
Fan_on.off_422_daily	ON	0.65063	0.73381	225.1078	233.2092
Heat_on.off_422_daily	intercept	0.00042	0.22762	226.1863	234.2877
Heat_on.off_422_daily	ON	-0.35997	0.2839	226.1863	234.2877
METAR_IcyPrecip_YorN	intercept	-0.1233	0.15526	226.0299	234.1313
METAR_IcyPrecip_YorN	Yes	-0.42725	0.36792	226.0299	234.1313
METAR_SnowEvent_YorN	intercept	0.0123	0.15501	222.0758	230.1772
METAR_SnowEvent_YorN	Yes	-0.67838*	0.27405	222.0758	230.1772
METAR_ThunderEvent_YorN	intercept	-0.46116*	0.20348	225.5637	233.6651
METAR_ThunderEvent_YorN	Yes	0.43384	0.29508	225.5637	233.6651
Wind_Dir_Hi	intercept	0.13428	0.76496	223.4322	240.8187
Wind_Dir_Hi	N	-0.10959	1.07349	223.4322	240.8187
Wind_Dir_Hi	NE	-0.02881	1.81877	223.4322	240.8187
Wind_Dir_Hi	NW	-0.07131	1.66267	223.4322	240.8187
Wind_Dir_Hi	S	-0.48523	1.66267	223.4322	240.8187
Wind_Dir_Hi	SW	-1.23374	1.07349	223.4322	240.8187
Wind_Dir_Hi	W	-0.38023	0.81373	223.4322	240.8187
Wind_Dir	intercept	-1.06069	0.8023	227.5532	246.6735
Wind_Dir	N	0.99958	1.20945	227.5532	246.6735
Wind_Dir	NE	0.93721	1.02787	227.5532	246.6735
Wind_Dir	NW	0.91933	0.9584	227.5532	246.6735
Wind_Dir	S	1.13065	1.15891	227.5532	246.6735

(continued)

**Table 6C-4. Time Series Analysis for 422 Basement South PCE: Categorical Predictor Variables, Period January 2011 to February 2012
(continued)**

Predictor Code ^a	Model Term	Coefficient	SE	AIC	BIC
Wind_Dir	SE	0.7445	1.38197	227.5532	246.6735
Wind_Dir	SW	1.39367	1.02267	227.5532	246.6735
Wind_Dir	W	0.51865	0.87499	227.5532	246.6735

^a Descriptions of predictor codes can be found in Table 6A-1.

* = significant at 5%

** = significant at 1%

Reference AC = OFF

Reference AC = OFF

Reference Fan = OFF

Reference Heat = OFF

Reference IcyPrecip = No

Reference SnowEvent = No

Reference Win Dir Hi = E

$$y(t) - y(t - 1) = \beta_0 + \beta_1 x_{ON}(t) + u(t) \text{ where } x_{ON}(t) = \begin{cases} 1 & \text{if predictor}_{iS} \text{ ON} \\ 0 & \text{if predictor}_{iS} \text{ OFF} \end{cases}$$

If X(t) = ON/OFF, then Off is reference cell

$$y(t) - y(t - 1) = \beta_0 + \beta_1 Wind_Dir_Hi_N(t) + \beta_2 Wind_Dir_Hi_{NE}(t) + \beta_3 Wind_Dir_Hi_{NW}(t) + \beta_4 Wind_Dir_Hi_{SE}(t) + \beta_5 Wind_Dir_Hi_S(t) + \beta_6 Wind_Dir_Hi_{SW}(t) + \beta_7 Wind_Dir_Hi_W(t) + u(t)$$

$$\text{where } x_d(t) = \begin{cases} 1 & \text{if } wind_{iS} \text{ in direction } d \\ 0 & \text{if } wind_{iS} \text{ not in direction } d \end{cases}$$

$$y(t) - y(t - 1) = \beta_0 + \beta_1 Wind_Dir_N + \beta_2 Wind_Dir_{NE}(t) + \beta_3 Wind_Dir_{NW}(t) + \beta_4 Wind_Dir_{SE}(t) + \beta_5 Wind_Dir_S(t) + \beta_6 Wind_Dir_{SW}(t) + \beta_7 Wind_Dir_W(t) + u(t)$$

$$\text{where } x_d(t) = \begin{cases} 1 & \text{if } wind_{iS} \text{ in direction } d \\ 0 & \text{if } wind_{iS} \text{ not in direction } d \end{cases}$$

**Attachment 6D. Chloroform Time Series Results—September 2012 through
April 2013**

Table 6D-1. Time Series Analysis for 422 Basement South Chloroform: Predictor Variables Requiring No Lag Terms, Period September 2012 to April 2013

Predictor Code ^a	Model Term	Coefficient	SE	R ²	Rel R ²	AIC
Abs_AMax_Change_dPdt	intercept	0.36673	0.21303	0.123429	0	17.34112
Abs_AMax_Change_dPdt	mitigation(t)	-0.10333	0.14939	0.123429	0.018338	17.34112
Abs_AMax_Change_dPdt	x(t)	-3.16961	1.8446	0.123429	0.105091	17.34112
Bar_drop_Hg.hr	intercept	0.08569	0.14281	0.024657	0	20.33073
Bar_drop_Hg.hr	mitigation(t)	-0.11723	0.15807	0.024657	0.02068	20.33073
Bar_drop_Hg.hr	x(t)	9.48802	27.17646	0.024657	0.003977	20.33073
Bar_in_Hg	intercept	-35.36332*	13.86233	0.223114	0	13.96087
Bar_in_Hg	mitigation(t)	-0.04988	0.14267	0.223114	0.01185	13.96087
Bar_in_Hg	x(t)	1.17744*	0.46044	0.223114	0.211264	13.96087
BP_Net_Change	intercept	0.08605	0.14282	0.024941	0	20.32257
BP_Net_Change	mitigation(t)	-0.11714	0.15799	0.024941	0.020671	20.32257
BP_Net_Change	x(t)	-0.05998	0.16688	0.024941	0.00427	20.32257
BP_Pump_Speed	intercept	0.38395	0.25242	0.092824	0	18.30207
BP_Pump_Speed	mitigation(t)	-0.14604	0.15371	0.092824	0.026328	18.30207
BP_Pump_Speed	x(t)	-1.48574	1.04807	0.092824	0.066496	18.30207
BP_Stroke_Length	intercept	0.33285	0.27452	0.061589	0	19.24989
BP_Stroke_Length	mitigation(t)	-0.16341	0.16185	0.061589	0.029081	19.24989
BP_Stroke_Length	x(t)	-0.29215	0.27722	0.061589	0.032509	19.24989
Cool_Degree_Day	intercept	0.10634	0.14112	0.044703	0	19.15316
Cool_Degree_Day	mitigation(t)	-0.11447	0.15232	0.044703	0.020153	19.15316
Cool_Degree_Day	x(t)	-0.01094	0.01322	0.044703	0.024549	19.15316
DepthToWater	intercept	0.58908	1.32344	0.025079	0	19.74285
DepthToWater	mitigation(t)	-0.10231	0.15551	0.025079	0.017893	19.74285
DepthToWater	x(t)	-0.03198	0.08331	0.025079	0.007186	19.74285

(continued)

Table 6D-1. Time Series Analysis for 422 Basement South Chloroform: Predictor Variables Requiring No Lag Terms, Period September 2012 to April 2013 (continued)

Predictor Code ^a	Model Term	Coefficient	SE	R ²	Rel R ²	AIC
Diff_T_420baseN.Out_F	intercept	-0.14933	0.26079	0.08593	0	21.8563
Diff_T_420baseN.Out_F	mitigation(t)	-0.08519	0.18809	0.08593	0.014932	21.8563
Diff_T_420baseN.Out_F	x(t)	0.0231	0.02019	0.08593	0.070998	21.8563
Diff_T_420baseS.Out_F	intercept	-0.17849	0.27789	0.088085		21.80673
Diff_T_420baseS.Out_F	mitigation(t)	-0.08784	0.18751	0.088085	0.015282	21.80673
Diff_T_420baseS.Out_F	x(t)	0.02354	0.02022	0.088085	0.072803	21.80673
Fall_Crk_Gage_ht_ft	intercept	0.03248	0.24127	0.022143		19.83003
Fall_Crk_Gage_ht_ft	mitigation(t)	-0.11182	0.15408	0.022143	0.019683	19.83003
Fall_Crk_Gage_ht_ft	x(t)	0.01401	0.0534	0.022143	0.00246	19.83003
Hum_out_.	intercept	0.35634	0.63278	0.027492		20.24922
Hum_out_.	mitigation(t)	-0.10657	0.15782	0.027492	0.01882	20.24922
Hum_out_.	x(t)	-0.00375	0.00848	0.027492	0.008673	20.24922
Max_Change_dPdt	intercept	0.0678	0.14304	0.042093		19.82566
Max_Change_dPdt	mitigation(t)	-0.09384	0.15798	0.042093	0.016711	19.82566
Max_Change_dPdt	x(t)	0.47634	0.62592	0.042093	0.025382	19.82566
Rain_In_met	intercept	0.10197	0.14754	0.025091		19.74247
Rain_In_met	mitigation(t)	-0.11525	0.1542	0.025091	0.02025	19.74247
Rain_In_met	x(t)	-0.03593	0.09352	0.025091	0.004841	19.74247
Rain_IPH	intercept	0.1565	0.17632	0.03828		19.93688
Rain_IPH	mitigation(t)	-0.16366	0.17302	0.03828	0.02716	19.93688
Rain_IPH	x(t)	-0.04059	0.05873	0.03828	0.01112	19.93688
StackEffect_420baseN	intercept	-0.30802	0.35242	0.097938	0	21.57859
StackEffect_420baseN	mitigation(t)	-0.0869	0.1864	0.097938	0.01517	21.57859
StackEffect_420baseN	x(t)	2.86115	2.28617	0.097938	0.082769	21.57859

(continued)

Table 6D-1. Time Series Analysis for 422 Basement South Chloroform: Predictor Variables Requiring No Lag Terms, Period September 2012 to April 2013 (continued)

Predictor Code ^a	Model Term	Coefficient	SE	R ²	Rel R ²	AIC
StackEffect_420baseS	intercept	-0.36804	0.39786	0.096997		21.60048
StackEffect_420baseS	mitigation(t)	-0.08984	0.18624	0.096997	0.01556	21.60048
StackEffect_420baseS	x(t)	3.12245	2.51136	0.096997	0.081438	21.60048
StdDev_Setra_420ss.base_Pa	intercept	0.07515	0.18864	0.034332		19.73633
StdDev_Setra_420ss.base_Pa	mitigation(t)	-0.13261	0.20699	0.034332	0.013915	19.73633
StdDev_Setra_420ss.base_Pa	x(t)	0.01596	0.02136	0.034332	0.020418	19.73633
StdDev_Setra_422base.out_Pa	intercept	-0.01723	0.13321	0.357476		9.259407
StdDev_Setra_422base.out_Pa	mitigation(t)	-0.17618	0.14427	0.357476	0.025431	9.259407
StdDev_Setra_422base.out_Pa	x(t)	0.057**	0.01584	0.357476	0.332045	9.259407
StdDev_Setra_422ss.base_Pa	intercept	0.0487	0.20983	0.01139		20.8936
StdDev_Setra_422ss.base_Pa	mitigation(t)	-0.082	0.19635	0.01139	0.009063	20.8936
StdDev_Setra_422ss.base_Pa	x(t)	0.00222	0.02125	0.01139	0.002327	20.8936
T_422first_C	intercept	0.29386	2.31113	0.017142		23.56665
T_422first_C	mitigation(t)	-0.10898	0.23087	0.017142	0.014775	23.56665
T_422first_C	x(t)	-0.0032	0.0353	0.017142	0.002367	23.56665
Wind_Run_mi	intercept	0.2486	0.20143	0.064324		18.55132
Wind_Run_mi	mitigation(t)	-0.13159	0.15181	0.064324	0.023298	18.55132
Wind_Run_mi	x(t)	-0.00022	0.0002	0.064324	0.041026	18.55132
Wind_Speed_Hi_MPH	intercept	0.82018*	0.33535	0.200808		14.75347
Wind_Speed_Hi_MPH	mitigation(t)	-0.26185	0.15577	0.200808	0.055118	14.75347
Wind_Speed_Hi_MPH	x(t)	-0.01979*	0.00832	0.200808	0.145691	14.75347

(continued)

Table 6D-1. Time Series Analysis for 422 Basement South Chloroform: Predictor Variables Requiring No Lag Terms, Period September 2012 to April 2013 (continued)

Predictor Code ^a	Model Term	Coefficient	SE	R ²	Rel R ²	AIC
Wind_Speed_MPH	intercept	0.32735	0.24984	0.071055		18.96603
Wind_Speed_MPH	mitigation(t)	-0.15421	0.15775	0.071055	0.027705	18.96603
Wind_Speed_MPH	x(t)	-0.05145	0.04385	0.071055	0.04335	18.96603

^a Descriptions of predictor codes can be found in Table 6A-1.

* = significant at 5%

** = significant at 1%

Full Model: $y(t) - y(t - 1) = \beta_0 + \beta_1 \text{mitigation}(t) + \beta_2 x(t) + u(t)$

Table 6D-2. Time Series Analysis for 422 Basement South Chloroform: Predictor Variables Requiring One Lag Term, Period September 2012 to April 2013

Predictor Code ^a	Model Term	Full Model					First Reduced Model				
		Coefficient	SE	R ²	Rel R ²	AIC	Coefficient	SE	R ²	Rel R ²	AIC
Dew_pt_422_F	intercept	0.08443	0.3456	0.126273336	0	19.2501284	0.28996	0.32812	0.03853		19.92962
Dew_pt_422_F	mitigation(t)	-0.03157	0.15963	0.126273336	0.01245162	19.2501284	-0.10476	0.15675	0.03853	0.018539	19.92962
Dew_pt_422_F	x(t)	-0.02015	0.01248	0.126273336	0.059948886	19.2501284	-0.00618	0.00888	0.03853	0.01999	19.92962
Dew_pt_422_F	x(t-1)	0.01806	0.01163	0.126273336	0.05387283	19.2501284					
Heat_Degree_Day	intercept	0.09474	0.18852	0.056414614	0	20.7954243	0.05678	0.18407	0.021516		19.84865
Heat_Degree_Day	mitigation(t)	-0.0886	0.15613	0.056414614	0.016614681	20.7954243	-0.10845	0.15453	0.021516	0.019045	19.84865
Heat_Degree_Day	x(t)	0.00069	0.00087	0.056414614	0.013935774	20.7954243	0.00015	0.00067	0.021516	0.00247	19.84865
Heat_Degree_Day	x(t-1)	-0.00086	9.00E-04	0.056414614	0.02586416	20.7954243					
Hum_422_.	intercept	0.13802	0.24107	0.172855774	0	17.7160501	0.24401	0.24733	0.043674		19.7794
Hum_422_.	mitigation(t)	-0.08184	0.15322	0.172855774	0.01693898	17.7160501	-0.13584	0.15873	0.043674	0.023958	19.7794
Hum_422_.	x(t)	-0.02286*	0.01102	0.172855774	0.08400026	17.7160501	-0.00504	0.00639	0.043674	0.019716	19.7794
Hum_422_.	x(t-1)	0.0196	0.01013	0.172855774	0.071916535	17.7160501					
Out_Wkly_Elect_radon	intercept	-0.24235	0.17208	0.441656419	0	11.632551	0.09353	0.16566	0.023645		19.79481
Out_Wkly_Elect_radon	mitigation(t)	0.06219	0.15365	0.441656419	0.011000154	11.632551	-0.11438	0.16716	0.023645	0.022327	19.79481
Out_Wkly_Elect_radon	x(t)	-0.37598	0.24025	0.441656419	0.041855964	11.632551	-0.02794	0.21875	0.023645	0.001318	19.79481
Out_Wkly_Elect_radon	x(t-1)	0.90625**	0.26017	0.441656419	0.388800301	11.632551					
Setra_420ss.base_Pa	intercept	0.07452	0.1172	0.649798127	0	-2.6213735	0.06156	0.17775	0.14346		16.73837
Setra_420ss.base_Pa	mitigation(t)	0.03267	0.16084	0.649798127	0.016980891	-2.6213735	0.13197	0.22526	0.14346	0.011588	16.73837
Setra_420ss.base_Pa	x(t)	0.05394**	0.0097	0.649798127	0.382537332	-2.6213735	0.02006	0.01083	0.14346	0.131872	16.73837
Setra_420ss.base_Pa	x(t-1)	-0.04556**	0.00933	0.649798127	0.250279904	-2.6213735					

(continued)

Table 6D-2. Time Series Analysis for 422 Basement South Chloroform: Predictor Variables Requiring One Lag Term, Period September 2012 to April 2013 (continued)

Predictor Code ^a	Model Term	Full Model					First Reduced Model				
		Coefficient	SE	R ²	Rel R ²	AIC	Coefficient	SE	R ²	Rel R ²	AIC
Setra_422base.out_Pa	intercept	0.09844	0.18875	0.090911806	0	21.2146434	0.02823	0.16194	0.059036		19.55993
Setra_422base.out_Pa	mitigation(t)	-0.15526	0.20437	0.090911806	0.020471437	21.2146434	-0.08338	0.17236	0.059036	0.010057	19.55993
Setra_422base.out_Pa	x(t)	0.01101	0.01242	0.090911806	0.047108743	21.2146434	0.00453	0.00409	0.059036	0.048979	19.55993
Setra_422base.out_Pa	x(t-1)	-0.00488	0.01143	0.090911806	0.023331625	21.2146434					
Setra_422base.upst_Pa	intercept	-0.05413	0.43134	0.38453811	0	13.7133752	-0.23636	0.37217	0.046783		21.35356
Setra_422base.upst_Pa	mitigation(t)	0.02549	0.22509	0.38453811	0.014635544	13.7133752	-0.01235	0.20432	0.046783	0.004932	21.35356
Setra_422base.upst_Pa	x(t)	1.72083*	0.62875	0.38453811	0.155184071	13.7133752	0.46432	0.5137	0.046783	0.041851	21.35356
Setra_422base.upst_Pa	x(t-1)	-1.70539**	0.53214	0.38453811	0.214718495	13.7133752					
Setra_422SGdp.ss_Pa	intercept	-0.05303	0.18135	0.24249904	\	16.4717934	0.05376	0.16464	0.015602		20.77832
Setra_422SGdp.ss_Pa	mitigation(t)	-0.13038	0.19842	0.24249904	0.017899068	16.4717934	-0.12136	0.19788	0.015602	0.013185	20.77832
Setra_422SGdp.ss_Pa	x(t)	-0.00464	0.00579	0.24249904	0.015244649	16.4717934	0.00191	0.00567	0.015602	0.002417	20.77832
Setra_422SGdp.ss_Pa	x(t-1)	0.0136*	0.00531	0.24249904	0.209355323	16.4717934					
Setra_422ss.base_Pa	intercept	0.12252	0.16915	0.29032411	0	14.7761661	0.0616	0.1628	0.013465		20.83687
Setra_422ss.base_Pa	mitigation(t)	-0.2752	0.22811	0.29032411	0.038823906	14.7761661	-0.06242	0.21066	0.013465	0.007275	20.83687
Setra_422ss.base_Pa	x(t)	0.02281	0.01224	0.29032411	0.069853178	14.7761661	0.0027	0.01091	0.013465	0.00619	20.83687
Setra_422ss.base_Pa	x(t-1)	-0.03604**	0.01232	0.29032411	0.181647027	14.7761661					
Snowdepth_daily	intercept	0.08015	0.14063	0.054377791	0	20.8579563	0.08114	0.13939	0.033661		19.48644
Snowdepth_daily	mitigation(t)	-0.13564	0.15669	0.054377791	0.024417269	20.8579563	-0.12359	0.15448	0.033661	0.021672	19.48644
Snowdepth_daily	x(t)	0.01561	0.05216	0.054377791	0.007096696	20.8579563	0.02966	0.04815	0.033661	0.011988	19.48644
Snowdepth_daily	x(t-1)	0.03867	0.05226	0.054377791	0.022863826	20.8579563					

(continued)

Table 6D-2. Time Series Analysis for 422 Basement South Chloroform: Predictor Variables Requiring One Lag Term, Period September 2012 to April 2013 (continued)

Predictor Code ^a	Model Term	Full Model					First Reduced Model				
		Coefficient	SE	R ²	Rel R ²	AIC	Coefficient	SE	R ²	Rel R ²	AIC
Soil_H2O_In6_cbar	intercept	0.17496	0.72403	0.020324586	0	21.8839233	0.15538	0.54207	0.020256		19.88596
Soil_H2O_In6_cbar	mitigation(t)	-0.11143	0.16731	0.020324586	0.018690138	21.8839233	-0.10912	0.15487	0.020256	0.019131	19.88596
Soil_H2O_In6_cbar	x(t)	7.00E-05	0.01266	0.020324586	0.000996671	21.8839233	-0.00044	0.00321	0.020256	0.001125	19.88596
Soil_H2O_In6_cbar	x(t-1)	-0.00062	0.01487	0.020324586	0.000637776	21.8839233					
Soil_H2O_Out3.5_cbar	intercept	0.12846	0.2267	0.06991649	0	20.3774624	0.13269	0.22788	0.022317		19.8249
Soil_H2O_Out3.5_cbar	mitigation(t)	-0.08399	0.17997	0.06991649	0.015494588	20.3774624	-0.08537	0.18093	0.022317	0.013963	19.8249
Soil_H2O_Out3.5_cbar	x(t)	-0.00173	0.00168	0.06991649	0.028219292	20.3774624	-3.00E-04	0.00112	0.022317	0.008353	19.8249
Soil_H2O_Out3.5_cbar	x(t-1)	0.00149	0.00132	0.06991649	0.02620261	20.3774624					
Soil_H2O_Out6_cbar	intercept	-0.15502	0.37866	0.038332688	0	21.3458937	-0.12135	0.35937	0.033834		19.48125
Soil_H2O_Out6_cbar	mitigation(t)	-0.17278	0.18254	0.038332688	0.028350625	21.3458937	-0.16854	0.179	0.033834	0.026251	19.48125
Soil_H2O_Out6_cbar	x(t)	0.00073	0.00196	0.038332688	0.004472022	21.3458937	0.00105	0.0017	0.033834	0.007583	19.48125
Soil_H2O_Out6_cbar	x(t-1)	0.00049	0.00142	0.038332688	0.005510042	21.3458937					
Soil_T_C_MW3.9	intercept	-0.85172	0.77625	0.080024295	0	19.5928888	-0.27043	0.6821	0.022761		20.03413
Soil_T_C_MW3.9	mitigation(t)	-0.0839	0.20365	0.080024295	0.006963991	19.5928888	-0.10581	0.20296	0.022761	0.010944	20.03413
Soil_T_C_MW3.9	x(t)	0.18396	0.44138	0.080024295	0.038626041	19.5928888	0.02304	0.04268	0.022761	0.011817	20.03413
Soil_T_C_MW3.9	x(t-1)	-0.12156	0.41987	0.080024295	0.034434263	19.5928888					
Soil_T_C_OTC.1	intercept	0.01867	0.19679	0.080461629	0	19.5819526	0.08583	0.19372	0.010053		20.35712
Soil_T_C_OTC.1	mitigation(t)	-0.0935	0.21923	0.080461629	0.009964568	19.5819526	-0.08913	0.21826	0.010053	0.008658	20.35712
Soil_T_C_OTC.1	x(t)	-0.02383	0.04265	0.080461629	0.016169292	19.5819526	-0.00145	0.01991	0.010053	0.001395	20.35712
Soil_T_C_OTC.1	x(t-1)	0.04112	0.03851	0.080461629	0.054327769	19.5819526					

(continued)

Table 6D-2. Time Series Analysis for 422 Basement South Chloroform: Predictor Variables Requiring One Lag Term, Period September 2012 to April 2013 (continued)

Predictor Code ^a	Model Term	Full Model					First Reduced Model				
		Coefficient	SE	R ²	Rel R ²	AIC	Coefficient	SE	R ²	Rel R ²	AIC
Soil_T_C_OTC.3.5	intercept	-0.04689	0.20688	0.11051349	0	18.8177217	0.02691	0.20449	0.03214		19.79302
Soil_T_C_OTC.3.5	mitigation(t)	-0.1449	0.21026	0.11051349	0.015319443	18.8177217	-0.1326	0.20782	0.03214	0.013862	19.79302
Soil_T_C_OTC.3.5	x(t)	0.03921	0.07814	0.11051349	0.051658137	18.8177217	0.01278	0.01793	0.03214	0.018278	19.79302
Soil_T_C_OTC.3.5	x(t-1)	-0.00855	0.0699	0.11051349	0.04353591	18.8177217					
Soil_T_C_OTC.6	intercept	-0.06951	0.21831	0.095517693	0	19.2022449	0.01968	0.21319	0.028158		19.89568
Soil_T_C_OTC.6	mitigation(t)	-0.13886	0.21317	0.095517693	0.014606017	19.2022449	-0.13075	0.20892	0.028158	0.013557	19.89568
Soil_T_C_OTC.6	x(t)	0.03015	0.0837	0.095517693	0.042168429	19.2022449	0.0127	0.01971	0.028158	0.014601	19.89568
Soil_T_C_OTC.6	x(t-1)	0.00031	0.07473	0.095517693	0.038743247	19.2022449					
StackEffect_422baseN	intercept	0.00557	0.39131	0.179922451	0	21.57762	-0.21706	0.37976	0.059894		22.4461
StackEffect_422baseN	mitigation(t)	-0.09381	0.1819	0.179922451	0.01669922	21.57762	-0.11037	0.18896	0.059894	0.018633	22.4461
StackEffect_422baseN	x(t)	3.49529	2.14754	0.179922451	0.085492215	21.57762	1.64854	1.87329	0.059894	0.041261	22.4461
StackEffect_422baseN	x(t-1)	-3.23418	2.05034	0.179922451	0.077731016	21.57762					
StackEffect_422baseS	intercept	-0.01102	0.37925	0.191127646	0	21.2887065	-0.2024	0.37982	0.05621		22.52821
StackEffect_422baseS	mitigation(t)	-0.09107	0.18085	0.191127646	0.016504856	21.2887065	-0.11532	0.18925	0.05621	0.019458	22.52821
StackEffect_422baseS	x(t)	3.64141	2.09876	0.191127646	0.090735604	21.2887065	1.44551	1.72627	0.05621	0.036752	22.52821
StackEffect_422baseS	x(t-1)	-3.34664	1.98743	0.191127646	0.083887186	21.2887065					
StackEffect_422first	intercept	-0.07828	0.37666	0.146608015	0	19.6027812	-0.13831	0.39707	0.039935		23.09739
StackEffect_422first	mitigation(t)	-0.13005	0.20147	0.146608015	0.01464159	19.6027812	-0.14345	0.21815	0.039935	0.020544	23.09739
StackEffect_422first	x(t)	3.9634	2.54956	0.146608015	0.085546389	19.6027812	1.12145	1.74712	0.039935	0.019391	23.09739
StackEffect_422first	x(t-1)	-3.10646	2.41613	0.146608015	0.046420036	19.6027812					

(continued)

Table 6D-2. Time Series Analysis for 422 Basement South Chloroform: Predictor Variables Requiring One Lag Term, Period September 2012 to April 2013 (continued)

Predictor Code ^a	Model Term	Full Model					First Reduced Model				
		Coefficient	SE	R ²	Rel R ²	AIC	Coefficient	SE	R ²	Rel R ²	AIC
StdDev_Setra_422base.upst_Pa	intercept	-0.27968	0.7702	0.102438767	0	22.3914665	-0.28885	0.43528	0.044746		21.4048
StdDev_Setra_422base.upst_Pa	mitigation(t)	0.06397	0.3387	0.102438767	0.011175901	22.3914665	0.0055	0.21465	0.044746	0.004864	21.4048
StdDev_Setra_422base.upst_Pa	x(t)	3.14057	2.7702	0.102438767	0.060079339	22.3914665	1.68541	1.92012	0.044746	0.039881	21.4048
StdDev_Setra_422base.upst_Pa	x(t-1)	-1.87872	1.96414	0.102438767	0.031183527	22.3914665					
StdDev_Setra_422SGdp.ss_Pa	intercept	0.02295	0.23866	0.045540758	0	22.4809169	0.00761	0.17073	0.045113		19.95652
StdDev_Setra_422SGdp.ss_Pa	mitigation(t)	-0.10196	0.22113	0.045540758	0.00994487	22.4809169	-0.09049	0.1735	0.045113	0.010882	19.95652
StdDev_Setra_422SGdp.ss_Pa	x(t)	0.00739	0.00921	0.045540758	0.0309152	22.4809169	0.00697	0.00752	0.045113	0.034231	19.95652
StdDev_Setra_422SGdp.ss_Pa	x(t-1)	-0.00102	0.00978	0.045540758	0.004680689	22.4809169					
T_422_F	intercept	-0.23089	1.65718	0.028836178	0	22.2105007	-0.4608	1.38702	0.025977		20.29281
T_422_F	mitigation(t)	-0.14066	0.17451	0.028836178	0.022828157	22.2105007	-0.13902	0.17113	0.025977	0.022807	20.29281
T_422_F	x(t)	0.01053	0.02273	0.028836178	0.004202827	22.2105007	0.008	0.02027	0.025977	0.00317	20.29281
T_422_F	x(t-1)	-0.00576	0.02168	0.028836178	0.001805194	22.2105007					
T_422baseN_C	intercept	0.42151	1.63965	0.086622996	0	23.8403661	0.46561	1.64803	0.022389		23.2676
T_422baseN_C	mitigation(t)	-0.02915	0.20648	0.086622996	0.012599045	23.8403661	-0.11095	0.19349	0.022389	0.018652	23.2676
T_422baseN_C	x(t)	-0.06001	0.05653	0.086622996	0.034876647	23.8403661	-0.00669	0.02876	0.022389	0.003737	23.2676
T_422baseN_C	x(t-1)	0.05243	0.04796	0.086622996	0.039147305	23.8403661					
T_422baseS_C	intercept	-0.25334	3.06035	0.020301571	0	25.3123837	-0.26977	2.86556	0.020278		23.31288
T_422baseS_C	mitigation(t)	-0.12147	0.20827	0.020301571	0.019602243	25.3123837	-0.12056	0.19753	0.020278	0.01986	23.31288
T_422baseS_C	x(t)	0.0066	0.0617	0.020301571	0.000410008	25.3123837	0.00583	0.04718	0.020278	0.000418	23.31288
T_422baseS_C	x(t-1)	-0.00101	0.05054	0.020301571	0.00028932	25.3123837					

(continued)

Table 6D-2. Time Series Analysis for 422 Basement South Chloroform: Predictor Variables Requiring One Lag Term, Period September 2012 to April 2013 (continued)

Predictor Code ^a	Model Term	Full Model					First Reduced Model				
		Coefficient	SE	R ²	Rel R ²	AIC	Coefficient	SE	R ²	Rel R ²	AIC
T_out_F	intercept	0.05385	0.29526	0.144613699	0	18.656125	0.2653	0.27756	0.041988		19.82871
T_out_F	mitigation(t)	-0.05225	0.15393	0.144613699	0.013410693	18.656125	-0.10165	0.15673	0.041988	0.01801	19.82871
T_out_F	x(t)	-0.01342	0.00789	0.144613699	0.065950164	18.656125	-0.00471	0.00621	0.041988	0.023978	19.82871
T_out_F	x(t-1)	0.01287	0.00759	0.144613699	0.065252842	18.656125					
T_out_Hi_F	intercept	-0.10741	0.39433	0.121793177	0	19.3933355	0.25487	0.32756	0.032871		20.09393
T_out_Hi_F	mitigation(t)	-0.05097	0.15896	0.121793177	0.012441666	19.3933355	-0.11883	0.1572	0.032871	0.021004	20.09393
T_out_Hi_F	x(t)	-0.00587	0.00501	0.121793177	0.031044322	19.3933355	-0.00273	0.00472	0.032871	0.011867	20.09393
T_out_Hi_F	x(t-1)	0.00821	0.00527	0.121793177	0.07830719	19.3933355					
T_out_Lo_F	intercept	0.03263	0.19474	0.156087783	0	18.2779934	0.16717	0.18892	0.037008		19.9739
T_out_Lo_F	mitigation(t)	-0.01078	0.16093	0.156087783	0.011817125	18.2779934	-0.08042	0.16371	0.037008	0.014599	19.9739
T_out_Lo_F	x(t)	-0.01695	0.00946	0.156087783	0.072034756	18.2779934	-0.00469	0.00704	0.037008	0.02241	19.9739
T_out_Lo_F	x(t-1)	0.01533	0.00833	0.156087783	0.072235903	18.2779934					
Wind_Chill_F	intercept	0.03335	0.25157	0.134398709	0	18.9885192	0.20991	0.23496	0.037295		19.96556
Wind_Chill_F	mitigation(t)	-0.05128	0.15532	0.134398709	0.013301266	18.9885192	-0.10063	0.15745	0.037295	0.017816	19.96556
Wind_Chill_F	x(t)	-0.01067	0.00674	0.134398709	0.057337835	18.9885192	-0.0036	0.00536	0.037295	0.019479	19.96556
Wind_Chill_F	x(t-1)	0.01061	0.00646	0.134398709	0.063759608	18.9885192					
X422baseN_Wkly_Elect_radon	intercept	0.38303	0.20497	0.591639019	0	3.22961784	-0.04	0.24557	0.062803		20.25656
X422baseN_Wkly_Elect_radon	mitigation(t)	-0.31523	0.17679	0.591639019	0.063329487	3.22961784	-0.03711	0.21832	0.062803	0.015576	20.25656
X422baseN_Wkly_Elect_radon	x(t)	0.05379**	0.01516	0.591639019	0.175615022	3.22961784	0.01678	0.0187	0.062803	0.047227	20.25656
X422baseN_Wkly_Elect_radon	x(t-1)	-0.07535**	0.01481	0.591639019	0.35269451	3.22961784					

(continued)

Table 6D-2. Time Series Analysis for 422 Basement South Chloroform: Predictor Variables Requiring One Lag Term, Period September 2012 to April 2013 (continued)

Predictor Code ^a	Model Term	Full Model					First Reduced Model				
		Coefficient	SE	R ²	Rel R ²	AIC	Coefficient	SE	R ²	Rel R ²	AIC
X422baseS_Wkly_Elect_radon	intercept	0.29397	0.16424	0.628601471	0	-1.7536206	-0.09373	0.22632	0.059405		19.86514
X422baseS_Wkly_Elect_radon	mitigation(t)	-0.22954	0.13603	0.628601471	0.053377238	-1.7536206	0.0087	0.19751	0.059405	0.009629	19.86514
X422baseS_Wkly_Elect_radon	x(t)	0.06063**	0.01412	0.628601471	0.206089807	-1.7536206	0.01859	0.01835	0.059405	0.049776	19.86514
X422baseS_Wkly_Elect_radon	x(t-1)	-0.08018**	0.01384	0.628601471	0.369134427	-1.7536206					
X422office2nd_Wkly_Elect_radon	intercept	0.18401	0.17719	0.41813784	0	9.91928466	-0.06006	0.19764	0.062567		19.77423
X422office2nd_Wkly_Elect_radon	mitigation(t)	-0.16539	0.15445	0.41813784	0.032676094	9.91928466	-0.01763	0.18117	0.062567	0.009776	19.77423
X422office2nd_Wkly_Elect_radon	x(t)	0.10906**	0.03559	0.41813784	0.164255095	9.91928466	0.03805	0.03611	0.062567	0.052791	19.77423
X422office2nd_Wkly_Elect_radon	x(t-1)	-0.13186**	0.03608	0.41813784	0.221206652	9.91928466					

^a Descriptions of predictor codes can be found in Table 6A-1.

* = significant at 5%

** = significant at 1%

Full Model: $y(t) - y(t - 1) = \beta_0 + \beta_1 \text{mitigation}(t) + \beta_2 x(t) + \beta_3 x(t - 1) + u(t)$

First Reduced Model: $y(t) - y(t - 1) = \beta_0 + \beta_1 \text{mitigation}(t) + \beta_2 x(t) + u(t)$

Table 6D-3. Time Series Analysis for 422 Basement South Chloroform: Categorical Predictor Variables, Period September 2012 to April 2013

Predictor Code ^a	Model Term	Coefficient	SE	R ²	AIC
Heat_on.off_422_daily	intercept	0.04763736	0.17675089	0.023822	19.78019432
Heat_on.off_422_daily	mitigation	-0.1302747	0.16410908	0.023822	19.78019432
Heat_on.off_422_daily	ON	0.0606044	0.17977249	0.023822	19.78019432
METAR_IcyPrecip_YorN	intercept	0.04763736	0.17675089	0.023822	19.78019432
METAR_IcyPrecip_YorN	mitigation	-0.1302747	0.16410908	0.023822	19.78019432
METAR_IcyPrecip_YorN	YES	0.0606044	0.17977249	0.023822	19.78019432
METAR_SnowEvent_YorN	intercept	0.06136205	0.1566704	0.023458	19.79101129
METAR_SnowEvent_YorN	mitigation	-0.1088824	0.15409885	0.023458	19.79101129
METAR_SnowEvent_YorN	YES	0.03772992	0.11704648	0.023458	19.79101129
METAR_ThunderEvent_YorN	intercept	0.09688769	0.14897846	0.022004	19.83416899
METAR_ThunderEvent_YorN	mitigation	-0.1145738	0.15466837	0.022004	19.83416899
METAR_ThunderEvent_YorN	YES	-0.0322192	0.12628619	0.022004	19.83416899
Wind_Dir_Hi	intercept	0.53427778*	0.22703548	0.22892	17.7508248
Wind_Dir_Hi	mitigation	-0.1776111	0.14956147	0.22892	17.7508248
Wind_Dir_Hi	S	-0.4866667	0.34162247	0.22892	17.7508248
Wind_Dir_Hi	SW	-0.2666667	0.34162247	0.22892	17.7508248
Wind_Dir_Hi	W	-0.45027778*	0.18449722	0.22892	17.7508248
Wind_Dir	intercept	0.15231707	0.14934916	0.612856	2.458957513
Wind_Dir	mitigation	-0.2084756	0.11869068	0.612856	2.458957513
Wind_Dir	NE	0.0001597**	0.25640116	0.612856	2.458957513
Wind_Dir	NW	-0.1105259	0.15057235	0.612856	2.458957513

(continued)

Table 6D-3. Time Series Analysis for 422 Basement South Chloroform: Categorical Predictor Variables, Period September 2012 to April 2013 (continued)

Predictor Code ^a	Model Term	Coefficient	SE	R ²	AIC
Wind_Dir	S	0.14615854	0.20414566	0.612856	2.458957513
Wind_Dir	SW	0.05449187	0.16009803	0.612856	2.458957513
Wind_Dir	W	-0.0770198	0.14861041	0.612856	2.458957513

^a Descriptions of predictor codes can be found in Table 6A-1.

* = significant at 5%

** = significant at 1%

Reference = Mitigation = OFF

Reference Snow Event = No

Reference ThunderEvent = No

Reference Wind Dir Hi = E

Reference Wind Dir = E

$$\text{Full Model: } y(t) - y(t - 1) = \beta_0 + \beta_1 \text{mitigation}(t) + \beta_2 x(t) + u(t)$$

$$y(t) - y(t - 1) = \beta_0 + \beta_1 \text{mitigation}(t) + \beta_2 x_{ON}(t) + u(t)$$

$$\text{where } x_{ON}(t) = \begin{cases} 1 & \text{if predictor is ON} \\ 0 & \text{if predictor is OFF} \end{cases}$$

If X(t) = ON/OFF, then Off is reference cell

$$y(t) - y(t - 1) = \beta_0 + \beta_1 \text{mitigation}(t) + \beta_2 \text{Wind_Dir_Hi}_N(t) + \beta_3 \text{Wind_Dir_Hi}_{NE}(t) + \beta_4 \text{Wind_Dir_Hi}_{NW}(t) + \beta_5 \text{Wind_Dir_Hi}_{SE}(t) + \beta_6 \text{Wind_Dir_Hi}_S(t) + \beta_7 \text{Wind_Dir_Hi}_{SW}(t) + \beta_8 \text{Wind_Dir_Hi}_W(t) + u(t)$$

$$\text{where } x_d(t) = \begin{cases} 1 & \text{if wind}_{iS} \text{ in direction } d \\ 0 & \text{if wind}_{iS} \text{ not in direction } d \end{cases}$$

$$y(t) - y(t - 1) = \beta_0 + \beta_1 \text{mitigation}(t) + \beta_2 \text{Wind_Dir}_N(t) + \beta_3 \text{Wind_Dir}_{NE}(t) + \beta_4 \text{Wind_Dir}_{NW}(t) + \beta_5 \text{Wind_Dir}_{SE}(t) + \beta_6 \text{Wind_Dir}_S(t) + \beta_7 \text{Wind_Dir}_{SW}(t) + \beta_8 \text{Wind_Dir}_W(t) + u(t)$$

$$\text{where } x_d(t) = \begin{cases} 1 & \text{if wind}_{iS} \text{ in direction } d \\ 0 & \text{if wind}_{iS} \text{ not in direction } d \end{cases}$$

Attachment 6E. PCE Time Series Results—September 2012 through April 2013

Table 6E-1. Time Series Analysis for 422 Basement SouthPCE: Predictor Variables Requiring No Lag Terms, Period September 2012 to April 2013

Predictor Code ^a	Model Term	Coefficient	SE	R ²	Rel R ²	AIC
Abs_AMax_Change_dPdt	intercept	1.22048	0.89542	0.07795	0	97.74926
Abs_AMax_Change_dPdt	mitigation	-0.41531	0.62792	0.07795	0.017287968	97.74926
Abs_AMax_Change_dPdt	x(t)	-9.84844	7.75331	0.07795	0.060661997	97.74926
Bar_drop_Hg.hr	intercept	0.33791	0.58665	0.020109	0	99.45284
Bar_drop_Hg.hr	mitigation	-0.43222	0.64932	0.020109	0.017904626	99.45284
Bar_drop_Hg.hr	x(t)	-23.02025	111.6363	0.020109	0.002204059	99.45284
Bar_in_Hg	intercept	-131.24289*	58.18286	0.185163	0	94.28815
Bar_in_Hg	mitigation	-0.21135	0.5988	0.185163	0.011251348	94.28815
Bar_in_Hg	x(t)	4.37081*	1.93256	0.185163	0.173911377	94.28815
BP_Net_Change	intercept	0.33823	0.58697	0.019453	0	99.47157
BP_Net_Change	mitigation	-0.43518	0.64932	0.019453	0.018029989	99.47157
BP_Net_Change	x(t)	0.11012	0.68583	0.019453	0.001423161	99.47157
BP_Pump_Speed	intercept	0.87741	1.06847	0.032276	0	99.103
BP_Pump_Speed	mitigation	-0.50364	0.65064	0.032276	0.020817944	99.103
BP_Pump_Speed	x(t)	-2.65207	4.43631	0.032276	0.011457795	99.103
BP_Stroke_Length	intercept	1.09667	1.13717	0.041269	0	98.84158
BP_Stroke_Length	mitigation	-0.59818	0.67047	0.041269	0.024484031	98.84158
BP_Stroke_Length	x(t)	-0.88597	1.14836	0.041269	0.016784647	98.84158
Cool_Degree_Day	intercept	0.43265	0.57884	0.043252	0	101.0131
Cool_Degree_Day	mitigation	-0.45782	0.62475	0.043252	0.019183379	101.0131
Cool_Degree_Day	x(t)	-0.04437	0.05422	0.043252	0.024068826	101.0131
DepthToWater	intercept	-1.34114	5.43194	0.022257	0	101.6426
DepthToWater	mitigation	-0.47332	0.63827	0.022257	0.019642849	101.6426
DepthToWater	x(t)	0.10656	0.34196	0.022257	0.00261458	101.6426

(continued)

Table 6E-1. Time Series Analysis for 422 Basement SouthPCE: Predictor Variables Requiring No Lag Terms, Period September 2012 to April 2013 (continued)

Predictor Code ^a	Model Term	Coefficient	SE	R ²	Rel R ²	AIC
Diff_T_420baseN.Out_F	intercept	-0.19491	1.074	0.038581	0	81.30412
Diff_T_420baseN.Out_F	mitigation	-0.36033	0.77459	0.038581	0.014153522	81.30412
Diff_T_420baseN.Out_F	x(t)	0.05317	0.08316	0.038581	0.024427482	81.30412
Diff_T_420baseS.Out_F	intercept	-0.31209	1.14302	0.043181	0	81.20341
Diff_T_420baseS.Out_F	mitigation	-0.3612	0.77126	0.043181	0.014203774	81.20341
Diff_T_420baseS.Out_F	x(t)	0.05865	0.08318	0.043181	0.028976833	81.20341
Fall_Crk_Gage_ht_ft	intercept	0.84646	0.98316	0.033377	0	101.3109
Fall_Crk_Gage_ht_ft	mitigation	-0.43683	0.62785	0.033377	0.018301341	101.3109
Fall_Crk_Gage_ht_ft	x(t)	-0.13716	0.2176	0.033377	0.015076147	101.3109
Hum_out_.	intercept	1.85992	2.58666	0.032481	0	99.09705
Hum_out_.	mitigation	-0.41081	0.64513	0.032481	0.017067451	99.09705
Hum_out_.	x(t)	-0.02088	0.03467	0.032481	0.01541401	99.09705
Max_Change_dPdt	intercept	0.23754	0.57656	0.073411	0	97.88677
Max_Change_dPdt	mitigation	-0.32351	0.63677	0.073411	0.01400441	97.88677
Max_Change_dPdt	x(t)	3.07248	2.52293	0.073411	0.059406184	97.88677
Rain_In_met	intercept	0.37066	0.60643	0.019444	0	101.7259
Rain_In_met	mitigation	-0.45072	0.63381	0.019444	0.018838917	101.7259
Rain_In_met	x(t)	-0.05732	0.38441	0.019444	0.000605509	101.7259
Rain_IPH	intercept	0.07616	0.72455	0.033153	0	99.07759
Rain_IPH	mitigation	-0.25607	0.71099	0.033153	0.011729382	99.07759
Rain_IPH	x(t)	0.14885	0.24134	0.033153	0.021424004	99.07759
StackEffect_420baseN	intercept	-0.66841	1.45297	0.049087	0	81.07337
StackEffect_420baseN	mitigation	-0.35644	0.76848	0.049087	0.014056878	81.07337
StackEffect_420baseN	x(t)	7.37447	9.42552	0.049087	0.035030442	81.07337

(continued)

Table 6E-1. Time Series Analysis for 422 Basement SouthPCE: Predictor Variables Requiring No Lag Terms, Period September 2012 to April 2013 (continued)

Predictor Code ^a	Model Term	Coefficient	SE	R ²	Rel R ²	AIC
StackEffect_420baseS	intercept	-0.86824	1.63761	0.051223	0	81.02616
StackEffect_420baseS	mitigation	-0.36146	0.76656	0.051223	0.014234411	81.02616
StackEffect_420baseS	x(t)	8.35968	10.33693	0.051223	0.036988152	81.02616
StdDev_Setra_420ss.base_Pa	intercept	0.50142	0.75756	0.033344	0	89.24936
StdDev_Setra_420ss.base_Pa	mitigation	-0.69528	0.83124	0.033344	0.032019203	89.24936
StdDev_Setra_420ss.base_Pa	x(t)	-0.00277	0.08577	0.033344	0.001324316	89.24936
StdDev_Setra_422base.out_Pa	intercept	0.27924	0.65019	0.10014	0	94.8681
StdDev_Setra_422base.out_Pa	mitigation	-0.70319	0.7042	0.10014	0.029886447	94.8681
StdDev_Setra_422base.out_Pa	x(t)	0.11136	0.07733	0.10014	0.070253452	94.8681
StdDev_Setra_422ss.base_Pa	intercept	-0.49322	0.80636	0.141733	0	93.59033
StdDev_Setra_422ss.base_Pa	mitigation	0.06677	0.75456	0.141733	0.011332684	93.59033
StdDev_Setra_422ss.base_Pa	x(t)	0.14921	0.08168	0.141733	0.130400733	93.59033
T_422first_C	intercept	-2.87808	8.81305	0.069557	0	77.1065
T_422first_C	mitigation	-0.99219	0.88037	0.069557	0.064796214	77.1065
T_422first_C	x(t)	0.05603	0.1346	0.069557	0.004761246	77.1065
Wind_Run_mi	intercept	0.90915	0.83173	0.050248	0	100.8003
Wind_Run_mi	mitigation	-0.51475	0.62685	0.050248	0.021619049	100.8003
Wind_Run_mi	x(t)	-0.00076	0.00081	0.050248	0.028628636	100.8003
Wind_Speed_Hi_MPH	intercept	1.49549	1.50247	0.044885	0	98.73577
Wind_Speed_Hi_MPH	mitigation	-0.67778	0.69789	0.044885	0.027238416	98.73577
Wind_Speed_Hi_MPH	x(t)	-0.03101	0.03727	0.044885	0.017646443	98.73577

(continued)

Table 6E-1. Time Series Analysis for 422 Basement SouthPCE: Predictor Variables Requiring No Lag Terms, Period September 2012 to April 2013 (continued)

Predictor Code ^a	Model Term	Coefficient	SE	R ²	Rel R ²	AIC
Wind_Speed_MPH	intercept	1.10345	1.03641	0.04826	0	98.63665
Wind_Speed_MPH	mitigation	-0.57432	0.6544	0.04826	0.023882224	98.63665
Wind_Speed_MPH	x(t)	-0.16097	0.18189	0.04826	0.024377662	98.63665

^a Descriptions of predictor codes can be found in Table 6A-1.

* = significant at 5%

** = significant at 1%

Full Model: $y(t) - y(t - 1) = \beta_0 + \beta_1 \text{mitigation}(t) + \beta_2 x(t) + u(t)$

Table 6E-2. Time Series Analysis for 422 Basement South PCE: Predictor Variables Requiring One Lag Term, Period September 2012 to April 2013

Predictor Code ^a	Model Term	Full Model					First Reduced Model				
		Coefficient	SE	R ²	Rel R ²	AIC	Coefficient	SE	R ²	Rel R ²	AIC
Dew_pt_422_F	intercept	0.96395	1.48279	0.04241555	0	100.8080671	1.17836	1.34599	0.036730282		98.97381406
Dew_pt_422_F	mitigation(t)	-0.33603	0.68488	0.04241555	0.015319291	100.8080671	-0.41238	0.64301	0.036730282	0.01714491	98.97381406
Dew_pt_422_F	x(t)	-0.03968	0.05352	0.04241555	0.022698396	100.8080671	-0.0251	0.03644	0.036730282	0.01958537	98.97381406
Dew_pt_422_F	x(t-1)	0.01884	0.04992	0.04241555	0.004397859	100.8080671					
Heat_Degree_Day	intercept	0.23712	0.78723	0.02042613	0	103.6968606	0.23473	0.75483	0.020417901		101.6971041
Heat_Degree_Day	mitigation(t)	-0.43245	0.65198	0.02042613	0.01804378	103.6968606	-0.4337	0.63371	0.020417901	0.01812644	101.6971041
Heat_Degree_Day	x(t)	0.00064	0.00365	0.02042613	0.002108764	103.6968606	0.00061	0.00276	0.020417901	0.00229146	101.6971041
Heat_Degree_Day	x(t-1)	-5.00E-05	0.00374	0.02042613	0.000273582	103.6968606					
Hum_422_	intercept	0.7374	1.03358	0.09469278	0	99.23615923	1.01158	1.01388	0.043226474		98.78434532
Hum_422_	mitigation(t)	-0.40181	0.65695	0.09469278	0.01821861	99.23615923	-0.54148	0.65067	0.043226474	0.02247309	98.78434532
Hum_422_	x(t)	-0.06718	0.04726	0.09469278	0.04840652	99.23615923	-0.02108	0.02619	0.043226474	0.02075339	98.78434532
Hum_422_	x(t-1)	0.05071	0.04341	0.09469278	0.028067652	99.23615923					
Out_Wkly_Elect_radon	intercept	-0.23849	0.78421	0.11114663	0	72.30218372	0.31501	0.61983	0.050662579		83.13073781
Out_Wkly_Elect_radon	mitigation(t)	-0.46293	0.70022	0.11114663	0.034543476	72.30218372	-0.66205	0.62545	0.050662579	0.05044627	83.13073781
Out_Wkly_Elect_radon	x(t)	0.37132	1.09492	0.11114663	0.01790837	72.30218372	0.07913	0.81845	0.050662579	0.0002163	83.13073781
Out_Wkly_Elect_radon	x(t-1)	0.90474	1.1857	0.11114663	0.058694781	72.30218372					
Setra_420ss.base_Pa	intercept	0.47951	0.67704	0.28571014	0	78.05457546	0.45745	0.74544	0.064971279		88.41771229
Setra_420ss.base_Pa	mitigation(t)	-0.3719	0.92913	0.28571014	0.020150347	78.05457546	-0.25847	0.94469	0.064971279	0.01823955	88.41771229
Setra_420ss.base_Pa	x(t)	0.1377*	0.05601	0.28571014	0.169634758	78.05457546	0.0392	0.04541	0.064971279	0.04673173	88.41771229
Setra_420ss.base_Pa	x(t-1)	-0.11815*	0.0539	0.28571014	0.095925033	78.05457546					

(continued)

Table 6E-2. Time Series Analysis for 422 Basement South PCE: Predictor Variables Requiring One Lag Term, Period September 2012 to April 2013 (continued)

Predictor Code ^a	Model Term	Full Model					First Reduced Model				
		Coefficient	SE	R ²	Rel R ²	AIC	Coefficient	SE	R ²	Rel R ²	AIC
Setra_422base.out_Pa	intercept	0.51544	0.7302	0.19891639	0	91.56651467	0.328	0.67114	0.049940087		96.33381283
Setra_422base.out_Pa	mitigation(t)	-0.8619	0.79066	0.19891639	0.034633191	91.56651467	-0.51301	0.71432	0.049940087	0.02140135	96.33381283
Setra_422base.out_Pa	x(t)	-0.06718	0.04805	0.19891639	0.052086449	91.56651467	0.01415	0.01695	0.049940087	0.02853874	96.33381283
Setra_422base.out_Pa	x(t-1)	0.08565	0.04424	0.19891639	0.112196748	91.56651467					
Setra_422base.upst_Pa	intercept	0.58298	2.11105	0.1103328	0	86.76320701	-0.00832	1.53535	0.021820296		89.37737961
Setra_422base.upst_Pa	mitigation(t)	-0.38149	1.10162	0.1103328	0.015541535	86.76320701	-0.35501	0.84291	0.021820296	0.01258146	89.37737961
Setra_422base.upst_Pa	x(t)	3.13228	3.07719	0.1103328	0.036630786	86.76320701	0.68875	2.11922	0.021820296	0.00923883	89.37737961
Setra_422base.upst_Pa	x(t-1)	-3.59823	2.60438	0.1103328	0.058160475	86.76320701					
Setra_422SGdp.ss_Pa	intercept	0.0717	0.73407	0.26923789	0	89.17770373	0.50802	0.67006	0.041496637		96.57270941
Setra_422SGdp.ss_Pa	mitigation(t)	-0.32562	0.80316	0.26923789	0.017381949	89.17770373	-0.28299	0.80532	0.041496637	0.01365841	96.57270941
Setra_422SGdp.ss_Pa	x(t)	-0.0431	0.02342	0.26923789	0.077484753	89.17770373	-0.01595	0.02306	0.041496637	0.02783822	96.57270941
Setra_422SGdp.ss_Pa	x(t-1)	0.05629*	0.02151	0.26923789	0.174371184	89.17770373					
Setra_422ss.base_Pa	intercept	0.59905	0.74411	0.19144008	0	91.80804057	0.42906	0.66622	0.02881943		96.92747168
Setra_422ss.base_Pa	mitigation(t)	-0.99407	1.00347	0.19144008	0.03422534	91.80804057	-0.34871	0.86205	0.02881943	0.01450354	96.92747168
Setra_422ss.base_Pa	x(t)	0.08241	0.05383	0.19144008	0.059059121	91.80804057	0.01781	0.04465	0.02881943	0.01431589	96.92747168
Setra_422ss.base_Pa	x(t-1)	-0.11453*	0.05421	0.19144008	0.098155624	91.80804057					
Snowdepth_daily	intercept	0.33009	0.58312	0.03207038	0	103.3500707	0.33103	0.5721	0.030963554		101.3832131
Snowdepth_daily	mitigation(t)	-0.50348	0.64973	0.03207038	0.021212882	103.3500707	-0.49207	0.63402	0.030963554	0.02052769	101.3832131
Snowdepth_daily	x(t)	0.10049	0.21628	0.03207038	0.00872116	103.3500707	0.1138	0.19763	0.030963554	0.01043587	101.3832131
Snowdepth_daily	x(t-1)	0.03664	0.21669	0.03207038	0.002136336	103.3500707					

(continued)

Table 6E-2. Time Series Analysis for 422 Basement South PCE: Predictor Variables Requiring One Lag Term, Period September 2012 to April 2013 (continued)

Predictor Code ^a	Model Term	Full Model					First Reduced Model				
		Coefficient	SE	R ²	Rel R ²	AIC	Coefficient	SE	R ²	Rel R ²	AIC
Soil_H2O_In6_cbar	intercept	1.66667	2.94696	0.03379673	0	103.2983014	1.70387	2.20627	0.033781973		101.2987444
Soil_H2O_In6_cbar	mitigation(t)	-0.40219	0.68097	0.03379673	0.016375483	103.2983014	-0.40658	0.63035	0.033781973	0.01703337	101.2987444
Soil_H2O_In6_cbar	x(t)	-0.00931	0.05151	0.03379673	0.010123996	103.2983014	-0.00834	0.01305	0.033781973	0.0167486	101.2987444
Soil_H2O_In6_cbar	x(t-1)	0.00118	0.06051	0.03379673	0.007297253	103.2983014					
Soil_H2O_Out3.5_cbar	intercept	0.4013	0.92497	0.07819472	0	101.9341348	0.42063	0.93553	0.019034517		101.7380296
Soil_H2O_Out3.5_cbar	mitigation(t)	-0.39628	0.7343	0.07819472	0.017315905	101.9341348	-0.40256	0.74277	0.019034517	0.01484413	101.7380296
Soil_H2O_Out3.5_cbar	x(t)	-0.00699	0.00686	0.07819472	0.025717775	101.9341348	-0.00049	0.00462	0.019034517	0.00419039	101.7380296
Soil_H2O_Out3.5_cbar	x(t-1)	0.00681	0.00537	0.07819472	0.035161043	101.9341348					
Soil_H2O_Out6_cbar	intercept	-1.19291	1.53216	0.06268327	0	102.4180648	-1.03695	1.45518	0.056936455		100.5953249
Soil_H2O_Out6_cbar	mitigation(t)	-0.84955	0.7386	0.06268327	0.036195032	102.4180648	-0.82993	0.7248	0.056936455	0.03308157	100.5953249
Soil_H2O_Out6_cbar	x(t)	0.00558	0.00793	0.06268327	0.016067762	102.4180648	0.00706	0.00686	0.056936455	0.02385489	100.5953249
Soil_H2O_Out6_cbar	x(t-1)	0.00225	0.00574	0.06268327	0.010420478	102.4180648					
Soil_T_C_MW3.9	intercept	-0.52035	3.13269	0.08417303	0	83.77096317	0.08596	2.7215	0.034398468		89.22206253
Soil_T_C_MW3.9	mitigation(t)	-0.59883	0.82188	0.08417303	0.026809873	83.77096317	-0.71456	0.80977	0.034398468	0.03373733	89.22206253
Soil_T_C_MW3.9	x(t)	-1.49175	1.78127	0.08417303	0.025738105	83.77096317	0.02697	0.17029	0.034398468	0.00066114	89.22206253
Soil_T_C_MW3.9	x(t-1)	1.53922	1.69445	0.08417303	0.031625055	83.77096317					
Soil_T_C_OTC.1	intercept	0.30168	0.78693	0.10126046	0	83.3377772	0.5478	0.76619	0.038757373		89.10895239
Soil_T_C_OTC.1	mitigation(t)	-0.51474	0.87667	0.10126046	0.024743267	83.3377772	-0.59064	0.86327	0.038757373	0.02687555	89.10895239
Soil_T_C_OTC.1	x(t)	-0.17428	0.17055	0.10126046	0.029174794	83.3377772	-0.02784	0.07874	0.038757373	0.01188183	89.10895239
Soil_T_C_OTC.1	x(t-1)	0.1938	0.154	0.10126046	0.047342398	83.3377772					

(continued)

Table 6E-2. Time Series Analysis for 422 Basement South PCE: Predictor Variables Requiring One Lag Term, Period September 2012 to April 2013 (continued)

Predictor Code ^a	Model Term	Full Model					First Reduced Model				
		Coefficient	SE	R ²	Rel R ²	AIC	Coefficient	SE	R ²	Rel R ²	AIC
Soil_T_C_OTC.6	intercept	0.13652	0.89557	0.06963586	0	84.13318118	0.37018	0.85135	0.038033088		89.12778251
Soil_T_C_OTC.6	mitigation(t)	-0.65464	0.87446	0.06963586	0.030704725	84.13318118	-0.77487	0.83432	0.038033088	0.0355073	89.12778251
Soil_T_C_OTC.6	x(t)	-0.12508	0.34338	0.06963586	0.014159463	84.13318118	0.0259	0.07869	0.038033088	0.00252579	89.12778251
Soil_T_C_OTC.6	x(t-1)	0.1782	0.30655	0.06963586	0.024771676	84.13318118					
StackEffect_422baseN	intercept	-0.10901	1.66749	0.07649438	0	82.4592142	-0.59489	1.54017	0.041040699		81.25032093
StackEffect_422baseN	mitigation(t)	-0.37818	0.77514	0.07649438	0.015176107	82.4592142	-0.41432	0.76634	0.041040699	0.01616068	81.25032093
StackEffect_422baseN	x(t)	9.16046	9.1512	0.07649438	0.040287208	82.4592142	5.13012	7.59733	0.041040699	0.02488002	81.25032093
StackEffect_422baseN	x(t-1)	-7.05825	8.73698	0.07649438	0.021031064	82.4592142					
StackEffect_422baseS	intercept	-0.13729	1.62093	0.08365779	0	82.2956873	-0.57407	1.53818	0.040075819		81.27143996
StackEffect_422baseS	mitigation(t)	-0.37439	0.77296	0.08365779	0.01519065	82.2956873	-0.42973	0.7664	0.040075819	0.01675795	81.27143996
StackEffect_422baseS	x(t)	9.63521	8.97008	0.08365779	0.043244161	82.2956873	4.62362	6.99093	0.040075819	0.02331787	81.27143996
StackEffect_422baseS	x(t-1)	-7.63789	8.49424	0.08365779	0.025222975	82.2956873					
StackEffect_422first	intercept	-0.34754	1.48134	0.21695057	0	71.63838656	-0.64684	1.48848	0.121701201		75.95303418
StackEffect_422first	mitigation(t)	-1.02645	0.79236	0.21695057	0.066495065	71.63838656	-1.03849	0.81775	0.121701201	0.07169757	75.95303418
StackEffect_422first	x(t)	17.86543	10.02697	0.21695057	0.110202326	71.63838656	7.15296	6.54933	0.121701201	0.05000363	75.95303418
StackEffect_422first	x(t-1)	-12.07194	9.5022	0.21695057	0.040253174	71.63838656					
StdDev_Setra_422base.upst_P a	intercept	1.23563	3.26923	0.02407285	0	88.891638	0.35884	1.7982	0.016999557		89.49536772
StdDev_Setra_422base.upst_P a	mitigation(t)	-0.74454	1.43765	0.02407285	0.016011335	88.891638	-0.44506	0.88677	0.016999557	0.01434564	89.49536772
StdDev_Setra_422base.upst_P a	x(t)	-0.39959	11.75849	0.02407285	0.004246069	88.891638	0.36533	7.9323	0.016999557	0.00265391	89.49536772
StdDev_Setra_422base.upst_P a	x(t-1)	-2.96142	8.33706	0.02407285	0.003815445	88.891638					

(continued)

Table 6E-2. Time Series Analysis for 422 Basement South PCE: Predictor Variables Requiring One Lag Term, Period September 2012 to April 2013 (continued)

Predictor Code ^a	Model Term	Full Model					First Reduced Model				
		Coefficient	SE	R ²	Rel R ²	AIC	Coefficient	SE	R ²	Rel R ²	AIC
StdDev_Setra_422SGdp.ss_Pa	intercept	-0.20743	0.96182	0.08729598	0	94.95811894	0.26354	0.70531	0.04198972		96.55881622
StdDev_Setra_422SGdp.ss_Pa	mitigation(t)	-0.20479	0.89116	0.08729598	0.011367877	94.95811894	-0.53521	0.71674	0.04198972	0.02232177	96.55881622
StdDev_Setra_422SGdp.ss_Pa	x(t)	0.0023	0.03712	0.08729598	0.010690416	94.95811894	0.02178	0.03108	0.04198972	0.01966795	96.55881622
StdDev_Setra_422SGdp.ss_Pa	x(t-1)	0.04189	0.03942	0.08729598	0.065237687	94.95811894					
T_422_F	intercept	0.83543	6.58063	0.08823246	0	99.43525938	-3.25906	5.66023	0.034244908		99.04596502
T_422_F	mitigation(t)	-0.64844	0.69297	0.08823246	0.024384401	99.43525938	-0.61917	0.69835	0.034244908	0.0244048	99.04596502
T_422_F	x(t)	0.09785	0.09028	0.08823246	0.022786842	99.43525938	0.0529	0.08271	0.034244908	0.0098401	99.04596502
T_422_F	x(t-1)	-0.10263	0.08609	0.08823246	0.041061212	99.43525938					
T_422baseN_C	intercept	1.4478	6.81636	0.02103693	0	83.68387198	1.41045	6.63197	0.018179479		81.74507858
T_422baseN_C	mitigation(t)	-0.48674	0.85838	0.02103693	0.017423003	83.68387198	-0.41746	0.77864	0.018179479	0.01621386	81.74507858
T_422baseN_C	x(t)	0.02641	0.23501	0.02103693	0.001404234	83.68387198	-0.01874	0.11574	0.018179479	0.00196561	81.74507858
T_422baseN_C	x(t-1)	-0.04441	0.19936	0.02103693	0.00220969	83.68387198					
T_422baseS_C	intercept	1.31187	11.99	0.06739298	0	82.66516172	-1.719	11.51721	0.018501039		81.73819965
T_422baseS_C	mitigation(t)	-0.62844	0.81597	0.06739298	0.022552785	82.66516172	-0.46041	0.79391	0.018501039	0.01754365	81.73819965
T_422baseS_C	x(t)	0.17482	0.24172	0.06739298	0.012337034	82.66516172	0.03399	0.18962	0.018501039	0.00095739	81.73819965
T_422baseS_C	x(t-1)	-0.18694	0.19802	0.06739298	0.032503162	82.66516172					
T_out_F	intercept	0.64957	1.27444	0.05119392	0	100.5502017	0.99079	1.1415	0.035281587		99.01589259
T_out_F	mitigation(t)	-0.32527	0.66439	0.05119392	0.014850685	100.5502017	-0.40498	0.64456	0.035281587	0.01683769	99.01589259
T_out_F	x(t)	-0.03092	0.03404	0.05119392	0.027227156	100.5502017	-0.01687	0.02554	0.035281587	0.0184439	99.01589259
T_out_F	x(t-1)	0.02077	0.03274	0.05119392	0.009116075	100.5502017					

(continued)

Table 6E-2. Time Series Analysis for 422 Basement South PCE: Predictor Variables Requiring One Lag Term, Period September 2012 to April 2013 (continued)

Predictor Code ^a	Model Term	Full Model					First Reduced Model				
		Coefficient	SE	R ²	Rel R ²	AIC	Coefficient	SE	R ²	Rel R ²	AIC
T_out_Hi_F	intercept	-0.25759	1.69656	0.03214691	0	101.1067261	0.32513	1.35239	0.018449552		99.50021288
T_out_Hi_F	mitigation(t)	-0.33396	0.68393	0.03214691	0.014079788	101.1067261	-0.44311	0.64904	0.018449552	0.01837115	99.50021288
T_out_Hi_F	x(t)	-0.00477	0.02157	0.03214691	0.001110826	101.1067261	0.00027	0.0195	0.018449552	7.84E-05	99.50021288
T_out_Hi_F	x(t-1)	0.0132	0.02265	0.03214691	0.016956295	101.1067261					
T_out_Lo_F	intercept	0.34255	0.85199	0.03828627	0	100.9285485	0.53429	0.77949	0.023886556		99.34468411
T_out_Lo_F	mitigation(t)	-0.27037	0.70405	0.03828627	0.013190534	100.9285485	-0.36962	0.67548	0.023886556	0.01506627	99.34468411
T_out_Lo_F	x(t)	-0.02832	0.04141	0.03828627	0.016481488	100.9285485	-0.01084	0.02903	0.023886556	0.00882028	99.34468411
T_out_Lo_F	x(t-1)	0.02185	0.03646	0.03828627	0.008614248	100.9285485					
Wind_Chill_F	intercept	0.50049	1.08481	0.04166871	0	100.8298963	0.75549	0.96678	0.029610088		99.18002029
Wind_Chill_F	mitigation(t)	-0.33356	0.66975	0.04166871	0.014967358	100.8298963	-0.40483	0.64784	0.029610088	0.01679942	99.18002029
Wind_Chill_F	x(t)	-0.02204	0.02908	0.04166871	0.019490877	100.8298963	-0.01183	0.02206	0.029610088	0.01281066	99.18002029
Wind_Chill_F	x(t-1)	0.01532	0.02787	0.04166871	0.007210474	100.8298963					
X422baseN_Wkly_Elect_radon	intercept	0.55821	0.8556	0.47336466	0	71.81747139	-1.06975	0.92672	0.071919955		89.3165776
X422baseN_Wkly_Elect_radon	mitigation(t)	-0.50885	0.73796	0.47336466	0.023561036	71.81747139	0.72274	0.82389	0.071919955	0.0158268	89.3165776
X422baseN_Wkly_Elect_radon	x(t)	0.21388**	0.0633	0.47336466	0.207839694	71.81747139	0.0938	0.07055	0.071919955	0.05609316	89.3165776
X422baseN_Wkly_Elect_radon	x(t-1)	-0.23396**	0.06181	0.47336466	0.241963935	71.81747139					
X422baseS_Wkly_Elect_radon	intercept	0.4604	0.83297	0.41207972	0	82.67796223	-0.62471	0.90347	0.088196961		94.61625387
X422baseS_Wkly_Elect_radon	mitigation(t)	-0.45966	0.6899	0.41207972	0.026285122	82.67796223	0.24219	0.78844	0.088196961	0.00969768	94.61625387
X422baseS_Wkly_Elect_radon	x(t)	0.23314**	0.0716	0.41207972	0.202568874	82.67796223	0.10112	0.07326	0.088196961	0.07849928	94.61625387
X422baseS_Wkly_Elect_radon	x(t-1)	-0.23836**	0.07017	0.41207972	0.183225719	82.67796223					

(continued)

Table 6E-2. Time Series Analysis for 422 Basement South PCE: Predictor Variables Requiring One Lag Term, Period September 2012 to April 2013 (continued)

Predictor Code ^a	Model Term	Full Model					First Reduced Model				
		Coefficient	SE	R ²	Rel R ²	AIC	Coefficient	SE	R ²	Rel R ²	AIC
X422first_Wkly_Elect_radon	intercept	0.32559	0.93329	0.37377688	0	80.04031205	-0.69935	0.96311	0.102040335		91.95828131
X422first_Wkly_Elect_radon	mitigation(t)	-0.40386	0.77016	0.37377688	0.01968515	80.04031205	0.24253	0.83577	0.102040335	0.0090676	91.95828131
X422first_Wkly_Elect_radon	x(t)	0.54809**	0.1864	0.37377688	0.195691022	80.04031205	0.26939	0.18026	0.102040335	0.09297273	91.95828131
X422first_Wkly_Elect_radon	x(t-1)	-0.53663**	0.18427	0.37377688	0.158400712	80.04031205					
Soil_T_C_OTC.3.5	intercept	0.15083	0.85578	0.06970928	0	84.13136614	0.3652	0.81695	0.041208202		89.04512984
Soil_T_C_OTC.3.5	mitigation(t)	-0.72874	0.86975	0.06970928	0.033482405	84.13136614	-0.79183	0.83025	0.041208202	0.03646982	89.04512984
Soil_T_C_OTC.3.5	x(t)	-0.02098	0.32325	0.06970928	0.015151221	84.13136614	0.03052	0.07165	0.041208202	0.00473838	89.04512984
Soil_T_C_OTC.3.5	x(t-1)	0.088	0.28915	0.06970928	0.021075653	84.13136614					

^a Descriptions of predictor codes can be found in Table 6A-1.

* = significant at 5%

** = significant at 1%

Full Model: $y(t) - y(t - 1) = \beta_0 + \beta_1 \text{mitigation}(t) + \beta_2 x(t) + \beta_3 x(t - 1) + u(t)$

First Reduced Model: $y(t) - y(t - 1) = \beta_0 + \beta_1 \text{mitigation}(t) + \beta_2 x(t) + u(t)$

Table 6E-3. Time Series Analysis for 422 Basement South PCE: Categorical Predictor Variables, Period September 2012 to April 2013

Predictor Code ^a	Model Term	Coefficient	SE	R ²	AIC
Heat_on.off_422_daily	intercept	0.17192308	0.72428618	0.02416307	101.586018
Heat_on.off_422_daily	mitigation	-0.53384615	0.67248283	0.02416307	101.586018
Heat_on.off_422_daily	ON	0.28346154	0.73666803	0.02416307	101.586018
METAR_IcyPrecip_YorN	intercept	0.17192308	0.72428618	0.02416307	101.586018
METAR_IcyPrecip_YorN	mitigation	-0.53384615	0.67248283	0.02416307	101.586018
METAR_IcyPrecip_YorN	YES	0.28346154	0.73666803	0.02416307	101.586018
METAR_SnowEvent_YorN	intercept	0.08123399	0.63351509	0.04943441	100.825107
METAR_SnowEvent_YorN	mitigation	-0.41873108	0.62311671	0.04943441	100.825107
METAR_SnowEvent_YorN	YES	0.43461001	0.47329112	0.04943441	100.825107
METAR_ThunderEvent_YorN	intercept	0.36469553	0.61150632	0.019058	101.737335
METAR_ThunderEvent_YorN	mitigation	-0.45023004	0.63486147	0.019058	101.737335
METAR_ThunderEvent_YorN	YES	-0.05673884	0.51836222	0.019058	101.737335
Wind_Dir_Hi	intercept	0.83588889	1.00180733	0.10612621	100.880286
Wind_Dir_Hi	mitigation	-0.39922222	0.65994872	0.10612621	100.880286
Wind_Dir_Hi	S	-1.84666667	1.5074291	0.10612621	100.880286
Wind_Dir_Hi	SW	-1.64666667	1.5074291	0.10612621	100.880286
Wind_Dir_Hi	W	-0.49388889	0.81410476	0.10612621	100.880286
Wind_Dir	intercept	1.35536585	0.74315741	0.42927816	92.3177316
Wind_Dir	mitigation	-0.13804878	0.59060162	0.42927816	92.3177316
Wind_Dir	NE	1.39268293	1.27584531	0.42927816	92.3177316
Wind_Dir	NW	-2.03207317*	0.74924397	0.42927816	92.3177316
Wind_Dir	S	-1.06731707	1.01582334	0.42927816	92.3177316
Wind_Dir	SW	-1.71898374*	0.79664353	0.42927816	92.3177316

(continued)

**Table 6E-3. Time Series Analysis for 422 Basement South PCE: Categorical Predictor Variables, Period September 2012 to April 2013
(continued)**

Predictor Code ^a	Model Term	Coefficient	SE	R ²	AIC
Wind_Dir	W	-1.01158537	0.73948142	0.42927816	92.3177316

^a Descriptions of predictor codes can be found in Table 6A-1.

* = significant at 5%

** = significant at 1%

Reference = Mitigation = OFF

Reference Heat = ON

Reference Icy Precip = No

Reference Snow Event = No

Reference ThunderEvent = No

Reference Wind Dir Hi = E

Reference Wind Dir = E

$$y(t) - y(t - 1) = \beta_0 + \beta_1 \text{mitigation}(t) + \beta_2 x_{ON}(t) + u(t)$$

$$\text{where } x_{ON}(t) = \begin{cases} 1 & \text{if predictor is } ON \\ 0 & \text{if predictor is } OFF \end{cases}$$

If X(t) = ON/OFF, then Off is reference cell

$$y(t) - y(t - 1) = \beta_0 + \beta_1 \text{mitigation}(t) + \beta_2 \text{Wind_Dir_Hi}_N(t) + \beta_3 \text{Wind_Dir_Hi}_{NE}(t) + \beta_4 \text{Wind_Dir_Hi}_{NW}(t) + \beta_5 \text{Wind_Dir_Hi}_{SE}(t) + \beta_6 \text{Wind_Dir_Hi}_S(t) + \beta_7 \text{Wind_Dir_Hi}_{SW}(t) + \beta_8 \text{Wind_Dir_Hi}_W(t) + u(t)$$

$$\text{where } x_d(t) = \begin{cases} 1 & \text{if wind}_{iS} \text{ in direction } d \\ 0 & \text{if wind}_{iS} \text{ not in direction } d \end{cases}$$

$$y(t) - y(t - 1) = \beta_0 + \beta_1 \text{mitigation}(t) + \beta_2 \text{Wind_Dir}_N(t) + \beta_3 \text{Wind_Dir}_{NE}(t) + \beta_4 \text{Wind_Dir}_{NW}(t) + \beta_5 \text{Wind_Dir}_{SE}(t) + \beta_6 \text{Wind_Dir}_S(t) + \beta_7 \text{Wind_Dir}_{SW}(t) + \beta_8 \text{Wind_Dir}_W(t) + u(t)$$

$$\text{where } x_d(t) = \begin{cases} 1 & \text{if wind}_{iS} \text{ in direction } d \\ 0 & \text{if wind}_{iS} \text{ not in direction } d \end{cases}$$

Attachment 6F. Time Series Analysis Results—Hartman Online GC Data, Daily Resolution

Table 6F-1. Time Series Analysis for First Difference of 422 Basement South PCE Concentration (GC) Variables That Did Not Need Lag Terms. Period December 2012 to March 2013

Predictor Code ^a	Model Term	Model: $Y(t) - Y(t - 1) = \beta_0 + \beta_1\text{mitigation}(t) + \beta_1x(t) + x(t)$	
		Coefficient	SE
Bar_drop_Hg.hr	intercept	0.081	0.207
	mitigation	-0.097	0.270
	x(t)	33.592**	11.506
BP_Net_Change	intercept	-46.888*	19.787
	mitigation	0.164	0.309
	x(t)	1.557*	0.656
BP_Pump_Speed	intercept	0.082	0.206
	mitigation	-0.111	0.270
	x(t)	-1.466**	0.500
Cool_Degree_Day	intercept	0.458	0.322
	mitigation	-0.062	0.280
	x(t)	-4.853	3.024
Rain_IPH	intercept	0.439	0.333
	mitigation	-0.085	0.280
	x(t)	-1.347	0.939
Wind_Dir	intercept	0.073	0.218
	mitigation	-0.087	0.285
	x(t)	0.266	5.396
Wind_Dir_Hi	intercept	-0.191	0.484
	mitigation	-0.038	0.299
	x(t)	0.061	0.099

^a Descriptions of predictor codes can be found in Table 6A-1.

Table 6F-2. Time Series Analysis for 422 Basement South PCE Concentration (GC). Variables that Needed a Lag-1 Day Term. Period December 2012 to March 2013

Predictor Code ^a	Model Term	Full Model: $y(t) - y(t - 1) = \beta_0 + \beta_1\text{mitigation}(t) + \beta_2x(t) + \beta_3x(t - 1) + u(t)$		First Reduced Model: $y(t) - y(t - 1) = \beta_0 + \beta_1\text{mitigation}(t) + \beta_2x(t) + u(t)$	
		Coefficient	SE	Coefficient	SE
Bar_in_Hg	intercept	1.684	21.681	-46.888*	19.787
	mitigation(t)	-0.107	0.281	0.164	0.309
	x(t)	2.428**	0.650	1.55729*	0.656
	x(t-1)	-2.482**	0.651		
BP_Stroke_Length	intercept	0.289	0.396	0.439	0.333
	mitigation(t)	-0.081	0.282	-0.085	0.280
	x(t)	-1.497	0.966	-1.347	0.939
	x(t-1)	0.686	0.964		
Fall_Crk_Gage_ht_ft	intercept	-0.186	0.507	-0.191	0.484
	mitigation(t)	-0.039	0.306	-0.038	0.299
	x(t)	0.066	0.190	0.061	0.099
	x(t-1)	-0.007	0.189		
GW_level_log_MW3_in	intercept	1.273	2.677	1.317	2.593
	mitigation(t)	-0.046	0.303	-0.045	0.299
	x(t)	-0.112	0.412	-0.080	0.165
	x(t-1)	0.035	0.408		
Heat_Degree_Day	intercept	-0.581	0.495	-1.297*	0.506
	mitigation(t)	-0.022	0.259	0.057	0.288
	x(t)	0.079**	0.017	0.043**	0.014
	x(t-1)	-0.059**	0.017		
Heat_Index_F	intercept	0.731	0.500	1.478**	0.501
	mitigation(t)	-0.027	0.262	0.088	0.289
	x(t)	-0.079**	0.017	-0.046**	0.015
	x(t-1)	0.058**	0.017		
Hum_422_.	intercept	-0.070	0.473	0.655	0.517
	mitigation(t)	-0.096	0.245	-0.042	0.289
	x(t)	-0.107**	0.027	-0.027	0.022
	x(t-1)	0.1134**	0.027		
Hum_out_.	intercept	1.023	1.218	2.138	1.139
	mitigation(t)	-0.055	0.262	-0.043	0.275
	x(t)	-0.049**	0.018	-0.027	0.015
	x(t-1)	0.037*	0.018		

(continued)

Table 6F-2. Time Series Analysis for 422 Basement South PCE Concentration (GC). Variables that Needed a Lag-1 Day Term. Period December 2012 to March 2013 (continued)

Predictor Code ^a	Model Term	Full Model: $y(t) - y(t - 1) = \beta_0 + \beta_1\text{mitigation}(t) + \beta_2x(t) + \beta_3x(t - 1) + u(t)$		First Reduced Model: $y(t) - y(t - 1) = \beta_0 + \beta_1\text{mitigation}(t) + \beta_2x(t) + u(t)$	
		Coefficient	SE	Coefficient	SE
Rain_In_met	intercept	0.073	0.236	0.092	0.230
	mitigation(t)	-0.087	0.293	-0.100	0.290
	x(t)	-0.288	0.830	-0.210	0.795
	x(t-1)	0.284	0.829		
Setra_422base.out_Pa	intercept	-0.024	0.376	-0.449	0.358
	mitigation(t)	-0.177	0.270	-0.152	0.288
	x(t)	-0.419**	0.142	-0.274*	0.130
	x(t-1)	0.338*	0.144		
Setra_422base.upst_Pa	intercept	-1.185	0.837	-2.108**	0.791
	mitigation(t)	0.243	0.352	0.507	0.355
	x(t)	5.094**	1.316	3.182**	1.078
	x(t-1)	-3.230*	1.345		
Setra_422SGdp.ss_Pa	intercept	0.292	0.261	0.172	0.239
	mitigation(t)	-0.086	0.328	-0.110	0.309
	x(t)	0.004	0.011	-0.004	0.009
	x(t-1)	-0.015	0.011		
Setra_422ss.base_Pa	intercept	0.180	0.268	0.133	0.249
	mitigation(t)	-0.097	0.881	-0.101	0.818
	x(t)	-0.034	0.053	0.003	0.047
	x(t-1)	0.042	0.042		
SGP11.13_GC3_PCE	intercept	0.107	0.226	0.062	0.222
	mitigation(t)	-0.223	0.357	-0.192	0.352
	x(t)	0.015	0.010	0.002	0.004
	x(t-1)	-0.013	0.009		
SGP2.9_GC3_PCE	intercept	0.102	0.444	0.317	0.479
	mitigation(t)	0.104	0.296	-0.002	0.322
	x(t)	-0.008*	0.003	-0.001	0.001
	x(t-1)	0.008*	0.003		
SGP8.9_GC3_PCE	intercept	-0.190	0.383	0.311	0.377
	mitigation(t)	-0.004	0.351	0.097	0.370
	x(t)	-0.017**	0.005	-0.001	0.002
	x(t-1)	0.018**	0.005		

(continued)

Table 6F-2. Time Series Analysis for 422 Basement South PCE Concentration (GC). Variables that Needed a Lag-1 Day Term. Period December 2012 to March 2013 (continued)

Predictor Code ^a	Model Term	Full Model: $y(t) - y(t - 1) = \beta_0 + \beta_1\text{mitigation}(t) + \beta_2x(t) + \beta_3x(t - 1) + u(t)$		First Reduced Model: $y(t) - y(t - 1) = \beta_0 + \beta_1\text{mitigation}(t) + \beta_2x(t) + u(t)$	
		Coefficient	SE	Coefficient	SE
SGP9.6_GC3_PCE	intercept	0.028	1.094	0.610	0.783
	mitigation(t)	0.051	0.866	-0.443	0.575
	x(t)	0.013	0.020	-0.002	0.003
	x(t-1)	-0.013	0.017		
Snowdepth_daily	intercept	0.066	0.251	0.078	0.242
	mitigation(t)	-0.075	0.303	-0.089	0.293
	x(t)	-0.033	0.168	-0.004	0.082
	x(t-1)	0.034	0.172		
Soil_H2O_In6._cbar	intercept	-0.548	3.782	-1.675	3.792
	mitigation(t)	-0.275	0.376	-0.203	0.382
	x(t)	0.255	0.192	0.011	0.024
	x(t-1)	-0.251	0.195		
Soil_H2O_Out6._cbar	intercept	0.060	1.222	0.165	1.113
	mitigation(t)	-0.086	0.295	-0.091	0.291
	x(t)	-0.001	0.006	0.000	0.004
	x(t-1)	0.001	0.006		
Soil_T_C_MW3.9	intercept	-0.531	2.704	0.220	2.676
	mitigation(t)	-0.067	0.298	-0.092	0.304
	x(t)	4.855	4.674	-0.009	0.171
	x(t-1)	-4.806	4.616		
Soil_T_C_OTC.1	intercept	-0.199	0.298	-0.099	0.305
	mitigation(t)	-0.073	0.275	-0.101	0.285
	x(t)	-0.236	0.182	0.065	0.080
	x(t-1)	0.330	0.181		
Soil_T_C_OTC.3.5	intercept	-0.012	0.502	-0.006	0.520
	mitigation(t)	-0.173	0.286	-0.079	0.292
	x(t)	1.942	0.998	0.016	0.092
	x(t-1)	-1.897	0.979		
Soil_T_C_OTC.6	intercept	-0.026	0.500	-0.063	0.548
	mitigation(t)	-0.182	0.270	-0.071	0.293
	x(t)	2.011**	0.695	0.024	0.087
	x(t-1)	-1.966**	0.683		

(continued)

Table 6F-2. Time Series Analysis for 422 Basement South PCE Concentration (GC). Variables that Needed a Lag-1 Day Term. Period December 2012 to March 2013 (continued)

Predictor Code ^a	Model Term	Full Model: $y(t) - y(t - 1) = \beta_0 + \beta_1\text{mitigation}(t) + \beta_2x(t) + \beta_3x(t - 1) + u(t)$		First Reduced Model: $y(t) - y(t - 1) = \beta_0 + \beta_1\text{mitigation}(t) + \beta_2x(t) + u(t)$	
		Coefficient	SE	Coefficient	SE
SSP2_GC3_PCE	intercept	-0.131	0.639	-0.082	0.632
	mitigation(t)	-0.169	0.406	-0.162	0.405
	x(t)	-0.104	0.307	0.040	0.152
	x(t-1)	0.154	0.286		
SSP4_GC3_PCE	intercept	-0.082	0.572	-0.017	0.610
	mitigation(t)	0.208	0.355	-0.122	0.360
	x(t)	-0.014**	0.005	0.000	0.001
	x(t-1)	0.013**	0.004		
SSP7_GC3_PCE	intercept	0.120	0.175	0.040	0.225
	mitigation(t)	0.006	0.260	-0.229	0.329
	x(t)	0.096**	0.019	0.014	0.015
	x(t-1)	-0.112**	0.019		
T_420baseN_C	intercept	-0.682	1.176	0.622	1.385
	mitigation(t)	-0.184	0.203	-0.118	0.246
	x(t)	-0.224**	0.053	-0.013	0.033
	x(t-1)	0.241**	0.051		
T_420baseS_C	intercept	-0.529	1.231	0.768	1.449
	mitigation(t)	-0.176	0.204	-0.110	0.247
	x(t)	-0.217**	0.053	-0.016	0.033
	x(t-1)	0.230**	0.052		
T_420first_C	intercept	0.150	0.873	1.221	0.972
	mitigation(t)	-0.144	0.205	-0.069	0.241
	x(t)	-0.123**	0.032	-0.028	0.023
	x(t-1)	0.120**	0.032		
T_422_F	intercept	8.152	13.785	-4.207	10.737
	mitigation(t)	-0.118	0.294	-0.070	0.291
	x(t)	0.111	0.154	0.060	0.151
	x(t-1)	-0.225	0.155		
T_422baseN_C	intercept	0.164	2.965	4.257	3.362
	mitigation(t)	-0.182	0.206	-0.070	0.242
	x(t)	-0.419**	0.089	-0.077	0.062
	x(t-1)	0.417**	0.087		

(continued)

Table 6F-2. Time Series Analysis for 422 Basement South PCE Concentration (GC). Variables that Needed a Lag-1 Day Term. Period December 2012 to March 2013 (continued)

Predictor Code ^a	Model Term	Full Model: $y(t) - y(t - 1) = \beta_0 + \beta_1\text{mitigation}(t) + \beta_2x(t) + \beta_3x(t - 1) + u(t)$		First Reduced Model: $y(t) - y(t - 1) = \beta_0 + \beta_1\text{mitigation}(t) + \beta_2x(t) + u(t)$	
		Coefficient	SE	Coefficient	SE
T_422baseS_C	intercept	-2.795	6.508	3.519	7.259
	mitigation(t)	-0.259	0.219	-0.110	0.248
	x(t)	-0.927**	0.220	-0.058	0.122
	x(t-1)	0.975**	0.215		
T_out_F	intercept	0.748	0.507	1.497**	0.506
	mitigation(t)	-0.023	0.264	0.093	0.289
	x(t)	-0.078**	0.017	-0.046**	0.015
	x(t-1)	0.057**	0.017		
T_out_Hi_F	intercept	0.932	0.529	1.656**	0.519
	mitigation(t)	-0.026	0.258	0.059	0.284
	x(t)	-0.061**	0.014	-0.041**	0.012
	x(t-1)	0.039**	0.014		
T_out_Lo_F	intercept	0.402	0.433	1.008*	0.423
	mitigation(t)	-0.016	0.275	0.146	0.294
	x(t)	-0.069**	0.018	-0.041*	0.016
	x(t-1)	0.055**	0.017		
Wind_Chill_F	intercept	0.742	0.396	1.206**	0.393
	mitigation(t)	0.006	0.265	0.108	0.284
	x(t)	-0.067**	0.015	-0.043**	0.012
	x(t-1)	0.042**	0.015		

^a Descriptions of predictor codes can be found in Table 6A-1.

7. Vapor Intrusion Forecasting Performance

Vapor intrusion site investigation costs are driven higher by the need for multiple samples per structure to characterize the commonly observed spatial and temporal variability in indoor, subslab, and deep soil-gas concentrations. However, relatively few vapor intrusion assessment data sets have been published that include both long-term monitoring and high-frequency sample collection for VOCs. Temporal variability in VOC concentrations in indoor air is expected to be driven by variation in barometric pressure, house operations, temperature, water table, and soil moisture. These phenomena have known but irregular cycles on multiple time scales.

Current state guidance documents generally call for sampling at times of the year believed to be associated with the highest vapor intrusion potential and for timing sampling events with respect to rain events. For example, California requires that soil gas sampling be delayed for 5 days after any rain of more than 1/2 inch (CA DTSC, 2012). From a practical standpoint, it would be ideal if the practitioner could determine the likelihood of a near-future vapor intrusion event. The average long-term exposure can be influenced by short, high-concentration events occurring at brief periods during the year, although this effect may not be large enough to change the risk management decision (Weinberg et al., 2014). Thus, it would be beneficial to the practitioner to be able to deploy a small number of short-term samplers during occasions when concentrations are most likely to produce a sharp increase or be at their worst.

Based on a limited number of studies, TCE is currently being managed in some EPA regions based on risk screening levels that are similar for both chronic cancer risk and shorter term reproductive effects, with exposure periods of 1 month or less. This change in risk screening criteria provides an additional impetus to better understand and, if possible, predict the highest vapor intrusion conditions.

7.1 Forecasting Approach

We expected the indoor air concentration (our dependent variable) to depend on the vapor intrusion flux from soil gas, which in turn is controlled or influenced by a number of other variables that can affect the vapor intrusion process. These variables were collected as follows.

- Weather-related variables, including air temperature, barometric pressure, and wind, were collected from standard National Weather Service (NWS) forecasts.
- Soil moisture; soil temperature; groundwater level; heating, ventilation, air conditioning operation; and mitigation system operation were measured on site as described in **Section 3**.
- Stream gauge information, previously shown to correlate with shallow groundwater levels at this site (U.S. EPA, 2013), was obtained real-time from the U.S. Geological Survey along with groundwater-level data from an on-site continuous groundwater level logger.
- Indoor AlphaGUARD real-time radon instruments, Safety Siren home radon sensors, SETRA and Voltran pressure monitoring devices were used to observe radon and differential pressure at a high time resolution.

The meteorological data were interpreted in terms of previous time series analysis results (as described in U.S. EPA [2013] and **Section 6.1** of this report) to predict the relative expected degree of vapor intrusion up to 7 days in advance. The results from previous studies used for this purpose are given primarily in Chapters 9 and 10 and summarized in Section 13.1.3 of U.S. EPA (2013). (Note that the analyses described in the rest of **Section 6** of this report had not been fully completed, so those results did not strongly influence the prediction approach described in this section.)

Intensive sampling was performed during the times of predicted high vapor intrusion events and during control times. These sampling events included TO-17 tubes for soil gas, short-term passive adsorbers, soil-gas radon, and groundwater sampling.

Testing our ability to predict peak vapor intrusion events in the duplex (as indicated by indoor air concentrations) based on these data required the following:

- A prediction guide (**Table 7-1**) with trigger points based on meteorological variables, differential pressure measurements, and radon concentrations was developed considering results from the previous years of intensive indoor air sampling for VOCs and radon. These variables and trigger points are based on the data analysis of previous data from the Indianapolis house described in U.S. EPA (2013).
- Forecasts of indoor air concentrations were made using meteorological variables given by the NWS in conjunction with the guide based on previous site-specific experience. The NWS forecasts were generally reviewed in the hourly weather forecast graph display, which provides information on temperature, wind direction, wind speed, precipitation potential, and amount. Note that barometric pressures are not part of that standard forecast and are not generated in the National Digital Forecast Database. The meteorological-based forecasts of vapor intrusion we made were modified in some cases based on real-time observations of radon and differential pressure on the day the forecast was prepared. Indoor air forecasts were made approximately 1 week in advance of sampling from November 8, 2013, to March 4, 2014.

We believed that it was unlikely that we would be able to forecast vapor intrusion conditions with more accuracy or lead time than is currently possible for weather forecasts, which are typically limited to 5 days or less. Weather forecast accuracy is not perfect even for fewer than 3 days in the United States, as shown for Indianapolis in **Table 7-2**. Weather forecast accuracy statistics for various U.S. locations can be obtained at <http://www.forecastadvisor.com/>.

Table 7-1. Meteorological Predictor Variables Used to Guide Prediction

Parameter	Proposed Trigger Point	Prediction Source	Monitoring Method
Exterior Temperature	Average daily temperature below 37°F; a differential temperature of 28 degrees °F between inside and outside	NWS, Indianapolis International Airport, available 5 days ahead	On-site weather station
Snowfall	Any observable snowfall at ground level	NWS, Indianapolis International Airport, available 5 days ahead (for snowfall probability of 0.1")	NWS, Indianapolis, National Climatic Data Center records for 24 hours a day, 7 days a week coverage; ARCADIS on-site observer when present (less than 24x7 coverage)
Snow or Ice Cover on Ground	Frozen shallow soils (precipitation or saturated soils followed by sustained cold weather, high moisture snowpacks)	National-level snow depth forecast at http://www.nohrsc.noaa.gov/nsa/ Weather channel predicts 48 hours out http://www.intellicast.com/Travel/Weather/Snow/SNOWcast.aspx	National climatic data center http://www.ncdc.noaa.gov/snow-and-ice/dly-data.php , supplemented with ARCADIS on site observations
Wind Direction	Winds predicted to be from SSW, SW, WSW, W, or WNW (five of 16 Cardinal directions)	NWS, Indianapolis International Airport, available 5 days ahead (for snowfall probability of 0.1")	On-site weather station

(continued)

Table 7-1. Meteorological Predictor Variables Used to Guide Prediction (continued)

Parameter	Proposed Trigger Point	Prediction Source	Monitoring Method
Differential Pressure (Mean)	Subslab vs. Indoor = 2 Pa Basement vs. Upstairs = 0.5 Pa	Not predicted, rather observed real time	Setra differential pressure measurements
Differential Pressure (Fluctuation Intensity) (Differential Pressure Standard Deviation/Differential Pressure Mean)	Subslab vs. Indoor = 3 Basement vs. Indoor = 4	Not predicted, rather observed real time	Setra differential pressure measurements
Radon Concentration	422 Basement radon concentration (AlphaGUARD) exceeding 8.5 pCi/L for a 4-hour average	Not predicted, rather observed real time	AlphaGUARD and/or SIRAD-106N instruments

Table 7-2. Ability to Forecast Weather of Major Providers in Indianapolis, IN^a

Weather Forecast Accuracy Data Last Year (2013)					
Provider	High Temp	Low Temp	Icon Precip	Text Precip	Overall
The Weather Channel	76.12%	75.25%	79.30%	79.30%	77.49%
MeteoGroup	73.03%	75.94%	80.40%	80.40%	77.44%
National Weather Service	70.86%	72.31%	77.15%	75.65%	73.99%
WeatherBug	68.52%	68.58%	79.32%	79.32%	73.94%
AccuWeather	67.16%	66.40%	78.81%	80.30%	73.17%
Weather Underground	68.36%	67.60%	79.54%	76.45%	72.99%
Foreca	72.58%	67.23%	75.77%	75.77%	72.84%
CustomWeather	67.16%	66.30%	77.71%	77.71%	72.22%
Persistence	30.27%	28.11%	57.43%	57.43%	43.31%

Source: ForecastAdvisor, 2014.

^aForecastadvisor.com describes their statistics as follows: "All the accuracy calculations that appear on ForecastAdvisor are averaged over one to three day out forecasts. The percentages you see for each weather forecaster are calculated by taking the average of four accuracy measurements. These accuracy measurements are the percentage of high temperature forecasts that are within three degrees of what actually happened, the percentage of low temperature forecasts that are within three degrees of actual, the percentage correct of precipitation forecasts (both rain and snow) for the forecast icon, and the percentage correct of precipitation forecasts for the forecast text. The percentages you see are specifically for the listed city. About 90 forecasts from each provider make up the monthly percent (30 days in a month times 3 days of forecasts per day), and over 1000 forecasts from each provider make up the yearly percent." <http://www.forecastadvisor.com/docs/accuracy/> downloaded 6/28/14

7.2 Assessment of Accuracy of Vapor Intrusion Predictions

As discussed in Section 6, multiple meteorological variables likely control VOC vapor intrusion at this duplex. The meteorological variables likely interact in complex ways that would make the system difficult to mathematically model completely. Such multiple variable effects are also known in the radon vapor intrusion literature. In their 1985 radon reference manual, Lewis and Houle stated:

"This paper identified about thirteen factors that can affect radon variation in the soil and house environment. The thirteen factors being soil moisture content, soil permeability, wind, temperature, barometric pressure, rainfall, frozen ground, snow

cover, earth tides, atmospheric tides, occupancy factors, season and time of day. One can see the complexity of understanding and studying radon variability in homes.”

We do not expect VOC vapor intrusion to be a significantly simpler process than radon vapor intrusion. VOC vapor intrusion is subject to the same building envelope factors that largely control radon vapor intrusion. However, because of their much longer half-life in the subsurface (see **Section 2**), VOCs are also subject to variability further away from the building as they migrate from more distant sources. The relationships among the variables may not be purely linear; they could be nonlinear (as discussed in Section 6) or synergistic. For example, the tetrachloroethylene (PCE) concentration curve vs. cold temperature-related variables appears to curve upward under the most extreme winter conditions, as we discuss in Section 6. That upward curve may reflect an additive or synergistic effect between related variables such as cold temperature, frozen ground, and snow cover. In other words, cold temperatures could influence vapor intrusion through several separate physical mechanisms, such as enhancement of the strength of the stack effect and formation of a lower-permeability frozen ground layer near the surface.

Using the factors described in **Table 7-1**, we attempted to forecast, on a weekly basis, the relative amount of vapor intrusion expected in the structure with a 1-day time resolution, expressing our prediction for each day on a scale of low to extremely high. The variables in Table 7-1 were considered as a totality according to professional judgment in formulating the prediction, with a somewhat greater weight given to the differential temperature. Although an algebraic approach was not used to prepare the forecast, the forecaster was cognizant of the strengths of relationships between these weather conditions and vapor intrusion concentrations observed previously. See:

- Figures 10-10 through 10-12 of U.S. EPA (2012) and Figures 9-42 and 9-43 of U.S. EPA (2013) regarding previously observed relationships between temperature and concentration;
- Figures 6-69, 6-70, and 9-45 through 9-47 of U.S. EPA (2013) regarding previously observed relationships between snow variables and concentration.
- Figures 9-50 through 9-52 of U.S. EPA (2013) regarding previously observed relationships between wind direction and concentration.

The predictions were converted to values according to this system (low =1, moderate = 3, moderately high = 4, high =5, very high = 6, extremely high = 7). Although at the time of prediction we did not expressly link these adjectival terms to numerical concentration ranges, the understood context was our previous observations in this duplex made without mitigation. The previously observed concentrations varied by a factor of 50x from “low” to “extremely high” (U.S. EPA, 2012, Chapter 5). Those daily adjectival predictions were then averaged for each week-long sampling interval and compared with the actual concentrations observed for PCE, chloroform, and radon (**Figures 7-1 through 7-3**).

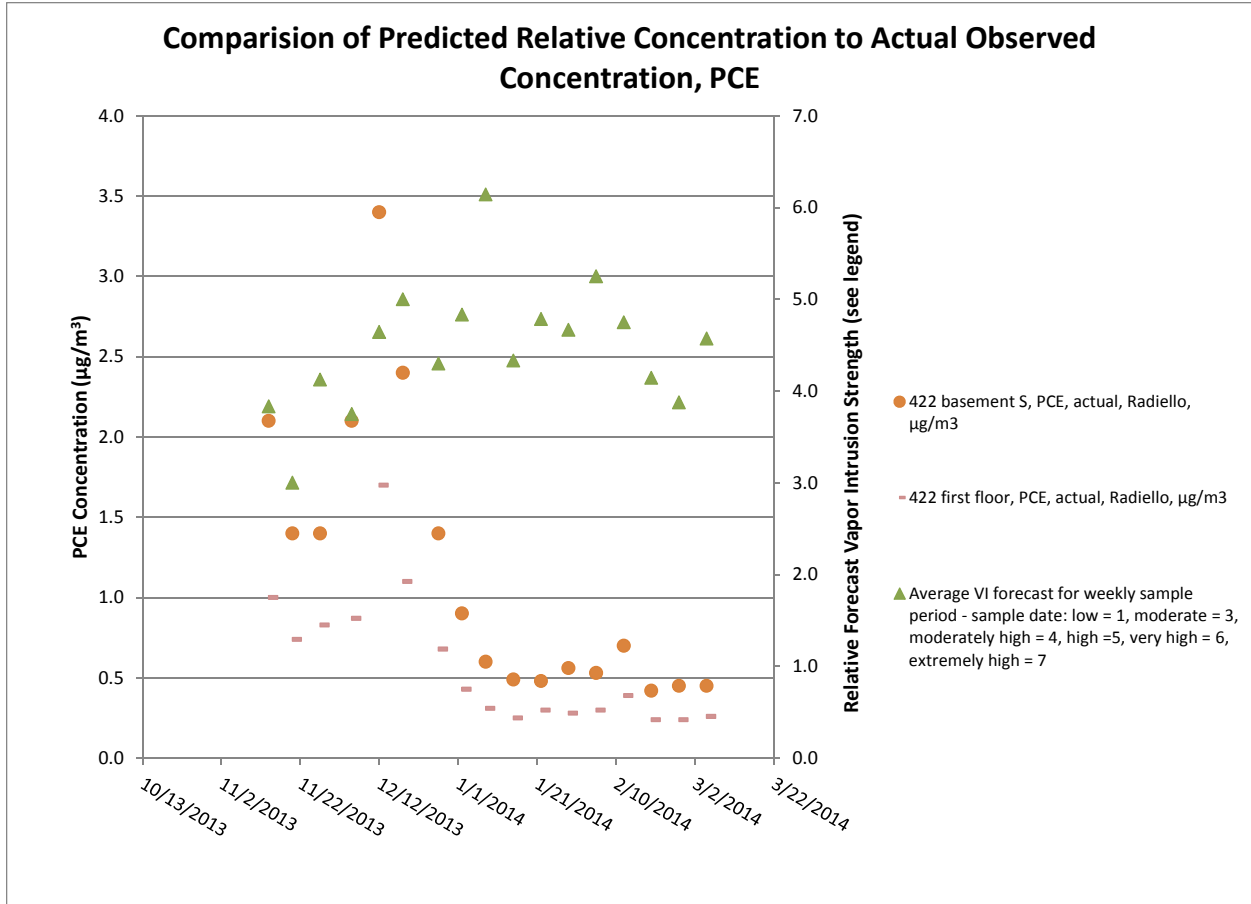


Figure 7-1. Comparison of predicted indoor air concentration to actual observed concentration, PCE.

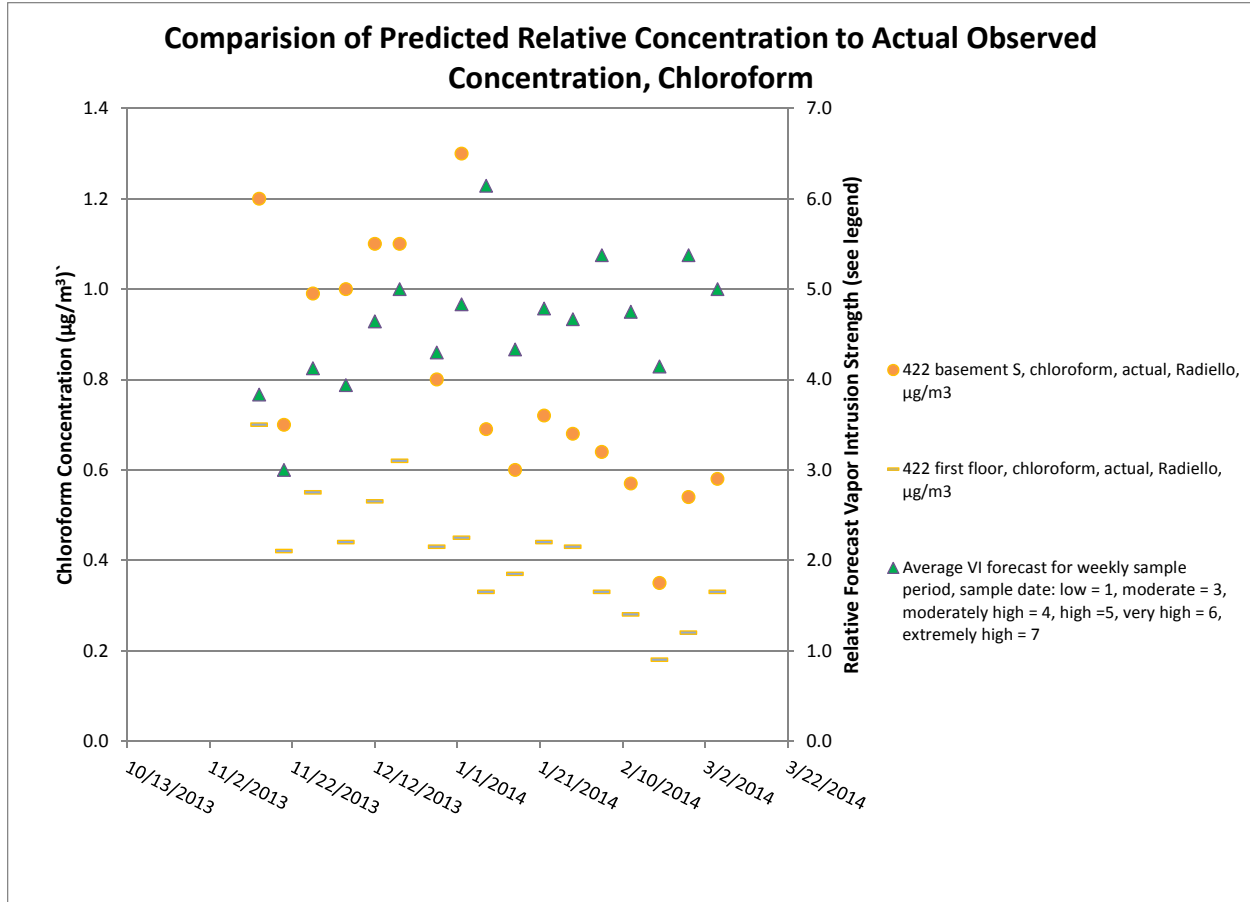


Figure 7-2. Comparison of predicted concentration to actual observed concentration, chloroform.

With regard to PCE (**Figure 7-1**) and chloroform (**Figure 7-2**), there is some agreement between the predicted and observed rises of indoor concentrations in November and December 2013. But unexpectedly, PCE indoor air concentrations started to decline after December 18, 2013. Chloroform also declined after December 18 with the exception of one high point on January 2, 2014. The decline in chloroform was less severe than for PCE. The declines occurred during a period of generally sustained, severe cold. The decline was not predicted.

Although the forecasts were focused on VOCs, the radon concentration was also plotted (**Figure 7-3**) as an indicator of vapor intrusion across the building envelope (see introductory material in Section 2). Radon concentrations had already reached high levels (> 5 pCi/L) typical of previously observed winters by the time prediction attempts began in November 2013 and stayed high (422 basement) or declined (422 first floor, 420 basement) until the mitigation system was restarted March 5, 2014. Thus, our prediction of rising concentrations in November and into December did not match the radon data either. There is some agreement in the predicted and observed slight fall in vapor intrusion due to gradual warming in February.

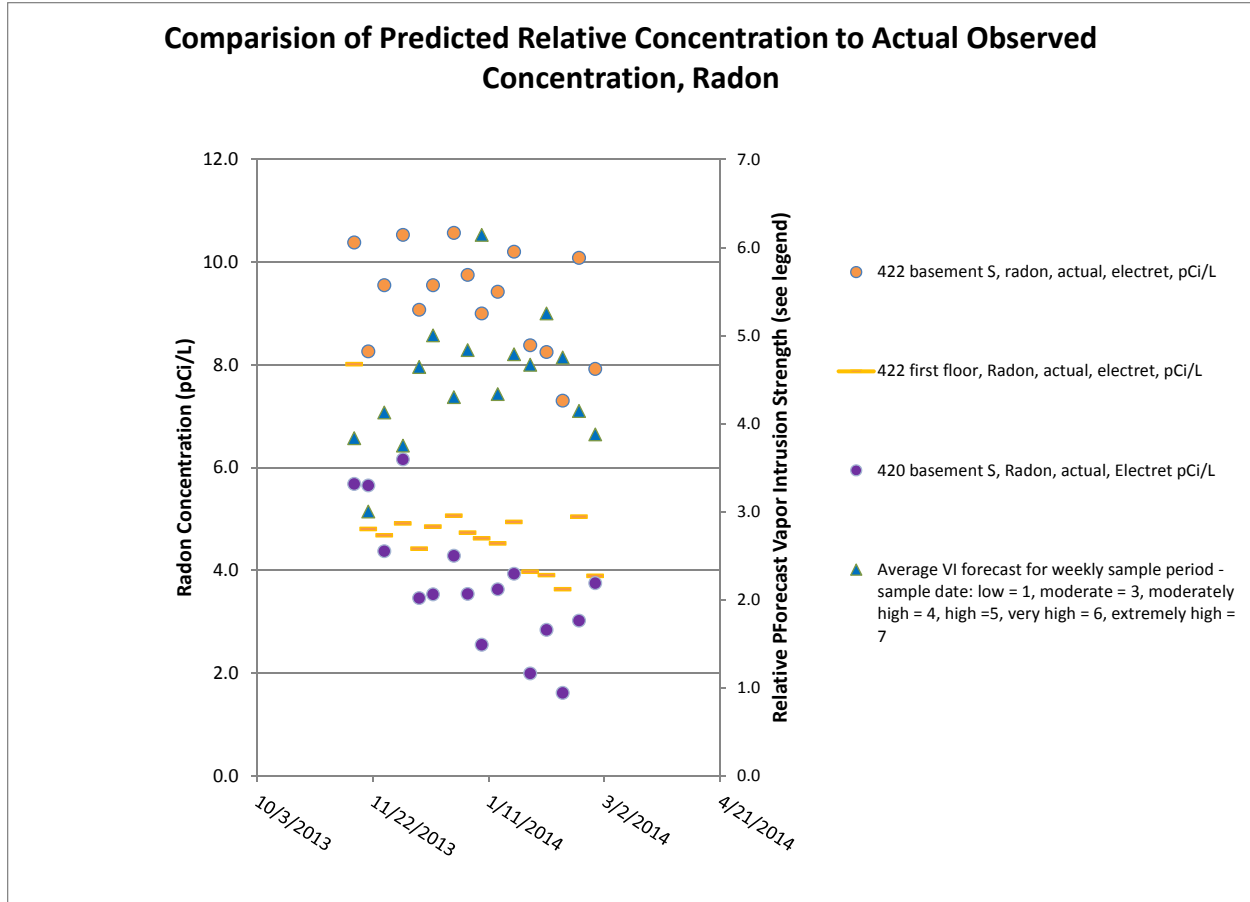


Figure 7-3. Comparison of predicted concentration to actual observed concentration, radon.

The long-term temporal PCE trends for the subslab ports (SSPs) show trends (**Figure 7-4**) that provide additional information about this late-winter decline in indoor air concentrations:

- The highest concentration port, SSP-1 (center of 422 side of duplex), reached a PCE peak of $1,100 \mu\text{g}/\text{m}^3$ on December 8, 2013, close to the previous maximum in early January 2011. This represents a substantial increase over the concentrations observed in October and November 2013. Late fall and early winter increases at that port were also seen between October 2012 and January 2012 as well as between June 2010 and January 2011.
- The second highest PCE port, SSP-4 (southern portion of 422 side of duplex), was at concentrations in October and November of 2013 similar to those observed in most of 2011.
- Both SSP-1 and SSP-4 PCE concentrations show a decline as the winter of 2013/2014 continued. SSP-4 starts declining in late November 2013, but SSP-1 does not start declining until early December 2013. Both ports appear to reach minimums in January 2014 and to begin increasing into February 2014. SSP-1 and SSP-4 PCE soil gas concentrations also went into late-winter dips in a previous winter, between November 2011 and February 2012. In that year, the dip in SSP-4 appears to start before the dip in SSP-1.

Thus, we observe reseasonal-scale trends in PCE soil gas, but they do not occur simultaneously at every location under this small duplex.

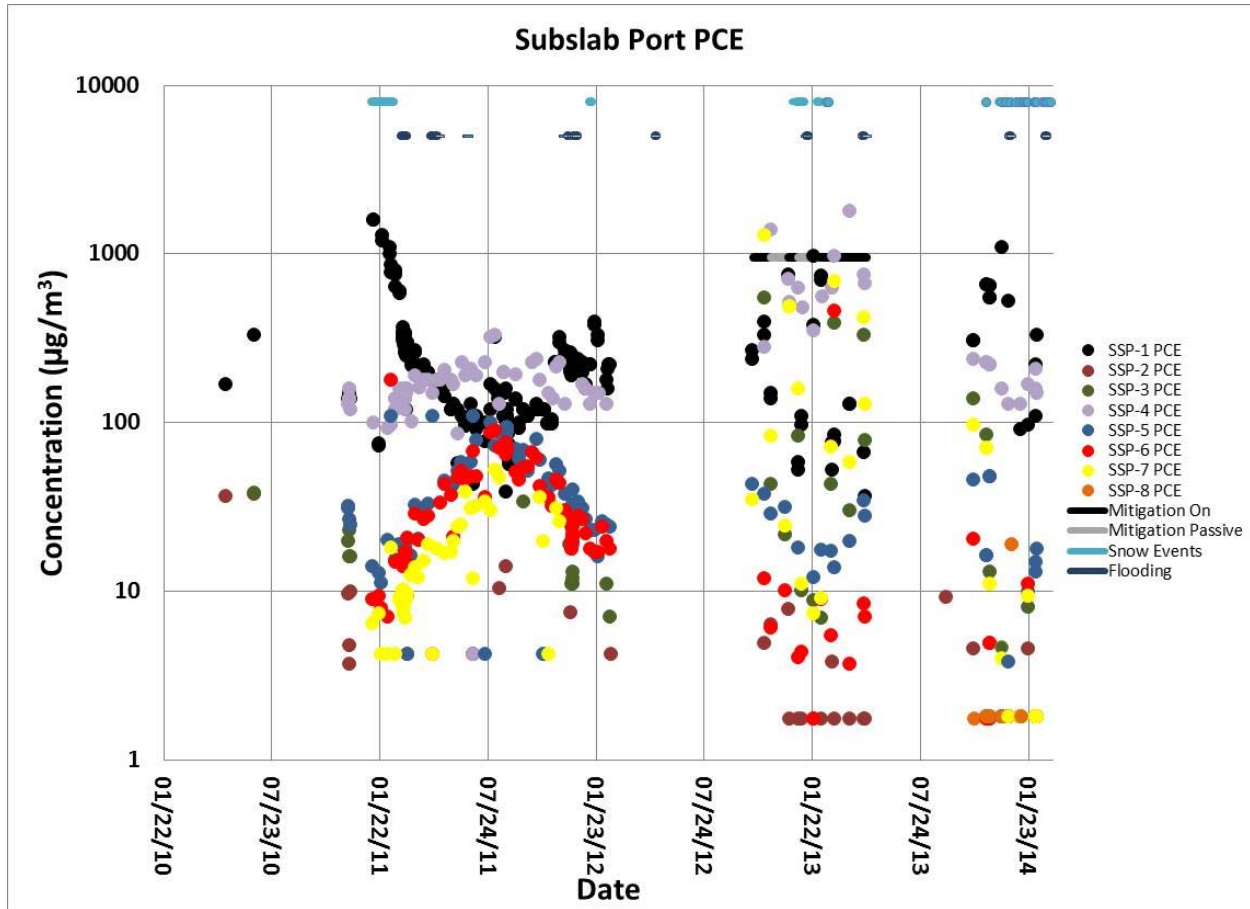


Figure 7-4. Subslab port PCE also showing flood periods (staggered dark blue lines below the light blue lines).

Chloroform also appears to exhibit some reseasonal trends in subslab soil gas (Figure 7-5):

- At SSP-1: A decline is observed from January to March 2011, December 2011 to February 2012, and November 2013 through March 2014
- At SSP-4: An increase is observed from December 2010 through May 2011, September 2011 to January 2012 (no observations after that date in 2012), and November 2013 to March 2014.

Note that the date ranges of these trends may be limited in some cases because sampling was not performed in all months because of resource limitations. Overall, however, the available data suggest that the highest chloroform concentrations consistently relocate from the central to southern portions of the 422 duplex in winter. It is unclear whether this represents a lateral movement of high-concentration soil gas or a change in the vertical migration routes from deep to shallower soil gas.

Given the limited temporal and spatial resolution of the data sets, it appears that there is a general correlation in time between the early-winter peaks observed in subslab soil gas (Figures 7-4 and 7-5) and indoor air (Figures 7-1 and 7-2). However, these observed seasonal trends in indoor air and soil gas do not strictly follow the air temperature, because as is typical, the lowest air temperatures occurred in January 2014.

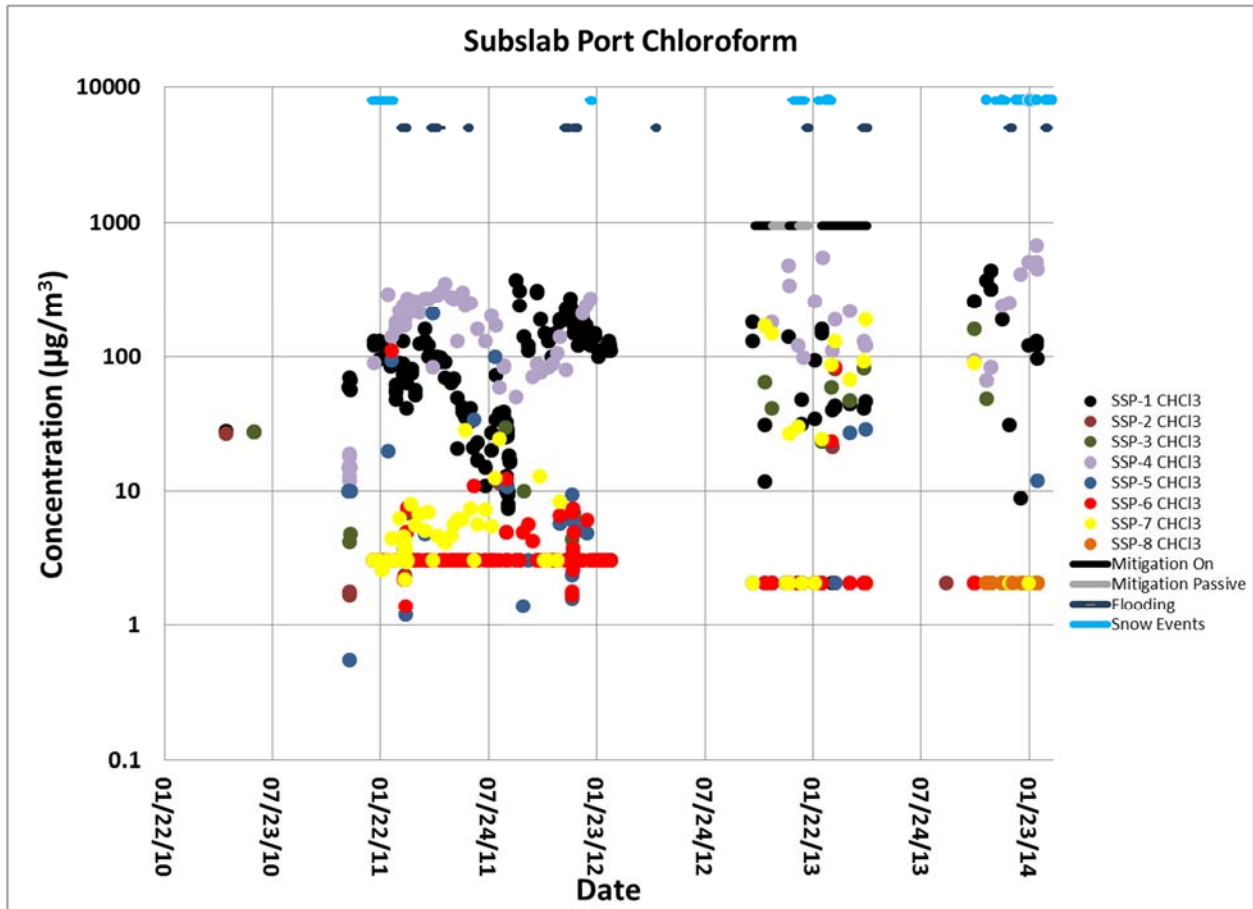


Figure 7-5. Subslab port chloroform also showing flood periods (staggered dark blue lines below the light blue lines).

Mechanisms that could potentially explain such seasonal-scale variations are now being explored such as cumulative “pumping” by the stack effect, temporary depletion of source concentrations, periodic flood events effecting groundwater, and gradual changes in soil temperature. For example, significant cyclical changes in soil gas concentrations due to water variations have been observed in tank experiments reported by Illangasekare and Petri (2013).

7.3 Potential Explanations of Differences between Forecast and Observations

Because the agreement between predicted and observed concentrations was disappointing, we reexamined the data set focusing on

- factors that may not have been well represented in the simple prediction methodology we used (which was focused on the predicted weather conditions for the day in question and less on long-term system behaviors) and
- how the winter of 2013–2014, during which we performed our prediction test, might have been different from the January 2011–April 2013 conditions on which the predictions were based.

7.3.1 Correlations to Change in Stack Effect Strength (as Opposed to Predicted Stack Effect Strength)

We observed a decline in indoor air VOC concentrations during the period of sustained cold weather that occurred during the winter of 2013–2014 in spite of our previous experience, suggesting that cold conditions would be associated with strong vapor intrusion. As discussed in Section 6.2.5.2 for chloroform, there is a potential explanation. The strength of the stack effect predicted by the temperature differential between the 422 basement south and outdoors was significant at the 1% level. A stronger stack effect in the current week was associated with higher concentrations of chloroform. Note, however, that the coefficient of the lagged term for the previous week is negative. Results of this type when the coefficients of the predictor variable in the current period and the lagged period are similar in magnitude but opposite in sign generally indicate that the change in the predictor variable is the factor related to the outcome variable rather than the predictor variable itself. So in this case, increasing values of the stack effect are associated with higher chloroform concentrations, not high values in and of themselves. This result may suggest why chloroform (and PCE) concentrations in our data sets tended to peak in late fall/early winter because that is the time of the year when cooling temperatures would be expected to result in an increasing stack effect. In the midwinter, conditions would be cold in an absolute sense but not as likely to be cooling in a relative sense. In late winter, conditions would be expected to be typically cool in an absolute sense but warming as compared with the proceeding weeks of midwinter. A physical explanation of this result may be that the stronger stack effects encourage advective chloroform migration but that sustained migration may temporarily deplete the source term (such as the concentration of chloroform at the interface between groundwater and soil gas). This behavior has been previously observed in the chamber-scale vapor intrusion experiments of Illangasekare and Petri (2013).

Although they do not reach statistical significance, the time series models for the PCE stack effect generally take the same form as was seen for chloroform. Positive coefficients are generally shown for the $x(t)$ terms, and negative coefficients for the 1-week lag $x(t - 1)$ and/or 2-week lag $x(t - 2)$ terms (see **Attachment 6C, Tables 6C-3, 6C-4, and Attachment 6E, Table 6E-3**). This suggests that for PCE as well increasing values for the stack effect may be associated with higher indoor air concentrations. Conversely, the model would also suggest that if the stack effect strength was still high, but declining, lower concentrations would be predicted.

7.3.2 Effects of Annual or Rarer Flooding Events (and high water table)

Since the beginning of the project at the 422/420 duplex, there have been several flood periods in nearby Fall Creek (defined as stream discharge greater than 2,000 cubic feet per second [cfs]). These periods are summarized in **Table 7-3**. Most of the floods occurred in early 2011, but one of the highest discharges occurred in late 2013.

As discussed in Section 11 of U.S. EPA (2013), there is a very strong relationship between Fall Creek gage height and groundwater levels under the duplex. **Figure 7-6** plots water-level depth below land surface (bls) versus time as recorded by the onsite well water-level logger. It has been in service since December 14, 2012. Four major flooding events are presented on this figure: January 15, 2013 (11.6 ft bgs); April 19, 2013 (12.3 ft bgs); December 23, 2013 (10.2 ft bgs); and February 22, 2014 (12.8 ft bgs). Each of these events corresponds well with a major 2013–2014 flooding event well over 3,000 cfs.

Figure 7-7 shows water-level depth for the entire project period, with the data before December 2012 based on a model fit to the stream gauge data from Fall Creek (blue dots), which accurately matched the manual water levels taken on site occasionally during that period (red dots). **Figure 7-7** shows that the December 2013 flood was one of the highest during the study and occurred unusually early in the winter; most major flood events (5,000 cfs peak flow in Fall Creek with corresponding water at 13 ft or above on site) occurred in late winter or early spring.

Table 7-3. Flooding Events During Project Period (stream discharge greater than 2,000 cfs in Fall Creek)

Start Date/Time	Stop Date/Time	Stream Discharge (cfs)
2/28/2011 2:30	3/3/2011 3:00	7,180
3/5/2011 4:30	3/8/2011 9:00	5,780
4/19/2011 13:30	4/22/2011 14:15	4,330
4/25/2011 23:30	4/29/2011 6:45	2,310
5/3/2011 16:00	5/4/2011 18:15	2,190
6/20/2011 9:15	6/21/2011 18:00	4,480
11/30/2011 0:15	12/1/2011 8:00	2,220
12/5/2011 22:45	12/7/2011 14:30	2,450
12/15/2011 12:15	12/17/2011 3:45	2,480
12/21/2011 12:15	12/22/2011 23:00	2,410
5/2/2012 10:15	5/3/2012 3:45	2,150
1/12/2013 23:00	1/16/2013 3:30	6,490
4/17/2013 1:45	4/21/2013 2:15	4,080
4/24/2013 12:00	4/25/2013 21:00	2,410
12/21/2013 13:30	12/25/2013 3:30	9,670
2/20/2014 23:15	2/23/2014 22:15	4,930
4/3/2014 12:15	4/5/2014 23:00	3,790

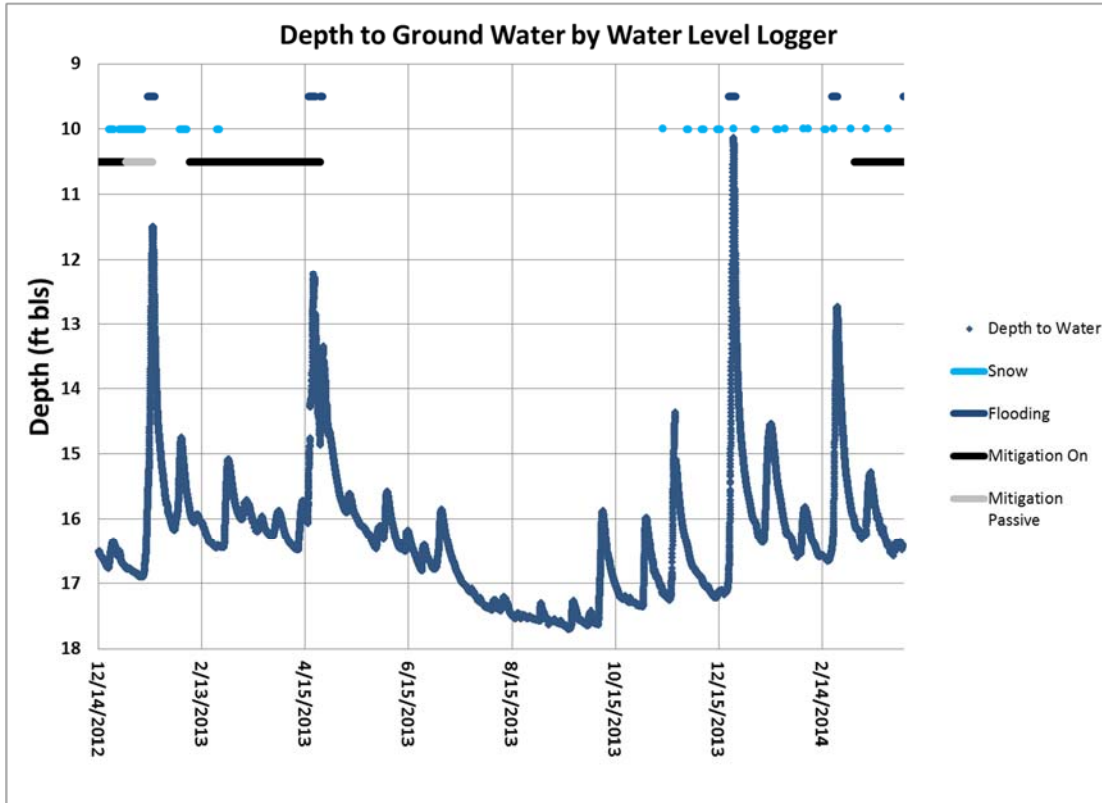


Figure 7-6. Depth to groundwater as measured by the 422 well water-level logger (2012–2014).

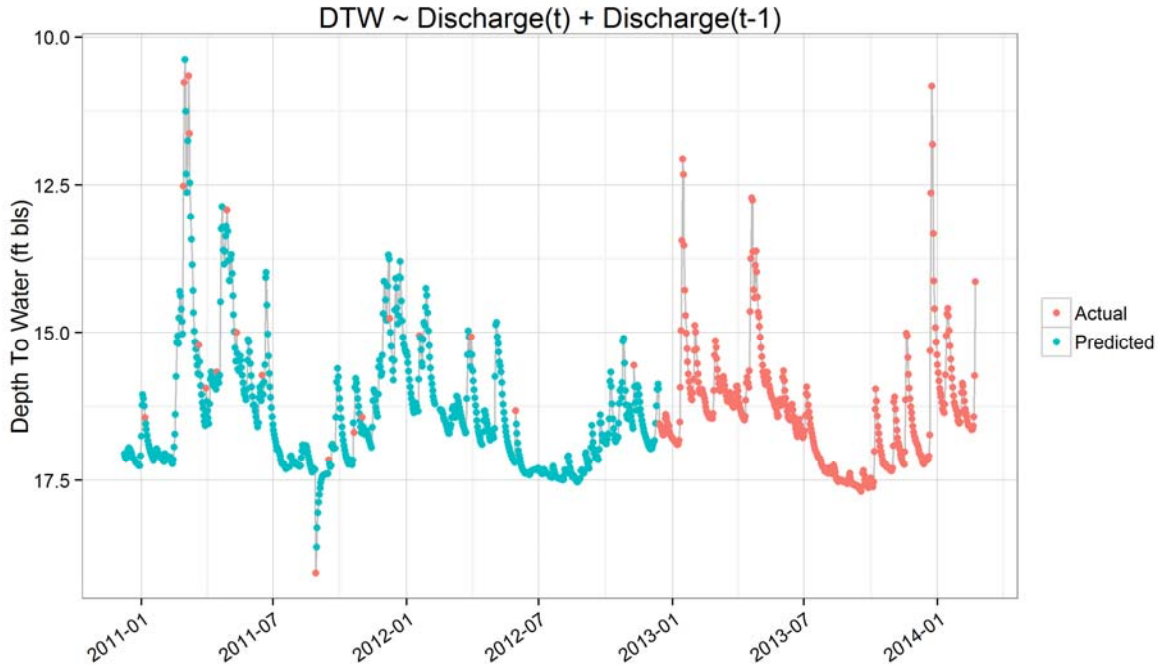


Figure 7-7. Depth to groundwater at duplex, including actual water-level logger and manual depth to water measurements and a predicted model based on Fall Creek stream gage data.

Figures 7-4 and 7-5 plot PCE and chloroform, respectively, for all the subslab ports found at the 422/420 house. Focusing on the time periods before and after the main mitigation on/off cycles (these cycles made patterns within the subslab data uncertain), there appears to be a suggestive relationship between subslab port VOC concentration and flood events (dark blue lines across the tops of the figures). This possible relationship can be best seen in wall ports 1 (black circles) and 4 (light purple circles), both on the 422 side of the duplex, in the central and southern basement segments, respectively. What is interesting is that both chloroform and PCE do not appear to behave the same way. Chloroform concentrations seem to increase at SSP-4 during periods of extended flooding, and concentrations seem to decrease at SSP-1 at roughly the same time. This “seesaw” effect may be due to mass movement in the subsurface from the central section of the 422 basement (SSP-1) to the southern section (SSP-4) (**Figure 7-5**). PCE, however, does not appear to behave in the same way (**Figure 7-4**). Both SSPs-1 and -4 seem to decrease to a greater or lesser extent during heavy or extended periods of flooding. For both compounds, one of the sharpest examples of this behavior can be found near the period of the December 23, 2013, flooding event (9,670 cfs), where concentrations fell by as much as an order of magnitude (**Figures 7-4 and 7-5**).

The time series analysis of water level did not reach statistical significance for the predictor variables “DepthToWater” and “Fall_Crk_Gage_ht_ft.” However, if the effect is due to extreme values of these variables that occur only occasionally the time series analysis, for which the longest continuous weekly data set was about 13 months, might not have been long enough to detect it. Note also that most of the time series analyses were done using indoor air rather than soil gas as the outcome variable. If soil gas concentrations were used as the outcome variable, it may have been more sensitive because building envelope effects would not complicate the analysis.

7.3.3 Winter to Winter Soil Gas Comparison

In an effort to understand how the winter of 2013–2014 may have differed from previous winters, we examined the temperature trend (**Figure 7-8**). The winter of 2013–2014 had the lowest temperatures and the most sustained low temperatures of any period since the beginning of the project (**Figures 7-8** and **7-9**). January 2014 also saw an unusually high snowfall and period of snowpack (**Figure 7-10**). If the response of indoor concentration to temperature is linear, then this would have been expected to result in the highest observed indoor concentrations. However, the potential for nonlinear effects (such as freezing) cannot be ruled out.

Note that in each year the lowest ambient temperatures are typically experienced in January.

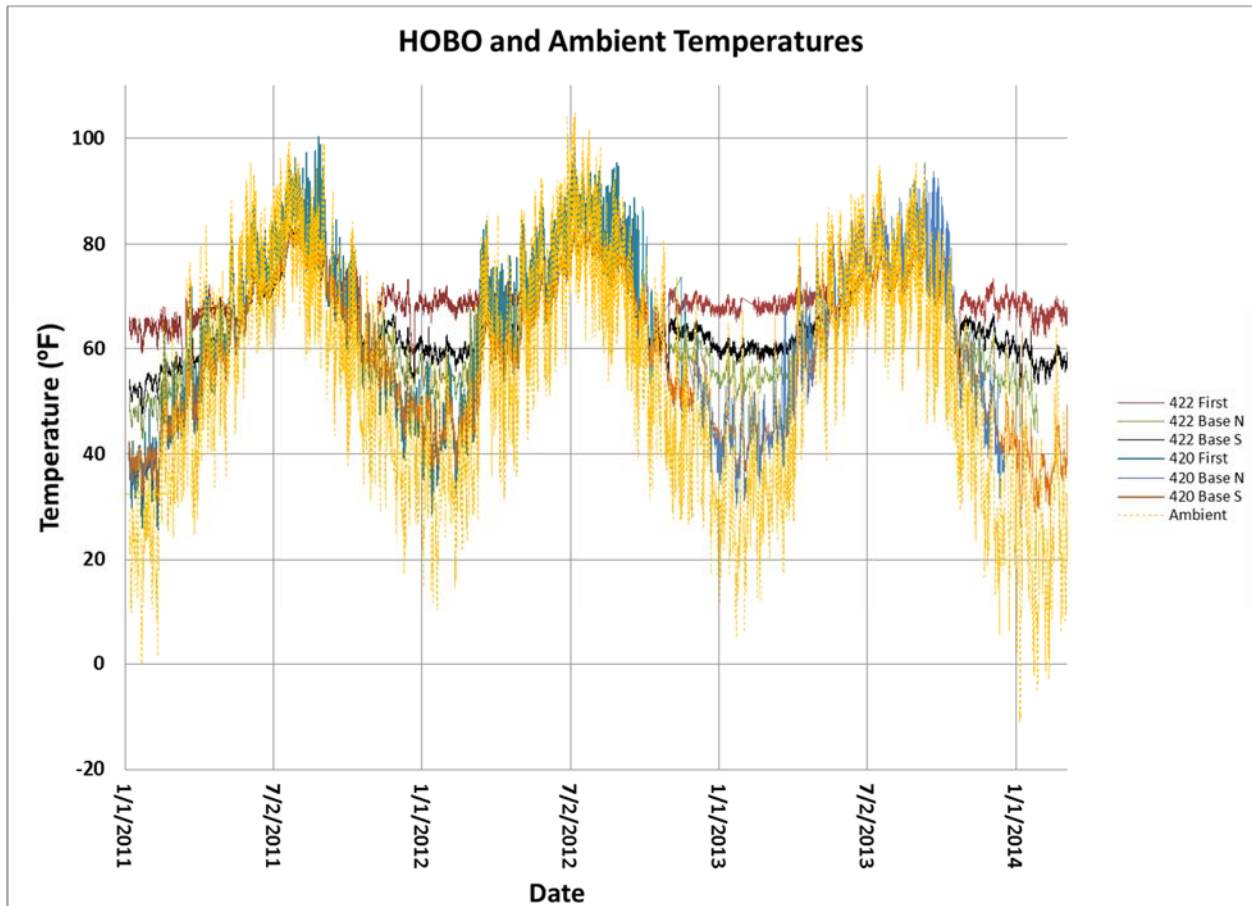


Figure 7-8. Indoor and ambient temperatures observed during project period (January 2011 through March 2014).

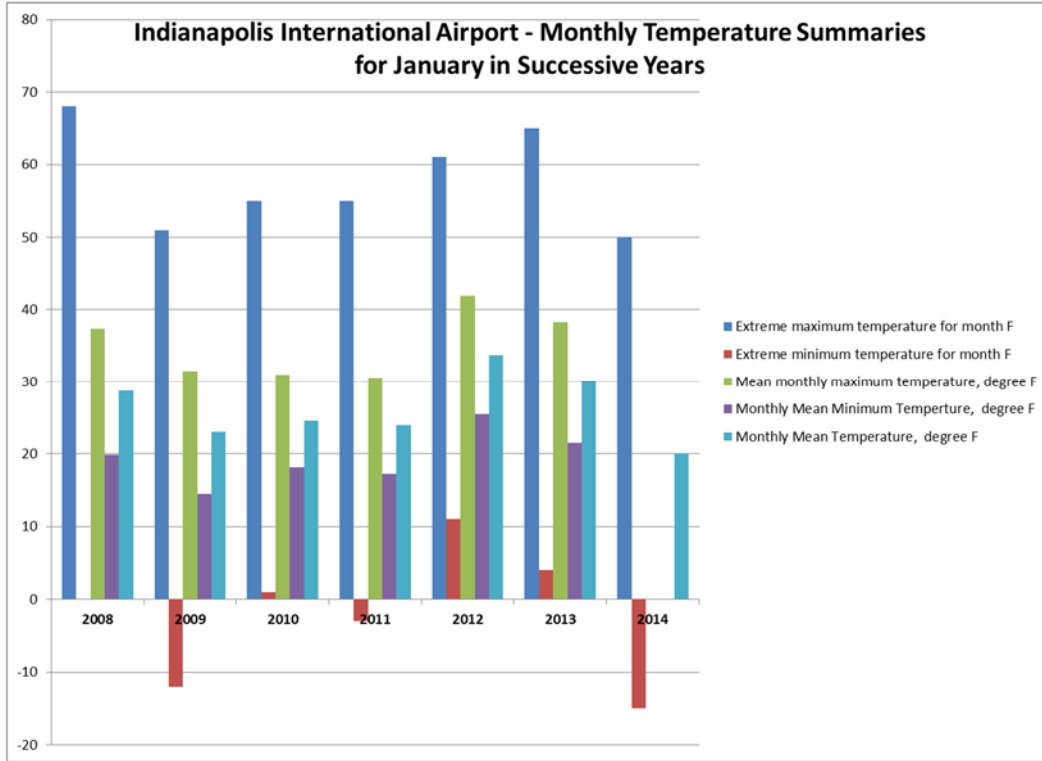


Figure 7-9. Comparison of monthly temperatures—extremes and means for January in 6 successive years.

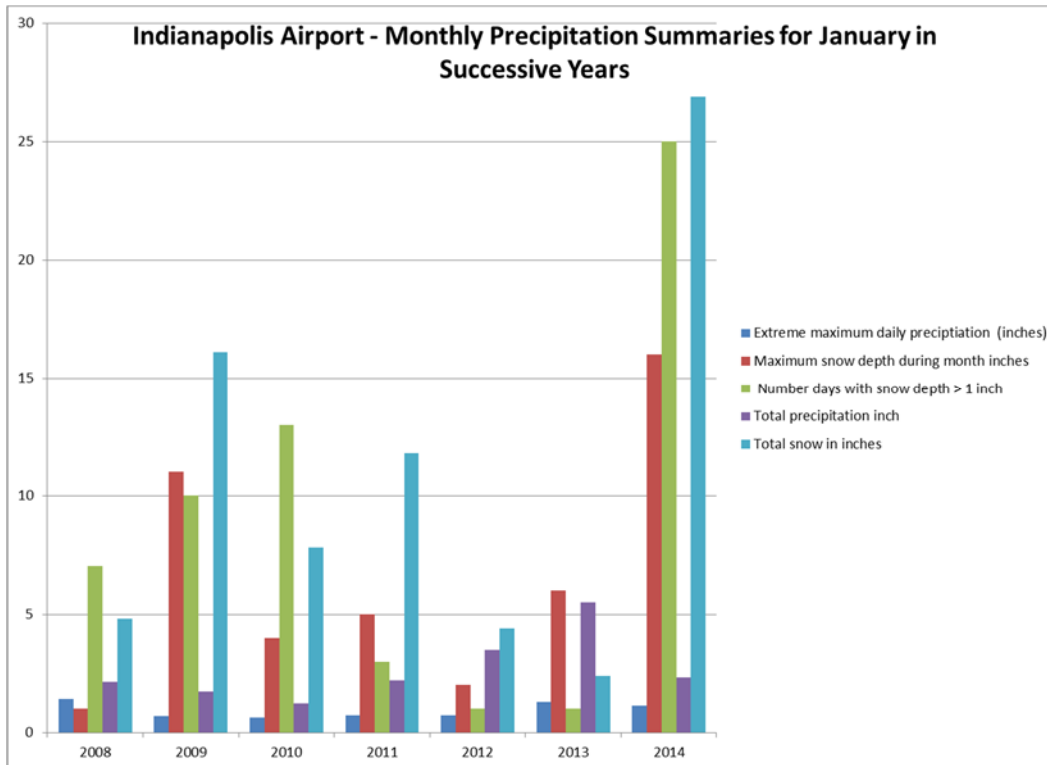


Figure 7-10. Comparison of monthly snowfall—extremes and means for January in 6 successive years.

A review of the indoor air data shows that the radon concentration in January in this duplex was virtually constant over 4 successive years (**Table 7-4**). Radon was also essentially constant in December and January of the four successive winters (**Tables 7-5** and **7-6**). This suggests as a first approximation that the radon source concentration and subslab to indoor air attenuation factors were relatively constant and thus not particularly sensitive to the year-to-year variation in winter conditions.

PCE concentrations were highly variable in indoor air (year-to-year variation of monthly average >15x). Subslab concentrations in January similarly varied year to year more than 15x. However, subslab concentrations in December were considerably less variable. This suggests that the differences in subslab concentrations from year to year are more pronounced in the midwinter than in early winter.

Chloroform’s behavior was intermediate between the consistency of radon and the variability of PCE. Average indoor air and subslab chloroform concentrations varied 3x between Januaries in the 4 years studied. These differences in the degree of year-to-year variability between radon, PCE, and chloroform in the same building over the same years suggest that differing mechanisms link weather and subslab/indoor concentrations for these three constituents. The conclusion of differing mechanisms also logically follows from the documented different distributions of PCE and chloroform at this site and the known short half life of radon that limits the distance over which it can travel.

Table 7-4. Comparison of Indoor Air Concentrations in Four Successive Januaries

	Screening Level	2011	2012	2013	2014
422 Basement South—January					
Radon (pCi/L)	4	9.4	8.8	9.5/3.6**	9.35
PCE (µg/m ³)	4.2	11.4	0.89	2.1/0.7**	0.606
Chloroform (µg/m ³)	0.11	1.2	0.7	0.69/0.29**	0.798
422 First Floor—January					
Radon (pCi/L)	4	5.3	4.4	4.1/1.6**	4.56
PCE (µg/m ³)	4.2	5.8	0.43	0.94/0.3**	0.314
Chloroform (µg/m ³)	0.11	0.65	0.3	0.38/0.22**	0.404

VOCs—residential RSL 10-6 Nov 2013

** Mitigation Off/On (or on in Passive mode)

Table 7-5. Comparison of Average Subslab Concentrations in Four Successive Decembers—422 Side of Duplex (µg/m³)

	2010	2011	2012	2013
422 Subslab—December				
Chloroform	27	180	NA/207**	49
Radon		1,265	1,253/569**	1132
PCE	90	202	NA/493**	131

**Table 7-6. Comparison of Average Subslab Concentrations in Four Successive Januarys—
422 Side of Duplex ($\mu\text{g}/\text{m}^3$)**

	2011	2012	2013	2014
422 Subslab—January				
Chloroform	105	133	71	49
Radon	1,179	1,184	1,240	1,212
PCE	591	230	341	36

A comparison of soil gas across depths for the heating seasons of the study at interior locations (**Figures 7-11** and **7-12**) suggests on the 422 side (SGP-8 and SGP-9 clusters) that the concentrations in the winter of 2013–2014 were typical for PCE and chloroform while the 2012–2013 concentrations (the period of mitigation testing) were outliers. PCE concentrations at SGP-10 (422 North), SGP-11 (420 Central), and SGP-12 (420 South) were lower in all periods than SGP-8 and SGP-9. For those three lower concentration locations, soil gas concentrations were even smaller in the 2013–2014 winter. Thus, the differences between high and low concentrations ports were more dramatic in the 2013–2014 winter than had previously been the case. Because the mass flux from a zone of the subslab is not necessarily proportional to the concentration in that zone, it is possible that these lower concentrations at SGP-10, SGP-11, and SGP-12 are mechanistically related to the lower indoor air concentrations observed in the winter of 2013–2014.

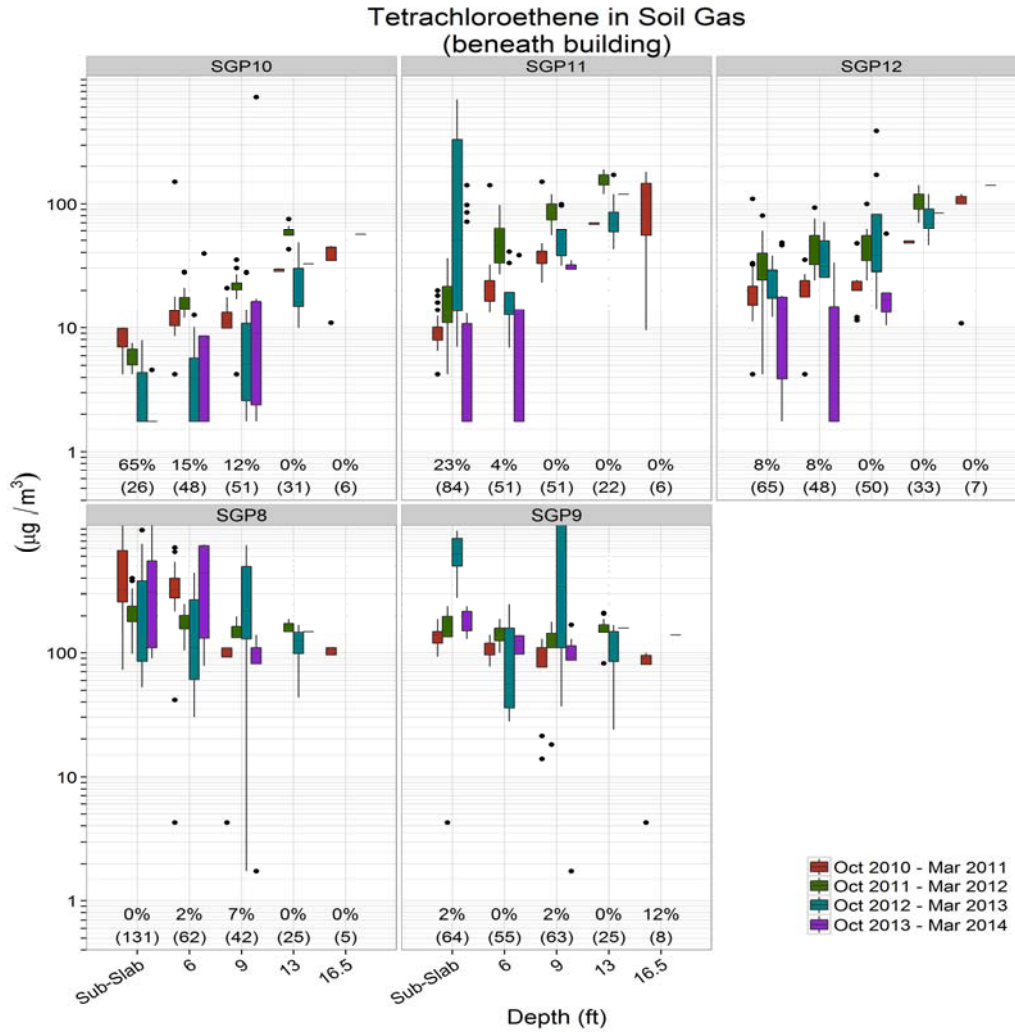


Figure 7-11. Box and whisker plot for PCE comparing four heating seasons (October to March) interior locations.^a For each location, five depths are plotted from subslab to 16.5’.

^aIn these plots, note that beneath each bar/whisker two numbers have been provided: the percentage of nondetects in the data set and the number of samples in the data set. Nondetects have been included in the plotted bar/whiskers. The top of each bar represents the third quartile (75th percentile) of the data, the line through the middle of the bar represents the median of the data set, and the bottom of each bar represents the lower quartile. The top of each whisker represents the largest value not considered an outlier. The bottom of each whisker represents the smallest value not considered an outlier. Data points beyond the whiskers are individually plotted as dots (although multiple nondetects will plot on top of one another). An “outlier” in a boxplot is any point greater than 1.5*Interquartile Range (1.5*q3-q1) or smaller than 0.5*IQR. In addition to plotting the four depths in each interior soil gas cluster, we have also plotted the corresponding nearest conventional subslab port as follows:

- SGP-8, with SSP-1
- SGP-9 with SSP-4
- SGP-10 with SSP-2
- SGP11 with SSP-3 and SSP-7 together
- SGP-12 with SSP-5”

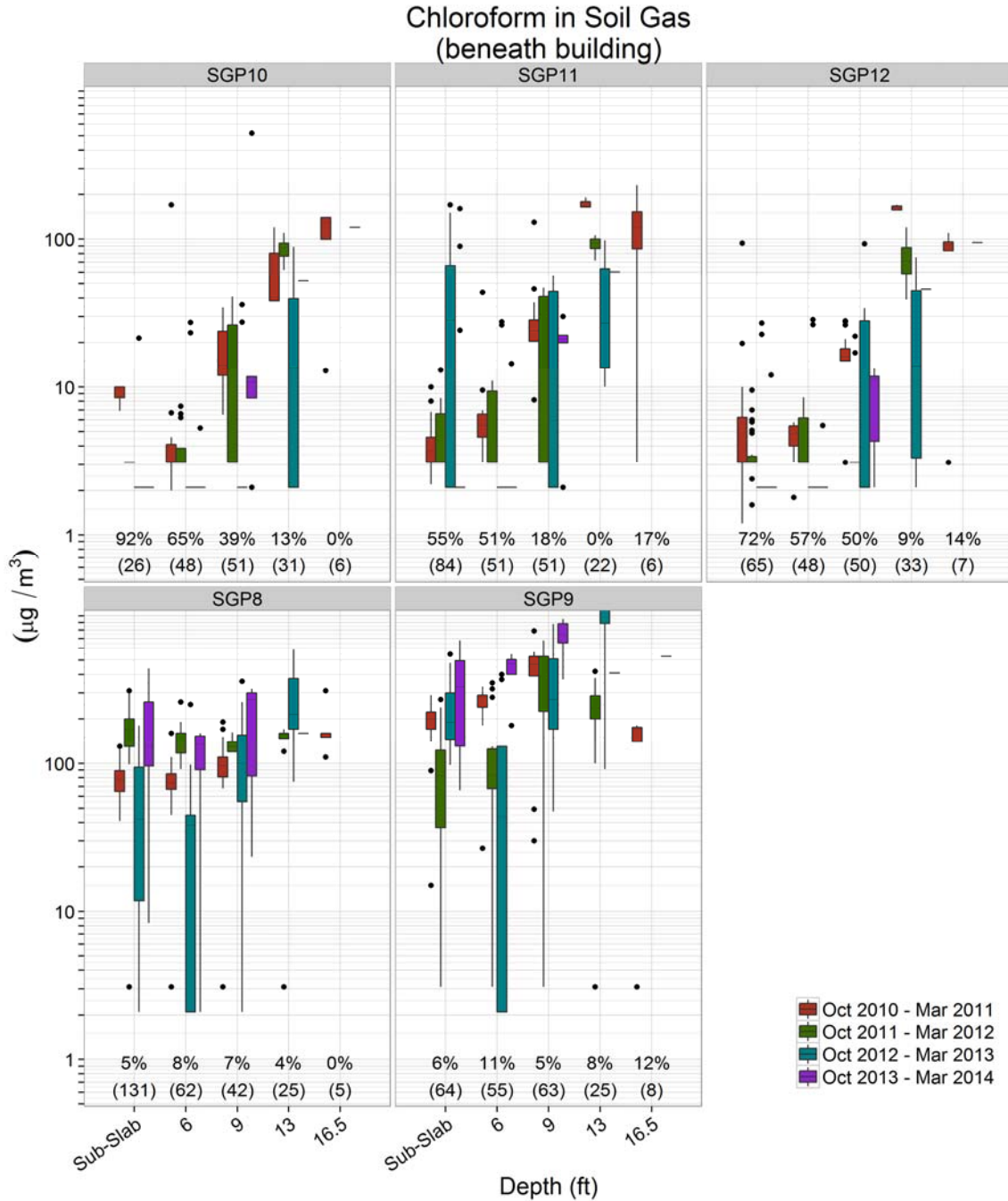


Figure 7-12. Box and whisker plot for chloroform comparing four heating seasons interior locations (October to March) for each location five depths are plotted from subslab to 16.5'.

A comparison of soil gas across depths for the heating seasons of the study at exterior locations (**Figures 7-13** and **7-14**) does not reveal any clear, consistent trends between years. Broadly, similar soil gas concentrations seem to have been available in these 4 years, but the indoor concentrations of PCE as seen before are highly variable.

7.4 Summary and Implications of Forecasting Results

The results in Sections 6 and this section suggest that although some meteorological variables have an association with higher indoor concentrations, our understanding of the interactions between these variables was not sufficient to predict peak indoor concentrations with a degree of uncertainty small enough to be useful, even in this highly studied duplex. Underlying gradual seasonal trends in subslab soil gas concentrations appear to be present in the data set that were not well predicted based on our 7-day forecasts. Specifically, PCE and chloroform concentrations peaked early in the winter of 2013–2014, before the winter’s coldest temperatures were experienced. Several mechanisms, such as temporary depletion of soil gas concentrations and periodic flood events affecting groundwater levels, could potentially explain such seasonal-scale variations.

The observed decreases in VOC concentration that started in mid-December 2013 have significant implications for sampling guidance if they can be replicated at other houses. Current state sampling guidance mostly assumes that any time in the winter heating season would be a near worst case sample, although California (CA DTSC, 2011; 2012) favors late winter/early spring. The slope of that observed decline in PCE in indoor air in this duplex is noticeably similar between the January through June 2011 sampling period as well as December 2013 through February 2014. Thus, we have observed in two winters a similar decline in indoor concentrations from an early winter peak. Based on our observations, early winter (falling temperatures) may be a more useful time to capture the peak vapor intrusion conditions than midwinter. However, in situations where changes in the depth to groundwater were dominant, a late winter/early spring peak water sampling round may also be useful.

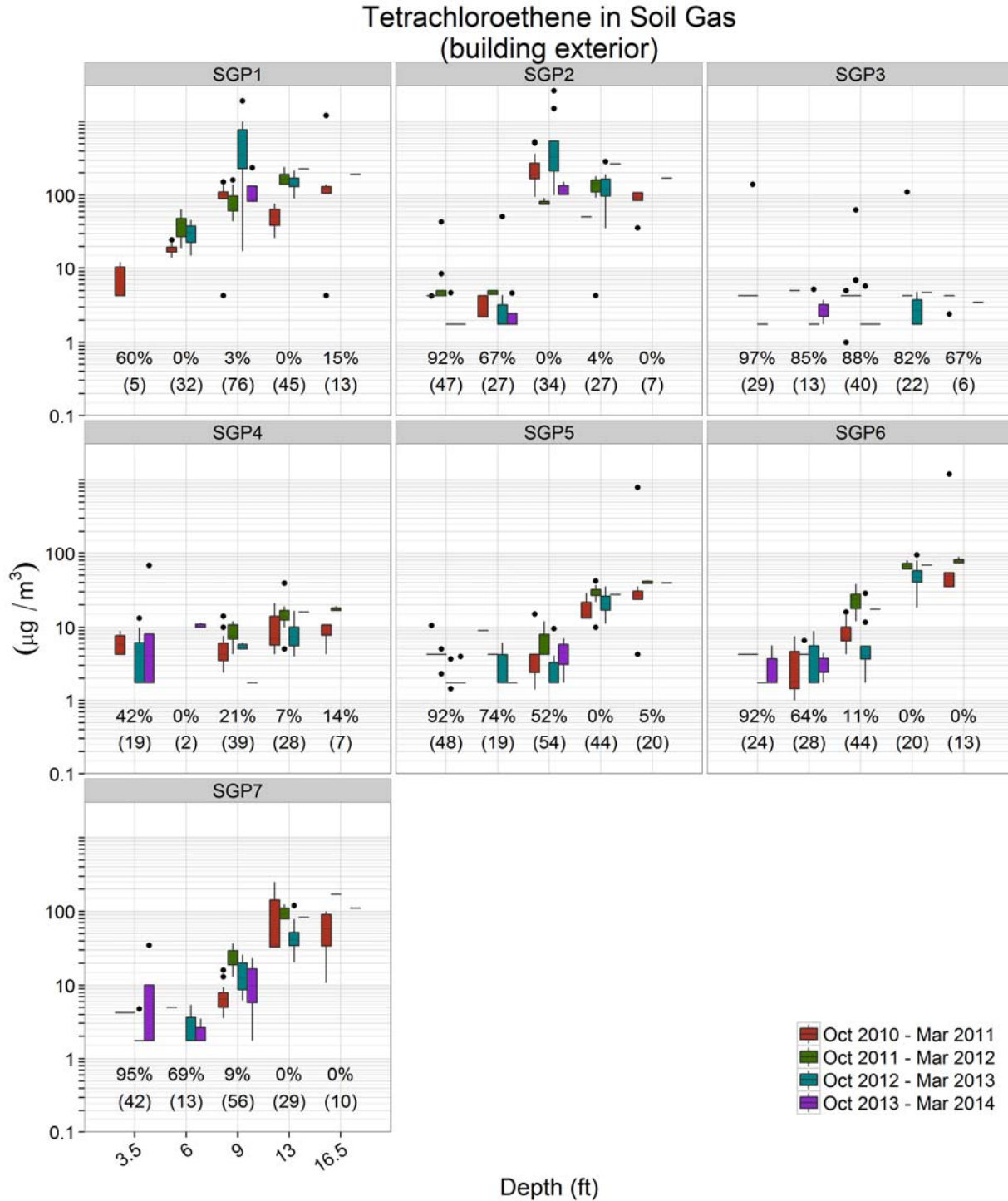


Figure 7-13. Box and whisker plot for PCE comparing four heating seasons (October to March) exterior locations; for each location five depths are plotted 3.5 to 16.5'.

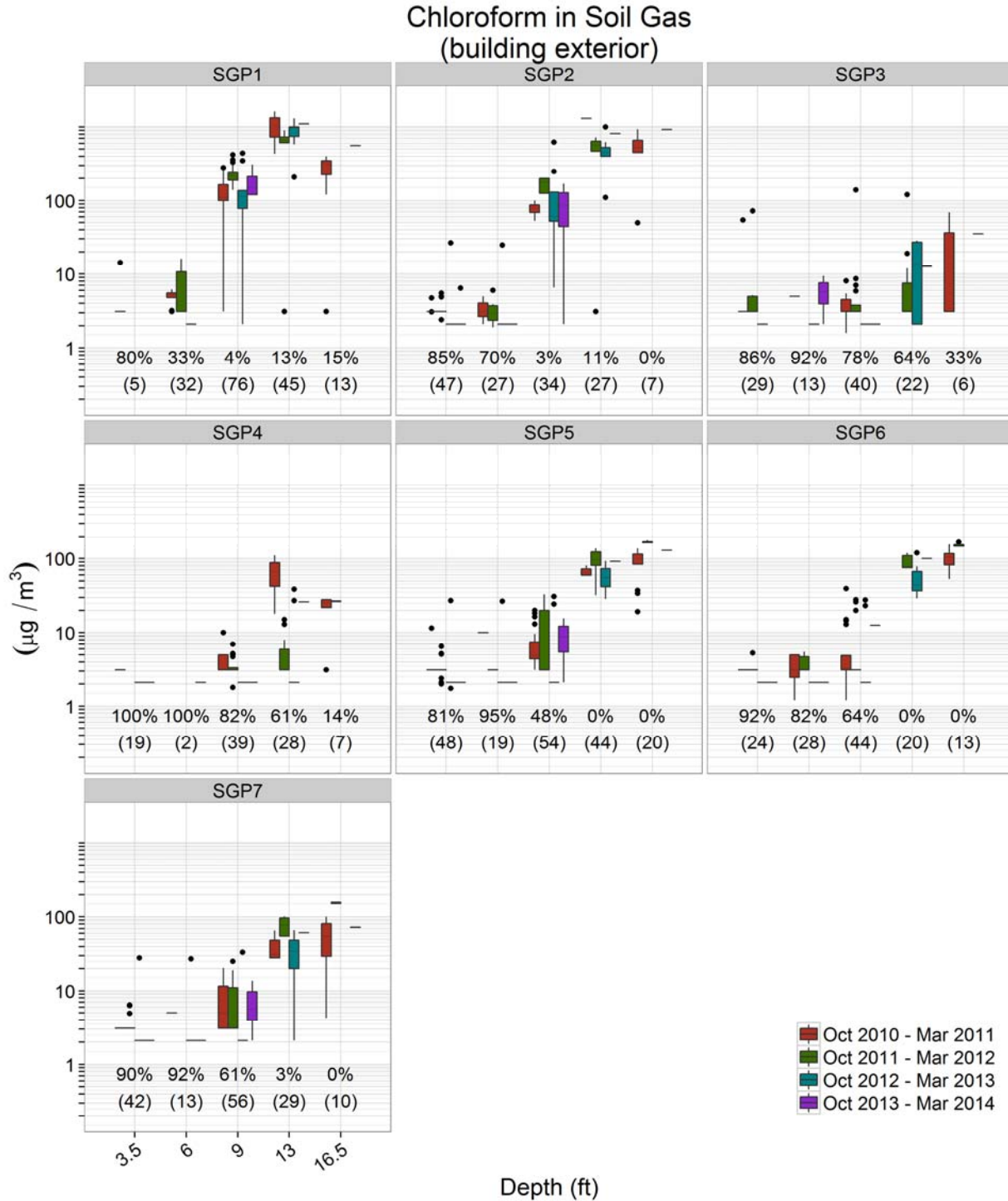


Figure 7-14. Box and whisker plot for chloroform comparing four heating seasons (October to March) exterior locations; for each location five depths are plotted 3.5 to 16.5'.

8. Groundwater Results

Section 11 in U.S. EPA (2013) assembled the available groundwater data (through May 2013) to determine whether groundwater concentrations at the site control soil gas and indoor air concentrations and whether the groundwater concentration trend is correlated to well or water depth. With respect to the latter, although a strong correlation between well depth and VOC levels was not evident, high PCE concentrations did correspond with the low groundwater levels observed in September–October 2011, which could be attributed to water decline or the lack of infiltration of freshwater.

In terms of groundwater as a VOC source, U.S. EPA (2013) concluded that there was more than enough PCE dissolved in the groundwater to serve as a source for the chemical vapor intrusion at the site, although the stability and narrow range of variability (less than an order of magnitude) in PCE concentrations made it unlikely that changes in groundwater concentrations are the causes of the changes in soil gas or indoor air concentrations over the course of the study. The study did conclude that groundwater was a likely source of the PCE vapors observed in the subsurface and indoor air during this study. However, the same conclusion could not be made about chloroform, where, based on limited data, groundwater concentrations did not appear sufficient to drive the soil gas and indoor air concentrations measured under and in the study duplex, suggesting that other sources may be responsible for the observed peak soil gas and indoor air chloroform concentrations.

This section updates the previous discussions and data summaries on groundwater levels and VOC concentrations (including better chloroform data), as well as additional spatial and temporal analyses of VOC concentrations in groundwater and their relationship to VOC vapor concentrations in soil gas.

8.1 Groundwater Level (Water Table) Changes beneath the Duplex

U.S. EPA (2013) describes how we took advantage of a strong correlation between depth to groundwater beneath the 422/420 house and the discharge and gage height of Fall Creek, which is about 300 ft south of the duplex, to develop a model to hindcast our continuous water-level data from the beginning of the project until November 9, 2012. Since that point, we have used a Solinst water Levelogger Model 3001 in the deepest well (MW1A) to record groundwater levels.

Figure 8-1 provides the full record of groundwater levels beneath the 420/422 duplex. As before, the lowest water levels were recorded in the summer months, with lows in the 17.5 ft bls range occurring each year (2011, 2012, and 2013). The hot and dry conditions in the summer of 2011 resulted in the lowest water depth recorded during this project (about 20 ft bls). The highest groundwater levels in the project occurred in response to heavy rain events in early March 2011, at about 9 ft bls. Fall Creek discharge flood events in early 2013 also were reflected in a higher water (12–13 ft bls), and in late December 2014, both the creek and groundwater water levels exhibited an 11 ft bls peak close to the March 2011 high water level of 10.5 ft bls.

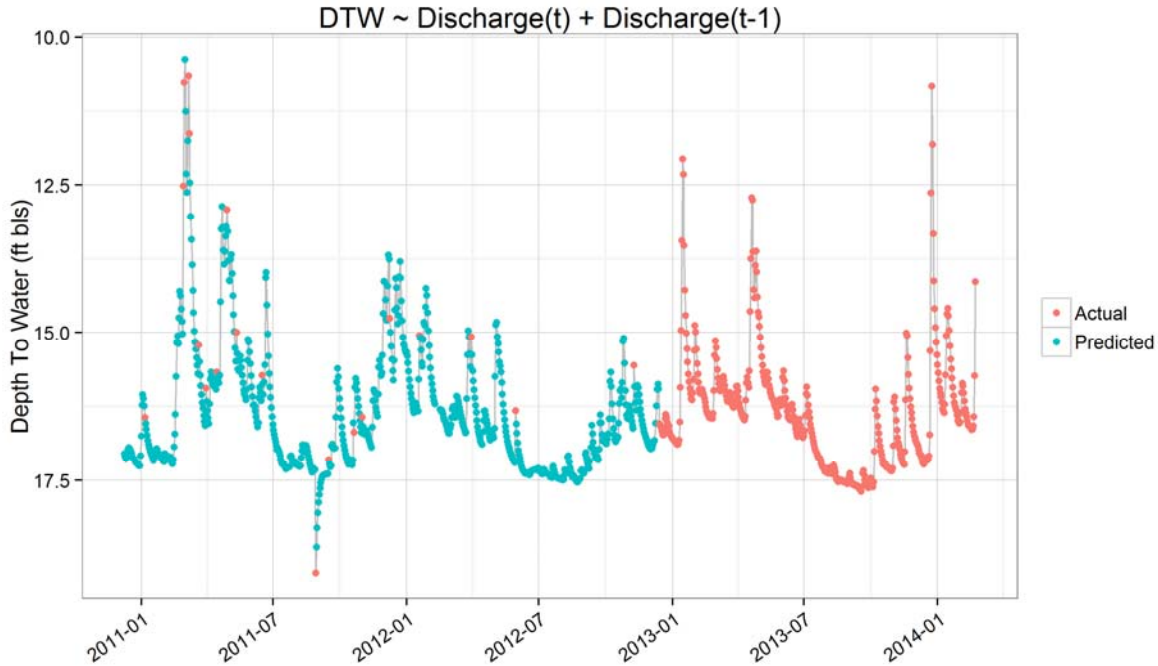


Figure 8-1. Depth to groundwater at duplex, including water-level logger data and manual depth to water measurements (red) and a predicted model based on Fall Creek stream gage data (blue).

8.2 Groundwater VOC Concentration Trends

During initial screening conducted in late spring 2010 at the site (U.S. EPA, 2012a), groundwater had detectable but low concentrations of PCE and chloroform, with PCE concentrations ranging from 0.46 to 0.61 $\mu\text{g/L}$ and chloroform levels ranging from 1.9 to 3.0 $\mu\text{g/L}$; although the data were subject to qualifiers related to the very low levels of analytes in the samples, the analyst believed that the analytes were present. In addition, a June 2005 groundwater sampling event associated with the nearby Mapleton-Fall Creek brownfields site found detectable chloroform (8.9 to 22.1 $\mu\text{g/L}$) in groundwater. However, regular groundwater sampling did not find comparable chloroform levels in groundwater, with only nondetects being seen in the first phase of this project (U.S. EPA, 2012a) and detectable concentrations lower than those observed during screening during this phase. PCE levels were similar to the screening levels during the first phase and remained so in this second project phase.

As described in **Section 3**, groundwater was sampled for VOC analysis approximately monthly during the active project. One hundred ninety groundwater samples were collected and analyzed over the two project phases from the six monitoring wells (two 3-well clusters) and from the flooded soil gas ports at 13 and 16.5 ft bls. **Table 8-1** (updated from U.S. EPA, 2013) shows the sampling locations, screened interval, and number of samples collected from each well and from the soil gas ports for the period of record of this project (February 28, 2011–April 2, 2014).

Table 8-1. Groundwater Monitoring Locations

Well ID	Screened Interval Depth (ft bls)	No. Measurements	Location
MW1A	24–26	9	Exterior South
MW1B	21–24	26	Exterior South
MW1C	16–21	30	Exterior South
MW2A	24–26	25	Exterior North
MW2B	21–24	20	Exterior North
MW2C	16–21	27	Exterior North
MW3	19.5–24.5	24	422 Basement
SGP GW points ^a	13–16.5	29	Various

^a Flooded soil gas ports

Figure 8-2 shows the groundwater concentrations of PCE and chloroform over the project to date. Nondetect samples are plotted at half the detection limit as open symbols for each chemical. Note the high detection limits for PCE (2.8 µg/L) and chloroform (2.0 µg/L) in the February 2011 to April 2012 time frame that are considerably higher than the detectable concentrations in the rest of the figure. EPA NERL improved the detection limits and instrument sensitivity for both chloroform and PCE later in 2012.

Chloroform was first detected on February 5, 2013, when it was detected at 1.25 µg/L in two samples (passive diffusion bag [PDB] and peristaltic pump collected samples) taken from the C (16–21 ft bls) level in MW1. A sample taken at the same time in the MW1 B (21–25 ft bls) level by peristaltic pump was below the detection limit of 2.5 µg/L. In late March through mid-April 2013, two samples showed detectable concentrations around 0.6 µg/L. Detectable mid-April chloroform concentrations otherwise ranged from 0.07 to 0.37 µg/L. After a June–November sampling hiatus, chloroform concentrations were markedly higher, ranging from 0.6 to over 3 µg/L in the period from December 5, 2013, through April 2, 2014. The reasons for this increase have not been discerned; although there was a prolonged cold snap during this period, PCE levels were not affected. Also, effects of this increase in chloroform groundwater levels did coincide with high subslab levels in SSP-4 but was not strongly reflected in the indoor air (see **Section 5**). Regardless, there does seem to be an increase in chloroform source concentrations that is reflected by the higher groundwater concentrations.

Overall, the chloroform groundwater data showed 53% nondetects (100 of 189), a decrease from the 84% observed in the 2013 report. Because of the improvement in detection limits and increase in groundwater concentrations, chloroform was detected in all but one sample taken since April 2013.

For PCE, groundwater concentrations remained consistent and fairly stable over the course of the project, with almost all detectable concentrations ranging between 0.2 and 0.8 µg/L. A single higher concentration event occurred in September–October 2011 when PCE concentrations in some wells ranged up to 1.3 µg/L. The consistent relationship of PCE concentrations observed in U.S. EPA (2013) between the wells and soil gas ports remains, with the soil gas points plotting well within the range of the more conventional monitoring wells (i.e., MW1A-C, MW2A-C, MW3). **Section 8.4** describes a statistical analysis that supports this temporal and spatial consistency across all groundwater samples, including monitoring wells and soil gas points.

Overall, there were 68 nondetects for PCE for a 36% detection rate. In 2013, PCE was detected in 13 of 40 samples, for a 33% detection rate.

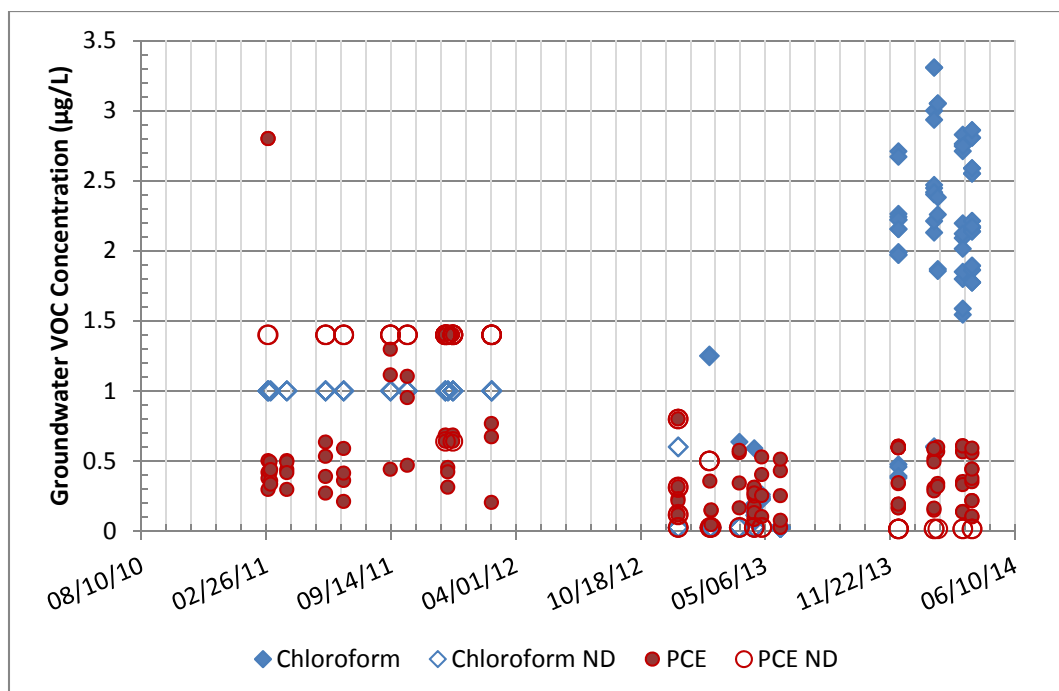


Figure 8-2. Groundwater VOC concentrations over time for Indianapolis duplex (open symbols represent nondetects plotted at one-half the detection limit).

8.3 Groundwater VOC Concentration, Well Depth, and Water Level

Figure 8-3 shows the relationship between monitoring well screen depth (top of screen) or soil gas port depth and PCE and chloroform groundwater concentration. As the figure shows, there does not appear to be a strong correlation, although the higher concentrations are associated with the deeper well screen depths (21, 24, and 26 ft bls to top of screen).

Figure 8-4 plots the groundwater PCE and chloroform concentration against the water level measured or estimated for the day the groundwater sample was taken. Again, a strong correlation is not visually apparent, but all of the higher chloroform concentrations occurred during the deeper groundwater levels observed in the late fall and early winter of 2014 (Figure 8-2). This could be related to the precipitation events, the high stream flow events, and groundwater level increases and decreases shown for this time period in Figure 8-1. Possible conceptual models related to this hypothesis include the following:

- When freshwater infiltrates into the aquifer, it is generally depleted in VOCs. Over time with a declining water table, VOCs slowly desorb off solids into the freshwater. Because this process happens faster than volatilization, the highest concentrations are when little freshwater has come in recently.
- When freshwater comes into the aquifer from rainfall, it is generally low in VOC concentration. Over time, the freshwater mixes with existing water and picks up VOCs at a rate faster than it can give them off through volatilization. Again, the maximum concentration is seen when little freshwater has come in recently and the water is low.

There also could be other factors related to the cold winter or changes in subsurface conditions (e.g., additional leaks from water mains or storm sewers containing chloroform) that could result in these higher chloroform concentrations observed since November 2013.

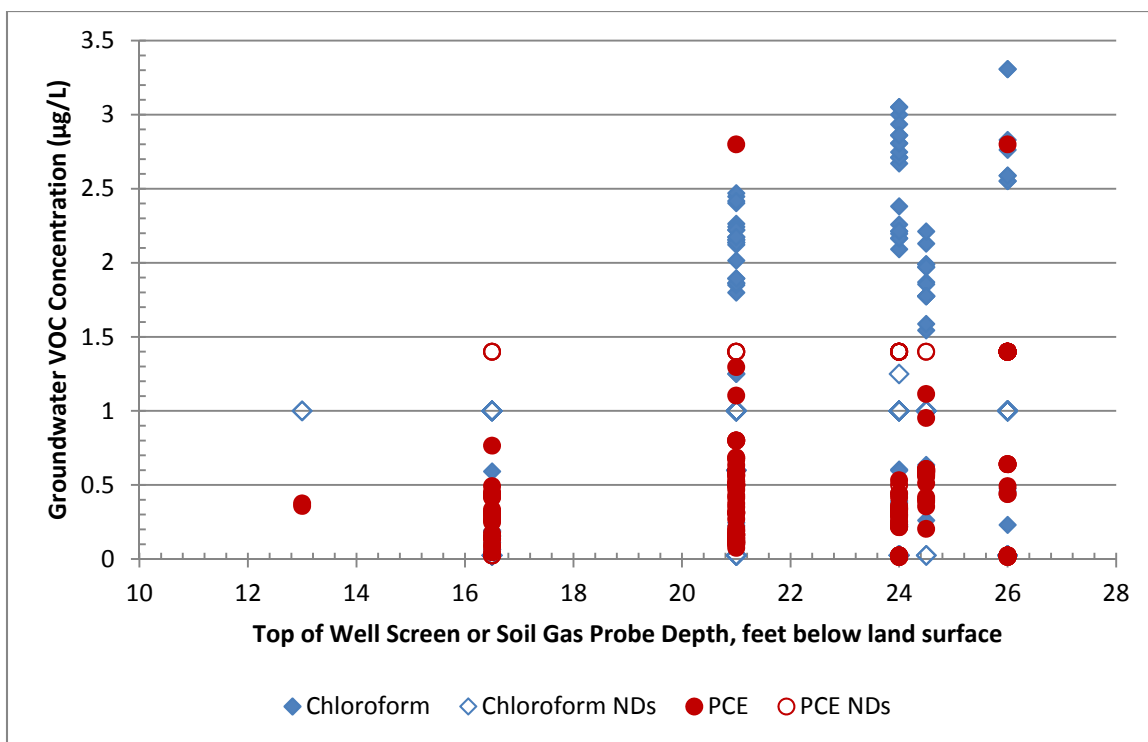


Figure 8-3. Plot of groundwater PCE and chloroform concentrations against well screen (or soil gas port) depth (well depth measured to top of screen; open symbols are nondetects plotted at one-half the detection limit) (data set over full study period discussed in this report).

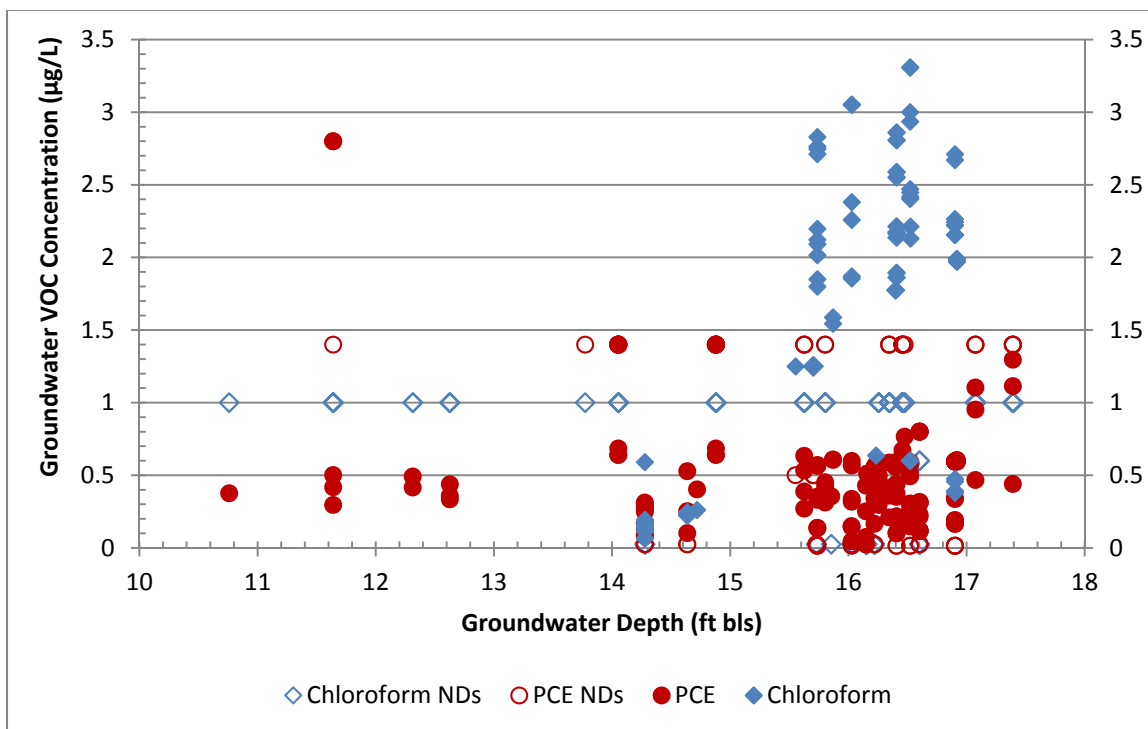


Figure 8-4. Plot of groundwater PCE and chloroform concentrations against groundwater depth (open symbols are nondetects plotted at one-half the detection limit) (data set over full study period discussed in this report).

8.4 Spatial Variability of Groundwater Samples

Occasionally the water rose high enough to take groundwater samples from the deeper (13–16.5 ft bls) soil gas ports in and around the duplex using peristaltic pump samplers. This provides additional spatial resolution to the groundwater levels under and around the house. **Figures 8-5** and **8-6** provide a snapshot of the spatial variability of groundwater VOC concentrations across the duplex on April 18, 2013, when most of the 16.5 ft soil gas probe groundwater samples contained detectable levels of VOCs. As shown in the figures, PCE concentrations varied by about a factor of 5 across the duplex, with highest concentrations ($0.25 \mu\text{g/L}$) in the south side and center of 422 and in the center of 420. Chloroform shows a different pattern on this date, with fewer high concentration points and the highest level ($0.45 \mu\text{g/L}$) in the south 422 basement.

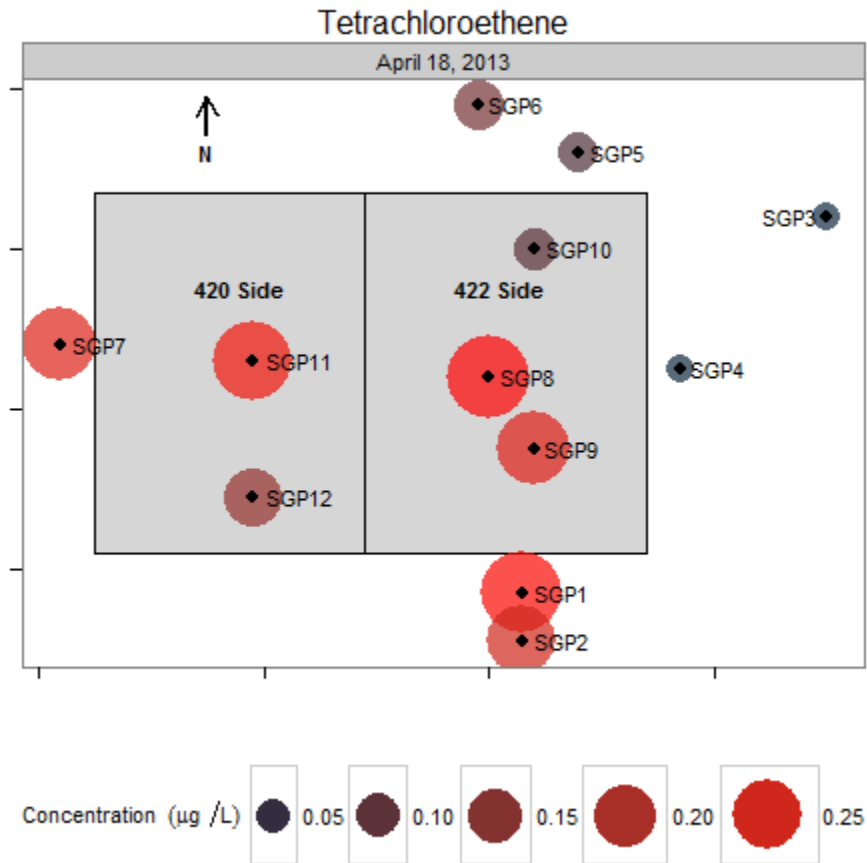


Figure 8-5. Spatial variability in groundwater PCE (tetrachloroethene) concentration, April 2013.

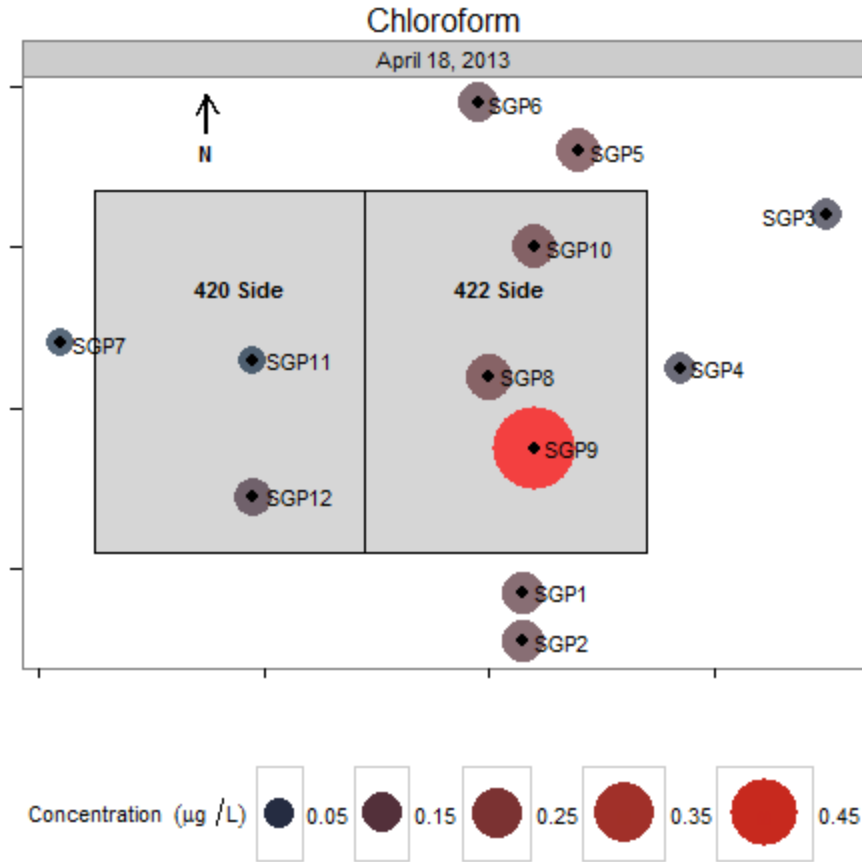


Figure 8-6. Spatial variability in groundwater chloroform concentration, April 2013.

8.5 Systematic Variability Due to Groundwater Sampling Method

Comparing measurements from the three types of groundwater sampling methods employed in this study (bailers, peristaltic pumps, and PDBs) required the definition of comparable measurements. As described in **Attachment 8A**, we employed a clustering algorithm called k-means clustering (Hartigan and Wong, 1979) to group the groundwater measurements into clusters of samples taken at similar locations and times. The purpose of the algorithm is to sort the data into k groups such that the within-group sum of squared errors (SSE) is minimized without a loss of information on the spatio-temporal variability of the data set. The clustering algorithm was applied to a data frame of each unique date/time and x-y-z location in the groundwater data and defined the four clusters in **Table 8-2** by their location in space and time.

Table 8-2. Four Clusters Defined for Indianapolis Groundwater Data

Cluster	Begin	End	N_locations	N_depths
4	February 28, 2011	June 30, 2011	6	9
2	September 13, 2011	February 22, 2012	8	10
3	December 17, 2012	May 30, 2013	15	8
1	December 05, 2013	April 02, 2014	3	7

As explained in **Attachment 8A**, because differences in concentration within each cluster were not correlated with location, depth, or time, these clusters are a suidefinition for “comparable” samples for this analysis. Within each cluster, there is no reason why any particular measurement should differ from the group average other than sampling/analysis error. If it is also true that sample method also does not drive any difference between individual measurements and the group average, we would expect the mean concentration difference for each sampling method to be zero. Indeed, all are very close to zero (**Table 8-3**), indicating that the methods produce essentially very similar results.

Table 8-3. Mean Difference in Concentration (Observed Mean – Group Mean) by Sampling Method

Compound	Method	Mean Concentration Difference (µg/L)
Chloroform	PDB	-0.02089
Tetrachloroethene	PDB	-0.01194
Trichloroethene	PDB	0.00135
Chloroform	Peristaltic Pump	0.0836
Tetrachloroethene	Peristaltic Pump	-0.06875
Trichloroethene	Peristaltic Pump	0.004545
Chloroform	Bailer	-0.03334
Tetrachloroethene	Bailer	0.1994
Trichloroethene	Bailer	-0.0165

This comparison can be made more mathematically using a simple analysis of variance (ANOVA) technique (or rather a nonparametric alternative to ANOVA), but first data from clusters with lots of nondetects should be removed to avoid biases related to data sets with large proportions of nondetects. **Table 8-4** shows the percentage of nondetects in the data by compound and cluster.

Table 8-4. Percent Nondetects by Compound and Cluster

Compound	Cluster	Percent_NDs
Chloroform	4	100
Tetrachloroethene	4	25
Trichloroethene	4	91
Chloroform	2	100
Tetrachloroethene	2	66
Trichloroethene	2	96
Chloroform	3	70
Tetrachloroethene	3	44
Trichloroethene	3	100
Chloroform	1	0
Tetrachloroethene	1	33
Trichloroethene	1	98

TCE has 90% or more nondetects in all four clusters, so it could not be considered in this analysis. Furthermore, 100% of chloroform measurements in clusters 4 and 2 are nondetects, so these also were excluded. The rest of the data were included in the analysis.

We performed a Kruskal-Wallis rank sum test on the PCE data from all remaining data clusters. This tests the null hypothesis that the concentration differences for each sample method follow the same distribution. The alternative is that at least one differs from the others.

Kruskal-Wallis Rank Sum Test: Concentration Difference by Groundwater Sampling Method, PCE

Test statistic	df	P value
26.52	2	1.739e-06 ***

Interestingly, this test returns a very small p-value, indicating that one of the sampling methods must have a different distribution from the others for PCE. A density plot of the concentration differences grouped by sampling method (**Figure 8-7**) reveals that bailer samples seem to be providing higher concentrations (i.e., they show a positive concentration difference) than the peristaltic pumps and PDB samples more often than they should assuming the sampling methods are comparable.

A similar test on the cluster 1 and 3 chloroform data reveals no bias in measuring chloroform concentration.

Kruskal-Wallis rank sum test: Concentration_Difference by Sampling Method, Chloroform

Test statistic	df	P value
2.999	2	0.2233

Given that VOC losses are more likely and prevalent than VOC increases in groundwater sampling, there is a small but statistically significant negative bias associated with PDB and peristaltic samplers when compared with bailer samplers at the low PCE concentrations measured during this study. Most field sampling method intercomparison studies (e.g., USGS, 2001; Maskarinac et al., 1989) are conducted at concentrations relevant for groundwater sampling—at or above the drinking water maximum contaminant level (MCL), rather than at the groundwater concentrations observed in this project (typically less than 2 µg/L). From physical first principles, we would expect the potential for small sorption or volatilization losses to be most significant on a percentage basis at low concentrations. Additional study may be necessary to determine if there are meaningful difference in sampling recoveries among sampling methods that are well accepted, when these methods are applied to the very low concentrations that can be of interest for vapor intrusion at shallow groundwater sites.

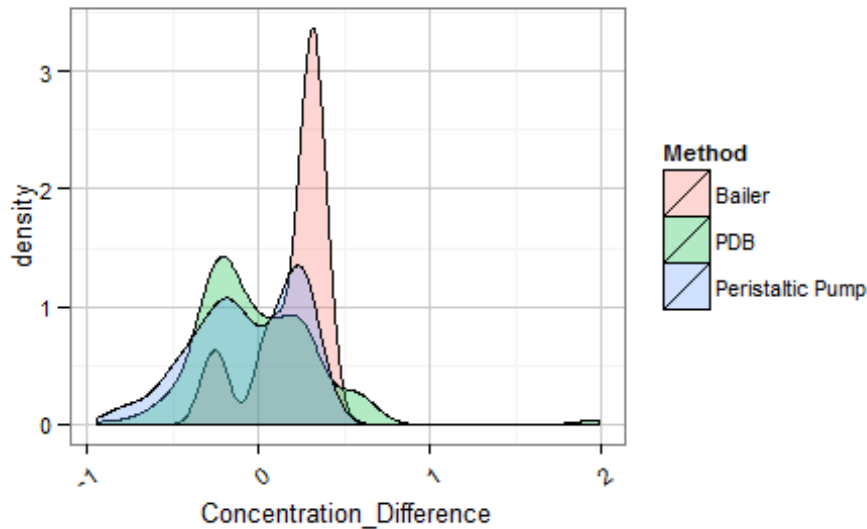


Figure 8-7. Distribution of concentration differences by sampling method—PCE.

8.6 Comparing Groundwater Samples with Soil Gas Samples

This section compares VOC vapor concentrations calculated from groundwater VOC measurements using Henry’s law with soil gas measurements. As a first step in the analysis, each groundwater sample was paired with the nearest soil gas sample in time and spatially.

8.6.1 Pairing of Groundwater Samples with Soil Gas Samples

Groundwater samples were assigned depth values as part of the description of the sample location. The PDB bags hang at a fixed depth, and the depth of those samples was determined by the tether length. Peristaltic pump samples and bailer samples were assigned a sample depth based on the screened interval of the well from which they came. They were assigned a sample depth of the minimum of the mean depth of the screened interval and the depth to water at the time of sampling.

Only the groundwater sample with the shallowest sample depth each day is included in this analysis for each sampling method. For example, if two peristaltic pump samples were taken on the same day at MW 1 and at MW 2, only the sample with the shallowest sample depth is included. If both samples had the same sample depth, both of them would be included and averaged.

Each groundwater sample was paired to a soil gas sample for the purpose of computing attenuation from groundwater to soil gas. The goal was to select the nearest soil gas sample to each groundwater sample—nearest both in distance and in time. The process for determining the “closest” soil gas sample to each groundwater sample was as follows:

- 1) Select only those soil gas samples that were taken between 14 days before the “start time” of the groundwater sample and 14 days after the collection time of the groundwater sample.
- 2) Select from the remaining eligible soil gas samples only those taken at the two sampling locations closest to the sampling location of the groundwater sample.
- 3) Select only those samples taken at the deepest depth of those remaining.
- 4) If there are still samples eligible from both of the closest sampling locations, select only those from the closest one.

- 5) If there are still multiple samples remaining, select the one closest in time to the collection time of the groundwater sample.

This process was consistently applied to all groundwater samples to match a single soil gas sample with each groundwater measurement.

Peristaltic pump samples and bailer samples had identical start times and collection times. PDB bag samplers are placed in the groundwater weeks before collection but are only representative of the groundwater composition in the days leading up to their collection. These samples were assigned a start time of 48 hours before their collection. The time window of eligibility for peristaltic pump samples and bailer samples is only 28 days, 14 days before and after the sample was taken. The window of eligibility for PDB bag samples is slightly longer, 16 days before their collection (14 days before their assigned start time) to 14 days after their collection.

The maximum time difference between groundwater sample date/time and soil gas sample date/time (well date/time – soil gas date/time) was set to be 28 days, the minimum time difference was –8 days, and the average absolute time difference between the two is 4 days. The following groundwater samples could not be paired with a soil gas sample within these constraints using the procedure detailed above: MW1, 03/18/2014 and 04/02/2014 and MW3, 05/30/2013, 03/18/2014, and 04/02/2014.

8.6.2 Pairing Depth with Groundwater Measurements to Soil Gas and Groundwater Samples

A depth-to-groundwater measurement was paired with both groundwater and soil gas samples from the water logger, hand measured, and imputed groundwater levels described in **Section 8-1**. For “instantaneous” samples (peristaltic pump samples, bailer samples, and TO-17 samples), the nearest depth-to-water measurement in time was used. For the longer exposure PDB bag groundwater samples, all depth-to-water measurements taken between the collection time minus 48 hours and the collection time were averaged to derive a representative depth-to-water value.

The difference in the depth-to-water value associated with each groundwater sample and the depth-to-water value accompanying its paired soil gas sample is a useful measure of similarity/dissimilarity of conditions when the two samples were taken. The average difference in depth to water at the time of the groundwater sample and the time of the soil gas sample paired to it is 9.8 inches. There are five sample pairings with a depth-to-water difference greater than 12 inches. These coincide with rapid changes in the water as shown in **Figure 8-8**.

8.6.3 Pairing Temperature Measurements with Groundwater Samples

For the groundwater measurements to be comparable to the soil gas measurements, they must be converted from liquid to vapor concentrations (i.e., groundwater measurements are reported in micrograms per liter of water [$\mu\text{g/L}$], and VOC concentrations in soil gas are reported in micrograms per cubic meter of soil gas [$\mu\text{g/m}^3$]). Henry’s law was used to convert liquid to gaseous concentrations. Because Henry’s law is dependent on temperature, each groundwater-soil gas sample pair was assigned the 16.5 ft bls temperature measurement in MW3 that was closest in time to the groundwater sampling time. The maximum absolute time difference between groundwater sample date/time and groundwater temperature measurement date/time was 14 days, and the average absolute time difference was 2 days.

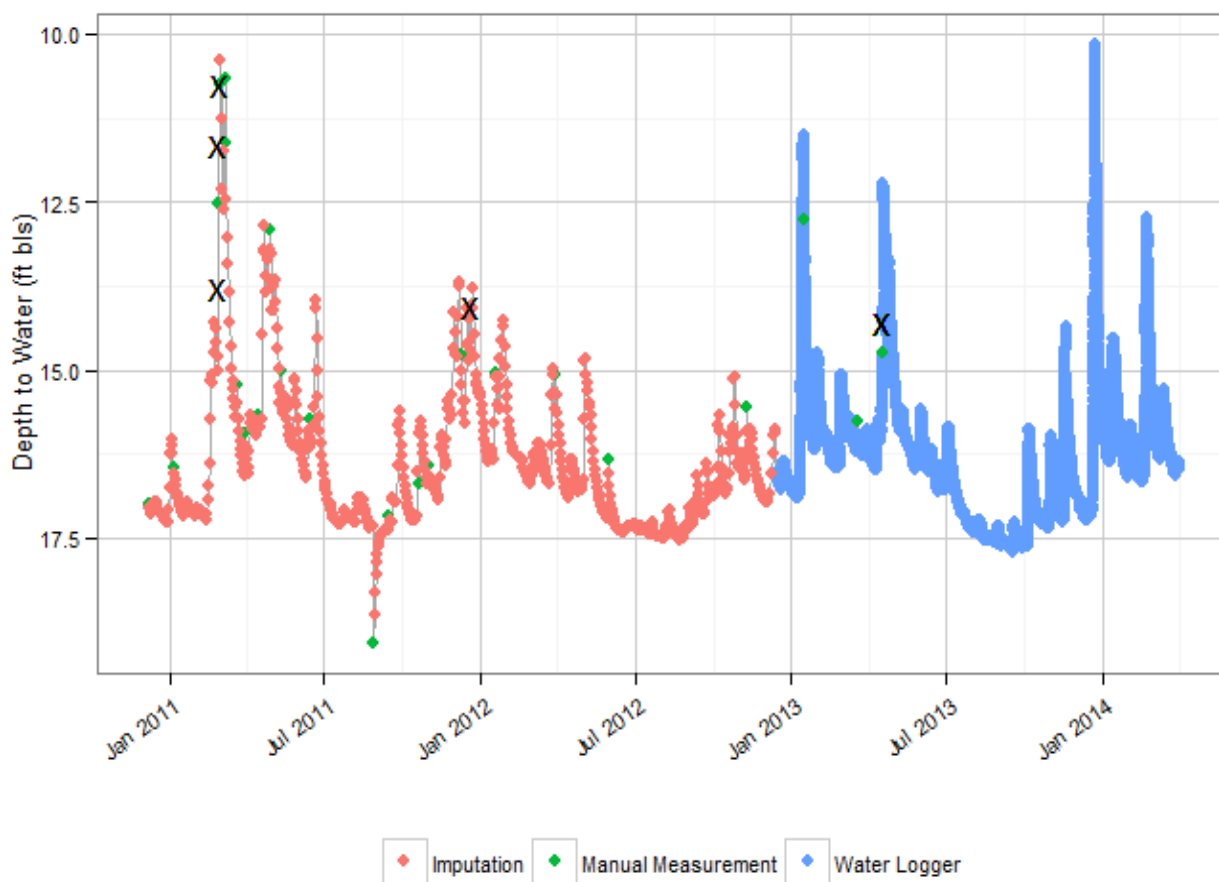


Figure 8-8. Groundwater level measurements used for depth-to-water. “X” indicates where groundwater sample and soil gas sample depth-to-water differ by more than 12 inches.

8.6.4 Henry’s Law Calculations

Assuming that the groundwater is in equilibrium with soil gas, Henry’s law predicts the expected deep soil gas concentration from the observed groundwater concentration. According to Henry’s law:

$$\text{Deep Soil Gas Concentration } (\mu\text{g}/\text{m}^3) = \frac{\text{Groundwater Concentration } (\mu\text{g}/\text{L})(H_L^*)(1000)}{(R)(K)}$$

where H_L^* is the Henry’s law conversion constant for the compound¹⁵, $R = 8.21E - 5 \frac{\text{atm}\cdot\text{m}^3}{\text{mol}\cdot\text{K}}$ is the molar gas constant, and K is the temperature in degrees Kelvin.

¹⁵ H_L^* (PCE) = 0.0027; H_L^* (TCE) = 0.009; H_L^* (chloroform) = 0.0023.

8.6.5 Results and Discussion

Figures 8-9 and **8-10** depict the observed VOC concentrations in groundwater, and **Table 8-5** presents summary statistics of these concentrations. Note the several samples that were taken on April 18, 2013. The water at that time was high enough to sample groundwater from the 16.5 ft deep soil gas monitoring ports, and samples were collected from several different ports and show the spatial distribution of VOCs between the ports. Note the large proportion of nondetect measurements (vertical lines) for trichloroethene (TCE) across the entire record and chloroform prior to December 2013. The improvement of the detection limit and increase in the groundwater concentration for chloroform shown in **Figure 8-9** was discussed earlier (see Section 8.2). **Figure 8-10** shows the lower variability in PCE (tetrachloroethene) data when compared with chloroform, which is also reflected by a standard deviation (0.35) that is less than half of the standard deviation of the chloroform data (0.75).

Because it comprises almost entirely nondetects, the TCE groundwater data are not discussed further.

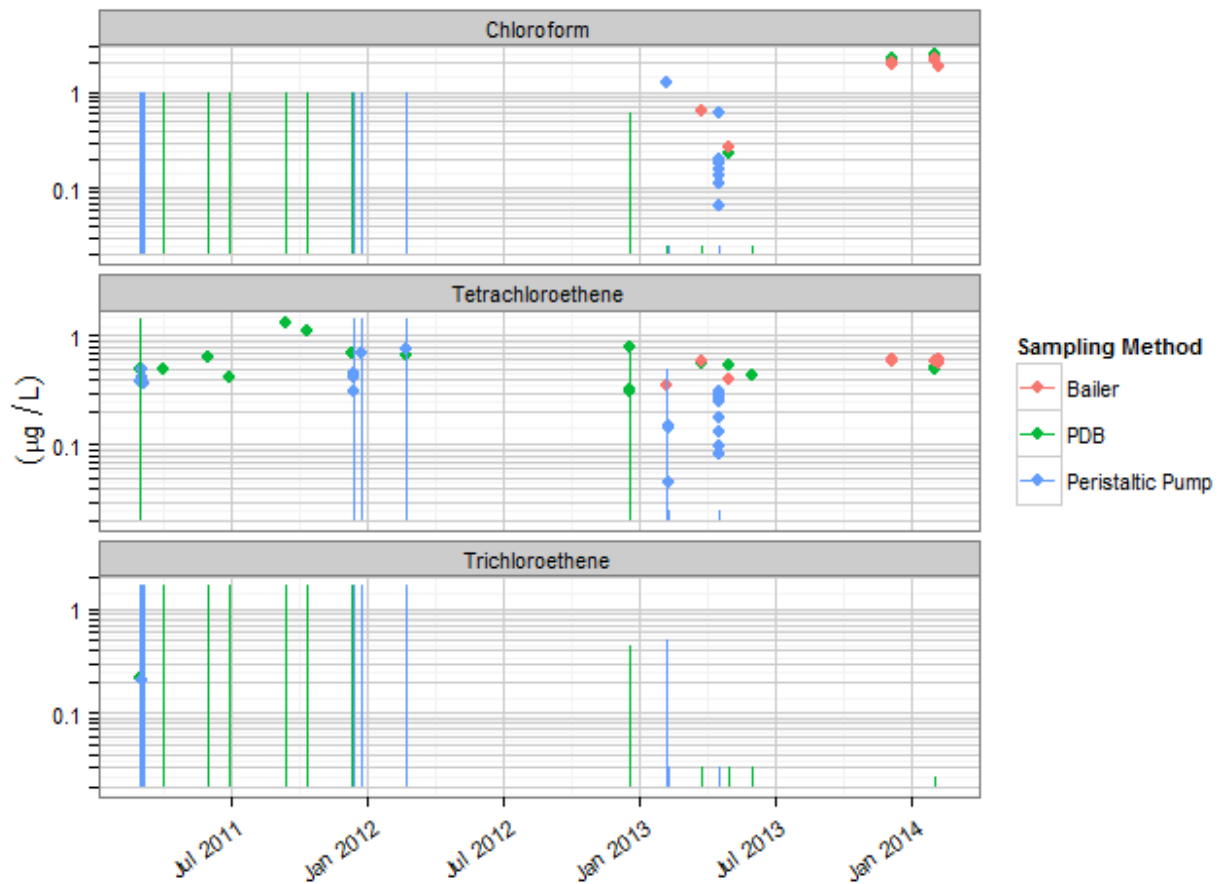


Figure 8-9. Measured VOC concentrations in groundwater by time and sampling method (vertical lines indicate nondetects plotted from zero to one-half the detection limit).

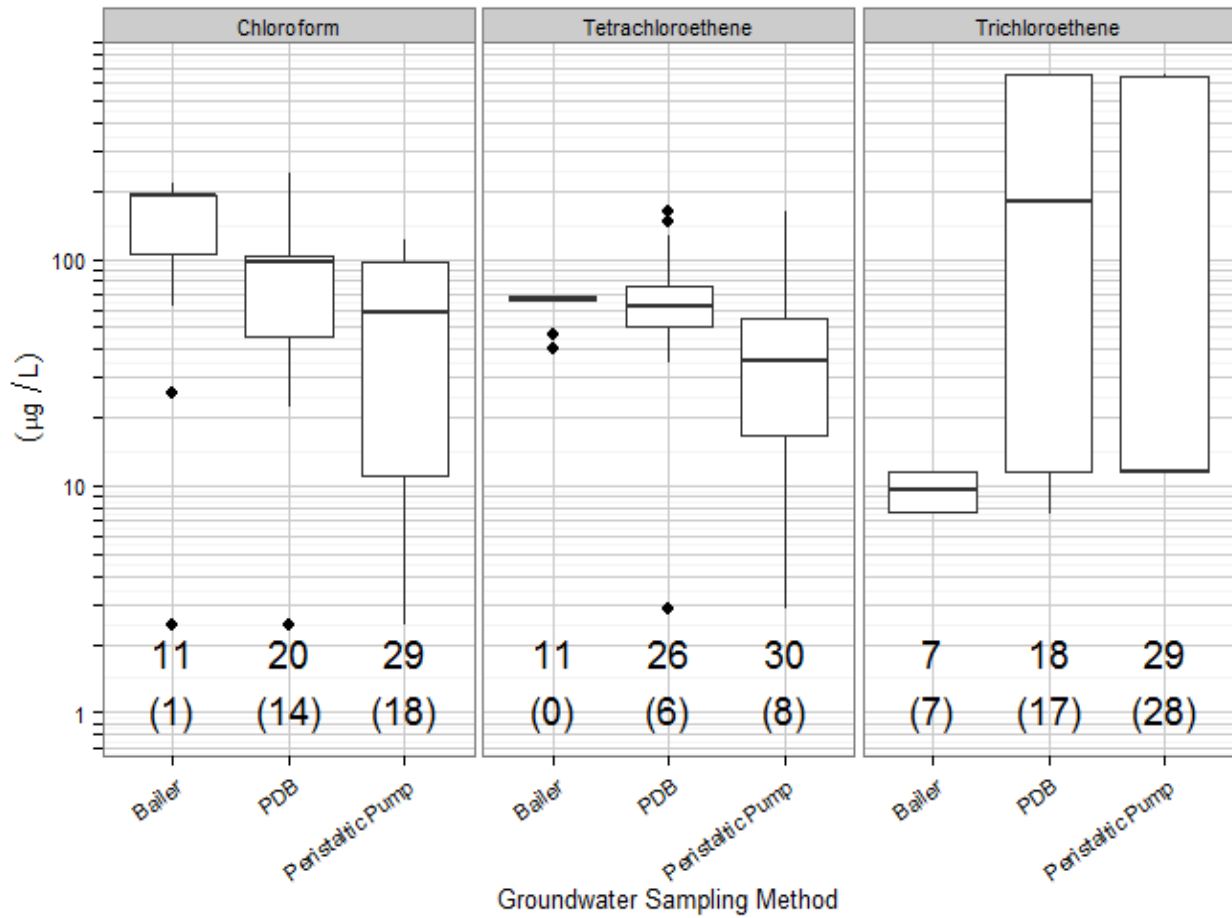


Figure 8-10. Box and whiskers plots of VOC concentrations in measured in groundwater, organized by sampling method. Boxes outline 25th and 75th percentiles with heavy bar representing the median (50th percentile) concentration. Number of measurements is given below bars along with the count of nondetects in parentheses.

Table 8-5. Summary of Groundwater Measurements (µg/L)

Compound	# of GW Samples	NDs	Flagged	Min	Q1	Median	Mean	Q3	Max	Standard Deviation of GW Samples	# of Unique Soil Gas Samples	Standard Deviation of Unique Soil Gas Samples
Chloroform	60	33	48	0.025	0.1561	1	0.8955	1	2.47	0.7451	31	407.5
PCE	67	14	53	0.025	0.31	0.5	0.5152	0.5968	1.4	0.3484	31	134.7
TCE	54	52	54	0.02	0.03	0.03	0.6795	1.7	1.7	0.7972	31	3.696

The expected concentration of VOCs in deep soil gas, although dependent on temperature, is almost a linear transformation of the observed groundwater concentrations, making the two very similar in variability. The expected deep soil gas concentrations predicted by Henry’s law are compared with the observed deep soil gas concentrations in **Figures 8-11, 8-12, and 8-13**. Although chloroform does not show a close agreement between the soil gas measurements and Henry’s law prediction, PCE does in terms of a similar pattern of values (**Figure 8-11**), a roughly linear correspondence in an xy plot (**Figure 8-12**), similar medians (**Figure 8-13**), and a range for the Henry’s law values that is, as expected, generally less than but within the observed range of soil gas measurements (**Figure 8-13**). With respect to chloroform, the lack of agreement between the predicted and measured concentrations is consistent with the hypothesis of additional nongroundwater subsurface sources for this contaminant. TCE shows no relationship or correlation because of the very low concentrations and very high percentage of nondetects in both the soil gas and groundwater measurements.

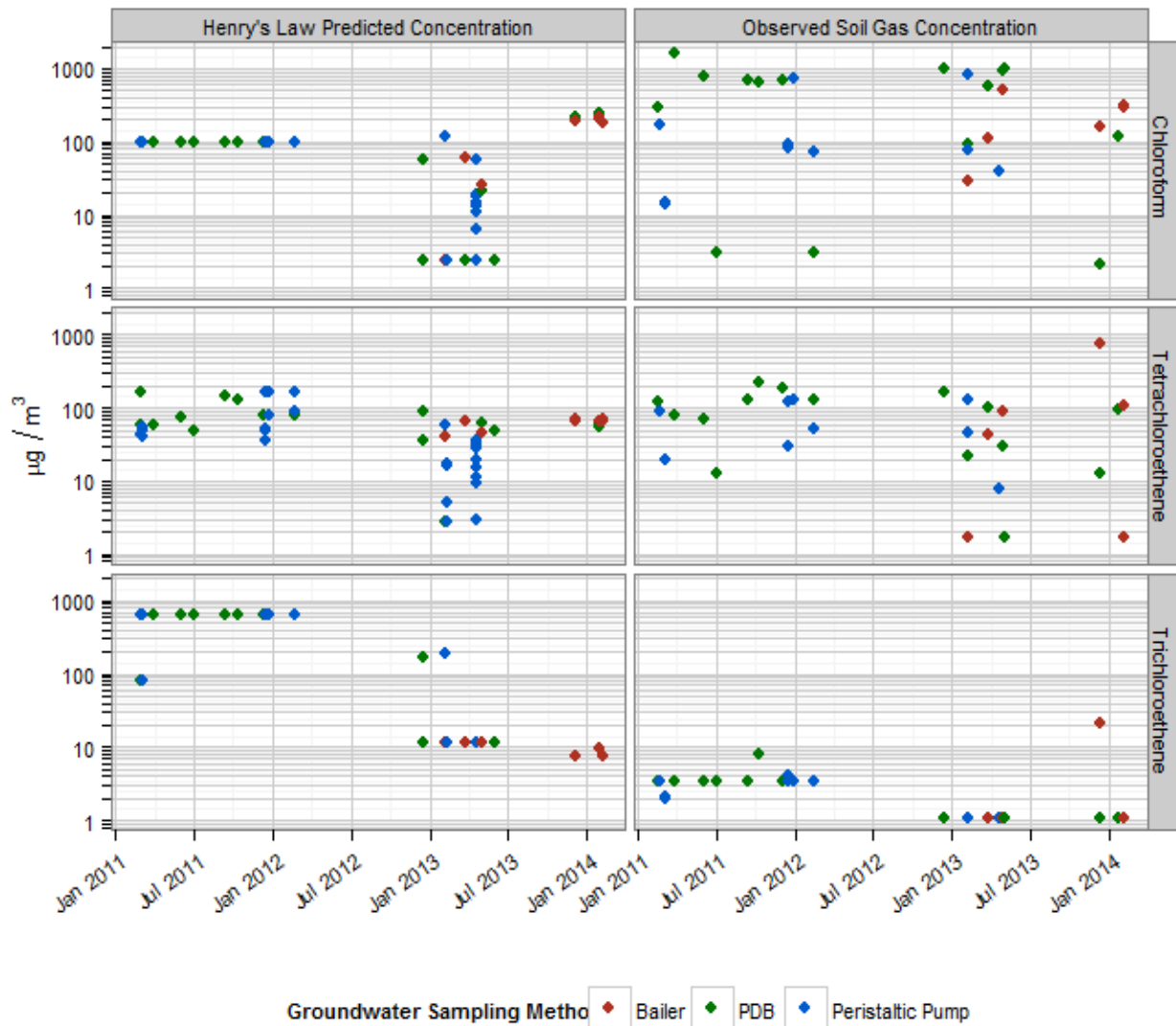


Figure 8-11. Expected and observed VOC concentrations in deep soil gas.

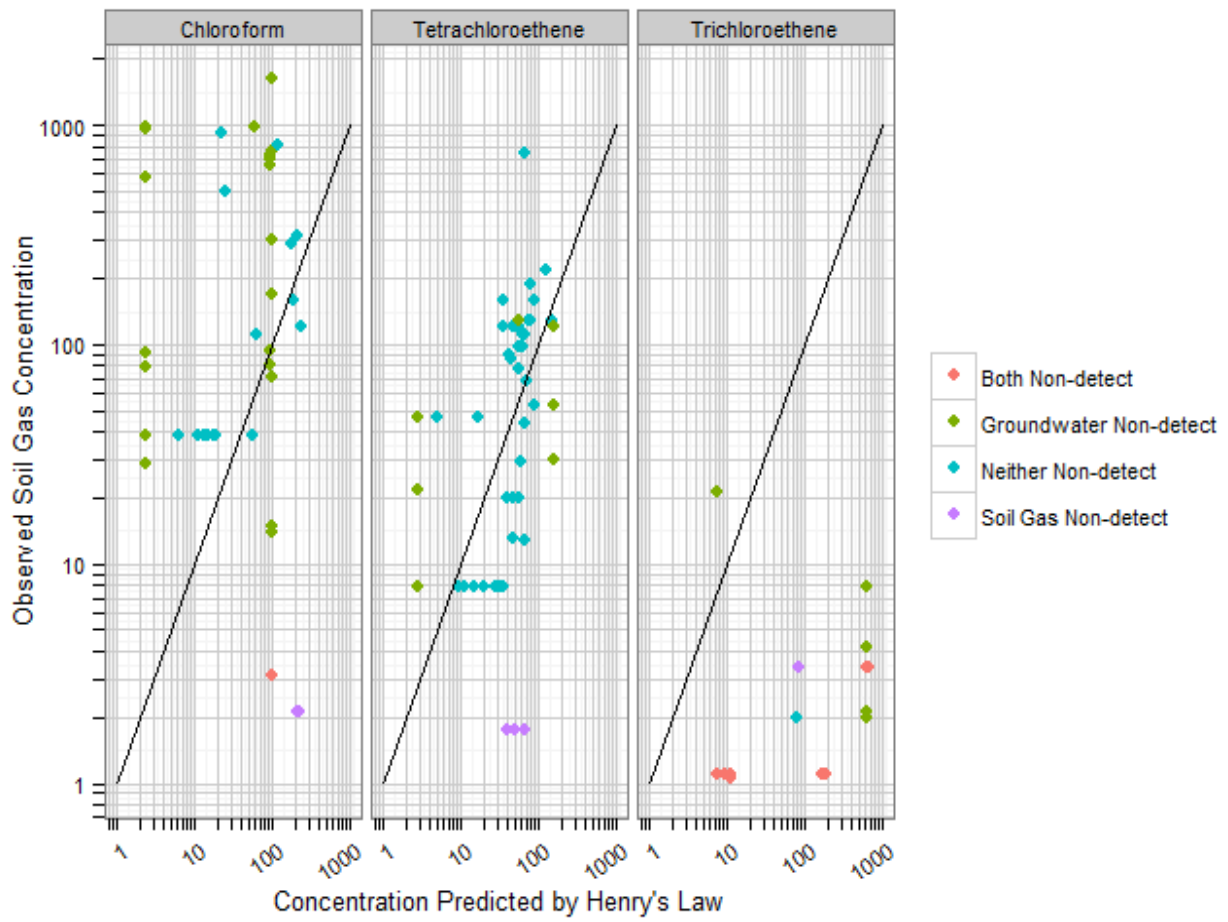


Figure 8-12. Expected vs observed VOC concentration.

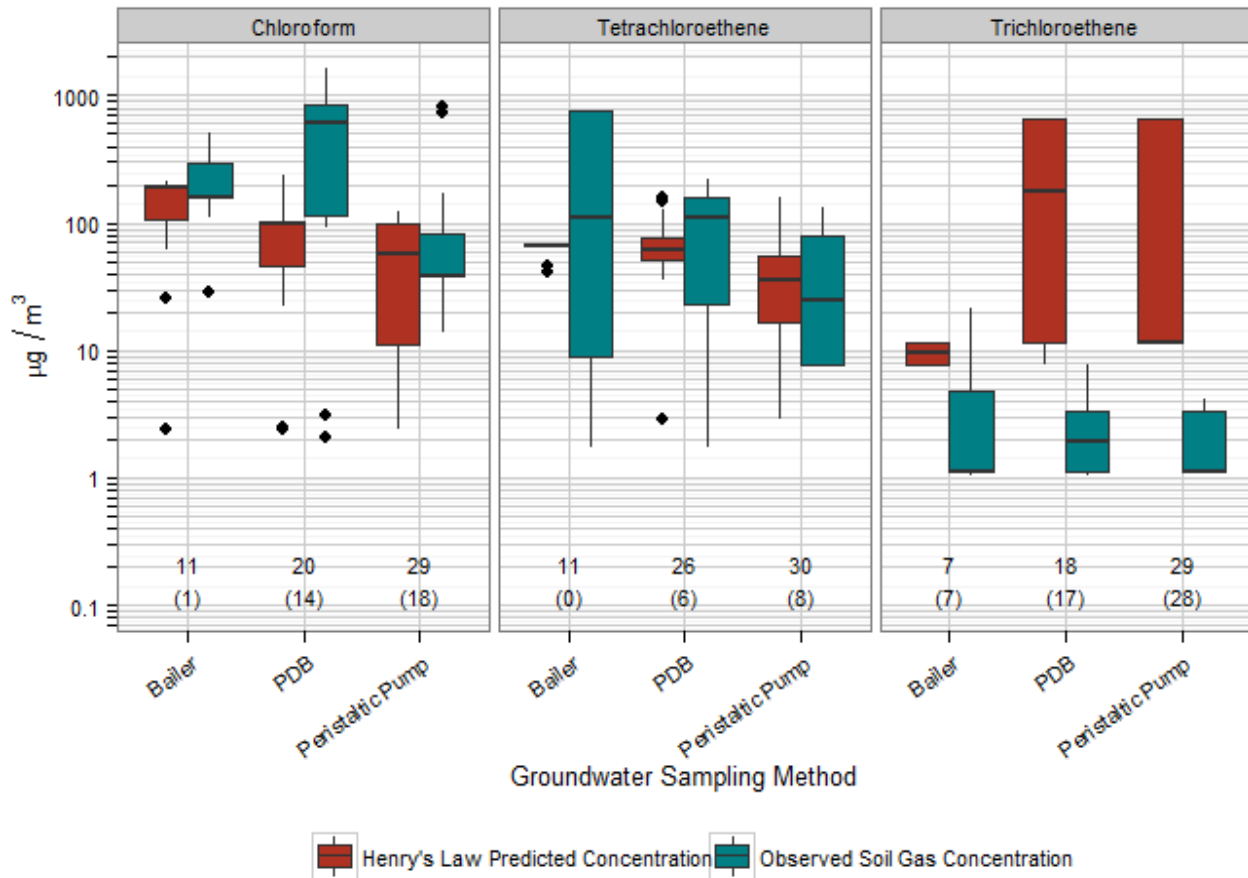


Figure 8-13. Measured VOC concentrations in groundwater, with the total number of soil gas measurements and number of nondetects below each set of boxes. Each box spans the 25th percentile to 75th percentile range with the median plotted as the bold line.

Recent literature (e.g., Carr et al., 2013) suggests that VOC volatilization from groundwater to soil gas is not solely a product of volatilization at the water table, but also can come from a pollutant-rich groundwater film left in the soil by a falling water table. This theory would suggest that an increase in depth to water preceding the soil gas sample could lead to a larger soil gas concentration and a larger difference between observed VOC concentrations and VOC concentrations predicted by modeling volatilization from the groundwater table. To test this hypothesis, the average depth to water was calculated for each day in the study period, and from this the change in depth to water was calculated by taking the first difference. These changes in depth-to-water values were matched by date to the collection date of the soil gas samples. Even in the PCE data, which has the fewest nondetects, no relationship is evident between change in the water elevation and deviation from expected soil gas concentration, as exhibited by the scatter of the data points in **Figure 8-14**.

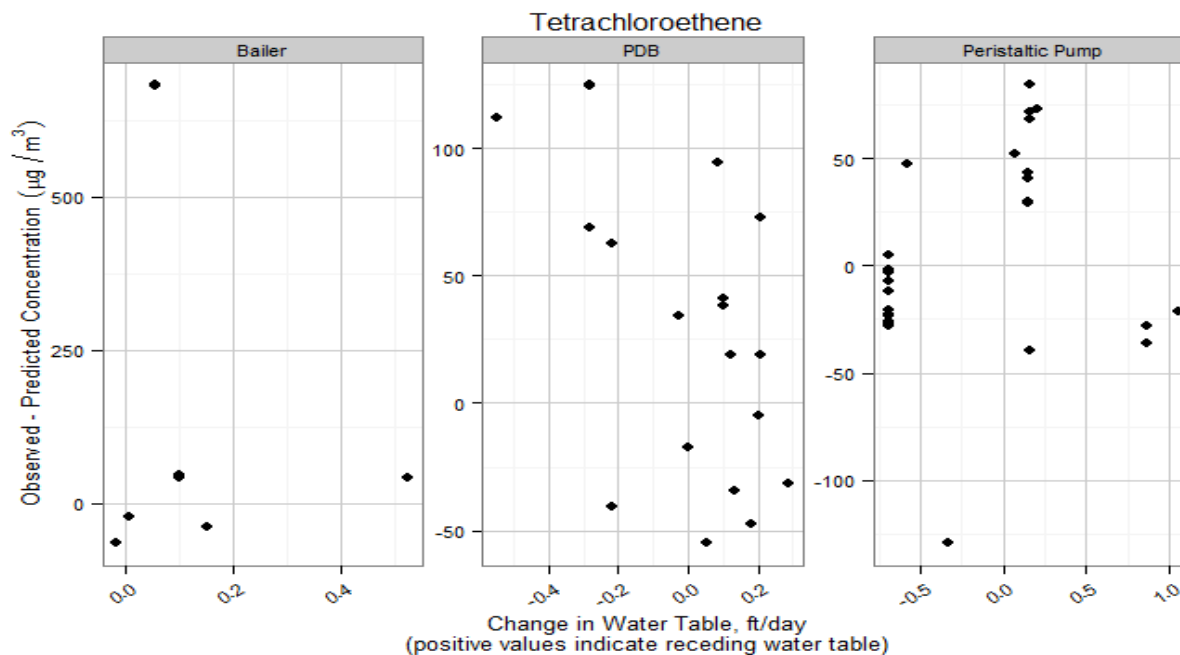


Figure 8-14. Change in water depth (ft/day) vs. deviation from Henry's law prediction.

8.7 The Relationship of Groundwater Concentration to Soil Gas and Indoor Air Concentrations

The monthly or longer groundwater sampling intervals make it very difficult to assess quantitatively the correlation of groundwater PCE against soil gas or indoor air concentrations, although the narrow range of variability in PCE concentrations (below an order of magnitude) and stability of this variability over time (see **Figures 8-2** and **8-3**) make it unlikely that changes in groundwater concentrations are strongly related to the changes in soil gas or indoor air concentrations over the time scales observed in this study. Chloroform's limited length of record for detectable concentrations in groundwater limits what can be assessed in that regard, although the high winter 2013–2014 chloroform measurements will provide a chance to see whether indoor air and subslab chloroform concentrations are elevated as well.

Although the groundwater concentrations are relatively sunder the site, there are sufficient data to evaluate the potential for groundwater to be the source of indoor air concentrations in the 420/422 duplex on the basis of Henry's law calculations. For PCE, the prevalent range of groundwater concentrations, from 0.2 to 0.8 $\mu\text{g}/\text{L}$, and mean of 0.4 $\mu\text{g}/\text{L}$, corresponds to vapor concentrations of 175, 579, and 275 $\mu\text{g}/\text{m}^3$, respectively, with the maximum groundwater concentration, 1.3 $\mu\text{g}/\text{L}$, corresponding to 941 $\mu\text{g}/\text{m}^3$. These concentrations are sufficient to produce the soil gas and indoor air concentrations observed in this study, especially considering the coarse-grained nature of the subsurface that allow ready diffusion and flow of contaminants from the water to the building. The agreement of Henry's law predictions with deep soil gas PCE levels described in **Section 8.6.5** confirms this relationship with actual measurements. Thus, the available groundwater data indicate that groundwater is a likely source of the PCE vapors observed in the subsurface and indoor air during this study, although additional vadose zone PCE sources cannot be ruled out based on the groundwater evidence alone.

As mentioned above, although the groundwater PCE concentrations are sufficient to be the primary source of the PCE measured in indoor air in this study, their observed variability does not explain the variability in the indoor air PCE measurements. As has been shown in this and other studies, the

variability in indoor air PCE concentrations is also influenced by subsurface, building-related, and meteorological variables that affect the concentration of PCE as it migrates from the water table, enters the building, and mixes with indoor air. In addition, other sources of PCE that may also exist in the vadose zone or sewer lines cannot be ruled out at this point, and variability in those sources could also influence the PCE concentrations in indoor air.

The same VOC source situation may not hold true for chloroform. In the earlier part of this study (U.S. EPA, 2013), most of the measured concentrations of chloroform in groundwater were nondetects, with the maximum groundwater concentration (0.64 µg/L) corresponding to a vapor concentration of 63 µg/m³ and the mean (0.12 µg/L) corresponding to 12 µg/m³. These groundwater concentrations were determined to be insufficient to drive the soil gas and indoor air concentrations measured in this study, suggesting that other sources, such as vadose zone sources from nearby former businesses using chloroform or disinfection by-products from leaky water mains, may be responsible for the observed peak soil gas and indoor air chloroform concentrations. Although the chloroform concentrations measured in the winter of 2013–2014 were almost an order of magnitude higher, ranging from 1.5 to 3.3 µg/L, and could be sufficient to drive vapor intrusion, the much lower groundwater concentrations observed in the early part of the study still support the likelihood that there are other sources for the chloroform vapor intrusion into the duplex.

8.8 Chapter Summary

The following conclusions can be drawn from the study of groundwater concentrations at the Indianapolis site and their relationship to soil gas concentrations and vapor intrusion.

- Observations and statistical tests of groundwater PCE and chloroform data indicate that groundwater VOC concentrations remain sand consistent at the Indianapolis site, especially for PCE. Chloroform also generally shows less than an order of magnitude variability, but concentrations did consistently increase by almost an order of magnitude in the latter part of this study during the winter of 2013–2014. This suggests different sources for chloroform and PCE, which is consistent with other lines of evidence in this study.
- Maximum observed groundwater concentrations for PCE and chloroform are sufficient in magnitude to be the source of the observed VOC levels in soil gas and indoor air through the vapor intrusion pathway. However, that fact is not sufficient to conclusively prove that the groundwater is the source. PCE shows a positive correlations between groundwater and deep soil gas concentrations, although chloroform does not, again supporting sources other than groundwater for chloroform.
- No correlation was observed or measured between groundwater sample depths, groundwater (water table) levels, and VOC concentrations in groundwater.
- A difference in arithmetic means suggests that bailers may control groundwater sample volatilization losses slightly better than PDBs or peristaltic pumps; although these differences are very significant, they are also very small.

The most important conclusion of this section is the reasonable fit for PCE between the observed deep soil gas concentrations and the deep soil gas concentrations calculated through Henry's law from groundwater concentrations and, in contrast, that chloroform is generally more concentrated in the deep soil gas than in groundwater. This is consistent with a conceptual site model in which (1) PCE is migrating to the immediate vicinity of the house in groundwater and vapor intrusion is driven by transport from groundwater and (2) chloroform is arriving at the immediate vicinity of the house at least in part from other sources, such as a buried storm sewer or sewer main, or a leaking city water main. Although the exact depth of the sewer and water lines in the vicinity of the house is not known, we know that these

are gravity sewers that must be substantially below the depth of our basement sewer lateral (approximately 7 ft bls). Therefore, any leaked water from these sewers would likely be discharged only a few feet above seasonal high water tables. Once discharged leaked water from the sewer line would have an opportunity to volatilize as it infiltrates more deeply. Thus, much of the dissolved chloroform probably volatilizes to contribute to soil gas concentrations before the water gets to the water and can be sampled. This would result in a higher concentration in deep soil gas than was observed in shallow groundwater.

Attachment 8A. Cluster Analysis for Evaluating Spatio-Temporal Variability

As shown in Section 8.2, there is little visual evidence of consistent spatial or temporal variability in the groundwater data collected at the Indianapolis duplex, other than a high chloroform groundwater concentration in the winter of 2013/2014. There was also no obvious relationship between groundwater depth or well depth and PCE or chloroform VOC levels. Given that groundwater was collected at a variety of depths and well locations during the course of this project, it was advantageous to perform a cluster analysis to demonstrate this formally in order to facilitate comparison using all of the groundwater samples. For example, there were a few instances when groundwater samples were taken from deeper soil gas ports because sampling was only possible when the water rose high enough to cover and enable sampling from the soil gas ports. Given the limited number of groundwater samples available, it would be good to be able to include these soil gas port groundwater samples with the more conventional well samples in subsequent analyses and comparisons of groundwater VOC data.

We employed a clustering algorithm called *k-means clustering* (Hartigan and Wong, 1979) to group the groundwater measurements into clusters of samples taken at similar locations and times. The purpose of the algorithm is to sort the data into k groups such that the within-group sum of squared errors (SSE) is minimized. The algorithm was applied to a data frame of each unique date/time and x-y-z location in the groundwater data.

It is common practice to normalize data before employing k-means clustering by centering (subtracting out the mean of each dimension) and scaling (dividing each dimension by its standard deviation). This ensures that each dimension contributes equally to cluster formation. However, given our preconceptions about the data, namely that the change in groundwater concentrations is greater over time than distance, we centered the data, but did not scale it before clustering. The clustering algorithm is designed for continuous data so we provided it location in the form of x, y, z, coordinates and converted date/time into hours since January 1st, 1970, before centering and clustering. This conversion into hours is an important and somewhat arbitrary decision. Dimensions with a larger range will tend to drive cluster formation more than dimensions with a smaller range. Certainly the range of hours in the groundwater data is much larger than the range of x, y, or z coordinates, so cluster formation will be largely driven by date/time. We chose hours as a suitable unit for date/time because we expect that a time difference of one hour between two samples might have approximately the same effect as a difference of one foot in the x, y, or z direction. As it turns out, using a conversion to hours, twelve hours, days, or two days yields a virtually identical set of clusters.

The next important decision in using k-means clustering to group the measurements is what value to choose for k . Should the data be grouped into 10 clusters or 9? Or five clusters or fifteen? As mentioned earlier, the algorithm groups the data into k clusters while minimizing the within-group SSE. Increasing the number of clusters from one to two yields a large reduction in within-group SSE, but eventually increasing k , the number of clusters, reaches a point of diminishing returns. The best achievable within-group SSE is plotted vs number of clusters below. As shown in **Figure 8A-1**, it appears that four clusters of measurements is a good choice for k .

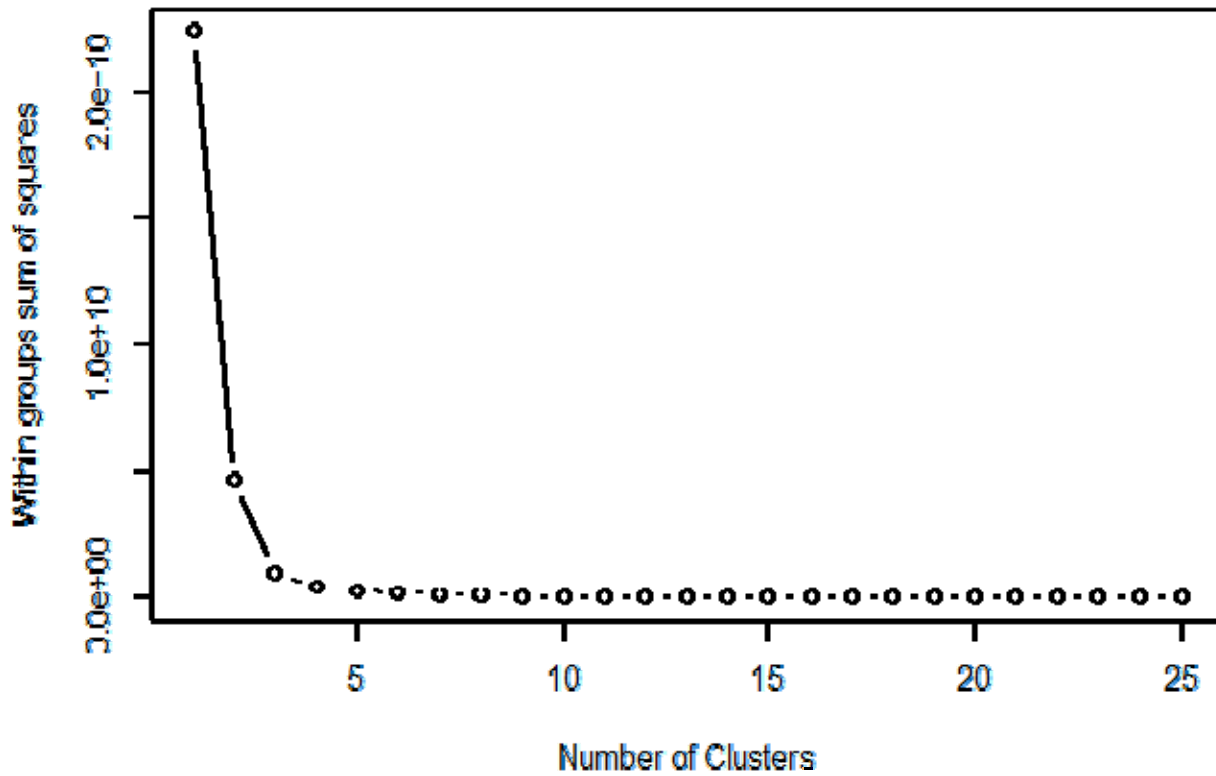


Figure 8A-1. Choosing k: How many clusters should the data be grouped into? Within group sum of squares by number of clusters for the Indianapolis groundwater data.

We grouped all of the date/time - location combinations into four clusters of geographically and temporally (but mostly temporally) similar clusters. The resulting clusters are plotted in **Figure 8A-2**. **Table 8A-1** shows the time period each cluster spans, as well as the number of different locations and sample depths in each cluster. Note that the high chloroform groundwater concentrations observed in the winter of 2013/2014 are all in Cluster 1.

Table 8A-1. Four Clusters Defined for Indianapolis Groundwater Data.

Cluster	Begin	End	N_locations	N_depths
4	February 28, 2011	June 30, 2011	6	9
2	September 13, 2011	February 22, 2012	8	10
3	December 17, 2012	May 30, 2013	15	8
1	December 05, 2013	April 02, 2014	3	7

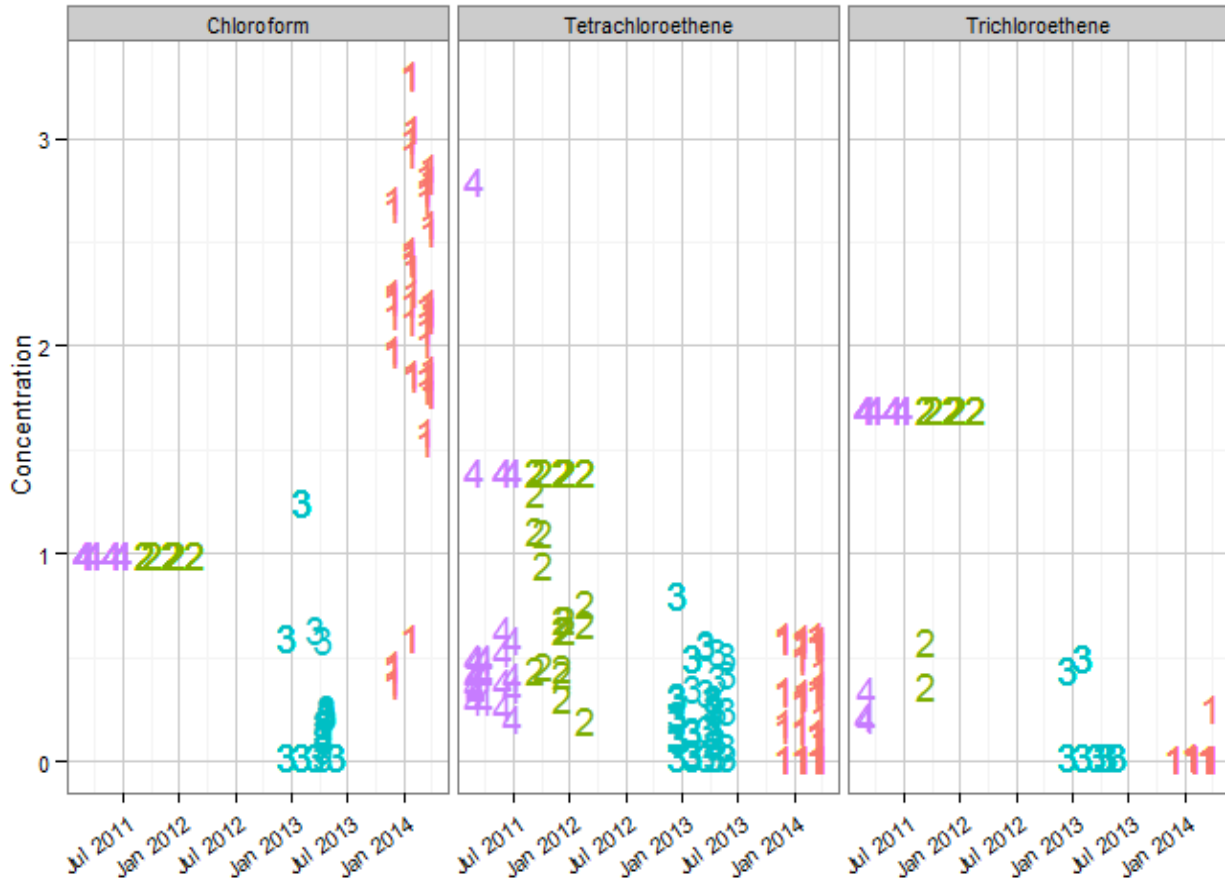


Figure 8A-2. Groundwater measurement clusters 1 – 4.

Table 8A-2 summarizes the variability within each cluster.

Table 8A-2. Concentration Variability within Each Indianapolis Groundwater VOC Measurement Cluster.

Compound	Cluster	N	NDs	SD	Geo_SD
Chloroform	4	32	32	0	1
Tetrachloroethene	4	32	8	0.68	2.022
Chloroform	2	53	53	0	1
Tetrachloroethene	2	53	35	0.3844	1.607
Chloroform	3	88	62	0.4376	4.76
Tetrachloroethene	3	88	39	0.2309	3.404
Chloroform	1	108	0	0.7198	1.701
Tetrachloroethene	1	108	36	0.2331	4.761

Now that we have allowed the data to "sort itself" into comparable clusters of data points in space and time, we can compare the concentrations measured by each sample to the group averages. We used the arithmetic mean to calculate group averages. Each cluster has a "center" - a mean date/time, x coordinate,

y coordinate, and z coordinate. We calculated the Euclidean distance between each samples' location and the mean location of its group, the time difference, in hours, between each measurement and the group center, and the difference in concentration between each sample and the mean of its group.

$$d(\text{point}, \text{center}) = \sqrt{(x_{\text{point}} - x_{\text{center}})^2 + (y_{\text{point}} - y_{\text{center}})^2 + (z_{\text{point}} - z_{\text{center}})^2}$$

When the X-Y distance from the cluster center (difference in location) is plotted against the concentration difference it is obvious that no relationship exists between the two (**Figure 8A-3**).

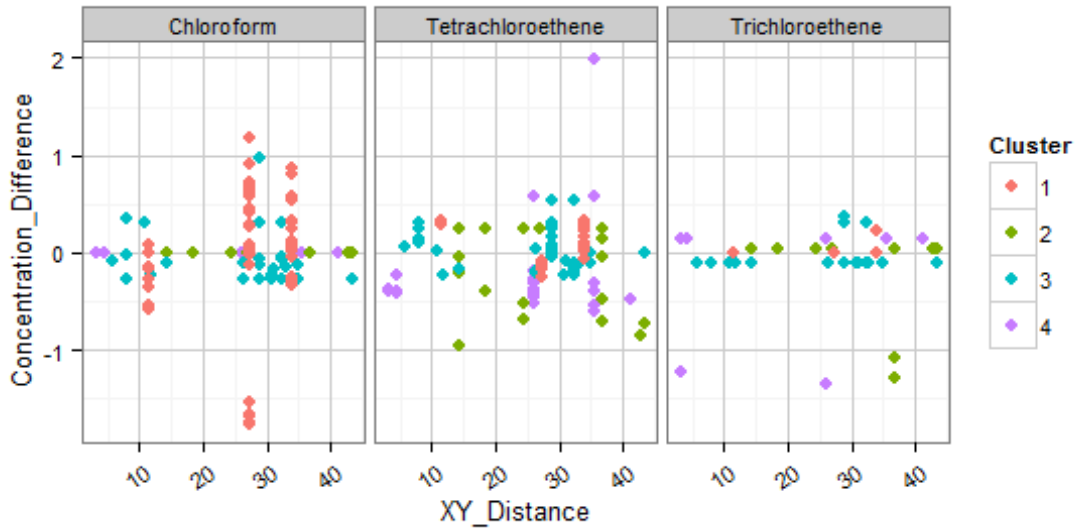


Figure 8A-3. X-Y distance (difference in location) does not explain difference in concentration.

Similarly, Z distance (difference in depth) is not obviously related to differing concentrations (**Figure 8A-4**).

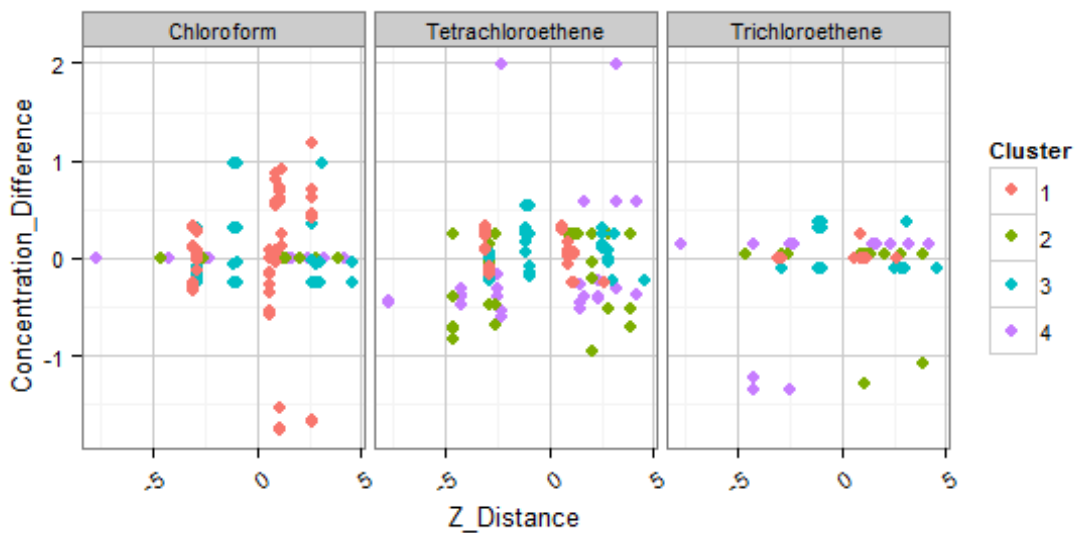


Figure 8A-4. Z distance (difference depth) does not explain difference in concentration.

Euclidean distance (X-Y-Z distance) does no better (**Figure 8A-5**).

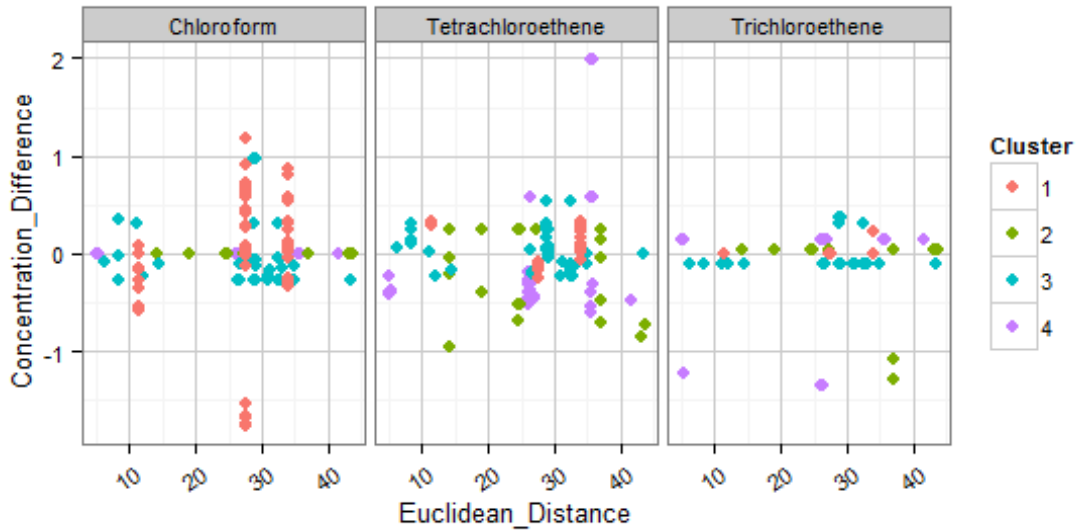


Figure 8A-5. Euclidean distance does not explain difference in concentration.

And finally, distance in time is also unrelated to concentration differences (**Figure 8A-6**).

Based on this analysis, we can confidently say that the 4 clusters defined in this analysis are valid groups of measurement points whose concentration differences are not due to sample location or depth or the time when the sample was taken.

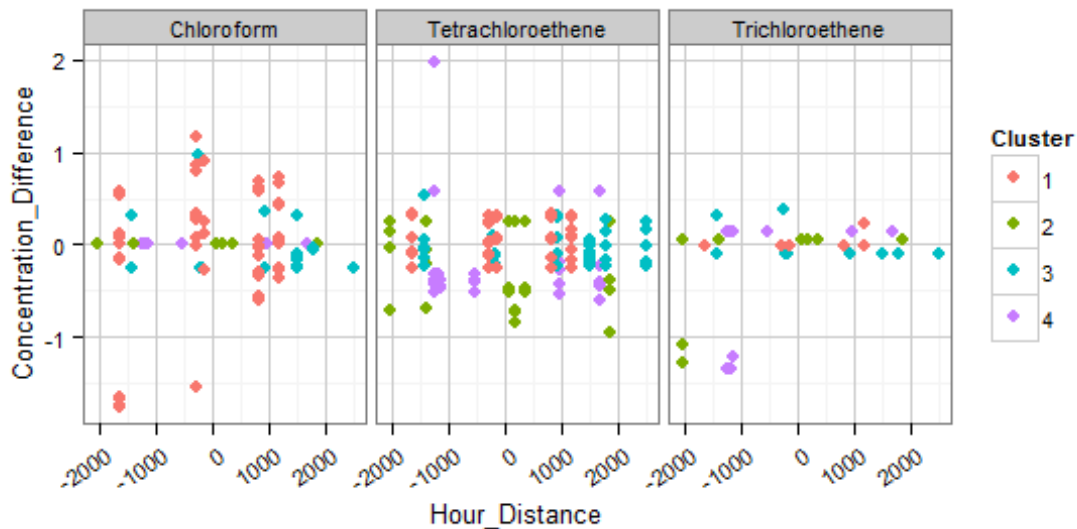


Figure 8A-6. Distance in time does not explain difference in concentration.

9. Conclusions and Practical Implications

9.1 Conclusions

9.1.1 Vapor Intrusion Prediction

In this project, we attempted to predict vapor intrusion up to 1 week into the future and then compare our predictions to observed indoor air concentrations. The prediction approach was based on the following:

- Previous analysis of 1-week scale data from this duplex (U.S. EPA, 2012a, 2013) that related indoor air concentrations to predictor variables, including exterior temperature, snowfall, and wind direction available from local weather forecasts. Because interior temperature in the 422 side of the duplex was being maintained by a thermostatically controlled heating system, exterior temperature would control the indoor/outdoor temperature differential and, thus, was expected to control the strength of the stack effect moving soil gas into the duplex.
- Human expert interpretation of “rules of thumb” derived from the previous studies in light of the next week’s weather forecast to predict vapor intrusion strength on an adjectival scale. The results from previous studies used for this purpose are given in Chapters 9 and 10 and summarized in Section 13.1.3 of U.S. EPA (2013).
- The use of real-time human observations of indoor radon concentrations and differential pressure on a weekly basis as an additional line of evidence for the vapor intrusion forecasts.
- An implicit mental model that the subsurface source term was relatively constant and, therefore, indoor air concentrations were primarily controlled by the current strength of the driving forces across the building envelope. Given the measured air exchange rates for the duplex are generally between 0.5 and 1.5 air exchanges per hour (U.S. EPA, 2012a, 2013), the indoor air concentration would be expected to respond to changes in the rate of infiltration of soil gas within several hours if the source strength in the subslab region was constant.

Some aspects of the observed trends in indoor air concentrations were predicted more accurately than others. Notably, an unpredicted decline in indoor air concentrations of VOCs was observed to begin in December despite sustained and even intensifying cold weather. Meanwhile, radon concentrations in indoor air stayed relatively high throughout the winter, suggesting that somewhat different mechanisms control VOC vs. radon vapor intrusion at this house. In our forecasting approach, the sustained cold weather was expected to lead to a continuing strong stack effect and consistently high indoor VOC concentrations, which did not occur during the winter of 2013–2014.

9.1.2 Additional Analysis: Vapor Intrusion Mechanisms and Driving Forces

The discrepancy between predicted and actual vapor intrusion led us to conduct a more in-depth analysis of the driving forces and mechanisms of vapor intrusion in this duplex. This analysis revealed the following:

- Dramatic differences between the range of indoor air VOC concentrations experienced in one winter to the next reemphasized that year-to-year meteorological or hydrogeological variations can be an important factor in vapor intrusion.
- The week-to-week change in the differential temperature (and thus the stack effect) was more significant than the absolute value of the differential temperature. In other words, indoor air concentrations of VOCs are expected to be high when the weather is suddenly getting colder but would not necessarily be expected to be as high during a period of sustained cold weather. This statistical finding agrees with a repeatable trend in the duplex indoor air data set in which the indoor air concentrations were observed to peak early in winter.

For example, increasing values of the calculated stack effect strength were statistically associated with higher chloroform indoor concentrations, but the stack effect strength values in and of themselves were not. This result may suggest why chloroform concentrations in our data sets tended to peak in late fall/early winter because that is the time of year when cooling temperatures would be expected to result in an increasing stack effect. A physical explanation of this result may be that an increasing stack effect encourages advective chloroform migration but that sustained migration may temporarily deplete the source (such as chloroform in vadose zone soils affected by a sewer or line the concentration of PCE at the interface between groundwater and soil gas). This behavior has been previously observed in the chamber-scale vapor intrusion experiments of Illangasekare and Petri (2013).

- Underlying, repeatable gradual seasonal trends in subslab soil gas concentrations appear to be present in the data set that were not well predicted based on our 7-day forecasts. These trends in subslab soil gas concentration correlate generally with trends in indoor concentrations. Although these trends repeated over several years, they did not have the same effect on two different subslab ports beneath the same side of the same duplex. Several mechanisms, such as temporary depletion of soil gas concentrations and periodic flood events affecting groundwater levels, could potentially explain such seasonal-scale variations.
- The relationships between several predictor variables and indoor air concentrations were apparently nonlinear. For example an inflection point was noted in the temperature data at approximately 52 to 55 °F. A U-shaped relationship between indoor air humidity and indoor PCE concentrations was noted with minimal PCE concentrations reached at intermediate humidities. A similar U-shaped relationship was noted between indoor air concentrations and continuous measurements of soil moisture directly beneath the basement floor. The relationships among the predictor variables may also be additive synergistic—this requires further analysis.
- In this report, we show that the most consistent relationship for barometric pressure is that an elevated (greater than 30 inches) and/or rising barometric pressure is associated with increasing vapor intrusion.
- In the time series analysis chapter of this report (**Section 6**), we show a strong statistical relationship between increases in radon concentration and VOC concentrations in indoor air. In some data sets, radon as a predictor was found to be statistically significant at the 1% level and to predict 40 to 60% of the variability in indoor air VOC concentrations (see specifically **Sections 6.2.5.4** and **6.2.5.5**).

The radon literature points to as many as 10 variables that continuously interact to control indoor radon concentrations. In this study, we found that the proportion of the VOC variability predicted by any one statistically significant predictor variables alone was modest (<30%). The ability of human experts to effectively predict such a complex multivariable process is expected to be limited. For example, despite more than a century of study, access to computerized forecasting tools, and large observational data sets weather forecasts can still be inaccurate.

9.1.3 Groundwater as a Vapor Intrusion Source

With respect to the continual study of groundwater concentrations at the Indianapolis site, perhaps the most important finding was the reasonable agreement between the observed deep soil gas PCE concentrations and those predicted by Henry's law from groundwater concentrations and, in contrast, that chloroform is generally more concentrated in the deep soil gas than in groundwater. This is consistent with a conceptual site model in which (1) PCE is migrating to the immediate vicinity of the house in groundwater and vapor intrusion is driven by transport from groundwater and (2) chloroform is arriving at the immediate vicinity of the house at least in part from other sources, such as a buried storm sewer or sewer main. Additional conclusions from the study of groundwater concentrations include the following:

- Observations and statistical tests of groundwater PCE and chloroform data indicate that ground VOC concentrations remain sand consistent at the Indianapolis site, especially for PCE.
- Chloroform also generally shows less than an order of magnitude variability, but concentrations did consistently increase by almost an order of magnitude in the latter part of this study during the winter of 2013–3014. This suggests different sources for chloroform and PCE, which is consistent with other lines of evidence in this study.
- No correlation was observed or measured between groundwater sample depths, groundwater (water table) levels, and VOC levels in groundwater.

These findings supplement the results of tracer tests reported in Sections 12.2 and 13.1.3 of our previous report (U.S. EPA, 2013). In those tracer tests, we showed migration in a few days of up to 20 ft laterally. The tracer tests also showed migration in a few days from 13 ft bls (near the water table) to 6 ft bls (basement floor elevation). In our first report on this project, we showed that the deep vs. shallow differential pressure responded strongly to the use of a box fan in the house to cause depressurization (U.S. EPA, 2012a, Section 12.2). These previous findings suggest that advective flow is a dominant influence on the vertical and lateral migration of soil gas to the house, at least within the horizontal and vertical limits of the well network installed on the duplex lot for this project.

9.2 Considerations for Practitioners

The following ideas are presented for consideration by vapor intrusion practitioners based on the research performed at the Indianapolis duplex site:

- Current indoor air sampling guidance that implicitly considers a sample collected at any time in any winter as a reasonable prediction of near-worst-case vapor intrusion should be reconsidered, especially when actual VOC concentrations are close ($\pm 30\%$) to the target exposure threshold values. Similarly, approaches that base an expectation for near-worst-case conditions on a single variable, such as indoor/outdoor temperature differential, are unlikely to lead to accurate predictions. One possible interim approach, based on our research site findings, would be to collect two samples in a winter, one in early to mid-winter and another later in the winter months. Prediction approaches that emphasize the week-to-week change in the values of the predictor variables, such as temperature differential and radon concentration, should be further tested.
- Should it be necessary to establish the worst-case short-term indoor air concentrations (with an exposure averaging period ranging from 1 week to 1 month), it will be necessary to consider year-to-year variations in meteorological conditions because it is possible to observe indoor air concentrations continuously for several months during one winter but miss by a factor of approximately 5 peak concentrations observed in prior and subsequent winters. Thus, to accurately measure the peak short-term concentrations expected over a long exposure period (e.g., years), one would likely have to sample various times during multiple years to capture the effect of extreme weather effects. Alternatively, an appropriate factor of safety could be applied to the available measurements.
- We continue to see no evidence of a statistically significant rain effect in our data set.
- Rather than expecting high radon concentrations at any given time to be predictive of high VOC concentrations, practitioners should consider *increasing* values of radon concentrations in indoor air as a strong predictor of *increasing* VOC vapor intrusion. Similarly, the rapid decrease in outdoor temperature appears to be a better predictor if vapor intrusion than cold temperature alone.

9.3 **Potential for Improvements in the Analysis and Prediction of Vapor Intrusion Temporal Variability**

Vapor intrusion strength appears to be a function of multiple independent weather and hydrological variables interacting in complex ways. There is no assurance that the most important variables in this single case study will be the most important variables at all residences in the United States. Most analyses of VOC vapor intrusion to date have attempted to correlate indoor concentrations directly to the current value of single variables. But the evidence from radon and this VOC study is clear that multiple variables—perhaps as many as 10—interact to control vapor intrusion. Therefore, we suggest that other detailed data sets be studied using a similar approach in which a formal statistical time series analysis is combined with graphical visualization of relationships *between changes in* predictor and outcome variables. These other data sets should encompass a range of geologic and climatic conditions as well as a variety of building construction styles. These time series analyses need also to be extended to consider the interaction of multiple predictor variables and the potential for nonlinear effects.

Our attempt to forecast worst-case vapor intrusion conditions based on human expert judgment and rules of thumb derived from previous data sets was not completely successful. As an international expert panel notes *“not only do people—including experts—suffer various forms of myopia; they also often are oblivious of the fact. Indeed, statistical linear models summarizing the relationship between a set of predictor variables and a predicted outcome often (repeatedly) perform better than intuitive expert judgments (or subjective expert opinions). Burgeoning empirical evidence suggests that humans, including experts, can be inept at making judgments, particularly under conditions of high uncertainty”* (McCarthy et al., 2001). Human forecasters also have a difficult time predicting phenomena that are controlled by numerous interacting variables. For example, Doswell and Shultz (2006) write in the context of severe weather forecasting that *“Forecasters and researchers generally acknowledge that any single diagnostic variable considered in isolation has little forecast value. Nevertheless, in our experience, we have seen instances where forecasters, often under forecast deadline pressure, will make forecast decisions based heavily, if not primarily, on a single diagnostic variable.”*

This information suggest that a more completely automated forecasting approach to vapor intrusion may perform better than a human expert’s judgment informed by rules of thumb derived from quantitative analysis of previous indoor air concentrations. This information also suggests that practitioners’ current attempts to select near-worst-case sampling conditions on the basis of guidance documents, rules of thumb, and experience at other sites are likely to be ineffective.

10. References

- Aaltonen, J., H. Pumpanen, T. Hakola, S. Vesala, R. Rasmus, and J. Back. 2012. Snowpack concentrations and estimated fluxes of volatile organic compounds in a boreal forest. *H. Biogeosciences* 9:2033–2044.
- Abreu, L.D., and P.C. Johnson. 2005. Effect of vapor source—building separation and building construction on soil vapor intrusion as studied with a three-dimensional numerical model. *Environmental Science and Technology* 39(12):4550–4561.
- Abreu, L.D., and P.C. Johnson. 2006. Simulating the effect of aerobic biodegradation on soil vapor intrusion into buildings: influence of degradation rate, source concentrations. *Environmental Science and Technology* 40(7):2304–2315.
- AFCEE (Air Force Center for Environmental Excellence). 2004. *Principles and Practices of Enhanced Anaerobic Bioremediation of Chlorinated Solvents*. Prepared for AFCEE, Brooks City-Base, TX. Available at http://costperformance.org/remediation/pdf/principles_and_practices_bioremediation.pdf.
- Akaike H., 1974, IEEE Trans. Auto. Control, 19, 716.
- Allen, M.K., D. Grande, and L. Pansch. 2007. *Evaluation of Passive Sampling Techniques for Monitoring Roadway and Neighborhood Exposures to Benzene and Other Mobile Source VOCs*. Wisconsin Department of Natural Resources (WDNR) Publication AM-384 2007. WDNR, Madison, WI. funded by U.S. EPA Community Scale Monitoring Grant. Available at <http://dnr.wi.gov/topic/AirQuality/documents/RoadwayStudyFinal.pdf>.
- Armstrong, R.L., and E. Brun. 2008. *Snow and Climate: Physical Processes, Surface Energy Exchange and Modeling*. Cambridge University Press.
- Arvela, H. 2008. *Radonsafe Foundation, Moisture Prevention and Air Exchange in a Healthy Building*. Finnish Research Programme on Environmental Health. Available at <http://www.ktl.fi/sytty/abstracts/arvela.htm>.
- ATSDR (Agency for Toxic Substances and Disease Registry). 1997. *Toxic Substances Portal—Toxicological Profile for Chloroform*. Available at <http://www.atsdr.cdc.gov/toxprofiles/tp.asp?id=53&tid=16>.
- Batterman, S., T. Metts, and P. Kalliokoski. 2002a. Diffusive uptake in passive and active absorbent sampling using thermal desorption tubes. *Journal of Environmental Monitoring* 4:870.
- Batterman, S., T. Metts, and P. Kalliokoski. 2002b. Low-flow active and passive sampling of VOCs using thermal desorption tubes: Theory and application at an offset printing facility. *Journal of Environmental Monitoring* 4:361–370.
- Begerow, J., E. Jermann, T. Keles, and L. Dunemann. 1999. Performance of two different types of passive samplers for the GC/ECD-FID determination of environmental VOC levels in air. *Fresenius Journal of Analytical Chemistry* 363:399–403.
- Bender., J.A. 1957. *Air Permeability of Snow*. Res. Rep. 37 Snow, Ice and Permafrost Research Establishment (U.S. Army Corps of Engineers) Wilmette, IL. p. 46–62.

- Bertoni, G., R. Tappa, and I. Allegrini. 2001. Internal consistence of the new “Analyst” diffusive sampler: a long term field test. *The Diffusive Monitor* 12:2–5.
- Bozkurt, O., K.G. Pennell, and E.M. Suuberg. 2007a. Evaluation of characterization techniques for vapor intrusion scenarios using a three-dimensional computational fluid dynamics (CFD) model. Air and Waste Management Association, Providence, RI, September.
- Bozkurt, O., K.G. Pennell, and E.M. Suuberg. 2007b. Characterizing vapor intrusion scenarios using a computational fluid dynamics model. ACS National Meeting. Boston, MA. August.
- Brenner, D. 2007. Effect of meteorological and site conditions on, and relationship of diurnal variation to, vapor intrusion at NASA Ames Research Center. Conference Proceeding from *Vapor Intrusion: Learning from the Challenges*—Air and Waste Management Association (AWMA), Providence, RI.
- Brown, V., and D. Crump. 1993. Appropriate sampling strategies to characterize VOCs in indoor air using diffusive samplers. Pp. 241–249 in *Proceedings of International Conference on VOCs*, London, October 27–28.
- Bruno, P., M. Caputi, M. Caselli, G. de Gennaro, and M. de Rienzo. 2005. Reliability of a BTEX radial diffusive sampler for thermal desorption: Field measurements. *Atmospheric Environment* 39:1347–1355.
- CA DTSC (California Department of Toxic Substances Control). 2011. *Final Guidance for the Evaluation and Mitigation of Subsurface Vapor Intrusion to Indoor Air (Vapor Intrusion Guidance)*. California Environmental Protection Agency, Sacramento. October. Available at http://www.dtsc.ca.gov/AssessingRisk/upload/Final_VIG_Oct_2011.pdf.
- CA DTSC (California Department of Toxic Substances Control). 2012. *Advisory Active Soil Gas Investigations*. California Environmental Protection Agency, DTSC, Los Angeles Regional Water Quality Control Board, San Francisco Regional Water Quality Control Board. Sacramento, CA April. Available at http://www.dtsc.ca.gov/SiteCleanup/upload/VI_ActiveSoilGasAdvisory_FINAL_043012.pdf.
- Cao, X.L., and C.N. Hewitt. 1994. Study of the degradation by ozone of adsorbents and hydrocarbons adsorbed during the passive sampling of air. *Environmental Science and Technology* 28:757–725.
- Carr, D.B., P.G., Laurent, C. Levy, and A.H. Horneman. 2011. Stylistic modeling of vadose zone transport insight into vapor intrusion processes. Presented at the *AEHS Workshop: Addressing Regulatory Challenges in Vapor Intrusion. A State of the Science Update*. San Diego CA, March 15.
- Case, J., and K. Gorder. 2006. The investigation of vapor intrusion at Hill AFB. Conference Proceeding from *Vapor Intrusion: The Next Great Environmental Challenge—An Update*. Air and Waste Management Association (AWMA), Los Angeles, CA.
- Christ, Maj John A. 2010. Vapor intrusion from entrapped NAPL sources and groundwater plumes: process understanding and improved modeling tools for pathway assessment. Presented at *SERDP Technical Exchange Meeting*, August 16.

-
- Cleveland, W.S. and S.J. Devlin. 1988. Locally-weighted regression: an approach to regression analysis by local fitting. *Journal of the American Statistical Association* 83(403):596–610.
- Cleveland, W.S. 1981. LOWESS: A program for smoothing scatterplots by robust locally weighted regression. *The American Statistician* 35(1):54.
- Cocheo, C., C. Boaretto, D. Pagani, F. Quaglio, P. Sacco, L. Zaratini, and D. Cottica. 2009. Field evaluation of thermal and chemical desorption BTEX radial diffusive sampler Radiello® compared with active (pumped) samplers for ambient air measurements. *Journal of Environmental Monitoring* 11:297–306.
- Cochrane, D., and G. H. Orcutt. 1949. Application of least squares regression to relationships containing autocorrelated error terms. *Journal of the American Statistical Association* 44:32–61,
- Cody, R.J., A. Lee, and R. Wiley. 2003. Use of radon measurements as a surrogate for relative entry rates of volatile organic compounds in the soil gas. Presented at the *AWMA Conference on Indoor Air Quality Problems and Engineering Solutions*. Research Triangle Park, NC, July 21–23.
- Cohen, A. B. 1971. *Concepts of Nuclear Physics*. McGraw-Hill.
- Colby College. 2009. *Regression: Patterns of Variation*. Colby College Biology Department. Available at <http://www.colby.edu/biology/BI17x/regression.html>.
- Conway, H. and J. Abrahamson. 1984. Air permeability as a textural indicator of snow. *Journal of Glaciology* 30(106):328-333.
- Coyne, L. 2010. Personal communication. SKC, Inc. August 17.
- Dawson, H. 2008. *US EPA's Vapor Intrusion Database—Preliminary Evaluation of Attenuation Factors for Chlorinated VOCs in Residences*. U.S. EPA Office of Superfund Remediation and Technology Innovation (OSRTI).
- Dawson, H., and H. Schuver. 2010. *US EPA's Vapor Intrusion Database: Preliminary Evaluation of Attenuation Factors for Chlorinated VOCs in Residences*. Presented at the 20th Annual International Conference on Soils, Sediments, Water and Energy, March 16.
- Defiant Technologies. 2012. FROG-4000™ Chemical Analysis System. Available at <http://www.defiant-tech.com/pdfs/FROG-4000%20Users%20Manual%202012%20V3.pdf>.
- DePersio, T., and J. Fitzgerald. 1995. Guidelines for the Design, Installation, and Operation of Sub-Slab Depressurization Systems. Massachusetts Department of Environmental Protection, Northeast Regional Office. Available at <http://www.mass.gov/dep/cleanup/laws/ssd1e.pdf>.
- DeVaull, G.E. 2012. Analysis and interpretation of time-variable vapor intrusion data: pressure-driven flow across building foundations. Proceedings paper, *AWMA Vapor Intrusion Conference*.
- DeVaull, G.E. 2013. Analysis and interpretation of time-variable vapor intrusion data: pressure driven flow across building foundations. Presented at *The 23rd Annual International Conference on Soil, Water, Energy, and Air*. San Diego, CA. March.
-

- Dickson, J., A. Lonegran, and R. Stetson. 2010. Characterization of multiple chlorinated solvent plumes due to the impact of TCE screening level reduction. *International Journal of Soil, Sediment and Water* 3(2): Section 11.
- Dietz, R.N., and E.A. Cote. 1982. Air infiltration measurements in a home using convenient perfluorocarbon tracer technique. *Environment International* 8(1-6):419–433.
- Dietz, R.N., et al. 1986. Detailed description and performance of a passive perfluorocarbon tracer system for building ventilation and air exchange measurements. Pp. 203–254 in *Measured Air Leakage of Buildings: A Symposium*. Heinz R. Trechsel, Peter L. Lagus, ASTM Committee E-6 on Performance of Building Constructions Contributor Heinz R. Trechsel, Peter L. Lagus. Published by ASTM International.
- DiGiulio, D., C. Paul, R. Cody, R. Willey, S. Clifford, P. Kahn, R. Mosley, A. Lee, and K. Christensen. 2006. *Assessment of Vapor Intrusion in Homes near the Raymark Superfund Site Using Basement and Subslab Air Samples*. EPA/600/R-05/147. U.S. EPA Office of Research and Development, Ada, OK, March.
- Distler, M., and P. Mazierski. 2010. Soil vapor migration through subsurface utilities. Proceedings 2010 AWMA Vapor Intrusion Specialty Conference. Chicago, IL. September. Available at <http://events.awma.org/education/Final%20Papers/6-Distler.PDF>.
- Division of Spill Prevention and Response Contaminated Sites Program. 2012. *Vapor Intrusion Guidance for Contaminated Sites*. October. Available at <http://dec.alaska.gov/spar/csp/guidance/Vapor%20Intrusion%20Guidance.pdf>.
- Dosewill, C.A., and D.M. Schultz. 2006. On the use of indices and parameters in forecasting, *E-Journal of Severe Storms Meteorology* 1(3). Available at <http://www.ejssm.org/ojs/index.php/ejssm/article/viewArticle/11/12>.
- Eklund, B., and D. Burrows. 2009. Prediction of indoor air quality from soil-gas data at industrial buildings. *Groundwater Monitoring and Remediation* 29(1):118–125.
- Environmental Quality Management. 2004. *Users Guide for Evaluating Subsurface Vapor Intrusion into Buildings*. Prepared for US EPA under EPA Contract Number: 68-W-02-33, WA No. 004, PN 030224.0002. Available at http://www.epa.gov/oswer/riskassessment/airmodel/pdf/2004_0222_3phase_users_guide.pdf.
- Folkes, D., W. Wertz, J. Kurtz, and T. Kuehster. 2009. Observed spatial and temporal distributions of CVOCs at Colorado and New York vapor intrusion sites. *Ground Water Monitoring & Remediation* 29(1):70–80.
- Forbes, J., J. Havlena, M. Burkhard, and K. Myers. 1993. Monitoring of VOCs in the deep vadose zone using multi-port soil gas wells and multi-port soil gas/ground-water wells. Pp. 557–571 in *Proceedings of the Seventh National Symposium on Aquifer Restoration, Ground-water Monitoring, and Geophysical Methods*, National Ground Water Association, Dublin, OH.
- ForecastAdvisor. 2014. Weather forecast accuracy details for Indianapolis, Indiana. Available at <http://www.forecastadvisor.com/detail/Indiana/Indianapolis/46201/>. Accessed June 28, 2014.

- Garbesi, K., and R.G. Sextro. 1989. Modeling and field evidence of pressure-driven entry of soil gas into a house through permeable below-grade walls. *Environmental Science and Technology* 23(12):1481–1487.
- Greiner, M.A., and R.M. Franza. 2003. Barriers and bridges for successful environmental technology transfer. *The Journal of Technology Transfer* 28(2):167–177(11).
- GSI Environmental. 2008. *Final Report: Detailed Field Investigation of Vapor Intrusion Processes*. ESTCP Project ER-0423, September.
- Hall, S.K., J. Chakraborty, and R.J. Ruch. 1997. *Chemical Exposure and Toxic Responses*. Boca Raton, FL: CRC Press.
- Hartman, B. 2006. *How to Collect Reliable Soil-Gas Data for Risk-Based Applications—Specifically Vapor Intrusion: Part 4 – Updates on Soil-Gas Collection and Analytical Procedures*. LUSTLine Bulletin 53.
- Hartigan, J.A., and M.A. Wong. 1979. Algorithm AS 136: A k-means clustering algorithm. *Journal of the Royal Statistical Society. Series C (Applied Statistics)* 28(1):100-108.
- Hosoda, M., A. Sorimachia, S. Tokonamia, T. Ishikawaa, S.K. Sahooa, N.M.M. Hassanb, M. Fukushib, and S. Uchidaa. 2008. Generation and control of radon from soil. *Proceedings of 12th International Congress of the International Radiation Protection Association*. Available at <http://www.irpa12.org.ar/fullpapers/FP0971.pdf>
- Hass, B.S., and R. Herrmann. 1998. Tracing volatile organic compounds in sewers. *Water Science and Technology* 37(1):295–301.
- Hayes, H. 2008. Air Toxics Ltd., personal communication to Chris Lutes, ARCADIS, August.
- Heggie, A.C., and B. Stavropoulos. 2019. Evaluating vapor intrusion risk using comparative dynamic and passive flux chambers at a TCE impacted site in Sydney Australia. Available at <http://events.awma.org/education/Final%20Papers/7-Heggie.pdf>. Paper presented at AWMA 2010 Vapor Intrusion Specialty Conference.
- Helsel, D.R. 2005. *Nondetects and Data Analysis: Statistics for Censored Environmental Data*. Hoboken, NJ: Wiley.
- Henry, N.W. 2001. R-square and standardization in regression. Virginia Commonwealth University. March. Available at <http://www.people.vcu.edu/~nhenry/Rsq.htm>.
- Hers, I., M. Lahvis, P. Dahlen, E. Hong Luo, G. DeVauil, and P. Johnson. 2011. *Cold Climate Vapor Intrusion Research Study – Results of Seasonal Monitoring of House at North Battleford, Saskatchewan*. <http://indoorairproject.files.wordpress.com/2011/03/sgs-attachment-4.pdf> cited as in preparation in http://www.epa.gov/oust/cat/pvi/PVI_Database_Report.pdf.
- Holton, C., H. Lou, P. Dahlen, K. Gorder, E. Dettenmaier, and P. Johnson. 2013a. Temporal variability in indoor air concentrations under natural conditions in a house overlying a dilute chlorinated solvent groundwater plume. *Environmental Science & Technology* 47(23):13347-13354.

- Holton, C., H. Luo, Y. Guo, P. Dahlen, P.C. Johnson, K. Gorder, and E. Dettenmaier. 2013b. Multi-year monitoring of a house over a dilute CHC plume: implications for pathway assessment using indoor air sampling and forced under-pressurization tests. Presented at *Looking Beyond Natural Variation in Vapor Intrusion: Understanding, Controlling, and Addressing Site Variables for Improved Practices and Effective Protection Strategies*. EPA Workshop at *The 23rd Annual International Conference on Soil, Water, Energy, and Air*, San Diego, CA. March. Available at https://iavi.rti.org/attachments/WorkshopsAndConferences/05_Johnson_03-19-13.pdf.
- Howard, P.H., R.S. Boethling, W.F. Jarvis, W.M. Meylan, and E.M. Michalenko. 1991. *Handbook of Environmental Degradation Rates*. Chelsea, MI: Lewis Publishers, Inc.
- Hui, S.C. 2003. *Lecture: Air Movement and Natural Ventilation*. Department of Mechanical Engineering, The University of Hong Kong. Used by Permission from Dr. Hui. Available at <http://www.arch.hku.hk/teaching/lectures/airvent/sect03.htm>.
- Illangasekare, T.H., and B. Petri. 2013. Climate and hydrogeologic factors contributing to variability of observed vapor concentrations in buildings due to vapor intrusion: experimental and modeling investigation. Presented at *REMTEC 2013*, Westminster, CO. March 4-6.
- IndyGov. 2012. *My Neighborhood*. Available at <http://maps.indy.gov/myneighborhood/>.
- Inside EPA. Regions Split Over Short-Term TCE Limit, Highlighting Need for EPA Guide. <http://insideepa.com/Superfund-Report/Superfund-Report-01/07/2013/regions-split-over-short-term-tce-limit-highlighting-need-for-epa-guide/menu-id-1094.html>
- ITRC (Interstate Technology and Regulatory Council). 2007. Vapor Intrusion Pathway: A Practical Guideline. Prepared by The Interstate Technology & Regulatory Council Vapor Intrusion Team. Available at <http://www.itrcweb.org/documents/VI-1.pdf>.
- Johnson, P.C., and R.A. Ettinger. 1991. Heuristic model for predicting the intrusion rate of contaminant vapors into buildings. *Environmental Science and Technology* 25:1445–1452.
- Johnson, P.C., E. Luo, C. Holton, P. Dahlen, Y. Guo, K. Gorder, and E. Dettenmaier. 2012. Vapor intrusion above a dilute CHC plume: lessons-learned from two years of monitoring. Presentation at AEHS Conference, March. Available at https://iavi.rti.org/attachments/WorkshopsAndConferences/09_P%20Johnson%20AEHS%20Talk%20032112.pdf.
- Johnson, P.C., C. Holton, Y. Guo, P. Dahlen, E. Luo, K. Gorder, and E. Dettenmaier. 2014. Lessons-learned from four years of intensive monitoring of a house over a dilute chlorinated hydrocarbon plume. Presented at: *Vapor Intrusion (VI) Exposures – The Challenges of, Need for, and Benefits of Long Term Stewardship*. The 24th Annual AEHS International Conference on Soil, Water, Energy, and Air—March 18, 2014, San Diego, CA. Available at https://iavi.rti.org/attachments/WorkshopsAndConferences/5_JohnsonSunDevil_031814.pdf.
- Jones, A. no date. Math 141, Reed College: Lecture 25: F-tests and R² examples and issues. Available at <http://people.reed.edu/~jones/Courses/P25.pdf>
- Judge, G.G, W.E. Griffiths, R.C. Hill, H. Lutkepohl, and T.C. Lee. 1985. *The Theory and Practice of Econometrics*, Second Edition. New York: Wiley.

- Jury, W.A., D. Russo, G. Streile, and H.E. Abd. 1990. Evaluation of volatilization by organic chemicals residing below the soil surface. *Water Resources Research* 26(1):13–20.
- Koontz, M.D., and H.E. Rector. 1995. *Estimation of Distributions for Residential Air Exchange Rates*. EPA Contract No. 68-D9-0166, Work Assignment No. 3-19. U.S. EPA Office of Pollution Prevention and Toxics. Washington, DC.
- Krewski, D., R. Mallick, J.M. Zielinski, and E.G. Létourneau. 2005. Modeling seasonal variation in indoor radon concentrations. *Journal of Exposure Analysis & Environmental Epidemiology* 15(3):234–243.
- Kuehster, T.E., D.J. Folkes, and E.J. Wannamaker. 2004. Seasonal variation of observed indoor air concentrations due to vapor intrusion. Presented at the *Midwestern States Risk Assessment Symposium*, Indianapolis, IN.
- Kurtz, J.P., and D.J. Folkes. 2008. Empirical data on lag time for vapor intrusion from a chlorinated VOC groundwater plume. Presented at *AEHS San Diego Conference*, March 12.
- Lau, P. 2008. Calculation of flow rate from differential pressure devices – orifice plates. Presented to the *European Metrology Association for Thermal Energy Measurement*, August 2–4.
- Lee, A., K. Baylor, P. Reddy, and M. Plate. 2010. EPA Region 9’s RARE opportunity to improve vapor intrusion indoor air investigations. Presented at the *20th Annual International Conference on Soils, Sediments, Water and Energy*, San Diego, CA. March 16.
- Lewis, R.K., and P.N. Houle. 1985. *A Living Radon Reference Manual*.
http://www.dep.state.pa.us/brp/radon_division/LivingRadonReferenceManual.htm reviewing Nazaroff, W. and Doyle, S. Radon Entry into Houses Having a Crawl Space. *Health Physics* 48:265–281.
- Liddle, A.R. 2004. How many cosmological parameters. *Monthly Notices of the Royal Astronomical Society* 351(3): L49-L53. Available at
<http://ned.ipac.caltech.edu/level5/March04/Liddle/Liddle2.html>.
- Linn, W., L. Appel, R. DeZeeuw, P. Doorn, J. Doyon, T. Evanson, J. Farrell, D. Hanson, R. Jurgens, J. So, C. Speigel, D. Switek, and S. Yankey. 2010. *Conducting Contamination Assessment Work at Drycleaning Sites*. State Coalition for Remediation of Drycleaners. Available at
<http://www.drycleancoalition.org/download/assessment.pdf>.
- Loureiro, C.O., and L.M. Abriola. 1990. Three-dimensional simulation of radon transport into houses with basements under constant negative pressure. *Environmental Science and Technology* 24(9):1338–1348.
- Luo, H., P. Dahlen, P. Johnson, T. Creamer, T. Peargin, P. Lundegard, B. Hartman, L. Abreau, and T. McAlary. 2006. Spatial and temporal variability in hydrocarbon and oxygen concentrations beneath a building above a shallow NAPL source. Presented at the *Battelle Conference on Remediation of Chlorinated and Recalcitrant Compounds*, Monterey, CA, May.
- Luo, H., P. Dahlen, P.C. Johnson, T. Peargin, and T. Creamer. 2009. Spatial variability of soil-gas concentrations near and beneath a building overlying shallow petroleum hydrocarbon-impacted soils. *Ground Water Monitoring & Remediation* 29(1):81–91.

- Lutes, C., Cosky, B., B. Schumacher, J. Zimmerman, H. Hayes, R. Truesdale, S. Lin, and B. Hartman. 2012a. Long-term detailed study of vapor intrusion temporal variability: implications for indoor air and soil gas sampling guidance. Oral Presentation and Short Paper: *AWMA Symposium on Air Quality Measurement Methods and Technology*, Durham, NC. April.
- Lutes, C., Cosky, B., L. Abreu, B. Schumacher, J. Zimmerman, R. Kapucinski, and R. Truesdale. 2012b. Can short-term fan testing provide insight into vapor intrusion. Oral Presentation and Short Paper: *AWMA Symposium on Air Quality Measurement Methods and Technology*, Durham, NC. April.
- Lutes, C., Cosky, B., Uppencamp, R., Abreu, L., Schumacher, B., Zimmerman, J. Truesdale, R., Lin, S., Hayes, H. and Hartman, B. 2012c. Recent observations on spatial and temporal variability in the field. Invited presentation at *EPA Workshop: Recent Advances to Vapor Intrusion Application and Implementation* at the 22nd Annual International Conference on Soil, Water, Energy & Air (AEHS) San Diego, March.
- Lutes, C., Cosky, B., Uppencamp, R., Abreu, L., Schumacher, B., Zimmerman, J. Truesdale, R., Lin, S., Hayes, H. and Hartman, B. 2012d. Short-term variability, radon tracer, and long-term passive sampler performance in the field. Invited presentation at *EPA Workshop: Recent Advances to Vapor Intrusion Application and Implementation* at the 22nd Annual International Conference on Soil, Water, Energy & Air (AEHS) San Diego, March.
- Lutes, C., P. Johnson, and R. Truesdale. 2013. Summary of evidence from “data-rich” studies and the challenges of using low-density monitoring data for vapor intrusion control. Presented at *Looking Beyond Natural Variation in Vapor Intrusion: Understanding, Controlling, and Addressing Site Variables for Improved Practices and Effective Protection Strategies*. EPA Workshop at The 23rd Annual International Conference on Soil, Water, Energy, and Air, San Diego, CA. https://iavi.rti.org/attachments/WorkshopsAndConferences/06_Truesdale_03-19-13.pdf.
- Lutes, C.C., R. Uppencamp, C. Singer, L. Abreu, R. Mosley, and D. Greenwell. 2009. *Radon Tracer as a Multipurpose Tool to Enhance Vapor Intrusion Assessment and Mitigation*. Poster presented at the Partners in Environmental Technology Technical Symposium and Workshop, Washington, DC, December.
- Lutes, C.C., R. Uppencamp, H. Hayes, D. Greenwell, and R. Mosley. 2010a. Long-term integrated samplers for indoor air and sub-slab soil gas at VI sites. Presented at the 2010 Battelle Conference, Monterey, CA.
- Lutes, C.C., R. Uppencamp, H. Hayes, R. Mosley and D. Greenwell. 2010b. Long-term integrating samplers for indoor air and subslab soil gas at VI sites. Presentation at *AWMA Specialty Conference: Vapor Intrusion 2010*, September 28–30, 2010. Chicago, IL. paper submitted to proceedings. Available at http://events.awma.org/education/Posters/Final/Lutes_RadonPoster.pdf or <http://events.awma.org/education/Final%20Papers/7-Lutes.pdf>
- Lutes, C.C., R. Uppencamp, H. Hayes, R. Mosley and D. Greenwell. 2010c. Long-term integrated samplers for indoor air and subslab soil gas at VI sites. Oral presentation at *Seventh International Remediation of Chlorinated and Recalcitrant Compounds Conference*, Monterey, CA; May 24–27.
- Lutes, C., R. Studebaker, and N. Weinberg. 2010d. *Optimal design of subslab depressurization systems for volatile organic compound vapor intrusion (VI) mitigation*. Poster presented at AWMA

- Specialty Conference: Vapor Intrusion 2010*, Chicago, IL, September 28–30. Available at http://events.awma.org/education/Posters/Final/Lutes_OptimalPoster.pdf.
- MacLeod, G., and J.M. Ames. 1986. Comparative assessment of the artifact background on thermal desorption of Tenax GC and Tenax TA. *Journal of Chromatography* 355:393–398.
- MADEP. 2002. *Indoor Air Sampling and Evaluation Guide*. Boston, MA: Commonwealth of Massachusetts Executive Office of Environmental Affairs, Office of Research and Standards, Department of Environmental Protection.
- Marotta, L., M. Snow, and S. Varisco. 2012. Extending the hydrocarbon range above naphthalene for soil vapor and air samples using automated thermal desorption/gas chromatography/mass spectrometry (ATD/GC/MS). Presented at *National Environmental Monitoring Conference*, Washington, DC, August 6–10.
- Maskarinec, M.P., C.K. Bayne, L.H. Johnson, S.K. Holladay, and R.A. Jenkins. 1989. *Stability of Volatile Organics in Environmental Water Samples: Storage and Preservation*. ORNL/TM-11300. Oak Ridge National Laboratory, Oak Ridge, TN. Available at <http://www.dtic.mil/get-tr-doc/pdf?AD=ADA412461>.
- Mazerolle, M.J. 2004. Appendix 1: Making sense out of Akaike's Information Criterion (AIC): its use and interpretation in model selection and inference from ecological data. In *Mouvements et reproduction des amphibiens en tourbières perturbées*. Available at <http://theses.ulaval.ca/archimede/fichiers/21842/apa.html>
- McAlary, T.A., P. Dollar, P. de Haven, R. Moss, G. Wilkinson, J. Llewellyn, and D. Crump. 2002. Assessment of subsurface vapour transport through Triassic sandstone and quarry fill into indoor air in Weston Village, Runcorn. Presented at Indoor Air 2002, Monterey, CA.
- McCarthy, J.J., et al. Eds. 2001. *Climate Change 2001: Impacts, Adaptation and Vulnerability, Working Group II: Impacts, Adaptation and Vulnerability*. Cambridge University Press, Cambridge, UK. Available at <http://www.ipcc.ch/ipccreports/tar/wg2/index.php?idp=109>.
- McHugh, T. E., and T.N. Nickels. 2007. Evaluation of spatial and temporal variability in VOC concentrations at vapor intrusion investigation sites. Conference Proceeding from *Vapor Intrusion: Learning from the Challenges*—Air and Waste Management Association (AWMA), Providence, RI.
- McHugh, T., P. De Blanc, and R. Pokluda. 2006. Indoor air as a source of VOC contamination in shallow soils below buildings. *Soil and Sediment Contamination* 15:103–22.
- McHugh, T.E., T.N. Nickels, and S. Brock. 2007. Evaluation of spatial and temporal variability in VOC concentrations at vapor intrusion investigation sites. Pp. 129–142 in *Proceeding of Air & Waste Management Association's Vapor Intrusion: Learning from the Challenges*, Providence, RI, September 26–28.
- McHugh, T.E., D.E. Hammond, T. N. Nickels, and B. Hartman. 2008. Use of radon measurements for evaluation of volatile organic compound (VOC) vapor intrusion. *Environmental Forensics* 9(1): 107-114.

- Middleditch, B.S. 1989. *Analytical Artifacts: GC, MS, HPLC, TLC and PC*. Journal of Chromatography Library Volume 44. Elsevier, Amsterdam. p. 668-669.
- Moses, H., H.F. Lucas and G.A. Zerbe. 1963. The effect of meteorological variables upon radon concentration three feet above the ground. *J. APCA*. 13(1):12-19.
- Mosley, R.B. 2007. Use of radon to establish a building-specific sub-slab attenuation factor for comparison with similar quantities measured for other vapor intrusion contaminants. Presented at the *National Environmental Monitoring Conference*, Cambridge, MA, August 19–25.
- Mosley, R.B., D. Greenwell, A. Lee, K. Baylor, M. Plate, and C. Lutes. 2008. Use of integrated indoor radon and volatile organic compounds (VOCs) to distinguish soil sources from above-ground sources. Extended abstract and oral presentation, *AWMA Symposium on Air Quality Measurement and Technology*, Chapel Hill, NC, November 6.
- Mosley, R.B., D. Greenwell, and C.C. Lutes. 2010. Use of integrated indoor concentrations of tracer gases and volatile organic compounds (VOCs) to distinguish soil sources from above-ground sources. Poster presented at the *Seventh International Remediation of Chlorinated and Recalcitrant Compounds Conference*, Monterey, CA, May 24–27.
- Murry, D.M., and D.E. Burmaster. 1995. Residential air exchange rates in the United States: Empirical and estimated parametric distributions by season and climatic region. *Risk Analysis* 15(4):459–65.
- NOAA (National Oceanic and Atmospheric Administration). 1998. *Automated Surface Observing System (ASOS) Users Guide*. In cooperation with Department of Defense, Federal Aviation Administration and United States Navy. March. Available at <http://www.nws.noaa.gov/asos/aum-toc.pdf>.
- National Weather Service. 2012. *Excessive Heat - An Underrated Problem*. National Weather Service Regional Office, Central Regional Headquarters. Available at <http://www.crh.noaa.gov/Image/lx/wcm/Heat/ExcessiveHeat.pdf>.
- Nau, R. 2005a. Duke University, Class Notes for Decision 411 Forecasting. Available at <http://people.duke.edu/~rnau/411diff.htm>.
- Nau, R. 2005b. Duke University, Class Notes for Decision 411 Forecasting. Available at <http://people.duke.edu/~rnau/411regou.htm>.
- Nazaroff, W.W. 1988. Predicting the rate of ²²²Rn entry from soil into the basement of a dwelling due to pressure-driven air flow. *Radiation Protection Dosimetry* 22(1/4):199–202.
- Nazaroff, W.W., and A.V. Nero (Eds.). 1988. *Radon and Its Decay Products in Indoor Air*. New York: John Wiley and Sons.
- Nazaroff, W.W., S.R. Lewis, S.M. Doyle, B.A. Moed, and A.V. Nero, 1987. Experiments on pollutant transport from soil into residential basements by pressure-driven airflow. *Environmental Science & Technology* 21:459–466.
- Neptune and Company. 2007. *Report for 2007 Annual Vapor Intrusion Sampling for Buildings N210 and 19 and Additional Baseline Sampling for Building 16*. Prepared for ISSi/SAIC NASA Ames Research Center Moffett Field, California 94035-1100 Neptune Project No 09501.

- New York Times*. 2012. *Toxic Waters: Indianapolis Water*. May 26. Available at <http://projects.nytimes.com/toxic-waters/contaminants/in/marion/in5249004-indianapolis-water>.
- Newton, E., and R. Rudela. 2007. Estimating correlation with multiply censored data arising from the adjustment of singly censored data. *Environmental Science and Technology* 41(1):221–228.
- NJ DEP (New Jersey Department of Environmental Protection). 2012. *Draft Vapor Intrusion Guidance*. January.
- NJ DEP (New Jersey Department of Environmental Protection). 2013. *Vapor Intrusion Technical Guidance*. January. Available at http://www.nj.gov/dep/srp/guidance/vaporintrusion/vig_main.pdf
- Odabasi, M. 2008. Halogenated volatile organic compounds from the use of chlorine-bleach-containing household products. *Environmental Science and Technology* 42:1445–1451.
- Odenchantz, J.E., H. O'Neill, S.J. Steinmacher, J.D. Case, and P.C. Johnson. 2008. Residential vapor intrusion evaluation: long duration passive sampling v. short duration active sampling. *Remediation Journal* 18(4):49–54. Available at <http://onlinelibrary.wiley.com/doi/10.1002/rem.20181/abstract>.
- Oury, B., F. Lhuillier, J. Protois, and Y. Moréle. 2006. Behavior of the GABIE, 3M3500, PerkinElmer Tenax TA, and RADIELLO 145 diffusive samplers exposed over a long time to a low concentration of VOCs. *Journal of Occupational and Environmental Hygiene* 3(10):547–557.
- Parker, G.B. 1985. Measurement of air exchange rates in residential and commercial buildings in the northwest: techniques and results. *PNL-SA-13507*. Presented at *Conference on Conservation in Buildings: Northwest Perspective*, Butte MT, May 20. Abstract available at http://www.osti.gov/energycitations/product.biblio.jsp?osti_id=5567459.
- Pennequin-Cardinala, A. et al. 2005. Performances of the Radiellos diffusive sampler for BTEX measurements: Influence of environmental conditions and determination of modeled sampling rates. *Atmospheric Environment* 39:2535–2544.
- Perron, P. 1988. Trends and random walks in macroeconomic time series. *Journal of Economic Dynamics and Control* 12:297–332.
- Provoost, J., F. Tillman, J. Weaver, L. Reijnders, J. Bronders, I. Van Keer, and F. Swartjes. 2010. Vapour Intrusion into Buildings – A Literature Review, Chapter 2. In: *Advances in Environmental Research*. Volume 5 ISBN: 978-1-61668-744-1 Editor: Justin A. Daniels ©2010 Nova Science Publishers, Inc.
- R Development Core Team. 2012. *R: A Language and Environment for Statistical Computing*. R Foundation for Statistical Computing, Vienna, Austria. Available at <http://www.R-project.org>.
- Razali, N., and Y.B. Wah. 2011. Power comparisons of Shapiro-Wilk, Kolmogorov-Smirnov, Lilliefors and Anderson-Darling tests. *Journal of Statistical Modeling and Analytics* 2(1):21–33. Available at <http://instatmy.org.my/downloads/e-jurnal%202/3.pdf>. Retrieved 5 June 2012.
- Revzan K.L., W.J. Fisk, and A.J. Gadgil. 1991. Modeling radon entry into houses with basements: model description and verification. *Indoor Air* 2:173–189.

- Robinson A.L., and R.G. Sextro. 1997. Radon entry into buildings driven by atmospheric pressure fluctuations. *Environmental Science and Technology* 31:1742–1748.
- Robinson, A.L., R.G. Sextro, and W.J. Fisk. 1997a. Soil-gas entry into an experimental basement driven by atmospheric pressure fluctuations—Measurements, spectral analysis and model comparison. *Atmospheric Environment*, 31(10):1477–1485.
- Robinson, A.L., R.G. Sextro, and W.J. Riley. 1997b. Soil-gas entry into houses driven by atmospheric pressure fluctuations - the influence of soil properties. *Atmospheric Environment* 31:1487–1495.
- Rorech, G. J. 2001. Vacuum Extraction and Bioventing, Chapter 3. In E.K. Nyer, et al. (Ed.). *In-situ Treatment Technology*, 2nd edition, Lewis.
- Ruiz, J., R. Bilbao, and M. Murillo. 1998. Adsorption of different VOC onto soil minerals from gas phase: influence of mineral, type of VOC, and air humidity. *Environmental Science and Technology* 32:1079-1084.
- Ryan, J.V, P.M. Lemieux, and W.T Preston. 1998. Near-real-time measurement of trace volatile organic compounds from combustion processes using an on-line gas chromatograph. *Waste Management* 18(6):403–410.
- Said, S.E. and D.A. Dickey. 1984. Testing for unit roots in autoregressive-moving average models of unknown order. *Biometrika* 71:599–607.
- Scheeringa, K., and K. Hudson. 2011–2013. *Monthly Climate Summaries*. Indiana State Climate Office. Available at <http://iclimate.org/summary.asp>.
- Scheeringa, K., and M. Price. 2013–2014. *Monthly Climate Summaries*. Indiana State Climate Office. Available at <http://iclimate.org/summary.asp>.
- Schumacher, B., J. Zimmerman, C. Lutes, B. Cosky, R. Truesdale, R. Norberg and B. Hartman. 2013. Indoor air and soil gas temporal variability: effects on sampling strategies evidence from controlled and uncontrolled conditions. Presented at *Looking Beyond Natural Variation in Vapor Intrusion: Understanding, Controlling and Addressing Site Variables for Improved Practices and Effective Protection Strategies*, at the 23rd Annual International Conference on Soil, Water, Energy and Air, San Diego, CA. March 19.
- Schumacher, B., J. Zimmerman, G. Swanson, J. Elliot, and B. Hartman. 2010. Field observations on ground covers/buildings. Presented at the 20th Annual International Conference on Soils, Sediments, Water, and Energy, San Diego, CA. March 16.
- Schuver, H. 2013. Radon as a tracer and risk driving co-contaminant in chemical vapor intrusion. Presentation at *RemTec 2013 Summit*, Westminster, CO, March 6.
- Schuver, H., and L. Siegel. 2011. Vapor intrusion: involved-stakeholder awareness of the uncertainty (and multiple benefits of controls). *Community Involvement Training Conference*, Crystal City VA, July. Available at http://epa.gov/ciconference/download/presentations/Wed_OpenTime%20Session_Salon6_SchuverSiegel.pdf.

- Schuver, H.J., and R.B. Mosley. 2009. Investigating vapor intrusion with confidence and efficiency (some observations from indoor air-based radon intrusion studies). *AWMA Vapor Intrusion 2009*, San Diego, CA.
- Schwarz, G. 1978. Estimating the dimension of a model. *The Annals of Statistics* 6(2): 461-464. March.
- Sigma-Aldrich. 2012. *Radiello Manual, Volatile Organic Compounds (VOCs) Chemically Desorbed with CS₂, Supelco Edition*. Available at http://www.sigmaaldrich.com/content/dam/sigmaaldrich/docs/Supelco/Application_Notes/radiello_d1_d6.pdf, accessed August 2012.
- Smajstrla, A.G., and D.S. Harrison. 1998. *Tensiometers for Soil Moisture Measurement and Irrigation Scheduling*. CIR487. Agricultural and Biological Engineering Department, Florida Cooperative Extension Service, Institute of Food and Agricultural Sciences, University of Florida. Available at <http://edis.ifas.ufl.edu/ae146>.
- Saint-Germain, M.A. 1997. Course notes for PPA 696 research methods lecture on simple regression. California State University Long Beach. Available at [http://www.csulb.edu/~msaintg/ppa696/696regs.htm#ELEMENTS OF A REGRESSION](http://www.csulb.edu/~msaintg/ppa696/696regs.htm#ELEMENTS_OF_A_REGRESSION). Accessed June 21, 2014.
- Steck, D.J. 2012. An update on the draft of “Lessons from radon for vapor intrusion research and programs”. Presented at EPA-AEHS Workshop, *Recent Advances to VI Application & Implementation*, San Diego, CA. March.
- The Polis Center. 2012. *Study Neighborhoods from the Project on Religion and Urban Culture: Mapleton-Fall Creek*. Footnote 2. The Polis Center, Indianapolis, IN. Available at http://www.polis.iupui.edu/RUC/Neighborhoods/MapletonFallCreek/MFCNarrative.htm#_ftn2.
- Thomas, R.G. 1990. Volatilization from Soil, Chapter 16. In W.J. Lyman, et al. (Eds.). *Handbook of Chemical Property Estimation Methods*. American Chemical Society.
- Tillman, F.D., and J.W. Weaver. 2005. Review of recent research on vapour intrusion, U. S. Environmental Protection Agency, Office of Research and Development, Washington, DC 20460, report EPA/600/R-05/106
- Truesdale, R., H. Dawson, and I. Hers. 2005. Vapor intrusion database status and updates. Presented at *Specialty Workshop on Integrating Observed and Modeled Vapor Attenuation, AEHS 15th Annual West Coast Conference on Soils, Sediments and Water*, San Diego, CA. March 14. Available at http://iavi.rti.org/attachments/Resources/1045_-_Truesdale_Vapor_Intrusion_Database_Status_and_Updates.pdf.
- U.S. DOE (Department of Energy). *Innovative Technology Summary Report: Frozen Soil Barrier*. DOE/EM-0483 October 1999.
- U.S. EPA (Environmental Protection Agency). 1989. *Risk Assessment Guidance for Superfund Volume I: Human Health Evaluation Manual (Part A)*. EPA/540/1-89/002. Office of Emergency and Remedial Response, Washington, DC. December. Available at <http://www.epa.gov/oswer/riskassessment/ragsa/index.htm>.

- U.S. EPA (Environmental Protection Agency). 1990. *NAREL Standard Operating Procedures for Radon-222 Measurement Using Diffusion Barrier Charcoal Canisters*. EPA 520/5-90/032 Stock Number PB91-179002. U.S. EPA National Air and Radiation Environmental Lab., Montgomery AL.
- U.S. EPA (Environmental Protection Agency). 1991. *Risk Assessment Guidance for Superfund Volume I: Human Health Evaluation Manual (Part B, Development of Risk-based Preliminary Remediation Goals)*. EP A/540/R-92/003, Publication 9285.7-01 B. Office of Emergency and Remedial Response, Washington, DC. December. Available at <http://www.epa.gov/oswer/riskassessment/ragsb/>.
- U.S. EPA (Environmental Protection Agency). 1992. *Indoor Radon and Radon Decay Product Measurement, Device Protocols*. EPA 402-R-92-004, Office of Radiation Programs, Washington, DC, July (revised).
- U.S. EPA (Environmental Protection Agency). 1993a. *Protocols for Radon and Radon Decay Product Measurements in Homes*. EPA-402-R-92-003, May 1993a.
- U.S. EPA (Environmental Protection Agency). 1993b. *Radon Reduction Techniques for Existing Detached Houses, Technical Guidance (third edition) for Active Soil Depressurization Systems*. EPA/625/R-93/011.
- U.S. EPA (Environmental Protection Agency). 1996a. *Aromatic and Halogenated Volatiles by Gas Chromatography Using Photoionization and/or Electrolytic Conductivity Detectors*. SW-846 Method 8021b. Office of Solid Waste and Emergency Response, Washington, DC. December. Available at <http://www.epa.gov/osw/hazard/testmethods/sw846/pdfs/8021b.pdf>.
- U.S. EPA (Environmental Protection Agency). 1996b. *Determinative Chromatographic Separations*. SW-846 Method 8000b. Office of Solid Waste and Emergency Response, Washington, DC. December. Available at <http://www.epa.gov/osw/hazard/testmethods/sw846/pdfs/8000b.pdf>.
- U.S. EPA (Environmental Protection Agency). 1999a. *Compendium of Methods for the Determination of Toxic Organic Compounds in Ambient Air, Second Edition, Compendium Method TO-14Ab: Determination of Volatile Organic Compounds (VOCs) in Ambient Air Using Specially Prepared Canisters With Subsequent Analysis By Gas Chromatography*. EPA/625/R-96/010b. Available at <http://www.epa.gov/ttnamti1/files/ambient/airtox/to-14ar.pdf>.
- U.S. EPA (Environmental Protection Agency). 1999b. *Compendium of Methods for the Determination of Toxic Organic Compounds in Ambient Air Second Edition Compendium Method TO-15 Determination of Volatile Organic Compounds (VOCs) in Air Collected in Specially-Prepared Canisters and Analyzed by Gas Chromatography Mass Spectrometry (GC/MS)*. EPA/625/R-96/010b. Available at <http://www.epa.gov/ttnamti1/files/ambient/airtox/to-15r.pdf>.
- U.S. EPA (Environmental Protection Agency). 1999c. *Compendium of Methods for the Determination of Toxic Organic Compounds in Ambient Air, Second Edition, Compendium Method TO-17, Determination of Volatile Organic Compounds in Ambient Air Using Active Sampling Onto Sorbent Tubes*. EPA/625/R-96/010b. Available at <http://www.epa.gov/ttnamti1/files/ambient/airtox/to-17r.pdf>.
- U.S. EPA (Environmental Protection Agency). 2002a. *OSWER Draft Guidance for Evaluating the Vapor Intrusion to Indoor Air Pathway from Groundwater and Soils (Subsurface Vapor Intrusion Guidance)*. EPA530-D-02-004. Available at <http://www.epa.gov/correctiveaction/eis/vapor.htm>

- U.S. EPA (Environmental Protection Agency). 2002b. *Guidance on Environmental Data Verification and Validation*. EPA QA/G-8 EPA/240/R-02/004. November. Available at <http://www.epa.gov/quality/qs-docs/g8-final.pdf>.
- U.S. EPA (Environmental Protection Agency). 2002c. *Calculating Upper Confidence Limits for Exposure Point Concentrations at Hazardous Waste Sites*. Office of Emergency and Remedial Response, Washington, D.C. December. <http://www.epa.gov/oswer/riskassessment/pdf/ucl.pdf>.
- U.S. EPA (Environmental Protection Agency). 2003. *A Standardized EPA Protocol for Characterization of Indoor Air Quality in Large Office Buildings*. U.S. EPA Indoor Air Division and Atmospheric Research and Exposure Assessment Laboratory. Available at http://www.epa.gov/iaq/base/pdfs/2003_base_protocol.pdf.
- U.S. EPA (Environmental Protection Agency). 2003b. *Purge-and-Trap for Aqueous Samples*. SW-846 Method 5030c, Revision 3. Office of Solid Waste and Emergency Response, Washington, DC. December. Available at <http://www.epa.gov/osw/hazard/testmethods/pdfs/5030c.pdf>.
- U.S. EPA (Environmental Protection Agency). 2005a. *Draft Standard Operating Procedure (SOP) for Installation of Sub-Slab Vapor Probes and Sampling Using EPA Method TO-15 to Support Vapor Intrusion Investigations*. Office of Research and Development. Ada, OK. Available at http://www2.epa.gov/sites/production/files/documents/epa_sub-slabvapor.pdf.
- U.S. EPA (Environmental Protection Agency). 2005b. *DRAFT Assessment of Vapor Intrusion in Homes Near the Former Raymark Superfund Site - Recommendations for Testing at Other Sites*.
- U.S. EPA (Environmental Protection Agency). 2008. *Engineering Issue: Indoor Air Vapor Intrusion Mitigation Approaches*. EPA/600/R-08-115. National Risk Management Research Laboratory, Cincinnati, OH. <http://www.clu-in.org/download/char/600r08115.pdf>
- U.S. EPA (Environmental Protection Agency). 2008b. *U.S. EPA Contract Laboratory Program National Functional Guidelines for Superfund Organic Methods Data Review*. EPA-540-R-08-01. Office of Superfund Remediation and Technology Innovation, Washington, DC. June. Available at <http://epa.gov/superfund/programs/clp/download/somnfg.pdf>.
- U.S. EPA (Environmental Protection Agency). 2009. *Risk Assessment Guidance for Superfund Volume I: Human Health Evaluation Manual (Part F, Supplemental Guidance for Inhalation Risk Assessment)*. EPA-540-R-070-002, OSWER 9285.7-82. Office of Superfund Remediation and Technology Innovation, Washington, DC. January. Available at <http://www.epa.gov/oswer/riskassessment/ragsf/index.htm>.
- U.S. EPA (Environmental Protection Agency). 2011. *Exposure Factors Handbook 2011 Edition (Final)*. EPA/600/R-09/052F. 2011. Office of Research and Development, Washington, DC.
- U.S. EPA (Environmental Protection Agency). 2012a. *Fluctuation of Indoor Radon and VOC Concentrations Due to Seasonal Variability*. EPA/600/R-12/673. Office of Research and Development, Las Vegas, NV. September. Available at <http://www.clu-in.org/download/contaminantfocus/vi/VI-EPA600-R-09-073.pdf>
- U.S. EPA (Environmental Protection Agency). 2012b. *EPA On-line Tools for Site Assessment Calculation: Johnson and Ettinger Attenuation Factor*. U.S. EPA Ecosystems Research, Athens, GA. Available at http://www.epa.gov/athens/learn2model/part-two/onsite/jne_alpha.htm.

- U.S. EPA (Environmental Protection Agency). 2012c. *EPA's Vapor Intrusion Database: Evaluation and Characterization of Attenuation Factors for Chlorinated Volatile Organic Compounds and Residential Buildings*. EPA 530-R-10-002. Office of Solid Waste and Emergency Response, Washington, DC. March. Available at http://www.epa.gov/oswer/vaporintrusion/documents/OSWER_2010_Database_Report_03-16-2012_Final_witherratum_508.pdf
- U.S. EPA (Environmental Protection Agency). 2012d. *Conceptual Model Scenarios for the Vapor Intrusion Pathway*. Office of Solid Waste and Emergency Response, Washington, DC. Available at <http://www.epa.gov/oswer/vaporintrusion/documents/vi-cms-v11final-2-24-2012.pdf>.
- U.S. EPA (Environmental Protection Agency). 2012e. *Drinking Water Contaminants*. Available at <http://water.epa.gov/drink/contaminants/index.cfm>.
- U.S. EPA (Environmental Protection Agency). 2012f. *Petroleum Hydrocarbons and Chlorinated Hydrocarbons Differ In Their Potential for Vapor Intrusion*. Information Paper. Office of Underground Storage Tanks, Washington, DC. March. Available at <http://www.epa.gov/oust/cat/pvi/pvicvi.pdf>.
- U.S. EPA (Environmental Protection Agency). 2012g. *A Citizen's Guide to Radon*. EPA 402-K-12-002. Office of Air and Radiation, Indoor Environments Division. Washington, DC. May. <http://www.epa.gov/radon/pubs/citguide.html>.
- U.S. EPA (Environmental Protection Agency). 2013. *Assessment of Mitigation Systems on Vapor Intrusion*. EPA/600/R-13/241. Office of Research and Development, National Exposure Research Laboratory. Las Vegas, NV. October.
- USGS (Geological Survey). 2001. *User's Guide for Polyethylene-Based Passive Diffusion Bag Samplers to Obtain Volatile Organic Compound Concentrations in Wells*. Water-Resources Investigations Report 01-4060. Columbia, SC. Available at: <http://sc.water.usgs.gov/publications/pdf/WRIR01-4060.pdf>.
- University of Minnesota. 2008. *Re-Arch: The Initiative for Renewable Energy in Architecture*. Fact Sheet. University of Minnesota Initiative for Renewable Energy in Architecture (re-ARCH). Available at <http://www.research.umn.edu/factsheets/VentilationFactSheet.pdf>.
- Wang, F., and I.C. Ward. 2000. The development of a radon entry model for a house with a cellar. *Building and Environment* 35:615–631.
- Wania, F., J.T. Hoff, C.Q. Jia, and D. Mackay. 1998. The effects of snow and ice on the environmental behaviour of hydrophobic organic chemicals. *Environmental Pollution* 102(1):25-41.
- Weinberg, N., C. Lutes, M. Bartee, R. Norberg, R. Truesdale, and B. Schumacher. 2014. A risk assessment comparison: evaluation of relevant indoor air exposure concentrations and periods and implications for developing indoor air sampling plans. *Proceedings of AWMA Vapor Intrusion, Remediation, and Site Closure Conference*, Cherry Hill, NJ. September.
- Wertz, W., and T. Festa. 2007. The patchy fog model of vapor intrusion. Pp. 28–36 in *Proceedings of AWMA Conference on Vapor Intrusion: Learning from the Challenges*, Providence, RI, September 26–28. Pittsburgh, PA: Air and Waste Management Association.

- White, R.G. 1964. Determination of carbon disulfide in benzene by ultraviolet spectrophotometry. *Applied Spectroscopy* 18(4):112-113.
- Whitmore, A., and R.L. Corsi. 1994. Measurement of gas-liquid mass transfer coefficients for volatile organic compounds in sewers. *Environmental Progress* May:114–123.
- Wickham, H. 2009. *ggplot2: Elegant Graphics for Data Analysis*. New York: Springer.
- Wilson, L.G., L.G. Everett, and S.J. Cullen (Eds.). 1995. *Handbook of Vadose Zone Characterization and Monitoring*. Boca Raton, FL: Lewis Publishers.
- Winberry, W. T., L. Forehand, N.T. Murphy, A. Ceroli, B. Phinney, and A. Evans. 1990. *Compendium of Methods for the Determination of Air Pollutants in Indoor Air*. EPA/600/4-90/010. U.S. Environmental Protection Agency, Office of Research and Development, Research Triangle Park, NC. April.
- Wisbeck D., C. Sharpe, A. Frizzell, C. Lutes, and N. Weinberg. 2006. Using naturally occurring radon as a tracer for vapor intrusion: a case study. ARCADIS, presented at the 2006 *Society of Risk Analysis (SRA) Annual Meeting*, Baltimore, MD.
- Yamazawa, H., T. Miyazaki, J. Moriizumia, T. Iida, S. Takeda, S. Nagarab, K. Satob, and T. Tokizawab. 2005. High levels of natural radiation and radon areas: radiation dose and health effects. *Proceedings of the 6th International Conference on High Levels of Natural Radiation and Radon Areas*. International Congress Series. 1276:221–222. February. Available at <http://www.sciencedirect.com/science/article/pii/S0531513104017947>
- Yao, Y., K.G. Pennell, and E.M. Suuberg. 2010. *Proceedings of the Air & Waste Management Association's Vapor Intrusion 2010 Conference*. September 29–30. Available at <http://www.clu-in.org/download/contaminantfocus/vi/The%20Influence%20of%20Transient%20Processes.pdf>
- Yeates, G.L., and D.M. Nielsen. 1987. Design and implementation of an effective soil gas monitoring program for four-dimensional monitoring of volatile organics in the subsurface. In *Proceedings of the NWWA Focus Conference on Ground Water Issues*. Indianapolis, IN. April 21–23.
- Zhao, Y., and C. Frey. 2006. Uncertainty for data with non-detects: air toxic emissions from combustion. *Human and Ecological Risk Assessment* 12:1171–1191.



Office of Research
and Development (8101R)
Washington, DC 20460

Official Business
Penalty for Private Use
\$300

EPA/600/R-15/070
October 2015
www.epa.gov

Please make all necessary changes on the below label, detach or copy and return to the address in the upper left hand corner.

If you do not wish to receive these reports CHECK HERE ; detach, or copy this cover, and return to the address in the upper left hand corner.

PRESORTED STANDARD
POSTAGE & FEES PAID
EPA PERMIT No. G-35



Recycled/Recyclable
Printed with vegetable-based ink on
paper that contains a minimum of
50% post-consumer fiber content
processed chlorine free